UNIVERSITY OF COPENHAGEN
FACULTY OF SCIENCE

NONLINEAR DYNAMICS IN GENERAL RELATIVITY

DOCTORAL THESIS

This thesis has been submitted to the PhD School of
The Faculty of Science, University of Copenhagen.

by

JAIME REDONDO-YUSTE

This thesis has been carried out at the Center of Gravity, Niels Bohr Institute. The Center of Gravity is a Center of Excellence funded by the Danish National Research Foundation under grant no. DNRF184. I also acknowledge support by the VILLUM Foundation (grant no. VIL37766), the DNRF Chair program (grant no. DNRF162) by the Danish National Research Foundation and the European Union's H2020 ERC Advanced Grant "Black holes: gravitational engines of discovery" grant agreement no. Gravitas–101052587.

ASSESMENT COMMITTEE

SUPERVISOR

prof. dr. V. Cardoso	Københavns Universitet Instituto Superior Técnico da Universidade de Lisboa

ASSESSMENT COMMITTEE

dr. E. Most	California Institute of Technology
dr. B. Bonga	Radboud University
dr. M. van de Meent	Københavns Universitet

NIELS BOHR INSTITUTE, UNIVERSITY OF COPENHAGEN

A Félix Yuste Latasa, el Carapo.

ABSTRACT / ABSTRAKT

The detection of gravitational waves has opened a new window into the strong-field regime of gravity and matter at extreme densities. This thesis investigates how the nonlinear character of Einstein's equations manifests itself in the relaxation of black holes to equilibrium and in the interaction between gravitational waves and matter.

The first part of the thesis is devoted to nonlinear effects in black hole ringdown. I show that perturbation theory predicts the excitation of higher harmonics arising from nonlinear couplings of the characteristic vibrational modes of the ringing black hole. I characterise the properties of these higher harmonics, identifying them as a new observable of interest for future gravitational wave detectors, and lay the groundwork towards analytically modelling them in the high-frequency regime. Next, I study how accretion of gravitational waves during the merger is imprinted onto the ringdown signal. Finally, I investigate nonlinear dynamics in exotic compact objects with stable light rings, demonstrating that long-lived gravitational waves can trigger turbulent behaviour, with striking analogies to turbulence in fluid dynamics.

The second part of the thesis focuses on the interaction between gravitational waves and matter. Particular emphasis is placed on dissipative relativistic hydrodynamics, as viscosity plays for gravitational waves a role analogous to conductivity for electromagnetic radiation. I develop the formalism to describe the relaxation to equilibrium of a perturbed viscous star within a well-posed relativistic Navier-Stokes theory. This formalism is then applied to study the reflection and absorption of gravitational waves by a compact neutron star, as well as the impact of viscosity on its characteristic oscillation modes. At a later stage I demonstrate that low-frequency gravitational waves can be superradiantly amplified when scattered off a rotating viscous star.

Overall, this thesis advances our knowledge of strong-field gravity along two complementary directions. On the one hand, it contributes to the development of a nonlinear paradigm for black hole spectroscopy, shedding light on the rich spacetime dynamics that unfold in the aftermath of black hole mergers. On the other hand, it establishes how dissipative effects in neutron star matter leave distinct imprints on gravitational wave signals. These signatures provide a new avenue for probing the microphysical properties of dense matter in neutron star interiors using gravitational wave observations.

Upcoming gravitational wave detectors will observe black holes ring down with unprecedented accuracy and detect mergers of neutron stars across the observable Universe. The resulting wealth of data carries pristine information about black holes, neutron stars, and the fundamental laws governing their dynamics. With an improved theoretical understanding of nonlinear gravitational phenomena and the role of dissipation in neutron star matter, this information can be decoded to address unanswered questions about gravity, matter, and the structure of spacetime.

Dansk oversættelse

Opdagelsen af gravitationsbølger har åbnet et nyt vindue ind til tyngdekraftens stærke feltregime og stof ved ekstreme densiteter. Denne tese undersøger, hvordan de ikke-lineære karakteristika i Einsteins ligninger manifesterer sig i sorte hullers afslapning mod ligevægt samt i interaktionen mellem gravitationsbølger og stof.

Den første del af tesen er afsat til ikke-lineære effekter i ringdown-fasen for et sort hul. Jeg viser, at perturbationsteori forudsiger exciteringen af højere harmoniske komponenter, som opstår gennem ikke-lineære koblinger mellem de karakteristiske vibrationsmoder i det afklingende sorte hul. Jeg karakteriserer egenskaberne af disse højere harmoniske komponenter ved at identificere dem som nye observerbare størrelser af interesse for fremtidige detektorer og lægge grundlaget for en analytisk model af dem i højfrekvensregimet. Herefter studerer jeg, hvordan akkretionsprocessen af gravitationsbølger under sammenstødet er indkodet i ringdown-signalet. Til sidst undersøger jeg ikke-lineære dynamikker i eksotiske kompakte objekter med stabile fotonringe, hvor jeg demonstrerer, at langtlevende gravitationsbølger kan medføre turbulent adfærd, med en tæt analogi til turbulens i væskedynamik.

Anden del af tesen fokuserer på interaktionen mellem gravitationsbølger og stof. Der lægges særligt vægt på relativistisk hydrodynamik med dissipative effekter, da viskositet for gravitationsbølger fungerer på en måde, der svarer til ledningsevne for elektromagnetisk stråling. Jeg udviklede en formulisme for at beskrive afslapningen til ekvilibrium af en perturberet viskøs stjerne under en veldefineret relativistisk Navier–Stokes-teori. Denne formulisme er derefter brugt til at studere refleksion og absorption af gravitationsbølger i en neutronstjerne samt virkningen af viskositet på dens karakteristiske oscillationer. Senere viser jeg, at gravitationsbølger med lav frekvens kan forstærkes superradiant, når de spredes fra en roterende stjerne.

Samlet set udvider denne tese vores forståelse af tyngdekraftens stærke feltregime i to komplementære retninger. På den ene side bidrager den til udviklingen af et ikke-lineært paradigme for sort hul-spektroskopi, der fortæller os noget om den komplekse rumtid-dynamik, der udfolder sig i kølvandet på sammenstødet mellem sorte huller. På den anden side viser den, hvordan dissipative effekter i neutronstjernemateriale efterlader tydelige aftryk i gravitationsbølgesignaler. Disse signaturer giver os en ny mulighed for at undersøge de mikrofysiske egenskaber af tæt stof i neutronstjerners indre ved hjælp af observationer af gravitationsbølger.

Fremtidige gravitationsbølgedetektorer vil observere ringdown-fasen af sorte huller med hidtil uset nøjagtighed og detektere sammenstød mellem neutronstjerner i hele det observerbare univers. De derved opnåede store mængder data rummer ren information om sorte huller, neutronstjerner og de fundamentale love, der styrer deres dynamik. Med en nu forbedret teoretisk forståelse af ikke-lineære gravitationsfænomener og rollen af dissipative effekter i neutronstjernemateriale kan denne information udnyttes til at belyse ubesvarede spørgsmål om tyngdekraft, stof og rumtidens struktur.

Oversat af Leart Sabani

PUBLICATIONS

The thesis is based on, and partially consists of reprints of these publications.

1. Jaime Redondo-Yuste et al. "Spin dependence of black hole ringdown nonlinearities." In: *Phys. Rev. D* 109.10 (2024), p. L101503. DOI: 10.1103/PhysRevD.109.L101503. arXiv: 2308.14796 [gr-qc]
   Presented in Chapter 5.

2. Bruno Bucciotti et al. "Ringdown nonlinearities in the eikonal regime." In: *Phys. Rev. D* 111.8 (2025), p. L081502. DOI: 10.1103/PhysRevD.111.L081502. arXiv: 2501.17950 [gr-qc]
   Presented in Chapter 5.

3. Kwinten Fransen, David Pereñiguez, and Jaime Redondo-Yuste. "Perturbations of Plane Waves and Quadratic Quasinormal Modes on the Lightring." In: *JHEP* 2025.12 (Dec. 2025), p. 148. DOI: 10.1007/JHEP12(2025)148. arXiv: 2509.03598. URL: https://doi.org/10.1007/JHEP12(2025)148
   Presented in Chapter 6.

4. Jaime Redondo-Yuste, David Pereñiguez, and Vitor Cardoso. "Ringdown of a dynamical spacetime." In: *Phys. Rev. D* 109.4 (2024), p. 044048. DOI: 10.1103/PhysRevD.109.044048. arXiv: 2312.04633 [gr-qc]
   Presented in Chapter 7.

5. Jaime Redondo-Yuste and Alejandro Cárdenas-Avendaño. "Perturbative and nonlinear analyses of gravitational turbulence in spacetimes with stable light rings." In: *Phys. Rev. D* 111.12 (2025), p. 124009. DOI: 10.1103/hy3r-ww3w. arXiv: 2502.18643 [gr-qc]
   Presented in Chapter 8.

6. Jaime Redondo-Yuste. "Perturbations of relativistic dissipative stars." In: *Class. Quant. Grav.* 42.7 (2025), p. 075012. DOI: 10.1088/1361-6382/adbfef. arXiv: 2411.16841 [gr-qc]
   Presented in Chapter 10.

7. Valentin Boyanov et al. "Dynamical Response of Viscous Objects to Gravitational Waves." In: *Phys. Rev. Lett.* 135.15 (2025), p. 151402. DOI: 10.1103/smlr-v7b2. arXiv: 2411.16861 [gr-qc]
   Presented in Chapter 11.

8. Jaime Redondo-Yuste and Vitor Cardoso. "Superradiant amplification by rotating viscous compact objects." In: *Phys. Rev. D* 112.6 (2025), p. L061501.

DOI: 10.1103/gvd3-lqkv. arXiv: 2506.13850 [gr-qc]
Presented in Chapter 12.

The following publications were also completed during the course of this PhD, although they do not form part of this thesis.

9. Finnian Gray et al. "Carrollian motion in magnetized black hole horizons." In: *Phys. Rev. D* 107.6 (2023), p. 064009. DOI: 10.1103/PhysRevD.107.064009. arXiv: 2211.13695 [gr-qc]

10. Jaime Redondo-Yuste and Luis Lehner. "Non-linear black hole dynamics and Carrollian fluids." In: *JHEP* 02 (2023), p. 240. DOI: 10.1007/JHEP02(2023)240. arXiv: 2212.06175 [gr-qc]

11. Jaime Redondo-Yuste et al. "Eternal binaries." In: *Phys. Rev. D* 107.12 (2023), p. 124025. DOI: 10.1103/PhysRevD.107.124025. arXiv: 2304.02039 [gr-qc]

12. Alessia Platania and Jaime Redondo-Yuste. "Diverging black hole entropy from quantum infrared non-localities." In: *Phys. Lett. B* 857 (2024), p. 138993. DOI: 10.1016/j.physletb.2024.138993. arXiv: 2303.17621 [hep-th]

13. Conor Dyson et al. "Relativistic aerodynamics of spinning black holes." In: *Phys. Rev. D* 109.10 (2024), p. 104038. DOI: 10.1103/PhysRevD.109.104038. arXiv: 2402.07981 [gr-qc]

14. Vitor Cardoso et al. "Hushing black holes: Tails in dynamical spacetimes." In: *Phys. Rev. D* 109.12 (2024), p. L121502. DOI: 10.1103/PhysRevD.109.L121502. arXiv: 2405.12290 [gr-qc]

15. Davide Gaiotto et al. "Twisted Traces on Abelian Quantum Higgs and Coulomb Branches." In: *Commun. Math. Phys.* 406.9 (2025), p. 202. DOI: 10.1007/s00220-025-05379-2. arXiv: 2308.15198 [hep-th]

16. Juno C. L. Chan et al. "Lensing and wave optics in the strong field of a black hole." In: *Phys. Rev. D* 112.6 (2025), p. 064009. DOI: 10.1103/6h6r-46cd. arXiv: 2502.14073 [gr-qc]

17. Emanuele Berti et al. "Black hole spectroscopy: from theory to experiment." In: (May 2025). arXiv: 2505.23895 [gr-qc]

ACKNOWLEDGMENTS

The past three years have been a thrilling ride, riddled with the joy of discovery and the chaos of nights and days spent out and about, full of hygge evenings, tasty pastries, and baggy-eyed mornings alike. To everyone that contributed to these moments, a heartfelt thank you.

Vitor has been the best supervisor I could have asked for. Thank you for believing in me. You have taught me a great deal of science, but the key lesson I take from you is that hard work goes a long way. I will always cherish those moments staring at the same blackboard, excited about figuring something out only to realise minutes later that we were wrong. Thank you for your generosity: so often I felt I could not tell whether an idea had been mine or yours all along. And finally, thank you for so many fascinating discussions that so often went beyond science into the realm of art or of pure craziness. We will build a black hole together.

The Strong group, as a whole, has felt like a family away from home. A family driven by a shared curiosity, and a shared excitement about life in a new place. Julie, you made this possible. The Strong years happened, and they were as wonderful as they could be. Your kindness, your hard work, your patience, and your readiness to fight our battles for us were essential for all of us, they certainly were for me. Thank you for the coffee, for the smiles, and for your friendship.

I had the fortune to engage with many brilliant colleagues during these years. However, David has become the best collaborator I could have asked for, and a better friend than I could possibly deserve. I have learned so much from you that I would be proud if I managed to teach back even 1/% of what you taught me. Thank you for all the belays, beers, and banter, and I only wish for the future our collaboration will continue, I am certain our friendship will. I must also thank my collaborators Alejandro, Caio, Emanuele, Gregorio, Kwinten, and Maarten. I learned from each of you, and working with you made me better in every possible way. Finally, a big thank you to Frans for welcoming me in Princeton and for always finding time to discuss and entertain every idea, no matter how crazy. A warm thanks to all the folks I met in the States, and especially to Alex and Carolina for welcoming me and opening their home to me when I had nowhere else to go.

In September 2022, I arrived in a city I had never been to, to work with a group that did not yet exist, and to live with two guys I had never met. Conor, Thomas: thank you for taking this gamble with me. These years have been an unbelievable adventure, and I would not have chosen different companions for this ride. Jose, you have been a true role model. I wish to be a little bit like you when I grow up. Thank you also to Marina and Juno for sharing this ride together, and for killing the spiders in the kitchen. To Luka: know that you are brilliant. Thank you for always being there, and for some of the most interesting conversations I have ever shared. Thank you to Francesco D. P. for jazzy nights, and to Francesco F. for all

the movie nights, sunbathing days, and for your gentleness and tenderness. Lastly, thanks to Lorenz and all of Batch 47-B for rolling dice together; to Vasco and João for making such a big impact in such a short time; to David for the wonderful moments shared climbing together; to Cristina and Emily for all the Friday beers, fun evenings, and shared confessions; and to Stéphanie, Trine, and Swantje for all the ice cream, Suits, and Sex and the City. Copenhagen has provided the perfect scenery for all this, and communities such as cph4water, the wonderfully curated program at the Cinemateket, and the bmos at Sinne Gas Bageri have played a major role in making my time here all the more enjoyable.

I also think now of the friendships I cherish all around the world. To Carlos and Diego, I owe you so much. Alicia, Miguel, Ivan, Silvia: I deeply miss your warmth; being with you feels like being home. Thanks to Tessa for welcoming me to New York again and again, and for inspiring me, I am so proud to be your friend. Thanks to Jordan, Sotiris, Eivind, and Charlie for being like siblings in pursuit of the same dream. Thanks as well to Matt for possibly the best road trip of my life. To Manu, Shawn, and Anna, thank you for bringing to life one of the craziest dreams I could ever imagine. Those long calls, discussing line after line, were some of the most frustrating, but also some of the most rewarding moments of these past years.

To Anna, words do not suffice to express my gratitude. You have been the lighthouse guiding my way back to shore every time I felt lost. Your sense of wonder is contagious, and you have inspired me to be a better scientist, and also a better human being. Thank you for making me change my mind: if forever were ours together, I would choose it.

Por último, no puedo dejar de agradecer la inestimable labor de mi maravillosa familia, las personas más importantes de mi vida. Gracias a mis abuelos, que me demostraron desde niño un ejemplo de esfuerzo, constancia, y sobre todo, amor – *lo importante, es que seáis buenas personas*. Mi hermano Sergio ha sido, es, y será mi modelo a seguir. Gracias por tu amistad, por compartir buenos y malos momentos, y por tu apoyo incondicional y constante. Ojalá algún día me parezca más a ti. Gracias de corazón a mis padres, Mario y Rosa. Ellos me enseñaron el valor del trabajo, ellos confiaron en mí antes que yo confiara en mí mismo, y ellos me apoyaron siempre y en todo momento para cumplir mis sueños. Gracias por vuestro amor. Gracias por vuestra fe en mi. Gracias por darme alas para volar mi propio vuelo.

CONTENTS

Part I

GRAVITATIONAL MUSINGS

The idea of infinity cannot be expressed in words or even described, but it can be apprehended through art, which makes infinity tangible. The absolute is only attainable through faith and in the creative act.

— *Andrei Tarkovsky,* Sculpting on Time

1

INTRODUCTION

Written while listening to music composed by Igor Stravinsky.

Barely a hundred steps from the Niels Bohr Institute lies Sortedams Sø. I often find myself walking along its shore. It takes about twenty to thirty minutes to circle the lake, which I find is just long enough for the mind to shed the last meeting or calculation and ready itself for something new. As I walk, I wonder about the lake's history. Sortedams Sø looks rather uninteresting: it is shallow, its water frequently has a foul smell, and its only landmark is Fugleøen, an artificial island where cormorants breed. Nonetheless, its history is quite fascinating. Originally built as a moat, it was later turned into a water reservoir, and now it sets the stage for swans, running clubs, ducks, and first dates. In 1944, a German BV 138 attempted an emergency landing here, ending in disaster for two crewmen and a remarkably unlucky passerby. In 1967, seven activists seized Fugleøen, declared themselves an anarchist republic, and applied for membership in the United Nations. After a day, they rowed back to shore.

Amid these human affairs, I wonder: has the water of Sortedams Sø always looked the same? In winter it sometimes freezes, and on those rare days it is different. But the surface I watch now must resemble what those seven activists saw before founding their nation, or the final glimpse of that doomed passerby in the spring of 1944. The world outside has changed: I do not walk in a Nazi-occupied Denmark, nor do many still hold the ideals of peace and love. Yet something remains.

That feeling explains my fascination with physics. What laws of nature remain immutable? What are the laws that allow us to look back and say with confidence that, on a sunny summer day, Sortedams Sø would not have looked much different than it does now? This pursuit of universality finds its full power in experiment and in the language of mathematics [461]. Centuries of work, and the vast efforts of brilliant men and women, have revealed that a handful of fundamental equations govern natural phenomena at scales ranging from the inhumanly tiny to the otherworldly enormous. We often speak of four fundamental interactions: electromagnetism, the weak force, the strong force, and gravity.

One aspect is particularly remarkable to me: three of these four interactions are nonlinear. By this I mean, simply, that their vacuum equations are nonlinear in the strict mathematical sense. As Stanisław Ulam famously remarked, "Using a term like nonlinear science is like referring to the bulk of zoology as the study of non-elephant animals." Extending the list beyond these interactions to include

the emergent laws of complex macroscopic systems, such as fluid dynamics or magnetohydrodynamics, we find that the vast majority of physical systems, from the oceans to the cytoplasm, from stellar nurseries to green laser pointers, are nonlinear.

Nonlinear equations predict a fascinating wealth of phenomena that, in one way or another, govern our lives. One such example is chaos: small disturbances can lead to dramatic consequences. Chaos manifests, for instance, in the context of what we dub turbulence. Defining turbulence in sufficient generality is itself a complex problem. The best definition I have heard in all these years I owe to Frans Pretorius, who, paraphrasing Supreme Court Justice Potter Stewart, claimed: "I know it when I see it" [1]. Turbulence has fascinated physicists for generations. Heisenberg is quoted as having said on his deathbed: "When I meet God, I am going to ask him two questions: Why relativity? And why turbulence? I really believe He will have an answer for the first." This is not a thesis about turbulence, but it is, perhaps, a thesis inspired by turbulent dynamics.

The other essential ingredient of this thesis is General Relativity. Einstein's theory of gravitation is remarkably beautiful and deeply challenging at the same time. One aspect that makes it beautiful is that, unlike most other physical theories, the background structure is itself the dynamical field. The motion of ocean currents is affected by the rotation of the Earth, yet it does not shorten the duration of a day. By contrast, the motion of a mass is affected by the local gravitational field and simultaneously modifies it. This mutual interaction is ultimately one of the reasons General Relativity is so challenging.

Beyond its mathematical elegance, the merit of Einstein's theory of gravitation lies in its extraordinary predictive power in describing the most energetic processes in the Universe. A paradigmatic example are black holes (BHs). BHs are nonlinear solutions of Einstein's equations, with no strict analogue in Newtonian gravity. A single equation, with only two free parameters, describing the geometry of a BH captures both the end state of massive stars and the dynamics of galactic centres. Very few solutions in physics explain a range of natural phenomena spanning seven orders of magnitude, which makes BHs truly exceptional.

A major milestone in General Relativity was the detection of gravitational waves (GWs) in 2015 by the LIGO collaboration [5]. Einstein had already predicted in 1916 that moving massive bodies could source ripples in spacetime that carry energy and angular momentum, and are therefore detectable [184, 185]. It is worth emphasizing how remarkable these detections are. The LIGO–Virgo–KAGRA collaboration has now detected more than one hundred GW events from the mergers of compact objects. Two black holes, already extraordinary objects on their own, find each other in a cosmic dance, orbiting and inspiraling until, in a fraction of a second, they emit an amount of energy that, if converted to visible light at Earth, would make the night sky appear as bright as day. Millions of years pass while these spacetime ripples propagate through the Universe, and we happen to live in the privileged

1 In *Jacobellis v. Ohio*, Stewart used these words to argue that the material at hand was not obscene.

generation that has measured, for the first time in human history, this new form of cosmic messenger.

Ten years after that first detection, interest in GWs has only grown. They offer vast discovery potential: in just a decade, we have learned that BHs exist with masses beyond previous expectations [2], that light propagates at the same speed as GWs [6], and that General Relativity remains extraordinarily accurate even in extremely strong and highly dynamical gravitational fields [3, 7]. Understanding and interpreting GWs, including nonlinear phenomena, is therefore the primary goal of this thesis.

There exists yet another class of compact objects that is as intriguing as BHs: *neutron stars*. These are extremely dense stars, compressing nearly twice the mass of the Sun into a sphere that would fit within the municipality of Copenhagen. In fact, they are so dense that atoms can no longer exist in their interiors; their cores are instead filled with a soup of neutrons, hence the name. Their extreme compactness means that General Relativity is essential for understanding their dynamics. At the same time, the matter in their interiors is cold and ultra-dense, pushing our knowledge of nuclear physics beyond its limits. All four fundamental interactions play a major role in describing neutron star dynamics, and by studying them we may not only answer questions about gravitation, but also gain insight into quantum chromodynamics and the physics of neutrinos. The final part of this thesis is concerned with the interaction between GWs and neutron stars.

Before turning to the technical details, we introduce two of the central concepts of this thesis, GWs and BHs, and outline its overall structure.

1.1 BASIC CONCEPTS

1.1.1 *What are Gravitational Waves?*

General Relativity describes the spacetime as a four-dimensional Lorentzian manifold $(\mathcal{M}, g)$, equipped with the Levi-Civita connection ∇_a. The dynamics is governed by the Einstein-Hilbert action

$$S = \int_{\mathcal{M}} d^4x \sqrt{-g} \Big(\frac{1}{2\kappa} R + \mathcal{L}_M \Big) \,, \tag{1.1}$$

where $\kappa = 8\pi G/c^4 = 8\pi$ in geometric units, R is the Ricci scalar, and $\mathcal{L}_M$ is the matter lagrangian. Demanding that the action is stationary, and assuming spacetime has no boundaries, we recover Einstein's equations

$$G_{ab} \equiv R_{ab} - \frac{1}{2} R g_{ab} = \kappa T_{ab} \,, \qquad T_{ab} = \frac{-2}{\sqrt{-g}} \frac{\delta(\sqrt{-g}\mathcal{L}_M)}{\delta g^{ab}} \,, \tag{1.2}$$

where T_{ab} is the *stress-energy tensor*. For day-to-day classical physics, the spacetime is well described by the Minkowski solution $g = \eta$

$$\eta_{ab} dx^a dx^b = -dt^2 + dx^2 + dy^2 + dz^2 \,, \tag{1.3}$$

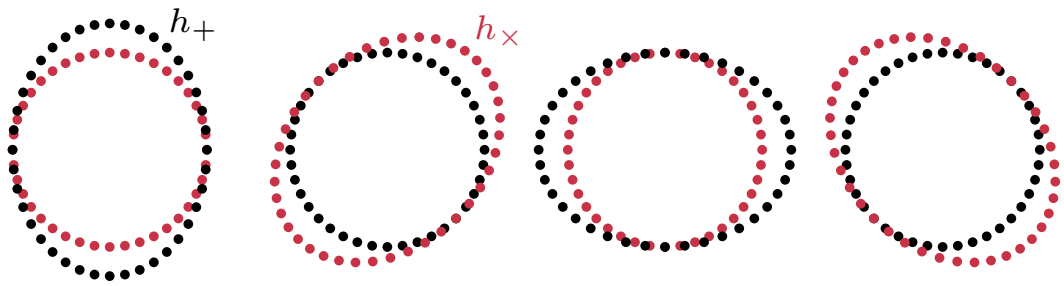

Figure 1 Schematic representation of the shape of a ring of freely falling particles under the passing of a + polarised GW (black), and a × polarised GW (red).

in the usual Cartesian coordinates. This is a vacuum solution of Einstein equations, meaning it solves (1.2) setting $T_{ab} = 0$, and all curvature tensors vanish. Hence we refer to this as *flat* spacetime. Small deviations around flat spacetime can be captured perturbatively, assuming that the spacetime geometry is everywhere close to the Minkowski spacetime, $g_{ab} = \eta_{ab} + \epsilon h_{ab}$, with $\epsilon \ll 1$. By appropriately choosing the coordinates up to order $\mathcal{O}(\epsilon)$, we can always assume the metric perturbation h_{ab} is in the transverse and traceless (TT) gauge:

$$\nabla^b h_{ab} = 0\,, \qquad \eta^{ab} h_{ab} = 0\,. \tag{1.4}$$

The linearised Einstein equations in vacuum lead to a wave equation for the metric perturbation

$$\Box h_{ab} = 0\,. \tag{1.5}$$

Thus, General Relativity predicts the existence of spacetime waves, propagating exactly at the speed of light (along null cones). It is possible to find two (and only two!) covariantly conserved polarisation tensors $\epsilon^+_{ab}, \epsilon^\times_{ab}$, that capture the two propagating degrees of freedom. If we consider GWs propagating along the z direction, we can write

$$h_{ab} = e^{i\omega(z-t)} \left(h_+ \epsilon^+_{ab} + h_\times \epsilon^\times_{ab} \right), \tag{1.6}$$

with $h_{+,\times}$ the *GW strain* in the $+, \times$ polarizations, and the polarisation tensors are

$$\epsilon^+_{ab} = \begin{pmatrix} 0 & 0 & 0 & 0 \\ 0 & 1 & 0 & 0 \\ 0 & 0 & -1 & 0 \\ 0 & 0 & 0 & 0 \end{pmatrix}, \qquad \epsilon^\times_{ab} = \begin{pmatrix} 0 & 0 & 0 & 0 \\ 0 & 0 & 1 & 0 \\ 0 & 1 & 0 & 0 \\ 0 & 0 & 0 & 0 \end{pmatrix}. \tag{1.7}$$

Now, consider a ring of particles free-falling in the xy plane. Select any two diametrically opposed particles, and let s^i be their separation vector. The geodesic deviation equation implies that their separation evolves as

$$\frac{D^2 s^i}{D\tau^2} = -R^i_{0j0} s^j = \frac{1}{2} \frac{\partial^2 h^i_j}{\partial t^2} s^j\,, \tag{1.8}$$

and in the TT gauge, proper and coordinate time coincide to first order, so the geodesic separation between freely falling particles is simply

$$s^i(t) = s^j(0)\left(\delta_{ij} + \frac{1}{2}h_{ij}(t)\right). \tag{1.9}$$

Therefore, propagating GWs stretch and compress the spacetime between two freely-falling points by an amount that is directly proportional to the GW strain. A visualization of this effect is shown in Fig. 1. This is, in essence, the physical mechanism used to detect GWs. GW detectors are based on a laser interferometer, where the mirrors that determine the laser paths behave like freely falling particles. Changes in the length along each of the arms of the interferometer lead to an excess power in the detector after the recombination of the two signals, and this excess power can be directly linked to the GW strain. Of course this is nothing but an extremely simplified version of what is, without a doubt, one of the most precise experiments of the history of humankind.

So far, we have only discussed the propagation of GWs. These are sourced by the dynamics of matter fields and gravity (such as moving BHs). Let us recover the presence of matter fluctuations, assume the perturbation is sourced by some (small) stress-energy tensor $T_{ab} = \epsilon t_{ab}$. In general, we can no longer assume that the metric perturbation is in the TT gauge. We can always ensure the transverse condition, though, so suffices to work instead with the trace-free metric perturbation $\bar{h}_{ab} = h_{ab} - h\eta_{ab}/2$.

$$\Box\bar{h}_{ab} = 2\kappa t_{ab}\,. \tag{1.10}$$

Using the flat space Green's function we can write

$$\bar{h}_{ab} = \frac{4G}{c^4}\int d^3x' \frac{t_{ab}(ct - |x - x'|, x')}{|x - x'|}\,. \tag{1.11}$$

At large distances from the source, using the multipolar decomposition of the stress energy tensor, we find that GWs are sourced by the second-derivative of the quadrupole moment of the matter fluctuation [327]

$$h^{\rm TT}_{ab} = \frac{2G}{c^4 r}\ddot{Q}_{ij}(t - r/c)\,. \tag{1.12}$$

Two massive bodies orbiting each other are the paradigmatic example of a changing quadrupole moment in nature. However notice that the constant in front is remarkably small, $Gc^{-4} \sim 10^{-45}\mathrm{s}^2/(\mathrm{kgm})$. Therefore, generating a measurable GW strain demands remarkably large quadrupole moments, changing very rapidly. The GW strain "only" decays as $1/r$, meaning that the main difficulty in exciting GWs is generating really large quadrupole moment changes, since otherwise GWs propagate and decay as usual waves. Therefore it stands to reason that *compact binary coalescences*, meaning the orbit and ultimate merger of compact gravitating bodies, is one of the leading sources of GWs in the Universe. There are a number of other

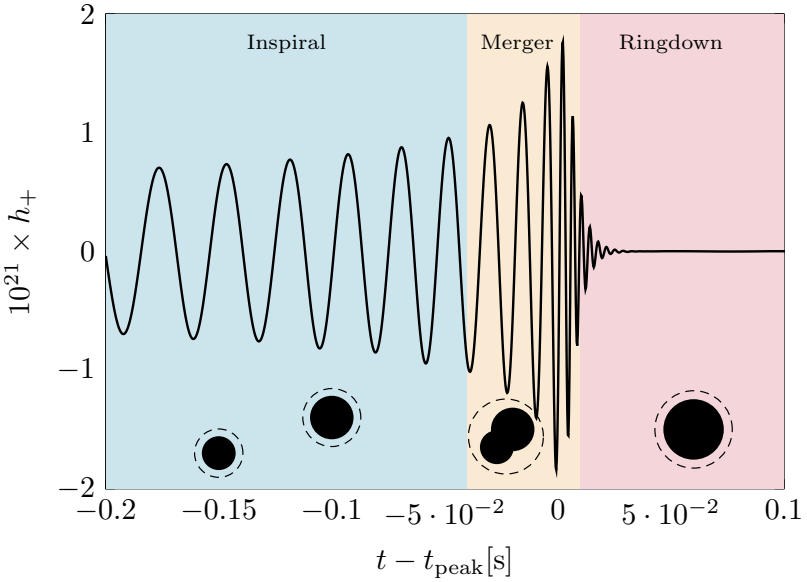

Figure 2 Characteristic GW strain at the detector for a compact binary coalescence. In this case, we consider the merger of two nonspinning BHs with masses $(m_1, m_2) = (33, 37)M_\odot$, which merged at a distance of $d_L = 410$Mpc. We highlight the three different stages of the coalescence.

physical processes which emit GWs, such as supernovae, mountains in neutron stars, superradiance, primordial GWs or phase transitions in the early Universe.

The typical GW strain emitted during a compact binary coalescence is shown in Fig. 2. Three distinct stages are highlighted in the figure: the inspiral, merger, and ringdown. This distinction is not a fundamental division, but mostly a practical one. The GWs emitted during the inspiral can be accurately modelled by the post-Newtonian or post-Minkowskian theory, in essence, refining (1.12) order by order, accounting for the relativistic motion of the source. This expansion is eventually not accurate anymore, and a numerical solution of the full Einstein equations is needed. Tackling this stage – the merger – was a profound technical and fundamental challenge, suffices to mention that the first efforts in this direction were initiated by Susan Hahn and Richard Lindquist in 1964 [234], and a complete solution describing the merger of orbiting BHs had to wait more than forty years, until the breakthroughs of 2005 [40, 96, 387]. Once the two BHs merge, the last stages of the GWs emission can be modelled perturbatively once again, albeit in a different manner. This is the ringdown regime, to which much of this thesis is devoted.

Finally, let us examine whether GWs can carry energy and angular momentum. This problem was brilliantly tackled by Isaacson [253, 254]. First of all, notice that we shall not consider GWs exclusively as perturbations to flat space, but in general as small fluctuations on some, yet-to-be-determined background, $g_{ab} = \bar{g}_{ab} + \epsilon h_{ab}$. But how do we distinguish the background from the foreground? The key idea is to consider simultaneously a split into a high-frequency sector and a low-frequency sector. Let Λ be the characteristic lengthscale of the background curvature, such that $\partial\bar{g} \sim \bar{g}/\Lambda$, and λ the lengthscale of the GWs, $\partial h \sim h/\lambda$. We now assume a

separation of scales, $\lambda \ll \Lambda$. Splitting the perturbed Einstein equations into low and high-frequencies, we encounter

$$\begin{aligned} \bar{R}_{ab} &= -\langle R^{(2)}_{ab}\rangle + \kappa\Big\langle T_{ab} - \frac{1}{2}T g_{ab}\Big\rangle\,, \\ R^{(1)}_{ab} &= -\Big[R^{(2)}_{ab}\Big]^{\text{High}} + \kappa\Big(T_{ab} - \frac{1}{2}T g_{ab}\Big)^{\text{High}}\,, \end{aligned} \tag{1.13}$$

where $\langle\cdot\rangle$ denotes the averaged quantity over a lengthscale l such that $\lambda \ll l \ll \Lambda$, effectively selecting the low-frequency content. The high superscript can be thought of as the deviations with respect to this mean field. In essence, this split is akin to how we can define waves in the ocean as small ripples with respect to an averaged water height. The second equation, omitting the higher-order term, is the one we already dealt with. But the first equation now shows that GWs can have an impact on the spacetime curvature. Notice that if we denote by $\bar{T}_{ab} = \langle T_{ab}\rangle$, and reversing the traces, then the first equation becomes

$$\bar{R}_{ab} - \frac{1}{2}\bar{R}\bar{g}_{ab} = \kappa\Big(\bar{T}_{ab} + t^{\text{GW}}_{ab}\Big)\,, \tag{1.14}$$

where t^{GW}_{ab} is the effective stress energy tensor associated to GWs, and is given by

$$t^{\text{GW}}_{ab} = -\kappa^{-1}\Big\langle R^{(2)}_{ab} - \frac{1}{2}R^{(2)}\bar{g}_{ab}\Big\rangle = \frac{1}{4\kappa}\langle \partial_a h_{cd}\partial_b h^{cd}\rangle\,, \tag{1.15}$$

where the last equality holds in the TT gauge. This demonstrates that, indeed, GWs are physical and carry energy-momentum.

1.1.2 *What are Black Holes?*

Often, the concept of a BH is introduced by first discussing the notion of escape velocity. Take a body of mass M and radius R, imagine the Earth, for instance. The escape velocity is the speed necessary for a small particle to escape the gravitational pull. Finding the kinetic energy that exactly balances the gravitational potential energy, one arrives to $v_e = \sqrt{2GM/R} \sim 11\text{km/s}$ on Earth. John Michell famously considered the thought experiment of computing the size of a body such that light could not escape from it: $R_S = 2GM/c^2$. Such an object would be a *dark star*, invisible to us, as no light could ever be emitted from it.

BHs turn into reality this back-of-the-envelope calculation. Schwarzschild first noted that Einstein's equations admitted, in vacuum, a simple static solution assuming spherical symmetry, given by

$$g_{ab}dx^a dx^b = -f(r)dt^2 + f^{-1}(r)dr^2 + r^2 d\Omega^2\,, \qquad f = 1 - \frac{2GM}{c^2 r}\,, \tag{1.16}$$

where $M > 0$ is some positive number. Asymptotically, this geometry is simply flat space. However, the geometry becomes pathological at two locations: $r = R_S$, and $r = 0$. The first pathology is due to a poor choice of coordinates. Replace

the time coordinate by the proper time of a null ray moving inwards, $v = t + r_*$, with $r_* = r + R_S \log(r/R_S - 1)$ the tortoise coordinate. Then, the Schwarzschild geometry takes the form

$$g_{ab}dx^a dx^b = -f(r)dv^2 + 2dvdr + r^2 d\Omega^2 \,. \tag{1.17}$$

The singularity at $r = R_S$ has disappeared. In fact, by investigating the causal structure, one notices that that radius is characterized by parametrizing surfaces of vanishing expansion: null rays, e. g., light, never escapes the surface $r = R_S$. Therefore, it defines the surface of the *dark star* region, what we know refer to as the *event horizon*. Its interior, we dub *black hole*. We emphasize, though, that this is a vacuum solution, where the energy content is contained in the curvature of spacetime itself.

Both event horizons and black holes admit a formal definition, which is independent of coordinate choices, and relies instead on the causal structure of the spacetime. Since this is only an introductory chapter, we avoid introducing additional terminology here, and refer the interested reader instead to, e. g., [157]. At this point, suffices to say that if we think of ourselves as asymptotic observers, then any physical event that occurs inside the BH, $r < R_S$, is inaccessible to us. Strictly speaking we cannot (classically) know whether event horizons exist in any finite amount of time.

The singularity at $r = 0$ did not disappear when changing coordinates and in fact it is unavoidable, as it is a true singularity. For instance, one may calculate the Kretschmann scalar, to find that it diverges

$$R_{abcd}R^{abcd} = \frac{48G^2M^2}{c^4 r^6} \xrightarrow{r\to 0} \infty \,. \tag{1.18}$$

Singularities are fascinating, as they predict the doom of General Relativity itself, which simply ceases to be an accurate description of the spacetime geometry close to that point. Nevertheless, this occurs inside the BH region, and any physical consequences are (classically) forbidden from influencing observers external to the BH. In this thesis we will always think about BHs as referring to the exterior spacetime geometry, i. e., the causal past of future null infinity.

Up to this point, BHs are an exciting possibility of General Relativity, showcasing interesting physics associated to the likely existence of horizons and singularities. All of these, nevertheless, lie within the realm of theoretical physics. However BHs are of paramount importance in astrophysics, for one major reason: they are the endpoint of gravitational collapse. Once a sufficiently massive star exhausts its nuclear fuel, it falls onto itself due to its own self-gravity, undergoing a *supernova* explosion. Depending on the initial mass of the star, and on the details of radiative processes taking place, gravitational collapse may be halted by neutron degeneracy pressure and strong-force repulsion, leading to a *neutron star*. However, if the initial star is massive enough, nothing can halt the collapse, and the end-point is inevitably a BH. A convincing argument, albeit based on a simplified model, was first presented by Oppenheimer and Snyder [362].

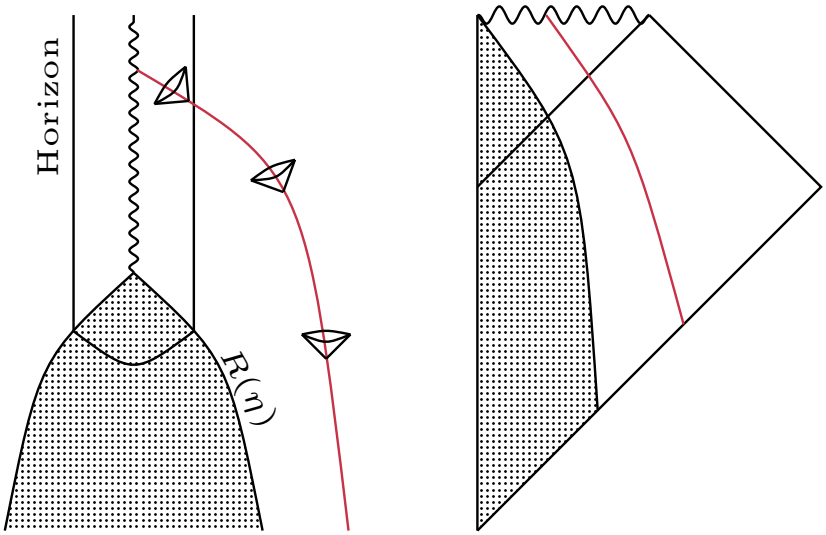

Figure 3 **Left:** Schematic representation of the gravitational collapse of a shell of matter, showing the formation of a singularity (wiggly line), and horizon. The motion of a representative infalling observer is shown in red, including the tilting of lightcones. **Right:** The same process, but shown as its Penrose diagram.

The Oppenheimer-Snyder model considers the gravitational collapse of a ball of dust (pressureless matter). Let R be the radius of this ball of dust, which begins to collapse from rest at $t = 0$, from a finite radius R_0. Geodesic motion leads to

$$R = \frac{R_0}{2}(1 + \cos\eta)\,, \qquad \tau = \sqrt{\frac{R_0^3}{8M}}(\eta + \sin\eta)\,, \tag{1.19}$$

which we have parametrized in terms of a parameter η, which is directly linked to the proper time of the surface τ. Clearly R decreases until $\eta = \pi$, at which point $R \to 0$ — all matter in this ball of dust is crushed at a single point of spacetime. However, any test particle experiences this collapse in a finite amount of proper time $\Delta\tau = \pi\sqrt{R_0^3/(8M)}$. The spacetime geometry in the exterior of the star is described by the Schwarzschild spacetime (1.16), for radii $r \geq R(\eta)$, where $t(\eta)$ can be found in [444]. Inside the ball of dust, the spacetime takes the form of a closed cosmological universe, in comoving coordinates,

$$ds^2 = -d\tau^2 + a^2(\tau)[d\chi^2 + \sin^2\chi d\Omega^2]\,, \qquad a(\tau) = \sqrt{\frac{R_0^3}{8M}}(1 + \cos\eta)\,, \tag{1.20}$$

with $\tau(\eta)$ given by (1.19). This geometry matches smoothly the exterior Schwarzschild spacetime. The density $\rho \sim a^{-3} \to \infty$ as the star collapses, indicating that all the matter is indeed focused onto a single point. A schematic representation of this collapse is shown in Fig. 3. Since the shell is forced to move along a timelike trajectory, and all timelike geodesics starting inside the event horizon inevitable terminate at $r = 0$, we can conclude that nothing can prevent the formation of a BH once all the matter has fallen inside its own gravitational radius.

This exercise illustrates that BHs are far from a theoretical divertimento, but rather a physical reality that influences stellar and galactic dynamics. Per se, we may never be able to confidently answer whether BHs, i. e., event horizons, exist. However, the astrophysical evidence for compact, dark objects, compatible with our knowledge of BHs from General Relativity, is astounding [7, 14, 15].

1.2 A HITCHHIKER'S GUIDE TO THIS THESIS

The main research output of this thesis is divided into two parts: Part II (*Nonlinear Dynamics in Black Hole Ringdown*) and Part III (*Interaction of Gravitational Waves with Viscous Matter*). Preceding these, Chapter 2 presents a collection of mathematical and methodological tools used throughout the thesis, including the spinor formulation of General Relativity and the Geroch-Held-Penrose formalism, numerical methods for solving partial differential equations, and Bayesian inference. Chapter 3 presents key results in BH perturbation theory for spherically symmetric BHs. Several of these results are also essential for understanding perturbations of spherically symmetric stars, which are studied in the latter half of the thesis.

The aim of Part II is to investigate nonlinear aspects of perturbed BHs. Following a BH merger, the remnant relaxes to equilibrium by emitting GWs in a superposition of damped harmonics, dubbed quasinormal modes. This description is rooted in linear perturbation theory, despite the fact that the merger itself is a highly nonlinear process. A central question motivating this part of the thesis is therefore: where are the nonlinearities?

Part II begins with Chapter 4, which introduces rotating BHs and their perturbations. While most of the material presented here has appeared previously in the literature, several results are rewritten within a covariant GHP framework. This includes two distinct metric reconstruction procedures and the derivation of the source term for the Teukolsky equation at second order in perturbation theory. Most of the technical calculations in this chapter are carried out using the `xAct` packages `SymSpin` and `xPert`, and the code reproducing these results is available in [1].

The genuinely novel contributions of the thesis begin in Chapter 5, which studies the excitation of driven higher harmonics (quadratic QNMs) arising from nonlinear mode coupling between the ringdown GWs. This requires solving second order perturbations of a rotating black hole and subsequently inferring the amplitudes of these driven modes from the data. We find that these amplitudes are largely independent of the initial conditions, suggesting a new avenue to test the nonlinear dynamics of General Relativity with GW data. The chapter concludes with a discussion of interesting features of quadratic QNMs in the high-frequency (eikonal) regime. Chapter 6 builds on these results by studying high-frequency perturbations of rotating BHs through their description as perturbations of plane-wave spacetimes, using the Penrose limit [374]. This chapter presents the first comprehensive formulation of first- and second-order gravitational perturbations on homogeneous plane waves and provides analytical predictions for the amplitudes of quadratic QNMs in the eikonal regime. Chapter 7 then examines a complementary nonlinear

effect during ringdown: the change in the remnant BH mass due to GW accretion, and the corresponding imprint this has on the emitted signal. Finally, Chapter 8 explores an alternative scenario in which the compact object is not a BH but a horizonless ultracompact object. Such models have been conjectured to exhibit a nonlinear instability associated with the stable trapping of GWs. Here we show that under certain conditions no instability arises. Instead, the presence of stable trapping (absent for astrophysical BHs) leads to turbulent dynamics.

Part III focuses on the interaction between GWs and matter. Nonlinear phenomena are not confined to vacuum spacetimes, and the coupling between strong gravity and complex physical systems such as neutron stars provides a rich laboratory in which to search for new physics. Chapter 9 introduces the framework of first-order relativistic hydrodynamics, discussing its well-posedness and causality. Central to this part is Chapter 10, which develops the formalism required to study perturbations of spherically symmetric viscous stars and derives the corresponding master equations. The physical implications of this framework are explored in Chapter 11, within spherical symmetry, and extended to include rotational effects in Chapter 12. Our results show that GW propagation is strongly influenced by viscous and dissipative processes in the cores of neutron stars, leading to GW absorption, viscosity-induced shifts in stellar oscillation frequencies, and superradiant amplification of low-frequency GWs. These results pave the way towards mapping transport coefficients into GW observables during neutron star mergers, providing a new angle through which to infer the composition of matter at extreme densities.

The thesis concludes in Part IV with a concise summary of results, and an outlook on future directions.

Conventions. This thesis makes use in its majority of the mostly plus metric signature $(-+++)$, with Wald's [455] convention for the Riemann curvature. The mostly minus $(+---)$ metric signatures, however, is used in Chapters 4 and **??**, which heavily rely on the 2-spinor calculus, where this metric signature choice is advantageous. Those chapters also make use of Penrose & Rindler's convention for the Riemann curvature, which unfortunately is the opposite of Wald's [375]. We always work in geometric units, where the speed of light c and the Gravitational constant G are both set to unity $c = 1 = G$. Throughout all this work we restrict to 4 spacetime dimensions.

Spacetime indices are labelled by lower-case latin letters $a, b, c, \cdots = 0, \ldots, 3$. Spinor indices are labelled with uppercase latin letters $A, B, \cdots = 0, 1$ with primes denoting the conjugate representation $A', B', \cdots = 0', 1'$. Uppercase latin letters beginning at $I, J, \cdots = 2, 3$ are used to denote spacetime indices with support on the sphere in spherically symmetric spacetimes.

2

MATHEMATICAL STRUCTURES

Written while listening to music composed by Maurice Ravel.

Geometry is the language of General Relativity. The gravitational field is encoded in the curvature of a spacetime metric, and matter moves along geodesics in this curved space, sourcing in turn gravitational fields. Our understanding of gravity is, thus, nonlinear, relying on the properties of complex systems of coupled partial differential equations. From the mathematical point of view, BH dynamics is described by a combination of differential geometry and analysis. Our experimental knowledge about BHs and GWs, however, is only probabilistic. Contrasting theoretical predictions against experimental data requires of knowledge of statistics and probability theory. This chapter is intended to present some of the fundamental mathematical tools of GW astronomy. There are, evidently, aspects of the mathematics of strong-field gravity that are not covered in this Chapter, or that may change in years to come as our understanding of physical phenomena and mathematics grows hand in hand.

This Chapter is intended as an overview of the mathematical foundations underlying this thesis, pointing to key references that I have found useful in my personal journey through these topics. In that sense, the presentation carried out here is not meant to be self-contained, nor exhaustive, but rather an introduction to the language that this thesis will use. First, I discuss the geometry of General Relativity, mostly from the lens of 2-spinor calculus. Next, I introduce some basic concepts of numerical analysis that are used repeatedly across this thesis, and some basic results on the well-posedness of systems of partial differential equations. Finally, I review briefly the foundations of Bayesian inference, and its application to GW data analysis.

2.1 GEOMETRY OF SPACETIME

Spacetime is described by a real Lorentzian manifold $(\mathcal{M}, g)$, with the unique metric-compatible Levi-Civita connection which we denote by ∇. In addition, if spacetime is globally hyperbolic, it admits a spinor structure. We will exploit this spinor structure to simplify the geometric description of four-dimensional spacetime. Next, we will introduce a null tetrad and discuss in detail the formulation of General Relativity due to Geroch, Held, and Penrose (GHP). Finally, we discuss spacetime symmetries on a particular class of spacetimes which includes astrophysical BHs.

2.1.1 *Spinor Calculus*

First of all, *what is a spinor?* Let us answer the question locally. The space of spin-vectors at a point, denoted by $\mathfrak{S}$, is a 2-dimensional vector space over $\mathbb{C}$, endowed with a symplectic structure $\{\cdot,\cdot\}$. This simplectic structure can be used to define musical operators mapping $\mathfrak{S}$ to its dual

$$\begin{aligned} &\mathfrak{S} \xrightarrow{\flat} \mathfrak{S}^* \xrightarrow{\sharp} \mathfrak{S} \\ &\xi \mapsto \xi^\flat \mapsto (\xi^\flat)^\sharp = \xi\,, \end{aligned} \tag{2.1}$$

where $\xi^\flat = \{\xi,\cdot\}$, and the inverse operator is, given some $\eta \in \mathfrak{S}^*$, the unique $\eta^\sharp \in \mathfrak{S}$ such that $\{\eta^\sharp,\zeta\} = \eta(\zeta)$ for all $\zeta \in \mathfrak{S}$. This establishes an isomorphism $\mathfrak{S} \simeq \mathfrak{S}^*$. We can use this to define the *complex conjugate* $\bar{\mathfrak{S}}$ as the dual space to the set of antilinear maps $\psi : \mathfrak{S} \to \mathbb{C}$ such that $\psi(a\xi + b\eta) = \bar{a}\xi + \bar{b}\eta$. Thus, the complex conjugate of a spinor $\xi \in \mathfrak{S}$ is $\bar{\xi}(\psi) = \{\psi^\sharp,\xi\}$.

By considering the direct product of multiple copies of $\mathfrak{S},\bar{\mathfrak{S}}$ and their duals we can construct spinor fields with arbitrary valence. Abstractly we assign a label to each of these copies, with $A,B,\ldots$ denoting copies of $\mathfrak{S}$ and its dual, and primed labels $A',B',\ldots$ denoting labels that "live" in the complex conjugate space. This defines an algebra $\mathfrak{S}^\bullet$, and elements of the algebra are graded by their valence, e. g., the spinor $\xi^{BC}_{AA'} : \mathfrak{S}\times\mathfrak{S}\times\mathfrak{S}^*\times\bar{\mathfrak{S}} \to \mathbb{C}$ has valence $(3,1)$.

Since $\mathfrak{S}$ is two-dimensional, the space of antisymmetric 2-forms, including the symplectic structure $\{\cdot,\cdot\}$, is one dimensional. Hence there exists a valence $(2,0)$ spinor $\epsilon_{AB} \in \mathfrak{S}^\bullet$ such that

$$\{\xi,\eta\} = \epsilon_{AB}\xi^A\eta^B\,, \qquad (\xi^A)^\flat = \epsilon_{BA}\xi^B\,, \qquad (\xi_A)^\sharp = \epsilon^{AB}\xi_B\,. \tag{2.2}$$

Thus, ϵ_{AB} is dubbed a *spin metric*. Notice the order in the contractions, taken to avoid introducing minus signs. A useful mnemonic to remember the contracted index of the spin metric is *left - lowering* and *right - raising*.

This construction of spinors at a point can be extended to spinor fields on spacetime as long as the given spacetime is *spin*, i. e., if it second Stiefel-Whitney class vanishes. Geroch [207] showed that this is the case for every globally hyperbolic spacetime by specifically constructing the algebra of associate spinor bundles that realizes the double cover structure of $\mathrm{Spin}(3,1) \simeq \mathrm{SL}(2,\mathbb{C}) \xrightarrow{2:1} \mathrm{SO}(1,3)$. A globally hyperbolic spacetime admits a Cauchy surface, meaning that topologically the manifold is $\mathcal{M} \simeq \mathcal{M}_3 \times \mathbb{R}$, and therefore the lift to this associate bundle trivializes. A visual illustration of this construction is shown in Fig. 4. We will denote by $\mathfrak{S}^\bullet(\mathcal{M})$ the algebra of spinors on spacetime.

Real spinor fields, i. e., those that are invariant under complex conjugation, are directly related to null vector fields. In particular, given a spinor ξ^A we can always construct a null vector field as $k^a = \xi^A\xi^{A'}$. Remarkably, $g_{ab} = \epsilon_{AB}\epsilon_{A'B'}$ is a symmetric, non-degenerate 2-form on $\mathcal{M}$, i. e., a Lorentzian metric. Moreover, if ∇_a is the covariant derivative associated to the Levi-Civita connection on $(\mathcal{M},g)$, then there exists a unique spinor derivative $\nabla_{AA'} : \mathfrak{S}^\bullet(M) \to \mathfrak{S}^\bullet(\mathcal{M})$ that is (i)

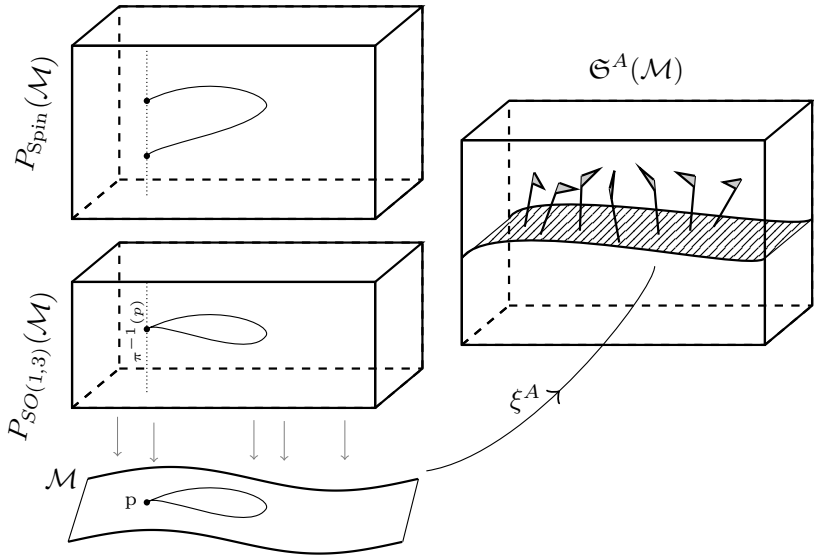

Figure 4 Schematic representation of the base manifold $\mathcal{M}$, the principal frame bundle $P_{SO(1,3)}\mathcal{M}$, and the spin bundle. By representing a closed loop in the base manifold and its corresponding lifts it becomes evident that the spin bundle is a double cover of the principal frame bundle. In the right we represent one of the associate spinor bundles $\mathfrak{S}^A(\mathcal{M})$, and a spinor field ξ^A is shown as a (smooth) section, where a spinor at each point is represented by a null flag.

linear, (ii) a derivation under multiplication of smooth scalar functions, i. e., satisfies a Leibnitz rule, (iii) torsion-free, and (iv) spin-metric compatible $\nabla_{AA'}\epsilon_{BC} = 0$. As this is unique, it reduces to the usual derivative when acting on real spinors, $\nabla_{AA'}(\xi^B\xi^{B'}) = \nabla_a k^b$.

A final ingredient will be the irreducible decomposition of spinors. Any spinor $\xi_{A\ldots BA'\ldots B'}$ is the sum of a symmetric spinor $\xi_{(A\ldots B)(A'\ldots B')}$ and outer products of spin metric's with symmetric spinors of lower valence. The proof of this result is given in Proposition 3.1 in [296] or Proposition (3.3.54) in [375]. In essence, the proof reduces to showing that one can symmetrize over two indices.

$$\xi_{\ldots AB\ldots} = \xi_{\ldots(AB)\ldots} + \frac{1}{2}\epsilon_{AB}\xi^{C}{}_{\ldots C\ldots}\,. \tag{2.3}$$

In order to show this, it suffices to show that the antisymmetric component of a spinor is proportional to the spin metric, which in turn follows from the Jacobi identity $\epsilon_{A[B}\epsilon_{CD]} = 0$. Therefore, we can reduce every spinor to symmetric spinors. Let us denote by $S_{(p,q)}$ the space of symmetric spinor fields with valence (p,q). The covariant derivative of a symmetric spinor can be decomposed into four irreducible parts: the divergence $\mathscr{D}$, curl $\mathscr{C}$, curl-dagger $\mathscr{C}^\dagger$, and twistor $\mathscr{T}$. Let us first define the symmetric product of symmetric spinors as

$$\begin{aligned} &\overset{i,j}{\odot} : S_{(k,l)} \times S_{(n,m)} \to S_{(k+n-2i,l+m-2j)}\,, \\ &\qquad (\eta,\xi) \to \eta \overset{i,j}{\odot} \xi = \eta_{(A_1\ldots A_{k-i-1}}{}^{(A'_1\ldots A'_{l-j-1}|B_1\ldots B_i B'_1\ldots B'_j|}\xi_{A_{k-i}\ldots A_{k+n-2i})B_1\ldots B_i B'_1\ldots B'_j}{}^{(A'_{l-j}\ldots A'_{l+m-2j})}\,. \end{aligned} \tag{2.4}$$

with $i \leq \min(k,n)$ and $j \leq \min(l,m)$. Then, the symmetric derivative operators are

$$\begin{aligned}
\text{Divergence:} \quad & \mathscr{D} : S_{(p,q)} \to S_{(p-1,q-1)}\,, \quad \mathscr{D}\xi \mapsto \nabla \overset{1,1}{\odot} \xi\,, \\
\text{Curl:} \quad & \mathscr{C} : S_{(p,q)} \to S_{(p+1,q-1)}\,, \quad \mathscr{C}\xi \mapsto \nabla \overset{0,1}{\odot} \xi\,, \\
\text{Curl dagger:} \quad & \mathscr{C}^\dagger : S_{(p,q)} \to S_{(p-1,q+1)}\,, \quad \mathscr{C}^\dagger\xi \mapsto \nabla \overset{1,0}{\odot} \xi\,, \\
\text{Twistor:} \quad & \mathscr{T} : S_{(p,q)} \to S_{(p+1,q+1)}\,, \quad \mathscr{T}\xi \mapsto \nabla \overset{0,0}{\odot} \xi\,.
\end{aligned} \tag{2.5}$$

For example, for a vector $\xi^a \equiv \xi^{AA'} \in S_{(1,1)}$, we have

$$\begin{aligned}
\mathscr{D}\xi =& \nabla_a \xi^a\,, \mathscr{T}\xi = \nabla_{(a}\xi_{b)} - \frac{1}{4} g_{ab} \nabla_c \xi^c \\
\mathscr{C}\xi =& (1 - i\star)\nabla_{[a}\xi_{b]}\,, \quad \mathscr{C}^\dagger\xi = (1 + i\star)\nabla_{[a}\xi_{b]}\,.
\end{aligned} \tag{2.6}$$

Let us show how this formulation simplifies the treatment of General Relativity. The curvature tensor can be decomposed in terms of the Weyl tensor C_{abcd}, a symmetric, rank-2 traceless tensor $R_{ab} - R g_{ab}/4$, and a Ricci scalar R. Each of these is associated to a symmetric spinor, given by

$$\begin{aligned}
&\text{Weyl:} && C_{abcd} = -\Psi_{ABCD}\epsilon_{A'B'}\epsilon_{C'D'} - \bar{\Psi}_{A'B'C'D'}\epsilon_{AB}\epsilon_{CD}\,, \\
&\text{Trace-free Ricci:} && S_{ab} = R_{ab} - \frac{1}{4} R g_{ab} = 2\Phi_{ABA'B'}\,, \\
&\text{Ricci scalar:} && R = -24\Lambda\,.
\end{aligned} \tag{2.7}$$

Vacuum Einstein equations simply read $\Phi = \Lambda = 0$. Hence, vacuum General Relativity, which describes BH spacetimes, is governed only by the dynamics of the Weyl or gravitational spinor Ψ. Its dynamics is fixed by Bianchi identities, which in spinor notation become

$$\begin{aligned}
\nabla^A_{B'} \Psi_{ABCD} =& \nabla^{A'}_{(B} \Phi_{CD)A'B'} \implies \mathscr{C}^\dagger \Psi = \mathscr{C}\Phi\,, \\
\nabla^{CA'} \Phi_{CDA'B'} =& -3\nabla_{DB'}\Lambda \implies \mathscr{D}\Phi = -3\mathscr{T}\Lambda\,.
\end{aligned} \tag{2.8}$$

Notice that in vacuum this is just $\nabla^{AA'}\Psi_{ABCD} = 0$. Taking an additional derivative, and commuting them, we obtain that vacuum gravity is governed by a nonlinear wave equation, often dubbed *Penrose wave equation*

$$\Box \Psi_{ABCD} = 6\Psi^{EF}_{(AB}\Psi^{EF}_{CD)}\,. \tag{2.9}$$

2.1.2 *GHP Formalism*

We introduce next the GHP formalism, first put forward in Ref. [208]. Let us start by introducing a spinor dyad (o_A, ι_A), normalized as $o_A \iota^A = 1$. This normalization implies that the spin metric is $\epsilon_{AB} = 2 o_{[A}\iota_{B]}$. This spin dyad can be mapped to a null tetrad in the complexified tangent space $(\ell_a, n_a, m_a, \bar{m}_a)$, with

$$\ell^a = o^A \bar{o}^{A'}\,, \qquad n^a = \iota^A \bar{\iota}^{A'}\,, \qquad m^a = o^A \bar{\iota}^{A'}\,, \qquad \bar{m}^a = \iota^A \bar{o}^{A'}\,, \tag{2.10}$$

satisfying that $\ell_a n^a = -m_a \bar{m}^a = 1$. The spacetime metric is

$$g_{ab} = \epsilon_{AB}\epsilon_{A'B'} = 2(\ell_{(a} n_{b)} - m_{(a}\bar{m}_{b)}) \,. \tag{2.11}$$

We recognize that (ℓ, n, m) defines a Newmann-Penrose (NP) tetrad [356]. Under a Lorentz transformation $L \in \mathrm{SL}(2,\mathbb{C})$, the spin dyad transforms as

$$\begin{pmatrix} \check{o}^A \\ \check{\iota}^A \end{pmatrix} = L \begin{pmatrix} o^A \\ \iota^A \end{pmatrix} \,, \qquad \check{o}_A \check{\iota}^A = \det L = 1 \,, \tag{2.12}$$

i. e., Lorentz transformations map spin dyads to spin dyads. It's useful to decompose Lorentz transformation in three classes, depending on how they act on the spin dyad

$$\begin{aligned} &\text{Class I:} \quad o \to o \,, \quad \iota \to \iota + \bar{a} o \,, \\ &\text{Class II:} \quad o \to o + b\iota \,, \quad \iota \to \iota \,, \\ &\text{Class III:} \quad o \to \sqrt{\Lambda e^{i\theta}} o \quad \iota \to \frac{1}{\sqrt{\Lambda e^{i\theta}}} \iota \,. \end{aligned} \tag{2.13}$$

Class I (respsectively II) transformations correspond to rotations along the o (respectively ι) spinors, parametrised by the complex functions a (respectiely b), whereas class III rotations are simultaneous boost-spin transformations, parametrised by the two real functions Λ, θ. Their action on the induced NP tetrad is simply

$$\begin{aligned} &\text{Class I:} \quad \ell \to \ell \,, \quad n \to a\bar{a}\ell + n + \bar{a}m + a\bar{m} \,, \quad m \to a\ell + m \,, \\ &\text{Class II:} \quad \ell \to \ell + \bar{b}m + b\bar{m} \,, \quad n \to n \,, \quad m \to bn + m \,, \\ &\text{Class III:} \quad \ell \to \Lambda\ell \quad n \to \Lambda^{-1}\ell \,, \quad m \to e^{i\theta} m \,, \end{aligned} \tag{2.14}$$

Class III transformations define a group action of $\mathbb{C}^\times$ on the spinor field algebra, with representations that can be labelled by two integers (p, q). A field $\xi_{A\ldots}$ is in the (p, q) representation, which we say to have *GHP Weight* (p, q), if it transforms in the following manner under a class III transformation:

$$\xi_{A\ldots} \overset{\circ}{=} (p,q) \iff \xi_{A\ldots} \xrightarrow{(o,\iota)\to(\lambda o, \lambda^{-1}\iota)} \lambda^p \bar{\lambda}^q \xi_{A\ldots} \,. \tag{2.15}$$

Equivalently we say that $\xi_{A\ldots}$ has boost weight $(p+q)/2$ and spin weight $(p-q)/2$. Formally, the (p, q)-representations of the $\mathbb{C}^\times$ group action induced by class III transformations can be used to define associate fiber bundles to the spinor algebra $\mathfrak{S}^\bullet_{(p,q)}$, whose sections are spinor fields with GHP weight (p, q). This bundle has an induced connection, sometimes dubbed GHP connection, which differs from the lifted Levi-Civita connection. The covariant derivative on $\mathfrak{S}_{(p,q)}$ is

$$\Theta_a = \nabla_a - p\omega_a - q\bar{\omega}_a \,, \tag{2.16}$$

where

$$\omega_a = \frac{1}{2}\Big(n^b \nabla_a \ell_b + m^b \nabla_a \bar{m}_b \Big) \,. \tag{2.17}$$

It is useful to introduce the projections of the GHP derivative onto the tetrad, which are operators with a well-defined GHP weight, i.e., they map $\mathfrak{S}_{(p,q)} \to \mathfrak{S}_{(p',q')}$, as

$$\text{þ} = \ell^a \Theta_a \,, \qquad \text{þ}' = n^a \Theta_a \,, \qquad \text{ð} = m^a \Theta_a \,, \qquad \text{ð}' = \bar{m}^a \Theta_a \,. \tag{2.18}$$

Their GHP weights can be read from (2.14)

$$\text{þ} \mathrel{\overset{\circ}{=}} (1,1) \,, \qquad \text{þ}' \mathrel{\overset{\circ}{=}} (-1,-1) \,, \qquad \text{ð} \mathrel{\overset{\circ}{=}} (1,-1) \,, \qquad \text{ð}' \mathrel{\overset{\circ}{=}} (-1,1) \,. \tag{2.19}$$

We have introduced the *prime* notation, which is one of the discrete internal symmetries of the spin dyad, given by

$$\text{Priming:} \qquad o^A \mapsto i\iota^A \,, \quad \iota^A \mapsto i o^A \,, \quad o^{A'} \mapsto -i\iota^{A'} \,, \quad \iota^{A'} \mapsto -i o^{A'} \,. \tag{2.20}$$

We will often make use of this symmetry, which in essence corresponds to changing the NP tetrad $(\ell, n, m)' \mapsto (n, \ell, \bar{m})$. Notice that it commutes with complex conjugation, so we write equivalently $\overline{X'} = \bar{X}'$. There is yet another discrete symmetry, first discovered by Sachs [416], dubbed the *starring* operation

$$\text{Starring:} \qquad o^A \mapsto o^A \,, \quad \iota^A \mapsto \iota^A \,, \quad o^{A'} \mapsto \iota^{A'} \,, \quad \iota^{A'} \mapsto -o^{A'} \,, \tag{2.21}$$

where notice that this does not commute with complex conjugation.

At this point, it is necessary to introduce the connection components. In addition to the GHP connection ω_a defined in (2.17), we need to introduce

$$\Gamma_a = m^b \nabla_a \ell_b \equiv \tau \ell_a + \kappa n_a - \rho m_a - \sigma \bar{m}_a \,, \tag{2.22}$$

where $(\tau, \kappa, \rho, \sigma)$, together with their primed versions, are the GHP *spin coefficients*. Indeed, they appear as the connection components in the GHP derivatives of the spin dyad

$$\Theta_a o^A = -\Gamma_a \iota^A \,, \qquad \Theta_a \iota^A = -\Gamma'_a o^A \,. \tag{2.23}$$

Equipped with these quantities, we can now derive the key equations of the GHP formalism: the Ricci transport equations, which relate the derivatives of spin coefficients to the spacetime curvature (and are equivalent to Cartan's structure equations), and the Bianchi identities. First, let us introduce the commutator $\Box_{AB}$

$$2\nabla_{[a}\nabla_{b]} = \epsilon_{A'B'} \Box_{AB} + \epsilon_{AB} \Box_{A'B'} \,, \qquad \Box = -\nabla \overset{0,1}{\odot} \nabla \,. \tag{2.24}$$

Notice that when acting upon a symmetric spinor $\xi \in S_{(n,m)}$ this is simply

$$\Box \overset{0,0}{\odot} \xi = -n\Psi \overset{1,0}{\odot} \xi - m\Phi \overset{0,1}{\odot} \xi \,. \tag{2.25}$$

Hence, if we let $\epsilon_{\mathbf{A}} = \{o, \iota\}$ be the spin dyad, we can write the Ricci transport equations compactly as

$$\Psi = \epsilon_{\mathbf{A}} \overset{0,0}{\odot} \Box \overset{0,0}{\odot} \epsilon^{\mathbf{A}} \,, \quad \Phi = \epsilon_{\mathbf{A}} \overset{0,0}{\odot} \bar{\Box} \overset{0,0}{\odot} \epsilon^{\mathbf{A}} \,, \qquad \Lambda = \frac{1}{6} \epsilon_{\mathbf{A}} \overset{1,0}{\odot} \Box \overset{1,0}{\odot} \epsilon^{\mathbf{A}} \,. \tag{2.26}$$

Writing these equations in terms of their dyad components leads to:

$$\begin{aligned}
(\text{Þ}-\rho)\tau =&\text{Þ}'\kappa-\bar{\tau}'\rho+(\bar{\tau}-\tau')\sigma+\Psi_1+\Phi_{01'}\,,\\
(\text{Þ}-\rho)\rho =&(\eth'-\tau')\kappa+\sigma\bar{\sigma}-\bar{\kappa}\tau+\Phi_{00'}\,,\\
(\text{Þ}'-\bar{\rho}')\rho =&(\eth'-\bar{\tau}')\rho'+\sigma\sigma'-\kappa\kappa'-\Psi_2-2\Lambda\,,\\
(\text{Þ}-\rho-\bar{\rho})\sigma =&(\eth-\tau-\bar{\tau}')\kappa-\Psi_0\,,\\
(\eth-\tau)\tau =&(\text{Þ}'-\rho')\sigma+\kappa\bar{\kappa}'-\rho\bar{\sigma}'+\Phi_{02'}\,,\\
(\eth-\tau)\rho =&\eth'\sigma-\bar{\rho}\tau+(\bar{\rho}'-\rho')\kappa-\Psi_1-\Phi_{12'}\,,
\end{aligned}\tag{2.27}$$

together with their primed versions, and their respective complex conjugates. Above, we have introduced the dyad components of the Weyl and Ricci spinors: for a spinor $X_{ij'}$ denotes the contraction of X with i-instances of ι with unprimed indices, and j-instances of ι with primed indices, the other indices being contracted with o. Bianchi identities (2.8) can also be written in terms of GHP scalars as

$$\begin{aligned}
(\text{Þ}-4\rho)\Psi_1 =&(\eth'-\tau')\Psi_0-(\eth-\bar{\tau}')\Phi_{00'}+(\text{Þ}-2\bar{\rho})\Phi_{01'}-\kappa(3\Psi_2-2\Phi_{11'})+\bar{\kappa}\Phi_{02'}-2\sigma\Phi_{10'}\,,\\
(\text{Þ}-3\rho)\Psi_2 =&(\eth'-2\tau')\Psi_1-(\eth-\bar{\tau}')\Phi_{10'}+(\text{Þ}-2\bar{\rho})\Phi_{11'}+\text{Þ}\Lambda+\sigma'\Psi_0-\kappa(2\Psi_3-\Phi_{21'})\\
&-\rho'\Phi_{00'}+\tau'\Phi_{01'}+\bar{\kappa}\Phi_{12'}-\sigma\Phi_{20'}\,,\\
(\text{Þ}-2\rho)\Psi_3 =&(\eth'-3\tau')\Psi_2-(\eth-\bar{\tau}')\Phi_{20'}+(\text{Þ}-2\bar{\rho})\Phi_{21'}+2\eth'\Lambda+2\sigma'\Psi_1-\kappa\Psi_4\\
&-2\rho'\Phi_{10'}+2\tau'\Phi_{11'}+\bar{\kappa}\Phi_{22'}\,,\\
(\text{Þ}-\rho)\Psi_4 =&(\eth'-4\tau')\Psi_3+(\eth'-2\tau')\Phi_{21'}-(\text{Þ}'-\bar{\rho})\Phi_{20'}+3\sigma'\Psi_2\\
&-2\kappa'\Phi_{10'}+2\sigma'\Phi_{11'}+\bar{\sigma}\Phi_{22'}\,,
\end{aligned}\tag{2.28}$$

together with their primed versions and their complex conjugates. We can also write additional equations for derivatives of the Ricci scalars following similar steps. The scalar equations provided by (2.27)-(2.28) will prove extremely useful when studying perturbations of rotating BHs, as we will discuss in Chapter 4.

2.1.3 *Algebraic Classification of Spacetimes*

Any symmetric spinor ξ admits a decomposition $\xi_{AB\dots C}=\zeta^{(1)}_{(A}\dots\zeta^{(n)}_{C)}$, which is unique up to proportionality constants and permutations [375]. In particular, the Weyl spinor admits such a decomposition

$$\Psi_{ABCD}=\kappa^{(1)}_{(A}\kappa^{(2)}_{B}\kappa^{(3)}_{C}\kappa^{(4)}_{D)}\,,\tag{2.29}$$

for 4 spinors $\kappa^{(1,\dots,4)}_{A}$. Each of these are dubbed *principal spinors*, and the null vectors they generate $k^{(i)}_{a}=\kappa^{(i)}_{A}\bar{\kappa}^{(i)}_{A'}$ are known as principal null directions (PNDs). Whenever two or more PNDs coincide, we say that it is a repeated PND. Spacetimes can be algebraically classified according to the number of repeated PNDs, leading to Petrov's algebraic classification [378]. Any spacetime belongs to one of five types depicted in Fig. 5. Of most focus in this thesis will be spacetimes of type D (corresponding to BH spacetimes). In Chapter 6 we will also consider type IV (sometimes named type N) spacetimes, corresponding to plane waves.

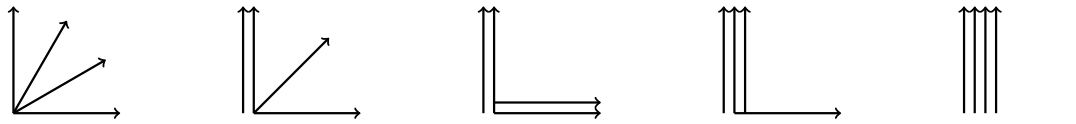

Type I $\Psi_{ABCD} = \alpha_{(A}\beta_B\gamma_C\delta_{D)}$ | Type II $\Psi_{ABCD} = \alpha_{(A}\alpha_B\gamma_C\delta_{D)}$ | Type D $\Psi_{ABCD} = \alpha_{(A}\alpha_B\beta_C\beta_{D)}$ | Type III $\Psi_{ABCD} = \alpha_{(A}\alpha_B\alpha_C\delta_{D)}$ | Type IV $\Psi_{ABCD} = \alpha_{(A}\alpha_B\alpha_C\alpha_{D)}$

Figure 5 Diagrammatic representation of the possible algebraic types, based on the number of repeated PNDs of the Weyl spinor.

2.1.4 *Symmetries of Vacuum Type D Spacetimes*

Let us focus now on spacetimes of type D. A theorem due to Goldberg and Sachs [220] establishes that in a type II spacetime, if a dyad is chosen such that o is aligned with the repeated principal spinor, then $\Psi_0 = \Psi_1 = \kappa = \sigma = 0$. Since type D spacetimes have two such repeated principal spinors, in a *principal dyad* such that both o and ι are aligned with the repeated principal spinors we have that

$$\Psi_0 = \Psi_1 = \Psi_3 = \Psi_4 = 0\,, \qquad \kappa = \sigma = \kappa' = \sigma' = 0,. \tag{2.30}$$

If the spacetime is also vacuum, this means that the only non-vanishing curvature component is Ψ_2. Let us introduce a rescaled version

$$\zeta = -\left(\frac{M}{\Psi_2}\right)^{1/3}, \tag{2.31}$$

where M can be thought of as a proportionality constant, which corresponds to the BH mass in the case of a Kerr spacetime, and is such that $\zeta \neq 0$ in the Minkowski limit. We will now show that this scalar governs a valence $(2,0)$ Killing spinor, which underpins the symmetries of BH spacetimes.

Let κ_{AB} be a symmetric spinor, and consider the Killing equation

$$\nabla^{A'}_{(A}\kappa_{BC)} = 0\,. \tag{2.32}$$

Taking another derivative, contracting, and symmetrizing we find an integrability condition

$$0 = \nabla^{A'}_{(B}\nabla_{A'A}\kappa_{CD)} = -\Box_{(AB}\kappa_{CD)} = 2\Psi^{D}_{(ABC}\kappa_{DE)}\,, \tag{2.33}$$

Let us show that type D spacetimes admit a valence $(2,0)$ Killing spinor. Let $\kappa_{AB} = \kappa_0\iota_A\iota_B - 2\kappa_1 o_{(A}\iota_{B)} + \kappa_2 o_A o_B$, and plug these into the integrability equation (2.33). The Goldberg-Sachs theorem (2.30) leads to $\kappa_0 = \kappa_2 = 0$. Using this, the Killing equation becomes

$$(\text{Þ} + \rho)\kappa_1 = 0\,, \quad (\eth + \tau)\kappa_1 = 0\,, \quad (\text{Þ}' + \rho')\kappa_1 = 0\,, \quad (\eth' + \tau')\kappa_1 = 0\,. \tag{2.34}$$

Bianchi identities (2.28) immediately lead to $\kappa_1 = \zeta$, i.e., vacuum type D spacetimes have a valence $(2,0)$ Killing spinor given by

$$\kappa_{AB} = -2\zeta o_{(A}\iota_{B)}\,. \tag{2.35}$$

This was first proven by Walker and Penrose [456]. Now notice that this Killing spinor leads immediately to a conformal Killing-Yano tensor $Y_{ab} = \kappa_{AB}\epsilon_{A'B'}$, satisfying

$$Y_{a(b;c)} = g_{bc}\xi_a - g_{a(b}\xi_{c)}\,, \qquad \xi_a = \frac{1}{3}\nabla^b Y_{ab}\,. \tag{2.36}$$

In fact, it is straightforward to check that the vector ξ_a is a proper Killing vector, given by

$$\xi_a = -\frac{1}{3}\nabla^B_{A'}\kappa_{AB} = \zeta(\rho'\ell_a - \rho n_a - \tau' m_a + \tau\bar{m}_a)\,, \tag{2.37}$$

and it is invariant under the prime operation, as one may expect of an isometry. For a quite general class of spacetimes (non-accelerating type D spacetimes, or spacetimes of the Kerr-NUT class), this Killing vector is proportional to a *real* Killing vector. Following the notation of [16], let $R = \Re\zeta$ and $I = \Im\zeta$ in that case. The conformal Killing-Yano tensor decomposes into a real 2-form f_{ab} and its dual, $\star f_{ab}$, the latter of which is a Killing-Yano tensor,

$$\star f_{ab} = \frac{1}{2i}(Y_{ab} - \bar{Y}_{ab}) = 2In_{[a}\ell_{b]} + 2iR\bar{m}_{[a}m_{b]}\,. \tag{2.38}$$

The Killing-Yano tensor can be thought of as the "square-root" of a Killing tensor $K_{ab} = \star f^c_a \star f_{cb}$, which satisfies the Killing equation $\nabla_{(a}K_{bc)} = 0$. This is given by

$$K_{ab} = 2\Big(I^2 n_{(a}\ell_{b)} + R^2\bar{m}_{(a}m_{b)}\Big)\,. \tag{2.39}$$

Finally, this structure leads to a last Killing vector

$$\eta^a = \xi_b K^{ab} = \zeta\Big[I^2(\rho'\ell^a - \rho n^a) - R^2(\tau\bar{m}^a - \tau' m^a)\Big]\,. \tag{2.40}$$

As we will discuss in Chapter 4, the two Killing vectors ξ^a and η^a are linearly independent, and together with the Killing tensor (2.39), lead to the conserved quantities that guarantee the integrability of geodesics in the spacetime of a rotating BH. Indeed, recall that if $T_{a_1a_2\ldots a_n}$ is a Killing tensor and $x^a(\lambda)$ a geodesic, the quantity $C_T = \dot{x}^{a_1}\dot{x}^{a_2}\ldots\dot{x}^{a_n}T_{a_1a_2\ldots a_n}$ is conserved along the geodesic. The proof is a simple calculation:

$$\dot{x}^b\nabla_b C_T = nT_{a_1a_2\ldots a_n}\dot{x}^{a_1}\dot{x}^{a_2}\ldots\dot{x}^b\nabla_b\dot{x}^{a_n} + \dot{x}^{a_1}\ldots\dot{x}^{a_n}\dot{x}^b\nabla_b T_{a_1\ldots a_n} = 0\,, \tag{2.41}$$

where the first term vanishes because x^a is a geodesic, and the second term vanishes due to T being a Killing tensor. Kerr-NUT spacetimes have 3 such conserved quantities:

$$\begin{aligned} C_\xi =& \dot{x}^a\xi_a = \zeta\Big(\rho' u^\ell - \rho u^n - \tau' u^m + \tau u^{\bar{m}}\Big)\,,\\ C_\eta =& \dot{x}^a\eta_a = \zeta\Big[I^2(\rho' u^\ell - \rho u^n) - R^2(\tau u^{\bar{m}} - \tau' u^m)\Big]\,,\\ C_K =& \dot{x}^a\dot{x}^b K_{ab} = I^2 u^n u^\ell + R^2 u^m u^{\bar{m}}\,. \end{aligned} \tag{2.42}$$

In the spacetime of a rotating BH these have the interpretation of energy, angular momentum along the spin direction, and Carter constant.

Remarkably, isometries can also be used to show that the wave equation is separable in Kerr-NUT spacetimes. Let us show this explicitly for the scalar wave equation. Let ϕ be a scalar field, with GHP weight $\phi \overset{\circ}{=} (0,0)$. In GHP form, the wave equation takes the form

$$\Box\phi = 2\Big[(\text{Þ} - \bar{\rho})(\text{Þ}' - \rho') - (\eth - \bar{\tau}')(\eth' - \tau') - \Psi_2\Big]\phi = 0\,. \tag{2.43}$$

The Lie derivatives generated by the isommetries ξ^a and η^a commute with the wave operator, $[\Box, \mathfrak{L}_\xi] = [\Box, \mathfrak{L}_\eta] = 0$. In addition, the Killing tensor generates an additional commuting operator $\mathcal{Q} = \nabla^a K_{ab} \nabla^b$. Thus, $(\Box, \mathfrak{L}_\xi, \mathfrak{L}_\eta, \mathcal{Q})$ are four mutually commuting operators, which guarantee the full separation of variables of the wave equation [113].

We have been able to characterize quite generically the conserved quantities and even separability of wave equations of Kerr-NUT spacetimes, simply starting from the existence of a valence $(2,0)$ Killing spinor leading to a real Killing vector. We will later return to this GHP formulation to study perturbations of algebraically special spacetimes. Understanding their algebraic structure and their symmetries, which become evident from the spinorial formulation of General Relativity, will allow us to simplify this problem greatly.

2.2 SOLVING DIFFERENTIAL EQUATIONS

Often in this thesis we encounter partial differential equations (or systems thereof) that do not admit analytic solutions. These are often *initial value problems*, where data is specified in a timelike initial slice, and we want to study its time-evolution. We often resort to numerical methods to tackle such problems. During the course of this thesis I have developed a number of different codes and routines, often based in different methods, but following the overarching principles discussed in this section. For this reason, I will omit (most) details about numerical implementation of solutions to differential equations from subsequent chapters of this thesis, unless directly relevant to the discussion, referring instead to the relevant references or to this Section. Before jumping into that, it is relevant to discuss when is a system of differential equations *well-posed*, a notion that will be especially important to discuss different formulations of relativistic hydrodynamics in Chapter 9.

2.2.1 *Well-posedness*

The notion of well-posedness is due to Hadamard [233]. A problem is said to be well-posed if (i) has a solution, (ii) said solution is unique, and (iii) the solution depends continuously on the problem's parameters, such as its initial data. These criteria seems minimal, yet often problems fail to meet them. A famous example is the formulation of Einstein's equations as an initial value problem: the "simplest"

formulation in terms of a $3+1$ split of spacetime (the so-called ADM decomposition) fails to be well-posed: it does not satisfy the last criteria, meaning that small numerical errors in the implementation of the equations move the numerical solution arbitrarily far away, in solution space, from the true solution.

Let us first analyze this concept with a simple problem:

$$\begin{aligned} \partial_t \phi^I =& P\phi \equiv A^{aI}_J \partial_a \phi^J \,, \\ \phi^I(x, t=0) =& \phi^I_0(x) \,, \end{aligned} \tag{2.44}$$

where A^{aI}_J are constants, and $x \in \mathbb{R}^d$. If the initial data is 2π-periodic, we can study the equivalent problem in a torus, and in particular we can safely take the Fourier transform. Denoting $\hat{\phi}$ and $\hat{\phi}_0$ the Fourier transformed fields, the problem admits a trivial solution as

$$\hat{\phi}^I(\omega, t) = \hat{\phi}^J_0(\omega) e^{i\omega_a A^{aI}_J t} \,. \tag{2.45}$$

The *principal symbol* of the differential operator that generates the equation is found in the exponent, and given by $\hat{P} = i\omega_a A^{aI}_J$. A problem is said to be *stable* if there exist positive constants K, α (independent on ω, t) such that

$$|e^{i\omega_a A^{aI}_J t}| \leq K e^{\alpha t} \,. \tag{2.46}$$

In this sense, we are not claiming that the problem does not have solutions that grow in time: linear instabilities of physical origin should be valid within a well-posed problem. The crucial aspect of this definition is that the constants K, α are independent of ω and t. This condition of stability is enough to prove that for such problem (2.45) is the unique solution (Theorem 3.1.1. in [232]). Now, how can we check for stability? A necessary condition is the *Petrovskii* condition, which establishes that the eigenvalues of the principal symbol (λ) satisfy $\Re\lambda \leq \alpha$ for some constant α. If in addition to the Petrovskii condition, the matrix that diagonalizes the principal symbol can be bounded by a constant K which is independent of ω, the problem is stable. These results lay out the rules of the game: we want to investigate the principal symbol of the equation as a linear operator, and its eigenvalues will encode crucial information. Thus, the following definitions should not come out as a surprise:

Let's consider a problem such as (2.44), where now A^{aI}_J are variable coefficients. Such problem is said to be *symmetric hyperbolic* if for every $\omega_a \in \mathbb{R}^d$, the matrix $\omega_a A^{aI}_J$ is Hermitian. If the matrix has real eigenvalues and is diagonalizable, the problem is *strongly hyperbolic*. A problem where the matrix has real eigenvalues but is not diagonalizable (there is no complete set of eigenvectors) is called *weakly hyperbolic*. Evidently, every symmetric hyperbolic system is strongly hyperbolic. The ADM formulation of General Relativity is an example of a weakly hyperbolic system that is not strongly hyperbolic.

Strong hyperbolicity is a necessary condition for well-posedness. In the quasilinear case, where $A^{aI}_J = A^{aI}_J(x^a, \phi^J)$ are also field-dependent, it is not sufficient, and one

also needs to require certain conditions on the smoothness of these functions [404]. Adding a forcing function to (2.44) does not make a well-posed problem ill-posed, and this can be proved using Duhamel's principle. We refer the reader to [232] for further details on how the hyperbolicity conditions here established lead to stability and, hence, well-posedness.

Finally, let us note that a related concept to that of well-posedness is that of causality of the propagation of perturbations. Whereas to establish whether a problem is well-posed we considered arbitrary frequencies $\omega \in \mathbb{R}^d$, to discuss causality we consider explicitly the high-frequency limit $|\omega| \gg 1$. In such case, consider a field of the form $\phi^I = u^I_\omega e^{\lambda_\omega t - \omega_a x^a}$, where u^I_ω is an eigenvector of $i\omega_a A^{aI}_J$ with eigenvalue λ_ω. In the high-frequency limit these fields are arbitrarily close to solutions to the equation (2.44), even in the case with variable coefficients (actually this argument can be generalized to quasilinear systems, see [404]). Therefore, the domain of dependence of the system is governed by the maximum propagation speed of these eigenvectors, i.e., by the largest eigenvalue $|\lambda_\omega|$ in the limit in which $\omega \to \infty$. Showing that the largest eigenvalue $\lim_{\omega\to\infty} |\lambda_\omega| < c$ is bounded by, e. g., the speed of light, is sufficient to ensure causality. As they both deal with the properties of eigenvalues of the principal symbol, violations of causality are intimately related to the well-posedness of a problem. We will get back to this topic in Chapter 9.

2.2.2 *Finite Differences*

In order to solve numerically a PDE of the form (2.44), we first ought to replace it by a system of coupled ODEs. We do so by introducing a discretization. For simplicity, let us assume that there is but one spatial dimension which we take to be 2π-periodic, and a single field $\varphi^I_I \equiv \varphi$. We introduce the following discretization of space and time:

$$x_j = jh\,, \qquad t_n = \lambda n h^p\,, \qquad \varphi^n_j = \varphi(x_j, t_n)\,, \qquad j \in \mathbb{Z}\,,\ n \in \mathbb{N} \cup \{0\}\,, \tag{2.47}$$

with $\lambda, p > 0$ positive constants, with p corresponding to the order of the spatial differential approximation. At each timestep, we replace the continuous function by a difference function $\varphi_j(t) = \varphi(t, x_j)$, which approximates the exact solution. Spatial derivatives are approximated by difference operators. These can be built directly in terms of the translation operator

$$\text{Translation}: \qquad (Ev)_j = v_{j+1}\,. \tag{2.48}$$

Clearly, the p-th power of the translation operator acts as $(E^p v)_j = v_{j+p}$, and its inverse acts as $(E^{-1}v)_j = v_{j-1}$, whereas $E^0 = I$ is the identity. In terms of these, we can define forward, backward, and central difference operators

$$D_+ = \frac{E - I}{h}\,, \qquad D_- = \frac{I - E^{-1}}{h}\,, \qquad D_0 = \frac{E - E^{-1}}{2h} = \frac{D_+ + D_-}{2}\,. \tag{2.49}$$

It is not hard to convince oneself that $D_\pm$ are first-order accurate approximations, whereas D_0 is a second-order accurate approximation to the derivative ∂_x. Higher derivatives can simply be approximated as products of these operators, i.e., D_+D_- is a second-order accurate approximation of ∂_x^2.

In order to obtain higher-order operators, let us consider the general form

$$Q_p = D_0 \sum_{r=0}^{p/2-1} (-1)^r q_r (h^2 D_+ D_-)^r \,. \tag{2.50}$$

We can enforce that $Q_p e^{i\omega x} = i\omega e^{i\omega x} + \mathcal{O}(\omega^{p+1}h^p)$ to find that the coefficients α_r must satisfy the recursion relation

$$\alpha_r = \frac{r}{4r+2}\alpha_{r-1}\,, \qquad r = 1, 2, \ldots, p/2-1\,, \qquad \alpha_0 = 1\,. \tag{2.51}$$

Of particular relevance will be fourth and sixth-order accurate operators, given by

$$\begin{aligned} Q_4 =& D_0\Big(I - \frac{h^2}{6}D_+D_-\Big)\,, \\ Q_6 =& D_0\Big(I - \frac{h^2}{6}D_+D_- + \frac{h^4}{30}D_+^2D_-^2\Big)\,. \end{aligned} \tag{2.52}$$

In terms of such a discretization, we can also introduce a discrete scalar product $(u,v)_h = \sum_j \bar{u}_j v_j h$, and its induced norm $||v||_h = \sqrt{(v,v)_h}$.

The time evolution is achieved via usual time-stepping methods in numerical analysis, see e.g. Chapter 1 in [232]. For simplicity, let us begin by considering explicit, one-step schemes, so that we can write the discrete version of the problem (2.44) as

$$\begin{aligned} \varphi_j^0 =& \varphi_0(x_j)\,, \\ \varphi_j^{n+1} =& Q(t_n)\varphi_j^n\,, \qquad n = 0, 1, \ldots\,. \end{aligned} \tag{2.53}$$

In particular, we can write a discrete solution operator $S_h(t,\tau)$ defined by $\varphi_j^n = S_h(t_n, t_m)\varphi_j^m$. Now we can extend the definition of stability (2.46) to the discrete setting: a difference approximation (2.53) is *stable* if there exist constants K, α independent of h, λ, p such that

$$||S_h(t_n, t_m)||_j \leq K e^{\alpha(t_n - t_m)}\,. \tag{2.54}$$

As in the previous case, we allow for exponential growth in our notion of stability, as long as the growth factors are independent of h. Suppose that $\varphi(t,x)$ is the exact smooth solution to the original problem. It will be useful to introduce a notion of *local truncation error* as

$$\lambda h^p \tau_j^n = \varphi(x_j, t_{n+1}) - Q\varphi(x_j, t_n)\,. \tag{2.55}$$

We say that a difference approximation is accurate of order $r = \min(p_1, pp_2)$ if there is a bounded function $L(t_n)$ such that for sufficiently small $h > 0$

$$||\tau^n||_h \leq L(t_n)(h^{p_1} + \lambda^{p_2} h^{pp_2})\,. \tag{2.56}$$

If an approximation scheme is *consistent*, i.e., if $r > 0$, and it is also *stable*, then we can prove on a finite interval $t \in [0, T]$ an error estimate

$$||\varphi^n - \varphi(\cdot, t_n)||_h \leq \mathscr{O}(h^r)\,, \tag{2.57}$$

see the proof of Theorem 4.2.3. in [232]. This justifies the replacement of a continuous problem for its discretized version, as long as we can prove the stability of the scheme, and that it leads to a consistent approximation. For problems with constant coefficients, we can formulate a discretized version of the Petrovskii necessary condition for stability: the eigenvalues of the Fourier transform version of the difference operator Q, say, $\hat{Q}$ must be bounded for some h-independent constant α. This is often called the von Neumann condition, and allows one to quickly verify the stability of a difference approximation.

Let us introduce one final concept: an approximation is said to be *dissipative of order* $2s$ if all the eigenvalues z_m of $\hat{Q}$ satisfy

$$|z_m| \leq (1 - \delta|\omega h|^{2s})e^{\alpha\lambda h^p}\,, \qquad |\omega h| \leq \pi\,, \tag{2.58}$$

where δ is a positive constant independent of h, ω. Intuitively, this means that high-frequency modes are damped. This definition of dissipation of an approximation can be easily generalized to hyperbolic problems with variable coefficients.

Now let us focus on hyperbolic systems, say, for simplicity, with constant coefficients, and replace the differential operator P by a difference operator Q_1 which is accurate of order $2r - 1$ with $r \geq 1$. This is not enough to guarantee stability, as we have not said anything about whether Q_1 is dissipative. However, consider instead the modification

$$Q = Q_1 + \sigma h^{2r-1} Q_2\,, \qquad \sigma = \text{const} > 0\,, \qquad Q_2 = (-1)^{r-1} D_+^r D_-^r\,. \tag{2.59}$$

The order of accuracy is unchanged, but Q_2 will make the approximation dissipative. The central result, which can be found in Theorem 5.7.2 in [232] is that, with a Runge-Kutta time-stepping method, the approximation (2.59) is stable, as long as σ is large enough, and λ is sufficiently small. Adding the operator Q_2 is often referred to as introducing Kreiss-Oliger dissipation. In essence, we are effectively adding higher-derivative terms to the equation which suppress high-frequency fluctuations that, otherwise, could spoil the stability of a numerical scheme. Similar stability results can be obtained for other time-stepping methods, although for the purposes of this thesis, we will most often use Runge-Kutta methods.

2.2.3 *Pseudospectral methods*

We now discuss another approach to solving a model problem (2.44) dubbed pseudospectral methods. The basic idea is to give up on having a uniform discretization, and instead approximate a function by a linear combination of certain polynomials with interesting properties

$$\varphi(t, x) \simeq \sum_{n=0}^{N} a_n(t) P_n(x)\,. \tag{2.60}$$

Finite difference methods appear when these polynomials are simply $P_n(x) = x^n$, and we recover the Taylor expansions that lead to the finite difference operators. However by choosing a different basis we can achieve a faster convergence. Indeed, the coefficients a_n of a certain series approximation may exhibit *spectral* or *exponential* convergence when $|a_n|$ decreases faster than n^{-k} for any finite fixed power k. Fourier series and Chebyshev polynomials (which are just a Fourier expansion in disguise) satisfy this property. Based on this, we may hope for an error estimate like

$$||\varphi(t_m, x) - \sum_{n=0}^{N} a_n(t_m) P_n(x)||_{w(x)} \leq \mathscr{O}(N^{-N}) \,, \tag{2.61}$$

where $||\cdot||_{w(x)}$ is the usual L_2-norm weighted with some $w(x)$. In general, most pseudospectral methods can't quite achieve (2.61), but they get remarkably close to such exponential convergence.

Broadly speaking there are two classes of spectral methods, which strive for this exponential convergence property. Here we focus on pseudospectral or collocation methods where, in essence, we define a discrete grid $(x_j)_{j=0}^N$ where we require the approximation to be exact, i.e.

$$\varphi(t, x_j) = \sum_{n=0}^{N} a_n(t) P_n(x_j) \,. \tag{2.62}$$

In such case, via quadrature we can interchangeably describe the function in terms of the coefficients $(a_n(t))$ or the function evaluated at the collocation points $(\varphi(t, x_j))$.

How to choose such collocation points? If our polynomial basis (P_n) is an orthonormal (under some scalar product) complete basis in some bound interval, say, $x \in [0, 1]$, a natural choice are the $N+1$-roots of $P_{N+1}(x)$. Alternative choices are possible, in particular, if we wish to include boundary points.

In most cases we will use a basis of Chebyshev polynomials. Only when studying problems on the sphere are spherical harmonics somewhat advantageous (we refer the reader to the First Moral Principle in Ref. [81]). Chebyshev polynomials are defined as

$$T_n(x) = \cos(n \arccos x) \,, \qquad x \in [-1, 1] \,. \tag{2.63}$$

There are two common choices for collocation points with Chebyshev polynomials:

- **Chebyshev nodes:** These are the $(N+1)$ roots of T_{N+1}. They are given by the following expression, where we also note how can we compute the coefficients of the expansion in terms of the values of the function at these points

$$x_n^{\mathrm{C}} = -\cos\Big(\frac{2n+1}{2(N+1)}\pi\Big) \,, \qquad a_n = \frac{2}{N+1} \sum_{k=0}^{N} \sigma_k \varphi(x_k)^{\mathrm{C}} T_n(x_k^{\mathrm{C}}) \,, \tag{2.64}$$

  where $\sigma_k = 1$ for $k = 1, \ldots, N$, and $\sigma_k = 1/2$ for $k = 0$.

- **Gauss-Lobatto points:** These include the boundary points and are given by

$$x_n^{\mathrm{GL}} = -\cos\left(\frac{n\pi}{N}\right), \qquad a_n = \frac{2}{N}\sum_{k=0}^{N}\hat{\sigma}_k \varphi(x_k^{\mathrm{GL}})T_n(x_k^{\mathrm{GL}}), \tag{2.65}$$

  where $\hat{\sigma}_k = \sigma_k$ for $k = 0, \ldots, N-1$, and $\hat{\sigma}_k = 1/2$ for $k = N$.

One advantage is that computing derivatives of a Chebyshev polynomial in terms of Chebyshev polynomials is straightforward, as

$$\frac{dT_{n+1}}{dx} = 2(n+1)T_n + \frac{n+1}{n-1}\frac{dT_{n-1}}{dx}. \tag{2.66}$$

This recursive relation can be efficiently implemented as a matrix operation mapping coefficients (a_n) of a function $\varphi(x)$ to the coefficients of the Chebyshev expansion of $\varphi'(x)$, say, (b_n), as $b_n = D_n^m a_m$.

We analyze now how to solve a particularly simple linear PDE with variable coefficients. Consider the initial value problem

$$\begin{aligned} \partial_t \varphi &= c(x)\partial_x \varphi, \\ \varphi(t=0,x) &= f(x), \end{aligned} \tag{2.67}$$

with $x \in [-1,1]$, and homogeneous boundary conditions, so we choose to work with Chebyshev nodes $x_n \equiv x_n^{\mathrm{C}}$. Let $\varphi_n^m = \varphi(t_m, x_n)$. Using a simple Euler method, the time evolution with step-size Δt is given by

$$\varphi_n^{m+1} = \varphi_n^m + \Delta t c(x_n)(D\varphi^m)(x_n). \tag{2.68}$$

Evaluating this takes only $\mathcal{O}(N)$ operations. Now, can we compute $(D\varphi^m)(x_n)$ efficiently? The answer is yes, thanks to the fast Fourier transform (FFT) — which when applied to Chebyshev polynomials, are often called *fast cosine transforms*. This is an efficient algorithm mapping $\varphi_n^m \overset{FFT}{\leftrightarrow} a_n(t_m)$, where $\varphi(t,x) = \sum_{n=0}^{N} a_n(t)T_n(x)$, only requiring $\mathcal{O}(N \log N)$ operations. In the Chebyshev basis, computing the derivative is an efficient step, taking only $\mathcal{O}(N)$ operations, thanks to the recursive relation (2.66). Without FFTs, using (2.64) would require matrix multiplication, i.e., $\mathcal{O}(N^2)$ operations: this alone would render pseudospectral methods not competitive against finite difference methods. An example of the algorithm described here is summarised in 1.

Both finite difference and pseudospectral methods are valid approaches to solve systems of differential equations. In general, finite difference methods are simpler to implement, but often cannot meet the accuracy and precision goals that spectral methods can. On the other hand, nonlinear problems quickly become challenging to implement in a stable way with pseudospectral methods. One common issue affecting pseudospectral techniques for nonlinear problems is *aliasing*: the product of two Chebyshev polynomials, say, $T_i(x)T_j(x)$ can be written as a sum of Chebyshev polynomials with degree up to $i+j$. Obviously, if $i+j > N$, a pseudospectral method will be losing high-frequency information, or rather aliasing this higher-frequency content to lower-frequency modes. There are ways to handle this issue, see e.g. Chapter 9 in Ref. [81].

Algorithm 1 Pseudo-code for solving (2.67) using a pseudospectral discretization.

$x_n \leftarrow \cos\left(\frac{\pi n}{N}\right)$ for $n = 0, \dots, N$ ▷ Chebyshev nodes
$c_n \leftarrow c(x_n)$ for $n = 0, \dots, N$
Initialize
$\varphi_n^0 \leftarrow f(x_n)$ for $n = 0, \dots, N$
$t \leftarrow 0$
for $m = 0$ **to** $M - 1$ **do**
    Forward fast cosine transform
    $a_k(t_m) \leftarrow \mathrm{FCT}\left[\{\varphi_n^m\}_{n=0}^N\right]$ for $k = 0, \dots, N$ ▷ $\mathscr{O}(N \log N)$ via FFT
    Chebyshev spectral differentiation
    $b_k \leftarrow 0$ for all k
    $b_N \leftarrow 0, \quad b_{N-1} \leftarrow 2N\, a_N$
    for $k = N - 2$ **down to** 1 **do**
        $b_k \leftarrow b_{k+2} + 2(k+1)a_{k+1}$
    end for
    $b_0 \leftarrow b_2 + a_1$
    $(D\varphi^m)_n \leftarrow \mathrm{IFCT}\left[\{b_k\}_{k=0}^N\right]$ for $n = 0, \dots, N$ ▷ $\mathscr{O}(N \log N)$
    Explicit Euler update at nodes
    $\varphi_n^{m+1} \leftarrow \varphi_n^m + \Delta t\, c_n\, (D\varphi^m)_n$ for $n = 0, \dots, N$ ▷ $\mathscr{O}(N)$
    $t_{m+1} \leftarrow t_m + \Delta t$
end for

2.3 BAYESIAN INFERENCE

Physics is, ultimately, an experimental science. Even though the scope of this thesis is theoretical, an understanding of how theoretical predictions meet experimental data is indispensable. This is especially true in the context of GW astrophysics, where the interpretation of GW data is often subtle. Therefore, in this section I briefly review some basic concepts of Bayesian inference: a rigorous statistical framework that allows us to interpret the information learned from a signal, while keeping explicit control of our models and prior assumptions and knowledge on the problem. Most of this section is based on [164, 430].

Suppose we measure certain random variable d, e.g., the time-sequence of GW strain measured by the LIGO detector. Suppose now we want to know whether such event was explained by a certain hypothesis H, e.g., a binary BH merger with certain physical parameters (θ_i) emitting GWs that reached Earth precisely at that time. Any time we tackle such a problem we also begin with some *prior* information, say, I, e.g., that BHs have a mass between, say, $2.5M_\odot$ and $250M_\odot$, since we know that astrophysical BHs forming from stellar collapse have a minimum mass, and we also know that our detector is only sensitive to certain frequencies. The principle of Bayesian inference is that our degree of belief of any given hypothesis H, given our prior information I and empirical evidence d is explained by some probability

distribution. Hence, we can assign a numerical degree of belief via Bayes theorem as

$$p(H|d,I) = \frac{p(d|H,I)p(H|I)}{p(d|I)}\,. \tag{2.69}$$

The left hand side is the *posterior distribution*, and it quantifies our degree of belief in favour of the hypothesis H given our prior information I, and the new empirical evidence d. In the numerator, we distinguish the *prior distribution* $p(H|I)$, that quantifies our prior degree of belief on the hypothesis H; and the *likelihood function* $p(d|H,I)$, i.e., given our prior information and assuming that our hypothesis is true, how likely d is. The denominator is often called the *evidence*. As the posterior distribution is indeed a probability distribution (and hence normalized), this denominator often factors out. However, as we will discuss later, it is important to perform *model selection*.

For concreteness, let us make the problem very concrete. We consider the inference of the mass and spin of the remnant BH after a binary BH merger through the GWs emitted during the last stage, i.e., the ringdown. Our data, therefore, is a GW strain time series, $d \equiv d(t)$. Our hypothesis will be that this data is a superposition of the fundamental mode of a Kerr BH and detector noise,

$$d(t) = h(t;\theta) + n(t)\,, \qquad h(t;\theta) = Ae^{-i(\omega t + i\phi)}\,, \tag{2.70}$$

where A, ϕ are an unknown amplitude and phase, and $\omega \equiv \omega(M,\chi)$ is a function which depends on the BH remnant mass M and spin χ. Here we take a very simplistic point of view where the ringdown signal is dominated by a single frequency, and where the amplitude and phase can be assumed to be constant. In practice, modelling the ringdown GWs is a more complicated problem and a topic of active research, see [68]. However this problem will be sufficient for the purposes of this section. Our hypothesis $H \equiv H(\theta)$ is parametrized by four numbers: $\theta : (A, \phi, M, \chi)$. Equivalently, we could simply parametrize the signal $h(t)$ in terms of the real and imaginary parts of the frequency, $\omega = 2\pi f - i/\tau$. These two parametrizations are equivalent, but as we will discuss soon, it matters (to some extent) which parametrization we choose.

This framework also shows that we need to specify some information on the noise, in order to compute the likelihood function. Noise emerging from stationary Gaussian processes is typically described in the frequency domain in terms of some power spectral density, which can be simulated or measured directly from the detector. In the time-domain, by virtue of the Wiener-Khinchin theorem, we can use instead the two-point autocovariance function [117]

$$C(\tau) = \int dt n(t) n(t+\tau)\,. \tag{2.71}$$

Then, we can prescribe the following likelihood function

$$\log p(d|\theta,I) = -\frac{1}{2}\int dt d\tau \Big[d(t) - h(t;\theta)\Big] C^{-1}(\tau) \Big[d(t+\tau) - h(t+\tau;\theta)\Big]\,. \tag{2.72}$$

We refer the reader to Ref. [430] for further justification on this likelihood function. Note that, in essence, we are marginalizing over the moments characterizing the Gaussian process from which the noise originated. Suppose that, instead of noise from a real detector, our data was generated from a numerical simulation. In that case we can directly estimate the "noise" through the difference between two runs with different (albeit sufficiently high) resolution, $n(t) \simeq E(t) = d_{\rm high}(t) - d_{\rm low}(t)$. In such case, we can prescribe directly a time-dependent likelihood function as [401]

$$\log p(d|\theta, I) = -\frac{1}{2}\int dt \left[\frac{d(t) - h(t;\theta)}{E(t)}\right]^2 . \tag{2.73}$$

Next, we need to prescribe priors on our hypothesis. These priors quantify our degree of belief on the model $h(t;\theta)$. Often, the goal when prescribing priors is to be as agnostic as possible. This leads to the *indifference principle*, dating back to Laplace, stating that if there is no reason to prefer any outcome, all outcomes should be equally probable. Mathematically this manifests into choosing *uniform* distributions for each of the parameters within certain bounds, e.g., $p(\phi) \sim U(0, 2\pi)$. Uniform distributions also maximize Shannon's information entropy, putting the previous principle into a rigorous framework (see Chapter 8 in [225]).

Now we can use Bayes' theorem to do *parameter estimation*, i.e., infer an estimate (an associated errors) given a data set. The denominator of Bayes' theorem can be computed as a normalization constant, simply as

$$Z_H \equiv p(d|I) = \int \prod_{j=1}^{N} d\theta_j p(d, \theta|I) = \int \prod_{j=1}^{N} d\theta_j p(d|\theta, I) p(\theta, I)\,, \tag{2.74}$$

where $N = 4$ in our case. Then, Bayes' theorem allows us to estimate, e.g., the mean of a single parameter θ_i, say, the BH mass, as

$$\langle \theta_i \rangle = \frac{\int \prod_{j\neq i}^{N} d\theta_j p(d|\theta, I) p(\theta, I)}{Z_H}\,. \tag{2.75}$$

Our model problem, which is already heavily simplified, is already 4-dimensional, meaning that evaluating the integrals in (2.75) is computationally quite costly. Unless we are interested in computing the *evidence*, i.e., the denominator $p(d|I)$, we can often avoid doing so by finding the maxima of the likelihood function. Nevertheless, finding extrema of nonlinear, high-dimensional functions is still a challenging problem. Remarkably clever strategies have been developed to solve this problem, ranging from Markov Chain Monte Carlo sampling, to nested sampling; and machine-learning based techniques such as simulation based inference are already a very efficient approach at tackling many problems. Explaining these methods in detail is out of the scope of this thesis. However, we note that in later chapters we will make use of *nested sampling*, an algorithm first introduced in [431], which allows fast and accurate estimation of both the posterior distribution and the evidence.

Computing the evidence (2.74) is interesting in order to perform *model selection*. Imagine that we have a competing model, say, $H_{\rm alt}$ to explain the data, e.g., the ringdown of a fuzzball. We wish to compare, based on our prior knowledge and on the data, our degree of belief in each of the models. Thus we are now not interested in a particular realisation of the model (a particular set of parameters θ_i), but on *any* combination of parameters within each model. Bayes' theorem once again provides a way to formalise this, defining the *odds ratio* as

$$O^{H}_{H_{\rm alt}}(d) = \frac{p(H|d,I)}{p(H_{\rm alt}|d,I} = \frac{p(H|I)}{p(H_{\rm alt}|I)}\frac{p(d|H,I)}{p(d|H_{\rm alt},I)}\,. \tag{2.76}$$

The second term in the product — the ratio of likelihoods — is known as *Bayes factor*

$$\mathcal{B}^{H}_{H_{\rm alt}}(d) = \frac{p(d|H,I)}{p(d|H_{\rm alt},I)} = \frac{Z_H}{Z_{H_{\rm alt}}}\,. \tag{2.77}$$

Here we need to be careful to not confuse these likelihoods with the previous discussion. In this case we want to weight in any possible realization of each model, so the Bayes factor is just the ratio of evidences. This is why nested sampling is a particularly valuable way of estimating the posterior distribution, as it allows us to also compute the evidence, and hence compare two given hypothesis.

There are many details we have omitted on spacetime geometry, numerical analysis of differential equations, and Bayesian inference. This chapter should be read as an approximately self-contained hitchhiker's guide to some of the mathematical concepts that will make an appearance at some point of this thesis, heavily supported in the references here cited. Each of these is a fascinating topic, about which I still learn and marvel often, and I hope this also serves as an invitation to the reader to explore them in depth.

3

BLACK HOLE PERTURBATION THEORY

Written while listening to music composed by W.A.Mozart.

The object of study of this thesis are gravitational waves (GWs) and their nonlinear interactions. Accessing this nonlinear regime typically requires numerical simulations of Einstein's equations. Despite the impressive progress of the field of Numerical Relativity, these simulations are often hindered whenever a disparity of scales is present, and their accuracy is limited by current computational capabilities. Alternatively, a perturbative scheme that incorporates order by order the nonlinear content of the theory is a very powerful tool, providing analytical or semi-analytical control that can be contrasted with targeted numerical simulations. Most of this thesis takes this point of view.

In this chapter we briefly review some fundamental aspects of black hole (BH) perturbations. For simplicity we restrict to non-spinning BHs, leaving a more detailed discussion of rotating BHs for chapter 4. First, we derive the equations governing linear perturbations, discussing their gauge-invariance. Next, we solve the scattering problem in the frequency domain, and introduce quasinormal modes (QNMs). Finally, we discuss the decomposition of time-domain waveforms into a prompt response, a *ringdown* stage dominated by QNMs, and a slowly-decaying tail. These constitute the basic foundations in which the work that follows is built.

3.1 GRAVITY IN SPHERICAL SYMMETRY

Physics is the science of exploiting symmetries. Hence, in order to study perturbations of spherically symmetric spacetimes we ought to exploit the spherical symmetry of the background. Gerlach and Sengupta first noticed this and used it to derive the equations governing perturbations about spherically symmetric spacetimes in a gauge invariant manner [205, 206]. Later works extended this to higher dimensions or to include particular matter models [228, 255, 281–283, 330, 332, 350, 376, 408]. We will use this same formulation to discuss the perturbations of viscous stars in Chapter 10, so we will keep this formulation sufficiently general for the time being.

A spherically symmetric spacetime in four spacetime dimensions can always be written as the warped product between a Lorentzian manifold $\mathcal{N}^2$ and the unit sphere $\mathcal{S}^2$, with a warping factor which we dub r^2, so that the global spacetime is

$\mathcal{M} = \mathcal{N}^2 \times_{r^2} \mathcal{S}^2$. In other words, if $\{y^a\}$ with $a = 0, 1$ are coordinates on $\mathcal{N}^2$, and $\{z^I\}$ with $I = 2, 3$ are coordinates on the sphere, the metric and stress energy tensor admit the decomposition

$$\begin{aligned} ds^2 &= g_{AB}(y)dy^A dy^B + r^2(y)q_{IJ}dz^I dz^J\,, \\ T &= T_{AB}(y)dy^A dy^B + r^2(y)\mathcal{T}q_{IJ}dz^I dz^J\,, \end{aligned} \tag{3.1}$$

where g_{AB} is the metric on $\mathcal{N}^2$, $r(y)$ is a real scalar field on $\mathcal{N}^2$, and the stress energy tensor is governed by the symmetric tensor $T_{AB}(y)$ and the scalar $\mathcal{T}$. Above, q_{IJ} is the metric of the round sphere. Notice that the Schwarzschild metric describing a spherically symmetric BH with mass M can always be cast in this form. For instance, in static and double null coordinates we have

$$\begin{aligned} &\text{Static:} \quad g_{AB}dy^A dy^B = -fdt^2 + f^{-1}dr^2\,, \quad r(t,r) = r\,, \quad f = 1 - \frac{2M}{r}\,, \\ &\text{Double null:} \quad g_{AB}dy^A dy^B = -fdudv\,, \quad r_\star = \frac{v-u}{2}\,, \end{aligned} \tag{3.2}$$

where in double null coordinates, the warping factor r is only given implicitly in terms of the tortoise coordinate $r_\star$ via

$$\frac{dr}{dr_\star} = f\,, \quad r_\star = r + 2M\log\Big(\frac{r}{2M} - 1\Big)\,. \tag{3.3}$$

Let ∇_A denote the covariant derivative on $(\mathcal{N}^2, g_{AB})$, and D_I the covariant derivative on the sphere. Let us also introduce the vector

$$v_A = \frac{1}{r}\nabla_A r\,. \tag{3.4}$$

Einstein equations, with the cosmological constant set to zero, take the form

$$\begin{aligned} \Big(3v^2 + 2\nabla_A v^A - \frac{1}{r^2}\Big)g_{AB} - 2\Big(v_A v_B + \nabla_A v_B\Big) &= 8\pi T_{AB}\,, \\ \nabla_A v^A + v^2 - \frac{1}{2}{}^{(2)}R &= 8\pi\mathcal{T}\,, \end{aligned} \tag{3.5}$$

where $v^2 = v_A v^A$, and we have made use of the fact that any 2 dimensional Lorentzian manifold has vanishing Einstein tensor. Notice how these equations (3.5) in vacuum are immediately satisfied for the Schwarzschild metric, which can be directly checked in either coordinate set (3.2).

3.2 LINEAR PERTURBATIONS

The approach taken in this thesis to understand the nonlinear dynamics of spacetime during BH relaxation relies on linearizing the field equations around a given exact solution. For the time being, it is sufficient to think that the spacetime metric admits the formal expansion

$$g_{ab} = \mathring{g}_{ab} + \varepsilon\dot{g}_{ab} + \mathcal{O}(\varepsilon^2)\,, \tag{3.6}$$

where $\mathring{g}_{ab}$ is a spherically symmetric metric of the form (3.1), and $\varepsilon \ll 1$ is a book-keeping small parameter. We will generically use the notation above to denote background and perturbed quantities, e. g., the perturbation of the stress energy tensor will be denoted by $\dot{T}_{ab}$, etc.

An arbitrary symmetric tensor, e. g.the metric perturbation $\dot{g}_{ab}$ has the following $2+2$ decomposition

$$\begin{aligned}
\dot{g}_{ab}dx^a dx^b =& \sum_{\ell,m}\left({}^{\mathrm{E}}\dot{g}^{\ell m}_{ab} + {}^{\mathrm{O}}\dot{g}^{\ell m}_{ab}\right),\\
{}^{\mathrm{E}}\dot{g}^{\ell m}_{ab}dx^a dx^b =& \dot{h}^{\ell m}_{AB}\mathcal{Y}^{\ell m}dy^A dy^B + 2\dot{h}^{\ell m}_{A}\mathcal{Y}^{\ell m}_{I}dy^A dz^I + r^2\left[\dot{h}^{\ell m}\mathcal{Y}^{\ell m}q_{IJ} + \dot{\tilde{h}}^{\ell m}\mathcal{Y}^{\ell m}_{AB}\right]dz^I dz^J,\\
{}^{\mathrm{O}}\dot{g}^{\ell m}_{ab}dx^a dx^b =& 2\dot{k}^{\ell m}_{A}\mathcal{X}^{\ell m}_{I}dy^A dz^I + \dot{k}^{\ell m}\mathcal{X}^{\ell m}_{AB}dz^I dz^J,
\end{aligned} \tag{3.7}$$

where we have introduced a split in *even* (or polar) and *odd* (or axial) tensor harmonics. The tensor spherical harmonics are defined in terms of the usual spherical harmonics $\mathcal{Y}^{\ell m}$, which are eigenfunctions of the spherical laplacian

$$D_I D^I \mathcal{Y}^{\ell m} = -\ell(\ell+1)\mathcal{Y}^{\ell m}, \tag{3.8}$$

with ℓ a non-negative integer, and $|m| \leq \ell$. These are orthonormal functions on the sphere. We can now drop the ℓ, m label, since different harmonics never mix in the linearised theory – but keeping in mind that we always refer to a concrete harmonic. The vector and tensor harmonics with even and odd parity introduced above are given by

$$\begin{aligned}
&\text{Even parity:} \quad \mathcal{Y}_I = D_I\mathcal{Y}, \quad \mathcal{Y}_{IJ} = D_I D_J\mathcal{Y} + \frac{\ell(\ell+1)}{2}\mathcal{Y}q_{IJ},\\
&\text{Odd parity:} \quad \mathcal{X}_I = \epsilon^J_I D_J\mathcal{Y}, \quad \mathcal{X}_{IJ} = D_{(I}D_{J)}\mathcal{Y}.
\end{aligned} \tag{3.9}$$

Whenever $\ell = 0, 1$ some of these harmonics are trivially zero. We refer to the monopole ($\ell = 0$) and dipole ($\ell = 1$) modes as non-radiative modes, and for this reason, they need to be treated separately, so we will assume for the time being that we work with radiative multipoles, $\ell \geq 2$.

3.2.1 *Gauge Fixing*

The form of this metric fluctuation is not invariant. Clearly we can perform a "small" gauge transformation, generated by the vector field $\Xi = \varepsilon\dot{\xi}^{\ell m}$, such that

$$\mathfrak{L}_\Xi g = \mathring{g} + \varepsilon\left(\dot{g} + \mathfrak{L}_{\dot{\xi}}\mathring{g}\right) + \mathscr{O}(\varepsilon^2). \tag{3.10}$$

We can use this freedom to our advantage. We will show now how given a general metric fluctuation $\dot{g}$, we can find a unique perturbation-dependent vector field $\xi[\dot{g}]$ that takes the metric to the so-called Regge-Wheeler (RW) gauge. Equivalently, the variables constructed in this manner are gauge invariants. The key aspect will be

that this is a complete gauge fixing, i. e., the gauge vector field is uniquely fixed by the metric perturbation, with no residual gauge freedom. In order to show this, notice that the gauge vector admits the decomposition

$$\dot{\xi} = \dot{\xi}_A \mathcal{Y} dy^A + \left(\dot{\xi}\mathcal{Y}_I + \dot{\chi}\mathcal{X}_I\right) dz^I \,. \tag{3.11}$$

The even and odd parity sectors transform separately. The gauge-transformed metric perturbation $\dot{g}' = \dot{g} + \mathfrak{L}_{\dot{\xi}} \mathring{g}$ is given by

$$\dot{k}'_A = \dot{k}_A - r^2 \nabla_A \dot{\chi} \,, \quad \dot{k}' = \dot{k}' - 2\dot{\chi} \,, \tag{3.12}$$

for the odd parity sector and

$$\begin{aligned} \dot{h}'_{AB} =& \dot{h}_{AB} - 2\nabla_{(B}\dot{\xi}_{A)} \,, \quad \dot{h}'_A = \dot{h}_A - \dot{\xi}_A - r^2 \nabla_A \dot{\xi} \,, \\ \dot{h}' =& \dot{h} + \ell(\ell+1)\dot{\xi} - 2v^A \dot{\xi}_A \,, \quad \dot{\tilde{h}}' = \dot{\tilde{h}} - 2\dot{\xi} \,, \end{aligned} \tag{3.13}$$

for the even parity perturbations. The RW gauge is defined by the conditions

$$\dot{k} = \dot{\tilde{h}} = 0 \,, \quad \dot{h}_A = 0 \,. \tag{3.14}$$

These conditions can be achieved by setting $\dot{k}' = \dot{\tilde{h}}' = \dot{h}'_A = 0$ in eqs. (3.12)-(3.13), and writing the perturbation-dependent gauge vector

$$\dot{\chi} = \frac{\dot{k}}{2} \,, \quad \dot{\xi} = \frac{\dot{\tilde{h}}}{2} \,, \quad \dot{\xi}_A = \dot{h}_A - \frac{r^2}{2}\nabla_A \dot{\tilde{h}} \,. \tag{3.15}$$

As anticipated this is a *complete* gauge fixing – there is no remaining freedom. A more detailed discussion of the issues of gauge freedom in perturbation theory can be found in Refs. [84, 330]. We can now assume that the metric perturbation is in the RW gauge, i. e., it takes the form

$$\dot{g}_{ab} dx^a dx^b = \dot{h}_{AB} \mathcal{Y} dy^A dy^B + 2\dot{k}_A \mathcal{X}_I dy^A dz^I + r^2 \dot{h} \mathcal{Y} q_{IJ} dz^I dz^J \,. \tag{3.16}$$

The stress energy tensor would allow for arbitrary fluctuations $\dot{T}_{ab}$ which are not constrained by gauge freedom. We will now proceed to study the linearised theory around a spherically symmetric background in the absence of matter fluctuations, i. e., $\dot{T}_{ab} = 0$. These will be dealt with in Chapter 10, in order to discuss the perturbations of viscous stars. Our goal now is to solve the homogeneous linearised Einstein equations $\dot{G}_{ab} = 0$. The Einstein tensor is a symmetric tensor, and thus can be decomposed in even and odd parity spherical harmonics. Let us denote $\dot{G}_{ab} = \dot{G}^{\mathrm{E}}_{ab} + \dot{G}^{\mathrm{O}}_{ab}$ to each of these sectors, which must vanish independently. Then, we have

$$\begin{aligned} \dot{G}^{\mathrm{E}}_{ab} dx^a dx^b =& \dot{H}_{AB} \mathcal{Y} dy^A dy^B + 2\dot{H}_A \mathcal{Y}_I dy^A dz^I + r^2 \left[\dot{H}\mathcal{Y} q_{IJ} + \dot{\tilde{H}}\mathcal{Y}_{AB}\right] dz^I dz^J \,, \\ \dot{G}^{\mathrm{O}}_{ab} dx^a dx^b =& \dot{K}_A \mathcal{X}_I dy^A dz^I + \dot{K}\mathcal{X}_{AB} dz^I dz^J \,. \end{aligned} \tag{3.17}$$

The linearised Einstein equations imply simply that each of these harmonic modes vanishes independently.

3.2.2 *Odd parity – Regge-Wheeler equation*

The only odd parity Einstein equations are $\dot{K} = \dot{K}_A = 0$, given by

$$\begin{aligned} \dot{K} \equiv& \nabla_A \dot{k}^A = 0\,, \\ \dot{K}_A \equiv& \frac{1}{r^2}\nabla_B\Big[r^4\nabla_{[A}\Big(r^{-2}\dot{k}_{B]}\Big)\Big] + \Big(\frac{\ell(\ell+1)-2}{r^2} + 8\pi\mathcal{T}\Big)\dot{k}_A = 0\,. \end{aligned} \tag{3.18}$$

Notice now that antisymmetric tensors on a 2-dimensional background span a 1-dimensional space, and hence we can write

$$\nabla_{[A}\Big(r^{-2}\dot{k}_{B]}\Big) = r^{-4}\Psi\epsilon_{AB}\,, \tag{3.19}$$

for some scalar function $\Psi = -(r^4/2)\epsilon^{AB}\nabla_A(r^{-2}\dot{k}_B)$. Let us further assume that we are in vacuum, i. e., $\mathcal{T} = 0$ [1]. Then, taking $\epsilon^{AB}\nabla_A\dot{K}_B$ we find a decoupled equation for Ψ

$$r^2\nabla_A\Big(r^{-2}\nabla^A\Psi\Big) - \frac{\ell(\ell+1)-2}{r^2}\Psi = 0\,. \tag{3.20}$$

This equation, first presented in Ref. [205], when evaluated in static coordinates reduces to the Regge-Wheeler equation [402] (albeit for a different variable $\psi_{\rm RW} = \Psi/r$)

$$-\partial_t^2\psi_{\rm RW} + f\partial_r(f\partial_r\psi_{\rm RW}) - V_{\rm RW}\psi_{\rm RW} = 0\,, \quad V_{\rm RW} = f\Big(\frac{\ell(\ell+1)}{r^2} - \frac{3f'}{r}\Big)\,. \tag{3.21}$$

3.2.3 *Even parity – Zerilli equation*

In the even parity sector, we begin by noticing that

$$\dot{\mathring{H}} = -\frac{1}{2r^2}\dot{h}^A_A = 0\,. \tag{3.22}$$

The even parity metric perturbation on $\mathcal{N}^2$ must be traceless. Next, we have an equation for the perturbation of the warping factor h

$$\dot{H}_A = \nabla^B\dot{h}_{AB} - \nabla_A\dot{h} = 0\,. \tag{3.23}$$

Using eq. (3.23) to eliminate derivatives of $\dot{h}$ and the traceless condition (3.22) immediately lead to $\dot{H} = 0$. The only remaining equation is $\dot{H}_{AB}$, given by

$$\begin{aligned} &2\nabla_B\nabla^C\dot{h}_{AC} + 2v^C\Big(\nabla_C\dot{h}_{AB} - 2\nabla_{(A}\dot{h}_{B)C}\Big) + 4v_{(A}\nabla^C\dot{h}_{B)C} - \Big(\frac{(\ell-1)(\ell+2)}{r^2} - 2v^2\Big)\dot{h}_{AB} \\ &+ \Big(2v^Cv^D\dot{h}_{CD} - 2v^C\nabla^D\dot{h}_{CD} - 2\nabla^C\nabla^D\dot{h}_{CD} + \frac{(\ell-1)(\ell+2)}{r^2}\dot{h}\Big)g_{AB} = 0\,. \end{aligned}$$

1 This term can be absorbed in a "master variable" which describes the odd-parity perturbations of the matter sector, see [376, 399].

(3.24)

In deriving this we have also used that the Einstein tensor vanishes in two dimensions for any metric, in particular, $G[h_{AB}] = 0$, to eliminate several second derivative terms. Taking the trace-free part we obtain an equation which only depends on h_{AB}:

$$2\nabla_B\nabla^C\dot{h}_{AC} - g_{AB}\nabla^C\nabla^D\dot{h}_{CD} + 2v^C\Big(\nabla_C\dot{h}_{AB} - 2\nabla_{(B}\dot{h}_{A)C}\Big) + 4v_{(A}\nabla^C\dot{h}_{B)C} - \Big(\frac{(\ell-1)(\ell+2)}{r^2} - 2v^2\Big)\dot{h}_{AB} = 0\,. \tag{3.25}$$

At this point one may be tempted to give up, as no further simplification seems possible. Since h_{AB} is traceless, it is determined by two real functions, which are fixed by the two coupled equations (3.25). Remarkably Zerilli [473] found a way to decouple both equations in terms of a single variable ψ_Z constructed from h_{AB} which satisfies a wave equation

$$-\partial_t^2\psi_Z + f\partial_r(f\partial_r\psi_Z) - V_Z\psi_Z = 0\,, \tag{3.26}$$

with the potential

$$V_Z = \frac{2f}{r^3}\Big[\frac{9M^3 + 3\lambda^2 Mr^2 + \lambda^2(1+\lambda)r^3 + 9\lambda M^2 r}{9M^2}\Big]\,, \quad \lambda = (\ell-1)(\ell+2)/2\,. \tag{3.27}$$

As for the RW equation, there is no unique choice for a master variable that satisfies the Zerilli equation (3.26). Common choices are the master function of Cunningham, Price, and Moncrief [154] in the odd parity sector [2], or the variable introduced by Moncrief [345] (often referred to as Zerilli-Moncrief variable), see [352] for a discussion on the possible choices of variables. Also notice that the time derivatives of these variables also satisfy the same equations, although in the presence of matter fluctuations, their source terms may exhibit different decay properties [247].

Despite their different appearance, the RW (3.21) and Zerilli (3.26) equations lead to the same physics – a phenomena known as isospectrality. In essence, there exists a change of variable that maps the RW equation into the Zerilli equation, and vice-versa [128], although further insights on this may be gained by analysing the problem in terms of the perturbations of the curvature [349]. Finally, we remark that both the RW and the Zerilli variables are directly related to the GWs measured by an observer asymptotically far away from the BH. We refer the interested reader to [330] for further details.

3.2.4 *Non-radiative Multipoles*

We conclude the derivation of the master equations governing linear perturbations on spherical BHs by discussing the non-radiative multipoles $\ell = 0, 1$. In order to do

2 Notice that this is related to our $\psi_{\rm RW}$ by a simple proportionality factor [399].

so, we must go back to eq. (3.7) and analyse the extra gauge-freedom gained for these multipoles.

First, for spherically symmetric perturbations, $\ell = 0$, notice that $\mathcal{Y} = \text{const}$ and hence $\mathcal{X}_I = \mathcal{X}_{IJ} = \mathcal{Y}_I = \mathcal{Y}_{IJ} = 0$. The metric perturbation has even parity and is solely generated by h_{AB} and h. In the $\ell = 0$ sector, a gauge transformation is only generated by (3.11) with $\xi = \chi = 0$. Choosing $\dot{\xi}_A$ such that $v^A \dot{\xi}_A = h/2$ eliminates the perturbation generated by $\dot{h}$. This is not a complete gauge fixing, as one can always add a gauge transformation generated by a timelike vector T_A orthogonal to v_A. This additional gauge freedom can be used to make $v^A T^B \dot{h}_{AB} = 0$. There is one remaining residual freedom in $n^A \dot{\xi}_A$, which can then be used to render the metric perturbation time-independent. Plugging this back into the linearised equations, one finds (see App.G in [472] for further details) that this perturbation corresponds to a small shift in the BH mass.

Next, let us examine the $\ell = 1$ modes. In this case we have both odd and even parity perturbations. In the odd sector, notice that $\mathcal{X}_{IJ} = 0$, meaning that now we can use the gauge transformation (3.12) to set, e. g. $T^A \dot{k}_A = 0$, where T^A is the Killing vector generating time-translations. Once again, there is certain residual gauge-freedom associated to a purely radial shift of $\dot{k}_A$. Further exploiting this, and solving the linearised equations, the $\ell = 1$ odd parity fluctuations are shown to correspond to adding a small angular momentum to the BH, taking the metric to the Hartle-Thorne metric [236].

Finally, the $\ell = 1$ even parity perturbations are pure gauge. Indeed, let us stare now at (3.13), where $\dot{\tilde{h}} = 0$ since $\mathcal{Y}_{IJ} = 0$ for $\ell = 1$. We can eliminate $\dot{h}, \dot{h}_A$ through appropriate choices of $\dot{\xi}, \dot{\xi}_A$, leaving only $\dot{h}_{AB}$. Plugging now this into the linearised equations one can show that $\dot{h}_{AB}$ is pure gauge by showing that it is a Lie derivative of a vector field (which one can identify with $\dot{\xi}_A$). Zerilli [472] found a physical interpretation of this gauge transformation as a translation to the center of mass, which generates this dipolar terms.

This shows how, in vacuum, the multipoles $\ell = 0, 1$ are not dynamical. If one considers matter coupled to gravity, e. g., Einstein-Klein-Gordon or Einstein-Maxwell theories, then there are non-trivial dynamics in the scalar and dipole sectors, respectively [376].

3.3 SOLVING THE LINEARISED EQUATIONS

We will now discuss the solutions to the RW and Zerilli equations, which describe perturbations of a Schwarzschild BHs. In the presence of matter fluctuations, e. g., a point-mass thrusted towards the BH, these equations become

$$-\partial_t^2 \Psi_\bullet + f \partial_r (f \partial_f \Psi_\bullet) - V_\bullet \Psi_\bullet = \mathcal{S}_\bullet \,, \qquad \bullet = \{\text{even}, \text{odd}\} \,, \tag{3.28}$$

where the even (respectively odd)-parity potential is given by eq. (3.27) (resp. (3.21)). Notice that the radial derivatives combine to be simply $\partial^2_{r_\star}$, with $r_\star$ the tortoise coordinate satisfying $dr = f dr_\star$. If we restrict to the case where the gravitational fluctuations are sourced by the motion of a point-mass with mass μ, along a

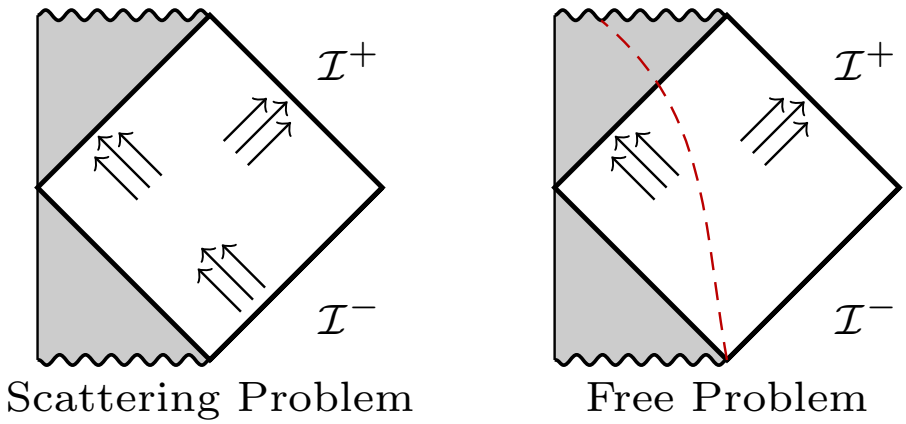

Figure 6 Sketch of the Penrose diagram of a Schwarschild BH representing the two kind of problems, as specified by the boundary conditions, that we will consider. In the scattering problem, waves are sent from $\mathcal{I}^-$, are absorbed at the event horizon, and out-going at $\mathcal{I}^+$. In the free problem there are no incoming waves from $\mathcal{I}^-$ – instead waves can be excited by a point-particle falling into the BH (represented by the dashed red line), or some fiducial initial perturbations. .

worldline $x^a = (t_p(\tau), r_p(\tau), \pi/2, \phi_p(\tau))$, with τ the proper time, then the source term takes the form

$$\mathcal{S}_\bullet = F_\bullet(t)\delta(r - r_p(t)) + G_\bullet(t)\delta'(r - r_p(t))\,. \tag{3.29}$$

The exact form of the functions F, G depends on the choice of master variable in each sector, see e.g. [247].

The problem at hand is an initial boundary value problem – we ought to specify both the behaviour of Ψ at the boundaries, $r \to 2M, \infty$, and evolve forward in time starting from some initial condition. The boundary conditions are enforced by the geometry of the background spacetime. In particular, perturbations must be purely in-coming at the event horizon. At null infinity, we can consider in general that there is a superposition of in-coming waves (from $\mathcal{I}^-$) and out-going waves (towards $\mathcal{I}^+$). This picture corresponds then to a *scattering problem*, where we study the response of the BH to certain in-coming waves. Alternatively we often consider the *free problem*, where there are no in-coming waves from $\mathcal{I}^-$. See Fig. 6 for a sketch of the differences between the scattering problem and the free problem.

In the frequency domain, i. e., denoting $\Psi = e^{-i\omega t}\psi$, and letting Z_ω be the Fourier transform of the source term, the full problem can be written

$$\begin{aligned} &\frac{d^2\psi}{dr_\star^2} + (\omega^2 - V)\psi = Z_\omega\,, \\ &\psi \xrightarrow{r_\star \to -\infty} Te^{-i\omega r_\star}\,, \quad \psi \xrightarrow{r_\star \to \infty} Ie^{-i\omega r_\star} + Re^{i\omega r_\star}\,. \end{aligned} \tag{3.30}$$

The factors T, I, R correspond to transmitted, incident, and reflected pieces. These are not independent, and in fact, satisfy

$$I^2 + R^2 = T^2\,. \tag{3.31}$$

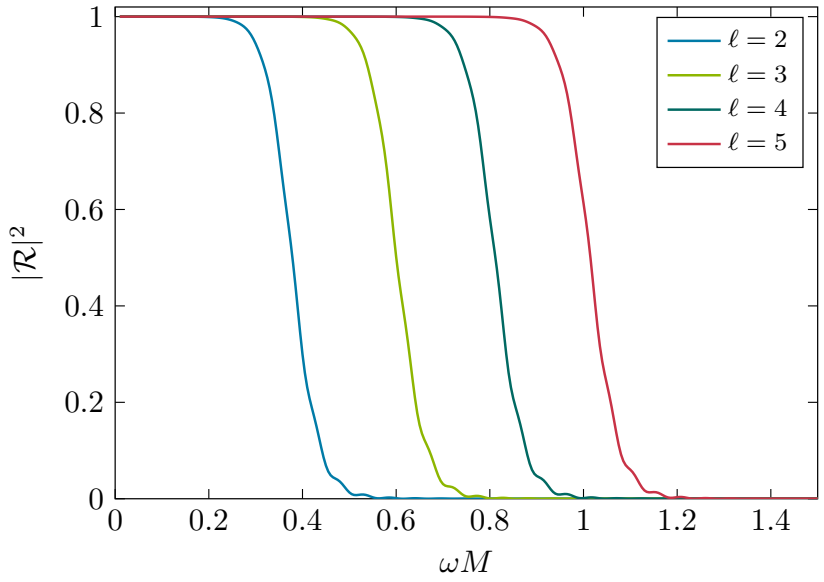

Figure 7 Reflectivity $|\mathcal{R}|^2$ as a function of the dimensionless frequency ωM for different values of ℓ. The reflectivity coincides for the even and odd parity sectors. For all values of ℓ there is a value such that frequencies larger than that value are mostly absorbed by the BH.

In the free problem we set $I = 0$. By going to the Fourier domain we have omitted the possible role of some initial conditions at a hypersurface $t = \text{const.}$. These can be accounted for using a Laplace transform instead (see [61, 400]).

3.3.1 *Scattering Problem*

Let us first examine briefly the scattering problem in the absence of sources, i. e., setting $Z = 0$. The problem then is homogeneous, so we can set without loss of generality $T = 1$. Then, the scattering problem is fully characterised by the *reflectivity* coefficients

$$\mathcal{R}_\ell(\omega) = \frac{R}{I}\,. \tag{3.32}$$

Physically this represents the amount of "energy" that is reflected by the BH. Propagation through flat space would lead simply to $|\mathcal{R}| = 1$, and zero-reflectivity corresponds to perfect absorption. One may thus think of BHs as spectral filters that imprint some information about their structure by scattering waves through the reflectivity factors. In fact, the amplification factor used to relate a lensed gravitational wave with its unlensed component can be written directly in terms of these factors, whenever the lens is a Schwarzschild BH [125, 299, 379, 418].

We solve for the reflectivity by directly integrating eq. (3.30) up to a large enough radius, and then extracting the incident and reflected wave coefficients. We set boundary conditions at a finite distance to the event horizon $r_{\text{min}} = 2M + \epsilon$, with

$0 < \epsilon \ll 1$. In order to have accurate enough boundary conditions, we solve the equation close to the horizon with an ansatz of the form

$$\psi = e^{-i\omega r_\star} \sum_{n=0}^{N} a_n (r-2M)^n \,, \tag{3.33}$$

where the a_n coefficients are functions only of ℓ, ω. We typically set $r_{\rm min} = 2M + 10^{-6}$ and $N = 10$. Doing this calculation reveals that isospectrality holds – the reflectivities obtained for the odd and even sectors are identical. The reflectivity is shown for different values of ℓ in Fig. 7. Notice that the transition occurs at some particular value of the frequency which scales with the number ℓ. We will later confirm that this frequency corresponds approximately to the real part of the fundamental quasinormal mode. We will return to the study of the scattering problem later in this thesis when we discuss the response of viscous stars.

3.3.2 *Free Problem*

Let us now focus on the free problem. For our purposes, as we are mostly interested in the free oscillations of the BH itself, it will be equivalent to consider either a source, e. g.given by a point-particle, or a source that emerges through the Laplace transform of some non-trivial initial data. Recall that if the initial data of an homogeneous second order equation is $\Psi(t=0) = \psi_0$ and $d\Psi/dr_\star(t=0) = \psi_1$, the Laplace transformed equation has a source term

$$Z_\omega = \psi_1 - i\omega\psi_0 \,. \tag{3.34}$$

Let us denote two independent homogeneous solutions as

$$\begin{aligned} &\text{In solution:} \quad \psi_{\rm in} \xrightarrow{r_\star \to -\infty} e^{-i\omega r_\star} \,, \\ &\text{Up solution:} \quad \psi_{\rm up} \xrightarrow{r_\star \to \infty} e^{i\omega r_\star} \,. \end{aligned} \tag{3.35}$$

These solutions can be understood from the boundaries of the characteristic problem: the "in" solution satisfies $\psi_{\rm in} = 0$ at the past event horizon $\mathcal{H}^-$, whereas the "up" solution satisfies $\psi_{\rm up} = 0$ at past null infinity $\mathcal{I}^-$. Notice that the $\psi_{\rm in}$ solutions are the ones that generate the scattering problem discussed before. Their asymptotic behaviour sufficiently far away is

$$\psi_{\rm in} \xrightarrow{r_\star \to \infty} I(\omega) e^{-i\omega r_\star} + R(\omega) e^{i\omega r_\star} \,. \tag{3.36}$$

The Wronskian formed by these solutions is

$$\mathrm{Wr} = \psi_{\rm in} \frac{d\psi_{\rm up}}{dr_\star} - \psi_{\rm up} \frac{d\psi_{\rm in}}{dr_\star} = 2i\omega I(\omega) \,. \tag{3.37}$$

The solution of eq. (3.30) can be written, then, as

$$\psi = \psi_{\rm up} \int_{-\infty}^{r} \left(\frac{\psi_{\rm in} Z_\omega}{2i\omega I(\omega)} f dr \right) + \psi_{\rm in} \int_{r}^{\infty} \left(\frac{\psi_{\rm up} Z_\omega}{2i\omega I(\omega)} f dr \right) \equiv C_{\rm up}\psi_{\rm up} + C_{\rm in}\psi_{\rm in} \,. \tag{3.38}$$

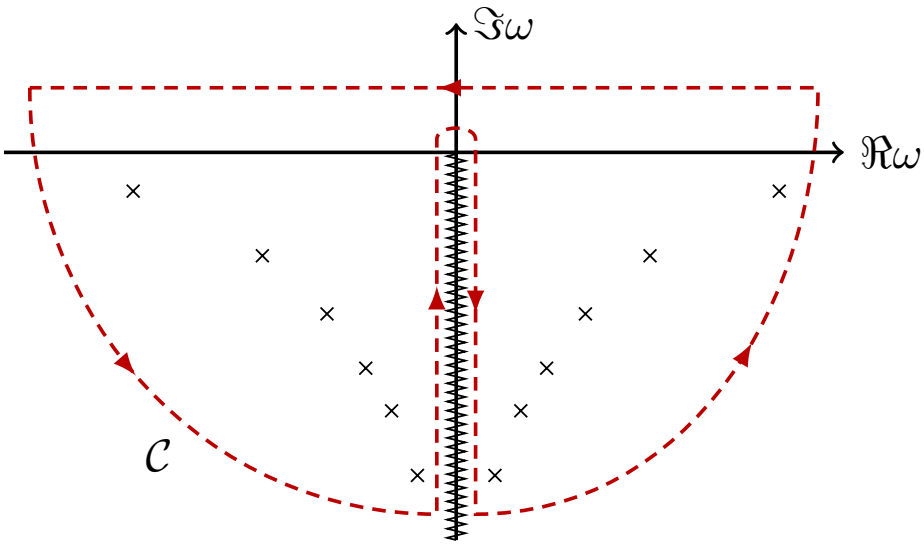

Figure 8 Integration contour $\mathcal{C}$ to perform the inverse Fourier (Laplace) transform. Crosses denote poles of the Green's function, i. e., zeros of $I(\omega)$. The jagged line at $\Im\omega = 0$ corresponds to a branch cut.

We recover the solution in the time-domain by taking the inverse Fourier (or Laplace) transform of (3.38),

$$\Psi = \int_{\mathcal{C}} \psi e^{-i\omega t} d\omega \,. \tag{3.39}$$

Special care is needed as the integration will not be fully convergent along the real axis unless the source term has compact support in ω. In particular notice that if we are considering the initial value problem, the source term (3.34) does not have compact support in ω. Then we ought to deform the integration contour $\mathcal{C}$ in the way shown in Fig. 8. Two features are evident from eq. (3.38): (i) there is an essential singularity at $\omega = 0$ and additionally, a branch cut extending all the way along the negative imaginary axis, and (ii) whenever $I(\omega) = 0$ (equivalently, whenever the reflectivity is divergent), there is a pole. These are also shown in Fig. 8. The branch cut leads to the late-time polynomial decay of Ψ (known as *tails*), whereas the poles correspond to the quasinormal modes (QNMs) of the BH. The contributions of the different part of the integration contour are analysed in further detail in Refs. [24, 138, 303, 358] (see more recent developments in [163] and references therein).

3.3.3 *Quasinormal Modes*

QNMs correspond to zeros of the incident amplitude. These are frequencies for which the two boundary conditions (in-going at the horizon and out-going at infinity) are satisfied simultaneously. Therefore one may think of QNMs as the natural frequencies of oscillation of the BH. These are similar to the normal modes of vibration of a string, but as evident from Fig. 8, they are complex numbers. This is a consequence of the fact that the problem (3.30) is not self-adjoint. Hence there

are no normal modes but quasinormal modes with complex frequencies, which do not span the full space of solutions, and which are not bounded. The consequences of the fact that the linearised perturbations of a BH are governed by a non-normal operator are far-reaching and still under deep scrutiny, see [12, 29, 69, 101, 139, 261, 359, 457] and references therein.

For each value of ℓ, m [3], let us label each of the poles of the reflectivity with an index $n = 0, 1, \ldots$ in increasing order of $|\Im\omega|$. With this ordering there are two QNMs for each label ℓmn with different sign in the real part of the frequency. We label the modes where $\mathrm{sgn}(\Re\omega_{\ell mn}) = \mathrm{sgn}(m)$ as *co-rotating* and annotate them with a $+$ label. Modes where the sign of the real part is the opposite as the sign of m are dubbed *counter-rotating*, and given a $-$ label. Hence, QNMs are characterised by four labels, $(\ell, m, n, \pm)$.

The contribution due to a given QNM enclosed in $\mathcal{C}$ to Ψ can be written exactly [61]. Since there is a degeneracy in m, and hence co and counter-rotating modes are physically equivalent for a Schwarzschild BH, let us label now the modes only with (ℓn). The excitation of the (ℓn) modes is given by the contribution due to the Residue Theorem to (3.39)

$$\Psi_{\ell n} = \frac{-e^{-i\omega_{\ell n} t}}{2\omega_{\ell n}} \left(\frac{dI}{d\omega}\right)^{-1}\Big|_{\omega=\omega_{\ell n}} \int_{2M}^{\infty} Z_{\omega_{\ell n}} \psi_{\rm in} f dr \equiv e^{-i\omega_{\ell n} t} B_{\ell n} \int_{2M}^{\infty} Z_{\omega_{\ell n}} \psi_{\rm in} f dr\,, \quad (3.40)$$

where the $B_{\ell n}$ are often referred to as *quasinormal excitation factors* (QNEF). Remarkably these are geometric factors, independent of the source term or the initial perturbation. Physically they can be thought of as susceptibilities which determine how "easy" it is to excite a given QNM. If the source term has compact support in r, the integral in (3.40) trivially amounts to a finite value. However, if the source does not have compact support, the integral diverges in general. Nevertheless, an appropriate deformation of the contour near the singular points (the horizon and infinity) can render the integral finite [217, 224, 303].

The second difficulty is finding the frequencies corresponding to these QNMs. The spectrum of frequencies is shown in Fig. 9. We distinguish three methods to compute them, although this does not aim to be an exhaustive list. Apart from the methods discussed here, there are a number of approximations one can use to estimate the QNM frequencies, e. g., in the large ℓ limit.

- **Shooting methods**. We can extend the procedure carried out for the scattering problem to find the frequencies ω for which $I(\omega) = 0$. A bisection method (or more sophisticated root-finding algorithms) can be used to find QNM frequencies, then. The main advantage of this method is that it is remarkably simple to implement, meaning it generalizes easily to other scenarios. However, it requires of an initial guess that must be sufficiently close to the real QNM frequency for the root-finding algorithm to converge. Additionally the numerical integration of eq. (3.30) is delicate and requires sufficient precision at high frequencies, or for large values of ℓ.

3 Notice that the m modes are all degenerate for a Schwarzschild BH. Rotation will break this degeneracy.

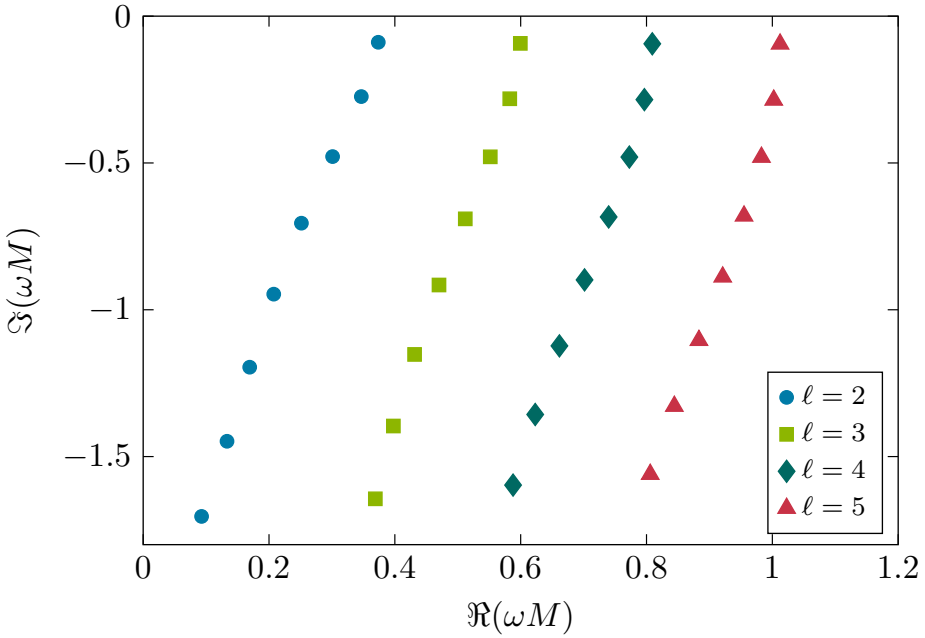

Figure 9 First 8 QNM frequencies of the Schwarzschild BH for $\ell = 2, 3, 4, 5$. The fundamental mode is the mode with the smallest value of $|\Im(\omega M)|$.. The real part of the frequency of this mode corresponds, for each ℓ, with the transition at which the reflectivity changes from 1 to 0 in Fig. 7.

- **Leaver's method**. This method [302] is based on noticing that one can reduce solving (3.30) to a three-term recursion relation. In order to do so, let us start by writing the ansatz

$$\psi = \left(\frac{r}{2M} - 1\right)^{\rho} \left(\frac{r}{2M}\right)^{-2\rho} e^{-\rho(r/2M-1)} \sum_{n=0}^{\infty} a_n \left(1 - \frac{2M}{r}\right)^n , \quad \rho = -2iM\omega \,. \tag{3.41}$$

This ansatz has the required ingoing behaviour at the event horizon. Plugging this into (3.30) yields the three-term recursion relation

$$\begin{aligned} \alpha_n a_{n+1} + \beta_n a_n + \gamma_n a_{n-1} &= 0 \,, \\ \alpha_n &= n^2 + 2(\rho+1)n + 2\rho + 1 \,, \\ \beta_n &= -\left(2n^2 + 2n(4\rho+1) + 8\rho^2 + 4\rho + (\ell+2)(\ell-1) - 1\right) , \\ \gamma_n &= n^2 + 4\rho n + 4\rho^2 - 4 \,. \end{aligned} \tag{3.42}$$

Above it is implied that $a_{-1} = 0$. The out-going boundary condition at large distances is satisfied if the series expansion is regular, i. e., if $\sum a_n < \infty$, which is true for minimal solutions to the recursion relation. Now, minimal solutions are given in terms of a continued fraction [202]

$$\frac{a_{n+1}}{a_n} = \frac{-\gamma_{n+1}}{\beta_{n+1} -} \frac{\alpha_{n+1}\gamma_{n+2}}{\beta_{n+2} -} \dots \,. \tag{3.43}$$

This can be thought of as an effective boundary condition for $n = \infty$. The ratio a_1/a_0 can be determined directly from the recursion relation (3.42) as $a_1/a_0 = -\beta_0/\alpha_0$. Combining these two equations we obtain a nonlinear *algebraic* equation for the QNM frequencies

$$0 = \beta_0 - \frac{\alpha_0\gamma_1}{\beta_1 -}\frac{\alpha_1\gamma_2}{\beta_2 -}\frac{\alpha_2\gamma_3}{\beta_3 -}\cdots . \tag{3.44}$$

This equation can be truncated at a sufficiently large n and solved numerically for the QNM frequencies. Leaver's method has shown to lead to highly accurate results.

- **Hyperboloidal method**. Another option in order to impose the boundary conditions is to find suitable coordinates such that the constant "time" slices become null close to infinity and the event horizon. These coordinates are dubbed *hyperboloidal coordinates* and are, arguably, the best suited coordinates to perform calculations in perturbation theory around BH spacetimes [471]. Such a change can be achieved by a transformation of the form $\tau = t - H(r)$, where $H(r)$ is dubbed a height function, and different choices for this height function are discussed in [369]. One may additionally compactify the radial coordinate, say, through the transform $\sigma = 4M/r - 1$, such that $r = [2M, \infty)$ is mapped to $\sigma \in [-1, 1]$. Then, regular solutions must automatically satisfy the in-going and out-going boundary conditions at the horizon and infinity, respectively. Spectral or pseudospectral methods discussed in the previous chapter become particularly useful in this context. The RWZ equations change form, but they still can be cast as an eigenvalue problem $\mathbf{L}\psi = \omega^2\psi$ for some linear operator $\mathbf{L}$. Under a spectral decomposition, the problem of finding QNMs reduces to finding the eigenvalues of a matrix. Obviously this is tremendously advantageous as it does not require any initial guess, and moreover, it produces the frequencies of several overtones in a single calculation. The main difficulty of carrying out this calculation is of a technical nature – as discussed previously, the RWZ equations are not self-adjoint, and hence numerical methods to find the eigenvalues of the non-normal matrix $\mathbf{L}$ are prone to instabilities. Highly accurate methods that work with sufficient precision are, thus, a strict requirement of the hyperboloidal approach.

3.3.4 *Time Domain Response*

To conclude this chapter, we consider the time-domain solution to the RWZ equations. For simplicity we focus on the source-free case, where the perturbations are sourced instead by some initial data, given by a Gaussian pulse located sufficiently far away. Based on (3.39), we expect the solution to take the form

$$\Psi_\ell = \underbrace{\sum_{n=0}^{\infty} \Psi_{\ell n} e^{-i\omega_{\ell n} t}}_{\text{QNMs}} + \Psi_{\mathcal{B}} + \Psi_F \,, \tag{3.45}$$

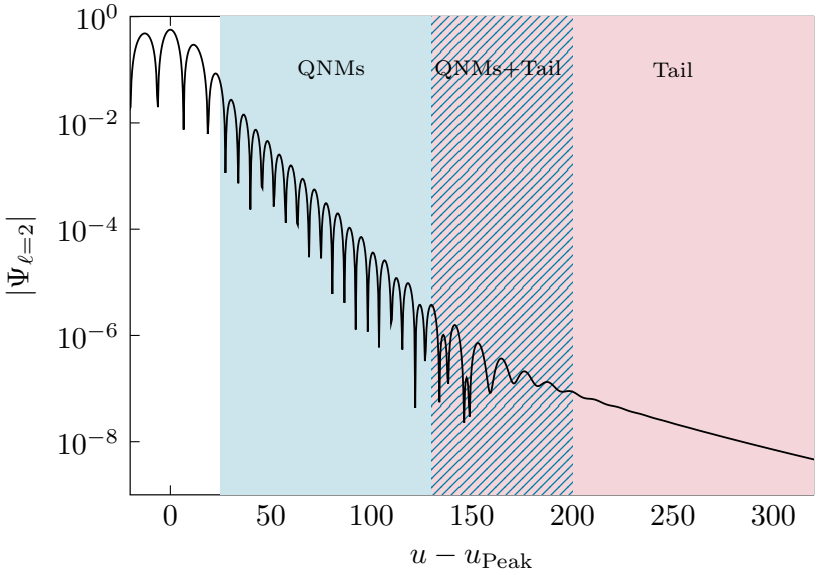

Figure 10 Ringdown extracted at future null infinity for $\ell = 2$, and compactly supported initial data. We observe a prompt signal followed by a QNM-driven relaxation, which at some point transitions to a power-law decay.

where $\Psi_{\mathcal{B},F}$ are the contributions of the branch-cut and of the two quarter-circles in the integration contour, respectively. If we extract Ψ_ℓ at $\mathcal{I}^+$, and at late times, the branch cut contribution becomes

$$\Psi_{\mathcal{B}}|_{\mathcal{I}^+}(u) = \sum_{p=0}^{\infty} \Psi_p^{\rm Tail} u^{-2-\ell-p} + \sum_{p=2}^{\infty} \Psi_p^{\rm Tail,Log} u^{-2-\ell-p} \log(u)\,, \tag{3.46}$$

where the leading order term, which dominates at late times, is often dubbed Price's law [229, 230, 389, 390], and the appearance of higher-order terms, including log-terms, is discussed [44, 45, 121, 242, 244]. Notice that the branch cut also has a contribution at early times due to the essential singularity at $\omega = 0$ [303]. Finally, the term Ψ_F corresponds to the direct propagation of the initial data and thus, if that is compactly supported, we have that the contribution of Ψ_F vanishes after a certain time.

We compare this expectation against the direct numerical solution of the RW equation in the time-domain (3.21), constructed using the general principles discussed in Chapter 2. Results are shown in Fig. 10, and details of the numerical implementation can be found in [229, 399].

The extracted ringdown signal close to $\mathcal{I}^+$ is shown in Fig. 10. We can visually identify three distinct regimes – an early-time response, with growing amplitude, a QNM-driven ringdown, and a slowly-decaying late-time tail. Let us now imagine that we detect this signal in a noisy detector with, say, stationary Gaussian noise with a fixed amplitude. We can use Bayesian inference to infer the leading QNM of the signal during the ringdown-dominated regime. In particular, following the

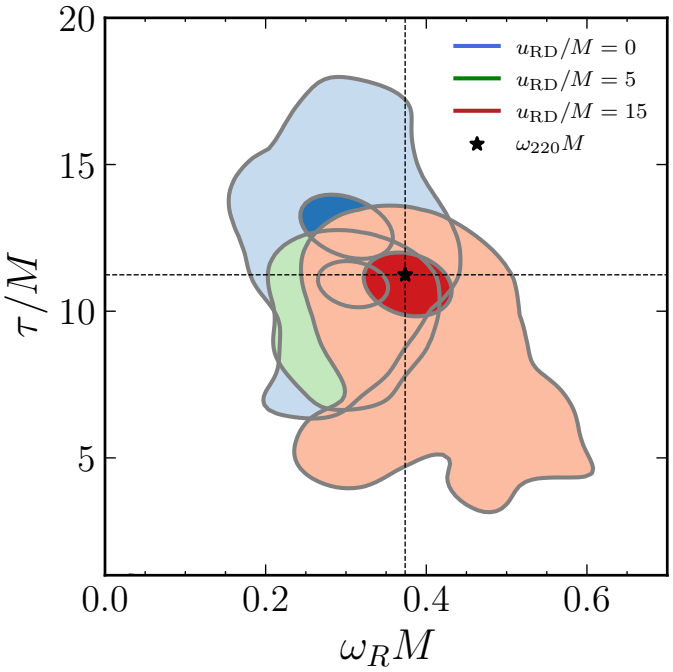

Figure 11 1 and 2σ confidence intervals on the marginalized (ω_R, τ)-distributions for a simulated signal injected in Gaussian noise. Different starting times are shown in different colors, as indicated in the legend.

discussion of Chapter 2, we try to model the signal between $u - u_{\rm Peak} \in [u_{\rm RD}, u_{\rm End}]$ as a single QNM

$$\Psi = Ae^{-i\omega t+\phi}\,, \qquad \omega = \omega_R - i/\tau\,, \tag{3.47}$$

and infer jointly the four parameters $(A, \phi, \omega_R, \tau)$. We set uniform priors and use nested sampling as implemented in `NestedSamplers.jl` [320], enabled via `Bat.jl` [421]. The 1 and 2σ confidence intervals of the marginal frequency distribution, for different ringdown start times $u_{\rm RD}$, are shown in Fig. 11. We now note clearly an important effect of BH ringdown, relevant even at the level of linear perturbations: models based on a superposition of damped sinusoids are not a consistent description of the signal very close to the peak [68]. This is but one of the many difficulties of ringdown data analysis.

- *When does each regime start and end?* From the frequency-domain analysis it is not possible to point down precisely when does, e. g., the contribution of the tail begin to be important. Exact knowledge of the initial data and the source is required for this, which in general is not available. A sensible and minimal requirement is that our inferred physical parameters are independent of the transition times that we define [39].

- *How many QNMs?* Our frequency-domain solution (3.45) contains formally an infinite amount of overtones. Most of these (those with $n \geq 3$ for $\ell = 2$) have a quality factor $\mathcal{Q} = \Re\omega/2\Im\omega < 1/2$, meaning that they are overdamped

modes, and thus extremely challenging to infer. On the other hand, they are generically excited [61, 162, 213]. A common way to avoid this issue is to only consider the QNM-driven regime after some time $u > u_{\rm RD}$ which is large enough for most of these overtones to be significantly damped, and therefore we can safely truncate the overtone sum in (3.45). On the other hand, doing so "throws away" the loudest part of the signal, making the data analysis challenge even more challenging [39, 70, 92, 116, 143, 147].

- *Fitting or projecting?* When working with Hermitian systems, whose solution can be expanded on a basis of normal modes, one can simply project the solution onto the subspace generated by one normal mode. A clear example is the projection onto spherical harmonics that we perform to decompose the GW signal. BH perturbations are not governed by a Hermitian problem. The most natural approach, then, is to *fit* the signal to some template model composed, e. g., by a superposition of QNMs. Some additional control can be achieved through Bayesian inference [116]. There are, nonetheless, alternative approaches to infer the QNM content of a GW signal which we do not discuss here [322, 475].

We will return to discuss these issues in more detail in Chapter 5 when discussing the extraction of quadratic QNMs from time-domain solutions to the second-order perturbations about a Kerr BH. We refer the interested reader to [68] and references therein for a comprehensive overview of this problem, and further details that have been omitted here.

Part II

NONLINEAR DYNAMICS IN THE BLACK HOLE RINGDOWN

Embrace beautiful lies
– the chronic insanity of the sane

— *Sarah Kane,* 4:48 Psicosis

4

PERTURBATIONS OF ROTATING BLACK HOLES

Written while listening to music composed by Dmitri Shostakovich.

4.1 INTRODUCTION

Solving Einstein equations is a daunting task even in highly symmetric settings. Just one year after the publication of Einstein's work on General Relativity, Schwarzschild found a solution describing a vacuum, static, and spherically symmetric spacetime [423]. Two years later, Lense and Thirring set the foundations to include the effects of rotation perturbatively [306]. However, an exact solution describing rotating, stationary spacetimes remained elusive for nearly 50 years. Kerr [274, 275] achieved this coinciding with the first astronomical hints of what we now recognize as BHs, sparking a surge of activity in General Relativity and the geometrodynamics of rotating BHs. One must not forget how remarkable this solution is. In Chandrasekhar's words: *In my entire scientific life [...] the most shattering experience has been the realization that an exact solution of Einstein's equations [...] provides the absolutely exact representation of untold numbers of massive black holes that populate the Universe.*

A major achievement in the dynamics of rotating spacetimes, i. e., Kerr BHs, was realizing that their (perturbative) dynamics is governed by a single equation. Teukolsky [441] showed that the perturbation to certain scalars constructed out of the Weyl curvature satisfied decoupled wave equations. Such decoupling should not come out as a surprise, but simply as a consequence of the special algebraic structure of the Kerr geometry [71, 415]. This equation is also separable, which once again should not come out as a surprise given the algebraic symmetries of the Kerr metric [113]. Nevertheless, the Teukolsky equation has proven foundational to study the dynamics of BHs and their emission of GWs.

In this chapter we revisit the problem of perturbations around Kerr BHs. First, we discuss some generalities about the Kerr geometry, including its algebraic structure, symmetries, and geodesic motion on the Kerr spacetime. Next, we focus on perturbations of Kerr BHs. We derive Teukolsky equation in vacuum, and discuss how to include arbitrary sources. We discuss two approaches to the metric reconstruction problem, and discuss the gauge and frame invariance of perturbations. Finally, we derive the second-order Teukolsky equation governing next to leading order vacuum perturbations to rotating BHs, which will be foundational to the following chapter of this thesis.

4.2 THE KERR METRIC

The Kerr spacetime, in Boyer-Lindquist coordinates (t, r, θ, ϕ), takes the form

$$\begin{aligned} ds^2 = &-\left(1-\frac{2Mr}{\Sigma}\right)dt^2 - \frac{4aMr\sin^2\theta}{\Sigma}dtd\phi + \frac{\Sigma}{\Delta}dr^2 \\ &+ \Sigma d\theta^2 + \left[\Delta + \frac{2Mr(r^2+a^2)}{\Sigma}\right]\sin^2\theta d\phi^2 \,, \end{aligned} \tag{4.1}$$

where

$$\Sigma = r^2 + a^2\cos^2\theta \,, \qquad \Delta = r^2 - 2Mr + a^2 = (r-r_+)(r-r_-) \,, \qquad r_\pm = M \pm \sqrt{M^2-a^2} \,, \tag{4.2}$$

where $r_\pm$ are the locations of the outer $(+)$ and inner $(-)$ horizons. The outer horizon is a Killing horizon. Indeed, it is generated by the null vector $\chi^a = (\partial_t)^a + \Omega_H(\partial_\phi)^a$, which is a linear combination of Killing vectors, where $\Omega_H = a/2Mr_+$ is the angular velocity of the horizon. As $\Omega_H = \text{const}$ we say that the Kerr horizon rotates rigidly.

Clearly, two horizons exists only when $a < M$. Such BHs are called *subextremal*. Whenever $a = M$ the two horizons coincide and the solution is dubbed *extremal*. We will not consider the case where $a > M$, which contains a naked singularity. We will also not pay much attention to the interior of the Kerr BH geometry $r < r_+$ for two main reasons: (i) it is causally disconnected from future null infinity, meaning it is inaccessible to exterior observers and thus of no observational significance within classical gravity; and (ii) the inner horizon is unstable due to mass inflation [382], casting doubts on the validity of the Kerr geometry to describe the interior spacetime, at least close to the inner horizon. Suffices to say that the Kerr BH has a *ring singularity* at $r = 0, \theta = \pi/2$ corresponding to the root of Σ.

By analyzing the metric at large distances, $r \gg M$ and $a/r \ll 1$ the Kerr spacetime takes the simple form

$$ds^2 = -\left(1-\frac{2M}{r}\right)dt^2 + \left(1+\frac{2M}{r}\right)dr^2 + r^2(d\theta^2 + \sin^2\theta d\phi^2) - \frac{4aM}{r}\sin^2\theta dtd\phi \,, \tag{4.3}$$

which is simply the asymptotic metric (weak field) of a mass M rotating with angular momentum $J = aM$. Thus, we can identify the parameters (M, a) with the mass and spin of the BH.

Another relevant surface of Kerr BHs is the *ergoregion*. The spacetime itself is rotating, resulting in dragging of inertial frames. In particular, this means that the timelike Killing vector $\xi = \partial_t$ becomes null *outside* the outer horizon. Physically this means that a timelike observer is forced to rotate in solidarity with the BH; and static observers cannot exist inside the ergoregion. The location of the ergoregion is thus defined by the roots of $\xi^a\xi_a = -g_{tt}$, i. e.,

$$r_O = M + \sqrt{M^2 - a^2\cos^2\theta} \,. \tag{4.4}$$

The presence of an ergoregion is a remarkable property of Kerr BHs, in particular enabling the Blandford-Znajek process which possibly powers galactic jets. A simple

version of this is the *Penrose process*: a particle launched from rest towards the ergoregion, with energy $\mathcal{E}_0$, fissions into two equal particles with mass $m_1 = q\mathcal{E}_0$. For an external observer, as $g_{tt} < 0$, one of the fission products may appear to have a negative energy. If that particle falls into the horizon, the escaping particle must have gained energy, due to energy and angular momentum conservation. Indeed, the efficiency of the process is, assuming equatorial motion [83]

$$\frac{\mathcal{E}_1}{\mathcal{E}_0} = \frac{1}{2}\Big(1 + \sqrt{\frac{2M(1-4q^2)}{r_{\rm fission}}}\Big)\,. \tag{4.5}$$

Clearly, for $\mathcal{E}_1 > \mathcal{E}_0$ the fission must take place at $r_{\rm fission} < 2M(1-4q^2) < 2M$, i. e., inside the ergoregion. An infalling particle with (apparent) negative energy density does not make the BH area decrease. That would be a blatant violation of Hawking's area theorem. Instead, the infalling particle decreases the BH mass M, but it also spins-down the BH, in such a way that the irreducible mass $M_{\rm irr} = \sqrt{Mr_+/2}$ grows.

4.2.1 *Coordinates*

The Boyer-Lindquist coordinates are geometric, in that they follow naturally from the symmetries of the spacetime: indeed, t and ϕ are parameters along integral curves of stationary Killing vectors. Other geometrically motivated choices are possible, such as the coordinates introduced by Doran [174], and coordinates constructed directly from the Killing spinor structure of the Kerr spacetime, see 2.5.2. in [16] or Appendix D in [198]. Other useful coordinates are *hyperboloidal* coordinates. We construct now horizon-penetrating hyperboloidal coordinates, which we also compactify. This will later allow for efficient numerical implementation of the Teukolsky equation, as hyperboloidal coordinates naturally account for the boundary conditions required to study BH perturbations.

First, let us write the spacetime in (ingoing) Eddington-Finkelstein coordinates

$$dv = dt + dr_\star - dr\,, \qquad d\varphi = d\phi + \frac{a}{r^2+a^2}dr_\star\,, \tag{4.6}$$

where we have generalized the tortoise coordinate $dr_\star = (r^2+a^2)/\Delta dr$. Next, we aim to find hyperboloidal coordinates $T = T(v,r)$ and $R = R(r)$. Following the *minimal gauge* prescription we want to change the time coordinate with a r-dependent height function, $T = v + h(r)$ such that the ingoing characteristic speed vanishes at $r = \infty$. As discussed in Appendix C3 of [409], this is achieved by the transformation

$$T = v - r - 4M\log r\,, \qquad R = \frac{r_h^2}{r}\,, \tag{4.7}$$

where we have chosen the compactification length such that $R \in [0, r_h]$.

4.2.2 *Algebraic Structure*

The Kerr metric is algebraically type D, meaning it has two repeated principal null directions. A principal NP tetrad is the *Carter* tetrad, which in Boyer-Lindquist coordinates is

$$\begin{aligned} \ell^a &= \frac{1}{\sqrt{2\Delta\Sigma}}\left(r^2+a^2, \Delta, 0, a\right), \\ n^a &= \frac{1}{\sqrt{2\Delta\Sigma}}\left(r^2+a^2, -\Delta, 0, a\right), \\ m^a &= \frac{1}{\sqrt{2\Sigma}}\left(ria\sin\theta, 0, 1, \frac{i}{\sin\theta}\right), \end{aligned} \tag{4.8}$$

where

$$\zeta = r - ia\cos\theta, \tag{4.9}$$

is the proportionality constant in front of the Killing spinor, i. e., if we choose a spin dyad (o_A, ι_A) aligned with the tetrad (4.8), then $\kappa_{AB} = -2\zeta o_{(A}\iota_{B)}$ is a Killing spinor. As discussed in Chapter 2 this means that the only non-vanishing Weyl scalar is

$$\Psi_2 = -\frac{M}{\zeta^3}. \tag{4.10}$$

Additionally, the only non-vanishing GHP spin coefficients are

$$\rho = -\rho' = -\zeta^{-1}\sqrt{\frac{\Delta}{2\Sigma}}, \qquad \tau = \tau' = -\frac{ia\sin\theta}{\zeta\sqrt{2\Sigma}}, \tag{4.11}$$

The Carter tetrad is related to the often-used Kinnersely tetrad by

$$\ell^a = \sqrt{\frac{\Delta}{2\Sigma}}\ell^a_{\mathrm{K}}, \quad n^a = \sqrt{\frac{2\Sigma}{\Delta}}n^a_{\mathrm{K}}, \quad m^a = \frac{\bar{\zeta}}{\sqrt{\Sigma}}m^a_{\mathrm{K}}. \tag{4.12}$$

From the existence of the valence $(2,0)$-Killing spinor, and the fact that the Killing vector $\xi^a = (\partial_t)^a$, which can be checked by simply evaluating (2.37) using (4.8)–(4.11), we deduce that Kerr also has a Killing tensor (2.39), and a second Killing vector η^a given by (2.40), which, in this case, is just $\eta^a = a^2(\partial_t)^a + a(\partial_\phi)^a$.

4.2.3 *Kerr Geodesics*

Let us now review briefly the problem of motion in the Kerr geometry. Let $u^a(\tau)$ be the 4-velocity of a given trajectory, which we take to be *timelike* or *null* depending on whether $u^a u_a = \epsilon = -1$ or $u^a u_a = 0$. Two conserved quantities are constructed from the Killing vectors

$$\mathcal{E} = -\xi_a u^a, \qquad \mathcal{L} = a^{-1}\left(\eta_a u^a + a^2\mathcal{E}\right), \tag{4.13}$$

corresponding to the energy and angular momentum (in the direction of the BH spin). The Killing tensor leads to an additional conserved quantity, the *Carter constant* [114]

$$\mathcal{Q} = u^a u^b K_{ab} - (\mathcal{L} - a\mathcal{E})^2 \,. \tag{4.14}$$

In terms of these conserved quantities, and with respect to the *Mino-Carter time* $d\lambda = \Sigma^{-1} d\tau$ [341], the geodesic equation is reduced to first-integrals

$$\begin{aligned}
\left(\frac{dr}{d\lambda}\right)^2 =& \mathcal{R}(r) \,, \\
\left(\frac{d\theta}{d\lambda}\right)^2 =& \Theta(\theta) \,, \\
\frac{dt}{d\lambda} =& \frac{r^2+a^2}{\Delta}\Big[\mathcal{E}(r^2+a^2) - a\mathcal{L}\Big] + a\Big(\mathcal{L} - a\mathcal{E}\sin^2\theta\Big) \,, \\
\frac{d\phi}{d\lambda} =& \frac{a}{\Delta}\Big[\mathcal{E}(r^2+a^2) - a\mathcal{L}\Big] + \frac{\mathcal{L}}{\sin^2\theta} - a\mathcal{E} \,,
\end{aligned} \tag{4.15}$$

where we have introduced the potentials [221, 338]

$$\begin{aligned}
\mathcal{R}(r) =& \Big[\mathcal{E}(r^2+a^2) - a\mathcal{L}\Big]^2 - \Delta\Big[\mathcal{Q} + (a\mathcal{E}-\mathcal{L})^2 - \epsilon r^2\Big] \,, \\
\Theta(\theta) =& \mathcal{Q} + a^2(\mathcal{E}^2 - \epsilon^2)\cos^2\theta - \mathcal{L}^2\cot^2\theta \,.
\end{aligned} \tag{4.16}$$

The motion of timelike and null geodesic is fully characterised in terms of the constants of motion $\mathcal{E}, \mathcal{L}, \mathcal{Q}, \epsilon$, and can be classified according to the number and location of the roots of the radial and polar polynomials. Analytical solutions to the geodesic equations exist in terms of elliptic functions [176, 221, 338].

A particularly interesting class of geodesics are bound, null geodesics, usually referred to as *lightrings*. These are closely linked to the high-frequency behaviour of GWs [103], and offer an interesting observational target with very large baseline interferometry, providing an alternative path to measuring the mass and spin of supermassive BHs [321]. We now focus on this case, and set $\epsilon = 0$. Since bound null orbits must be spherical, we seek orbits located at zeros of the radial potential $\mathcal{R}(r_{\rm LR}) = \mathcal{R}'(r_{\rm LR}) = 0$. The only physically admissible class of solutions to these two equations is [440]

$$\begin{aligned}
\frac{\mathcal{L}}{\mathcal{E}} =& -\frac{r_{\rm LR}^3 - 3Mr_{\rm LR}^2 + a^2(r_{\rm LR}+M)}{a(r_{\rm LR}-M)} \,, \\
\frac{\mathcal{Q}}{\mathcal{E}^2} =& -\frac{r_{\rm LR}^3\Big(r_{\rm LR}^3 - 6Mr_{\rm LR}^2 + 9M^2 r_{\rm LR} - 4a^2 M\Big)}{a^2(r_{\rm LR}-M)^2} \,.
\end{aligned} \tag{4.17}$$

Physical solutions to these equations are confined to a finite range, which we denote by $r_{\rm LR} \in [r_{\rm LR_+}, r_{\rm LR_-}]$. The two extremes are achieved for equatorial orbits, when $\mathcal{Q} = 0$. In fact, these are just the *prograde* and *retrograde* lightrings

$$r_{\rm LR_\pm} = 2\left[1 + \cos\left(\frac{2}{3}\arccos\left(\mp\frac{|a|}{M}\right)\right)\right] , \tag{4.18}$$

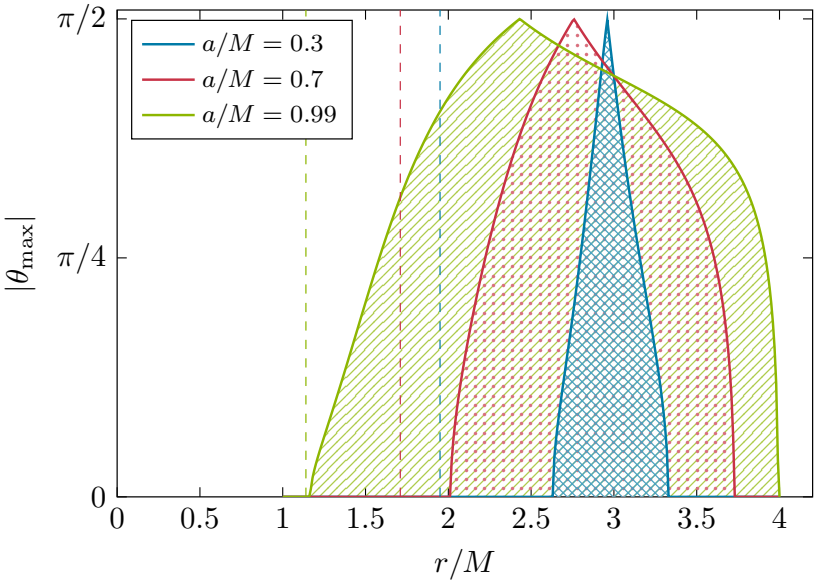

Figure 12 Shape of the photon shell as a function of the lightring radius for three different values of the dimensionless spin, represented with different colors. The dashed lines represent the location of the outer horizon for each spin.

and satisfy $M \leq r_{\mathrm{LR}_+} \leq 3M \leq r_{\mathrm{LR}_-} \leq 4M$. Those are lightrings which are purely equatorial (since $\mathcal{Q} = 0$), and degenerate to the Schwarzschild unique lightring $r_{\mathrm{LR}}(a = 0) = 3M$, which is the unique double root of the radial potential when $a = 0$. However, there is a continuous spectrum of lightrings spanning a *photon shell* between $[r_{\mathrm{LR}_+}, r_{\mathrm{LR}_-}]$ for Kerr black holes, which perform certain polar libration, and are fully characterized by (4.17) [1]. The polar libration can be characterized by the roots of the polar potential. If we let $z = \cos\theta$, these roots are given by

$$z^2 = \frac{(a^2\mathcal{E}^2 - \mathcal{Q} - \mathcal{L}^2) + \sqrt{(a^2\mathcal{E}^2 - \mathcal{Q} - \mathcal{L}^2)^2 + 4a^2\mathcal{Q}}}{2a^2}\,. \tag{4.19}$$

The maximum angular libration allowed as a function of the lightring radius is shown in Fig. 12 for different values of the dimensionless BH spin. Chapter 6 will discuss in detail the connection between lightrings and perturbations of rotating BHs.

4.3 LINEAR PERTURBATIONS

We now consider linear perturbations of the Kerr geometry, i.e., let the metric and the stress energy tensor be

$$g_{ab} = g^{\mathrm{Kerr}}_{ab} + \varepsilon \dot{h}_{ab} + \mathscr{O}(\varepsilon^2)\,, \qquad T_{ab} = \varepsilon \dot{T}_{ab} + \mathscr{O}(\varepsilon^2)\,, \tag{4.20}$$

1 Notice that the sign of $\mathcal{E}$ matters only to determine a time orientation for the null geodesic. Otherwise, $\mathcal{E}$ merely corresponds to a choice of units, and $\mathcal{L}/\mathcal{E}$ and $\mathcal{Q}/\mathcal{E}^2$ are the dimensionless quantities which parametrize null geodesics.

where $\varepsilon \ll 1$ is a book-keeping small number. First, we will show that vacuum perturbations are governed by the Teukolsky equation. Next, we discuss Wald's identity, which relates to Teukolsky equation in the presence of sources, and use it to reconstruct the metric by the method of Hertz potentials. We review an additional method of metric reconstruction, and finally tackle the problem of gauge and frame invariance to linear order.

4.3.1 *Teukolsky Equation*

Let us begin with the Penrose Wave Equation (2.9), and project it with $o^A o^B o^C o^D$. Doing so, we obtain an equation for $\Psi_0 = o^A o^B o^C o^D \Psi_{ABCD}$,

$$\mathscr{O}_0[\Psi_0] + \mathscr{O}_1[\Psi_1] + \mathscr{O}_2[\Psi_2] = 0\,, \tag{4.21}$$

where $\mathscr{O}_i$ are given by

$$\begin{aligned}
\mathscr{O}_0 =& \text{Þ}\text{Þ}' - \eth\eth' - \bar{\rho}\text{Þ} - (4\rho + \bar{\rho})\text{Þ}' + \tau'\eth + (4\tau + \bar{\tau}')\eth' \\
&+ 4(\rho\rho' + \kappa\kappa' - \tau\tau' - \sigma\sigma') - 2\Psi_2\,, \\
\mathscr{O}_1 =& 10\Psi_1 - 4(\kappa\bar{\rho}' - \sigma\bar{\tau}) + 4(\text{Þ}'(\kappa\cdot) - \eth'(\sigma\cdot))\,, \\
\mathscr{O}_2 =& 3\Big[(\rho + \bar{\rho})\sigma - (\tau + \bar{\tau}')\kappa + \eth\kappa - \text{Þ}\sigma + \Psi_0\Big]\,.
\end{aligned} \tag{4.22}$$

Linearising (4.21) around a type D background immediately leads to

$$\mathring{\mathscr{O}}_0[\dot{\Psi}_0] + \dot{\mathscr{O}}_2[\mathring{\Psi}_2] = 0\,. \tag{4.23}$$

However, notice that one of Ricci identities is

$$\eth\kappa - \text{Þ}\sigma - \kappa(\tau + \bar{\tau}') + \sigma(\rho + \bar{\rho}) + \Psi_0 = 0\,. \tag{4.24}$$

This is just $\mathscr{O}_2$. Hence, $\mathscr{O}_2 = 0$ in vacuum, at all orders. We have arrived at Teukolsky's equation

$$\mathring{\mathscr{O}}_0[\dot{\Psi}_0] \equiv \mathcal{O}_0\dot{\Psi}_0 = 0\,, \tag{4.25}$$

where the Teukolsky operator is simply $\mathscr{O}_0$ on a type D background, which can be rewritten as

$$\mathcal{O}_0 = (\text{Þ} - 4\rho - \bar{\rho})(\text{Þ}' - \rho') - (\eth - 4\tau - \bar{\tau}')(\eth' - \tau') - 3\Psi_2\,. \tag{4.26}$$

Taking primes of this equation we obtain the equivalent operator for Ψ_4

$$\mathcal{O}_4 = (\text{Þ}' - 4\rho' - \bar{\rho}')(\text{Þ} - \rho) - (\eth' - 4\tau' - \bar{\tau})(\eth - \tau) - 3\Psi_2\,, \qquad \mathcal{O}_4\dot{\Psi}_4 = 0\,, \tag{4.27}$$

and satisfies the Teukolsky equation with spin weight $s = -2$. Equivalently, we could have started taking the $\iota^A\iota^B\iota^C\iota^D$ projection of (2.9), and we would have arrived at the same point mirroring these steps.

The Teukolsky operator (4.26) coincides with the wave operator $\Box$ up to lower order terms. Thus it should not come out as a surprise that one can also find a complete set of commuting operators, building upon the separability of the wave equation discussed in Chapter 2. In fact, we can write a generalized Teukolsky equation for spin s perturbations,

$$\mathcal{O}_{(s)} = (\text{þ} - 2s\rho - \bar{\rho})(\text{þ}' - \rho') - (\text{ð} - 2s\tau - \bar{\tau}')(\text{ð}' - \tau') - (2s^2 - 3s + 1)\Psi_2\,, \tag{4.28}$$

which reduces to the Klein-Gordon equation when $s = 0$, and $\mathcal{O}_{(+2)} = \mathcal{O}_0, \mathcal{O}_{(-2)} = \mathcal{O}_4$. This operator commutes with the two Killing vectors ξ^a, η^a, and with the two operators [16]

$$\begin{aligned} \mathcal{R}_s =& \zeta\bar{\zeta}(\text{þ} - \rho - \bar{\rho})(\text{þ}' - 2s\rho') + \frac{2s-1}{2}(\zeta + \bar{\zeta})\mathfrak{L}_\xi\,, \\ \mathcal{S}_s =& \zeta\bar{\zeta}(\text{ð} - \tau - \bar{\tau})(\text{ð}' - 2s\tau') + \frac{2s-1}{2}(\zeta - \bar{\zeta})\mathfrak{L}_\xi\,, \end{aligned} \tag{4.29}$$

where in terms of GHP quantities, acting on a quantity $X \overset{\circ}{=} (p, q)$, the Lie derivative along ξ^a is

$$\mathfrak{L}_\xi = -\zeta(-\rho'\text{þ} + \rho\text{þ}' + \tau'\text{ð} - \tau\text{ð}') - \frac{p}{2}\zeta\Psi_2 - \frac{q}{2}\bar{\zeta}\bar{\Psi}_2\,. \tag{4.30}$$

The spin-s Teukolsky operator can thus be written simply as

$$\zeta\bar{\zeta}\mathcal{O}_{(s)} = \mathcal{R}_s - \mathcal{S}_s\,. \tag{4.31}$$

When $s = 0$, we have that $\mathcal{R}_0 = \mathcal{Q}$ is just the Carter operator. The key observation is that, upon global factors that can be absorbed appropriately, the operators $\mathcal{R}_s, \mathcal{S}_s$ depend only on the radial and angular coordinate, respectively, apart from the (Killing-generated) coordinates t, ϕ. Thus (4.31) implies immediately the separation of variables of Teukolsky equation. For convenience, we write the separated equations now in terms of the Kinnersley tetrad for $s = 2$. Letting

$$\dot{\Psi}_0 = e^{-i\omega t}\sum_{\ell,m} {}_{+2}R_{\ell m\omega}(r)\,{}_{+2}S_{\ell m}(\theta, \phi; a\omega)\,, \tag{4.32}$$

where ℓ, m are spherical harmonic indices, meaning $\ell \geq 2$ and $m \in [-\ell, \ell]$, the radial and angular functions satisfy the separated equations

$$\begin{aligned} \left[\frac{d}{dz}\left((1-z^2)\frac{d}{dz}\right) + a^2\omega^2 z^2 - \frac{(m+sz)^2}{1-z^2} - 2a\omega sz + C\right]{}_sS_{\ell m}(\theta, \phi; a\omega) =& 0\,, \\ \left[\Delta^{-s}\frac{d}{dr}\left(\Delta^{s+1}\frac{d}{dr}\right) + \frac{K^2 - 2is(r-M)K}{\Delta} + 4is\omega r - {}_s\lambda_{\ell m}\right]{}_sR_{\ell m\omega} =& 0\,, \end{aligned} \tag{4.33}$$

where we remind that $z = \cos\theta$, and we have introduced $C = {}_s\lambda_{\ell m} + 2a\omega m - a^2\omega^2$, and $K = \omega(r^2 + a^2) - am$. The eigenvalue ${}_s\lambda_{\ell m}$ is sometimes dubbed the angular separation constant. Notice that as ϕ is a Killing vector, the spheroidal harmonics are eigenfunctions

$${}_sS_{\ell m}(\theta, \phi; a\omega) = {}_sS_{\ell m}(\theta, 0; a\omega)e^{im\phi}\,. \tag{4.34}$$

4.3.2 *Wald's Identity*

We could have decided to work with the Penrose wave equation in the presence of sources. In the symmetric spinor notation, this is just the curl of (2.8), i. e., $\mathscr{C}\mathscr{C}^{\dagger}\Psi = \mathscr{C}\mathscr{C}\Phi$. The perturbations of the Ricci tensor can be related to the matter perturbations, i. e., the perturbations of the stress-energy tensor, via Einstein equations, $\mathcal{E}[\dot{h}]_{ab} = 8\pi\dot{T}_{ab}$, where $\mathcal{E}[\dot{h}]$ is, in essence, the Lichnerowicz operator,

$$\mathcal{E}[\dot{h}_{cd}]_{ab} = -\nabla_a\nabla_b\dot{h}^c_c - \nabla^2\dot{h}_{ab} + 2\nabla^c\nabla_{(a}\dot{h}_{b)c} + \mathring{g}_{ab}\left(\nabla^2\dot{h}^c_c - \nabla^c\nabla^d\dot{h}_{cd}\right). \tag{4.35}$$

Keeping track of the source terms in our derivation of Teukolsky equations we would find a non-vanishing right-hand side,

$$\mathcal{O}_0\Psi_0 = \mathcal{S}_0[\dot{T}_{ab}]\,, \qquad \mathcal{O}_4\Psi_4 = \mathcal{S}_4[\dot{T}_{ab}]\,. \tag{4.36}$$

In order to do so, it is useful to relate the NP components of the perturbed stress-energy tensor with the spinor components of the perturbed Ricci tensor,

$$\begin{aligned} \dot{T}_{ll} =& \dot{\Phi}_{00'} \equiv o^A o^B \bar{o}^{A'} \bar{o}^{B'} \Phi_{ABA'B'}\,, \qquad T_{ln} = \Phi_{11'} + \frac{\Lambda}{4}\,, \qquad T_{lm} = \Phi_{01'}\,, \\ \dot{T}_{nn} =& \dot{\Phi}_{22'}\,, \qquad T_{nm} = \dot{\Phi}_{12'}\,, \qquad T_{mm} = \dot{\Phi}_{02'}\,, \qquad T_{m\bar{m}} = \dot{\Phi}_{11'} - \frac{\Lambda}{4}\,. \end{aligned} \tag{4.37}$$

A lengthy calculation, which simply mirrors the steps taken in the previous section, leads to

$$\begin{aligned} \mathcal{S}_0 =& \frac{1}{2}(\eth - \bar{\tau}' - 4\tau)\Big[(\text{þ} - 2\bar{\rho})\dot{T}_{lm} - (\eth - \bar{\tau}')\dot{T}_{ll}\Big] \\ &+ \frac{1}{2}(\text{þ} - 4\rho - \bar{\rho})\Big[(\eth - 2\bar{\tau}')\dot{T}_{lm} - (\text{þ} - \bar{\rho})\dot{T}_{mm}\Big]\,, \\ \mathcal{S}_4 =& \frac{1}{2}(\eth' - \bar{\tau} - 4\tau')\Big[(\text{þ}' - 2\bar{\rho}')\dot{T}_{nm} - (\eth' - \bar{\tau})\dot{T}_{nn}\Big] \\ &+ \frac{1}{2}(\text{þ}' - 4\rho' - \bar{\rho}')\Big[(\eth' - 2\bar{\tau})\dot{T}_{nm} - (\text{þ}' - \bar{\rho}')\dot{T}_{mm}\Big]\,. \end{aligned} \tag{4.38}$$

Finally, notice that we can also write the Weyl scalars as some operator acting on the metric perturbation, i. e., $\mathcal{T}_0[\dot{h}_{ab}] = \dot{\Psi}_0$, and equivalently for $\dot{\Psi}_4$. A short-cut to finding this operator is to project onto components (2.26). Alternatively, one may work directly from the definition to obtain

$$\begin{aligned} 2\mathcal{T}_0 =& (\eth - \bar{\tau}')(\eth - \bar{\tau}')\dot{h}_{ll} + (\text{þ} - \bar{\rho})(\text{þ} - \rho')\dot{h}_{mm} \\ &- \Big[(\text{þ} - \bar{\rho})(\eth - 2\bar{\tau}') + (\eth - \bar{\tau}')(\rho - 2\bar{\rho})\Big]\dot{h}_{lm}\,, \end{aligned} \tag{4.39}$$

and $\mathcal{T}_4 = \mathcal{T}_0'$. Putting all of this together, we obtain an operator identity

$$\mathcal{O}_0\Big[\mathcal{T}_0(\dot{h}_{ab})\Big] = \mathcal{S}_0\Big[\mathcal{E}(\dot{h}_{cd})_{ab}\Big]\,, \tag{4.40}$$

together with its primed version. This is sometimes referred to as Wald's identity, as it was first written in this form by Wald in [454]. Nevertheless, this is based on a

series of remarkbale works by Cohen and Kegeles [144, 268], and Chrzanowski [141], who deserve no less credit. The identity itself, nevertheless, is already contained in Teukolsky's original work [441]. The usefulness of this identity, which was the original goal of these authors, is to generate a metric perturbation $\dot{h}_{ab}$ which is a solution to the linearised Einstein equations, given a solution to Teukolsky equation, say, $\dot{\Psi}_0$. This is the topic of the next subsection.

4.3.3 *Metric Reconstruction via Hertz potentials*

The problem of metric reconstruction is the following: suppose we have a solution of the (vacuum) Teukolsky equation, say, $\mathcal{O}_0\psi = 0$. Can we use it to generate a metric perturbation $\dot{h}_{ab}$ that is a solution to the linearised Einstein equations, $\mathcal{E}[\dot{h}_{ab}] = 0$? Moreover, what is the connection between $\mathcal{T}_{0,4}[\dot{h}_{ab}]$ and the original solution ψ? This is the matter of this section. The method we present here is based on Hertz potentials, and sometimes is referred to as Cohen, Chrzanowski, and Kegeles (CCK) metric reconstruction [141, 144, 268].

Let us begin with the abstract operator identity $\mathcal{O}\mathcal{T} = \mathcal{S}\mathcal{E}$, where these are linear differential operators acting on some functional space, say, of scalar fields (for simplicity). Before moving forward, we ought to define the *adjoint* of an operator $\mathcal{L}$, which we denote $\mathcal{L}^\dagger$. This is nothing but the unique operator satisfying

$$\varphi\mathcal{L}[\phi] - \mathcal{L}^\dagger[\varphi]\phi = \nabla_a \mathcal{J}^a\,, \tag{4.41}$$

for some current $\mathcal{J}^a$. This definition generalizes trivially to tensor fields, and to tensorial operators. Thus, it follows easily that the GHP connection is skew-adjoint $\Theta_a^\dagger = -\Theta_a$ (and so is the usual covariant derivative). Using this and the definition of the GHP spin coefficients, it is straightforward to find that

$$\begin{aligned} \text{Þ}^\dagger &= -\text{Þ} + \rho + \bar{\rho}\,, \qquad (\text{Þ}')^\dagger = -\text{Þ}' + \rho' + \bar{\rho}'\,, \\ \eth^\dagger &= -\eth + \tau + \bar{\tau}'\,, \qquad (\eth')^\dagger = -\eth' + \tau' + \bar{\tau}\,. \end{aligned} \tag{4.42}$$

Let us now assume that the operator $\mathcal{E}$ is self-adjoint, $\mathcal{E} = \mathcal{E}^\dagger$. This is true for the Einstein equations, as $\mathcal{E}$ is quadratic in the skew-adjoint operator ∇_a (4.35).

Now, let us go back to the operator identity, and assume that we have a solution ψ_H satisfying $\mathcal{O}^\dagger\psi_H = 0$. We will call this a *Hertz* potential. Then, $\varphi = \mathcal{S}^\dagger\psi_H$ satisfies $\mathcal{E}^\dagger\varphi \equiv \mathcal{E}\varphi = 0$, i. e., we found a solution to the equation $\mathcal{E}\varphi = 0$. Applying this to the identity (4.40) we find that

$$\mathcal{E}[\dot{h}_{ab}] = 0 \impliedby \dot{h}_{ab} = 2\Re\mathcal{S}_i^\dagger[\psi_H]_{ab}\,, \qquad \mathcal{O}_i^\dagger\psi_H = 0\,, i = 0, 4\,. \tag{4.43}$$

A few observations are in order. First of all, this is only valid for vacuum perturbations. Recently, an extension of this formalism that accounts for matter fluctuations by correcting the metric perturbation appropriately has been put forward, but it is yet to be implemented in complex scenarios [223, 245, 448]. Secondly, the resulting metric fluctuation is in a very particular gauge, in particular, either in the ingoing radiation gauge (IRG) if we use $i = 0$ in (4.43), or in the outgoing radiation

gauge (ORG) if $i = 4$. The IRG (respectively ORG) satisfies $\ell^a \dot{h}_{ab} = 0$ (respectively $n^a \dot{h}_{ab} = 0$). To avoid confusion, let us summarise this explicitly:

$$\begin{aligned} \dot{h}^{\text{IRG}}_{ab} &= 2\Re \mathcal{S}_0^\dagger \psi^{\text{IRG}}\,, \qquad \mathcal{O}_0^\dagger \psi^{\text{IRG}} = 0\,, \qquad \ell^a \dot{h}^{\text{IRG}} = 0\,, \\ \dot{h}^{\text{ORG}}_{ab} &= 2\Re \mathcal{S}_4^\dagger \psi^{\text{ORG}}\,, \qquad \mathcal{O}_4^\dagger \psi^{\text{ORG}} = 0\,, \qquad n^a \dot{h}^{\text{ORG}} = 0\,. \end{aligned} \tag{4.44}$$

The third observation is that if we compute the Weyl scalars $\dot{\Psi}_{0,4}$ associated to $\dot{h}_{ab}$ obtained from (4.43), we do not recover the Hertz potential ψ_H. Instead, we find the radial and angular inversion equations:

$$\begin{aligned} \dot{\Psi}_0 &= \frac{1}{4}\text{þ}^4 \bar{\psi}^{\text{IRG}}_H = \frac{1}{4}\text{ð}^4 \bar{\psi}^{\text{ORG}}_H + \frac{3M}{4\zeta^4}\mathfrak{L}_\xi \psi^{\text{ORG}}_H\,, \\ \dot{\Psi}_4 &= \frac{1}{4}\text{ð}'^4 \bar{\psi}^{\text{IRG}}_H = \frac{3M}{4\zeta^4}\mathfrak{L}_{\tilde{\xi}} \psi^{\text{IRG}}_H = \frac{1}{4}\text{þ}'^4 \bar{\psi}^{\text{ORG}}_H\,. \end{aligned} \tag{4.45}$$

Here we have just uncovered the Teukolsky-Starobinski identities relating Hertz potentials in ingoing/outgoing radiation gauges.

4.3.4 *Metric Reconstruction via Transport Equations*

The above construction works quite generically, but inverting the equations (4.45) is, in general, complicated. Separable solutions like QNMs can be more easily dealt with (see e.g. [59] and references therein), but the implementation of the CCK method quickly becomes complicated when dealing with an initial value problem. For that purpose, constructive procedures that directly obtain the metric perturbation $\dot{h}_{ab}$ in terms of some Weyl scalar which solves Teukolsky equations $\dot{\Psi}_{0,4}$ are preferred. Such was the approach first taken by Chandrasekhar [128], and also in Ref. [22]. Here we revisit the presentation of this approach by [319], which we will later apply in Chapter 5. In particular, we reproduce the results of [319] in terms only of GHP quantities and equations, somewhat simplifying all the calculation.

To make things concrete, we will assume in this case knowledge of $\dot{\Psi}_4$. Moreover we fix a frame following Campanelli & Lousto [95]

$$\dot{l}_a = \frac{1}{2}\dot{h}_{ll} n_a\,, \quad \dot{n}_a = \frac{1}{2}\dot{h}_{nn}\ell_a + \dot{h}_{ln} n_a\,, \quad \dot{m}_a = \dot{h}_{nm}\ell_a + \dot{h}_{lm} n_a - \frac{1}{2}(\dot{h}_{m\bar{m}} m_a + \dot{h}_{mm}\bar{m}_a)\,, \tag{4.46}$$

where the perturbed tetrad legs with upper indices are obtained by swapping the sign of the h_{xy} components. We also want to reconstruct the metric in the ORG. This is not the unique choice possible, but it is possibly the simplest. The ORG condition $n^a \dot{h}_{ab} = 0$ together with the traceless condition $g^{ab}\dot{h}_{ab}$ (which can always be assumed for radiation gauges of type II spacetimes in vacuum, see [388]) implies immediately

$$\dot{h}_{nl} = \dot{h}_{nn} = \dot{h}_{nm} = 0\,, \qquad \dot{h}_{m\bar{m}} = 0\,. \tag{4.47}$$

One can check that all is consistent by writing the metric perturbation in terms of (4.46) as

$$\dot{h}_{ab} = 2\dot{\ell}_{(a}n_{b)} + 2\ell_{(a}\dot{n}_{b)} - 2\dot{m}_{(a}\bar{m}_{b)} - 2m_{(a}\dot{\bar{m}}_{b)} \,. \tag{4.48}$$

Moreover, this frame choice together with the ORG condition guarantees that $\dot{\kappa}' = \dot{\rho}' = 0$. The rest of the perturbed spin coefficients can be written in a straightforward manner in terms of the metric perturbations. For completeness, we list them here. First, the unprimed coefficients are

$$\begin{aligned}
2\dot{\kappa} =& 2(\text{þ} - \bar{\rho})\dot{h}_{lm} - (\text{ð} + \tau - \bar{\tau}')\dot{h}_{ll} \,, \\
2\dot{\sigma} =& (\text{þ} + \rho - \bar{\rho})\dot{h}_{mm} + 2(\bar{\tau}' - \tau)\dot{h}_{lm} \,, \\
2\dot{\rho} =& (\text{ð}' + \tau')\dot{h}_{lm} - (\text{ð} - \bar{\tau}' + 2\tau)\dot{h}_{lm} - \rho'\dot{h}_{ll} \,, \\
2\dot{\tau} =& (\text{þ}' - \rho')\dot{h}_{lm} + \tau'\dot{h}_{mm} \,,
\end{aligned} \tag{4.49}$$

and for the primed coefficients

$$\begin{aligned}
2\dot{\sigma}' =& (\text{þ}' + \rho' - \bar{\rho}')\dot{h}_{\bar{m}\bar{m}} \,, \\
2\dot{\tau}' =& (\text{þ}' - \bar{\rho}')\dot{h}_{l\bar{m}} + \tau\dot{h}_{\bar{m}\bar{m}} \,.
\end{aligned} \tag{4.50}$$

Now we introduced perturbed GHP derivative operators. These satisfy a Leibnitz rule with respect to the metric perturbations, so that we can write

$$(\mathscr{D}\eta)^{\cdot} = \mathscr{D}\dot{\eta} + \dot{\mathscr{D}}\eta \,, \qquad \mathscr{D} \in \left\{\text{þ}, \text{þ}', \text{ð}, \text{ð}'\right\} , \tag{4.51}$$

when acting on any GHP scalar η. The perturbed operators are defined by their action on GHP scalars with weight, say, $\eta \mathrel{\overset{\circ}{=}} (p, q)$.

$$\begin{aligned}
\dot{\text{þ}}\eta =& \dot{\ell}^a\Theta_a\eta - \ell^a\left(p\dot{\omega}_a + q\dot{\bar{\omega}}_a\right)\eta \,, \qquad \dot{\text{þ}}'\eta = \dot{n}^a\Theta_a\eta - n^a\left(p\dot{\omega}_a + q\dot{\bar{\omega}}_a\right)\eta \,, \\
\dot{\text{ð}}\eta =& \dot{m}^a\Theta_a\eta - m^a\left(p\dot{\omega}_a + q\dot{\bar{\omega}}_a\right)\eta \,, \qquad \dot{\text{ð}}'\eta = \dot{\bar{m}}^a\Theta_a\eta - \bar{m}^a\left(p\dot{\omega}_a + q\dot{\bar{\omega}}_a\right)\eta \,,
\end{aligned} \tag{4.52}$$

where $\dot{\omega}_a$ is the perturbed GHP connection (which is a GHP field itself, unlike the original connection ω_a, the same manner that the perturbation of the Christoffel symbols is a tensor while the Christoffel symbols themselves are not), given by

$$\begin{aligned}
4\ell^a\dot{\omega}_a =& -(\text{þ}' + \rho' - \bar{\rho}')\dot{h}_{ll} - (\text{ð} + 2\tau - \bar{\tau}')\dot{h}_{l\bar{m}} + (\text{ð}' - 2\bar{\tau} + 3\tau')h_{lm} \,, \\
n^a\dot{\omega}_a =& 0 \,, \\
4m^a\dot{\omega}_a =& -(\text{þ}' - \rho' - 2\bar{\rho}')\dot{h}_{lm} + (\text{ð}' + \tau' - \bar{\tau})\dot{h}_{mm} \,.
\end{aligned} \tag{4.53}$$

Using these, we can mimic the steps of [319] to find a hierarchy of transport equations, starting from $\dot{\Psi}_4$. As a first step, we use one of Ricci identities (2.27) to find $\dot{\sigma}'$, and one of Bianchi identities (2.28) to find $\dot{\Psi}_3$:

$$(\text{þ}' - \rho' - \bar{\rho}')\dot{\sigma}' = \dot{\Psi}_4 \,, \qquad (\text{þ}' - 4\rho')\dot{\Psi}_3 = (\text{ð} - \tau)\dot{\Psi}_4 \,. \tag{4.54}$$

Now we can use (4.50) to directly find $\dot{h}_{\bar{m}\bar{m}}$ in terms of $\dot{\sigma}'$. Recall now that $\dot{h}_{mm} = \overline{\dot{h}_{\bar{m}\bar{m}}}$. With this in mind, we can return to Ricci identities, and after some algebra, obtain an equation for $\dot{\tau}'$ in terms of known quantities, while the linearised Bianchi identities gives an equation for $\dot{\Psi}_2$

$$\text{Þ}'\dot{\tau}' = \dot{\Psi}_3 - \frac{1}{2}(2\dot{\sigma}' - \dot{h}_{\bar{m}\bar{m}}\rho')(\tau - \bar{\tau}')\,, \qquad (\text{Þ}' - 3\rho')\dot{\Psi}_2 = (\eth - 2\tau)\dot{\Psi}_3\,. \tag{4.55}$$

Once again, the second equation of (4.50) now allows us to find $\dot{h}_{l\bar{m}} = \overline{\dot{h}_{lm}}$. Finally, there are multiple approaches to find an equation for $\dot{h}_{ll}$. Mimicking the previous structure, we can find a first order transport equation. However, this equation may not have the most desirable decay properties. Second-order equations like the one discussed in [319] may be better suited for analytical calculations or proving decay estimates. By working with the linearised Einstein equations, and in terms of the perturbed GHP derivatives, we find

$$(\text{Þ}' + \rho' - \bar{\rho}')\dot{h}_{ll} = (\eth' + \tau')\dot{h}_{lm} - (\eth + 2\tau - \bar{\tau}')\dot{h}_{l\bar{m}} + \frac{2}{\rho'}\left[\dot{\Psi}_2 - (\dot{\eth} - \dot{\tau}')\tau' - (\eth - \bar{\tau}')\dot{\tau}'\right]. \tag{4.56}$$

This completely reconstructs the metric perturbation in ORG in terms of first-order transport equations in Þ′, starting from $\dot{\Psi}_4$. Although these transport equations were already presented in NP form in [319], this derivation, which is GHP covariant at all steps, is novel. Writing the equations in GHP form not only simplifies the algebra, but introduces a sanity check at all steps (checking that the GHP weights of both sides of every equation match), and the discrete symmetries such as the prime operation allow us to relate certain equations to each other in a simple way.

4.3.5 *Gauge and Frame Invariance*

Finally, let us consider whether the perturbations to the Weyl scalars $\dot{\Psi}_{0,4}$ have any physical significance. In particular, a desirable property would be their invariance under gauge transformations, as well as under Lorentz rotations of the NP frame. Suppose we act with a small diffeomorphism $\Xi = \varepsilon\dot{\Xi}$, and with NP frame rotations of type I, II, and III generated by small parameters $a = \varepsilon\dot{a}$, $b = \varepsilon\dot{b}$, $\Lambda = 1 + \varepsilon\dot{\Lambda}$, and $\theta = \varepsilon\dot{\theta}$, where the transformations are defined in (2.14). An arbitrary transformation for a Weyl scalar, say, Ψ_0, is simply given by

$$\begin{aligned}\Psi_0 \to& \mathfrak{L}_\Xi\left(R_{III}R_{II}R_I o^A o^B o^C o^D \Psi_{ABCD}\right)\\ =& \mathfrak{L}_\Xi R_{III}\left(\Psi_0 + b\Psi_1 + b^2\Psi_2 + b^3\Psi_3 + b^4\Psi_4\right)\\ =& \mathfrak{L}_\Xi\left(\Lambda^2 e^{2i\theta}\Psi_0 + b\Lambda e^{i\theta}\Psi_1 + b^2\Psi_2 + b^3\Lambda^{-1}e^{-i\theta}\Psi_3 + b^4\Lambda^{-2}e^{-2i\theta}\Psi_4\right).\end{aligned} \tag{4.57}$$

Similar expressions can be found for all other components. If we now expand to first order, and retaining all possible terms, we find

$$\begin{aligned}
&\mathring{\Psi}_0 \to \mathring{\Psi}_0 + \mathfrak{L}_{\dot{\Xi}}\mathring{\Psi}_0 + 2(\dot{\Lambda} + i\dot{\theta})\mathring{\Psi}_0 + 4\dot{b}\mathring{\Psi}_1 = \dot{\Psi}_0\,,\\
&\mathring{\Psi}_1 \to \mathring{\Psi}_1 + \mathfrak{L}_{\dot{\Xi}}\mathring{\Psi}_1 + \dot{a}\mathring{\Psi}_0 + (\dot{\Lambda} + i\dot{\theta})\mathring{\Psi}_1 + 3\dot{b}\mathring{\Psi}_2 = \dot{\Psi}_1 + 3\dot{b}\mathring{\Psi}_2\,,\\
&\mathring{\Psi}_2 \to \mathring{\Psi}_2 + \mathfrak{L}_{\dot{\Xi}}\mathring{\Psi}_2 + 2\dot{a}\mathring{\Psi}_1 + 2\dot{b}\mathring{\Psi}_3 = \dot{\Psi}_2 + \mathfrak{L}_{\dot{\Xi}}\mathring{\Psi}_2\,,\\
&\mathring{\Psi}_3 \to \mathring{\Psi}_3 + \mathfrak{L}_{\dot{\Xi}}\mathring{\Psi}_3 + 3\dot{a}\mathring{\Psi}_2 - (\dot{\Lambda} + i\dot{\theta})\mathring{\Psi}_3 + \dot{b}\mathring{\Psi}_4 = \dot{\Psi}_3 + 3\dot{a}\mathring{\Psi}_2\,,\\
&\mathring{\Psi}_4 \to \mathring{\Psi}_4 + \mathfrak{L}_{\dot{\Xi}}\mathring{\Psi}_4 + 4\dot{a}\mathring{\Psi}_3 - 2(\dot{\Lambda} + i\dot{\theta})\mathring{\Psi}_4 = \dot{\Psi}_4\,,
\end{aligned} \tag{4.58}$$

where the last equality holds on a type D background and a principal NP tetrad. Thus, for the Kerr spacetime, $\dot{\Psi}_0$ and $\dot{\Psi}_4$ are invariant under gauge transformations and under frame transformations.

4.4 SECOND ORDER PERTURBATIONS

Finally, let us briefly discuss second-order fluctuations around the Kerr metric in vacuum. In particular we consider the problem where

$$g_{ab} = g^{\text{Kerr}}_{ab} + \varepsilon \dot{h}_{ab} + \frac{1}{2}\varepsilon^2 \ddot{h}_{ab}\,, \tag{4.59}$$

and the stress energy tensor vanishes at all orders. As we have discussed in the previous section, the first order problem is fully described by either $\dot{\Psi}_0$ or $\dot{\Psi}_4$, and the metric perturbation $\dot{h}_{ab}$ can be reconstructed in a radiation gauge following either of the two procedures described above.

We can follow similar steps as in the previous section to derive the equation that governs second order fluctuations. Starting from (4.21) and proceeding schematically, the following equation holds

$$\mathring{\mathscr{O}}_0[\ddot{\Psi}_0] = -\dot{\mathscr{O}}_0[\dot{\Psi}_0] - \dot{\mathscr{O}}_1[\Psi_1] \equiv \mathcal{S}^{(2)}_0[\dot{h}, \dot{h}]\,, \tag{4.60}$$

where the right hand side is, effectively, a quadratic functional of the metric perturbation $\dot{h}_{ab}$, and the perturbed operators are simply the linearisation of (4.22). For completeness we write here the source term in terms of GHP operators

$$\begin{aligned}
-\frac{1}{2}\mathcal{S}^{(2)}_0[\dot{h}, \dot{h}] =& 4\Big[\dot{\sigma}(\eth' - \tau') - \dot{\kappa}(\text{Þ}' - \rho') + \Big((\eth - \bar{\tau}')\rho\Big)^{\cdot} - \Big((\text{Þ} - \bar{\rho})\tau\Big)^{\cdot}\Big]\dot{\Psi}_1\\
&+ \Big[\Big(\eth\eth' - \text{Þ}\text{Þ}'\Big)^{\cdot} + \Big(4\rho(\text{Þ}' - \rho') + \bar{\rho}\text{Þ}' - \rho'\text{Þ}\Big)^{\cdot}\\
&\qquad - \Big(4\tau(\eth' - \tau') + \bar{\tau}'\eth' + \tau'\eth\Big)^{\cdot} + 2\dot{\Psi}_2\Big]\dot{\Psi}_0\,,
\end{aligned} \tag{4.61}$$

where a dot after a bracket denotes the perturbation of the whole bracket.

In order to know the dynamics of second order fluctuations in vacuum, it suffices to solve an inhomogeneous Teukolsky equation, with source term (4.61). This is sufficient in order to infer, e.g., the GW strain at future null infinity, as it can be read directly from $\ddot{\Psi}_4$ in an appropriate gauge. However, the problem of computing the

second-order metric fluctuation $\ddot{h}_{ab}$ from $\ddot{\Psi}_4$ is more complicated. Although similar techniques as the ones discusses in the previous section may apply, this remains an open problem at the time of writing this thesis.

Finally, let us briefly discuss the gauge and frame invariance of $\ddot{\Psi}_0$ (a similar discussion applies to $\ddot{\Psi}_4$). Going to second-order in (4.57), and using that the background is type D leads to

$$\ddot{\Psi}_0 \to \ddot{\Psi}_0 + 2\mathfrak{L}_{\underline{\ddot{\Xi}}}\Psi_0 + 4(\dot{\Lambda} + i\dot{\theta})\Psi_0 + 8\dot{b}\Psi_1 + 2\dot{b}^2\mathring{\Psi}_0\,. \tag{4.62}$$

Thus, $\ddot{\Psi}_0$ is, per se, neither gauge nor frame invariant. Campanelli and Lousto devised a prescription to add a quadratic piece in $\dot{h}_{ab}$ that compensates for this freedom, building a second-order frame and gauge invariant object. We refer the interested reader to Section IV of [95] for further details on this construction.

5

QUADRATIC QUASINORMAL MODES

Written while listening to music composed by Olivier Messiaen.

5.1 INTRODUCTION

The BH ringdown is an especially appealing dynamical setting to test our understanding of General Relativity and BH physics in the strong gravity regime. The BH spectroscopy program is concerned with the details of the relaxation to equilibrium of a BH after a merger, and it requires precise theoretical predictions to be compared against data [65, 67, 68]. In particular, the frequencies of the quasinormal modes (QNMs) are a benchmark prediction of General Relativity, and they have been used to validate the consistency of theoretical calculations based on Kerr BHs against LIGO-Virgo-KAGRA observations [5, 7, 8, 82, 115, 117, 120, 149, 150, 193, 429].

Most prior work on ringdown was done within linear perturbation theory, which is valid when the backreaction of the perturbations on the spacetime is negligible. However, right after the merger of two BHs backreaction is significant, and nonlinear phenomena have been identified in several studies (see e.g. [9, 39, 134, 318, 342, 419, 477]). In order to achieve high-precision ringdown tests, it is critical to understand the transition between the nonlinear and the linear regime.

A paradigmatic nonlinear effect are quadratic quasinormal modes (QQNMs): loosely speaking, these are driven, quadratic (and therefore, nonlinear) combinations of QNMs. The presence of these driven modes is predicted by second-order perturbation theory [85, 218, 252, 300, 319, 354, 372, 409], and they play an important role in particular in the higher harmonics of the GW strain waveform emitted during a binary BH merger [134, 318, 342]. The space-based interferometer LISA will likely observe these modes [464], confirming a nonlinear prediction of General Relativity and enhancing the BH spectroscopy program.

In this chapter we study the excitation of QQNMs of a Kerr BH using second-order perturbation theory, building upon the framework of Chapter 4. We show that (i) second-order perturbation theory predicts the excitation of QQNMs, with an amplitude in agreement with Numerical Relativity simulations, (ii) the amplitude ratio is largely independent of the initial conditions, and therefore, can be tested against observations, paving the way towards nonlinear BH spectroscopy, and (iii) the high-frequency excitation of QQNMs is subtle, with results hinting towards a possible

breakdown of perturbation theory for fine-tuned initial conditions, motivating a further scrutiny of this regime, which we carry out in Chapter 6.

5.2 WHAT ARE QUADRATIC QNMS?

First of all, let us discuss in detail what are QQNMs with a simple example which is, nevertheless, physically motivated. Consider a one–dimensional string with extremes fixed at $x = 0, L$, restricted to move in the (x, y)–plane. The position of each infinitesimal element of mass of the string $\vec{r}$ at a time t is given by

$$\vec{r}(t) = (x + \xi(x,t), \eta(x,t)) \,, \tag{5.1}$$

The equation of motion governing the dynamics of the string is

$$\rho_0 \frac{\partial^2}{\partial t^2}\vec{r} = \frac{\partial}{\partial x}\Big(\tau \hat{s}\Big) \,, \qquad \hat{s} = \frac{\vec{r}'}{||\vec{r}'||} \tag{5.2}$$

where the prime denotes a derivative with respect to x, ρ_0 is the (constant) density of the string, and τ is the stress. Usually the stress is taken to be constant, but this is strictly speaking not true. In fact we can write

$$\frac{\tau}{\rho_0} = c_T^2 + c_L^2\Big(||\vec{r}'|| - 1\Big) \,, \qquad c_T^2 = \frac{\tau_0}{\rho_0} \,, \quad c_L^2 = \frac{\tau_0 + E}{\rho_0} \,, \tag{5.3}$$

with E the Young modulus of the material of the string, and τ_0 the stress of the string at equilibrium. The equations of motion for longitudinal and transverse perturbations take the form

$$\begin{aligned} \frac{\partial^2 \xi}{\partial t^2} - c_L^2 \xi'' &= (c_L^2 - c_T^2)\eta' \Delta \,, \\ \frac{\partial^2 \eta}{\partial t^2} - c_L^2 \eta'' &= (c_T^2 - c_L^2)(1 + \xi')\Delta \,, \end{aligned} \tag{5.4}$$

where

$$\Delta = \frac{(1+\xi')\eta'' - \eta'\xi''}{\Big[(\eta')^2 + (1+\xi')^2\Big]^{3/2}} \,. \tag{5.5}$$

Now let us consider small transverse perturbations $\eta = \epsilon\dot{\eta} + \dots$, and suppose $\xi = \epsilon^2\ddot{\xi} + \dots$. To leading order, we have that transverse fluctuations just satisfy a one-dimensional wave equation, as expected:

$$\frac{\partial^2 \dot{\eta}}{\partial t^2} - c_L^2 \dot{\eta}'' = 0 \implies \dot{\eta} = \eta_n \sin\Big(\lambda_n x\Big) e^{-i\omega_n^{(T)} t} \,, \quad \omega_n^{(L/T)} = c_{L/T}\lambda_n \,, \tag{5.6}$$

where $\lambda_n = n\pi/L$. To leading order $\Delta = \dot{\eta}'' + \mathscr{O}(\epsilon^2)$, so the non-linear transverse fluctuations are dominated by

$$\frac{\partial^2 \ddot{\xi}}{\partial t^2} - c_L^2 \ddot{\xi}'' = (c_L^2 - c_T^2)\dot{\eta}'\dot{\eta}'' \,. \tag{5.7}$$

The solution is simply given by

$$\ddot{\xi} = \frac{c_T^2 - c_L^2}{2\lambda_n^3}\left[\frac{2\eta_n\bar{\eta}_n}{(\omega_{2n}^{(L)})^2} + \frac{\eta_n^2 e^{-i\omega_{2n}^{(T)}t}}{\left((\omega_{2n}^{(L)})^2 - (\omega_{2n}^{(T)})^2\right)} + \frac{\bar{\eta}_n^2 e^{i\omega_{2n}^{(T)}t}}{\left((\omega_{2n}^{(L)})^2 - (\omega_{2n}^{(T)})^2\right)}\right]. \tag{5.8}$$

Remarkably we observe that small transverse vibrations to the string source longitudinal fluctuations oscillating at twice the frequency. This is often referred in acoustics and in nonlinear optics as *higher harmonic generation*. In particular, the modes oscillating with frequency $\omega_{2n}^{(T)} = 2\omega_n^{(T)}$ are the *second harmonics*. In the presence of dissipation, these would become QQNMs. We emphasize that these are longitudinal modes oscillating with (twice) the characteristic frequency of transverse modes, i. e., these modes are oscillating with frequencies that are not in the longitudinal spectrum. Whenever this is the case, $\omega_{2n}^{(T)} \to \omega_{2n}^{(L)}$, the denominators diverge and the system is said to be in resonance. Nevertheless any (small) dissipation in the equations destroys the resonance condition, so this will not be a concern when discussing BH QQNMs.

A similar discussion holds for BH perturbations. Suppose the first-order perturbations are governed by two QNMs,

$$\Psi_4 = \sum_{I=1,2} A_I e^{-i\omega_{\ell_I m_I n_I} t} R_{\ell_I n_I}(r)\, {}_{-2}S_{\ell_I m_I}(\theta,\phi; a\omega_{\ell_I m_I n_I})\,, \tag{5.9}$$

following the notation of the previous chapter. The second-order perturbations are governed by

$$\mathcal{O}_4\ddot{\Psi}_4 = \mathcal{S}_4[\dot{h},\dot{h}]\,. \tag{5.10}$$

It is not hard to convince oneself that as source term is quadratic in the metric perturbation, it must be of the form

$$\mathcal{S}_4[\dot{h},\dot{h}] \supset \sum_{I,J=1,2} A_I A_J e^{-i(\omega_{\ell_I m_I n_I} + \omega_{\ell_J m_J n_J})t} \tilde{R}_{I\times J}(r)\tilde{S}_{I\times J}(\theta) e^{i(m_I+m_J)\phi}\,. \tag{5.11}$$

Other combinations involving the complex conjugates are also possible and expected. In any case, we are now dealing with an inhomogeneous wave equation, with a source term which drives the system with frequency $\omega_{\ell_1 m_1 n_1} + \omega_{\ell_2 m_2 n_2}$. As time-translations are a symmetry of the Teukolsky equation, $[\mathcal{O}_4, \mathfrak{L}_{\xi}] = 0$, it follows that the inhomogeneous solution contains terms of the form

$$\ddot{\Psi}_4 \supset \sum_{\ell,m}\sum_{I,J=1,2} \mathcal{R}_{I\times J}^{(\ell,m)} A_I A_J e^{-i(\omega_{\ell_I m_I n_I} + \omega_{\ell_J m_J n_J})t} \ddot{R}(r)\, {}_{-2}Y_{\ell m}(\theta,\phi)\delta^m_{m_I+m_J}\,, \tag{5.12}$$

where we choose to re-express the solution as a sum over spherical harmonics. The quantities $\mathcal{R}_{I\times J}^{(\ell,m)}$ are dubbed *QQNM ratios* and measure the susceptibility of certain mode combinations to be excited. We refer to the modes (ℓ_1, m_1, n_1) and (ℓ_2, m_2, n_2) as *parent modes*, and the QQNM oscillating with frequency $\omega_{\ell_1 m_1 n_1} + \omega_{\ell_2 m_2 n_2}$ as

daughter mode. We also notice that there angular selection rules apply: the azimuthal number of the daughter mode must satisfy $m = m_1 \pm m_2$ (the negative sign arising from the case where a mode couples to the complex conjugate of another mode). Due to the spherical-spheroidal mixing of Kerr BHs, there is no constraint on the polar number ℓ beyond $|\ell| \geq m$. For nonrotating BHs ($a = 0$), spherical symmetry enforces a selection rule on ℓ, given by $|\ell_1 - \ell_2| \leq \ell \leq \ell_1 + \ell_2$. The angular harmonics that do not satisfy this selection rule are not significantly excited for moderately rotating BHs.

Computing and understanding the dependence of these QQNM ratios on the initial conditions, the BH spin, and the parent mode harmonic numbers is the goal of this Chapter, and one of the major contributions of this thesis. We highlight that these can play a role akin to QNM frequencies in BH spectroscopy since they can be computed quite accurately with perturbative methods, and then compared against GW observations, providing a clean test of General Relativity in the strong-field regime, and based on nonlinear effects.

5.3 METHODS

We tackle this problem through a two step-process: first, we solve numerically the first- and second-order Teukolsky equations as an initial value problem. Secondly, we extract posterior probability distributions for the amplitudes of parent and daughter modes, and use them to estimate the QQNM ratio.

5.3.1 *Time-domain Evolution of Second Order Teukolsky Equation*

We numerically solve the linear and quadratic Teukolsky equations employing the code described in Ref. [409]. The code solves the Teukolsky equation and metric reconstruction equations on a horizon-penetrating, hyperboloidally compactified domain (4.7). At each time step, we first solve the linear Teukolsky equation for $\dot{\Psi}_4$, then we solve the transport equations to reconstruct the metric perturbation $\dot{h}_{ab}$ in the ORG, as explained in Chapter 4, and use them to source the second order Teukolsky equation.

Initial data for $\dot{\Psi}_4$ is given by:

$$\dot{\Psi}_4(t=0) = \phi_0 \, {}_{-2}P^m_\ell(\vartheta) e^{im\phi}\,, \tag{5.13}$$
$$\phi_0 = A\left(\tfrac{r-r_l}{r_u-r_l}\right)^2\left(\tfrac{r_u-r}{r_u-r_l}\right)^2 \exp\left(-\tfrac{1}{r-r_l} - \tfrac{2}{r_u-r}\right)\theta(r-r_l)\theta(r_u-r)\,.$$

Above, ${}_sP^m_\ell$ denotes the spin-weighted associated Legendre function, the numbers ℓ and m are constants which characterize the angular structure of the initial data, and θ denotes the Heaviside step function. The parameters $\{A, r_l, r_u\}$ characterize the initial profile, fixing respectively its amplitude, lower and upper radius. The initial velocity profile, $\partial_t \dot{\Psi}_4$, is chosen so that the pulse moves towards the BH. We additionally set $\dot{h}_{ab}\,(t=0) = 0$. While these initial data do not satisfy the Einstein constraint equations, so long as $|m| \geq 2$ the constraint violating modes propagate

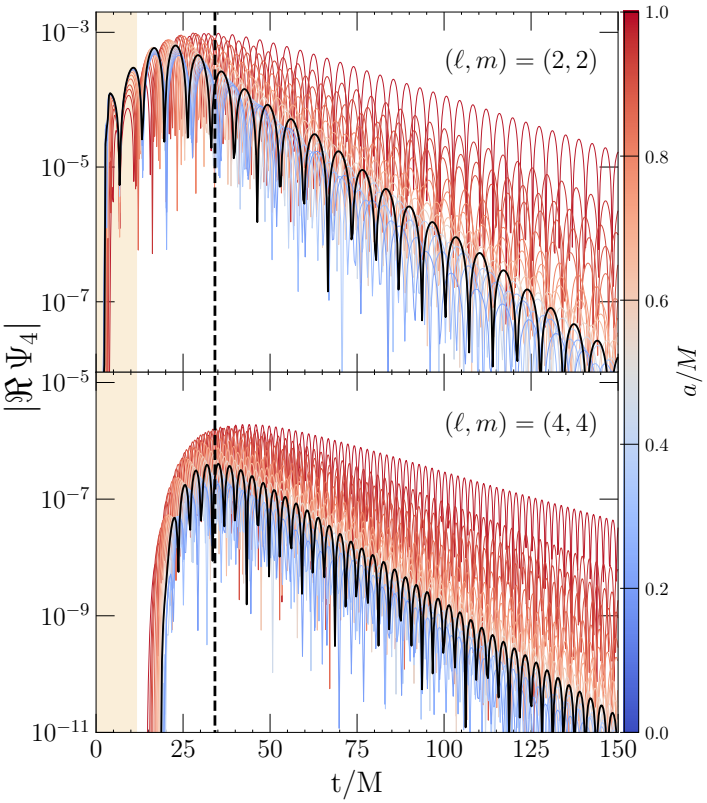

Figure 13 Linear (top) and quadratic (bottom) perturbation to the Weyl scalar Ψ_4 at future null infinity for $(\ell, m) = (2, 2)$ (top) and $(4, 4)$ (bottom), and for different BH spins, as indicated by the colorbar. The perturbation is sourced by an incoming initial profile with $\{A, r_l/r_h, r_u/r_h\} = \{0.01, 1.5, 2.5\}$ in the notation of (5.13). For the black line ($a/M = 0.5$) we show the reference time when the quadratic mode attains its maximum (dashed), and the constraint-violating region (in beige).

off of our computational domain in a finite amount of time T_R [409]. We set $\ddot{\Psi}_4 = 0$, $\ddot{h}_{ab} = 0$, which satisfies the second-order Einstein constraint equations.

As the numerical grid represents a hyperboloidal slicing of the Kerr background, we can extract $\dot{\Psi}_4$ and $\ddot{\Psi}_4$ directly at future null infinity. We then project those quantities onto spin-weighted spherical harmonics. We show the representative evolution for different BH spins in Fig. 13. In that figure, the BH is initially perturbed by an incoming mode with $\ell = m = 2$. The largest daughter harmonic is the $\ell = m = 4$, shown in the lower panel. Its excitation is delayed, as we wait to initialise the evolution until constraint violating modes have abandoned our computational domain. Nevertheless, this has no impact on our ability to study second-order modes.

The simulations were run with a spin-dependent base grid resolution, because higher resolution is needed as the BH approaches extremality. For each run we used two different (but close-by) resolutions. The number of radial and angular points used in the runs, (N_x, N_y), is listed in Table 1. In order to test the numerical convergence of our code, we fix the BH spin to $a/M = 0.7$ and we assume initial conditions such that $r_l = 1.5 r_h$, $r_u = 2.5 r_h$. We consider three runs with $(N_x, N_y) = (188, 24), (190, 24), (192, 24)$. In Fig. 14 we show an independent residual test for these three runs. The residual $\mathcal{H} \sim \Im h_{ll}$ checks that the reconstructed metric is real, and should be zero by virtue of (4.56). As usual, the time axis in the figure is such that $t = 0$ denotes the peak of the second-order perturbations. Constraint violations leave our computational domain at times $T_R < 0$ (i.e., in the region marked by hatched gray lines); at later times, the residuals converge rapidly to zero. Higher

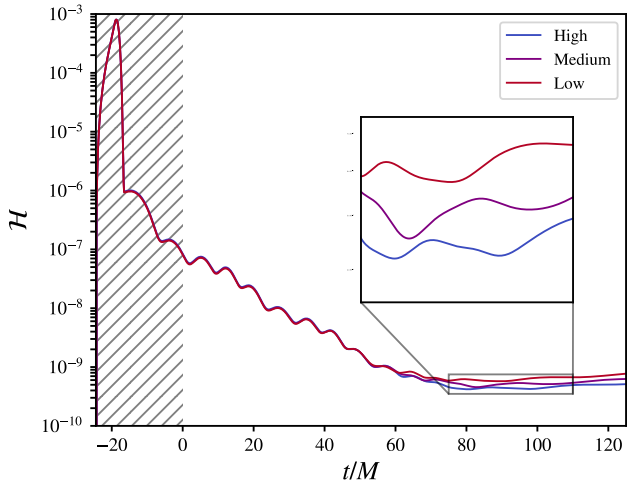

Figure 14 Independent residual stemming from the reality of the reconstructed metric components $\mathcal{H}$ (see Ref. [409]) as a function of time, for a BH spin $a/M = 0.7$, and for high $(N_x, N_y) = (192, 24)$, medium $(N_x, N_y) = (190, 24)$ and low $(N_x, N_y) = (188, 24)$ resolutions. The hatched region at $t < 0$ (where $t = 0$ is the peak of the second order perturbations) is not used for the Bayesian inference. At times $t > 0$ the residuals are small and converging to zero. The inset shows that the residuals are smaller for higher resolutions as expected, although the difference is small, because the resolutions are very close to each other.

a/M	Low Resolution	High Resolution
$0 \ldots 0.5$	$(184, 24)$	$(186, 24)$
$0.5 \ldots 0.9$	$(190, 24)$	$(192, 24)$
$0.9 \ldots 1$	$(196, 28)$	$(198, 28)$

Table 1: Resolution levels (N_x, N_y) for different BH spins.

resolutions generally lead to smaller values of the residuals, as expected. Notice that the chosen resolutions are very close to each other and the convergence of the code is exponential, therefore the difference between resolutions is only visible in the inset. Even though the residuals are small and converging to zero at times $t \geq T_R$, some truncation error is inevitably present in the simulations. We use this truncation error, which we estimate by computing the difference between the high and low resolutions defined in Table 1, to construct a time-dependent likelihood function, as already introduced in Chapter 2.

5.3.2 *Bayesian Inference of Mode Amplitudes*

To compare our results with Numerical Relativity results, such as Refs. [134, 342], we study the strain amplitude h instead of Ψ_4. Our numerical simulations end before we observe a power-law tail, and the modeling starting time imposed by the metric reconstruction implies that the initial burst should not affect our calculations. Hence,

for each of the spherical modes we consider a template consisting of a superposition of damped sinusoids

$$h_{\ell m}(t) = \sum_{\ell'=2}^{\infty}\sum_{n=0}^{\infty}\Big[\mathcal{A}_{\ell' mn}\, e^{-i(\omega_{\ell' mn}(t-t_0)+\phi_{\ell' mn})} + \mathcal{A}_{\ell' -mn}\, e^{-i(\omega_{\ell' -mn}(t-t_0)+\phi_{\ell' -mn})}\Big]\,, \tag{5.14}$$

with $t > t_0$ and the complex frequencies $\omega_{\ell' mn}$ correspond to the QNMs of a perturbed Kerr BH.[1] All amplitudes and phases are defined with respect to the reference time $t_0 = 0$, which we choose to coincide with the peak of the second-order perturbation (see Fig. 13). The sum on ℓ' is due to spherical-spheroidal mode mixing [65, 66, 89, 273, 315]. We compute the mixing coefficients using the Black Hole Perturbation Toolkit [74]. The first term in (5.14) corresponds to "corotating" (prograde) modes with $\Re\omega_{\ell mn} > 0$, while the second corresponds to "counterrotating" (retrograde) modes with $\Re\omega_{\ell -mn} < 0$, which are increasingly suppressed for large values of a/M [65, 307, 309]. As our model assumes a QNM-driven regime, we can analyze $\psi_{4,\ell m}$ and reconstruct the strain amplitudes by a simple frequency rescaling: $\mathcal{A}_{\ell mn} = (2\omega^2_{\ell mn})^{-1}\mathcal{A}^{\Psi}_{\ell mn}$, at future null infinity. This rescaling is in good agreement with an alternative calculation in which we compute the strain h through two direct integrations in time of Ψ_4, and then extract the amplitude of h, but it avoids the integrations (which increase numerical noise).

We refer to each of the two contributions to a given (ℓm) multipole of h as a "mode," each with an amplitude $\mathcal{A}_{\ell mn}$ and a phase $\phi_{\ell mn}$, treated as two unknown parameters to be inferred from the numerical data.

Properly accounting for errors on the fitting parameters is crucial, because some of the subdominant contributions can be comparable to the numerical resolution (this is true, e.g., for counterrotating modes and near-extremal spins). For this reason, we address the fitting problem through Bayesian inference [262]. In this way the numerical error is folded in the inferred parameters, yielding not only a point estimate of the quantities of interest, but the full information available at a given resolution (including the uncertainties).

The complex QNM frequencies are uniquely determined by the Kerr BH mass (which enters only as a scaling factor) and spin of each simulation. We choose uniform priors on all sampling parameters within the ranges $\ln\mathcal{A} \in [-15, 0]$ for the linear contributions, $\ln\mathcal{A} \in [-35, -5]$ for the quadratic contributions, and $\phi \in [0, 2\pi]$. The dominant uncertainty in the reconstruction is introduced by the resolution error, so we consider a gaussian likelihood, with an error at each time given by the difference between the two highest resolutions available. This choice guarantees a conservative and unbiased mode extraction, as we verified by simulating and recovering mock ringdown signals superimposed to the numerical error. To

1 The frequencies correspond to a Kerr BH with mass and spin fixed by the initial conditions. Changes in the mass and spin are proportional to $(\dot{h}_{ab})^2$, and thus, they do not affect the evolution of $\dot{\Psi}$ and $\ddot{\Psi}$ to second order in perturbation theory. Higher-order perturbations (starting at cubic order, i.e., $\dddot{\Psi}$) would be sensitive to this effect [399, 419].

perform the extraction, we developed a dedicated `python` package, `bayRing`, which we make publicly available [1].

The waveform model is interfaced through `pyRing` [118], the QNM frequencies are computed through the `qnm` [436] package, and the high-dimensional parameter space exploration is achieved through the parallel nested sampling algorithm [431], as implemented in `raynest` [165]. We use 128 live points, and 256 maximum Markov Chain Monte Carlo (MCMC) steps. For each analysis, we run 4 parallel explorations, and combine them in a unique posterior distribution by weighting them through their Bayesian evidence. This last step is crucial to ensure that our estimate does not depend on the random initial seed (the most challenging fitting models contain up to 14 free parameters).

A challenging step is how to decide which modes to include in the analysis. The vast range of initial conditions and BH spins that we explore implies that some modes will be well above numerical uncertainties, while others (in particular, counterrotating modes) will be comparable to numerical uncertainties. Including all such contributions in every case is computationally prohibitive, so we adopt a more practical approach. Rather than assuming that a given set of modes is present in the data, we first agnostically extract the spectral content of the simulations.

We start by focusing on three representative simulations, with low-mid-high spins $a/M = \{0.3, 0.5, 0.7\}$, and analyze each of them (for the linear and quadratic sectors separately) using a "free modes" model:

$$h(t) = \sum_{i=0}^{N} \mathcal{A}_i \, e^{-i[\omega_i (t-t_0)+\phi_i]} \,, \tag{5.15}$$

where $\omega_{\rm R}^i = {\rm Re}(\omega_i)$, $\tau_i = 1/{\rm Im}(\omega_i)$, A_i, and ϕ_i are now all free parameters. To ensure that we are in the QNM-driven regime, we set $t_0 = 10M$. Note that $t_0 = 0$ corresponds to the peak of the quadratic mode, which is typically $\sim 20M$ after the peak of the linear modes, ensuring that we are well into the QNM-driven regime. Besides the standard settings stated in the main text, we choose additional priors on the frequency and damping time in the ranges $M\omega_{\rm R} \in [-2, 2]$, $\tau/M \in [1, 50]$. To prevent "mode switching" during sampling, we order the modes by decreasing frequency.

As expected, the free modes posteriors latch onto the predicted Kerr frequencies (uniquely determined by the known mass and spin for each simulation) of several dominant contributions, e.g. $\{220, 2\text{-}20, 320, 3\text{-}20, 221\}$ in the linear case. All the modes we consider have a clear overlap with a single GR prediction, making their identification unambiguous. We keep adding modes as long as the Bayesian evidence favours their inclusion. Equivalently, we stop adding modes once the residuals that we obtain are smaller than the error induced by the numerical resolution. By this procedure we conclude that we must include $N = 4$ modes.

Now that we have agnostically singled out the dominant contributions, we repeat the fit using Eq. (5.14). However, now we fix the complex frequency to the predicted Kerr value and we vary the starting time $t_0 \in [0, 25]M$, in steps of M. We start by fixing the dominant mode (the 220 in the linear case) and we add the modes

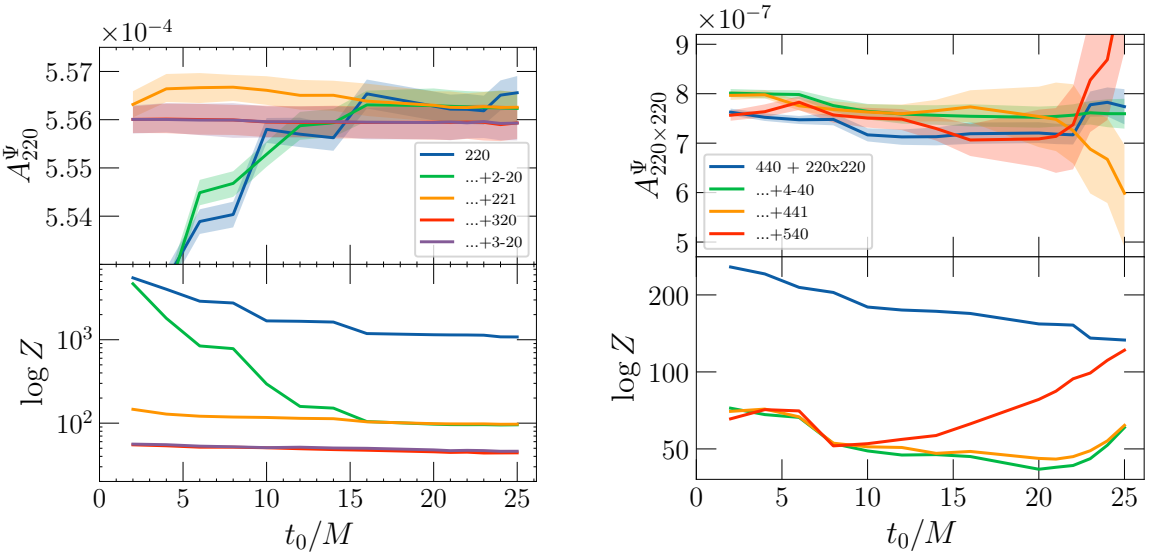

Figure 15 **Left:** Amplitude of the 220 mode (top) and Bayesian evidence $-\log Z$ as a function of the starting time of the fit, t_0, for a black hole with spin $a/M = 0.7$. Each line corresponds to a different mode content; the legend indicates the last mode added to the template (in order: 220, 2-20, 221, 320, 3-20). Shaded regions represent the 90% Bayesian inference confidence interval, including numerical uncertainties. **Right:** Same as in the left panel, for the $\ell = m = 4$ sector. The bottom panel shows that adding modes beyond 440, 4-40, 220 × 220 reduces the Bayesian evidence, and the extracted amplitude of the quadratic mode becomes less stable, with larger oscillations.

selected above one by one in order of decreasing amplitude, as determined by the free-frequency modes fit. This procedure has proven to be successful in a wide range of QNM extraction problems, ranging from perturbation theory to full binary simulations [39].

In the top left panel of Fig. 15 we show how the amplitude of the 220 mode is impacted by the addition of other modes (as indicated in the legend). When fitting using only the 220 mode, the amplitude displays large variations at early times (shaded regions indicate the uncertainty induced by the numerical resolution). When including the first overtone (221) mode, the amplitude variation is greatly reduced, and the 220 late-time amplitude varies by 1%. Adding the 320 mode further reduces the amplitude variation. On the contrary, adding the next dominant mode 3-20 has a negligible impact on the 220 mode amplitude (which remains constant), and instead decreases the evidence very slightly (due to the logarithmic scaling in Fig. 15, this is not immediately evident in the figure). Our mode-addition procedure has reached convergence and no more additional modes need to be included.

The same method is then applied to the quadratic sector, this time quantifying the impact on the extraction of the 220 × 220 mode amplitude. In this case, comparatively larger variations of the amplitudes are present, which are however compatible with the wide error bars (dictated by the numerical resolution), shown as shaded regions in Fig. 15. Again, saturation of the evidence is observed for all times considered. Remarkably, this occurs when only the fundamental prograde

and retrograde mode 440 and 4-40 are present, in addition to the quadratic mode 220×220. Including any other mode only decreases the Bayesian evidence. This procedure sets the "default" set of modes used in this work. In order to correctly resolve the physical QNM content of the system in the quadratic sector, we must take into account 7 modes (corresponding to 14 free parameters).

Finally, we estimate the error by "marginalizing" over the starting time in the following way. For each run, we extract the amplitude posteriors at starting times $t_0/M = \{15, 17.5, 20, 22.5, 25\}$. Earlier times are excluded because we observe large variations in the parameters, indicating that a pure QNM description is not applicable yet. The final estimate of the amplitude is then constructed by combining all of the posterior samples from each of the inferences, and extracting the mean and standard deviation of the combined posterior samples. This amounts to considering each of the inferences as part of the same random process. Such procedure results in a conservative estimation of the error bars, since small variations due to the starting times or mode inclusion will enlarge the tails of the distribution.

5.4 RESULTS

Using the method described in the previous section, from each numerical evolution we can infer the value of the nonlinear ratio as

$$\mathcal{R}^{(\ell',m')}_{(\ell_1,m_1,n_1)\times(\ell_2,m_2,n_2)} = \frac{\mathcal{A}^{(\ell',m')}_{(\ell_1,m_1,n_1)\times(\ell_2,m_2,n_2)}}{\mathcal{A}_{(\ell_1,m_1,n_1)} \times \mathcal{A}_{(\ell_2,m_2,n_2)}}\,, \tag{5.16}$$

where $\mathcal{A}^{(\ell',m')}_{(\ell_1,m_1,n_1)\times(\ell_2,m_2,n_2)}$ denotes the amplitude of the mode oscillating with frequency $\omega_{(\ell_1,m_1,n_1)} + \omega_{(\ell_2,m_2,n_2)}$ extracted in the (ℓ', m') harmonic. We have produced a catalog of runs with varying initial conditions and BH spins, as well as different initially excited angular harmonics. We now summarize our results on each of these effects.

5.4.1 *Independence on Initial Conditions*

Let us focus simply on the case where the only excited harmonic is $(\ell, m) = (2, 2)$. The leading order nonlinearity in this case is captured by the QQNM ratio $\mathcal{R}^{(4,4)}_{(2,2,0)\times(2,2,0)} \equiv \mathcal{R}_{(2,2,0)\times(2,2,0)}$. We have explored a range of initial conditions, and our results are summarized in Fig. 16.

The overall amplitude A of the initial perturbation is a scaling factor, hence it must factor out of the ratio, but there could be nontrivial dependence of this ratio on other parameters, such as the location of the inner boundary, r_l, and the "width" of the initial pulse, $w = r_u - r_l$. In Fig. 16 we show that the ratio is only mildly dependent (if at all) on r_l and w. The figure shows that the mild dependence on initial conditions is valid for all values of the spins. Notice that for smaller spins, due to the increased relevance of counterrotating modes, the uncertainties in the extraction are larger.

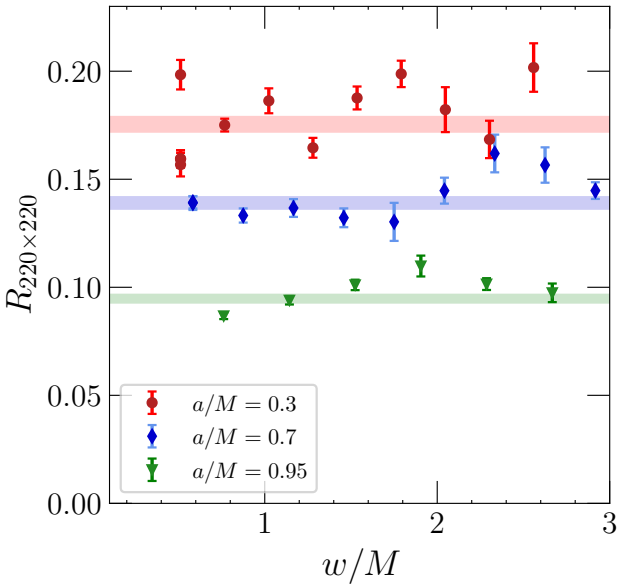

Figure 16 Ratio $\mathcal{R}_{220\times220}$ as a function of the width of the initial pulse $w = r_u - r_l$, for a BH spin $a/M = [0.3, 0.7, 0.95]$ (in red, blue, green, respectively) and $r_l = 1.5r_h$. When a given value of w represents multiple points, those are computed using different values of r_l, further showing that the ratio depends only very mildly on the initial conditions.

The uncertainties in the extraction also become larger as the pulse becomes wider ($w \geq 3r_h$) or it is placed further away from the horizon ($r_l \geq 2r_h$). This is due to two reasons: the numerical evolution code uses a compactified grid, and thus it needs more resolution to resolve features that are further away from the horizon. Moreover, initial pulses located far away correspond to a larger value of T_R, and this affects the time window of the signal available for the fit.

Although from the point of view of a frequency-domain calculation this ratio is naturally independent of the initial conditions [79, 86, 87, 277], it is nevertheless a nontrivial consistency check that time-domain evolutions confirm this. In fact, this shows that the QQNM excitation is insensitive to the prompt response, or to nonlinear couplings between prompt and QNM excitations.

5.4.2 *Dependence on the BH Spin*

The dependence on the spin can be studied in a similar way. We now assume the pulse to be at $r_l = 1.5r_h$, with width $w = r_h$. In this case, a frequency domain argument immediately shows that the QQNM ratio should naturally depend on the BH spin, for the same reason as the QNM excitation factors depend on the BH spin.

This expectation is confirmed in Fig. 17: the ratio $\mathcal{R}_{220\times220}$ is indeed spin-dependent and decreases with spin, ranging roughly between $\mathcal{R}_{220\times220} = 0.16$ for $a/M = 0.2$ and $\mathcal{R}_{220\times220} = 0.08$ for $a/M = 0.98$. These variations are much larger than the estimated uncertainties, or than possible variations due to the mild dependence on the initial conditions. The values that we extract, moreover,

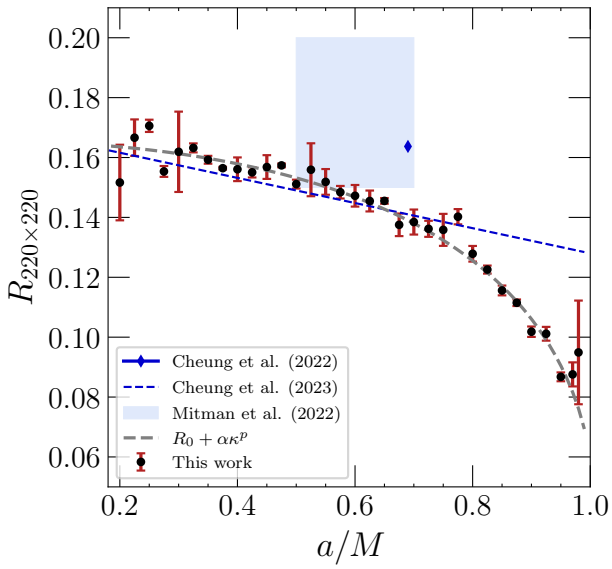

Figure 17 Ratio $\mathcal{R}_{220\times220}$, as a function of the spin of the remnant BH, showing a clear dependence with the spin. The gray dashed line represents the best fit to a power law in terms of the surface gravity, $\mathcal{R}_{220\times220} = R_0 + (M\kappa)^p$, see (5.17). We also represent the values for the QQNM ratio obtained originally from NR in [134] (referred to as Cheung et al.) and [342] (referred to as Mitman et al.). The blue dashed line corresponds to the linear hyperfit reported in [135], based on a catalogue of NR simulations.

are remarkably close to the resulting nonlinear ratio reported in [134, 342]. The spin-dependence of $\mathcal{R}_{220\times220}$ is well explained by a power law of the surface gravity $\kappa = \frac{\sqrt{M^2-a^2}}{2M(M+\sqrt{M^2-a^2})}$: our results are well fitted to an expression of the form $\mathcal{R}_{220\times220} = R_0 + (M\kappa)^p$, with

$$R_0 = 0.058 \pm 0.003, \quad p = 1.61 \pm 0.03\,. \tag{5.17}$$

Uncertainties in the ratio extraction become smaller for rapidly spinning BHs, since at low spins counterrotating modes are as important as corotating ones. As a consequence, especially for the quadratic modes, our template should be enhanced with all the counterrotating contributions [65, 135, 307, 309], including the highly damped overtone and mode-mixing ones [65, 66, 89, 273, 315], severely complicating the inference problem and increasing computational cost. These contributions include, for example, mode-mixing terms such as the 640 mode or the 541 overtone, as well as additional quadratic terms such as 220 $\times$ 2-20 mode. Frequency domain calculations [87, 277] are better suited to achieve an accurate calculation of the QQNM ratio. Our results, on the other hand, demonstrate that in an initial value problem with remarkably different initial conditions as after a binary BH merger, the excitation of QQNMs is governed by the same physics.

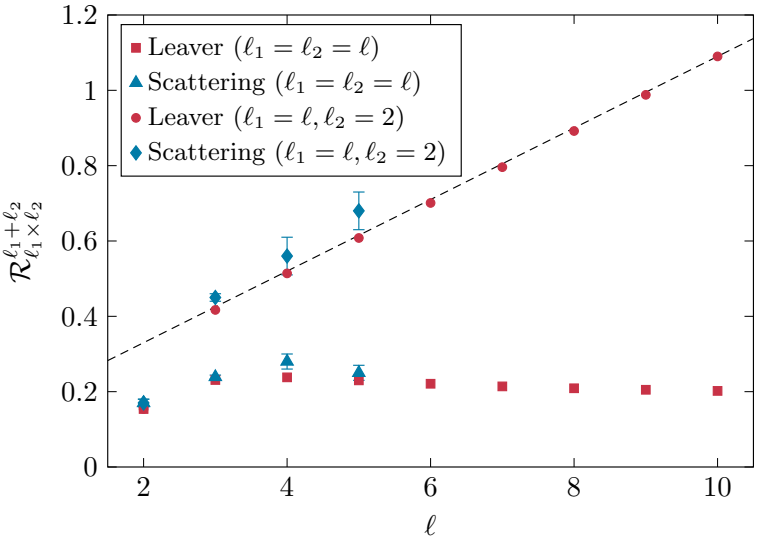

Figure 18 QQNM ratio (5.18) obtained through the Leaver method (blue) and scattering method (red), for $\ell_1 = \ell_2 = \ell$ (squares and triangles), and for $\ell_1 = \ell, \ell_2 = 2$ (circles and diamonds). The black dashed line represents a linear scaling with ℓ.

5.4.3 *Dependence on the Angular Harmonic*

Finally, we aim to investigate how does the QQNM ratio behave when one approaches the high-frequency or *eikonal* regime, corresponding to $\ell \gg 1$. This limit can be associated to a null geodesic congruence centered at the light ring (LR) with an expansion determined by Lyapunov's exponent [103, 333, 422]. It can also be understood as fluctuations about the Penrose limit adapted to the LR, made precise in [196], an approach which we study in Chapter 6.

To simplify the problem, we will restrict to Schwarzschild BHs. Moreover, we focus on the mode-coupling between fundamental modes $n_1 = n_2 = 0$, for $\ell_1 = m_1$ and $\ell_2 = m_2$. Thus, we denote the short-hand

$$\mathcal{R}^{\ell}_{\ell_1\times\ell_2} = \mathcal{R}^{(\ell,\ell)}_{(\ell_1,\ell_1,0)\times(\ell_2,\ell_2,0)}\,. \tag{5.18}$$

Notice that since we work with non-spinning BHs, we can easily recover the m-dependence from $\mathcal{R}^{\ell}_{\ell_1\times\ell_2}$, since this dependence is fully captured by $3j$ symbols, which govern the overlap of three (possibly spin weighted) spherical harmonics,

$$\mathcal{R}^{\ell}_{\ell_1 m_1\times\ell_2 m_2} \propto \begin{pmatrix} \ell_1 & \ell_2 & \ell \\ m_1 & m_2 & -m_1-m_2 \end{pmatrix}. \tag{5.19}$$

Now, estimating the $\ell \to \infty$ limit of $3j$ symbols allows us to rescale our results giving

$$\mathcal{R}^{2\ell}_{\ell m_1\times\ell m_2} \simeq (-1)^{m_1+m_2}\left(\frac{2}{\ell\pi}\right)^{1/4} e^{-\frac{(m_1-m_2)^2}{4\ell}}\mathcal{R}^{2\ell}_{\ell\ell\times\ell\ell}\,, \tag{5.20}$$

valid when $m_1, m_2 \lesssim \sqrt{\ell}$, for the case when $\ell_1 = \ell_2$. For the second case that we will study in detail, $\ell_1 = \ell, \ell_2 = 2$, we have instead

$$\mathcal{R}^{\ell+2}_{\ell m_1 \times 22} \simeq \frac{(-1)^{\ell+m_1}}{4}\left(1+\frac{m_1}{\ell}\right)^2 \mathcal{R}^{\ell+2}_{\ell\ell\times 22}\,, \tag{5.21}$$

uniformly in $|m_1| \leq \ell$.

In order to avoid the difficulties associated to the excitation of multiple counter-rotating modes, we infer the amplitudes using a minimization algorithm — `jaxqualin` [135]. We have validated this against our results based on Bayesian inference, finding very good agreement in the extraction of QQNM ratio. Moreover, pushing to higher values of the angular number ℓ requires a very high resolution in the angular direction, increasing rapidly the computational cost. We refer to this method of extracting the QQNM amplitude as *Scattering*, as it is based on the time-domain scattering of Gaussian pulses off a non-spinning BH.

We compare our results with calculations in the frequency domain, based on [86, 87]. This method (dubbed *Leaver* onward) is based on a solution of the Regge-Wheeler-Zerilli equations at second order with QNM boundary conditions using the Leaver algorithm, extending the method introduced in Chapter 3. The solutions are obtained as an infinite series whose coefficients can be computed with arbitrary precision in `Mathematica`. This means that the accuracy of the method is very high.

Our results are summarized in Fig. 18. We have focused on two distinct ratios, $\mathcal{R}^{2\ell}_{\ell\times\ell}$, and $\mathcal{R}^{\ell+2}_{\ell\times 2}$. In the first case, the ratio seems to approach a constant value as $\ell \to \infty$ — therefore motivating whether a calculation of the QQNM in the eikonal regime could directly estimate analytically this constant. The second case is more puzzling: the ratio seems to grow linearly with ℓ. We obtain $\mathcal{R}^{\ell+2}_{22\times\ell\ell} \propto \ell$, hinting towards a divergence as $\ell \to \infty$. Naturally one could worry that such a divergence would imply that perturbation theory is not valid at high enough frequencies, since the second order modes could in principle have a much larger amplitude than the leading order modes. Here we argue that this can not be the case, at least for physically reasonable initial conditions.

The perturbative expansion on which linear and quadratic modes is based is not necessarily guaranteed to converge. It can break down if certain resonances between modes are present [41, 72, 73, 260, 463]. Upon direct examination, one can conclude that such resonances do not occur, at least for the lower ℓ modes, with low overtone number, for Schwarzschild. However, a breakdown of perturbation theory can still occur if the nonlinear ratio describing the coupling between several incoming modes with wave number k_i, and resulting in a mode with wave number $k \gtrsim k_i$, diverges as $k \to \infty$. Let us be more precise. Suppose that the nonlinearity is quadratic, hence leading to a three wave interaction [355], or equivalently, a vertex in a Feynman diagram with valence 3. Assume that the coupling coefficient in that vertex, i.e., the nonlinear ratio between the amplitude of the outgoing (quadratic) mode, and the incoming (linear) modes, scales as $\mathcal{R}(k) \sim |k|^\alpha$ for some positive power α. If the initial conditions are such that $A_k \sim k^{-(\alpha-\delta)}$ for any positive value of δ, perturbation theory will break down for sufficiently high wave number, regardless of how small the initial perturbations are.

How does this translate to our original problem? For a Schwarzschild BH, the angular number ℓ plays the role of the wave number k, and the leading order nonlinearity is quadratic. The amplitudes that are important in order to describe a breakdown of perturbation theory are the amplitudes of the metric perturbation, A_ℓ. Let us examine the $\ell \times 2$ coupling discussed above, where we observe precisely a linear growth with wave number $\mathcal{R}(\ell) \propto \ell$. Thus, if we could excite the BH with initial data such that $\ell A_\ell \to \infty$ as $\ell \to \infty$, perturbation theory would break down. We argue that such an initial spectrum is not physical. Indeed, consider a point particle being shot radially towards a Schwarzschild BH. If it is shot exactly towards the center, in the ultrarelativistic regime, this leads to a spectrum $A_\ell \sim \ell^{-2}$ [432]. Thus, this is clearly not enough to trigger an instability, since the high-frequency modes are not sufficiently excited. We can imagine an enhancement of this high-frequency content by increasing the impact parameter with which the particle is thrown into the BH, until reaching the critical impact parameter. Close to that value, we would expect the spectrum to be bounded by that of a massless particle orbiting the LR. In that case, the total energy diverges [47], but from the energy flux computed in a single orbit, we can estimate $A_\ell \sim \ell^{-3/2}$. Once again, this does not meet the condition we established to trigger a breakdown of perturbation theory.

A possible interpretation of this impossibility is that the nonlinear ratio in this case scales as $\mathcal{R}(\ell) \sim \omega(\ell)$, since, in the eikonal regime, $\omega_\ell = \Omega\ell + \mathcal{O}(\ell^0)$, where Ω is the orbital frequency of the LR. Thus, a breakdown of perturbation theory only occurs if the initial spectrum satisfies $A_\ell \omega_\ell \to \infty$. The Rayleigh-Jeans spectrum, typically associated with thermal states in hydrodynamics, is given by $A_\ell \omega_\ell = \text{const.}$ [355]. Therefore, not even a thermal state would be enough to trigger an instability. Perturbation theory of nonspinning BHs is safe.

5.5 CONCLUSIONS

The full nonlinear content of Einstein's equations is currently accessible only via simulations in numerical relativity. However, essential insight can be obtained with various degrees of approximation. The next step in a BH spectroscopy program requires the understanding of second-order effects. We uncovered essential aspects of such higher-order terms, demonstrating independence on initial conditions, and a strong but predictable dependence on the BH spin.

Remarkably, our results concerning the spin-dependence of the quadratic vs linear amplitudes ratio are in good agreement with the values reported from full nonlinear numerical simulations. These results are in agreement with numerical relativity simulations of scattering of wavepackets [476], and with frequency-domain perturbative calculations [277]. The predictability of the QQNM ratio from perturbation theory, and its solid observational prospects with LISA and third-generation detectors [464], make it an exciting prospect for testing General Relativity in the nonlinear regime, and expanding the breadth of BH spectroscopy to account for nonlinear effects.

Moreover, we have demonstrated that the QQNM ratios scale in a nontrivial way with the angular harmonic ℓ. Some of the angular mixing channels asymptote

constant values, hinting that calculations in the eikonal regime may be able to provide analytical estimates which are relatively accurate at moderate frequencies too. On the other hand, other angular channels such as the QQNM ratio $\mathcal{R}^{\ell+2}_{22\times\ell\ell}$ studied here appear to grow linearly with ℓ. This might seem to imply a breakdown of BH perturbation theory for some specific initial conditions. However, as argued above, these initial conditions need to be fine tuned and do not seem to be excited by simple physical processes, such as high-energy sources plunging into a BH. This opens a window towards exploring analytical methods to understand the high-frequency limit of the nonlinear ratio that excites quadratic modes in more generic configurations, as well as for Kerr BHs. The next chapter of this thesis 6 is devoted precisely to this, studying second-order perturbations of Kerr BHs in the high-frequency regime, by mapping the problem to studying perturbations on plane wave spacetimes, clarifying some of these questions.

6

QUADRATIC QUASINORMAL MODES AT THE LIGHTRING

Written while listening to music composed by Franz Schubert.

6.1 INTRODUCTION

Quadratic quasinormal modes (QQNMs) are an exciting prospect to probe gravity in the nonlinear regime. Chapter 5 showcased both the predictive power of perturbation theory and its rapidly increasing difficulty beyond linear order. In particular, the computational difficulty, and necessity to deal with numerical results, is not a desirable feature of a perturbative approach which is precisely implemented to avoid solving Einstein's equations numerically, but in their full glory.

Within the regime of linear perturbation theory, the high-frequency or eikonal limit provides a clear correspondence that allows for both analytical (or semianalytical) calculations with remarkable accuracy, as well as a powerful intuition, in order to understand the QNM frequencies of rotating BHs. This is based on a correspondence between QNMs and bound null geodesics (lightrings), which can be made precise by studying the high-frequency limit of the perturbation theory equations [68, 103, 219, 333, 358, 385, 422]. The question that we tackle in this chapter is whether this correspondence extends to QQNMs, and if so, whether the high frequency limit can allow for a tractable perturbation theory of rotating BHs beyond linear order. We anticipate that the answer is positive in both cases.

The key realization is that capturing non-linear effects perturbatively is most straightforward when the linearized problem is itself simple or under excellent control. On this account, the perturbation theories on curved space that are best understood are those on Lorentzian symmetric spaces: Minkowski [186, 451], Anti-de Sitter (AdS) [13, 112, 168, 170, 182, 214, 263, 314, 394, 412, 413], de Sitter (dS) [30, 56], or Cahen-Wallach (a class of plane waves [91]) spacetimes [212, 248, 334].

More recently, it has been appreciated that a version of the eikonal limit and the corresponding quasinormal modes can be captured by the physics of plane waves [196, 265]. The reason is that these plane waves appear in the limit of a geometry near null geodesics; a construction formalized by Penrose [373]. In particular, the Penrose limit near the lightring of a BH maps the local curvature dynamics, directly tied to high-frequency QNMs, to the dynamics of perturbations around a plane wave. This correspondence is particularly simple for the class of equatorial lightrings. In that case, the corresponding plane wave spacetime is a

Cahen-Wallach plane wave. It is thus reasonable to expect that a perturbation theory can be developed comparable in detail to those on AdS and dS backgrounds which, at least to some approximation, can be connected to an interesting aspect of BH mergers. It is this that we set out to do here more systematically. Notice that the high-frequency limit also has interesting observational perspectives, both connecting dynamical GW emission with lightring measurements [15, 264, 321], or in hierarchical triples [99, 418].

In this Chapter, we develop the framework to study second-order perturbations around plane waves. In particular we propose a partial gauge and frame fixing based on the geometry of algebraically type N spacetimes which we dub geodesic, parallel, and transverse (GPT) gauge. This gauge and frame fixing guarantees that the amplitudes of QQNMs on the Weyl scalar are physically meaningful, and invariant under the residual gauge freedom. We also present a complementary approach for second-order perturbations restricted to homogeneous plane waves, based on the construction of metric harmonics. Both frameworks are used to study the excitation of QQNMs in homogeneous plane waves arising as Penrose limits of the equatorial lightring of Kerr. We compute the ratio describing the excitability of QQNMs for arbitrary mode-coupling combinations, including all overtone indices, and uncover a set of selection rules, inherited from the algebraic properties of the background. Special cases of these ratios have also been discussed recently in Refs. [269, 377].

The remainder of this chapter is structured as follows. First, in section 6.2, we review plane wave spacetimes, and discuss how certain classes of plane waves emerge as approximate descriptions of lightrings for BH spacetimes. We emphasize that the approximation in particular captures an eikonal branch of quasinormal modes. Next, in section 6.3 we discuss perturbation theory up to second order, including a novel geometric gauge and frame-fixing approach on plane waves. Then we further restrict to homogeneous plane waves, specifically those describing equatorial lightring physics. We discuss mode solutions for this case, establishing their relationship with the simple and inverted harmonic oscillator in section 6.4, as well as discussing an alternative approach based on metric perturbations. Finally, we discuss the excitation of QQNMs, first for a nonlinear scalar toy model, and then for the full case of Einstein gravity in section 6.5.

Conventions. Notably this chapter uses a mostly minus metric signature $(+,-,-,-)$ and the Riemann tensor's sign given by $[\nabla_a, \nabla_b]V_c = R_{abcd}V^d$.

6.2 PLANE WAVES

In this work we consider nonlinear fluctuations about a family of background spacetimes that belong to the class of *plane waves*. In Brinkmann coordinates, the line element reads

$$ds^2 = -A_{ij}(u)x^i x^j du^2 + 2dudv - dx^2 - dy^2 \,. \tag{6.1}$$

where $x^i, x^j \in \{x, y\}$ and A_{ij} is an arbitrary symmetric matrix depending on the coordinate u. A more general discussion of parallel, plane-fronted waves can be found in [437]. That the spacetime metric (6.1) indeed describes a type of parallel, plane-fronted wave can be seen as follows. First, the metric takes the form of flat space (in double null coordinates) plus a gravitational deformation $\sim du^2$. In addition, the null vector field $\ell^a = (\partial_v)^a$ is covariantly-constant (or *parallel*),

$$\nabla_a \ell_b = 0\,, \tag{6.2}$$

so it is also a Killing vector field ($\nabla_{(a}\ell_{b)} = 0$). This shows that the gravitational deformation $\sim du^2$ propagates at the speed of light along ℓ^a. Finally, eq. (6.1) is plane-fronted in the sense that transverse surfaces of constant u, v are flat. It should be stressed, though, that the spacetimes (6.1) are not asymptotically flat, since the gravitational deformation extends infinitely along ℓ^a (see [251] for a discussion on the causal structure of pp-waves). The quadratic dependence in x and y of the deformation $\sim du^2$ is sometimes called the *plane-wave* condition. It allows us to interpret the spacetime (6.1) quite literally as a two-dimensional (potentially time-dependent) harmonic oscillator. This is seen easily in the case that $A_{ij}(u) = A_{ij}$ is a constant matrix. In that case, as it is also symmetric, without loss of generality it can also be taken to be diagonal. Denoting the eigenvalues to be $-\Omega^2$ and Λ^2, the metric has the following (complex-valued) Killing vectors,

$$a_\pm = \frac{e^{\pm i\Omega u}}{\sqrt{2\Omega}}\left(\pm i\Omega x \partial_v + \partial_x\right)\,, \quad b_\pm = \frac{e^{\mp \Lambda u}}{\sqrt{2\Lambda}}\left(\mp \Lambda y \partial_v + \partial_y\right)\,, \quad \mathbf{1} = i\partial_v\,. \tag{6.3}$$

These Killing vectors span the Heisenberg algebras of the simple and inverted harmonic oscillators,

$$[a_-, a_+] = \mathbf{1}\,, \quad [b_-, b_+] = i\mathbf{1}\,, \tag{6.4}$$

where all other commutators vanish. In the case of arbitrary $A_{ij}(u)$ one loses the isometry generated by ∂_u, but it can be shown that (6.1) still enjoys a Heisenberg Killing algebra (see e.g. [437]). We will distinguish three subcases within the geometry (6.1),

1. *General*: $\delta^{ij}A_{ij}(u) \neq 0$ and $A_{ij}(u) \neq$ constant.
2. *Vacuum*: $\delta^{ij}A_{ij}(u) = 0$,
3. *Homogeneous*: $A_{ij}(u) =$ constant.[1]

Whenever the vacuum condition holds, then eq. (6.1) is a Ricci-flat geometry for any u-dependence of $A_{ij}(u)$. The homogeneous case will still be of interest even when it

1 Note that this class should more properly be referred to as symmetric (or Cahen-Wallach [91]), homogeneous plane waves being slightly more general [77]. However, we believe that the analysis we do for this case would generalize to the broader class of homogeneous plane waves, although at an algebraic cost which we avoid in this work.

is not a solution of vacuum Einstein's equations, as it involves an additional Killing vector containing the u-direction. However, it is the vacuum and homogeneous case with ∂_u a Killing vector that will be of most relevance in this work.

In general, plane-wave spacetimes emerge naturally in several physical scenarios. Most importantly for our purposes, the geometries (6.1) appear as *Penrose limits* [76] as reviewed next.

6.2.1 *Penrose Limits*

In a precise sense, the spacetime in the neighborhood of a null geodesic γ resembles a gravitational plane wave. This observation follows after performing a specific "zoom-in" of the spacetime close to γ, known as a *Penrose limit* [373]. This is introduced by first writing the spacetime metric in Penrose coordinates (u, V, Y^i) adapted to the geodesic,[2]

$$ds^2 = 2dudV + a(u, V, Y^i)dV^2 + 2b_i(u, V, Y^i)dVdY^i + g_{ij}(u, V, Y^i)dY^i dY^j\,, \quad (6.5)$$

with $i, j = 1, 2$, and where $\partial_u = \nabla V$ is tangent to a twist-free null geodesic congruence. The latter can always be taken such that γ corresponds to the curve $(u, V = 0, Y^i = 0)$. Next, the idea consists in performing a "zoom-in" towards γ while "blowing-up" the spacetime metric in such a way that one recovers a finite, well-defined geometry. Precisely, this is realised by performing an inhomogeneous, constant coordinate re-scaling

$$(u, V, Y^i) = (u, \lambda^2\tilde{V}, \lambda\tilde{Y}^i)\,, \quad \lambda \in \mathbb{R}\,, \quad (6.6)$$

and then taking the limit

$$ds^2_\gamma := \lim_{\lambda\to 0} \lambda^{-2} ds^2 = 2dud\tilde{V} + g_{ij}(u, 0, 0)d\tilde{Y}^i d\tilde{Y}^j\,. \quad (6.7)$$

We say that ds^2_γ, obtained this way, is the Penrose limit of the original metric ds^2 along γ. Given that the Ricci tensor is invariant under constant conformal transformations, $R_{ab}(g) = R_{ab}(\lambda^2 g)$, it is guaranteed that if ds^2 is Ricci-flat, then so are its Penrose limits ds^2_γ. The coordinates $(u, \tilde{V}, \tilde{Y}^i)$ are known as *Einstein–Rosen* coordinates for the plane wave. These have the advantage of exhibiting manifestly many of the symmetries of spacetime but, in general, they are not globally defined. Instead, we choose to work in *Brinkmann coordinates* (u, v, x^i), which preserve γ as the curve $(u, v = 0, x^i = 0)$, are global coordinates, and cast the metric in the form of eq. (6.1) (see e.g. [77] for an explicit construction)

$$ds^2_\gamma = -A_{ij}(u)x^i x^j du^2 + 2dudv - dx^2 - dy^2\,. \quad (6.8)$$

Furthermore, it can be shown that in these coordinates the symmetric matrix $A_{ij}(u)$ is given by [78]

$$A_{ij}(u) = \mathrm{R}_{abcd}E^a_i E^b_+ E^c_j E^d_+\Big|_{\gamma(u)}\,, \quad (6.9)$$

2 Here we follow [76], where one can also find a description of the Penrose limit based on null Fermi normal coordinates.

where R_{abcd} is the Riemann tensor of the *original* spacetime, and (E^a_+, E^a_-, E^a_i) is a null frame where E^a_+ is tangent to a null congruence containing γ and E^a_-, E^a_i are parallelly-propagated along E^a_+. Equation (6.9) shows explicitly and covariantly the amount of information retained about the original spacetime, which is the same tidal information as encoded in the null geodesic deviation equation. In addition, it allows one to think of the Penrose limit formally as a map $(ds^2, \gamma) \mapsto A_{ij}(u)$ and yields a powerful way of computing it (especially using the 2-spinor formulation of (6.9), see [133, 445]). For example, the Penrose limit along an equatorial null geodesic in a Kerr BH reads [133] (see also [196, 246, 298, 371]),

$$ds^2 = -\frac{3Mb^2}{r(u)^5}\left(y^2 - x^2\right)du^2 + 2dudv - dx^2 - dy^2\,, \tag{6.10}$$

where M is the BH mass, $r(u)$ is a solution to the Kerr geodesic equation for the radial coordinate, and $b = \mathcal{L}/\mathcal{E}$ is the geodesic's "impact parameter", with $\mathcal{E}, \mathcal{L}$ its conserved energy and azimuthal angular momentum. In general, this is an inhomogeneous plane wave, but it becomes homogeneous if one chooses the equatorial geodesic to be one of the lightrings, where $r(u) = constant$. In that situation, the coordinates x and y can be thought of as measuring the distance away from the original geodesic along the polar and radial directions, respectively. This case is discussed in detail in Section 6.4, and is of special importance due to the correspondence between these lightrings and the eikonal regime of QNMs.

6.2.2 *Algebraic Description*

According to Petrov's classification (see Chapter 2), the plane wave spacetime (6.1) is of type IV (also known as type N) where the unique principal null direction (PND) is defined by the parallel null vector ∂_v. Consequently, the geometry (6.1) has a very simple description in terms of the GHP formalism. Indeed, in terms of the null frame

$$\ell = \partial_v\,, \quad n = \partial_u + \frac{A_{ij}(u)}{2}x^i x^j \partial_v\,, \quad m = \left(\partial_x + i\partial_y\right)/\sqrt{2}\,, \tag{6.11}$$

all spin coefficients and Weyl scalars vanish except for

$$\kappa' = \frac{1}{2\sqrt{2}}(\partial_x - i\partial_y)\left(A_{ij}(u)x^i x^j\right)\,, \qquad \Psi_4 = -\frac{1}{4}(\partial_x - i\partial_y)^2\left(A_{ij}(u)x^i x^j\right)\,, \tag{6.12}$$

and their complex conjugates. In particular, this means that the directional GHP derivatives are just the ordinary directional derivatives along the null frame (6.11), since the GHP connection vanishes. One can easily verify the GHP-covariant expressions,

$$\text{Þ}\kappa' = 0\,, \qquad \text{Þ}\Psi_4 = 0\,, \qquad \eth'\kappa' = -\Psi_4\,, \tag{6.13}$$

which will be useful in the next sections. Other useful expressions that only hold in the particular frame (6.11) are

$$\kappa' = \frac{1}{2}\eth'\left(A_{ij}(u)x^i x^j\right)\,, \qquad \Psi_4 = -\frac{1}{2}\eth'^2\left(A_{ij}(u)x^i x^j\right)\,, \qquad \eth\kappa' = \frac{1}{2}\delta^{ij}A_{ij}(u)\,,$$

(6.14)

and the wave operator is

$$\Box \equiv \nabla^a \nabla_a = 2(\text{þ}'\text{þ} - \text{ð}'\text{ð})\,. \tag{6.15}$$

As is often the case in algebraically special spacetimes, the fact that most GHP quantities of the background vanish will drastically simplify the analysis of gravitational fluctuations. This is therefore the approach to perturbation theory that we take next.

6.3 PERTURBATION THEORY

Throughout this section we will consider vacuum plane waves, thus setting $\delta^{ij}A_{ij}(u) = 0$ in eq. (6.1). Our goal is to describe the propagation of linear and quadratic gravitational fluctuations on such backgrounds. The approach presented here focuses on solving for the fluctuations of the spacetime curvature, rather than the fluctuations of the metric itself, given that these capture the physical degrees of freedom of the gravitational field. In section 6.4.2 we will instead show how to address the problem from a pure metric perspective in the special case of homogeneous background plane waves.

Our formalism follows as closely as possible the formalism introduced for perturbations of Kerr BHs in Chapter 4. However, the gauge choices are adapted to the geometry of plane waves. This is made manifest by our choice of a perturbed tetrad, which does not match the choice of Ref. [95], see (4.46).

Our starting point is the projection of the Penrose Wave equation (2.9) onto the spin dyad leg parallel to the PND, which we already wrote in (4.21). We remind the reader of our notation, where every quantity $\mathcal{Q}$ is assumed to admit a formal perturbative expansion

$$\mathcal{Q} = \mathcal{Q}^\circ + \epsilon\dot{\mathcal{Q}} + \frac{1}{2!}\epsilon^2\ddot{\mathcal{Q}} + ... \tag{6.16}$$

Here $\mathcal{Q}^\circ$ denotes the value of $\mathcal{Q}$ in the plane wave background, $\epsilon \ll 1$ is a perturbative book-keeping parameter (that we omit in general) and the over-dot notation stands for the operators $\dot{\mathcal{Q}} = d\mathcal{Q}/d\epsilon|_{\epsilon=0}$, $\ddot{\mathcal{Q}} = d^2\mathcal{Q}/d\epsilon^2|_{\epsilon=0}$, etc, and should not be confused with a total space or time derivative of $\mathcal{Q}$. We will sometimes abuse the notation and write $\mathcal{Q}^\circ = \mathcal{Q}$ if there is no risk of confusion.

Taking into account that the only non-vanishing GHP quantities of our background are κ' and Ψ_4 given by (6.12), eq. (**??**) expanded at first- and second-order readily gives

$$\text{First order:} \quad (\text{þ}'\text{þ} - \text{ð}'\text{ð})\,\dot{\Psi}_0 = 0\,, \tag{6.17}$$

$$\text{Second order:} \quad (\text{þ}'\text{þ} - \text{ð}'\text{ð})\,\ddot{\Psi}_0 = -2\left(\dot{\mathscr{O}}_0\dot{\Psi}_0 + \dot{\mathscr{O}}_1\dot{\Psi}_1 + \dot{\mathscr{O}}_2\dot{\Psi}_2\right)\,. \tag{6.18}$$

At first order, one encounters a decoupled equation for $\dot{\Psi}_0$, which is analogous to Teukolsky's equation for $\dot{\Psi}_0$ [441], see (4.26). However, as in the case of perturbations of Kerr, the second order equation requires knowledge of the full metric perturbation at first order. Before computing this, let us begin by discussing the gauge freedom at first and second order in perturbation theory.

6.3.1 *Gauge Considerations*

Following the general transformation rules (recall (4.57)), in a plane wave background, the Weyl scalar Ψ_0 is fully gauge-invariant at first order, but not at second and higher orders,

$$\ddot{\Psi}_0 \mapsto \ddot{\Psi}_0 + 2\mathfrak{L}_{\dot{\xi}}\ddot{\Psi}_0 + 8\dot{b}\dot{\Psi}_1 + 4(\dot{\Lambda} + i\dot{\theta})\dot{\Psi}_0\,, \tag{6.19}$$

where the notation for frame rotations was introduced in (2.14). In particular, only first-order gauge parameters contribute to the transformation, but not second-order ones $(\ddot{\xi}^a, \ddot{a}, ...)$. This is due to the fact that $\ddot{\Psi}_0$ is itself gauge-invariant. Our approach to deal with gauge symmetry in this work consists in fixing partially the *linear* gauge freedom, by imposing some conditions that are both physically and mathematically well-defined. This ensures that several quantities we compute related to $\ddot{\Psi}_0$ are physically meaningful, and invariant under the residual gauge freedom. This applies specially to the QQNM excitation ratios computed in section 6.5.

Consider a spacetime that is a vacuum deformation of our plane wave. We chose our frame so that ℓ^a is tangent to a twist free geodesic null congruence, and n^a and m^a are parallelly-propagated along ℓ^a, that is,

$$\ell_a = \nabla_a u\,, \quad \ell^a\nabla_a\ell^b = \ell^a\nabla_a n^b = \ell^a\nabla_a m^b = 0\,, \tag{6.20}$$

where u is a function satisfying $\nabla^a u\nabla_a u = 0$ (which implies $\ell^a\nabla_a\ell_b = 0$ automatically). Notice this frame can always be constructed, at least locally. Thus, eqs. (6.20) are exact statements that are valid to all orders, in particular they hold for our background frame (6.11), and imply the vanishing of several spin coefficients and their fluctuations. With this choice, we will be able to impose three geometric conditions that define our linear gauge, up to certain residual freedom. We describe them next, showing that each condition can always be met for any solution to the linear equations, and identifying the remaining gauge transformations that preserve them.

1. *Geodesic condition*: Our first gauge choice is to set

$$\dot{\ell}_a = 0\,. \tag{6.21}$$

That this is always possible can be seen as follows. Linearising the first equation in (6.20), we find $\dot{\ell}_a = \nabla_a\dot{u}$, and this can be set to zero through a diffeomorphism with $\dot{\xi}_v = -\dot{u}$ (where $\dot{\xi}_v = \ell^a\dot{\xi}_a$). Notice that the choice (6.21) is equivalent to taking the function u, which satisfies $\nabla^a u\nabla_a u = 0$ nonperturbatively, as a coordinate. This fact motivates calling eq. (6.21) the geodesic condition.

The gauge parameters that leave (6.21) invariant satisfy

$$0 = \mathfrak{L}_{\dot{\xi}}\ell_a + \dot{\bar{b}}m_a + \dot{b}\bar{m}_a + \dot{\Lambda}\ell_a\,, \tag{6.22}$$

and projecting this equation along the null frame, we find

$$\partial_v\dot{\xi}_v = 0\,, \quad \dot{b} = m^a\nabla_a\left(\dot{\xi}_v\right)\,, \quad \dot{\Lambda} = -n^a\nabla_a\left(\dot{\xi}_v\right)\,. \tag{6.23}$$

That is, the generators of class II and class III rotations $\dot{b}$ and $\dot{\Lambda}$ cannot act independently, but only together with a diffeomorphism whose component $\dot{\xi}_v$ is v-independent. Finally, we remark that in this gauge $h_{vv} = -(g^{ab}\ell_a\ell_b)^{\cdot} = 0$.

2. *Transverse condition*: The next gauge choice is

$$\ell^a h_{ab} = 0\,. \tag{6.24}$$

To show that this gauge can always be achieved, consider acting on any solution h_{ab} with a diffeomorphism whose component $\dot{\xi}_v$ is constant, while the remaining components are generic and denoted $\dot{\xi}_I \equiv \{\dot{\xi}_u, \dot{\xi}_x, \dot{\xi}_y\}$. This satisfies (6.23) so it preserves (6.21). Then, imposing that the transformed metric satisfies (6.24) one immediately finds

$$0 = \ell^a(h_{ab} + 2\nabla_{(a}\dot{\xi}_{b)}) \quad \Longrightarrow \quad \dot{\xi}_I = -\int h_{vI}dv\,, \quad \text{with} \quad I = \{u, x, y\}\,. \tag{6.25}$$

In obtaining this, it is useful to notice that in our coordinates $\Gamma^a_{bv} = 0$, and that since (6.21) holds then $h_{vv} = 0$. Now, imposing that the gauge parameters leave invariant (6.21) (so $\partial_v\dot{\xi}_v = 0$) and (6.24), it readily follows that

$$\dot{\xi}_I = -v\partial_I\dot{\xi}_v + \dot{C}_I\,, \quad \partial_v\dot{C}_I = 0\,, \quad \text{with} \quad I = \{u, x, y\}\,, \tag{6.26}$$

where $\dot{C}_I$ are v-independent functions that arise as integration constants. Thus, the diffeomorphisms allowed by (6.21) and (6.24) are entirely fixed by the v-independent functions $\dot{\xi}_v$ and $\dot{C}_I$ through (6.26), although we notice that in general $\dot{\xi}_I$ can exhibit a linear dependence on v. We also remark that in this gauge $(\ell^a)^{\cdot} = \left(g^{ab}\ell_b\right)^{\cdot} = -h^{ab}\ell_b = 0$. For a discussion on the transverse gauge condition in more general (type II) spaces we refer the reader to [388].

3. *Parallel condition*: The final requirement follows by consistency with our non-perturbative choice eq. (6.20), that the frame is parallelly propagated along ℓ_a. At linear order, that statement reads

$$\left(\ell^b\nabla_b X_a\right)^{\cdot} = \ell^b\nabla_b\dot{X}_a - \dot{\Gamma}^c{}_{ab}X_c\ell^b = 0\,, \tag{6.27}$$

where we used that $(\ell^a)^{\cdot} = 0$ and defined

$$\dot{\Gamma}^a{}_{bc} \equiv \frac{1}{2}g^{ad}\left(\nabla_b h_{cd} + \nabla_c h_{bd} - \nabla_d h_{bc}\right)\,, \quad X_a \equiv \{\ell_a, n_a, m_a\}\,. \tag{6.28}$$

Assuming that the geodesic and transverse conditions (eqs. (6.21) and (6.24)) hold, it can be verified by direct computation that

$$\begin{aligned}\dot{n}^a &= \frac{1}{2}\left(-h_{nn}\ell^a + h_{n\bar{m}}m^a + h_{nm}\bar{m}^a\right)\,,\\ \dot{m}^a &= \frac{1}{2}\left(-h_{nm}\ell^a + h_{m\bar{m}}m^a + h_{mm}\bar{m}^a\right)\,,\end{aligned} \tag{6.29}$$

is parallely propagated along ℓ^a, i.e., it satisfies eq. (6.27), and it is also a well-defined perturbed GHP frame since it satisfies

$$h_{ab} = 2\left(\ell_{(a}\dot{n}_{b)} - \dot{m}_{(a}\bar{m}_{b)} - m_{(a}\dot{\bar{m}}_{b)}\right) . \tag{6.30}$$

We notice that this frame can also be obtained by applying to the frame in Ref. [95] a linear class II rotation with parameter $\dot{a} = (1/2)h_{nm}$. Finally, requiring that the gauge parameters leave invariant the parallel condition eq. (6.27) only imposes two new constraints,

$$\partial_v \dot{a} = \partial_v \dot{\theta} = 0\,, \tag{6.31}$$

as can be readily checked.

In sum, we have found that at linear order it is always possible to impose the geodesic, parallel and transverse conditions (equations (6.21), (6.24) and (6.27) respectively), and we should call this the geodesic, parallel and transverse (GPT) gauge. We have also shown that the gauge parameters generating the residual gauge freedom are fixed by the v-independent (but otherwise arbitrary) functions $\dot{\xi}_v, \dot{C}_I, \dot{a}, \dot{\theta}$, through equations (6.23) and (6.26).

The fact that the GPT gauge is based on a frame parallelly-propagated along a null geodesic ensures that the associated curvature scalars are physically meaningful (the choice of a non-inertial null frame could induce unphysical features on the corresponding Weyl scalars). In addition, although the GPT gauge still allows a significant amount of gauge freedom, we will see that the corresponding transformation of $\ddot{\Psi}_0$ (given in (6.19)) leaves invariant the observables we will focus on in section 6.5.

6.3.2 *First-order Perturbations*

In order to reconstruct the metric perturbation $\dot{h}_{ab}$ in terms of the linearised curvature fluctuation $\ddot{\Psi}_0$, we follow the adjoint operator method (CCK metric reconstruction) already presented in Chapter 4. Given a GHP scalar $\Psi_H \overset{\circ}{=} (-4, 0)$ that satisfies the wave equation

$$\left(\text{þ}'\text{þ} - \text{ð}'\text{ð}\right)\Psi_H = 0\,, \tag{6.32}$$

one can generate a solution for the metric perturbation in the transverse gauge (6.24) by simply acting on Ψ_H with differential operators. We refer to Ψ_H as the *Hertz potential*. In turn, from the reconstructed metric perturbation and benefiting from the work done in Section 6.3.1, the complete solution for the GHP quantities in the GPT gauge can be obtained in terms of Ψ_H. Once we have the action of the adjoint operator $\mathcal{S}_0^\dagger$, we find the metric perturbation, and from that, everything follows in a straightforward manner. We list the solution next, where the quantities that vanish are omitted:

- *Metric perturbation*:

$$\begin{aligned}\dot{h}_{ab} = &- \ell_a\ell_b\left(\eth^2\Psi_H + \eth'^2\bar{\Psi}_H\right) + 2\ell_{(a}m_{b)}\text{Þ}\eth\Psi_H + 2\ell_{(a}\bar{m}_{b)}\text{Þ}\eth'\bar{\Psi}_H \\ &- m_am_b\text{Þ}^2\Psi_H - \bar{m}_a\bar{m}_b\text{Þ}^2\bar{\Psi}_H\,,\end{aligned} \tag{6.33}$$

  which satisfies the transverse condition $\ell^a h_{ab} = 0$.

- *Frame perturbations*:

$$\dot{n}_a = \frac{1}{2}\left(\ell_a\eth^2\Psi_H - m_a\text{Þ}\eth\Psi_H\right) + \text{c.c.}\,, \quad \dot{m}_a = \frac{1}{2}\left(\ell_a\text{Þ}\eth'\bar{\Psi}_H - \bar{m}_a\text{Þ}^2\bar{\Psi}_H\right)\,, \tag{6.34}$$

  which follow by plugging (6.33) into eq. (6.29), and is automatically in the geodesic and parallel gauge.

- *GHP spin coefficients*:

$$\dot{\kappa}' = \frac{1}{2}\eth'^3\bar{\Psi}_H\,, \quad \dot{\rho}' = \frac{1}{2}\eth'^2\text{Þ}\bar{\Psi}_H\,, \quad \dot{\sigma} = -\frac{1}{2}\text{Þ}^3\bar{\Psi}_H\,, \quad \dot{\tau} = -\frac{1}{2}\eth'\text{Þ}^2\bar{\Psi}_H\,, \tag{6.35}$$

  which follow by simply perturbing their definitions and plugging (6.33) and (6.34) in the resulting expressions. We also used the equation satisfied by the Hertz potential (6.32) in order to simplify expressions and show that several perturbations of spin coefficients vanish. As expected, $\dot{\kappa} = \dot{\rho} = 0$, signalling that ℓ remains a geodesic, twist-free congruence in the perturbed spacetime.

- *GHP connection 1-form*:

$$\dot{\omega}_a = -\frac{1}{2}\left(\eth'^2\text{Þ}\bar{\Psi}_H\right)\ell_a + \frac{1}{2}\left(\eth'\text{Þ}^2\bar{\Psi}_H\right)\bar{m}_a\,, \tag{6.36}$$

  which again follows by perturbing the definition of ω_a and using (6.33) and (6.34).

- *Weyl Scalars*:

$$\dot{\Psi}_n = -\frac{1}{2}\text{Þ}^{(4-n)}\eth'^n\bar{\Psi}_H\,, \tag{6.37}$$

  obtained again by perturbing their definitions and using (6.33) and (6.34). In order to present the Weyl scalars in this simple form, we also used the Hertz potential equation (6.32).

Before considering second order perturbations, let us show how from (6.37) a version of the *Teukolsky-Starobinsky identities* on type N spacetimes follows:

$$\text{Þ}^m\eth'^{4-m}\dot{\Psi}_n = \text{Þ}^{4-n}\eth'^n\dot{\Psi}_{4-m}\,, \quad (0 \leq m, n \leq 4)\,, \tag{6.38}$$

which relate the perturbations of the various Weyl scalars among themselves. Although these expressions have been obtained by working in the GPT gauge, we remark that the only ones that are not gauge-invariant in general are those involving $\{\dot{\Psi}_3, \dot{\Psi}_4\}$.

6.3.3 *Second-order Perturbations*

With the solution and operators introduced in Section 6.3.2, it is straightforward to obtain the source term of the second-order Teukolsky equation. The procedure is not too different than in obtaining (4.61), where we make extensive use of the perturbed GHP operators, in order to keep GHP covariance order by order. We find

$$\left(\text{þ}'\text{þ}-\text{ð}'\text{ð}\right)\dot{\Psi}_0=-2\left(\dot{\mathscr{O}}_0\Psi_0+\dot{\mathscr{O}}_1\Psi_1+\dot{\mathscr{O}}_2\Psi_2\right)\equiv\mathcal{S}_+ +\mathcal{S}_-\,, \tag{6.39}$$

where

$$\begin{aligned}2\mathcal{S}_+ =&\left(\text{þ}^6\bar{\Psi}_H\right)\left(\text{ð}'^2\bar{\Psi}_H\right)+4\left(\text{þ}^5\bar{\Psi}_H\right)\left(\text{ð}'^2\text{þ}\bar{\Psi}_H\right)+6\left(\text{þ}^2\text{ð}'^2\bar{\Psi}_H\right)\left(\text{þ}^4\bar{\Psi}_H\right)\\&+4\left(\text{þ}^3\bar{\Psi}_H\right)\left(\text{ð}'^2\text{þ}^3\bar{\Psi}_H\right)+\left(\text{þ}^2\bar{\Psi}_H\right)\left(\text{ð}'^2\text{þ}^4\bar{\Psi}_H\right)-2\left(\text{ð}'\text{þ}\bar{\Psi}_H\right)\left(\text{ð}'\text{þ}^5\bar{\Psi}_H\right)\\&-6\left(\text{ð}'\text{þ}^3\bar{\Psi}_H\right)^2-8\left(\text{ð}'\text{þ}^2\bar{\Psi}_H\right)\left(\text{ð}'\text{þ}^4\bar{\Psi}_H\right),\end{aligned} \tag{6.40}$$

$$2\mathcal{S}_- =\left(\text{þ}^2\Psi_H\right)\left(\text{ð}^2\text{þ}^4\bar{\Psi}_H\right)+\left(\text{ð}^2\Psi_H\right)\left(\text{þ}^6\bar{\Psi}_H\right)-2\left(\text{ðþ}\Psi_H\right)\left(\text{ðþ}^5\bar{\Psi}_H\right). \tag{6.41}$$

It is useful to distinguish these two terms depending on whether they involves products of $\bar{\Psi}_H$ with itself (in $\mathcal{S}_+$), or combinations of Ψ_H with $\bar{\Psi}_H$ (in $\mathcal{S}_-$). These will lead to source terms which oscillate with different frequencies, so we refer to these as the $++$ and the $+-$ channels. The master equation (6.39) describes generic second order curvature fluctuations on a non-homogeneous plane wave background, in terms of the Hertz potential which generates the first order metric fluctuations. We note that, when written in coordinates, our source term reduces to previous results in the literature [269], although this agreement was not entirely expected given that frame gauges are different.

6.4 HOMOGENEOUS PLANE WAVES

The previous discussion and results are valid for the general vacuum plane waves (6.1), which have arbitrary symmetric $A_{ij}(u)$ of vanishing trace. From now on we will restrict to homogeneous plane waves of the form

$$ds^2=-\left(\Lambda^2y^2-\Omega^2x^2\right)du^2+2dudv-dx^2-dy^2\,, \tag{6.42}$$

for which the analysis simplifies. However, as noted in Section 6.2.1, such spacetimes still capture physical regimes of great interest – they emerge as the Penrose limit along the equatorial LRs of a Kerr BH.

In more detail, the LR Penrose limit of a Kerr BH with mass M and dimensionless angular momentum a/M yields the metric (6.42) with $\Lambda = \Omega$, and[3]

$$\Omega_{\rm p,r} = \Lambda_{\rm p,r} = \frac{12M\left(r_{\rm p,r}^2 - 2Mr_{\rm p,r} + a^2\right)}{(r_{\rm p,r} - M)^2 r_{\rm p,r}^3}\,, \qquad r_{\rm p,r} = 2M\left[1 + \cos\left(\frac{2}{3}\arccos(\mp a/M)\right)\right], \tag{6.43}$$

where $r_{\rm p,r}$ are the prograde and retrograde radii of the equatorial LRs. We notice that the vacuum condition $\Lambda = \Omega$ holds in (6.43), since the Penrose limit of a Ricci-flat solution like Kerr is Ricci-flat, too. However, below we will retain some more generality by allowing $\Lambda \neq \Omega$ and assume $\Lambda, \Omega > 0$, unless stated otherwise.

6.4.1 *Scalar Wave Equation*

The wave equation in a general plane wave $\Box\Phi = 0$ is simply given by

$$2\Phi_{,uv} - \Phi_{,xx} - \Phi_{,yy} + A_{ij}x^i x^j \Phi_{,vv} = 0\,. \tag{6.44}$$

Thus, if $A_{ij}x^i x^j = \Lambda^2 y^2 - \Omega^2 x^2$, we can find solutions of the form

$$\Phi = e^{ip_u u + ip_v v} X(x) Y(y)\,, \tag{6.45}$$

for (at this point) arbitrary values of p_u, p_v. Solutions of the form (6.45) are just one of several ways to separate the wave equation on plane wave spacetimes. Notably, a separation in Rosen coordinates (6.7) is also possible, which has a slightly different flavour. However, it will be solutions of the form (6.45) that most explicitly have a close connection to QNMs. Plugging in the ansatz (6.45) leads to two separated equations

$$\begin{aligned} X'' - p_v^2\Omega^2 x^2 X &= (C - p_u p_v)X\,, \\ Y'' + p_v^2\Lambda^2 y^2 Y &= -(C + p_u p_v)Y\,, \end{aligned} \tag{6.46}$$

where C is a separation constant. We immediately recognise the equations for the simple and inverted harmonic oscillators (SHO and IHO, respectively), with an extra term. We comment on the well-known algebraic relation between modes on symmetric plane waves and the SHO and IHO below. For now, we simply remark that the general solution can be written in terms of parabolic cylindric functions.

If we see these plane waves as corresponding to the Penrose limit of a LR, then the x direction corresponds to the periodic θ direction, whereas the y direction is the radial direction with respect to the BH. In [196] it was argued that mode

3 Remark that, from the perspective of the plane wave (6.42), one can always scale $u \to cu$ and $v \to v/c$. From the perspective of the Penrose limit, this would amount to choosing a different affine time parameter. The choice (6.43) chooses this affine time to relate directly to the asymptotic Killing time with respect to which the quasinormal modes in the BH spacetime are defined, to straightforwardly compare.

solutions that are regular (bounded) along the x direction, and purely outgoing (and in fact asymptotically divergent) along the y direction oscillate at the same QNM frequencies as eikonal QNMs in Kerr. This is the class of solutions we will be focusing on. To that aim, let us first introduce the following family of off-shell modes,

$$\Phi^{(p_u,p_v,n_x,n_y)} \equiv e^{iup_u+ivp_v-|p_v|\Omega\frac{x^2}{2}-ip_v\Lambda\frac{y^2}{2}}\mathcal{N}_{(p_v,n_x,n_y)}H_{n_x}\left(\sqrt{|p_v|\Omega}x\right)H_{n_y}\left(\sqrt{ip_v\Lambda}y\right), \tag{6.47}$$

with n_x, n_y non-negative integers, $H_{n_{x,y}}(\xi)$ denote Hermite polynomials, and we choose normalization factors $\mathcal{N}_{(p_v,n_x,n_y)}$ given by

$$\mathcal{N}_{(p_v,n_x,n_y)} = \begin{cases} \frac{1}{2^{n_x+n_y}\pi}\Gamma\left(\frac{1-n_x}{2}\right)\Gamma\left(\frac{1-n_y}{2}\right), & n_x, n_y \text{ even}, \\ \frac{1}{2^{n_x+n_y}\pi n_y}\Gamma\left(\frac{1-n_x}{2}\right)\Gamma\left(1-\frac{n_y}{2}\right), & n_x \text{ even}, n_y \text{ odd}, \\ \frac{1}{2^{n_x+n_y}\pi n_x}\Gamma\left(1-\frac{n_x}{2}\right)\Gamma\left(\frac{1-n_y}{2}\right), & n_x \text{ odd}, n_y \text{ even}, \\ \frac{1}{2^{n_x+n_y}\pi n_x n_y}\Gamma\left(1-\frac{n_x}{2}\right)\Gamma\left(1-\frac{n_y}{2}\right), & n_x, n_y \text{ odd}. \end{cases} \tag{6.48}$$

This normalization guarantees that when evaluated at the location of the central geodesic $x = y = 0$, corresponding to the original geodesic whenever the plane wave spacetime is a Penrose limit, the mode is normalized to 1 when it is non-vanishing. If instead the mode vanishes there, the constant guarantees that its x- and y-derivatives at $x = y = 0$ are given by a natural dimensionful quantity, independent of the mode number ($\sqrt{|p_v|\Omega}$ for the x-direction and $\sqrt{ip_v\Lambda}$ for the y-direction). The modes (6.47) are eigenfunctions of the wave operator,

$$\Box\Phi^{(p_u,p_v,n_x,n_y)} = 2p_v\left[\text{sgn}(p_v)\Omega\left(n_x+\frac{1}{2}\right)+i\Lambda\left(n_y+\frac{1}{2}\right)-p_u\right]\Phi^{(p_u,p_v,n_x,n_y)}, \tag{6.49}$$

so, solutions to the free wave equation (or similarly the equation for the Hertz potential (6.32)) are simply eigenfunctions corresponding to the zero eigenvalue. This imposes a quantization condition for p_u:

$$p_u = \text{sgn}(p_v)\Omega\left(n_x+\frac{1}{2}\right)+i\Lambda\left(n_y+\frac{1}{2}\right). \tag{6.50}$$

Since we are assuming $\Omega, \Lambda > 0$, these modes are purely outgoing in the y-direction and decay exponentially along u, while their real frequencies p_v can have arbitrary sign.

The quantization condition allows us to establish a dictionary between the modes of a plane wave which emerges as the Penrose limit of the equatorial LR of a Kerr BH, with the high frequency or eikonal limit of the BH QNMs. Indeed, let $p_v = m\Omega_{\text{p,r}}$ correspond to the azimuthal harmonic number, and let $n_x = \ell - |m|$, $n_y = n$. Here, ℓ is the polar spherical harmonic index, and n is used to denote

the overtone index. Using this dictionary, and plugging in the value of Ω and Λ given in Eq. (6.43), we find that $p_u = \omega_{\ell mn}$ becomes the subleading correction to the frequency of QNMs in the eikonal or high frequency regime [196].

A more algebraic approach to the modes (6.47) starts from the observation that, in homogeneous plane waves, the isometry algebra generators are

$$\begin{aligned} a_\pm =& \frac{e^{\pm i\Omega u}}{\sqrt{2\Omega}} \left(\pm i\Omega x \partial_v + \partial_x\right) , \quad b_\pm = \frac{e^{\mp \Lambda u}}{\sqrt{2\Lambda}} \left(\mp \Lambda y \partial_v + \partial_y\right) , \\ \mathbf{1} =& i\partial_v , \quad H_{\Omega,\Lambda} = \mp i\partial_u . \end{aligned} \tag{6.51}$$

These span the harmonic oscillator algebra

$$[a_-, a_+] = \mathbf{1} , \quad [H_\Omega, a_\pm] = \pm\Omega a_\pm , \quad [b_-, b_+] = i\mathbf{1} , \quad [H_\Lambda, b_\pm] = \mp i\Lambda b_\pm . \tag{6.52}$$

This implies in particular that $a_\pm$ and $b_\pm$ act, through the Lie derivative, as "raising" and "lowering" operators for the n_x and n_y modes (6.47). Specifically, defining the number operators $N_x = -\mathfrak{L}_{a_+}\mathfrak{L}_{a_-}$ and $N_y = i\mathfrak{L}_{b_+}\mathfrak{L}_{b_-}$ these modes are such that

$$\begin{aligned} N_x \Phi^{(p_u,p_v,n_x,n_y)} &= -\mathfrak{L}_{a_+}\mathfrak{L}_{a_-}\Phi^{(p_u,p_v,n_x,n_y)} = n_x p_v \Phi^{(p_u,p_v,n_x,n_y)} , \\ N_y \Phi^{(p_u,p_v,n_x,n_y)} &= i\mathfrak{L}_{b_+}\mathfrak{L}_{b_-}\Phi^{(p_u,p_v,n_x,n_y)} = n_y p_v \Phi^{(p_u,p_v,n_x,n_y)} , \\ \mathfrak{L}_{\partial_u}\Phi^{(p_u,p_v,n_x,n_y)} &= i p_u \Phi^{(p_u,p_v,n_x,n_y)} , \\ \mathfrak{L}_{\partial_v}\Phi^{(p_u,p_v,n_x,n_y)} &= i p_v \Phi^{(p_u,p_v,n_x,n_y)} . \end{aligned} \tag{6.53}$$

Up to the normalization, for $p_v > 0$, they could have thus been generated by acting with $\mathfrak{L}_{a_+}$ and $\mathfrak{L}_{b_+}$ on the fundamental (Gaussian) mode $\Phi^{(p_u,p_v,0,0)}$. However, for $p_v < 0$, it is in fact a_+ that acts as a lowering operator while a_- is the raising operator.

This algebraic approach to the mode functions (6.47) is of course well-known, so we will not go into further details here. However, before using these modes, together with the simple form of the wave operator acting on them (6.49), to go to higher order in perturbation theory by solving the master equation (6.39), we will discuss how the same algebraic approach can just as well be used to approach the metric perturbations head-on. We should point out here that in a different ("coherent state" as opposed to "number") basis, not particularly well-suited to the description of QNMs, tensor harmonics on plane wave spacetimes have also been described for instance in [10, 334].

The above discussion is strictly only valid for the symmetric plane waves (6.42), which are a special case of homogeneous plane waves of special interest in relation to the Penrose limit of equatorial lightrings. However, any homogeneous plane wave has an additional Killing vector involving (though not necessarily identically to) ∂_u to extend the Heisenberg algebra (6.52) common to all plane waves. Thus, while not as simple as (6.53), we expect that the above discussion as well as the remainder of this section can be generalized beyond the symmetric plane waves to homogeneous plane waves [77, 78, 192].

6.4.2 *Metric Perturbations*

Just as the scalar wave equation reduced to an algebraic expression when acting on the modes satisfying (6.53), the linearized Einstein equations around a homogeneous plane wave will turn out to reduce to algebraic equations in terms of (symmetric) tensor modes $h_{ab}^{(p_u,p_v,n_x,n_y)}$ which satisfy[4]

$$\begin{aligned} N_x h_{ab}^{(p_u,p_v,n_x,n_y)} &= -\mathfrak{L}_{a_+}\mathfrak{L}_{a_-} h_{ab}^{(p_u,p_v,n_x,n_y)} = n_x p_v h_{ab}^{(p_u,p_v,n_x,n_y)} , \\ N_y h_{ab}^{(p_u,p_v,n_x,n_y)} &= i\mathfrak{L}_{b_+}\mathfrak{L}_{b_-} h_{ab}^{(p_u,p_v,n_x,n_y)} = n_y p_v h_{ab}^{(p_u,p_v,n_x,n_y)} , \\ \mathfrak{L}_{\partial_u} h_{ab}^{(p_u,p_v,n_x,n_y)} &= i p_u h_{ab}^{(p_u,p_v,n_x,n_y)} , \\ \mathfrak{L}_{\partial_v} h_{ab}^{(p_u,p_v,n_x,n_y)} &= i p_v h_{ab}^{(p_u,p_v,n_x,n_y)} . \end{aligned} \tag{6.54}$$

For each set of mode numbers (p_u, p_v, n_x, n_y), there will be ten independent such modes. Four of those, generated by similarly constructed vector modes $V_a^{(p_u,p_v,n_x,n_y)}$

$$\begin{aligned} N_x V_a^{(p_u,p_v,n_x,n_y)} &= -\mathfrak{L}_{a_+}\mathfrak{L}_{a_-} V_a^{(p_u,p_v,n_x,n_y)} = n_x p_v V_a^{(p_u,p_v,n_x,n_y)} , \\ N_y V_a^{(p_u,p_v,n_x,n_y)} &= i\mathfrak{L}_{b_+}\mathfrak{L}_{b_-} V_a^{(p_u,p_v,n_x,n_y)} = n_y p_v V_a^{(p_u,p_v,n_x,n_y)} , \\ \mathfrak{L}_{\partial_u} V_a^{(p_u,p_v,n_x,n_y)} &= i p_u V_a^{(p_u,p_v,n_x,n_y)} , \\ \mathfrak{L}_{\partial_v} V_a^{(p_u,p_v,n_x,n_y)} &= i p_v V_a^{(p_u,p_v,n_x,n_y)} , \end{aligned} \tag{6.55}$$

are pure gauge. Four more will be eliminated by the vacuum Einstein equations, and the final two dynamical, gravitational degrees of freedom turn out to be generated by the Hertz potential method (6.33), when taking the Hertz potentials to be proportional to the scalar modes $\Phi^{(p_u,p_v,n_x,n_y)}$.

6.4.2.1 *First-order perturbations*

The diagonalization of $\mathfrak{L}_{\partial_u}$ and $\mathfrak{L}_{\partial_v}$ is readily achieved. Therefore, motivated additionally by our expectations from the scalar modes, define

$$\begin{aligned} V_a^{(p_u,p_v,n_x,n_y,I)} &= e^{iup_u+ivp_v} e^{-\frac{|p_v|\Omega}{2}x^2 - i\frac{p_v\Lambda}{2}y^2} \tilde{V}_a^{(p_u,p_v,n_x,n_y,I)}(x,y) , \\ h_{ab}^{(p_u,p_v,n_x,n_y,IJ)} &= e^{iup_u+ivp_v} e^{-\frac{|p_v|\Omega}{2}x^2 - i\frac{p_v\Lambda}{2}y^2} \tilde{h}_{ab}^{(p_u,p_v,n_x,n_y,IJ)}(x,y) . \end{aligned} \tag{6.56}$$

We expect to find four independent vector modes, which we therefore label by an additional index $I \in \{n, \ell, x, y\}$ as well as the labels of the representation (p_u, p_v, n_x, n_y) defined by the (vector version of the) relations (6.55). Similarly, we expect ten independent tensor modes for each (p_u, p_v, n_x, n_y), such that in eq. (6.56) we have added a symmetric IJ label to the tensor modes.

There are two complementary approaches that are useful for constructing modes satisfying eqs. (6.55) and (6.54). The first is to start by finding the "ground states" or

4 Although here we can proceed formally with $\Lambda \neq \Omega$, we remark that gravitational fluctuations are only sensible if the background is on-shell, $\Lambda = \Omega$.

fundamental modes and subsequently raising the mode number using the properties of the algebra (6.52). The second approach simply relies on solving the differential equations implied by (6.55) and (6.54). In order to do this explicitly for the different vector and tensor modes, it is useful to decompose in components with respect the frame $(n, \ell, E^{(x)}, E^{(y)})$, where in terms of the principal null frame (6.11)

$$E^{(x)} = \frac{1}{\sqrt{2}}(m + \bar{m}) = \partial_x \,, \quad E^{(y)} = \frac{1}{i\sqrt{2}}(m - \bar{m}) = \partial_y \,. \tag{6.57}$$

Explicitly, we decompose

$$V_a = V_\ell n_a + V_n \ell_a - V_x E^{(x)}_a - V_y E^{(y)}_a \,, \tag{6.58}$$

and so on. Note in particular the sign choices.

To cross-check, we have applied both the algebraic and differential equations methods. However, as both methods are straightforward we do not enter into further details about these derivations. Instead, we simply quote the result

$$\begin{aligned}
\tilde{V}_a^{(p_u,p_v,n_x,n_y,n)} &= \mathcal{N}_{(p_v,n_x,n_y,n)} H_{n_x}(\sqrt{|p_v|\Omega}x) H_{n_y}(\sqrt{ip_v\Lambda}y)\ell_a \,, \\
\tilde{V}_a^{(p_u,p_v,n_x,n_y,x)} &= \mathcal{N}_{(p_v,n_x,n_y,x)} H_{n_x}(\sqrt{|p_v|\Omega}x) H_{n_y}(\sqrt{ip_v\Lambda}y) E^{(x)}_a \\
&\quad - i\sqrt{\Omega/4|p_v|}\left(-2n_x H_{n_x-1}(\sqrt{|p_v|\Omega}x) + H_{n_x+1}(\sqrt{|p_v|\Omega}x)\right) H_{n_y}(\sqrt{ip_v\Lambda}y)\ell_a \,, \\
\tilde{V}_a^{(p_u,p_v,n_x,n_y,y)} &= \mathcal{N}_{(p_v,n_x,n_y,y)} H_{n_x}(\sqrt{|p_v|\Omega}x) H_{n_y}(\sqrt{ip_v\Lambda}y) E^{(y)}_a \\
&\quad - i\sqrt{i\Lambda/4p_v} H_{n_x}(\sqrt{|p_v|\Omega}x)\left(-2n_y H_{n_y-1}(\sqrt{ip_v\Lambda}y) + H_{n_y+1}(\sqrt{ip_v\Lambda}y)\right)\ell_a \,, \\
\tilde{V}_a^{(p_u,p_v,n_x,n_y,\ell)} &= \mathcal{N}_{(p_v,n_x,n_y,\ell)} H_{n_x}(\sqrt{|p_v|\Omega}x) H_{n_y}(\sqrt{ip_v\Lambda}y) n_a \\
&\quad - i\sqrt{i\Lambda/4p_v} H_{n_x}(\sqrt{|p_v|\Omega}x)\left(-2n_y H_{n_y-1}(\sqrt{ip_v\Lambda}y) + H_{n_y+1}(\sqrt{ip_v\Lambda}y)\right) E^{(y)}_a \\
&\quad - i\sqrt{\Omega/4|p_v|} H_{n_y}(\sqrt{ip_v\Lambda}y)\left(-2n_x H_{n_x-1}(\sqrt{|p_v|\Omega}x) + H_{n_x+1}(\sqrt{|p_v|\Omega}x)\right) E^{(x)}_a \\
&\quad + \frac{1}{2p_v^2}\left(2p_u p_v + p_v^2(\Lambda^2 y^2 - \Omega^2 x^2)\right) H_{n_x}(\sqrt{|p_v|\Omega}x) H_{n_y}(\sqrt{ip_v\Lambda}y)\ell_a \,.
\end{aligned} \tag{6.59}$$

Here we have kept the normalizations $\mathcal{N}_{(p_v,n_x,n_y,I)}$ arbitrary for now.

The mode $\tilde{V}^{(p_u,p_v,n_x,n_y,\ell)}$ is clearly the most complicated, it is also the only one which can contribute to $\ell^a V_a \neq 0$. Conveniently, it turns out that this mode is pure gauge (for $p_v \neq 0$)

$$V_a^{(p_u,p_v,n_x,n_y,\ell)} = \frac{\mathcal{N}_{(p_v,n_x,n_y,\ell)}}{ip_v\mathcal{N}_{(p_v,n_x,n_y)}} \partial_a \left(\Phi^{(p_u,p_v,n_x,n_y)}\right) \,. \tag{6.60}$$

As a result, in the above formulation, it is particularly convenient to impose the gauge $\ell^a V_a = 0$. Tensor modes are given instead by

$$
\begin{aligned}
\tilde{h}_{ab}^{(p_u,p_v,n_x,n_y,nn)} &= \mathcal{N}_{(p_v,n_x,n_y,nn)} H_{n_x}(\sqrt{|p_v|\Omega}x) H_{n_y}(\sqrt{ip_v\Lambda}y)\ell_a\ell_b\,,\\
\tilde{h}_{ab}^{(p_u,p_v,n_x,n_y,xn)} &= \mathcal{N}_{(p_v,n_x,n_y,xn)} H_{n_x}(\sqrt{|p_v|\Omega}x) H_{n_y}(\sqrt{ip_v\Lambda}y) E^{(x)}_{(a}\ell_{b)}\\
&\quad - i\sqrt{\frac{\Omega}{4|p_v|}}\left(H_{n_x+1}(\sqrt{|p_v|\Omega}x) - 2n_x H_{n_x-1}(\sqrt{|p_v|\Omega}x)\right) H_{n_y}(\sqrt{ip_v\Lambda}y)\ell_a\ell_b\,,\\
\tilde{h}_{ab}^{(p_u,p_v,n_x,n_y,yn)} &= \mathcal{N}_{(p_v,n_x,n_y,yn)} H_{n_x}(\sqrt{|p_v|\Omega}x) H_{n_y}(\sqrt{ip_v\Lambda}y) E^{(y)}_{(a}\ell_{b)}\\
&\quad - i\sqrt{\frac{i\Lambda}{4p_v}} H_{n_x}(\sqrt{|p_v|\Omega}x)\left(H_{n_y+1}(\sqrt{ip_v\Lambda}y) - 2n_y H_{n_y-1}(\sqrt{ip_v\Lambda}y)\right)\ell_a\ell_b\,,\\
\tilde{h}_{ab}^{(p_u,p_v,n_x,n_y,xx)} &= \mathcal{N}_{(p_v,n_x,n_y,xx)} H_{n_x}(\sqrt{|p_v|\Omega}x) H_{n_y}(\sqrt{ip_v\Lambda}y) E^{(x)}_a E^{(x)}_b\\
&\quad - 2i\sqrt{\frac{\Omega}{4|p_v|}}\left(H_{n_x+1}(\sqrt{|p_v|\Omega}x) - 2n_x H_{n_x-1}(\sqrt{|p_v|\Omega}x)\right) H_{n_y}(\sqrt{ip_v\Lambda}y) E^{(x)}_{(a}\ell_{b)}\\
&\quad - \Omega^2 x^2 H_{n_x}(\sqrt{|p_v|\Omega}x) H_{n_y}(\sqrt{ip_v\Lambda}y)\ell_a\ell_b\,,\\
\tilde{h}_{ab}^{(p_u,p_v,n_x,n_y,xy)} &= \mathcal{N}_{(p_v,n_x,n_y,xy)} H_{n_x}(\sqrt{|p_v|\Omega}x) H_{n_y}(\sqrt{ip_v\Lambda}y) E^{(x)}_{(a} E^{(y)}_{b)}\\
&\quad - i\sqrt{\frac{i\Lambda}{4p_v}} H_{n_x}(\sqrt{|p_v|\Omega}x)\left(H_{n_y+1}(\sqrt{ip_v\Lambda}y) - 2n_y H_{n_y-1}(\sqrt{ip_v\Lambda}y)\right) E^{(x)}_{(a}\ell_{b)}\\
&\quad - i\sqrt{\frac{\Omega}{4|p_v|}}\left(H_{n_x+1}(\sqrt{|p_v|\Omega}x) - 2n_x H_{n_x-1}(\sqrt{|p_v|\Omega}x)\right) H_{n_y}(\sqrt{ip_v\Lambda}y) E^{(y)}_{(a}\ell_{b)}\\
&\quad - \sqrt{\frac{i\Lambda}{4p_v}} H_{n_x}(\sqrt{|p_v|\Omega}x)\left(H_{n_y+1}(\sqrt{ip_v\Lambda}y) - 2n_y H_{n_y-1}(\sqrt{ip_v\Lambda}y)\right)\\
&\quad \times\sqrt{\frac{\Omega}{4|p_v|}}\left(H_{n_x+1}(\sqrt{|p_v|\Omega}x) - 2n_x H_{n_x-1}(\sqrt{|p_v|\Omega}x)\right)\ell_a\ell_b\,,\\
\tilde{h}_{ab}^{(p_u,p_v,n_x,n_y,yy)} &= \mathcal{N}_{(p_v,n_x,n_y,yy)} H_{n_x}(\sqrt{|p_v|\Omega}x) H_{n_y}(\sqrt{ip_v\Lambda}y) E^{(y)}_a E^{(y)}_b\\
&\quad - 2i\sqrt{\frac{i\Lambda}{4p_v}} H_{n_x}(\sqrt{|p_v|\Omega}x)\left(H_{n_y+1}(\sqrt{ip_v\Lambda}y) - 2n_y H_{n_y-1}(\sqrt{ip_v\Lambda}y)\right) E^{(y)}_{(a}\ell_{b)}\\
&\quad + \Lambda^2 y^2 H_{n_x}(\sqrt{|p_v|\Omega}x) H_{n_y}(\sqrt{ip_v\Lambda}y)\ell_a\ell_b\,.
\end{aligned}
\tag{6.61}
$$

The reason for introducing modes satisfying (6.54) is that they do not mix under the linearized wave equation and, moreover, render them algebraic. Consider for the vector example the Maxwell equations[5]

$$F_{ab}^{(p_u,p_v,n_x,n_y)} = \nabla_a A_b^{(p_u,p_v,n_x,n_y)} - \nabla_b A_a^{(p_u,p_v,n_x,n_y)}, \quad \nabla^a F_{ab}^{(p_u,p_v,n_x,n_y)} = 0, \tag{6.62}$$

where we take $A^{(p_u,p_v,n_x,n_y)}$ to be a sum of the modes (6.55) with constant coefficients A_I for the relevant mode labeled by $I \in \{n, \ell, x, y\}$. Just like the scalar wave equation, the Maxwell equations (6.62) impose the mass-shell or dispersion relation (6.50) ($p_v \neq 0$)

$$p_u = \mathrm{sgn}(p_v)\Omega\left(n_x + \frac{1}{2}\right) + i\Lambda\left(n_y + \frac{1}{2}\right). \tag{6.63}$$

In addition, they eliminate one further ("longitudinal") combination of the vector modes. We are left with the expected two physical "transverse" electromagnetic polarizations for each set of spacetime mode numbers:

$$A_a^{(p_u,p_v,n_x,n_y)} = A_x V_a^{(p_u,p_v,n_x,n_y,x)} + A_y V_a^{(p_u,p_v,n_x,n_y,y)}. \tag{6.64}$$

These two physical degrees of freedom can be generated by a Hertz potential Φ_H satisfying the massless scalar wave equation as in the gravitational case.

Analogously to the Maxwell equations for the vector modes, the Einstein equations impose eq. (6.63) and eliminate all but two gravitational polarizations. These polarizations are captured exactly by one scalar Hertz potential and its conjugate mode. It is of course precisely this description in terms of scalar Hertz potentials, and closely related Weyl scalars that were used in the GHP formulation in Section 6.3.2. We find that the GHP formulation is ultimately more efficient to discuss the non-linearities. Nevertheless, let us conclude our discussion of a more directly metric-based approach by discussing non-linearities in this formulation.

6.4.2.2 *Second-order perturbations*

The crux of perturbation theory on homogeneous plane waves at non-linear orders is that it trivializes as soon as the source terms can be decomposed into modes such as (6.47), (6.55), or (6.54). While this is true regardless of whether we are dealing with scalars, vectors, or tensors, the actual decomposition naturally becomes more difficult at higher spin. However, *if* the source is again in the form of a sum of eigenfunctions of the wave operator, solutions to the inhomogeneous equation become readily available. For the scalar wave equation, the above claim is immediate. Consider

$$\Box\Phi = S\Phi^{(p_u,p_v,n_x,n_y)}, \tag{6.65}$$

5 We use A instead of V to emphasize the difference between electromagnetic gauge potentials, for which we impose equations of motion, and general vector fields V for which we do not.

for some constant S. Then using (6.49), a particular solution is given by

$$\Phi = \frac{S\Phi^{(p_u,p_v,n_x,n_y)}}{2p_v\left[\mathrm{sgn}(p_v)\Omega\left(n_x+\frac{1}{2}\right)+i\Lambda\left(n_y+\frac{1}{2}\right)-p_u\right]}. \tag{6.66}$$

In the next section, we will discuss how a source of the form (6.65), or in general a linear combination of such sources, can be found for a toy example and the master equation (6.39).

Consider instead the sourced Maxwell equations

$$\nabla^a\left(\nabla_a A_b - \nabla_b A_a\right) = \mathcal{A}^{(\hat{I})} V_a^{(p_u,p_v,n_x,n_y,\hat{I})}, \tag{6.67}$$

where $\mathcal{A}^{(\hat{I})}$ are constants and $\hat{I} \in \{x, y, \|\}$ runs over the three divergence free combinations [6] of the modes, which in particular for a non-resonant source (meaning p_u does not satisfy eq. (6.63))

$$V_a^{(p_u,p_v,n_x,n_y,\|)} = V_a^{(p_u,p_v,n_x,n_y,n)} - \frac{p_v}{2p_u-(2n_y+1)i\Lambda-(2n_x+1)\Omega} V_a^{(p_u,p_v,n_x,n_y,\ell)}, \tag{6.68}$$

where we have assumed that $\mathcal{N}_{(p_v,n_x,n_y,n)} = \mathcal{N}_{(p_v,n_x,n_y,\ell)}$ in eq. (6.55). Up to the decomposition of the right-hand side into the mode sum, eq. (6.67) is the form that second-and higher order perturbation equations will take. The solution to (6.67) is given by

$$A_a = \frac{\mathcal{A}^{(\hat{I})}\left(V_a^{(p_u,p_v,n_x,n_y,\hat{I})} - c_{(p_u,p_v,n_x,n_y,\hat{I})} V_a^{(p_u,p_v,n_x,n_y,\ell)}\right)}{2p_v\left[\mathrm{sgn}(p_v)\Omega\left(n_x+\frac{1}{2}\right)+i\Lambda\left(n_y+\frac{1}{2}\right)-p_u\right]}, \tag{6.69}$$

which is a simple generalization of the scalar case (6.66). The second term in (6.69) comes from the gauge ambiguity in inverting the wave equation. To stay in our preferred gauge despite the appearance of the $V_a^{(p_u,p_v,n_x,n_y,\ell)}$ modes in divergence free combination $V_a^{(p_u,p_v,n_x,n_y,\|)}$ for the source, we would simply choose $c_{(p_u,p_v,n_x,n_y,\ell)}$ to cancel that component while $c_{(p_u,p_v,n_x,n_y,y)} = c_{(p_u,p_v,n_x,n_y,x)} = 0$. For the case of electromagnetic perturbations, one may imagine non-linearities arising from an effective Heisenberg-Euler Lagrangian but our ultimate interest is of course in tensor perturbations and General Relavity, which we discuss next.

For the linearized Einstein equation[7] with a single mode source no new complications arise with respect to the Maxwell example. That is, the solution to

$$\dot{G}[h_{ab}] = \mathcal{A}^{(\hat{K})} h_{ab}^{(p_u,p_v,n_x,n_y,\hat{K})}, \tag{6.70}$$

6 We need the right-hand side to be a conserved current, or more directly, because of the divergence of the left-hand side $[\nabla_b, \nabla_a]F^{\nu\mu} = 2R_{\alpha\mu}F^{\alpha\mu} = 0$.

7 While not necessary in general, when discussing the Einstein equations, we will always set $\Lambda = \Omega$ in order for the vacuum Einstein equation of the background to be satisfied.

where $\dot{G}$ is the linearized Einstein tensor, is given by

$$h_{ab} = -\frac{2\mathcal{A}^{(\hat{K})} h_{ab}^{(p_u,p_v,n_x,n_y,\hat{K})}}{2p_v\left[\mathrm{sgn}(p_v)\Omega\left(n_x+\frac{1}{2}\right)+i\Lambda\left(n_y+\frac{1}{2}\right)-p_u\right]}\,. \tag{6.71}$$

Here we have left implicit a further projection associated to the gauge choice, resulting from the fact that divergence free modes labeled by $\hat{K}$, which are the allowed sources to (6.70) as in the Maxwell example, are not in our chosen gauge. In conclusion, as advertised, the core problem is to find the mode decomposition of any given source. Subsequently, the solution of the wave equation is trivial.

As a simple illustration consider the example of two linear $n_x = n_y = 0$, $p_v > 0$, on-shell gravitational modes sourcing a second order mode

$$h_{ab} = \sum_{i\in\{a,b\}}\left(h_+^{(i)} h_{ab}^{(p_u^{(i)},p_v^{(i)},0,0,+)} + h_\times^{(i)} h_{ab}^{(p_u^{(i)},p_v^{(i)},0,0,\times)}\right), \tag{6.72}$$

where, for the sake of this example, $p_v^{(a)}, p_v^{(b)} > 0$ and eq. (6.63) is satisfied. In addition, for clarity, we introduce the following (divergence free) combinations of the tensor harmonics starting from the definitions in (6.54)

$$\begin{aligned} h_{ab}^{(p_u^{(i)},p_v^{(i)},n_x,n_y,+)} &= h_{ab}^{(p_u^{(i)},p_v^{(i)},n_x,n_y,xx)} - h_{ab}^{(p_u,p_v,n_x,n_y,yy)} \\ &\quad + \frac{(2n_x+1)\Omega - i(2n_y+1)\Lambda}{p_v^{(i)}} h_{ab}^{(p_u^{(i)},p_v^{(i)},n_x,n_y,nn)}\,, \\ h_{ab}^{(p_u^{(i)},p_v^{(i)},n_x,n_y,\times)} &= 2h_{ab}^{(p_u^{(i)},p_v^{(i)},n_x,n_y,xy)}\,, \end{aligned} \tag{6.73}$$

which, combined with (6.63), solve the homogeneous, linearized Einstein equations. A direct computation one can find the second order Einstein tensor $\ddot{G}$ to be

$$\begin{aligned} \ddot{G}_{ab}[h_+^{(a)}, h_+^{(b)}] &= \frac{ih_+^{(a)}h_+^{(b)}}{2(p_v^{(a)}+p_v^{(b)})}\left\{\frac{\Omega\,(1-i)}{2p_v^{(a)}p_v^{(b)}}\right[\\ &\left(2i(p_v^{(a)})^4 + (1+4i)(p_v^{(a)})^3 p_v^{(b)} + 6i(p_v^{(a)})^2(p_v^{(b)})^2 + (1+4i)(p_v^{(b)})^3 p_v^{(a)} + 2i(p_v^{(b)})^4\right) h_{ab}^{(xx)} \\ &- \left(2i(p_v^{(a)})^4 - (1-4i)(p_v^{(a)})^3 p_v^{(b)} + 6i(p_v^{(a)})^2(p_v^{(b)})^2 - (1-4i)(p_v^{(b)})^3 p_v^{(a)} + 2i(p_v^{(b)})^4\right) h_{ab}^{(yy)}\Big] \\ &+ \frac{\Omega^2}{p_v^{(a)}p_v^{(b)}(p_v^{(a)}+p_v^{(b)})}\left(2(p_v^{(a)})^4 + (p_v^{(a)})^3 p_v^{(b)} + 2(p_v^{(a)})^2(p_v^{(b)})^2 + p_v^{(a)}(p_v^{(b)})^3 + 2(p_v^{(b)})^4\right) h_{ab}^{(nn)} \\ &+ \left((p_v^{(a)})^2 + p_v^{(a)}p_v^{(b)} + (p_v^{(b)})^2\right)\left(h_{ab}^{(\ell\ell)} - \frac{2\Omega(1+i)}{p_v^{(a)}+p_v^{(b)}} h_{ab}^{(n\ell)}\right)\Bigg\}\,, \end{aligned} \tag{6.74}$$

and similarly for the $(+,\times)$ and $(\times,\times)$ polarizations (which we omit for brevity). For definiteness we have fixed the normalizations $\mathcal{N}_{(p_v,n_x,n_y,IJ)} = 1$ and for simplicity

we distinguish the following three contributions from different polarizations: $h_+^{(a)}h_+^{(b)}$, $h_+^{(a)}h_\times^{(b)}$ (yielding also $(a) \leftrightarrow (b)$), and $h_\times^{(a)}h_\times^{(b)}$ as well as labeling the modes only with their tensor index, not including the common mode label which are implicitly $(p_u^{(a)} + p_u^{(b)}, p_v^{(a)} + p_v^{(b)}, 0, 0)$.

More important than the explicit expression is that it is decomposed solely in terms of modes $h_{ab}^{(p'_u, p'_v, 0, 0)}$ with $n_x = n_y = 0$. As a result $\mathfrak{L}_{a\_}\ddot{G} = \mathfrak{L}_{b\_}\ddot{G} = 0$. To see that this must have been the case, note that $\ddot{G}$ is built as a linear combination of terms including products of g_{ab}, h_{ab}, and its covariant derivatives. Now for isometries ξ, $[\mathfrak{L}_\xi, \nabla_a] = 0$. Therefore, together with $\mathfrak{L}_{a\_}h_{ab} = \mathfrak{L}_{b\_}h_{ab} = 0$ for the parent mode, by our choice of the linear perturbations (6.72), it indeed follows that $\mathfrak{L}_{a\_}\ddot{G} = \mathfrak{L}_{b\_}\ddot{G} = 0$. In turn, this implies that $\ddot{G}$ satisfies the conditions of (6.54) with $n_x = n_y = 0$. Thus, it can be decomposed in such modes as shown explicitly in (6.74). Finally, after performing this decomposition into the $n_x = n_y = 0$ modes (6.61), the second order metric perturbations are immediately found using (6.71).

While a similar direct computation is still possible for more complicated modes, it naturally becomes more tedious. Therefore, we avoid working with the linearized Einstein equations and tensor harmonics in favor of the master equation (6.39) of the GHP formulation and scalar harmonics (6.47).

6.5 QUADRATIC QUASINORMAL MODES

Linear perturbations on certain homogeneous plane waves can be related to the high-frequency regime of the QNMs of a Kerr BH, through the Penrose limit identification. This motivates exploring a similar connection between second order perturbations on the plane wave and BH QQNMs. The particular solution to the second order Teukolsky equation on the plane wave will contain source-driven modes, which oscillate with frequencies that correspond to the sum or the difference of the frequencies of linear QNMs. Recent works [269, 377] have taken some first steps towards analysing these QQNMs and relate them to the QQNMs of Kerr BHs, albeit restricting to modes with $n_x = n_y = 0$, and only those generated by the $\mathcal{S}_+$ term. In this section, we will discuss the QQNMs on the plane wave arising from all possible mode combinations, and identifying general selection rules. In order to do so, we first introduce the solutions of a scalar toy model that showcases most of the technical difficulties in a simpler setting, and then discuss our results in the gravitational case.

6.5.1 *Scalar QQNMs*

Before addressing the full gravitational case, it is illustrative to consider as a toy model a nonlinear wave equation for a scalar field. We consider the cubic self-interaction leading to the equation of motion

$$\Box\Phi + \Phi^2 = 0\,, \tag{6.75}$$

where we look for solutions of the form $\Phi = \epsilon\dot{\Phi} + \frac{1}{2}\epsilon^2\ddot{\Phi}$. The leading order solution corresponds to modes of the homogeneous plane wave, as discussed before. Generically, we can assume the leading order solution to be a superposition of two modes (as defined in (6.47))

$$\dot{\Phi} = \mathcal{A}_a \Phi^{(p_v^{(a)}, n_x^{(a)}, n_y^{(a)})} + \mathcal{A}_b \Phi^{(p_v^{(b)}, n_x^{(b)}, n_y^{(b)})}\,, \tag{6.76}$$

where, when not listed, it is implied that p_u is fixed by (6.63), as required to be a leading order solutions to the wave equation (we also note that a, b are merely labels, and not indices running in any set).

The next-to-leading order, which is the first order sensitive to the nonlinearity, satisfies the equation

$$\begin{aligned}\Box\ddot{\Phi} =& -2\mathcal{A}_a^2\left(\Phi^{(p_v^{(a)}, n_x^{(a)}, n_y^{(a)})}\right)^2 - 2\mathcal{A}_b^2\left(\Phi^{(p_v^{(b)}, n_x^{(b)}, n_y^{(b)})}\right)^2 - 4\mathcal{A}_a\mathcal{A}_b\Phi^{(p_v^{(a)}, n_x^{(a)}, n_y^{(a)})}\Phi^{(p_v^{(b)}, n_x^{(b)}, n_y^{(b)})} \\ =& \mathcal{S}_{aa} + \mathcal{S}_{bb} + 2\mathcal{S}_{ab}\,.\end{aligned} \tag{6.77}$$

The particular solution can be decomposed in three pieces $\ddot{\Phi} = \ddot{\Phi}_{aa} + \ddot{\Phi}_{bb} + 2\ddot{\Phi}_{ab}$ where $\Box\ddot{\Phi}_{IJ} = \mathcal{S}_{IJ}$ for $I, J = a, b$. It turns out that the source term can be generally written in terms of a linear combination of infinitely many eigenfunctions of the wave operator $\Phi^{(p_u, p_v, n_x, n_y)}$, as

$$\mathcal{S}_{IJ} = \sum_{n_y'=0}^{n_y^{(I)}+n_y^{(J)}} \sum_{n_x'=0}^{\infty} s_{IJ}^{(n_x', n_y')} \mathcal{A}_I\mathcal{A}_J\Phi^{(p_u', p_v', n_x', n_y')}\,, \qquad I, J = a, b\,, \tag{6.78}$$

where $p_u' = p_u^{(I)} + p_u^{(J)}$ and $p_v' = p_v^{(I)} + p_v^{(J)}$, and

$$\begin{aligned} s_{IJ}^{(n_x', n_y')} &= -2\mathcal{I}_x\mathcal{I}_y\,, \\ \mathcal{I}_x &= \int_{-\infty}^{\infty} \frac{\sqrt{|p_v'|\Omega}dx}{2^{n_x'} n_x'! \sqrt{\pi}} H_{n_x^{(I)}}\left(\sqrt{|p_v^{(I)}|\Omega}x\right) H_{n_x^{(J)}}\left(\sqrt{|p_v^{(J)}|\Omega}x\right) H_{n_x'}\left(\sqrt{|p_v'|\Omega}x\right) e^{-(|p_v'|+\frac{\Delta}{2})\Omega x^2}\,, \\ \mathcal{I}_y &= \int_C \frac{\sqrt{ip_v'\Omega}dy}{2^{n_y'} n_y'! \sqrt{\pi}} H_{n_y^{(I)}}\left(\sqrt{ip_v^{(I)}\Omega}y\right) H_{n_y^{(J)}}\left(\sqrt{ip_v^{(J)}\Omega}y\right) H_{n_y'}\left(\sqrt{ip_v'\Omega}y\right) e^{-ip_v'\Omega y^2}\,, \end{aligned} \tag{6.79}$$

where $\Delta = |p_v^{(I)}| + |p_v^{(J)}| - |p_v'|$ is only non-zero whenever $\text{sign}(p_v^{(I)}) \neq \text{sign}(p_v^{(J)})$ and we will comment on the $\mathcal{I}_y$ integration contour C later. As discussed in the previous section, by performing this decomposition in eigenfunctions of $\Box$, the solution to the second order equation becomes trivial, since $\ddot{\Phi}$ can then be written as a superposition of eigenfunctions. We translate the difficulty from solving an inhomogeneous differential equation, to expanding the source term in terms of the $\Phi^{(p_u', p_v', n_x', n_y')}$, i.e., computing the integrals $\mathcal{I}_{x,y}$.

The structure of these integrals shows why the sum in Eq. (6.78) only includes a finite amount of terms in the y direction, whereas it includes (in general) an infinite

amount of terms in the x-direction – if $n_y' > n_y^{(I)} + n_y^{(J)}$ then $\mathcal{I}_y = 0$, since it is the projection of a lower degree polynomial onto a higher order degree Hermite polynomial. Moreover, as it is exactly this polynomial decomposition we need, we can avoid the subtleties in choosing the appropriate integration contour in (6.79), by defining $\mathcal{I}_y$ in terms of this polynomial decomposition. We cannot use such a finite polynomial decomposition for the x-integral $\mathcal{I}_x$ in general, but here the integral over the real line is always absolutely convergent.

The application of various identities of Hermite polynomials would allow us to write the integrals in (6.79) more explicitly. Alternatively, we can observe that

$$\int dx x^k e^{-ax^2} = \frac{1+(-1)^k}{2} a^{-\frac{1+k}{2}} \Gamma\Big(\frac{1+k}{2}\Big) . \tag{6.80}$$

Thus, we can expand the integrands in (6.79) in terms of expressions of the form (6.80), and solve it analytically, once we know the Taylor coefficients of the product of Hermite polynomials. Abstractly we can write

$$\begin{aligned}
\mathcal{I}_x =& \frac{1}{2^{n_x} n_x! \sqrt{\pi}} \sum_{\alpha=0}^{n_x^{(I)}} \sum_{\beta=0}^{n_x^{(J)}} \sum_{\gamma=0}^{n_x'} \chi_{n_x^{(I)},\alpha} \chi_{n_x^{(J)},\beta} \chi_{n_x',\gamma} \Big(\frac{1+(-1)^{\alpha+\beta+\gamma}}{2}\Big) \Gamma\Big(\frac{1+\alpha+\beta+\gamma}{2}\Big) \\
&\times \sqrt{\frac{|p_v^{(I)}|^\alpha |p_v^{(J)}|^\beta |p_v'|^{\gamma+1}}{(|p_v'| + \Delta/2)^{\alpha+\beta+\gamma+1}}} , \\
\mathcal{I}_y =& \frac{1}{2^{n_y'} n_y'! \sqrt{i\pi \mathrm{sgn}(p_v')}} \sum_{\alpha=0}^{n_y^{(I)}} \sum_{\beta=0}^{n_y^{(J)}} \sum_{\gamma=0}^{n_y'} \chi_{n_y^{(I)},\alpha} \chi_{n_y^{(J)},\beta} \chi_{n_y',\gamma} \Big(\frac{1+(-1)^{\alpha+\beta+\gamma}}{2}\Big) \Gamma\Big(\frac{1+\alpha+\beta+\gamma}{2}\Big) \\
&\times \sqrt{\frac{(p_v^{(I)})^\alpha (p_v^{(J)})^\beta}{(p_v')^{\alpha+\beta}}} ,
\end{aligned} \tag{6.81}$$

where $\chi_{n,k}$ are simply the coefficients of the Hermite polynomials, i.e., $H_n(x) = \sum \chi_{n,k} x^k$. Whenever $\Delta = 0$ (which is the case for the $\mathcal{S}_{aa}, \mathcal{S}_{bb}$ terms, and for $\mathcal{S}_{ab}$ whenever $p_v^{(a)}$ and $p_v^{(b)}$ have the same sign), the sum only contains a finite amount of terms in the x direction as well. We will come back to the physical interpretation of this issue in terms of overtone excitations when discussing the gravitational case. However, another point of view from the perspective of the Hermite polynomials is that one can formally absorb a change in sign in p_v in the mode number condition (6.53) and the quantization condition (6.63) by analytically continuing in x and n_x. While generalization of Hermite polynomials with non-integer n_x can be made sense of, they are no longer polynomials. In any case, once the $s_{IJ}^{(n_x', n_y')}$ have been

determined, for instance using (6.79) and (6.81), the second order perturbation is found to be

$$\begin{aligned}\ddot{\Phi}_{IJ} &= \sum_{n'_x,n'_y} \mathcal{R}^{(n'_x,n'_y)}_{I\times J}\mathcal{A}_I\mathcal{A}_J\Phi^{(p'_u,p'_v,n'_x,n'_y)}\,,\\ \mathcal{R}^{(n'_x,n'_y)}_{I\times J} &= \frac{s^{(n'_x,n'_y)}_{IJ}}{|p'_v|\Omega(1+2n'_x)+ip'_v\Omega\left(1+2n'_y\right)-2p'_vp'_u}\,,\end{aligned} \tag{6.82}$$

where the denominator in $\mathcal{R}^{(n'_x,n'_y)}_{I\times J}$ is just the eigenvalue of the wave operator corresponding to $\Phi^{(p'_u,p'_v,n'_x,n'_y)}$. Notice that there are no resonances at second order. A resonance would occur if p'_u satisfies the on-shell condition (6.50), which would make the denominator in (6.82) vanish. However, since $p'_u = p^{(a)}_u + p^{(b)}_u$, the resonance condition would correspond to

$$\begin{aligned}\operatorname{sgn}(p'_v)\left(n'_x+\frac{1}{2}\right)+i\left(n'_y+\frac{1}{2}\right) =&\operatorname{sgn}(p^{(a)}_v)\left(n^{(a)}_x+\frac{1}{2}\right)+\operatorname{sgn}(p^{(b)}_v)\left(n^{(b)}_x+\frac{1}{2}\right)\\ &+i\left(n^{(a)}_y+n^{(b)}_y+1\right),\end{aligned} \tag{6.83}$$

which has no solution for any combination of positive integers $n^{(a,b)}_{x,y}, n'_{x,y}$. Above we have introduced the nonlinear ratios $\mathcal{R}^{(n'_x,n'_y)}_{I\times J}$. It is important to emphasize that these ratios are dependent on the normalization of the mode functions $\Phi^{(p_u,p_v,n_x,n_y)}$. If one were to choose a different normalization for the modes Φ^λ, the ratios are also transformed,

$$\tilde{\Phi}^\lambda = \alpha_\lambda\Phi^\lambda \implies \tilde{\mathcal{R}}^{(n'_x,n'_y)}_{I\times J} = \frac{\alpha_{\lambda_I}\alpha_{\lambda_J}}{\alpha_{\lambda'}}\mathcal{R}^{(n'_x,n'_y)}_{I\times J}\,. \tag{6.84}$$

However, despite this arbitrariness they still encode physically meaningful information. For example, consider a single parent mode $\dot{\Phi}_a = \dot{\Phi}_b = \mathcal{A}\Phi^{(p_v,n_x,n_y)}$ that does not vanish at the central geodesic γ (the LR from the Penrose limit perspective). Then, the quantity $\ddot{\Phi}_{aa}|_\gamma / \left(\dot{\Phi}_a|_\gamma\right)^2$ which is independent of any normalisation choice, is given by

$$\frac{\ddot{\Phi}_{aa}|_\gamma}{\left(\dot{\Phi}_a|_\gamma\right)^2} = \sum_{n'_x,n'_y}\mathcal{R}^{(2n'_x,2n'_y)}_{a\times a}\,, \tag{6.85}$$

as follows from (6.82) (notice self-couplings only connect to even modes). We note that this can be extended straightforwardly to more general parent mode configurations.

Further care is needed whenever $p'_v = 0$. This can occur whenever $p^{(a)}_v = 0$ or $p^{(b)}_v = 0$, or whenever $p^{(a)}_v = -p^{(b)}_v \equiv p_v$. The first case is trivial, and never appears by our choice of linear modes. The second case is potentially interesting, as it corresponds to two oscillatory modes, whose non-linear combination is a

non-oscillatory mode. This is clear since the source term does not depend on v, and is a purely damped contribution in the u direction

$$\begin{aligned}\mathcal{S}_{ab} =& e^{-2\Omega(n_y^{(a)}+n_y^{(b)}+1)u} e^{-|p_v|\Omega x^2} H_{n_x^{(a)}}\left(\sqrt{|p_v|\Omega}x\right) H_{n_x^{(b)}}\left(\sqrt{|p_v|\Omega}x\right) \\ & \times H_{n_y^{(a)}}\left(\sqrt{ip_v\Omega}y\right) H_{n_y^{(b)}}\left(\sqrt{-ip_v\Omega}y\right) .\end{aligned} \tag{6.86}$$

In this sense, these modes could be related to a nonlinear memory effect [343, 344]. If the source term does not depend on v, then the particular solution to the sourced wave equation does not depend on v either. While the wave equation is readily solved, the solutions take on a very different character than the quadratic quasinormal modes, which are our main interest in the remainder. Moreover, they can take us out of the Penrose limit approximation (contribute at a higher eikonal order [253, 254]) and are best understood as renormalizing the background spacetime within a class of spacetimes which retain ∂_v as an isometry. We leave a more complete discussion of these contributions to future work. In addition, the existence of such perturbations indicates that there are likely driven quasi-resonances at third-order in perturbation theory, which would also be interesting to investigate further.

6.5.2 *Gravitational QQNMs*

The gravitational case shares many similarities with the scalar toy model discussed above. In precise terms we consider a linear fluctuation of $\dot{\Psi}_0$, which is the superposition of two distinct modes

$$\dot{\Psi}_0 = \mathcal{A}_a \Phi^{(p_v^{(a)}, n_x^{(a)}, n_y^{(a)})} + \mathcal{A}_b \Phi^{(p_v^{(b)}, n_x^{(b)}, n_y^{(b)})} . \tag{6.87}$$

Whenever $p_v^{(a/b)} \neq 0$, such perturbation is generated by the Hertz potential

$$\Psi_H \equiv \Psi_H^{(a)} + \Psi_H^{(b)} = -\frac{2}{\left(p_v^{(a)}\right)^4}\bar{\mathcal{A}}_a \bar{\Phi}^{(p_v^{(a)}, n_x^{(a)}, n_y^{(a)})} - \frac{2}{\left(p_v^{(b)}\right)^4}\bar{\mathcal{A}}_b \bar{\Phi}^{(p_v^{(b)}, n_x^{(b)}, n_y^{(b)})} , \tag{6.88}$$

by virtue of Eq. (6.37).

The second order Teukolsky equation for $\ddot{\Psi}_0$ is, in terms of the Hertz potential

$$\Box\ddot{\Psi}_0 = 2(\mathcal{S}_+ + \mathcal{S}_-) , \tag{6.89}$$

with $\mathcal{S}_\pm$ defined in Eqs. (6.40)-(6.41), and the factor of 2 appears since $\mathcal{O}_0 = \text{þ}'\text{þ} - \text{ð}'\text{ð} = \frac{1}{2}\Box$.

Now, writing $\Psi_H^{(I)} = e^{-ip_v^{(I)}v}\psi_H^{(I)}$, and making use of the fact that $\text{Þ}\Psi_H^{(I)} = -ip_v^{(I)}\Psi_H^{(I)}$, with $I = a, b$, we can rewrite the equation as

$$
\begin{aligned}
\Box\ddot{\Psi}_0 &= \sum_{I,J=a,b}\left(\mathcal{S}_{IJ}^{+} + \mathcal{S}_{IJ}^{-}\right), \\
\mathcal{S}_{IJ}^{+} &= -\frac{1}{2}e^{i(p_v^{(I)}+p_v^{(J)})v}\Bigg[-2\Big((p_v^{(I)})^5 p_v^{(J)} + 4(p_v^{(I)})^4(p_v^{(J)})^2 + 3(p_v^{(I)})^2(p_v^{(J)})^2\Big)\eth'\bar{\psi}_H^{(I)}\eth'\bar{\psi}_H^{(J)} \\
&\quad + \Big((p_v^{(I)})^6 + 4(p_v^{(I)})^5 p_v^{(J)} + 6(p_v^{(I)})^4(p_v^{(J)})^2 + 4(p_v^{(I)})^3(p_v^{(J)})^3 + (p_v^{(I)})^2(p_v^{(J)})^4\Big)\bar{\psi}_H^{(I)}\eth'^2\bar{\psi}_H^{(J)}\Bigg] \\
&\quad + (I \leftrightarrow J)\,, \\
\mathcal{S}_{IJ}^{-} &= -(p_v^{(I)})^4 e^{i(p_v^{(I)}-p_v^{(J)})v}\Big[(p_v^{(I)})^2\bar{\psi}_H^{(I)}\eth^2\psi_H^{(J)} + (p_v^{(J)})^2\psi_H^{(J)}\eth^2\bar{\psi}_H^{(I)} + 2p_v^{(I)}p_v^{(J)}\eth\bar{\psi}_H^{(I)}\eth\psi_H^{(J)}\Big]\,.
\end{aligned}
\tag{6.90}
$$

The source, hence, decomposes into two possible channels: an additive channel (+) and a difference channel (−). Thus, if the linear fluctuations are excited with two different frequencies, these drive a total of 6 different QQNM frequencies: 3 in the additive channel (*aa*, *bb*, and *ab* = *ba* channels), and 3 in the difference channel (*ab*, *ba*, and the "zero-frequency" channel with contributions from both *aa* and *bb*).

Notice that the source term hence involves quadratic combination of the linear solutions, with up to second order spatial derivatives, due to the action of the ð operator. Building upon the results of the scalar toy model, we postulate that each of the source terms can be written uniquely as

$$
\begin{aligned}
\mathcal{S}_{IJ}^{+} &= \sum_{n_y'=0}^{n_y^{(I)}+n_y^{(J)}+2}\sum_{n_x'=0}^{\infty} s_{IJ}^{(n_x',n_y')}\mathcal{A}_I\mathcal{A}_J\Phi^{(p_u',p_v',n_x',n_y')}\,, \quad p_u' = p_u^{(I)} + p_u^{(J)}\,, \quad p_v' = p_v^{(I)} + p_v^{(J)}\,, \\
\mathcal{S}_{IJ}^{-} &= \sum_{n_y'=0}^{n_y^{(I)}+n_y^{(J)}+2}\sum_{n_x'=0}^{\infty} t_{IJ}^{(n_x',n_y')}\mathcal{A}_I\bar{\mathcal{A}}_J\Phi^{(p_u',p_v',n_x',n_y')}\,, \quad p_u' = p_u^{(I)} - p_u^{(J)}\,, \quad p_v' = p_v^{(I)} - p_v^{(J)}\,.
\end{aligned}
\tag{6.91}
$$

Each of the source coefficients $s_{IJ}^{(n_x',n_y')}, t_{IJ}^{(n_x',n_y')}$ can be written as a product of two integrals in the x and y direction, respectively. However, the integrals will involve more general polynomials than the product of two Hermite polynomials – indeed notice that the maximum degree in the y direction is now $n_y^{(I)} + n_y^{(J)} + 2$, since there are up to two derivatives. Additional care is needed to deal with the Gaussian exponential factor which is present whenever $p_v^{(a)}$ and $p_v^{(b)}$ have the same (different) sign in $t_{ab}^{(n_x',n_y')}$ (respectively $s_{ab}^{(n_x',n_y')}$).

The solution is then readily written in terms of the source coefficients as

$$\ddot{\Psi}_0 = \sum_{I,J=a,b} \sum_{n'_y=0}^{n_y^{(I)}+n_y^{(J)}+2} \sum_{n'_x=0}^{\infty} \left({}^{++(n'_x,n'_y)}_{\quad I\times J}\mathcal{R}\, \mathcal{A}_I \mathcal{A}_J \Phi^{(p_u^{(I)}+p_u^{(J)}, p_v^{(I)}+p_v^{(J)}, n'_x, n'_y)} + {}^{+-(n'_x,n'_y)}_{\quad I\times J}\mathcal{R}\, \mathcal{A}_I \bar{\mathcal{A}}_J \Phi^{(p_u^{(I)}-p_u^{(J)}, p_v^{(I)}-p_v^{(J)}, n'_x, n'_y)} \right),$$

$$ {}^{++(n'_x,n'_y)}_{\quad I\times J}\mathcal{R} = \frac{s_{IJ}^{(n'_x,n'_y)} \mathcal{N}^{-1}_{(p_v^{(I)}+p_V^{(J)}, n'_x, n'_y)}}{|p_v^{(I)}+p_v^{(J)}|\Omega(1+2n'_x) + i(p_v^{(I)}+p_v^{(J)})\left[2i(p_u^{(I)}+p_u^{(J)}) + \Omega(1+2n'_y)\right]},$$

$$ {}^{+-(n'_x,n'_y)}_{\quad I\times J}\mathcal{R} = \frac{t_{IJ}^{(n'_x,n'_y)} \mathcal{N}^{-1}_{(p_v^{(I)}-p_V^{(J)}, n'_x, n'_y)}}{|p_v^{(I)}-p_v^{(J)}|\Omega(1+2n'_x) + i(p_v^{(I)}-p_v^{(J)})\left[2i(p_u^{(I)}-p_u^{(J)}) + \Omega(1+2n'_y)\right]}. \tag{6.92}$$

As in the BH case, there are no contributions which oscillate with a frequency $\propto e^{-i(p_u^{(a)}+p_u^{(b)})u}$, i.e., modes that could be associated to a $--$ channel. Notice that the fact that there is no $--$ channel follows from Eq. (6.39) and $\ddot{\Psi}_i \sim \bar{\Psi}_H$ (Eq. (6.37)). Additionally we highlight that the denominator never vanishes, i.e., the system is never resonant up to second order in perturbation theory away from $p'_v = 0$ (see discussion above for the scalar case).

Here it is worth to emphasise two aspects about the physical significance of our quadratic ratios. First, even though they transform non-trivially under a different choice of mode normalisation (see eq.(6.84)), they still measure invariantly the quadratic excitations of the curvature scalar Ψ_0 at the LR, i.e., $x = y = 0$, as compared to the first order fluctuations. Just as in the scalar case (see discussion below eq.(6.84)), one can define

$$\ddot{\Psi}_0|_{x=y=0} = \sum_{I,J=a,b} \left({}^{++}_{I\times J}\mathcal{R} \left(\Psi_{0,I}|_{x=y=0}\right)\left(\Psi_{0,J}|_{x=y=0}\right) + {}^{+-}_{I\times J}\mathcal{R} \left(\Psi_{0,I}|_{x=y=0}\right)\left(\bar{\Psi}_{0,J}|_{x=y=0}\right) \right), \tag{6.93}$$

where the light ring ratios are

$$ {}^{++}_{I\times J}\mathcal{R} = \sum_{n'_x,n'_y} {}^{++(2n'_x,2n'_y)}_{\quad I\times J}\mathcal{R}, \qquad {}^{+-}_{I\times J}\mathcal{R} = \sum_{n'_x,n'_y} {}^{+-(2n'_x,2n'_y)}_{\quad I\times J}\mathcal{R}. \tag{6.94}$$

These expressions are a priori particular to our choice of normalization (6.48), which was specifically taken for the (even-even) modes to be unit at $x = y = 0$. However,

taking as an example the oscillating second order component related to a single parent mode, one has[8]

$$\frac{\ddot{\Psi}^{++}_{0,aa}|_{x=y=0}}{\left(\dot{\Psi}_{0,a}|_{x=y=0}\right)^2} = \overset{++}{\mathcal{R}}_{a\times a} = \sum_{n'_x,n'_y} \overset{++(2n'_x,2n'_y)}{\mathcal{R}}_{a\times a} \,. \tag{6.95}$$

The left-hand-side is a physically meaningful quantity, independent of any mode-normalisation choice, and is given merely by the sum of our quadratic ratios. In fact, this is what motivates our choice of normalisation. Had we chosen a different one, then the right-hand-side of (6.95) would be an artificially-weighted sum of ratios instead.

The second aspect to emphasize is the behaviour of these ratios under gauge transformations. Our GPT gauge, introduced in Section 6.3.1, is adapted to a null frame that is parallelly-propagated along a twist-free, null geodesic congruence. This choice of "inertial" null frame ensures that the associated curvature scalars are physically meaningful. In addition, the quadratic curvature ratios are invariant under the residual gauge symmetry within the GPT gauge. To see this, we recall that at second order $\ddot{\Psi}_0$ transforms, in general, according to (6.19). However, in order to respect the GPT gauge, the gauge parameters must be fixed by the v-independent (but otherwise arbitrary) functions $\dot{\xi}_v, \dot{C}_l, \dot{a}, \dot{\theta}$, via equations (6.23) and (6.26). If at linear level one has two excited QNMs, so that $\dot{\Psi}_0$ is of the form

$$\dot{\Psi}_0 = \mathcal{A}_a \Phi^{(p_v^{(a)}, n_x^{(a)}, n_y^{(a)})} + \mathcal{A}_b \Phi^{(p_v^{(b)}, n_x^{(b)}, n_y^{(b)})} = \mathcal{A}_a e^{i p_v^{(a)} v} \psi_a(u,x,y) + \mathcal{A}_b e^{i p_v^{(b)} v} \psi_b(u,x,y)\,, \tag{6.96}$$

then none of the residual gauge transformations acting on $\ddot{\Psi}_0$ via (6.19) can have a v-dependence of the forms $e^{i(p_v^{(a)}+p_v^{(b)})v}$ or $e^{\pm i(p_v^{(a)}-p_v^{(b)})v}$, so they leave the $++$ and $+-$ channels invariant. The only exception is the fine-tuned configuration $2p_v^{(I)} = p_v^{(J)}$, since in that case the QQNM frequency $p_v^{(J)} - p_v^{(I)}$ in the $+-$ channel is precisely $p_v^{(I)}$, one of the parent-mode frequencies, so that particular QQNM would be affected by the residual gauge transformations.

The computation of the ratios proceeds in the same fashion as for the scalar toy model. Our code, written in `Mathematica`, is available in [1].

6.5.3 *Selection Rules*

Before directly calculating the excitation of QQNMs we comment on certain *selection rules* that determine which modes are excited for any given mode combination. Let us consider the quadratic combination of two modes, $(p_v^{(a)}, n_x^{(a)}, n_y^{(a)}) \times (p_v^{(b)}, n_x^{(b)}, n_y^{(b)})$. We must distinguish two cases, depending on the relative sign

8 Note that only parent modes with even overtone indices contribute to (6.93), as these are non-vanishing on the LR, and similarly (6.95) is only defined for such even mode, but similar ratios could be defined for spatial derivatives at $x = y = 0$ that would be sensitive to odd overtones.

between $p_v^{(a)}$ and $p_v^{(b)}$. As discussed in the previous section, the QQNMs (the source-driven solution to the second order Teukolsky equation) can be decomposed in eigenvalues of the wave operator (6.66), labelled by (p'_u, p'_v, n'_x, n'_y). The allowed values for these labels are:

- $\mathrm{sgn}(p_v^{(a)}) = \mathrm{sgn}(p_v^{(b)})$. In this case we have

$$\begin{aligned}
++: &\quad p'_u = p_u^{(a)} + p_u^{(b)}, \quad p'_v = p_v^{(a)} + p_v^{(b)}, \quad 0 \leq n'_\bullet \leq n_\bullet^{(a)} + n_\bullet^{(b)}, \qquad \bullet = \{x, y\}, \\
+-: &\quad p'_u = p_u^{(a)} - p_u^{(b)}, \quad p'_v = p_v^{(a)} - p_v^{(b)}, \quad 0 \leq n'_x < \infty, \quad 0 \leq n'_y \leq n_y^{(a)} + n_y^{(b)}, \\
-+: &\quad p'_u = p_u^{(b)} - p_u^{(a)}, \quad p'_v = p_v^{(b)} - p_v^{(a)}, \quad 0 \leq n'_x < \infty, \quad 0 \leq n'_y \leq n_y^{(a)} + n_y^{(b)},
\end{aligned} \tag{6.97}$$

  where the $-+$ channel is obtained by swapping $a \leftrightarrow b$ in the $+-$ channel. There is an additional selection rule related to the parity of the overtones, which applies in all channels,

$$n'_\bullet \mod 2 = n_\bullet^{(a)} + n_\bullet^{(b)} \mod 2, \qquad \bullet = \{x, y\}, \tag{6.98}$$

  which simply follows from the well-defined parity of the linear modes.

- $\mathrm{sgn}(p_v^{(a)}) \neq \mathrm{sgn}(p_v^{(b)})$. In this case, the overtone selection rules for the $++$ and $+-$ channels flip:

$$\begin{aligned}
++: &\quad p'_u = p_u^{(a)} + p_u^{(b)}, \quad p'_v = p_v^{(a)} + p_v^{(b)}, \quad 0 \leq n'_x < \infty, \quad 0 \leq n'_y \leq n_y^{(a)} + n_y^{(b)}, \\
+-: &\quad p'_u = p_u^{(a)} - p_u^{(b)}, \quad p'_v = p_v^{(a)} - p_v^{(b)}, \quad 0 \leq n'_\bullet \leq n_\bullet^{(a)} + n_\bullet^{(b)},
\end{aligned} \tag{6.99}$$

  where we don't write the $-+$ channel for brevity, and the parity selection rule (6.98) still applies.

The selection rules for p'_u, p'_v trivially follow from the structure of linear modes (6.47). The parity rule, once again, simply follows from the fact that these are quadratic combinations of functions with well-defined parities. The only selection rules which are not trivial are those affecting the overtone excitation.

Already in the scalar toy model 6.5.1 we emphasized that there are two distinct cases which could lead to the excitation of either a finite or an infinite number of n'_x overtones, which we refer to respectively as "finite (excitation) channels" or "infinite (excitation) channels". This is related to whether the factor Δ in eq. (6.79) vanishes, or not. Whenever $\Delta \neq 0$, which occurs whenever $\mathrm{sgn}(p_v^{(a)}) = \mathrm{sgn}(p_v^{(b)})$ in the $+-$ channel, or whenever $\mathrm{sgn}(p_v^{(a)}) \neq \mathrm{sgn}(p_v^{(b)})$ in the $++$ channel, the absolute value in the x-dependent Gaussian exponential acts as an obstruction, and the decomposition of the source term in Hermite polynomials now requires and infinite amount of terms. This explains why n'_x can be arbitrarily large in the $+-$ and $-+$ cases in (6.97), and in the $++$ case in (6.99).

Focusing now on the finite excitation channels,a naive counting of the polynomial powers gives that an overtone of mode number up to $n' = n^{(a)} + n^{(b)} + 2$ could be excited, where the $+2$ is a consequence of the spatial derivatives in (6.40)–(6.41). On the other hand, we find that the maximal overtone number is, instead, $n' \leq n^{(a)} + n^{(b)}$. A special case of this selection rule is that the coupling between fundamental modes does not excite overtones. This was already observed and explained on symmetry grounds in metric perturbation approach of Section 6.4.2. Next, we extend this argument, in terms of the Einstein tensor, to the Weyl scalar and subsequently generalize it.

The argument we used to show that the second order metric sourced by fundamental modes was itself composed only of fundamental tensor modes made use of the following statements,

$$\mathfrak{L}_{a_-}\ddot{G} = \mathfrak{L}_{b_-}\ddot{G} = 0\,, \qquad [\mathfrak{L}_\xi, \nabla_\mu] = 0\,, \quad \xi \text{ an isometry.} \tag{6.100}$$

Before continuing, we should emphasise that we considered the case where $p_v^{(a)}, p_v^{(b)} > 0$ and complex metric perturbations or, equivalently, just the $++$ channel. If the signs of both p_v are flipped, the role of a_+ and a_- is reversed, but the argument still holds. On the other hand, if one of the contributing linear modes is lowered by a_- while the other is lowered by a_+, such as when $\mathrm{sgn}(p_v^{(a)}) \neq \mathrm{sgn}(p_v^{(b)})$ in the $++$ channel, the argument is bound to fail, as expected given that this would correspond to an infinite excitation channel. For brevity, we will not continuously emphasize these different mode combinations. Rather we again just present the argument for the $++$ channel with $p_v^{(a)}, p_v^{(b)} > 0$, leaving implicit the analysis with $a_+ \leftrightarrow a_-$ for the other finite excitation channels.

First, we want to show that the a_-, b_- operators anhilate the quadratic $\ddot{\Psi}_0$ [9]. The Weyl tensor $\ddot{C}_{abcd}$ is so anhilated by the same argument that we applied to the Einstein tensor. Therefore the only remaining question is to establish how do $\mathfrak{L}_{a_-}$ and $\mathfrak{L}_{b_-}$ act on the background and perturbed frames. We find, by a direct computation

$$\begin{aligned} &\mathfrak{L}_{a_\pm}\ell = \mathfrak{L}_{b_\pm}\ell = 0\,, \quad \mathfrak{L}_{a_\pm} m = \pm\frac{-i}{2}e^{\pm i\Omega u}\ell\,, \quad \mathfrak{L}_{a_\pm}\bar{m} = \pm\frac{-i}{2}e^{\pm i\Omega u}\ell\,, \\ &\mathfrak{L}_{b_\pm} m = \pm\frac{i}{2}e^{\pm\Lambda u}\ell\,,\,, \quad \mathfrak{L}_{b_\pm}\bar{m} = \pm\frac{-i}{2}e^{\pm\Lambda u}\ell\,. \end{aligned} \tag{6.101}$$

Therefore $\mathfrak{L}_{a_-}$ and $\mathfrak{L}_{b_-}$ clearly annihilate $\ddot{C}_{abcd}\ell^a m^b \ell^c m^d$ by the symmetries of the Weyl tensor. On the other hand, noting $\dot{\ell} = 0$ in the GPT gauge we adopted and, using eq. (6.34)

$$\dot{C}_{abcd}\ell^a \dot{m}^b \ell^c m^d = -\frac{1}{2}\dot{C}_{abcd}\ell^a \bar{m}^b \ell^c m^d \text{þ}^2\bar{\Psi}_H\,. \tag{6.102}$$

9 Here we assume that we can always isolate the $++$ contribution in second-order quantities with well-defined p_u, p_v, such as $\ddot{\Psi}_0$.

This too is annihilated by $\mathfrak{L}_{a_-}$ or $\mathfrak{L}_{b_-}$ since both $\text{þ}^2\bar{\Psi}_H$ and $\dot{C}_{abcd}\ell^a\bar{m}^b\ell^c m^d$ are (again when restricted to the $p_v^{(a)} + p_v^{(b)}$ modes and using (6.101) as well as symmetries of the Weyl tensor). Finally,

$$C_{abcd}\ddot{\ell}^a m^b \ell^c m^d = C_{abcd}\ell^a \ddot{m}^b \ell^c m^d = C_{abcd}\ell^a \dot{m}^b \ell^c \dot{m}^d = 0\,, \tag{6.103}$$

because, for the background, only $\Psi_4 \neq 0$. We conclude that two parent modes with $n_y^{(a)} = n_y^{(b)} = 0$ can only couple to a mode of $n_y' = 0$ and, similarly, two parent modes with $n_x^{(a)} = n_x^{(b)} = 0$ in a finite excitation channel can only couple to a mode of $n_x' = 0$.

Running through the same logic for $n_y^{(a)}, n_y^{(b)} \neq 0$ and acting with more than $n_y^{(a)} + n_y^{(b)}$ derivatives, we similarly conclude that $n_y' \leq n_y^{(a)} + n_y^{(b)}$ and analogously for $n_x^{(a)}, n_x^{(b)} \neq 0$ in a finite excitation channel. This represents a rather remarkable cancellation. In fact, minor changes of the source terms (6.40)-(6.41) would break this selection rule. In fact, it is a prime example of a feature that is more readily understood from the metric perturbation approach of Section 6.4.2, even though the master equation (6.39) is typically more convenient for calculations. Confirming that this selection rule is satisfied serves as a consistency check both in the derivation of the source term for the second order master equation, as well as for our calculation of the excitation of QQNMs.

Let us now connect these selection rules with the selection rules for QQNMs for Kerr BHs. Recall that QNMs are labelled by three indices (ℓ, m, n), which are related to the plane wave representations via $p_v = m\Omega$, $n_x = \ell - |m|$, and $n_y = n$, where the QNM frequencies are $\omega_{\ell mn} = p_u$, with p_u satisfying (6.63). Moreover the plane wave approximation requires $|\ell - |m|| \ll \ell$. For QQNMs we have [277, 401] that $(\ell^{(a)}, m^{(a)}, n^{(a)}) \times (\ell^{(b)}, m^{(b)}, n^{(b)}) \to (\ell', m')$, with $m' = m^{(a)} \pm m^{(b)}$ (in the $++$ and $+-$ channels), and $\ell' \geq |m'|$ is arbitrary. The QQNM has frequency $\omega' = \omega^{(a)} \pm \omega^{(b)}$. Notice that QQNMs in Kerr cannot be easily decomposed in radial overtones, unlike the decomposition we achieve here. Our results hence suggest that such a decomposition may be possible, likely following the construction of a radial scalar product following [316, 317], or the bilinear form of [224]. Leaving aside the issue of the overtone decomposition, our selection rules for p_u', p_v' are identical to the selection rules for ω', m', as expected.

Interpreting the selection rules for the overtones is more subtle. First, as noted, no decomposition of the BH QQNMs is usually made in the radial overtones, corresponding to n_y in the Penrose limit. Therefore, these selection rules are likely an emergent phenomenon in the high-frequency limit, although it would be interesting to investigate this further. Similarly, at least for a Kerr BH, with potentially unbounded ℓ', the selection rules for n_x are likely emergent. On the other hand, for a Schwarzschild BH, the situation of the n_x modes is more transparent. In that case, ℓ' is additionally constrained to satisfy $|m'|, |l^{(a)} - l^{(b)}| \leq \ell' \leq l^{(a)} + l^{(b)}$. Therefore, it follows that at most $l^{(a)} + l^{(b)} - \max\left(|m^{(a)} \pm m^{(b)}|, |l^{(a)} - l^{(b)}|\right) + 1$ modes are excited. In the $++$ channel, by the relation $n_x = \ell - |m|$, this becomes

exactly the $n_x^{(a)} + n_x^{(b)} + 1$ modes that are excited in the finite excitation channels. On the other hand, for the +- channel, this becomes instead $n_x^{(a)} + n_x^{(b)} + 1 + \left(|m^{(a)}| + |m^{(b)}| - \max\left(|m^{(a)} - m^{(b)}|, |l^{(a)} - l^{(b)}|\right)\right)$ number of modes that are excited with $|m^{(a)} - m^{(b)}| \leq \max(m^{(a)}, m^{(b)})$ and $|l^{(a)} - l^{(b)}| \leq \max(l^{(a)}, l^{(b)})$. Therefore, because by assumption $l^{(a)} \sim |m^{(a)}| \gg 1$ and $l^{(b)} \sim |m^{(b)}| \gg 1$, it follows that the number of modes excited is large, or in fact infinite in the geometrical optics approximation. This is indeed what is found for the corresponding infinite excitation channels.

6.5.4 *QQNM Excitation*

The simplicity of the homogeneous plane wave background allows us to provide analytical formulas for the ratios describing the QQNM excitation in quite general cases. We first examine the coupling of fundamental modes with different values of $p_v^{(a)} \neq p_v^{(b)}$, and then discuss the self-coupling of overtones.

6.5.4.1 *Fundamental modes*

We begin by examining the coupling between fundamental modes, i.e., couplings of the form $(p_v^{(a)}, 0, 0) \times (p_v^{(b)}, 0, 0)$, where $p_v^{(a)} \neq p_v^{(b)}$, generically. We must distinguish two cases, depending on whether the signs of the eigenvalues in v coincide or differ. Our results can be summarized in the following concise formulas. For the $++$ sector, we have

$$\begin{aligned}
\overset{++(0,0)}{\mathcal{R}}_{(p_v^{(a)},0,0)\times(p_v^{(b)},0,0)} =& \frac{i(p_v^{(a)} + p_v^{(b)})^4}{(p_v^{(a)})^3 (p_v^{(b)})^3} \qquad \left(\text{with} \quad p_v^{(a)} \geq p_v^{(b)} > 0\right), \\
\overset{++(2n,0)}{\mathcal{R}}_{(p_v^{(a)},0,0)\times(p_v^{(b)},0,0)} =& -\binom{-1/2}{n} \left(\frac{i + 2(1+i)n}{1 + 2(1+i)n}\right) (p_v^{(a)})^{1-n} (p_v^{(b)})^{n-3} \left(1 + \frac{p_v^{(b)}}{p_v^{(a)}}\right)^{9/2}, \\
& \left(\text{with} \quad p_v^{(a)} \geq |p_v^{(b)}| > 0 > p_v^{(b)}\right),
\end{aligned} \tag{6.104}$$

where n is any non-negative integer. For the $+-$ sector instead we find

$$\begin{aligned}
\overset{+-(2n,0)}{\mathcal{R}}_{(p_v^{(a)},0,0)\times(p_v^{(b)},0,0)} =& 2^{1-2n} \binom{2n}{n} \left(\frac{i + 2(1+i)n}{1 + 2(1+i)n}\right) (p_v^{(a)})^{1-n} (p_v^{(b)})^{n-3} \left(1 - \frac{p_v^{(b)}}{p_v^{(a)}}\right)^{1/2}, \\
& \left(\text{with} \quad p_v^{(a)} \geq p_v^{(b)} > 0\right), \\
\overset{+-(0,0)}{\mathcal{R}}_{(p_v^{(a)},0,0)\times(p_v^{(b)},0,0)} =& -\frac{2i p_v^{(a)}}{(p_v^{(b)})^3}, \qquad \left(\text{with} \quad p_v^{(a)} > |p_v^{(b)}| > 0 > p_v^{(b)}\right).
\end{aligned} \tag{6.105}$$

The scaling for the ratios leading to the fundamental mode is shown in figure 19.

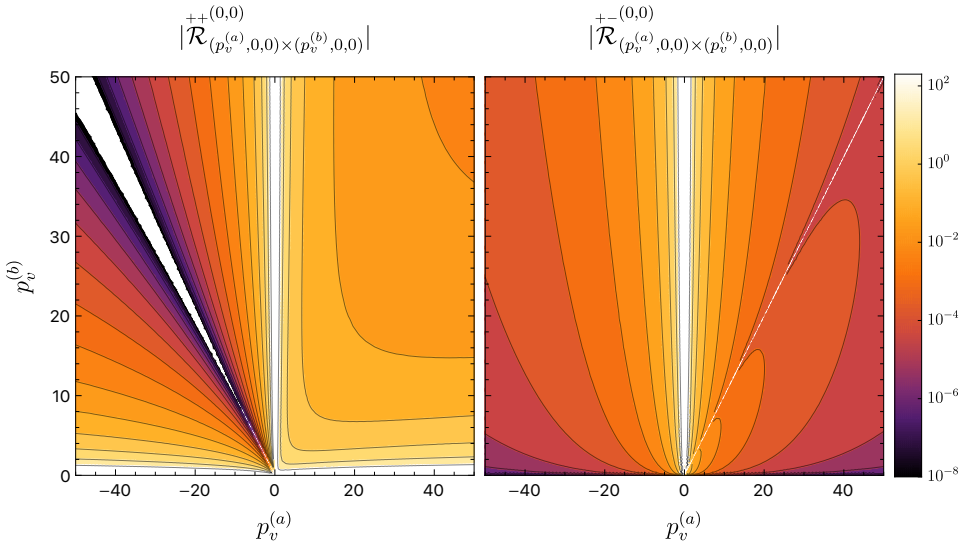

Figure 19 Absolute value of the ratios $\overset{++}{\mathcal{R}}, \overset{+-}{\mathcal{R}}$ for the coupling between $(p_v^{(a)},0,0)\times(p_v^{(b)},0,0)\to(0,0)$, exciting the fundamental mode, in logarithmic scale. We exclude the cases where $p_v^{(a)}+p_v^{(b)}=0$ (for $++$) and $p_v^{(a)}-p_v^{(b)}=0$ (for $+-$), since those correspond to zero frequency modes, as well as the zero-frequency parent modes.

We find that generically these ratios decay as $p_v^{(a)}\sim|p_v^{(b)}|\to\infty$, but they can grow to be large whenever one of the two eigenvalues becomes large, while the other one remains finite. We examine the asymptotic behavior later.

Notice that as required by the selection rules, the overtone number is conserved in the y-direction. Therefore, the combination of fundamental modes only leads to the excitation of overtones in the x-direction within the infinite-excitation channels. As $n\gg 1$, the amplitude of the n–th overtone decays as

$$\left|\overset{++}{\mathcal{R}}{}^{(2n,0)}_{(p_v^{(a)},0,0)\times(-|p_v^{(b)}|,0,0)}\right|\sim\left|\overset{+-}{\mathcal{R}}{}^{(2n,0)}_{(p_v^{(a)},0,0)\times(|p_v^{(b)}|,0,0)}\right|\sim n^{-1/2}\left(\frac{\left|p_v^{(b)}\right|}{p_v^{(a)}}\right)^n. \tag{6.106}$$

In the high-frequency regime, i.e., taking $p_v^{(a)},|p_v^{(b)}|\sim p_v\to\infty$, but keeping $p_v^{(a)}-|p_v^{(b)}|=\delta$ fixed and finite, the ratios scale as

$$\begin{aligned}
\overset{++}{\mathcal{R}}{}^{(0,0)}_{(p_v,0,0)\times(p_v-\delta,0,0)} =&\frac{16i}{p_v^2}\left(1+\frac{\delta}{p_v}\right)+\mathcal{O}(p_v^{-4}),\\
\overset{+-}{\mathcal{R}}{}^{(0,0)}_{(p_v,0,0)\times(\delta-p_v,0,0)} =&-\frac{2i}{p_v^2}\left(1+\frac{3\delta}{p_v}\right)+\mathcal{O}(p_v^{-4}),\\
\overset{++}{\mathcal{R}}{}^{(2n,0)}_{(p_v,0,0)\times(\delta-p_v,0,0)} =&(-1)^n\binom{-1/2}{n}\left(\frac{i+2(1+i)n}{1+2(1+i)n}\right)\sqrt{\frac{\delta^9}{p_v^{13}}}+\mathcal{O}(p_v^{-15/2}),\\
\overset{+-}{\mathcal{R}}{}^{(2n,0)}_{(p_v,0,0)\times(p_v-\delta,0,0)} =&2^{1-2n}\binom{2n}{n}\left(\frac{i+2(1+i)n}{1+2(1+i)n}\right)\sqrt{\frac{\delta}{p_v^5}}+\mathcal{O}(p_v^{-7/2}),
\end{aligned} \tag{6.107}$$

where $p_v \gg \delta > 0$. Thus, in the high-frequency limit all of these ratios vanish, albeit not at the same rate. Moreover, whenever we take $\delta \ll p_v$, the contributions to one of the channels – the one responsible for the infinite excitation channels – become highly suppressed. In the limit $\delta \to 0$, corresponding to $p_v^{(a)} \pm p_v^{(b)} = 0$, the ratio in this channel vanishes identically. As discussed previously, additional care is needed to treat these modes, since they do not depend on v. In a way, they play a similar role as the metric-completion piece when reconstructing the second-order metric perturbation in Kerr and we leave their study to future work.

Finally we note that if $p_v^{(a)} \to \infty$ keeping $p_v^{(b)}$ fixed, the ratios grow linearly with $p_v^{(a)}$. This is reminiscent of the result for a similar mode combination found for Schwarzschild BHs in the high-frequency regime in [88]. This reinforces the expectation that the exploration of QQNMs in plane waves may shed light towards the structure and excitation of QQNMs in BHs, although further work is necessary to connect these two in a precise manner.

6.5.4.2 *Self-excitation*

Next we discuss the self-excitation of overtones, i.e., couplings with $p_v^{(a)} = p_v^{(b)} = p_v$, $n_x^{(a)} = n_x^{(b)} = n_x$, and $n_y^{(a)} = n_y^{(b)} = n_y$. We focus on the $++$ sector and assume for simplicity that $p_v > 0$. This means that we restrict to study the coupling of overtones within finite excitation channels. We emphasize that the code that we make available [1] can compute arbitrary couplings. We find

$$\overset{++}{\mathcal{R}}{}^{(2n_x,0)}_{(p_v,n_x,0)^2} = \frac{(-1)^{n_x} i\alpha_{n_x}}{p_v^2}\,, \qquad \overset{++}{\mathcal{R}}{}^{(n_x,0)}_{(p_v,n_x,0)^2} = (1+(-1)^{n_x})\frac{\beta_{n_x}}{2p_v^2}\,, \qquad \overset{++}{\mathcal{R}}{}^{(0,0)}_{(p_v,n_x,0)^2} = \frac{\gamma_{n_x}}{p_v^2}\,, \tag{6.108}$$

where $\alpha_n, \beta_n, \gamma_n$ are coefficients whose behavior is illustrated in figure 20. We notice that $|\gamma_{n_x}| = \alpha_{n_x}$, while $|\beta_{n_x}| < \alpha_{n_x}$ for all $n_x > 0$. This hints that the excitation of different overtones occurs in a symmetric way – the minimum and maximum overtone number possible are excited with the same amplitude up to a phase. Figure 20 also shows that $\alpha_{n_x}, |\beta_{n_x}| \to$ const. seemingly as $n_x \to \infty$ for odd and even n_x separately. Notice also that these ratios scale as p_v^{-2}, which is the same scaling found for the fundamental modes. This scaling depends on the fact that we are normalizing the Weyl scalar $\dot{\Psi}_0$ of the modes at the LR, and different normalizations would lead to somewhat different scalings, as discussed in Eq. (6.84), although see again also the ratio (6.95) for the invariant physical implication of this result.

For the excitation of overtones in the y direction, we note the following crossing symmetry between $x \leftrightarrow y$:

$$\overset{++}{\mathcal{R}}{}^{(n_x',n_y')}_{(p_v,n_x,n_y)^2} = -\left(\overset{++}{\mathcal{R}}{}^{(n_y',n_x')}_{(p_v,n_y,n_x)^2}\right)^* . \tag{6.109}$$

In fact, this holds even if the two parent modes have different p_v, as long as they are in the finite excitation channel. Clearly, the x and y directions behave differently

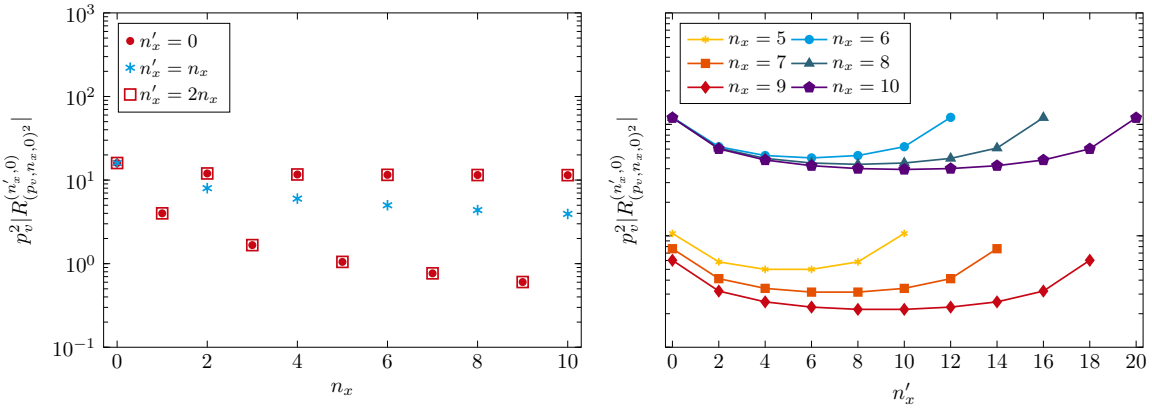

Figure 20 **Left.** Scaling of the self-coupling ratios $|\overset{++}{\mathcal{R}}{}^{(n'_x,0)}_{(p_v,n_x,0)^2}|$ as a function of the *parent* overtone n_x, for different values of n'_x. Red squares, blue stars, and red points correspond to $\alpha_{n_x}, \beta_{n_x}, \gamma_{n_x}$ in Eq. (6.108) respectively. Remark $|\gamma_{n_x}| = \alpha_{n_x}$. **Right.** Scaling of the same self-coupling ratios as a function of the *child* overtone index n'_x, for different values of the parent overtone number n_x. The same behavior is found when swapping the x and y directions, see also (6.109).

in the infinite excitation channel. Regardless (6.109) implies that for the couplings in (6.108), we can restrict our discussion to self-excitation of overtones in the x-direction. These are analyzed in more detail in figure 20. The panels in this figure show the absolute values of the coefficients $\alpha_n, \beta_n, \gamma_n$ from (6.108) as a function of n_x (left) and the excitation of different overtones, as given by their value of n'_x, due to the self-coupling $(p_v, n_x, 0) \times (p_v, n_x, 0) \to (n'_x, 0)$ (right). We observe that the spectrum of overtone excitations is symmetric with respect to the parent overtone. It leads to a somewhat flat spectrum, slightly favoring the excitation of the most extreme overtone numbers $n'_x = 0$ and $n'_x = 2n_x$. The odd and even parity overtones group themselves, yielding somewhat quantitatively different values. Again, this difference is sensitive to our choice of normalization of the modes. We have opted for a "local" choice of normalization which is physically based on the values the Weyl scalar (even) or its derivatives (odd) takes at the reference geodesic ($x = y = 0$).

6.6 CONCLUSIONS

Probing the non-linear regime of gravity is a challenging task. In this chapter we have taken one further step in this direction by studying the back-reaction of perturbations on plane wave spacetimes. Plane wave geometries are not only interesting in their own right, they also appear ubiquitously as approximate geometries near null geodesics. Specifically, near equatorial light-rings of Kerr black holes, a special class of Lorentzian symmetric (Cahen-Wallach) plane waves emerge, which capture an asymptotic branch of quasinormal modes. The non-linearities around such plane waves can thus be interpreted in terms of quadratic quasinormal modes.

We have studied second-order perturbations on general plane wave spacetimes, using a purely GHP-covariant formalism. We reduce the problem of studying second-

order perturbations to solving a sourced master wave equation, where the source is written in terms of a Hertz potential generating the first-order metric perturbations. Along the way, we also derive Teukolsky-Starobinsky identities for generic plane-wave spacetimes. Additionally, we present a complementary framework built upon metric perturbations for the case of plane waves with additional Killing vectors. While we expect this approach to work for the entire class of homogeneous plane waves, we work it out explicitly for the previously mentioned Lorentzian symmetric plane waves. Here, the algebraic structure of the plane waves reduces to that of simple and inverse harmonic oscillators, and the Killing vectors can be used to generate tensor harmonics, which in turn reduce Einstein's equations to mere algebraic equations. Such an approach based on metric perturbations, evades entirely the difficulty of reconstructing the metric from curvature perturbations.

Finally, we use our perturbation frameworks to define and compute the excitation of quadratic quasinormal modes, and measure their excitation in the second-order fluctuations of the Weyl scalar Ψ_0. Our work here extends previous work [269, 377], by computing the excitation of QQNMs for arbitrary combinations of linear modes. The second-order fluctuations of the curvature scalar Ψ_0 can always be written as a (possibly infinite) sum of eigenfunctions of the wave operator – this allows us to uncover emergent selection rules in the overtone numbers of the quadratic quasinormal modes. We provide analytical formulas for some relevant mode couplings as well as providing a code in [1], which can compute them more generally.

The excitation of QQNMs presented here is motivated by and related to the high-frequency limit of QQNMs of rotating BHs. The linear modes of symmetric plane waves correspond to the high frequency limit of Kerr QNMs through a particular identification of quantum numbers. Therefore, we can put in (approximate) correspondence the QQNMs excited in the plane wave spacetime to certain QQNMs in a Kerr black hole – indeed, their frequencies would match. Our results capture the second order curvature fluctuations evaluated exactly at the equatorial LR of the Kerr black hole. Moreover, as discussed in previous sections, our results depend on a gauge (and frame) which builds upon the geometric properties of homogeneous plane waves. Therefore, the main steps that should be taken to perform a precise match with the black hole quadratic quasinormal modes are: (i) matching the gauge and frame used in describing perturbations of Kerr to the GPT gauge presented here, and (ii) translating the ratio extracted at the lightring to the ratio extracted at future null infinity. We leave this for future work.

Another aspect of the second order perturbations which we leave to future work are zero-frequency modes, which appear in certain quadratic combinations. These zero-frequency modes likely cannot be interpreted as QQNMs of a black hole. Nevertheless, it would be interesting to better understand these contributions simply from the point of view of plane wave perturbation theory in its own right as well as in relation to the effective gravitational stress-energy tensor for the background that should be solved self-consistently with geometrical optics perturbations, as discussed already in [253, 254].

In addition to the immediate extensions of the present work suggested above, there is significant potential to bring more of the existing literature on plane wave spacetimes, sometimes already containing higher order perturbative results, to bear on or reinterpret them in light of the non-linear ringdown. To be sure, such extensions would only represent a highly particular limit of the ringdown problem and, in many instances, it will only be a toy model. Yet, it may not be entirely unfair to say that the Cahen-Wallach plane wave stands to the ringdown as the de Sitter space does to the cosmic microwave background. Thus, we believe that it would be a worthwhile pursuit.

7

RINGDOWN OF A DYNAMICAL SPACETIME

Written while listening to music composed by Sergei Rachmaninoff.

7.1 INTRODUCTION

The excitation of higher harmonics during the ringdown is an exciting prospect. However, this is not the only nonlinear effect present in the relaxation of BHs to equilibrium. Borrowing from nonlinear optics, one may also expect effects such as spectral broadening, manifesting e. g., as time-varying QNM frequencies. This effect is evident if one takes into account that the BH horizon changes its area by several percent in the early ringdown stages [348]. If the BH mass and spin are dynamical, so are its QNMs, and a model based on a superposition of linear QNMs with fixed frequencies and amplitudes is *not* the best model. This is one of the (multiple) reasons why ringdown models based on a superposition of QNMs, such as the model used in Chapter 3 or Chapter 5, are only accurate several cycles after the peak of the GW emission [5, 117, 119, 148, 149]. In this chapter we attempt to understand how does a BH with a varying mass relax to equilibrium, and how to model its ringdown emission.

Given the violent merger process, leading to considerable luminosities in GWs, accounting for the changing mass and spin in the early stages of the ringdown is necessary in order to have waveform models that accurately describe the early postmerger stage. It turns out that a dynamically changing BH mass and spin can excite a plethora of modes [419] (see also [42, 450]). The analysis of these effects has been performed focusing on scalar fields in anti-de Sitter space, thus providing only a qualitative picture and guide for how would the mechanism work in asymptotically flat space, where the structure of infinity and the dynamics are drastically different. It is therefore important to include asymptotically flat BHs in the framework. We will significantly improve and extend previous studies, by considering a setup where backreaction due to absorption can be modelled exactly, at the cost of restricting to configurations that are close to spherical symmetry.

More precisely, we consider linear fluctuations of gravitational and pure radiation fields around Vaidya's spacetime, the latter being an exact solution to Einstein's equation describing accretion of radiation by a BH. This setup allows us to discuss in detail the effects of the mass change in the ringdown waveform. In particular, we provide a model that, by coupling the amplitudes, frequencies and phases to the

evolving mass of the BH, is able to accurately capture the whole waveform, even in regimes where the timescale of the mass change is comparable to the oscillation frequency of the QNMs. An open question which we are also able to answer – in the negative – concerns possible echoes of GWs [100, 106], caused by reflections off the infalling matter. We find no evidence for such a phenomena within our setup. Previous studies of perturbations on Vaidya spacetime [9, 140] were restricted to scalar perturbations, which do not couple to neither the gravitational nor the pure radiation fluctuations. These studies already showed the coupling between the ringdown frequencies and the instantaneous mass of the BH. We extend them in several directions, by considering gravitational perturbations and uncovering the coupling to matter fluctuations, as well as by providing heuristic and accurate models of the ringdown signal on a Vaidya spacetime.

The chapter is organized as follows: first, in section 7.2 we provide a simple heuristic argument that nevertheless captures some of the main features of ringdown in an accreting spacetime. In section 7.3 we discuss the exact framework that we will be working with (gravitational perturbations in Vaidya spacetime), obtaining the master equation describing axial perturbations and discussing our numerical methods. We study our solutions in section 7.4, including extracting the mode content from the signal and finally proposing a novel waveform model based on time–varying amplitudes and frequencies, which captures better the waveform in the presence of accretion. We summarize our findings in Section 7.5.

7.2 HEURISTICS

As a first exercise, we consider a simplified problem that may, however, illustrate some of the main features of BH relaxation in the presence of accretion. In particular, we will deal with the case of a very quick accretion process. The regime of very slow or adiabatic accretion presents additional difficulties due to the presence of possible secular effects, and we leave its study for future work.

Take a BH with initial mass m_1 relaxing in a ringdown process. The metric perturbation h can be recovered, up to gauge redundancies [141, 454], from the Weyl scalar $\dot{\Psi}_4^{[1]} \equiv \dot{\Psi}$, where we remind that dotted quantities refer to linear perturbations. In addition, the superscript $[1]$ indicates that the perturbation is to be taken with respect to the BH spacetime with mass m_1. For simplicity we take the curvature perturbation to be a pure quadrupole QNM, with angular number $\ell = 2$.

Now consider that at some time, t_1, the BH undergoes an "instantaneous" mass increase $m_1 \to m_2$ with $m_2 > m_1$. Then, the evolution of the Weyl scalar at $t > t_1$, denoted by $\dot{\Psi}^{[2]}$, is governed by the wave operators of the BH with mass m_2, $\mathcal{O}^{[2]}\dot{\Psi}^{[2]} = 0$, subject to the initial conditions at t_1 given by a QNM of the BH with mass m_1, that is, $\dot{\Psi}^{[1]}(t = t_1)$. At intermediate times $t > t_1$ the solution can be approximated by a superposition of QNMs $\psi_n^{[2]}$ of the larger BH

$$\dot{\Psi}^{[2]}(t, r) = \sum_{n=0}^{\infty} c_n^{[2]} e^{-i\omega_n^{[2]}(t-t_1)} \psi_n^{[2]}(r) \tag{7.1}$$

where $c_n^{[2]}$ are excitation factors to be determined from the initial conditions at $t = t_1$, $\omega_n^{[2]}$ are the QNM frequencies of the BH with mass m_2 and $\psi_n^{[2]}$ are the radial wavefunctions of the QNMs with frequency $\omega_n^{[2]}$. In [224] (see also [419]) it was shown that such QNM excitation coefficients can be computed from the initial conditions by projecting them onto QNMs using a bilinear form, denoted $\langle\langle \cdot\,, \cdot \rangle\rangle$, with respect to which QNMs with different frequencies are orthogonal. This bilinear arises from the conserved current induced by the definition of the adjoint operator, together with the discrete $\mathbb{Z}_2$ symmetry of Kerr mapping $(t, \phi) \mapsto (-t, -\phi)$ in Boyer-Lindquist coordinates 4. Indeed, the Teukolsky operator defines a current π_a via

$$\mathcal{O}_4^\dagger(\mathrm{Y})\tilde{\mathrm{Y}} - \mathrm{Y}\mathcal{O}_4(\tilde{\mathrm{Y}}) = \nabla^a \pi_a[\tilde{\mathrm{Y}}, \mathrm{Y}]\,, \tag{7.2}$$

for some $\mathrm{Y}, \tilde{\mathrm{Y}}$. This current is trivially conserved if $\mathcal{O}_4^\dagger \mathrm{Y} = \mathcal{O}_4 \tilde{\mathrm{Y}} = 0$. A symmetry operator $\mathcal{C}$ mapping solutions of the adjoint to solutions of the original operator defines now a bilinear form

$$\langle\langle \mathrm{Y}_1\,, \mathrm{Y}_2 \rangle\rangle \equiv \int_\Sigma \star\pi[\mathcal{C}\mathrm{Y}_1, \mathrm{Y}_2]\,. \tag{7.3}$$

Taking $\mathcal{C}$ to be precisely the time-azimuthal angle simultaneous reversal frequency (corresponding to simultaneously reversing time and the direction of the BH spin) leads to the bilinear form defined in [224]. For nonrotating BHs, in Schwarzschild coordinates and relative to a Kinnersley tetrad, this is

$$\begin{aligned}\langle\langle \mathrm{Y}_1\,, \mathrm{Y}_2 \rangle\rangle =& m_2^{4/3} \int_\Sigma dr\, d\theta d\phi\, \frac{\sin\theta}{r^4 f^2} \Bigg\{ \mathrm{Y}_1\Big|_{\substack{t\to -t \\ \phi \to -\phi}} \left(\frac{r^2}{2f}\partial_t - 2\left(r - \frac{m_2}{2f}\right)\right) \mathrm{Y}_2 \\ &+ \mathrm{Y}_2 \left[\left(\frac{r^2}{2f}\partial_t - 2\left(r - \frac{m_2}{2f}\right)\right) \mathrm{Y}_1\right]_{\substack{t\to -t \\ \phi \to -\phi}} \Bigg\}\,,\end{aligned} \tag{7.4}$$

where $2f = 1 - 2m_2/r$. This bilinear is not well-defined for solutions that do not have compact support on the spacelike constant-time slice Σ. However, its definition can be extended by appropriately deforming the integration contour in the radial coordinate, analytically continuing this into the complex plane. By doing this, the QNM excitation coefficients are simply recovered as

$$\mathrm{Y} = \sum_{\ell m n} c_{\ell m n} \mathrm{Y}_{\ell m n}\,, \iff c_{\ell m n} = \frac{\langle\langle \mathrm{Y}\,, \mathrm{Y}_{\ell m n} \rangle\rangle}{\langle\langle \mathrm{Y}_{\ell m n}\,, \mathrm{Y}_{\ell m n} \rangle\rangle}\,, \tag{7.5}$$

with $\mathrm{Y}_{\ell m n}$ being QNMs labelled by the usual angular and overtone numbers 3.

Making use of this bilinear form, if $\dot{\Psi}^{[1]}(t = t_1)$ are initial conditions, then we can write

$$c_n^{[2]} = \frac{\langle\langle \dot{\Psi}^{[1]}(t = t_1)\,, \psi_n^{[2]} \rangle\rangle}{\langle\langle \psi_n^{[2]}\,, \psi_n^{[2]} \rangle\rangle}\,. \tag{7.6}$$

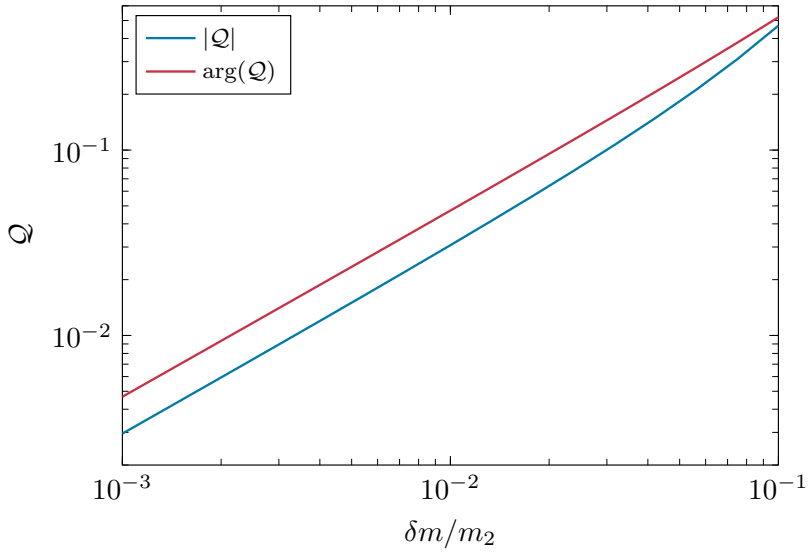

Figure 21 Decoherence factor $\mathcal{Q} = |C_{00} - 1|$ as a function of the relative change of mass $\delta m/m_2$, in absolute value (blue), and argument (red), written as $\mathcal{Q} = |\mathcal{Q}|e^{-i\mathrm{Arg}(\mathcal{Q})}$.

Now if for simplicity we take the initial perturbation to consist only of the fundamental mode ($n = 0$), the solution at all times can be written as

$$\Psi(t) = A_0 \begin{cases} e^{-i\omega_0^{[1]}t}\psi_0^{[1]}\,, & t < t_1\,, \\ \sum_{n=0}^{\infty} e^{-i(\omega_0^{[1]}-\omega_n^{[2]})t_1} C_{0n} e^{-i\omega_n^{[2]}t}\psi_n^{[2]}\,, & t > t_1\,. \end{cases} \tag{7.7}$$

Above we have defined the mixing coefficients C_{kn},

$$C_{kn} = \frac{\langle\langle \psi_k^{[1]}, \psi_n^{[2]} \rangle\rangle}{\langle\langle \psi_n^{[2]}, \psi_n^{[2]} \rangle\rangle}\,. \tag{7.8}$$

Thus, at late times we can observe two distinct effects: (i) the off-diagonal terms C_{0n} excite overtones of the final BH from the initial fundamental mode. This can be seen as an absorption induced mode excitation (AIME) effect [419]. (ii) The diagonal term, C_{00}, can be generically different than 1. This results in a renormalization of the amplitude of the fundamental mode, a similar effect to that of second order perturbation theory [300]. We refer to this process as a *decoherence* effect, since in practice the absorption is causing the initially coherent signal of a single mode to become a superposition of several modes, with different amplitudes.

We can then quantify which fraction of the initial QNMs amplitude projects into the fundamental mode of the BH after accretion, and which fraction is transmitted into certain number of overtones through AIME. We define the decoherence factor $\mathcal{Q}$ as

$$\mathcal{Q} \equiv C_{00} - 1 = \frac{\langle\langle \psi_0^{[1]}, \psi_0^{[2]} \rangle\rangle}{\langle\langle \psi_0^{[2]}, \psi_0^{[2]} \rangle\rangle} - 1\,. \tag{7.9}$$

This factor estimates how different is the amplitude that we would measure of the fundamental mode before and after accretion. Figure 21 shows that the decoherence

grows approximately linearly with the change of mass $\delta m = m_2 - m_1$ (although higher order terms become important as δm becomes larger), consistently with [419]. Moreover, the decoherence degree can be as large as $\sim$ 10% for an accretion process where the mass changes only by a few percent. Although we will discuss in Section 7.5 in more detail the phenomenological implications of our work, this already suggests that absorption can have a large effect in the amplitude evolution of QNMs.

The mass transition considered in this section is "instantaneous", and thus should only be regarded as an illustrative example. In what follows we consider instead a physically well-defined set up, where the effects of accretion on GWs are incorporated nonperturbatively.

7.3 FRAMEWORK

The aim of this chapter is to explore the effects of accretion on the free oscillations of a BH. To do so we will consider fluctuations of exact solutions of GR that describe BHs accreting high frequency radiation, e.g. GWs. This set up allows us to account for the non-linear interactions between gravity and in-falling matter, while retaining the relative simplicity of perturbation theory.

7.3.1 *Pure Radiation Fields and Vaidya spacetimes*

A *pure radiation field*, or *null dust* [437], is a spacetime satisfying

$$G_{ab} = \Phi K_a K_b \,, \quad K^a K_a = 0 \,, \tag{7.10}$$

where K^a and Φ are a null vector and a function. Conservation of the energy-momentum tensor (an immediate consequence of (7.10)) implies that K^a is geodesic, and without loss of generality, by simultaneous rescalings of Φ and K^a, it can be chosen to be affinely parametrised

$$K^a \nabla_a K^b = 0 \,. \tag{7.11}$$

Physically, this is a spacetime describing the high-frequency (eikonal) approximation to unpolarized radiation, with energy density Φ, propagating along the null direction K^a. This class of spacetimes was introduced by Vaidya [452], and have proved useful in a wide range of physical scenarios ever since.

In double null coordinates (u, v, θ, ϕ), the spherically symmetric line element reads [216] [1]

$$ds^2 = -2f(u,v)dudv + r^2(u,v)d\Omega^2 \,, \tag{7.12}$$

which are well-defined coordinates as long as $f(u,v) \neq 0$. Above, r is the area radius function, and $d\Omega^2$ denotes the metric on the unit round 2–sphere. Without

1 The factor 2 is perhaps unconventional, but we choose to include it to follow the convention of [9, 216]. For the Schwarzschild geometry with mass m, $2f = (1 - 2m/r)$.

loss of generality, K^a can be taken to point along one of the null directions, say $K \sim \partial_u$. Then, up to rescalings of K^a that depend on v only, Eq. (7.11) fixes

$$K = \frac{1}{f(u,v)}\partial_u \,. \tag{7.13}$$

The remaining equations do not fix the solution completely, and allow the free choice of a "mass-profile function" $m(v)$ (in terms of the Riemann tensor, $m = \frac{1}{2}r^3 R^{\theta\phi}_{\theta\phi}$)[458]. Restricting to mass profiles with $\partial_v m(v) \neq 0$, Einstein's equations can be reduced to a transport equation for $r(u,v)$ along ∂_v (the direction transverse to the null dust K^μ),

$$\partial_v r = -\varepsilon\left(1 - \frac{2m(v)}{r}\right), \qquad \varepsilon \equiv -\frac{\partial_v m(v)}{2|\partial_v m(v)|}, \tag{7.14}$$

which has a unique solution once an initial condition $r(u,v_0)$ is prescribed. Then, the functions f and Φ are[2]

$$f = 2\varepsilon\partial_u r\,, \qquad \Phi = -4\varepsilon\frac{\partial_v m}{r^2} = 2\frac{|\partial_v m|}{r^2}\,. \tag{7.15}$$

Notice that the second of these equations implies that the weak-energy condition holds automatically. We shall restrict to solutions with $f > 0$ in the regime of validity of the double null coordinates, and fix the time orientation by declaring K^a in (7.13) to be future-oriented (so that ∂_u and ∂_v are future-oriented, too). Along the trajectories of K^a the area-radius function $r(u,v)$ varies according to

$$K^a\nabla_a r = 2\varepsilon\,. \tag{7.16}$$

Therefore, increasing ($\varepsilon < 0$) or decreasing ($\varepsilon > 0$) profiles of $m(v)$ correspond to in-going or out-going pure-radiation fields, respectively. We will consider smooth mass profiles that interpolate between constant initial and final values

$$m\,(v \to \pm\infty) = \underset{1}{m_2}\,, \tag{7.17}$$

and will choose the asymptotic condition for the flow equation (7.14) of $r(u,v)$ as follows. At a slice $v = v_{\max}$, where $v_{\max} \gg 1$ is taken large enough to achieve the condition

$$\left|\frac{m_2 - m(v_{\max})}{m_2}\right| \ll 1\,, \tag{7.18}$$

we demand that $r(u,v_{\max})$ satisfies

$$r(u,v_{\max}) = \frac{m_2 - m_1}{|m_2 - m_1|}\frac{v_{\max} - u}{2} \tag{7.19}$$

$$- 2m(v_{\max})\ln\left|\frac{r(u,v_{\max})}{2m(v_{\max})} - 1\right|\,. \tag{7.20}$$

2 We have implicitly made some non-generic choices in reducing the equations of motion to (7.14) and (7.15) [458], but the class of solutions considered here are general enough for our purposes.

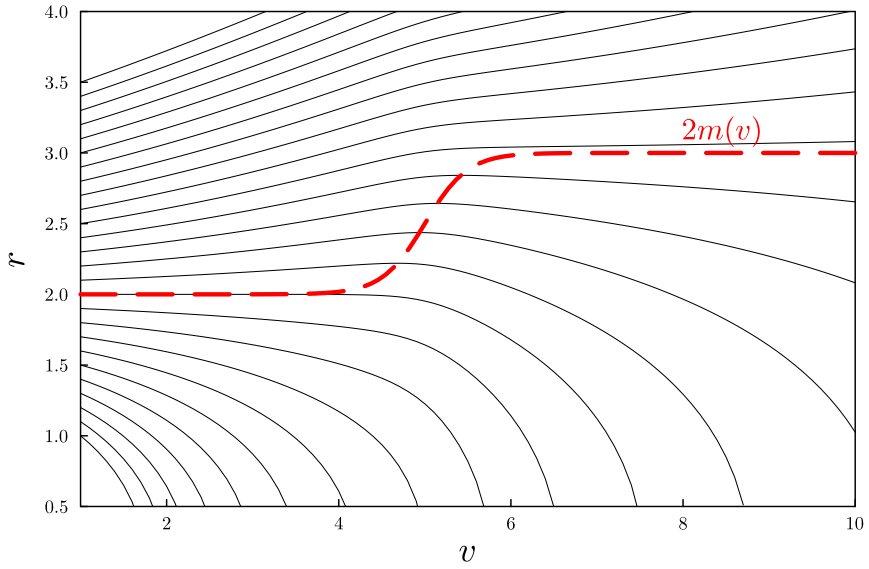

Figure 22 Lines of constant u for the mass profile (7.21), with $m_2 = 1.5m_1$, $v_1 = 5$, and $\tau = 0.5$. The red line shows the evolution of the mass profile $2m(v)$. Lines below this mass profile have always $r' < 0$ and fall inevitably towards the singularity.

This choice allows us to interpret (u, v), at large v, as the usual retarded and advanced times corresponding to the asymptotic state of the Vaidya background. The future event horizon and future null infinity are located at $u \to \infty$, $v \to \infty$, respectively.

Before considering a specific example, we notice that given an in-going pure-radiation solution associated to $r(u, v)$ with increasing mass profile $m(v)$ (i.e. where $f, \Phi, K...$ are constructed from $r(u, v)$ and $m(v)$ using the equations above), there is an out-going pure-radiation solution associated to $\tilde{r}(u, v) \equiv r(-u, -v)$ with decreasing mass profile $\tilde{m}(v) \equiv m(-v)$. As a case study, consider a mass function of the form

$$m(v) = m_1 + \frac{m_2 - m_1}{2}\left(1 + \tanh\left[\frac{v - v_1}{\tau}\right]\right), \tag{7.21}$$

where the mass increases from $m_1 \to m_2$ in a time-scale controlled by the parameter τ. This allows us to easily model different kinds of situations: ranging from the almost adiabatic increase of mass to very sudden changes. Integrating equation (7.14) numerically subject to condition (7.19), one finds a solution that describes a spherically symmetric BH increasing its mass from m_1 to m_2, as illustrated in the causal diagram in Fig. 22.

7.3.2 *Linear Fluctuations*

Fluctuations of pure radiation fields consist of a gravitational perturbation $\dot{h}_{ab}$ and the matter fields perturbations $\dot{\Phi}$ and $\dot{K}_a$, governed by equations (7.10) linearised on the background introduced above. While our background is spherically-symmetric,

the fact that it is not vacuum entails a coupling between $\dot{h}_{ab}$, $\dot{\Phi}$ and $\dot{K}_a$ that makes the analysis considerably more involved. Here we build on the formalism already introduced in Chapter 3 to derive the equations of motion in a gauge-invariant manner. Being concerned mostly with free oscillations of BHs, in this work it will suffice to restrict to the axial sector of the fluctuation. Since the spacetime is non-vacuum, our starting point must be the linearised Einstein equations (3.18). Introducing the Regge-Wheeler (RW) master variable Ψ as in (3.19), the linearised Einstein equations lead to a (sourced) master equation for Ψ [3]

$$\begin{aligned} r^2\nabla_A\left(r^{-2}\nabla^A(r\Psi)\right) - \frac{\ell(\ell+1)-2}{r}\Psi = r^2\varepsilon^{AB}K_B\nabla_A\left(\Phi\mathsf{v}\right), \\ K^A\nabla_A\left(r^2\Phi\mathsf{v}\right) = 0, \end{aligned} \tag{7.22}$$

where v is the odd-parity perturbation to the null vector $\dot{K}_a$,

$$\dot{K}_a = \mathsf{v}\mathcal{X}_I dz^I, \tag{7.23}$$

and the second equation in (7.22) is the linearised conservation of the stress energy tensor.

In double-null coordinates, evaluating the above equations on the background implies that we can substitute the derivatives of $r(u,v)$ by

$$\partial_v r = -\varepsilon\left(1-\frac{2m(v)}{r}\right), \quad \partial_u r = \frac{f(u,v)}{2\varepsilon}, \quad \partial^2_{uv} r = -\frac{m(v)f(u,v)}{r^2}. \tag{7.24}$$

Remarkably, the second of Eqs. (7.22) can be solved exactly for v, giving

$$\mathsf{v} = \frac{F(v)}{r^2\Phi}, \tag{7.25}$$

where $F(v)$ is a free function of v, which corresponds to an initial condition for v. In parallel, the first equation in (7.22) gives

$$\left[\partial^2_{uv} - \frac{f}{r}\left(\frac{3m(v)}{r^2} - \frac{\ell(\ell+1)}{2r}\right)\right]\Psi = \frac{2f}{r^2}\varepsilon F(v), \tag{7.26}$$

which is the master wave equation we are seeking for. In a static background of mass m one recovers the classic RW equation (in particular, the only consistent choice in that case is $F(v)=0$, as follows from (7.25) and the fact that for constant m one has $\Phi = 0$).

Equations (7.25)–(7.26) are one of our main results. Matter perturbations are completely determined once $F(v)$ is prescribed and do not depend on the gravitational sector Ψ. Axial GWs, on the other hand, are sourced by matter fluctuations in a very simple way. We can contrast this behaviour to axial perturbations of perfect fluids in

3 Here, upper case latin indices run from 0 to 1, and all the geometric pieces (such as the volume form ε_{AB} and covariant derivative ∇_A) are associated to the metric g_{AB} induced on surfaces of constant spherical angles.

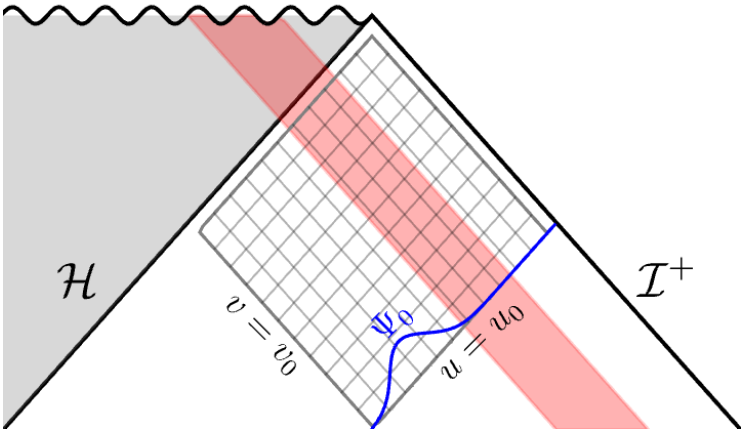

Figure 23 Upper half of the Penrose diagram describing Vaidya spacetime. The horizon grows due to absorption of null matter falling (red shaded region). Here, $\{u_0, v_0\}$ represent the region where we impose the initial conditions (blue curve), and $\{u_{\max}, v_{\max}\}$ control how close does our grid get to the horizon and null infinity, respectively.

stationary backgrounds [42, 108, 109, 131, 443], where the gravitational fluctuation satisfies an homogeneous equation. In the other extreme are *polar* fluctuations (not considered here) which couple efficiently to the matter sector even in static spacetimes [108, 109]. Thus, results (7.25)–(7.26) are an interesting outcome of dealing with a special type of matter, null radiation, in a non-stationary background.

7.3.3 *Numerical Framework*

We will solve the previous master equation numerically, making use of a characteristic algorithm. Here, we present the details of the numerical evolution, as well as the class of initial conditions that we will consider. The master equation that we are dealing with has the general form

$$\partial^2_{uv}\Psi + V(u,v)\Psi = \mathcal{S}[F]\,, \tag{7.27}$$

where Ψ is the master variable, $V(u,v)$ is the potential and $\mathcal{S}$ is a source term that depends on the matter fluctuations F. We consider a finite discrete grid in the range $[u_0, u_{\max}] \times [v_0, v_{\max}]$, as shown in Fig. 23.

In order to prescribe initial conditions, we assume that the $v = v_0$ surface is located far enough that we can set $\Psi(u, v_0) = 0$, giving initial data only in the $\Psi(u_0, v)$ surface. We consider a Gaussian wave packet

$$\Psi(u_0, v) = \Psi_0 \exp\Big(-\frac{(v - v_\Psi)^2}{\sigma^2_\Psi}\Big)\,. \tag{7.28}$$

Whenever we consider nonvanishing matter fluctuations, the profile $F(v)$ will also be given by a Gaussian of the form (7.28).

The evolution proceeds through the usual characteristic algorithm [229]. We integrate the equations from left to right at each new constant v slice. The first order

equations of the background (7.14)–(7.15) are solved using a fourth order finite difference approximation. The time update for the wave equation is given by

$$\Psi_N = \Psi_E + \Psi_W - \Psi_S + \frac{\Delta_u \Delta_v}{2} V_S (\Psi_E + \Psi_W) - \mathcal{S}_S \,, \tag{7.29}$$

where N, E, S, W denote the north, east, south and west points as seen from the Penrose diagram, and Δ_u, Δ_v are the grid resolutions in the u and v directions. A challenging point of the evolution appears when solving the radial equation Eq. (7.14), which needs instant conditions given by Eq. (7.19). In order to efficiently solve for the initial conditions, we combine two different algorithms, depending on whether $r_\star = (v-u)/2$ is large enough [229]. When $r_\star$ is large, a simple root–finding algorithm converges quickly. When $r_\star \lesssim 0$, we iterate the equation in its form $r/2m_2 = 1 + \exp[(r_\star - r)/2m_2]$ until the desired accuracy is achieved. We denote the solution close to the horizon as $\Psi_{\mathcal{H}} \sim \Psi(u_{\max}, v)$, and at infinity $\Psi_{\mathcal{I}^+} \sim \Psi(u, v_{\max})$. We have tested the accuracy of our algorithm by recovering the Schwarzschild QNM frequencies to good accuracy, as well as Price's law tail exponents, as will be discussed below. Moreover, our code shows the expected convergence rate when increasing resolution. The code is implemented in `Julia` and is made available in [1].

7.4 RESULTS

Once we have set up our problem and described the numerical methods employed to solve it, we move towards our goal of understanding ringdown processes in an accreting spacetime. First, we discuss the general features of the problem, including the excitation of a ringdown process by matter fluctuations. Secondly, we attempt to extract the mode characteristics on short timescales. Finally, we introduced a novel model, adapted to dynamical scenarios, and show convincing evidence that it outperforms the usual damped sinusoids framework.

7.4.1 *General Features*

The evolution of the master variable Ψ (directly related to the GW strain h), is shown in Fig. 24, for a background (7.21) with $(v_1/m_1, \tau/m_1) = (100, 10)$ and different intensity of accretion, as measured by m_2/m_1. In the following, we focus on the dominant quadrupolar $\ell = 2$ mode. For $m_2 = m_1$ we are simply describing the dynamics of slightly disturbed vacuum Schwarzschild BHs. For $m_2/m_1 = 1.5$ on the other hand, we are discussing a violently accreting spacetime, which saw a 50% increase in its mass on a very short timescale (roughly 5 light-crossing times).

Consider first a sourceless evolution, where matter fluctuations are set to zero (F in Eq. (7.26) vanishes). The top panels show the evolution for different values of the final mass m_2, with the black line corresponding to the evolution on a purely Schwarzschild background $m_2 = m_1$. This relaxation process is known as quasinormal ringdown and can be understood as leakage from the light ring [64,

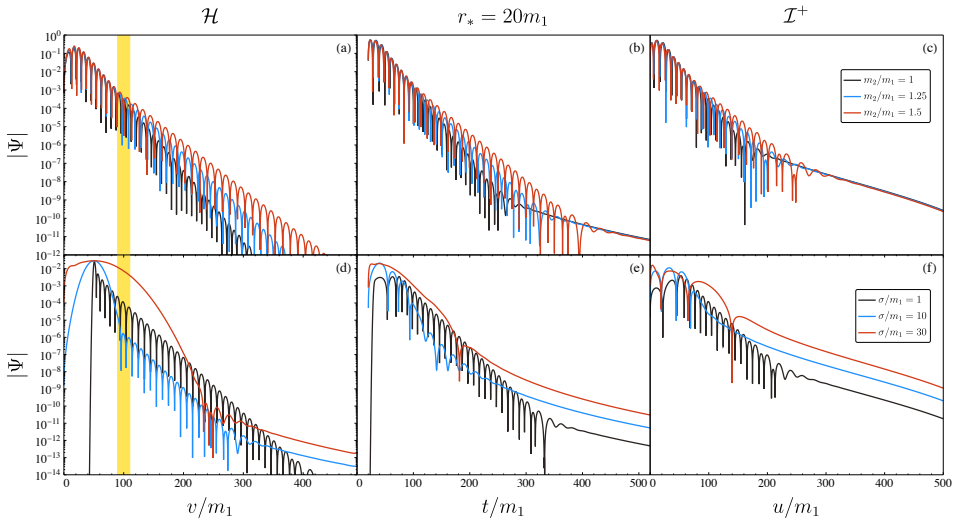

Figure 24 **Top:** Evolution of the quadrupolar gravitational master variable Ψ extracted at **a.** the horizon, **b.** a fixed radius $r_* = 20m_1$, and **c.** null infinity. Matter fluctuations vanish, while initial conditions are given by (7.28) with $(\Psi_0, v_\Psi/m_1, \sigma_\Psi/m_1) = (1, 15, 2.5)$, evolving on a Vaidya background (7.21) with $(v_1/m_1, \tau/m_1) = (100, 10)$ and m_2/m_1 as indicated in the legend. The shaded yellow region representswhere the background is most dynamical. **Bottom:** Evolution of Ψ with trivial initial conditions, $\Psi_0 = 0$, sourced only by matter fluctuations. In this case, $m_2 = 1.2m_1$.

65, 173, 191, 219, 333, 439]. At early times it is the same for all backgrounds, since all backgrounds have same m_1; thus the light ring properties are identical early on. During this stage,

$$\Psi \sim e^{-i\omega_{\rm QNM} t} = e^{-t/\tau_{\rm QNM}} \cos(\omega^R_{\rm QNM} t + \phi)\,, \tag{7.30}$$

where we assumed that there is a dominant QNM frequency which we write as

$$\omega_{\rm QNM} = \omega^R_{QNM} - i/\tau_{\rm QNM}\,. \tag{7.31}$$

One might therefore expect that early relaxation is described as above with $m \to m_1$, an expectation which is consistent with our results.

However, once accretion starts, the region near the light ring changes and so does the relaxation of the spacetime. Spacetimes with larger mass relax with a lower frequency and over longer timescales. Indeed, from Fig. 24, we observe that at early and late times the behaviour is as in Eq. (7.30) with $m \to m_{1,2}$, respectively, with a transient in between. We will explore this in more detail below. Notice, also, that the relaxation changes both in the waveforms extracted at the horizon (panel **a**) and in the waveform extracted at future null infinity (panel **c**). The frequency change as seen from $\mathcal{I}^+$ is a direct consequence of the fact that the light ring grows.

We also see power-law tails at very late times, when the field decays as $\Psi \sim t^{-p}$ [137, 138, 303, 390] at fixed radius and at null infinity. Similar power law tails form at the horizon, but only at much later times, for the class of initial conditions

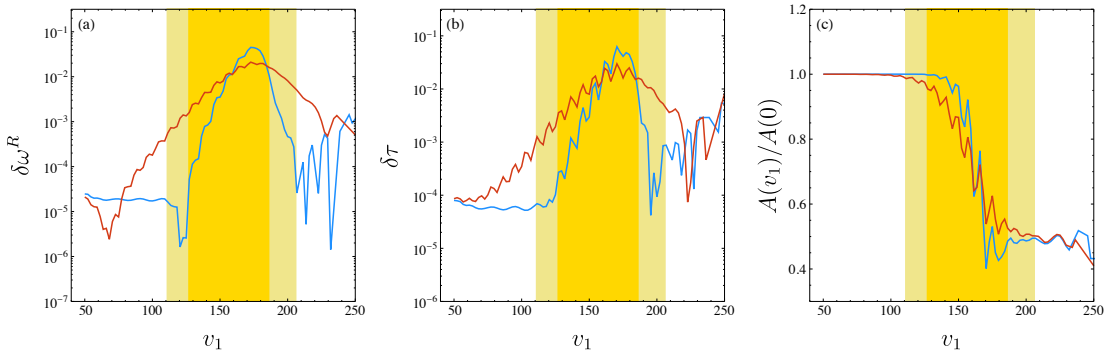

Figure 25 **a**. Relative error in the frequency δf compared to the Schwarzschild value, see Eq. (7.32). **b**. Same, but for the damping time. **c**. Extracted amplitude, normalized with respect to the initial amplitude. The shaded regions represent starting times such that the fitting window overlaps with the region where spacetime is most dynamical. Oscillations of the extracted values at late times are due to contamination with numerical noise of the signal. In all panels, we take $m_2/m_1 = 1.05$ and $\tau = 5(25)$ in blue (red), and fit over a window containing 6 half-periods with a template containing one free damped sinusoid.

considered here. The exponent of the tail in this case is in agreement with Price's law [390], (t^{-7} for this case) when extracting at a fixed radius (panels **b-e**). Despite the spacetime being dynamical, it asymptotes towards a Schwarzschild background, hence we expect Price's law to be satisfied [229, 243].

The bottom panels of Fig. 24 show the excitation of gravitational perturbations due to a matter fluctuation. We consider a matter profile for $F(v)$ given by a Gaussian pulse analogue to (7.28), centered at $v_1 = 50m_1$, with fixed amplitude and vary the width σ (see legend in panel **f**). We find that very thin profiles excite a larger overtone contribution, as can be seen from the rapid decay at early times at the horizon, whereas wider pulses excite the tail more efficiently, as is clearly seen in panels **d–f**, consistently with [61]. It is important to remark that in this case the matter fluctuations satisfy a first-order evolution equation that could be solved analytically, so there are no "matter" modes. As a consequence, the evolution of the gravitational perturbations Ψ is qualitatively equivalent to having a non–zero initial condition for Ψ.

7.4.2 *Mode Content of a Dynamical Ringdown*

Once we have numerical evolutions of gravitational perturbations in the Vaidya background, we consider the problem of modelling those waveforms. Since the matter fluctuations do not add additional dynamical modes, for simplicity we consider only the case where the matter fluctuations vanish (therefore, the equation is homogeneous), and the gravitational perturbations are sourced by some initial conditions. Moreover, the frequency content should be independent on whether the perturbations are extracted at infinity or at the horizon. Since the matter that is

accreted into the BH falls along the ∂_u null direction, studying the waveform at the horizon (which is transverse to ∂_u) provides a cleaner picture. Thus, in the following we will study the metric perturbation at the horizon, $\Psi \equiv \Psi_{\mathcal{H}}$.

Ultimately we are describing a ringdown process, therefore, the fundamental ingredient of the waveform model used to describe the signal is expected be a combination of damped sinusoids, as in Chapter 3. We define the amplitudes with respect to the peak of the waveform. We employ a least squares fitting algorithm [195, 313], with performance boosted via automatic differentiation. We choose initial conditions for the algorithm by sampling from uniform priors in the ranges $A \in [0,1]$, $\phi \in [0, 2\pi]$, $m_1\omega_R \in [0,1]$ and $\tau/m_1 \in [1,20]$. We iterate on the algorithm until the mismatch between the reconstructed waveform Ψ_R (i.e. the waveform evaluated at the best fit parameters) and the numerical signal is below a certain threshold. We have tested our algorithm by simulating mock data and extracting accurately the parameters, even in the presence of Gaussian noise.

By looking at Fig. 24-**a**, we can already observe that the waveform changes behaviour during the transient, in a way that depends on the value of the change of mass $\delta m = m_2 - m_1$. When the mass changes, the oscillation frequencies and the damping time change. This is to be expected: intuitively the behaviour at early times should be governed by some combination of QNMs of the BH with mass m_1, and at late times the same should be true for a BH with mass m_2: hence, the dimensionless quantity $\omega_R\, m(v)$ should be the same at early and late times, although it may oscillate in the transient.

In order to test this, we extract the average frequency over a time span $[v_1, v_1 + v_N]$, where v_N is chosen such that the signal contains approximately N half-periods, and we choose $N = 6$ [4]. This serves as an estimate for the "instantaneous" frequency, amplitude, and phase of the signal. We do so using different starting times, and show our results in Fig. 25. We use only one damped sinusoid in these fits.

First, we define the frequency and damping time shifts

$$\delta\omega^R = \left|1 - \frac{m(v)\omega_R}{m_1\omega_R^{\rm QNM}}\right|, \quad \delta\tau = \left|1 - \frac{m_1\tau}{m(v)\tau_{\rm QNM}}\right|, \tag{7.32}$$

where ω_R and τ are the extracted oscillation frequency and damping time, and $m_1\omega_R^{\rm QNM}$, $m_1\tau_{\rm QNM}$ are their QNM values for Schwarzschild with mass m_1. Since we are re–scaling by the appropriate mass dimension, we expect, as Fig. 25 shows, that these errors go to zero as $v_1 \to 0, \infty$. As one could naturally expect, when the mass absorption occurs more adiabatically (red line), the error in the frequency extraction is larger for a larger fraction of the evolution. On the other hand, when the mass absorption occurs very abruptly, the frequency errors $\delta\omega^R$ and $\delta\tau$ are quite small (of the order of $\sim 10^{-4}$ or below, notice that the scale is logarithmic), except for a very short time, related to the time when the background is dynamical, where they become larger than for their adiabatic counterpart.

4 This was the smaller value of N capable of recovering accurate enough the frequencies in tests containing Schwarzschild waveforms.

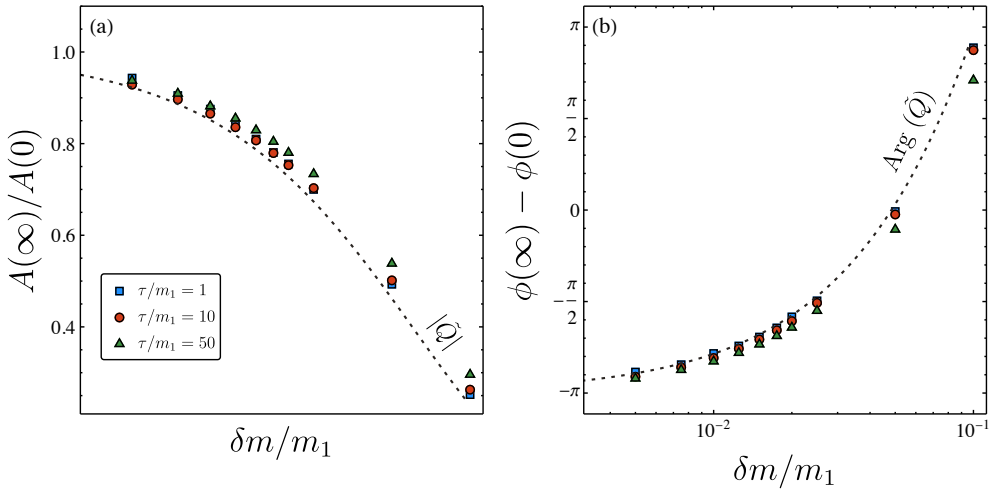

Figure 26 **Left:** Ratio between the final amplitude, $A(\infty)$, extracted at $v \geq v_1 + 4\tau$, and the initial amplitude, extracted at $v = 50$, for different values of the background profile $\{m_2, \tau\}$, as indicated in the legend. The dashed black line represents the (absolute value of the) re–scaled decoherence factor $\tilde{\mathcal{Q}}$, as defined in Eq. (7.33). **Right:** Same, but for the phase difference. In this case the black dashed line represents the complex argument of the decoherence factor.

The right panel in Fig. 25 shows the evolution of the amplitude of the fundamental mode, $A(v_1) \equiv A_0$, where the fit occurs over 6 half–periods starting at v_1. For convenience we normalize the amplitude with respect to the amplitude measured at early times (but once it is compatible with a constant), which we label as $A(0)$. We observe that at early times it is constant, which hints that a single damped sinusoid is providing an accurate representation of the signal. It is only at very late times that it becomes constant again, but the final value of the amplitude is substantially smaller than the initial one. Remarkably, it does *not* depend on the timescale at which the background changes, τ.

We remark that at all times the mismatch between the reconstructed waveform and the numerical data is always below $\sim 10^{-3}$. The mismatch achieves its largest values whenever the fitting window overlaps with the timescale where the BH mass is growing more significantly.

Taking one step further towards modelling the signal, we extract directly the final (initial) amplitudes and phases, $A(\infty)$ ($A(0)$), $\phi(\infty)$ ($\phi(0)$), in the regime where they are approximately constant. If the discussion in Sec. 7.2 is a good approximation, these should be related directly to the QNM decoherence factor $\mathcal{Q}$, as defined in Eq. (7.9). However, that factor relates the amplitudes as referred to the time at which the mass changes (that time is given by v_1 in the mass profile (7.21)). On the other

hand, the amplitudes and phases extracted from the fits are referred to the peak of the waveform, $v_{\rm peak}$. Thus, we would expect a relation given by

$$\frac{\tilde{A}(\infty)}{\tilde{A}(0)} = (1+\mathcal{Q})\frac{e^{i\omega(\infty)(v_1-v_{\rm peak})}}{e^{i\omega(0)(v_1-v_{\rm peak})}} \equiv \tilde{\mathcal{Q}}\,, \tag{7.33}$$

where $\tilde{A} = Ae^{i\phi}$ is the complex amplitude, and $\omega(\infty)$ (resp. $\omega(0)$) are the final (initial) ringdown frequencies of the fundamental mode. Fig. 26 shows the extracted values for the absolute value and the phase from three different regimes: $\tau = 1, 10, 50$, ranging from non–adiabatic, to a more adiabatic situation, as a function of the mass increase $\delta m = m_2 - m_1$. Our extracted values from the fit agree surprisingly well with the rescaled decoherence factor $\tilde{\mathcal{Q}}$. The agreement is remarkably good for all values of τ considered. On the other hand, the largest value of τ considered is only comparable to a few decades of decay of the fundamental mode frequency, and thus it is not yet exploring the really adiabatic regime. Pushing beyond this regime would require specifically targeted numerical methods that go beyond the scope of this work.

7.4.3 *A Dynamical Ringdown Model*

The previous analysis motivates a template that goes beyond damped sinusoids with fixed amplitudes and frequencies. Having knowledge of the mass function $m(v)$, and some analytical control as given by the decoherence factor $\mathcal{Q} \sim \alpha\delta m e^{-i\beta\delta m}$ (with $\alpha \sim 4.19$ and $\beta \sim 5.03$), obtained by fitting the results of Fig. 21), we propose the following model, with only two free parameters:

$$\begin{aligned} \Psi =& \Re\Big(A(v)e^{i\omega(v)v}\Big)\,, \\ A(v) =& \tilde{A}\Big[1+\tilde{Q}\frac{\delta m(v)}{m_2-m_1}\Big]\,, \quad \omega(v) = \frac{m_1\omega_{220}}{m(v)}\,, \end{aligned} \tag{7.34}$$

this is, the (complex) amplitude interpolates between some initial value $\tilde{A}$ (which contains the two free parameters of the model), and a final amplitude given by $\tilde{Q}\tilde{A}$, and the ringdown frequency evolves according to $m_1\omega_{220}/m(v)$. In the above, $\delta m(v) = m(v) - m_1$, and $m(v)$ is the time–varying mass, and ω_{220} is the (dimensionfull, complex) ringdown frequency of the Schwarzschild fundamental mode with mass m_1. We refer to this model as the *dynamical ringdown* (DR) model, to distinguish it from the usual (linear) ringdown templates with constant amplitudes and frequencies. At this stage, this model is only adapted to a single mode. However, extending it to contain overtones and capture their time dependence, as well as the AIME effect, is possible, but we leave that for future explorations.

In order to compare this model with the usual damped sinusoids, we consider a situation that resembles somewhat more closely what could happen after merger. We consider a reasonably mild accretion process, $m_2/m_1 = 1.05$. The accretion occurs "shortly" after the peak of the waveform, since we set $v_1 \sim 27$, with a timescale comparable to the decay rate of the fundamental mode, $\tau = 10m_1$. We

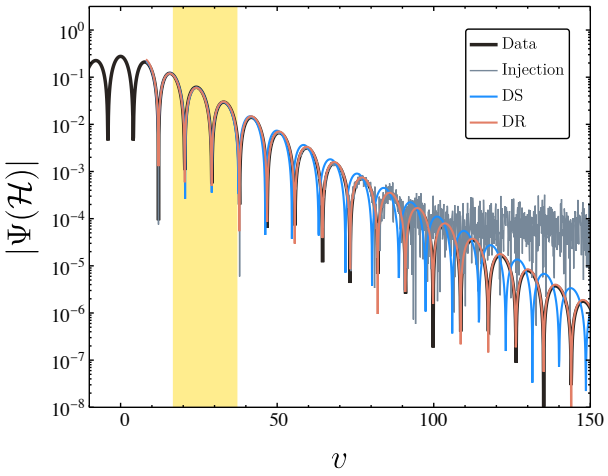

Figure 27 Numerical waveform (black) for a BH accreting 5% of its initial mass $m_2/m_1 = 1.05$ with $v_1 = 40$ and $\tau = 10$, extracted at the horizon. The initial data has $(A_\Psi, v_\Psi, \sigma_\Psi) = (1, 10, 2)$. Overlapped, we show the injected waveform into Gaussian white noise and the reconstructed waveforms using the damped sinusoids (DS) model (blue) and the dynamical ringdown (DR) model (red), starting the fit at $v_{\rm start} = 10$. The yellow band represents the times at which spacetime is highly dynamical.

inject our numerical waveforms into Gaussian white noise, defining at each timestep t_j

$$\Psi_{\rm injection}[t_j] = \Psi_{\rm num}[t_j] + \varepsilon[t_j]\,, \qquad \varepsilon \sim \mathcal{N}(0, \sigma = 10^{-4})\,. \tag{7.35}$$

We fit the waveform with both a damped sinusoids model containing one single damped sinusoid (we refer to this as the DS model), and with the DR model defined above. Comparing the performance of both models using the mismatch would not be completely fair, since they also contain different number of parameters. For this reason, we compute the Bayes factor between both models, defined as

$$\mathcal{B}_{\rm DR/DS} = \frac{p(d|{\rm DR})}{p(d|{\rm DS})}\,, \tag{7.36}$$

where $p(d|{\rm DR(DS)})$ is the evidence for the model DR (DS) when observing the data d (see Chapter 2). As in Chapter 3, we compute the evidence sampling from the posterior distribution using nested sampling [431]. Our priors are uninformative uniform distributions in the ranges $\ln A \in [-5, 2]$ [5], $f \in [0, 1]$, $\tau \in [1, 20]$ and $\phi \in [0, 2\pi]$. We sample using 64 live points, achieving fast convergence.

The reconstructed waveform for the different models, compared to the injected waveform (including noise) as well as the numerical waveform, is shown in Fig. 27. A simple visual inspection shows that the DR model captures much better the

5 For efficiency we sample on $\ln A$ rather than on the amplitude itself.

dynamical evolution of the waveform, even in the presence of noise. While the DS model is not able to capture the change in, e.g., the frequency and damping time of the ringdown due to accretion, this is perfectly captured by the DR model. Moreover, the amplitude and phase is consistent all throughout the evolution. The Bayes factor further supports this, obtaining a value of

$$\log \mathcal{B}_{DR/DS} \sim 3 \times 10^4 \,. \tag{7.37}$$

This is very strong quantitative evidence, beyond the qualitative evidence provided by Fig. 27, that in the presence of accretion a model containing varying amplitudes and frequencies is preferred with respect to a damped sinusoids (with fixed amplitudes and frequencies).

7.5 DISCUSSION

We have studied gravitational perturbations of accreting spacetimes, namely a Vaidya geometry describing a BH growing through accretion of null radiation fields. This setup mimics that of a highly dynamical spacetime – like that resulting from the coalescence of equal-mass BHs. Our interest in this problem is to complete our knowledge of the relaxation stage of BHs, and to understand whether one can extend a ringdown description based on (dynamical) damped sinusoids to earlier stages of the coalescence.

We showed that axial matter perturbations can be freely specified, and that they in turn source gravitational fluctuations that relax in a ringdown at late times. However, for the setups we considered, with null radiation being accreted, we find no evidence of other effects, such as echoes, that can arise in some situations due to the coupling to matter.

Our results indicate that accreting BHs have quasi-characteristic modes, which are now a function of their mass, as might be expected for mass-changing spacetimes. Their ringdown process is qualitatively described by damped sinusoids, but with varying frequencies and amplitudes. By coupling these to the BH mass we provide a template, which might be useful in interpreting results from full nonlinear simulations of BH spacetimes. Another interesting question regards the behaviour of fluctuations when the accretion happens very slowly. For the timescales considered here we find that the accretion timescale does not seem to play a significant role, but a careful analysis of the adiabatic limit is left for future explorations.

Breaking down the stationarity assumption of the background metric opens the way for new physics, of interest in realistic astrophysical scenarios. The framework developed here can be a starting point to study the gravitational dynamics in the presence of accretion in several configurations, such as its imprint on the inspiral of small bodies, or extending our findings to include a (time–varying) BH spin.

8

TURBULENCE OF TRAPPED GRAVITATIONAL WAVES

Written while listening to music composed by Manuel de Falla.

8.1 INTRODUCTION

So far in this thesis we have worked only under the assumption that General Relativity is correct at all relevant astrophysical scales, and that merging compact objects are Kerr BHs. From the theoretical point of view it is interesting to entertain alternative hypothesis to understand generic smoking guns that deviations of General Relativity will exhibit, in order to search for them. We emphasise that current data from GW measurements and very long baseline interferometry are all compatible with Kerr BHs [7, 14, 15, 36, 321].

One possibility is to consider compact objects that evade the final state conjecture, i. e., that can arise as alternatives to BHs as the end state of gravitational collapse, for instance. Classic examples are geons [460], boson stars [266, 308, 414], or more exotic alternatives such as fuzzballs [335], gravastars [336], or black bubbles [159–161, 215]. We refer generically to all these models as BH mimickers [106]. In this chapter, we analyze whether nonlinear effects can render generic BH mimickers unstable, or source interesting turbulent dynamics, that could potentially lead to distinct observational signatures.

GW observations from compact binary mergers directly test the Kerr hypothesis against varios BH mimicker models [100, 106], for instance, searching for GW echoes [106, 190, 286, 326], reporting only negative results thus far [7]. An alternative approach is to investigate the generic dynamical properties of these objects. This implies questioning, e.g., how would such an object form dynamically, and its linear and nonlinear stability. Generically, horizonless objects that are also compact possess a stable lightring (LR). These are circular orbits where light rays can remain trapped indefinitely. Ref. [272] showed that the presence of stable LRs was associated to a slow decay of linear perturbations, and it was conjectured that this would lead to a nonlinear instability. The physical insight was that the trapping of high frequency modes for a very long time could trigger BH formation, collapse, or disperse of the whole configuration. We refer to this as the LR instability conjecture. The goal of this work is to examine some of its fundamental aspects in the nonlinear regime.

Following the publication of [272], Ref. [104] investigated the perturbative properties of BH mimickers with stable LRs. In particular, as it was already known

for some stellar models [191], these objects have long-lived modes. Heuristic arguments favouring the presence of a nonlinear instability were discussed, as well. This problem has also been investigated from the numerical point of view, focusing on particular classes of mimickers that are solutions of well posed equations of motion. Ref. [231] showed that radial perturbations of scalarized, charged BHs with a stable LR, do not trigger any instability. In the context of boson stars, Ref. [153] claimed a generic instability for rotating boson stars with stable LRs, with a moderate timescale. The fate of the instability depends on the model under consideration, in some cases resulting in the collapse to a BH, while in others the star migrates towards a less compact configuration, without LRs. However, recent works [189, 329, 426–428] have failed to reproduce this instability in different regimes.

This problem is also directly related to the stability of higher dimensional black strings and black rings which also can possess stable LRs. Ref. [57] proved in that case the slow decay of linear perturbations, and conjectured a similar nonlinear instability. Morally, this problem is closely related to the turbulent instability of pure anti-de Sitter (AdS) space with reflective boundary conditions [41, 72, 73, 168, 171], albeit the presence of focusing due to the gravitational potential in AdS single out that scenario.

This chapter is motivated by a recent study [58], which investigates the dynamics of a defocusing cubic wave equation on a spacetime with stable trapping. That worked demonstrated a direct turbulent cascade in angular modes from numerical evolutions of localised initial data. Based on their numerical results, the authors of [58] conjectured that higher-order norms of the solution can grow unbounded in time for generic initial data, in stark contrast with the decay properties typically seen when trapping is unstable (as in asymptotically flat black hole spacetimes like Schwarzschild). We start this chapter by proving the aforementioned conjecture using perturbation theory and improved numerical simulations. Moreover, we demonstrate the development of a turbulent regime comparing perturbative analyses, dimensionally reduced models, and numerical simulations. Our results demonstrate that stable light rings do not confine as AdS does: even at high frequencies, the radiation can be distributed in a number of overtones, which are long-lived and localized not at the LR itself, but within a "light shell" with non negligible thickness. Therefore, arguments based on the hoop conjecture to invoke the formation of BHs at the LR are bound to fail.

The structure of the chapter is as follows. First, we revisit the model spacetime and nonlinear wave equation of Ref. [58] in Sec. 8.2. In Sec. 8.3 we solve the linear problem, studying the quasinormal mode spectrum of the system, and identify properties of the long-lived modes. We then examine the stability question from a mathematical point of view in Sec. 8.4. We compute the growth rate of higher-order norms within the perturbative regime for a simplified configuration. Furthermore, we show how this calculation accurately estimates the growth of the norms obtained from the numerical evolution of the nonlinear wave equation in a spacetime with stable trapping. Lastly, we examine the development of a turbulent regime, and the

end state of this process, in Sec. 8.5, and we conclude with a brief discussion of future prospects in Sec.8.6.

8.2 A SIMPLE GEOMETRY WITH A STABLE LIGHT RING

The LR instability is conjectured generically for many scenarios, based only on the existence of a closed, compact region with null trapping, such as a stable LR. However, the dynamics of different BH mimicker models are vastly different, since they involve different additional matter fields, or modified equations of motion. In order to isolate the role of stable trapping at triggering a nonlinear instability, we design a simple geometry (which is *not* a solution of Einstein equations) with a single stable LR. The nonlinear wave equation we consider on this spacetime captures some of the features of Einstein equations [58]:

$$\Box_g \Phi = \kappa \Phi^3 \,, \tag{8.1}$$

where κ is a positive coupling constant that controls the strength of the nonlinearity, $\Phi : \mathcal{M} \to \mathbf{R}$ is a real field taking values in the manifold $\mathcal{M}$, endowed with the Lorentzian metric g. The operator $\Box_g$ is the d'Alembertian of the spherically symmetric metric

$$g_{\mu\nu} dx^\mu dx^\nu = -f(r) dt^2 + f^{-1}(r) dr^2 + r^2 d\Omega^2 \,, \tag{8.2}$$

where the radial function $f(r)$ will be specified below, and $d\Omega^2$ is the area element of the unit 2-sphere. The choice of a cubic nonlinearity is motivated by the form of Einstein's equations in vacuum. While the spacetime we are considering is not a solution of vacuum Einstein's equations, we motivate the choice of the function f by requiring that it has a pair of LRs at tunable locations. A simple functional choice that achieves this behaviour is

$$f = 1 - \frac{8r^2}{R^2(4-\alpha^2) + \frac{(2+\alpha)^2}{R^2} r^4} \,, \tag{8.3}$$

where R is the location of the stable LR, and $0 < \alpha < 1$ is a parameter that controls how "deep" is the cavity that forms at the stable LR. Notice that this spacetime has a vanishing ADM mass. This will further show that the features associated to the so called LR instability are exclusively due to the presence of the stable trapping region, and not sensitive to the low frequency structure of the geometry.

We can reduce the problem to a set of coupled ODEs by expanding the field in spherical harmonics. Additionally, to simplify the problem even further, and focus on the same scenario as [58], we will restrict to axisymmetric modes. Thus, we can write

$$\Phi = \sum_\ell \frac{\phi_\ell}{r} \mathcal{Y}_{\ell,0}(\theta) \,. \tag{8.4}$$

Under this expansion, the nonlinear wave equation (8.1) becomes

$$\mathcal{O}_\ell \phi_\ell = \kappa \sum_{\ell_1 \ell_2 \ell_3} \mathcal{I}^\ell_{\ell_1 \ell_2 \ell_3} \frac{f}{r^2} \phi_{\ell_1} \phi_{\ell_2} \phi_{\ell_3} \,, \tag{8.5}$$

where $\mathcal{I}$ is the overlap between the spherical harmonics, defined as

$$\mathcal{I}^\ell_{\ell_1 \ell_2 \ell_3} = \int_{4\pi} d\Omega \mathcal{Y}_{\ell_1,0} \mathcal{Y}_{\ell_2,0} \mathcal{Y}_{\ell_3,0} \mathcal{Y}_{\ell,0} \,, \tag{8.6}$$

which can be shown to be given by the following sum of products of Wigner $3j$-symbols

$$\begin{aligned} \mathcal{I}^{\ell_1 \ell_2 \ell_3}_\ell &= \sum_{j=|\ell_1-\ell_2|}^{\ell_1+\ell_2} \frac{2j+1}{4\pi} \mathcal{C}^\ell_{\ell_1 \ell_2 \ell_3} \begin{pmatrix} \ell_1 & \ell_2 & j \\ 0 & 0 & 0 \end{pmatrix}^2 \begin{pmatrix} j & \ell_3 & \ell \\ 0 & 0 & 0 \end{pmatrix}^2 , \\ \mathcal{C}^\ell_{\ell_1 \ell_2 \ell_3} &= \sqrt{(2\ell_1+1)(2\ell_2+1)(2\ell_3+1)(2\ell+1)} \,. \end{aligned} \tag{8.7}$$

The system is, thus, governed by the following linear operator

$$\mathcal{O}_\ell = -\partial_t^2 + f\partial_r\Big(f\partial_r\Big) - \mathcal{V}_\ell \,, \qquad \mathcal{V}_\ell = f\Big(\frac{\ell(\ell+1)}{r^2} - \frac{\partial_r f}{r}\Big) \,. \tag{8.8}$$

The normalized potential for different values of ℓ is shown in Fig. 28. The geometry, by construction, possesses a stable LR at $r = R$, which leads to trapping of radiation, as well as an unstable LR located at $r \geq R$.

Despite the nonlinear term, global solutions to Eq. (8.1) in the spacetime of a Schwarzschild black hole exist [37, 357], and these arguments can be extended to our model spacetime. For this kind of nonlinearity, global existence follows from the conservation of energy, and the rate of decay of linear perturbations plays no role. The conserved energy norm is simply

$$\mathbf{E}_{\rm nl}[\Phi](t) = \int_{\Sigma_t} d^3x \sqrt{-g}\, T^{tt} \,, \tag{8.9}$$

where Σ_t is a $t =$ const. hypersurface, and T^{tt} is a component of the stress-energy tensor, given by

$$T_{ab} = \partial_a\Phi\partial_b\Phi - \frac{1}{2} g_{ab}\Big(\partial_c\Phi\partial^c\Phi + \frac{\Phi^4}{2}\Big) \,. \tag{8.10}$$

Energy conservation can be proven directly by taking the time derivative of (8.9), applying the equations of motion and integrating by parts. Additionally, we can define high-order norms of order k, which can be seen as norms on the Sobolev space defined at each temporal slice, namely

$$\Big\| D^{(k)}\Phi(t) \Big\|^2 = \int_{\Sigma_t} d^3x \gamma^{ij} \partial_i^{(k)}\Phi \partial_j^{(k)}\Phi \,, \tag{8.11}$$

where γ_{ij} is the spatial metric on the $t =$ const slice labeled by Σ_t. If we turn off the nonlinearity, i.e., when $\kappa = 0$, these nonlinear norms are bound uniformly, and

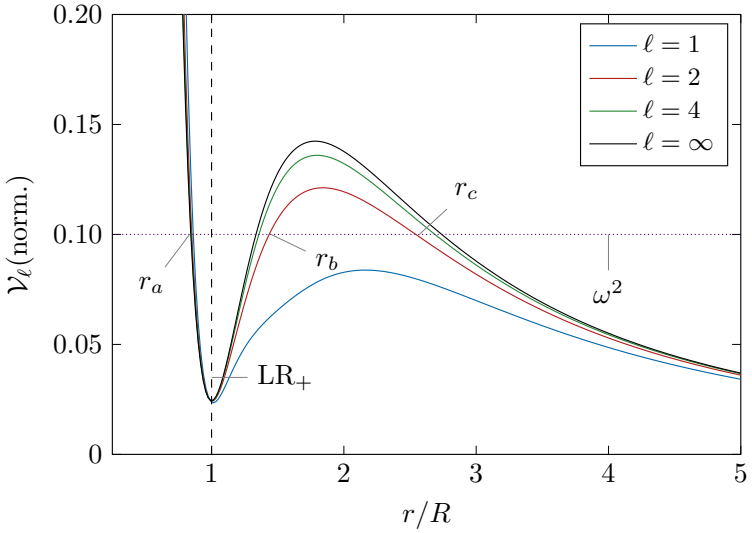

Figure 28 Normalized potential $\tilde{\mathcal{V}}_\ell = \ell^{-1}(\ell+1)^{-1}r^{-2}\mathcal{V}_\ell$, defined in Eq. (**??**), with $\alpha = 0.05$, for different values of the angular number ℓ, including the eikonal limit (in black). The stable LR (denoted with a plus sign) is located at $r = R$. There is always another (unstable) LR, associated to the local maximum of the potential, at $r > R$. Additionally, we show for an arbitrary value of ω^2 (purple dotted line), the three classical turning points $r_{a,b,c}$ which define the boundaries between the classically allowed and forbidden regions in the WKB approximation.

the local energy decays. More precisely, if Ω is a non-empty and bounded compact region, which does not change with time, and we denote by $\left\|D^{(k)}_\Omega \Phi(t)\right\|^2$, the norm defined in Eq. (8.11), but integrating only over the compact region, i.e., $\Sigma_t \cap \Omega$, we have [58]

$$\left\|D^{(k)}_\Omega \Phi(t)\right\|^2 \overset{\kappa=0}{\leq} \frac{C_{\Omega,k}}{\log(2+t)^2} \sum_{s=0}^{k+1} \left\|D^{(s)}\Phi(0)\right\|^2 . \tag{8.12}$$

However, as evidenced from the numerical simulations presented in [58], this property no longer holds in the presence of the nonlinear term. This is one of the major attributes we analyze in the following sections.

8.3 LINEAR PERTURBATIONS

Before analysing the nonlinear problem, it is important to understand key aspects of the linearised problem. In this Section, we will discuss the spectrum of the linearised problem, showing that there exists a family of long-lived modes associated with the stable LR. We characterise the frequencies and damping times of these modes by combining exact numerical methods with approximate methods valid in the eikonal regime.

8.3.1 *Direct Integration*

Let us solve the linear equation $\mathcal{O}_\ell \phi_\ell = 0$ subject to out-going boundary conditions as $r \to \infty$, and look for solutions that are regular at the origin. This regularity condition can be seen as $\phi_\ell \sim r^{\ell+1}$ as $r \to 0$ [1]. Solutions satisfying these boundary conditions are QNMs. Using a shooting method as described in Chapter 3, we solve the equation in the frequency domain by writing $\phi_\ell = e^{-i\omega_{\ell n} t} e_{\ell n}(r)$.

$$f\partial_r\Big(f\partial_r(e_{\ell n})\Big) + (\omega_{\ell n}^2 - \mathcal{V}_\ell) e_{\ell n} = 0\,, \tag{8.13}$$

subject to $e_{\ell n} \sim r^{\ell+1}$ as $r \to 0$, and $e_{\ell n} \sim e^{i\omega_{\ell n} r_\star}$ as $r \to \infty$, where the tortoise coordinate $r_\star$ is defined as the coordinate which satisfies $dr_\star = f^{-1} dr$. We "shoot" for the QNM frequencies $\omega_{\ell n}$ by requiring that the solutions constructed from each boundary match smoothly at some intermediate radius [63, 127]. This unveils an infinite set of QNM frequencies and radial functions, labeled by the integer n, for each angular harmonic. The $n = 0$ mode is the longest-lived, and therefore called the fundamental mode. Modes with $n > 0$ have successively shorter damping times, and are referred to as the overtones of the system. This method is only efficient for the first few angular harmonics. For higher angular harmonics, we evaluate the QNM frequencies using two different approximate methods, described below.

8.3.2 *WKB Approximation*

Let us briefly review the application of the Werners–Kramers–Brillouin (WKB) approximation to find the long-lived modes of a system. The approximation in this case corresponds to a perturbative expansion in $1/\ell$, and thus is accurate for high wavenumbers. However, it has also been shown to be very accurate [367] in the presence of long-lived modes, i.e., in order to capture modes of the system with very large quality factors.

Let us begin by considering the WKB ansatz, $\phi_\ell \sim e^{pS_p(r) - i\omega_p t}$, with $p = \ell + 1/2$ so that the linear equation becomes

$$\frac{S''}{p^2} + (S')^2 + \Big(\tilde{\omega}_p^2 - \mathcal{U}\Big) = \frac{\chi}{p^2}\,, \tag{8.14}$$

where the prime denotes derivatives with respect to the tortoise coordinate, i.e., $S' = f\partial_r S$, the rescaled frequency is $\tilde{\omega} = \omega/p$, and the potential splits into the WKB potential $\mathcal{U} = f r^{-2}$ and the correction χ, given by

$$\chi = \frac{f}{4r^2} - \frac{f'}{r}\,. \tag{8.15}$$

The solution between the turning points r_a and r_b can be found as an asymptotic series in $1/p$. Indeed, writing $S = S_0 + pS_1 + p^2 S_2$, one gets

1 Irregular solutions behave as $\phi_\ell \sim r^{-\ell}$.

$$
\begin{aligned}
S_0 &= \pm\, i \int_{r_a}^{r} \sqrt{|\mathcal{Q}(x)|}\,\frac{dx}{f(x)}\,, \qquad S_1 = -\frac{1}{4}\log|\mathcal{Q}| \\
S_2 &= \pm\,\frac{i}{8}\int_{r_a}^{r}\left[\frac{\mathcal{U}''(x)}{\mathcal{Q}(x)^{3/2}} + \frac{5}{4}\frac{\mathcal{U}'(x)}{\mathcal{Q}(x)^{5/2}} - \frac{4\chi(x)}{\sqrt{\mathcal{Q}(x)}}\right]\frac{dx}{f(x)}\,,
\end{aligned}
\tag{8.16}
$$

where $\mathcal{Q}(x) = \tilde{\omega}_p^2 - \mathcal{U}(x)$. Remarkably, the first two terms in the expansion do *not* depend on the source term χ [171]. Therefore, we will truncate the expansion at the first order in p.

We now can use this expression to construct the solution in the four regions in which our problem is divided. We start from the outermost region, which we label region IV, where $r_c \leq r < \infty$. In general, the solution in that region, which is classically allowed, has the form

$$
\phi_\ell^{IV} = \frac{\mathcal{A}}{\sqrt{p}\mathcal{Q}^{1/4}} e^{ip\eta_+(r,r_c)} + \frac{\mathcal{B}}{\sqrt{p}\mathcal{Q}^{1/4}} e^{-ip\eta_+(r,r_c)}\,, \quad \eta_\pm(r,r_a) = \int_{r_a}^{r}\sqrt{\pm\mathcal{Q}(x)}\frac{dx}{f(x)}\,.
\tag{8.17}
$$

As $r \to \infty$, $\mathcal{Q} \to \tilde{\omega}$ becomes constant. Outgoing boundary conditions correspond to

$$
\phi_\ell \to e^{i\omega r_\star}\,,
\tag{8.18}
$$

as $r \to \infty$. Thus, out-going boundary conditions are equivalent to requiring that $\mathcal{B} = 0$. For simplicity, we will then put $\mathcal{A} = 1$, which is just an overall normalization constant.

The solution in region III, $r_b \leq r \leq r_c$, can be written as

$$
\phi_\ell^{III} = \frac{C_1}{\sqrt{p}|\mathcal{Q}|^{1/4}} e^{p\eta_-(r,r_b)} + \frac{C_2}{\sqrt{p}|\mathcal{Q}|^{1/4}} e^{-p\eta_-(r,r_b)}\,.
\tag{8.19}
$$

The constants C_1 and C_2 are not independent, but instead are fixed by connection formulas, which match this solution to the solution in region IV. The connection formulas in this case yield

$$
C_1 = -ie^{-(p\eta_{cb} - i\pi/4)}\,, \qquad C_2 = \frac{1}{2}e^{(p\eta_{cb} + i\pi/4)}\,,
\tag{8.20}
$$

where $\eta_{cb} = \eta_-(r_c, r_b)$. Following the same logic, the solution in region II, $r_a \leq r \leq r_b$, has the form

$$
\phi_\ell^{II} = \frac{C_3}{\sqrt{p}\mathcal{Q}^{1/4}} e^{i\eta(r,r_a)} + \frac{C_4}{\sqrt{p}\mathcal{Q}^{1/4}} e^{-i\eta(r,r_a)}\,,
\tag{8.21}
$$

where the connection formulas now yield

$$
C_3 = e^{-i(p\eta_{ba} - \pi/4)}\left(C_2 - \frac{i}{2}C_1\right)\,, \qquad C_4 = e^{i(p\eta_{ba} - \pi/4)}\left(C_2 + \frac{i}{2}C_1\right)\,.
\tag{8.22}
$$

Finally, the solution in region I, $0 < r \leq r_a$, is given by

$$\phi_\ell^I = \frac{C_5}{\sqrt{p}|\mathcal{Q}|^{1/4}} e^{p\eta_-(r,r_a)} + \frac{C_6}{\sqrt{p}|\mathcal{Q}|^{1/4}} e^{-p\eta_-(r,r_a)}\,, \tag{8.23}$$

with

$$C_5 = -i\Big(C_3 e^{i\pi/4} + C_4 e^{-i\pi/4}\Big)\,, \qquad C_6 = \frac{1}{2}\Big(C_3 e^{i\pi/4} - C_4 e^{-i\pi/4}\Big)\,. \tag{8.24}$$

As $r \to 0$ the WKB phase becomes divergent, due to the divergence of the potential. Thus, in order to have a regular solution at $r \to 0$, we need $C_6 = 0$. Inserting the connection formulas the regularity condition becomes

$$e^{2ip\eta_{cb}}\Big(1 + e^{2ip\eta_{ba}}\Big) + i\Big(e^{2ip\eta_{ba}} - 1\Big) = 0\,, \tag{8.25}$$

which, in the large p limit is dominated by the first term, yielding

$$e^{ip\eta_{ba}} + e^{-ip\eta_{ba}} = 0\,. \tag{8.26}$$

This condition is just the Bohr–Sommerfeld quantization rule

$$p\eta_{ba} \equiv \int_{r_a}^{r_b} \sqrt{\omega^2 - \mathcal{V}_\ell}\,\frac{dr}{f(r)} = \pi\Big(n + \frac{1}{2}\Big)\,, \tag{8.27}$$

where n denotes the overtone index.

We can now compute the leading order scaling of the frequencies with the angular number ℓ. Indeed, by expanding around the stable light ring $r \sim R$, and keeping only the leading order term, $V \sim \ell^2 f(R)/R^2$, the Bohr–Sommerfeld condition yields

$$\omega = \Omega\ell + \mathcal{O}(\ell^0)\,, \tag{8.28}$$

where $\Omega = \sqrt{f(R)}/R$ is the frequency of the stable LR. Similarly, the imaginary part scales as the tunnelling probability between regions II and IV

$$\log\tau \sim 2\eta_{bc} \sim \gamma\ell + \mathcal{O}(\ell^0)\,, \qquad \gamma = \frac{\pi(f_{\mathrm{LR}_-} - \Omega^2)}{\sqrt{2Q^{(2)}_{\mathrm{LR}_-}}}\,. \tag{8.29}$$

8.3.3 *Breit-Wigner Resonances*

We usually think of QNMs as poles of the scattering matrix, but an alternative viewpoint is to think them as Breit–Wigner resonances in the scattering amplitude. Using this idea, Chandrasekhar and Ferrari [129, 130] designed an efficient algorithm to find the frequencies of the longest lived modes.

We start by integrating outwards, ensuring that the solution is regular at the origin. At large distances, the outgoing solution takes the form $\phi_\ell \sim A\cos(\omega r) + B\sin(\omega r)$.

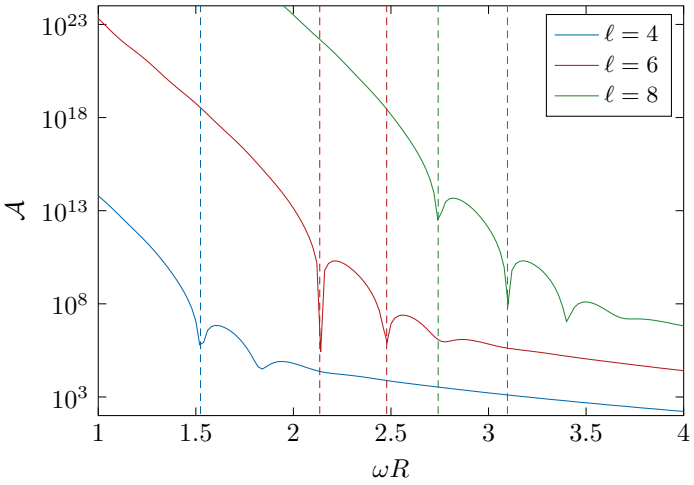

Figure 29 Breit–Wigner function $\mathcal{A}(\omega)$ for $\ell = 4, 6, 8$ and $\alpha = 0.2$. Each local minimum corresponds to a long-lived QNM. The dashed lines correspond to the calculation of the real part of the frequency using the WKB method, showing a good agreement between both methods.

Near the frequency of a long-lived mode, the scattering amplitude has the following behaviour:

$$\mathcal{A}(\omega) \equiv A^2 + B^2 \sim (\omega - \omega_R)^2 + \omega_I^2 \,, \tag{8.30}$$

where the real part of the frequency ω_R acts as the effective energy of the state, and ω_I as its decay rate. Then, the longer lived modes can be found by identifying the minima of $\mathcal{A}(\omega)$, which correspond to ω_R. Then, the imaginary part can be computed as

$$\omega_I = \sqrt{\frac{2\mathcal{A}(\omega_R)}{\mathcal{A}''(\omega_R)}} \,. \tag{8.31}$$

It is important to note that this approach makes no approximations on the potential, as opposed to the WKB approach. Its main advantage with respect to the direct integration method, discussed below, is that in order to find the modes we just need to search for the minima of $\mathcal{A}$ along the real line, whereas in the direct integration case we search for zeros of the Wronskian in the complex plane, which is computationally more involved. The characteristic behaviour of $\mathcal{A}(\omega)$, from where the real part of the QNM frequencies can easily be read, is shown in Fig. 29.

The Breit–Wigner method refines the frequency obtained from the WKB method. However, it requires significantly more numerical precision for higher angular numbers to accurately resolve the small imaginary part of the QNMs.

8.3.4 *Spectrum*

These methods allow us to obtain the fundamental QNM frequency for both the first angular harmonics (via direct integration) and higher harmonics (via WKB or

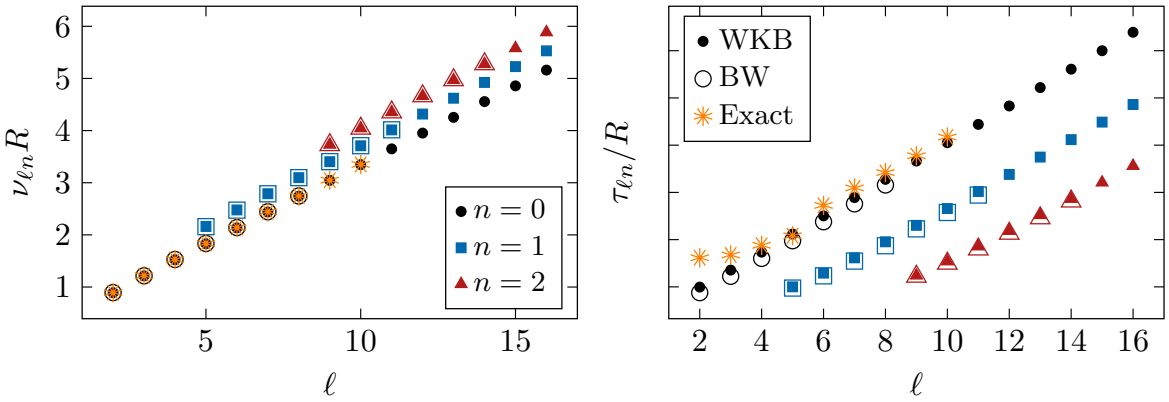

Figure 30 Oscillation frequency (left) and damping time (right) of the first few QNMs for the modeled spacetime with $\alpha = 0.166$. The exact values, computed with a direct integration, are shown as orange stars. Filled markers are computed using the WKB approximation, whereas the empty markers have been computed through the Breit–Wigner (BW) method. As expected, all three methods start showing good agreement for the higher harmonics $\ell \gtrsim 6$.

Breit–Wigner). The results can be visualised by writing $\omega_{\ell n} = \nu_{\ell n} - i/\tau_{\ell n}$, where $\nu_{\ell n}$ is the real part of the frequency of the QNM, and $\tau_{\ell n}$ its damping time. In particular, Fig. 30 shows how the damping time $\tau_{\ell n} R \sim e^{\gamma \ell}$ grows exponentially with ℓ, with γ given by (8.29). These results confirm the intuition that modes with higher multipolar index ℓ are more efficiently trapped by the potential. Additionally, we confirm that the oscillation frequency scales linearly with ℓ as $\nu_\ell \approx \Omega \ell$.

For the higher angular harmonics, Fig. 30 shows that these numerical solutions are in agreement with the WKB approximation, as well as a method based on Breit–Wigner resonances. Notice that the direct integration method requires higher numerical precision to accurately resolve the higher ℓ harmonics. Since this becomes quickly a computationally expensive task, we only compute up to $\ell = 10$.

These frequencies can also be extracted from the numerical simulations of Ref. [58], when using small initial data, to stay within the regime of validity of the linear theory. We highlight that for each ℓ, there is a finite number of long-lived modes with different overtone index $n = 0, \ldots, N_\ell$. The highest possible overtone index for a long-lived mode N_ℓ can be estimated in the WKB approximation, as the largest integer such that

$$N_\ell + \frac{1}{2} \leq \frac{1}{\pi} \int_{r_a}^{r_{\mathrm{LR}_-}} \frac{dr}{f} \sqrt{\frac{f(r_{\mathrm{LR}_-})}{r^2_{\mathrm{LR}_-}} - \mathcal{V}_\ell}\,. \tag{8.32}$$

Evaluating this expressions for the considered geometry, reveals that $N_\ell \lesssim \alpha \ell$ where $\alpha \in [1/3, 1/2]$. Thus, in the high frequency regime, where all the damping times can be assumed to be much larger than any relevant dynamical timescale, there is not just one, but a large number of long-lived modes.

8.4 GROWTH OF THE NORMS

Let us now examine the stability of the nonlinear problem, i.e., when $\kappa \neq 0$. While the nonlinear energy norm (8.9) is conserved, the higher order Sobolev norms (8.11) may not be conserved. Note that one can also can define higher order energy-like norms as

$$\mathbf{E}^{(k)}_{\rm nl}[\Phi](t) = \int_{\Sigma_t} d^3x \sqrt{-g}\ (T^{(k)})^{tt}\,, \tag{8.33}$$

with

$$T^{(k)}_{ab} = \partial^{(k)}_a \Phi \partial^{(k)}_b \Phi - \frac{1}{2} g_{ab}\left(g^{cd} \partial^{(k)}_c \Phi \partial^{(k)}_d \Phi + \frac{\Phi^2}{2} \right). \tag{8.34}$$

These norms, as opposed to the Sobolev norms (8.11), involve time derivatives, as well as the potential term. Ref. [58] presented numerical evidence that second order derivatives (related to the second order Sobolev norms) grow within their simulation time for sufficiently large initial data. It was conjectured that all norms with $k > 1$ grow for arbitrarily small initial data. In this Section we address this question by computing the rate at which both Sobolev and energy-like higher order norms grow, in the perturbative regime (therefore, for arbitrarily small initial data), in a simplified model. Lastly, we show, with additional numerical evidence, that the growth of the norms in the $3+1$ dimensional model follows a similar rate.

8.4.1 *Two-Dimensional Model*

Let us begin by considering a simplified scenario. We consider the nonlinear wave equation on the circle $\mathbf{S}^1$. This system is not dissipative, and its spectrum of normal modes can be computed analytically. Concretely, let us solve the initial value problem

$$\begin{cases} -\partial_t^2 \Phi + \partial_x^2 \Phi &= \Phi^3\,, \\ \Phi(t=0,x) &= \phi_0(x)\,, \quad \partial_t \Phi(t=0,x) = 0\,, \end{cases} \tag{8.35}$$

where $x \in \mathbf{S}^1$, or equivalently, $\Phi(t,x) = \Phi(t,x+2\pi)$. We will make one more simplifying assumption: let us assume that the initial data is composed of a single mode. This means that we choose ϕ_0 to be

$$\phi_0 = \epsilon \cos(nx)\,, \quad n \in \mathbb{N}\,. \tag{8.36}$$

We will further assume that we are in the perturbative regime, so that $\epsilon \ll 1$. The solution, up to next to next to leading order (NNLO), can be written as

$$\Phi = \epsilon \phi^{(1)} + \epsilon^3 \phi^{(3)} + \epsilon^5 \phi^{(5)} + \mathcal{O}\left(\epsilon^6\right)\,, \tag{8.37}$$

where

$$\begin{aligned}\phi^{(1)} =& \cos(nx)\,,\\ \phi^{(3)} =& a_1(t)\cos(nx) + a_3(t)\cos(3nx)\,,\\ \phi^{(5)} =& b_1(t)\cos(nx) + b_3(t)\cos(3nx) + b_5(t)\cos(5nx)\,.\end{aligned} \tag{8.38}$$

This results from expanding the higher-order equations into the normal modes of the circle with static initial data, represented by a cosine series. The nonlinearity is captured by the dependence of the modes on time. In particular, the time dependent coefficients satisfy the following equations of motion

$$\begin{aligned}\ddot{a}_1 + n^2 a_1 =& -\frac{3}{4}\cos^3(nt)\,, \qquad \ddot{a}_3 + (3n)^2 a_3 = -\frac{1}{4}\cos^3(nt)\,,\\ \ddot{b}_1 + n^2 b_1 =& -\frac{3}{4}\cos^2(nt)(3a_1 + a_3)\,, \quad \ddot{b}_3 + (3n)^2 b_3 = -\frac{3}{4}\cos^2(nt)(a_1 + 2a_3)\,,\\ \ddot{b}_5 + (5n)^2 b_5 =& -\frac{3}{4}\cos^2(nt)a_3\,.\end{aligned} \tag{8.39}$$

This system admits an analytic solution up to this order, but we omit the exact expressions for brevity. What is important for the current discussion is that the resonant terms on the right side of the above equations cause terms that grow secularly. To NLO we find linear growth in time, e.g., $a_1 \propto t\sin(nt)$, and to NNLO we observe terms that grow like t^2. This means that the NLO solution is only valid up to times when $t \leq \mathscr{O}(\epsilon^{-1})$, and the NNLO solution is only valid up to $t \leq \mathscr{O}(\epsilon^{-1/2})$. A two-timescale expansion [276] would be necessary to find a solution valid for larger timescales.

We can now calculate the equivalents of the Sobolev and energy-like higher-order norms in this situation. While the computation is straightforward, it is somewhat lengthy, and details are omitted (see Appendix C in [396]). In this case, the Sobolev and energy higher-order norms are expressed as follows:

$$\begin{aligned}\left\|D^{(k)}\Phi\right\|^2 =& \int_{\mathbf{S}^1} dx \left(\partial_x^{(k)}\Phi\right)^2\,,\\ \mathbf{E}_{\text{nl}}^{(k)}[\Phi](t) =& \int_{\mathbf{S}^1} dx \left[\left(\partial_t^{(k)}\Phi\right)^2 + \left(\partial_x^{(k)}\Phi\right)^2 + \frac{\Phi^4}{4}\right],\end{aligned} \tag{8.40}$$

and the Sobolev norm, up to NNLO is given by

$$\begin{aligned}\left\|D^{(k)}\Phi\right\|^2 =& \epsilon^2\pi n^{2k}\Big[\cos^2(nt) + 2\epsilon^2\cos(nt)a_1(t)\\ &+ \epsilon^4\left(2\cos(nt)b_1(t) + a_1(t)^2 + 3^{2k}a_3(t)^2\right)\Big]\,.\end{aligned} \tag{8.41}$$

As we can see, the NNLO contribution has terms that grow like t^2 with slope 3^{2k} which depends on the order of the norm that we are considering. Let us be more

explicit about this. If we define the rolling average over a period T of the initial mode as

$$\langle f(t)\rangle_T \equiv \frac{n}{2\pi}\int_{T-\pi/n}^{T+\pi/n} dt f(t)\,, \tag{8.42}$$

for any function $f(t)$, then, the rolling average of the Sobolev norm, after considering the time dependent mode coefficients is

$$\langle \left\| D^{(k)}\Phi \right\|^2 \rangle_T = \frac{\pi}{2}\epsilon^2 n^{2k}\left(1+\frac{3\epsilon^2}{64^2}\Big[6\cos(2nT)-1\Big]+\frac{72\epsilon^4}{n^2}\Big[(360+3^{2k})T^2+\mathscr{O}(T)\Big]\right). \tag{8.43}$$

It is now explicit that $\langle \left\| D^{(k)}\Phi \right\|^2 \rangle_T \supset \epsilon^6 3^{2k} T^2$, whereas the other terms are either constants, or purely oscillatory terms. Thus, if we fix the period T and the amplitude of the initial data ϵ, we find that the higher-order norms have grown more relative to the lower-order norms. This is consistent with a direct energy cascade: if energy is flowing towards higher frequency modes, this must lead to faster growth of the higher energy norms since those weigh more heavily than the high-frequency content.

A similar behavior occurs for the energy-like higher-order norms. Indeed, we find that

$$\begin{aligned}\langle \mathbf{E}^{(k)}_{\mathrm{nl}}[\Phi]\rangle_T =& \pi n^{2k}\epsilon^2\left(1+\frac{3\epsilon^2}{64}\Big[\frac{3}{n^{2k}}+n^{-2}\Big(6k-1+3(1+(-1)^k)\cos(2nT)\Big)\Big]\right.\\ &\left.+\epsilon^4\Big[\frac{3^{2(k-1)}-1}{1024n^2}T^2+\mathscr{O}\Big(T,T^2\cos(nT)\Big)\Big]\right).\end{aligned} \tag{8.44}$$

By setting $k=1$ we recover a constant value, as expected,

$$\langle \mathbf{E}^{(1)}_{\mathrm{nl}}[\Phi]\rangle_T = \pi n^2\epsilon^2+\frac{3\epsilon^4}{8} = \text{constant}\,. \tag{8.45}$$

We have also checked that the NNLO term vanishes exactly, even before taking the average. However, for the higher-order norms, we observe the same behaviour for both the Sobolev and energy-like norms, i.e., the norms grow as $\epsilon^6 c_k T^2$, where c_k is some monotone function of k, which depends on the precise definition of the norm. Note that the energy-like norms must have $c_{k=1}=0$, whereas this restriction does not apply to the Sobolev norms, which can grow even at first order.

8.4.2 *Four-dimensional Model*

Building on our analysis of the two-dimensional model, we now return to the original four-dimensional setup to apply the insights gained and further explore its behavior. Unlike the simpler nonlinear wave equation on a circle, the four-dimensional system exhibits several key differences. First, it is dissipative: because

the scalar field can escape to infinity rather than remain perfectly trapped at the stable LR, the mode frequencies are complex. Second, in the 2-dimensional case, frequencies of normal modes are commensurate. In contrast, for the four-dimensional setup, the sum of two (or more) QNM frequencies does not generically match the frequency of any other QNM, so the system is not at an exact resonance.

Although notable differences exist between the previous model (the nonlinear wave on the circle) and the physical scenario of interest, we can still examine whether the signature of growing higher-order norms emerges here. A key similarity is evident: if we excite the system with the $\ell = L, n = 0$ mode, modes with $\ell = 3L, 5L, \ldots$ subsequently appear, hinting at a direct cascade of energy.

Estimating the full higher-order Sobolev or energy norms from numerical solutions is a complicated task. Extracting reliable estimates of higher derivatives–and thus higher-order norms–from numerical solutions can quickly become cumbersome, as each (numerical) differentiation compounds the approximation error. One may also require (numerical) interpolation for the (numerical) integration over the domain. Nonetheless, building on the results of [58], we know that angular derivatives at the LR can grow rapidly for large initial data, which indicates that the angular terms in both Sobolev and energy norms might increase as well.

We solve the nonlinear wave equation (8.1), for axisymmetric initial data, using the numerical method described in Ref. [58]. We prescribe initial data localised around the stable LR. Since this is a trapping region, the field is confined at the LR, and its radial structure remains largely unchanged. Therefore, we can confidently estimate the total energy norm by extracting only the norm at the LR itself. We define, assuming additionally an axisymmetric configuration, the norm at the LR as

$$\left\| D^{(k)}\Phi(t) \right\|^2_{\rm LR} = \int_{r=R} \sin\theta d\theta d\phi \left(|\partial^{(k)}_\theta \Phi|^2 \right) , \tag{8.46}$$

and conjecture that all the norms scale in a similar manner, i.e., $\mathbf{E}^{(k)}_{\rm nl}[\Phi(t)] \sim \left\| D^{(k)}\Phi(t) \right\|^2 \sim \left\| D^{(k)}\Phi(t) \right\|^2_{\rm LR}$. Now, if the field at the LR is expanded in spherical harmonics (assuming axisymmetry)

$$\Phi = \sum_\ell c_\ell \mathcal{Y}_{\ell,0}(\theta) , \tag{8.47}$$

then one can compute the localized norm at the LR, up to a positive numerical factor b, as

$$\left\| D^{(k)}\Phi(t) \right\|^2_{\rm LR} = 2\pi b \sum_\ell \ell^{2k} c^2_\ell . \tag{8.48}$$

Without loss of generality, we will now set $b = 1$. The challenging part about extracting the behavior of these norms from numerical simulations is that, due to numerical errors, we only have access to the lower order multipoles, roughly, $\ell \lesssim 16$. In particular, for the values of α, R that we choose for numerical purposes, $\alpha = 0.166$

and $R = 0.229$ (chosen to agree with [58], which make it simpler for the potential well to be numerically resolvable after compactification), the damping time of the $\ell = 2$ mode is only $\tau_{20}/R \sim 10^3$ (see Fig. 30). If we excite initially the $\ell = 2$ mode, we will only see the norm growth on timescales shorter than this decay timescale, $t \ll \tau_{20}$. From the 2-dimensional model, we may expect that the norm grows as $\epsilon^4 t^2$, as shown in 8.44. The high power of the amplitude ϵ in this scaling makes it challenging to observe the norm growth for small initial data, even for the higher order norms.

We examine the norm ratio

$$\mathcal{R}^{(k)}_{\rm LR} \equiv \frac{\left\| D^{(k)}\Phi(t) \right\|^2_{\rm LR}}{\left\| D^{(k)}\Phi(0) \right\|^2_{\rm LR}}, \tag{8.49}$$

in Fig. 31, for different values of k, and an initial amplitude of $\epsilon = 1.5$ (which sets us away from the perturbative regime). Figure 31 shows how this norm ratio grows in an approximately linear fashion with $\epsilon^4 t^2$ (mind this scaling for the horizontal axes), during timescales shorter than the linear decay time of the fundamental mode. However, since the amplitude of the initial data may not be considered small, the agreement between this Figure and Eq. (8.44) is remarkable. Moreover, we can observe how the higher order norms (larger values of k) grow faster than the lower values of k. This is the same feature present already in the two-dimensional model. The ratio does not initially start at 1 for the higher-order norms because we average over multiple time points, and the rapid energy exchange between modes makes this transient phenomenon difficult to resolve.

These results provide analytical evidence that in the presence of stable trapping, nonlinear dynamics lead to a direct energy cascade, which in turn results in growing higher-order norms. In particular, higher-order norms grow faster than lower-order norms, and the growth rate seems to be polynomial in time. The norms do not diverge in finite time–it has been already established the global existence of solutions for this equation. This implies, in particular, that for any initial data ϵ and finite time T, we can always find an integer $K(\epsilon, T)$ such that norms with order $k \geq K$ have grown more than a certain factor of their initial value, regardless of how small this initial data is.

8.5 THE END STATE OF THE GRAVITATIONAL TURBULENT CASCADE

The previous discussion throws light to answer a question posed in previous work [58] related to the behaviour of higher-order norms in nonlinear systems in the presence of stable trapping. As we have found, all these norms grow, regardless of how small the initial data is. These higher order norms do not have a clear physical interpretation. In fact, the only norm with a well-defined physical meaning is the energy norm (8.9), which is actually conserved. The growth of these norms is interpreted as a consequence of the direct energy cascade. However, major significant questions remain unanswered. How does this cascade develop, and what are its

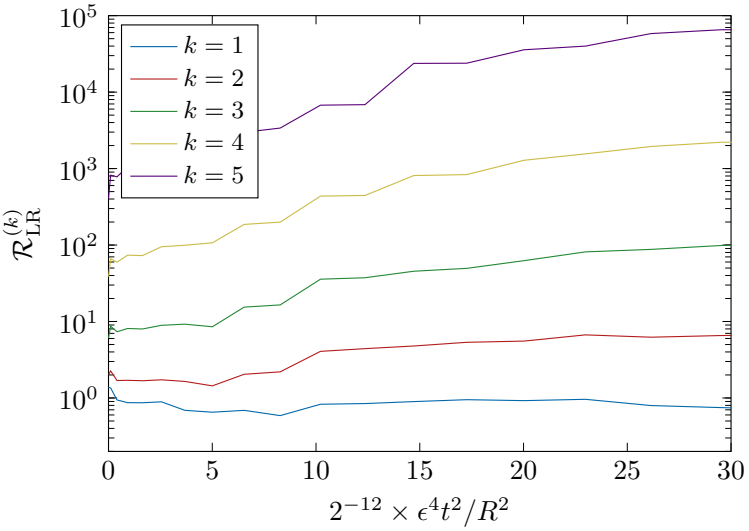

Figure 31 Ratio of the k-th order norm with respect to its initial value for different values of k, as indicated in the legend. The initial values are defined as in Eq. (8.49), at different times, with respect to the rescaled time $\propto \epsilon^4 t^2/R^2$, a factor based on Eq. (8.44). We choose a relatively large amplitude $\epsilon = 1.5$, in principle outside of the regime of validity of perturbation theory, where the initial data excites only the $\ell = 2$ mode. We set $\alpha = 0.166$ and $R = 0.229$ in (8.3).

properties? What is the end state of this dynamic process? In this section, we set ourselves to address these questions.

8.5.1 *Two-Dimensional Model*

As done in the previous Section, let us start with the lower-dimensional model, i.e., the nonlinear cubic wave equation in the circle. We evolve numerically the system of Eq. (8.35) with a pseudospectral strategy, following Chapter 2. We use the `ApproxFun.jl` package [361] to compute the nonlinear term in real space, and then evolve the Fourier representation of the equation in time using an explicit, fourth order Runge–Kutta method. After each step, we dealias the latter half of the Fourier modes to filter out contributions that can numerically contaminate the lower-frequency modes [81]. An important test is to check the accuracy and convergence of our implementation. We do so by estimating the lowest order norm of the residual, defined as

$$||\Phi^{(N_1)} - \Phi^{(N_2)}|| \equiv \left(\sum_{n \in \min(N_1,N_2)} |\phi_n^{(N_1)} - \phi_n^{(N_1)}|^2 \right)^{1/2} , \tag{8.50}$$

where $\Phi^{(N)}$ is the solution obtained using a total N modes, and ϕ_n^N is the coefficient of each of the modes for that particular solution. In Fig. 32 we show that the resolution error is several orders of magnitude below the norm of the solution, which estimates the accuracy of our method. Further, we show that doubling the

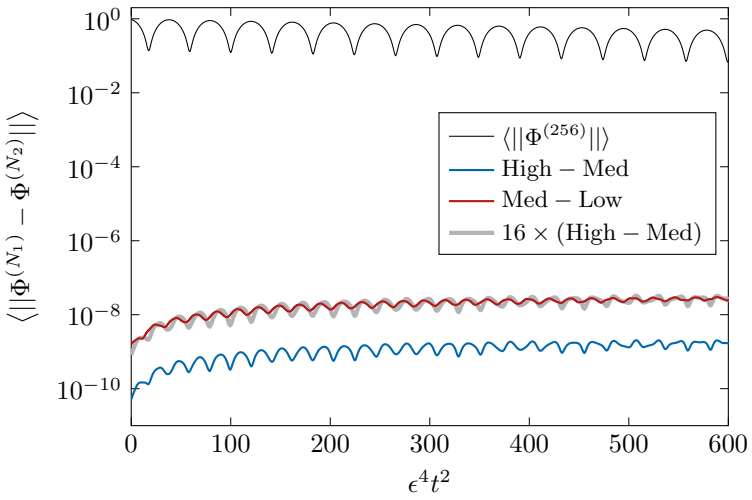

Figure 32 The norm defined in Eq. (8.50) for the highest resolution solution (using $N = 256$) in solid, black line, compared with the residuals between medium and high resolutions ($N = 128, 256$, respectively) in blue, and the residual between medium and low resolutions ($N = 128, 64$, respectively), in red. Overlapped and as a thicker, translucent gray line, we represent the rescaled residual between the medium and high resolutions, scaled by the convergence factor consistent with fourth-order convergence.

resolution decreases the error by a factor of 2^4, as expected for a fourth order method.

We prepare the evolution by exciting the two modes $n = 10, 11$, both with amplitude $\epsilon = 20$ (i.e., far away from the expected regime of validity of perturbation theory), and evolve the system until (long times) $T \gtrsim \epsilon^{-2}$. In Fig. 33 we present the evolution of the resulting spectrum, where we can see the development of an inertial range, characterized by a polynomial law, which can be interpreted as a direct energy cascade towards higher frequencies.

The development of an inertial range in the long- term dynamics of this nonlinear equation suggests an interpretation in terms of wave turbulence [290, 355, 467, 468]. We follow the derivation presented in [355]. Assuming that we treat small fluctuations with respect to the trivial solution, we can trade tracking the exact value of field modes $\{\phi_k(t)\}$ for the average particle number $n_k(t) \sim \langle |\phi_k(t)|^2 \rangle$. The evolution equations for the field are replaced, then, by the kinetic wave equation

$$\frac{dn_k}{dt} = \mathcal{C}[n_k]\,, \tag{8.51}$$

where $\mathcal{C}[n_k]$ is the collision integral. We refer the interested reader to [355] for further details. A cubic nonlinearity leads to a so called four wave kinetic process. One way of seeing this is that, if we would draw the perturbative problem of the excitation of NLO modes from linearized solutions using Feynman diagrams, we would draw a vertex with four legs (three incoming linear modes can excite a NLO mode). Building upon this intuition, we can decompose the collision integral

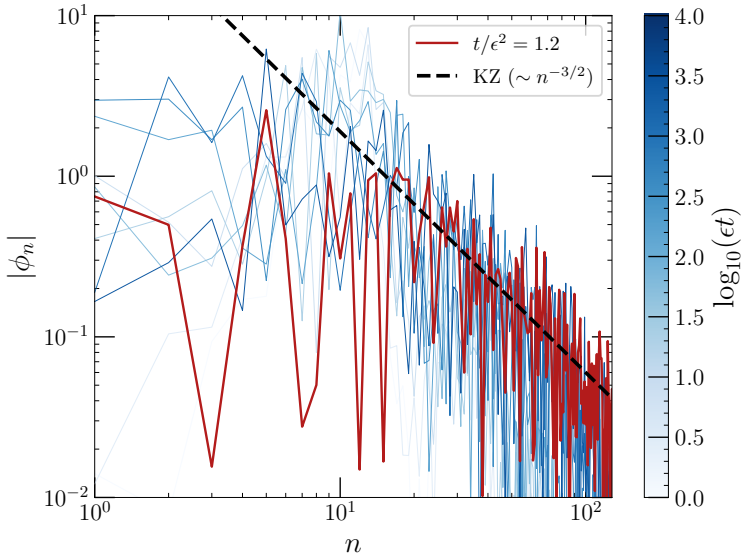

Figure 33 Field spectrum $|\phi_n|$ at different wavenumber n for large initial data with amplitude $\epsilon = 20$, initially excited in the modes $n = 10, 11$. The different colors indicate the field spectrum at different times, as indicated by the colorbar. The spectrum at the final time of the simulation, $t = 5000 \approx \epsilon^2$ is shown as a wider, red line. It agrees with the predicted Kolmogorov–Zakharov scaling $n^{-3/2}$ (dashed black line). The resolution of this simulation is $N = 1024$ modes.

into two different contributions, $\mathcal{C}[n_k] = \kappa_{2\leftrightarrow 2}\mathcal{C}_{2\leftrightarrow 2}[n_k] + \kappa_{3\leftrightarrow 1}\mathcal{C}_{3\leftrightarrow 1}[n_k]$, where the κ coefficients are numbers and of minor importance. Each of these is given by

$$\begin{aligned}\mathcal{C}_{2\leftrightarrow 2}[n_k] &= \int dk_1 dk_2 dk_3 W_{2\leftrightarrow 2}\Big[(n_1+n_2)n_3 n_k - n_1 n_2 (n_3 + n_k)\Big]\,,\\ \mathcal{C}_{3\leftrightarrow 1}[n_k] &= \int dk_1 dk_2 dk_3 W_{3\leftrightarrow 1}\Big[(n_1+n_2)n_3 n_k - n_1 n_2 (n_3 - n_k)\Big]\,,\end{aligned} \tag{8.52}$$

where the weights of the integrals are

$$\begin{aligned}W_{2\leftrightarrow 2} =& \delta(k_1+k_2+k_3-k)\delta(\omega_1+\omega_2-\omega_3-\omega_k)\,,\\ W_{3\leftrightarrow 1} =& \delta(k_1+k_2+k_3-k)\delta(\omega_1+\omega_2+\omega_3-\omega_k)\,.\end{aligned} \tag{8.53}$$

Recall that for the wave equation in the circle, the dispersion relation is just $\omega_k = |k|$. Thus, the $\mathcal{C}_{2\leftrightarrow 2}$ operator corresponds to processes that conserve the particle number, while $\mathcal{C}_{3\leftrightarrow 1}$ to processes that violate particle number conservation. Therefore, as opposed to other systems which also involve three wave interactions, such as the nonlinear Schrödinger equation [187], or a model for gravitational waves propagating in flat space [201, 203, 204], the system only has one conserved quantity (the energy presented in (8.9)). This implies that the only possible inertial regime in the turbulent state must be a direct cascade. On the other hand, if $\kappa_{3\leftrightarrow 1} = 0$, then there would be an additional conserved quantity (particle number), which would be associated to an inverse cascade.

There are special solutions to the kinetic wave equation which are stationary, i.e., $\dot{n}_k = 0$, under the assumption that there is dissipation acting at low and high

frequencies, and the system is being injected energy at some scale [290, 467] (which is not the case for the model we are interested). In this scenario, there exist solutions of the form $n_k \sim k^{-\nu}$, in the regime bounded by the dissipation scales, which is known as the inertial regime. These spectra are known as Kolmogorov-Zakharov (KZ) spectra, and there are many techniques devoted to compute the power of these spectra ν precisely. For four wave equations, the direct energy cascade is associated to a power $\nu = 3/2$ [145]. In Fig. 33 we find good agreement between the late time solution and this prediction.

Equipped with these expectations, we can now address the question about the end state of the nonlinear wave equation in this two-dimensional model, for small initial data. If there is no dissipation, a direct energy cascade towards higher energies ensues, ultimately spreading energy across all possible modes. In the asymptotic state, $t \to \infty$ all modes are excited with negligible amplitude (since the initial amount of energy in the system was finite), and the solution loses regularity in the asymptotic time, as evidenced by the fact that the higher order norms diverge as $t \to \infty$. However, in most physical situations we expect the system to dissipate energy beyond some scale $k \geq k_{\text{Diss}}$. The development of a KZ-like inertial range requires of continuous injection of energy, precisely to compensate this dissipation. In the absence of energy injection, the end state would just be $\Phi = 0$, i.e., the trivial solution. We emphasise that other nonlinear equations (for example, those for which the global existence of solutions is not guaranteed) or initial data very far from the perturbative regime, where this analysis based on weak wave turbulence does not hold, might exhibit different phenomenology at late times, such as, e.g., time-periodic solutions.

8.5.2 *Nonlinear Waves on the Sphere*

The previous model allowed for a straightforward analysis of the end state but has several limitations. One of the main limitations, in particular, is that the dispersion relation $\omega_k^2 = k^2$ only matches the dispersion relation of the long-lived modes in the eikonal regime. On the other hand, there is a physically motivated approximation that does not add much complexity, and can be put in closer contact with our original problem more directly.

After analysing the radial structure of numerical solutions to the nonlinear wave equation on the model spacetime [58], it is apparent that the waves are confined to a region close to the stable LR, i.e., at $r = R$. Indeed, Fig. 34 shows the radial profile of the $\ell = 2$ (the initially excited mode), and the $\ell = 4$ mode (excited nonlinearly) at late times. The localisation near the LR can be explained by comparing it with the radial profile of the fundamental modes, shown as dashed lines, which show good agreement (improved with increasing ℓ values).

Accordingly, we can consider a simplified model, which consists of the dimensional reduction of our original problem to the sphere located at the LR (as done in Ref. [58] to measure the evolution of the ℓ-spectrum). As we will show, eliminating the radial direction of the problem allows for significant simplifications. The

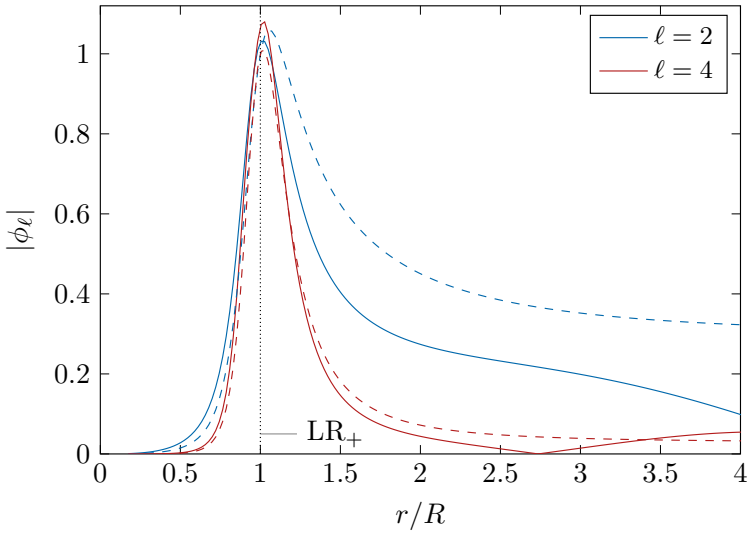

Figure 34 Normalised radial profile of the $\ell = 2$ and $\ell = 4$ modes extracted for a numerical simulation with weak coupling, $\epsilon = 0.1$, after $t/R = 10^3$, where the initial data excites only the $\ell = 2$ mode (solid lines). The dashed lines represent the radial profile of the fundamental mode associated to each ℓ mode. The agreement between both lines shows that most of the content of both linearly and nonlinearly excited modes, at large times, is contained in the fundamental mode, and peaks close to the stable LR.

radial dimension is important insofar as it provides the mechanism for dissipation through radiation leaking toward infinity. However, this dissipation can also be seen as a tunnelling process, akin to quantum mechanics, without needing to resolve the dynamics in the radial direction. We can always add these tunnelling rates a posteriori as dissipation coefficients, which are given by the damping times of the fundamental spherical harmonic modes.

To be precise, let us focus at the surface $r = R$, where the induced metric is

$$ds^2_{r=R} = -f(R)dt^2 + R^2 d\Omega^2 = -dT^2 + R^2 d\Omega^2 \,, \tag{8.54}$$

where we have re-scaled time as $T = \sqrt{f(R)}t$. We examine the nonlinear wave equation in this geometry, i.e., $\Box_{g_R}\Phi = \kappa\Phi^3$, where now $\Phi : \mathcal{S}^2 \times \mathbf{R} \to \mathbf{R}$ is a real field. Expanding in spherical harmonics, and assuming axisymmetry, we can write $\Phi = \sum_\ell \phi_\ell(T)\mathcal{Y}_{\ell,0}(\theta)$, so that the nonlinear wave equation reads

$$\frac{d^2\phi_\ell}{dT^2} + \frac{\ell(\ell+1)}{R^2}\phi_\ell = \kappa \sum_{\ell_1\ell_2\ell_3} \mathcal{I}_\ell^{\ell_1\ell_2\ell_3}\phi_{\ell_1}\phi_{\ell_2}\phi_{\ell_3} \,. \tag{8.55}$$

Assuming that the initial data has small amplitude ϵ, we can find perturbative solutions up to next to leading order. As in Sec. 8.4, we write $\phi_\ell = \epsilon\phi_\ell^{(1)} + \epsilon^3\phi_\ell^{(3)}$, and for initially static initial data, we have that the leading order solution is just

$$\phi_\ell^{(1)} = \mathcal{A}_\ell \cos(\omega_\ell T) \,, \qquad R\omega_\ell = \sqrt{\ell(\ell+1)} \,. \tag{8.56}$$

Going back to the original time coordinate, we find that the oscillation frequency $\omega_\ell T = \nu_\ell t$, with $\nu_\ell^2 = \Omega\ell(\ell+1)$, matching the WKB result, which is also obtained

when fitting the QNM frequencies obtained through direct integrations. Therefore, the reduction to the sphere captures accurately the real part of the frequency of the fundamental, long-lived modes. To NLO, writing $\Lambda = \{\ell \mid \mathcal{A}_\ell \neq 0\}$, we obtain the equation

$$\ddot{\phi}^{(3)}_\ell + \frac{\ell(\ell+1)}{R^2}\phi^{(3)}_\ell = \frac{\kappa}{4}\sum_{j\in\Lambda^3} \mathcal{I}^j_\ell \mathcal{A}_{j_1}\mathcal{A}_{j_2}\mathcal{A}_{j_3}\mathcal{F}_j(T)\,, \tag{8.57}$$

where $j = (j_1, j_2, j_3)$, and

$$\mathcal{F}_j(T) = \sum_{\sigma_1,\sigma_2=\pm 1} \cos(\Omega_j^{\sigma_1\sigma_2} T)\,, \qquad \Omega_j^{\sigma_1\sigma_2} = \omega_{j_1} + \sigma_1\omega_{j_2} + \sigma_2\omega_{j_3}\,. \tag{8.58}$$

The ℓ-th mode would be resonant if one of $\Omega_j^{\sigma_1\sigma_2} = \omega_\ell$ for some $j \in \Lambda^3$. If $j = \ell$, then $\Omega_\ell^{+-} = \Omega_\ell^{-+} = \omega_\ell$, which is actually the only possibility. In particular, if the initial data consists of a single mode, $\Lambda = \{\ell_0\}$, the only resonant mode at next to leading order is itself, ℓ_0. For this case, we can then write the third order solution, as

$$\phi^{(3)}_\ell = \begin{cases} \frac{\kappa \mathcal{I}^{\ell_0}_\ell \mathcal{A}^3_{\ell_0}}{4}\sum_{\sigma_1,\sigma_2=\pm 1}\mathcal{G}^{\sigma_1,\sigma_2}_{\ell,\ell_0}(T)\,, & \ell \neq \ell_0\,, \\ \frac{\kappa \mathcal{I}^{\ell_0}_{\ell_0} \mathcal{A}^3_{\ell_0}}{8\omega_{\ell_0}} t\sin(\omega_{\ell_0} t) + \mathscr{O}(t^0)\,, & \ell = \ell_0\,, \end{cases} \tag{8.59}$$

where

$$\mathcal{G}^{\sigma_1,\sigma_2}_{\ell,\ell_0}(T) = \frac{\cos(\omega_\ell T) - \cos(\Omega^{\sigma_1\sigma_2}_{\ell_0} T)}{\omega_\ell^2 - (\Omega^{\sigma_1\sigma_2}_{\ell_0})^2}\,, \tag{8.60}$$

is a purely oscillatory term, which combines the homogeneous modes and the non-linearly excited (cubic) modes. Note that we write $\Omega^{\sigma_1\sigma_2}_{\ell_0} = \Omega^{\sigma_1\sigma_2}_{(\ell_0,\ell_0,\ell_0)}$. Therefore, for $\ell \neq \ell_0$ (e.g., for $\ell = 3\ell_0$) the solution is purely oscillatory, and it excites both homogeneous and cubic modes with an amplitude which is cubic in the linear amplitude $\mathcal{A}_{\ell_0}$. The $\ell = \ell_0$ mode, however, features a secular linear growth in time, as well as sub-leading, oscillatory pieces. The results are the same for a general set of initially excited modes, $\tilde{\Lambda}$. Generically we have that $\phi^{(3)}_\ell \sim t\sin(\omega_\ell T)$ if $\ell \in \tilde{\Lambda}$, and otherwise, $\phi^{(3)}_\ell \sim \cos(\omega_\ell T)$ whenever $\ell \notin \tilde{\Lambda}$. This implies that all energy norms grow at the same rate, independently of the order of the norm.

Although resonances only occur exactly within each mode separately, at large values of ℓ we have that $R\omega_\ell \approx \ell + 1/2$. Then, in the large ℓ limit, we have

$$\Omega_j^{+-} = \omega_{j_1+j_2-j_3}\,, \qquad \Omega_j^{++} = \omega_{j_1+j_2+j_3+1}\,, \tag{8.61}$$

and similarly for the other two possible combinations. Therefore, as ℓ grows more modes become almost exactly resonant. This dispersion relation is also the dispersion relation of linear waves on the Möbius open strip. Intuitively, this can be seen as arising from the fact that axisymmetric waves on the sphere are waves in the

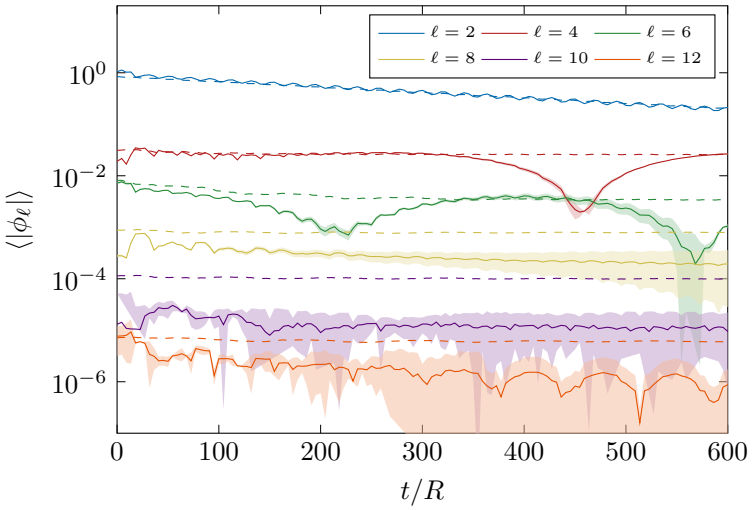

Figure 35 Root mean square value of the amplitude of each mode ϕ_ℓ extracted at the LR for an evolution of the complete spacetime, with amplitude $\epsilon = 1/2$ in the notation of Ref. [58] (solid lines), and for a comparable amplitude, including artificial dissipation, for the nonlinear wave equation on the sphere (dashed lines). The shaded bands denoted an estimate of the numerical error for the $3+1$ evolution, obtained by comparing two different resolutions. The agreement is remarkable for the most dominant modes at early times, but it breaks down at later times, and for the higher ℓ modes.

closed interval $[0, \pi]$, subject to the periodicity relation $\Phi(\theta) = \Phi(\theta + 2\pi)$. A simple way to achieve this is by requiring the anti-periodicity condition $\Phi(\theta) = -\Phi(\theta + \pi)$, which under an appropriate rescaling is the condition naturally satisfied by sections of the fibre bundle associated to the Möbius strip double cover of the circle.

To understand the dynamics at longer time scales, we will solve the equations numerically. To facilitate a better comparison with the complete system, we will include the dissipation rate for each mode by formulating the evolution equation for each mode as follows:

$$\ddot{\phi}_\ell + \frac{\ell(\ell+1)}{R^2}\phi_\ell + \frac{2}{\hat{\tau}_\ell}\dot{\phi}_\ell = (\Phi)^3_\ell\,, \tag{8.62}$$

where the right hand side contains the nonlinear term, and we have added a dissipative term with a timescale $\hat{\tau}_\ell = \tau_\ell/(\Omega R^2)$, with τ_ℓ the damping time obtained by fitting the WKB results to an exponential law. This equation is solved numerically using the same code as for the two dimensional scenario, but expanding instead on a basis of Legendre polynomials. We first test that, by doing this, we can reproduce the dynamics of the four-dimensional problem, at least in the regime where the initial data is small enough.

Figure 35 shows the numerical solution to the four-dimensional problem extracted at the LR as solid lines, and the numerical solution to (8.62) as dashed lines, after matching the amplitude of the initial data and rescaling the time appropriately. The uncertainty due to numerical error is shown as solid translucent bands, and is estimated by comparing two runs with resolution $\Delta x = 2.5 \times 10^{-3}$, and $\Delta x/2$. Clearly the numerical error is significant for the large ℓ modes after $t/R \gtrsim 100$.

However, even the $\ell = 8, 10$ modes are reasonably well resolved up to the times shown in the Figure, and we can draw some conclusions by comparing with the $2+1$ model.

The agreement for the lower ℓ modes is very good, especially at early times. At late times, even for low ℓ, we observe oscillations which are not present in the $2+1$ model. These are likely due to the excitation of different overtones within each angular harmonic ℓ, which have different amplitude at the LR. We also observe that the agreement is much worse for the higher ℓ modes, even at early times. There is a physical reason why we should not expect the higher ℓ modes to agree as well as the lower ℓ modes to a dimensionally reduced problem: higher ℓ modes support several long-lived modes (overtones), where only the fundamental mode is confined at the LR.

On the one hand, the fundamental mode $n = 0$ is always a long-lived mode, and has a radial support centered around the LR, with a radial spread $\delta^{(r)}_{\ell,n=0} \sim \ell^{-1/2}$ [104]. On the other hand, the highest overtone which is still long lived [2], $n = N_\ell$, has a radial support which does not depend on ℓ, $\delta^{(r)}_{\ell,n=N_\ell} \sim r_{\mathrm{LR}_-}$. The modes with intermediate overtone number, for a fixed value of ℓ, have a radial width which is proportional to its overtone number. Therefore, once these higher overtones start to play an important role in the nonlinear dynamics, the problem is not confined to a sphere located *exactly* at the LR, but rather at a spherical shell with finite thickness, that supports a finite amount of modes for each angular harmonic ℓ. We can see this phenomenon in Fig. 36.

This analysis implies that the dimensional reduction to the sphere might not be a good approximation for high-frequency modes since long-lived overtones may play a significant role. However, we can still gain some insights by analysing the behaviour at large times outside of the perturbative regime. In comparison to the two-dimensional model, we can anticipate a difference: In $1+1$ dimensions the dispersion relation was simply $\omega_k^2 = k^2$, hence, $\omega_{k_1+k_2+k_3} = \omega_{k_1} + \omega_{k_2} + \omega_{k_3}$, and as a consequence, the kinetic wave equation received contributions from the collision operator $\mathcal{C}_{3\leftrightarrow 1}$. However, in the sphere the dispersion relation is $R^2\omega_\ell^2 = \ell(\ell+1)$, and the combination of three modes onto a single mode is not resonant.

We can also observe this behaviour by analysing the NLO in perturbation theory. In particular, since the kinetic wave equation does not receive contributions from $\mathcal{C}_{3\leftrightarrow 1}$, and this term was responsible for the violation of the conservation of particle number, in its absence, we expect that the system undergoes both a direct energy cascade and an inverse cascade governed by the particle number (also known as *waveaction*) [204, 355]. We can find hints of this process happening in Fig. 37, e.g., in the form of "revivals" of low ℓ modes. These appear, for example, in the form of changes in the amplitudes of a lower ℓ mode and a decay of the amplitude of higher ℓ modes. For example, near $t/R \sim 400$ we see the amplitude of the $\ell = 2, 4$ modes grow significantly, while there is a decay in the amplitude of $\ell = 6$. Notice, for

2 By this, we mean the highest overtone, such as its damping time being larger than a certain threshold, or simply the largest overtone number that can be found as a solution to the Bohr-Sommerfeld quantization condition in the WKB regime.

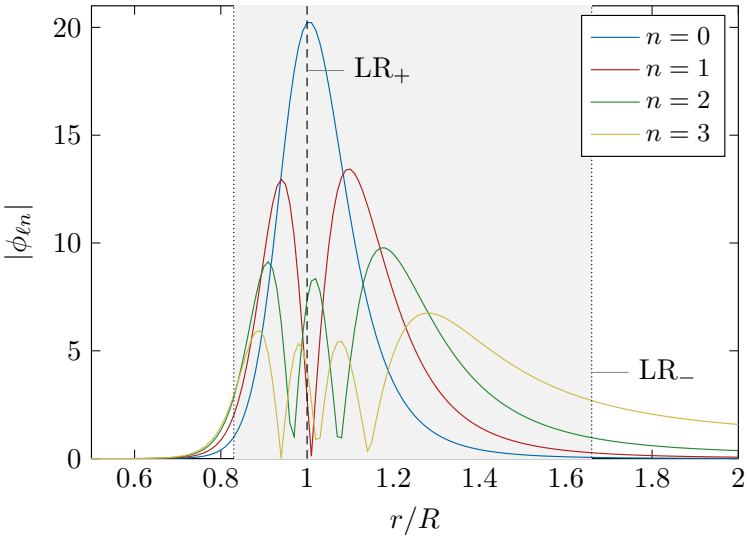

Figure 36 Normalised radial profile of the long-lived overtones of the $\ell = 10$ angular harmonic. Although the fundamental mode is localised very close to the LR (vertical-black dashed line), the higher overtones span a larger radial width, approximately ranging between the unstable LR, and its symmetric point in the potential, occupying all the filled gray region.

instance, the similarities between the dynamics of these modes, and the dynamics of radial modes of a scalar field in AdS for initial conditions within islands of stability [41], where also an inverse cascade is present.

The long-term dynamics of nonlinear waves on the sphere, in the presence of artificial dissipation in the manner of Eq. (8.62), results of a combination of several effects. On the one hand, we have a dual cascade: energy cascade, from low to high frequencies, and particle number cascade, from high to low frequencies. However, we also have dissipation, which is (exponentially) more efficient at low frequencies. Due to the presence of this low-frequency dissipation, the inverse energy cascade just facilitates the dissipation of energy at low frequencies in the system. The resulting turbulent behavior is, thus, only dominated by the direct energy cascade, as can be seen in Fig. 38. The Figure shows that the high frequency sector seems described by a KZ scaling. Although it is rather difficult to extract precise information about the KZ exponent, the scaling $\phi_\ell \sim \ell^{-3/2}$, characteristic of a direct energy cascade on a four wave interaction [231], appears as a good approximation. On the other hand, at low frequencies we observe the effect of dissipation, which suppresses significantly the spectrum for $\ell \lesssim 10$.

The development of an inertial range requires the dissipation of high-frequency radiation. However, the nonlinear wave model considered here lacks any intrinsic mechanism to provide this. In realistic scenarios, such dissipation can arise from the absorption of scalar waves or GWs by matter [80, 188, 226, 279, 280, 370, 395], or from quantum effects.

For a KZ spectrum to persist in the inertial range, energy must be injected at a constant rate. One possible mechanism for this is accretion, which could inject GWs

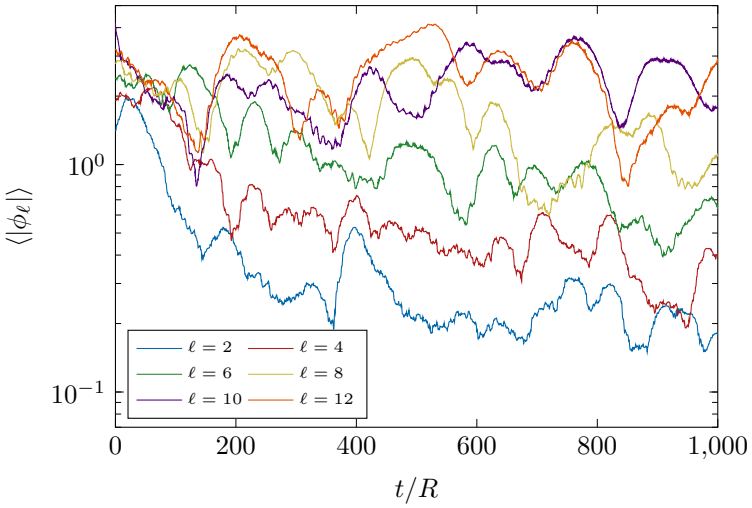

Figure 37 Evolution of the root mean square value of the mode amplitudes for some modes of the system, as depicted in the legend. The system is initialized in the $\ell = 10, 11$ modes, both with equal amplitude $\epsilon = \sqrt{10}$, evolved with a total resolution $N = 256$. We observe hints of an inverse cascade, as a correlated growth/decay of the amplitudes of lower ℓ / higher ℓ modes. For example, this explains the rapid growth of the $\ell = 2$ mode near $t/R = 400$, together with a decay of the $\ell = 6$ mode.

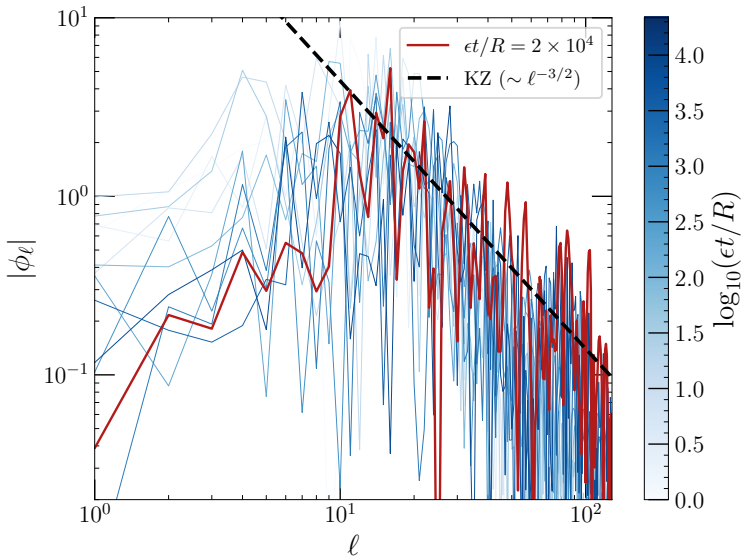

Figure 38 The power spectrum $|\phi_\ell|$ at different times (as indicated by the colorbar), for the same configuration presented in Fig. 37. The latest time available is represented with a thick-dark red line. At high frequencies, the spectrum is consistent with a Kolmogorov–Zakharov-type scaling $\phi_\ell \sim \ell^{-3/2}$ (black dashed line), as in the two dimensional model.

into the stable LR and sustain the KZ spectrum. However, this requires additional physical ingredients beyond the mere existence of a stable LR. In the absence of continuous energy injection, dissipation–inevitable at low frequencies, even in vacuum–dominates, and the KZ spectrum is not a stationary solution. Consequently, in the regime of validity of weak wave turbulence, we conjecture that the end state is always the trivial one, $\Phi = 0$.

8.6 DISCUSSION AND OUTLOOK

Several horizonless black hole mimickers and higher-dimensional spacetimes are known to admit stable light rings, which can efficiently trap high-frequency radiation, including gravitational waves. Consequently, small perturbations in such spacetimes decay slowly [57, 272]. While it has been conjectured that this slow decay could trigger a nonlinear instability, the existing numerical and analytical evidence remains inconclusive.

Recent numerical work [58] has provided evidence that a stable LR can induce a turbulent cascade capable of transferring energy to higher frequencies. In this work, we extend this analysis by further investigating the dynamics of this cascade in the perturbative regime. Our results indicate that the sole presence of a stable LR does not necessarily lead to instability. In particular, for the nonlinear cubic wave equation considered here, we argue that the trivial solution $\Phi = 0$ remains stable under small perturbations.

One important aspect of our analysis concerns the regularity of solutions. Nonlinear wave equations are generally prone to energy-cascading phenomena. By examining a two-dimensional model, we have confirmed that higher-order norms of the solution grow rapidly, with a rate that increases with wave number. This growth leads to a gradual loss of smoothness over time. We find that a similar behaviour occurs in the presence of a stable LR, reinforcing the evidence for a direct energy cascade. However, while such turbulence redistributes energy, it does not necessarily imply a global instability. In particular, the absence of an uncontrolled energy accumulation in any particular mode suggests that the system does not undergo a catastrophic breakdown.

A key question is whether this turbulent cascade could still lead to a physical instability over sufficiently long timescales. To address this, we have studied the long-term dynamics of a dimensionally reduced system, which describes waves propagating exactly at the LR. This model effectively captures the dynamics of low-ℓ modes, and our numerical simulations reveal hints of a dual cascade, where energy flows both towards higher frequencies (direct cascade) and towards lower frequencies (inverse cascade). When artificial dissipation is introduced at high frequencies, an inertial range emerges, characterised by a Kolmogorov–Zakharov spectrum. However, it is important to recognise that this model may not accurately describe the high-frequency behaviour. In particular, a family of long-lived radial overtones exists for large angular numbers, supported within a finite-thickness

spherical shell centered around the light rings. This suggests that conclusions from the reduced model should be treated cautiously, and further research is needed.

If the considered system with a stable light ring, were to be unstable, and the nonlinear back-reaction of the scalar field on the geometry were included, at least the following possible outcomes could be expected: the formation of a black hole at the LR; the emergence of time -periodic solutions (e.g., quasimode solutions exhibiting an uniform decay rate slower than inverse logarithmically in time); or the evolution toward a state *without* a stable LR altogether (as, e.g., conjectured in Ref. [153] for spinning boson stars but recently reconsidered in Ref. [329]). Regarding the first scenario, since radiation is only partially trapped within a finite-width shell, the formation of a black hole starting from arbitrarily small initial data appears inconceivable. This expectation aligns with the arguments presented in [58]. Unlike the case of pure AdS, where nonlinear wave interactions lead to the focusing of energy at a single point [73], in this type of spacetimes, the energy remains distributed across an extended region. Additionally, we find no evidence for the formation of time-periodic solutions, which require both (i) high-frequency dissipation and (ii) a continuous energy injection mechanism. In the absence of sustained energy input, they must eventually decay. Our results suggest that, after a sufficiently long time, the radiation either escapes the light ring or disperses into high-frequency modes with negligible amplitude. Based on this analysis, nonlinear waves propagating in spacetimes with stable light rings appear dynamically stable within the framework considered here.

Several aspects remain unexplored: what is the role of horizons in this turbulent cascade? On the one hand, a horizon would enhance dissipation, reinforcing the arguments against the instability. On the other hand, topological considerations imply that in four-dimensional asymptotically flat spacetimes, the presence of a horizon and a stable light ring necessitates a second unstable light ring, leading to additional complexity. Additionally, our analysis is simply based on a scalar field model while capturing some essential nonlinear dynamics, does not account for full gravitational interactions. Since trapped radiation at the light ring can, in principle, modify the light ring's properties, the backreaction effects in a fully relativistic setting could introduce additional dynamical features that the nonlinear behavior arising solely from the self-interaction of the scalar field does not capture. Lastly, rotation can amplify radiation, either through partial absorption at the surface of the black hole mimicker or via the presence of ergoregions [83]. Studying these effects in a well-posed matter model remains an important next step. Recent work [427, 428, 435] supports the picture drawn in this Chapter.

Part III

INTERACTION OF GRAVITATIONAL WAVES WITH VISCOUS MATTER

Well, there's so many sinking
Now you've got to keep thinking
You can make it through these waves

— *Joni Mitchell,* Blue

9

DISSIPATIVE RELATIVISTIC HYDRODYNAMICS

Written while listening to music composed by Ludwig van Beethoven.

9.1 INTRODUCTION

This second part of the thesis is devoted to understanding the interaction between gravitational waves (GWs) and matter. This is motivated for two main reasons. First, to understand the dynamics of neutron stars. These stars are extremely compact, and the properties of the cold and ultradense matter in their interior remain an open question. GW observations of merging neutron stars can help us understand their composition, but in order to do so we must achieve an excellent understanding of the interplay between stellar dynamics and GW emission.

The second motivation is the propagation of GWs through the Universe. The Universe is hardly empty, and less so the environments where BHs likely merge: galactic centers, globular cluster, or active galactic nuclei are filled with dust, accreted gas, dark matter, and other compact objects. The presence of these environments leaves imprints modifying the two-body dynamics during binary coalescences [46, 167, 175, 178, 433], but it also may affect how GWs are propagated. One way in which this occurs is through gravitational lensing [420]. However, the nature of GWs means that there are other possible signatures, e. g., bright counterparts to BH mergers, which carry important information about the astrophysical cradles where GW signals are born.

A crucial observation is that GWs couple dynamically to fluids through their viscosity. Therefore, this part of the thesis is particularly dedicated to the interaction of GWs with *viscous* matter. This was originally observed by Hawking [237], and Weinberg [459] in the context of propagation of GWs through cosmological history, but also applies to the propagation of GWs through slabs of matter [188, 226, 325, 370, 384]. Indeed, a GW propagating through a perfect fluid is not altered (except for a possible redshift due to the fluid's self-gravity). On the other hand, a GW propagating through a viscous fluid is partially absorbed and reflected by it. Dissipative effects in hydrodynamics play the same role as conductivity does with respect to the propagation of electromagnetic waves.

Fortunately, the same physical description applies both to neutron stars and to astrophysical environments, to a large extent. Both regimes fall within the regime of hydrodynamics, i. e., complex macroscopic material bodies that, close to equilibrium,

can be described in terms of thermodynamic variables. In order to account for viscous effects, we study hydrodynamics as an effective field theory [292, 293]. In this chapter we introduce our viewpoint on hydrodynamics, and we present the relativistic version of the Navier-Stokes equation that we will work with in subsequent chapters. In particular, we discuss in some depth the well-posedness of dissipative hydrodynamics. This builds heavily on recent works by Bemfica, Disconzi, Noronha [54], and Kovtun [293], and therefore this well-posed, causal, and stable theory of relativistic and dissipative fluid dynamics is often dubbed BDNK hydrodynamics.

9.2 HYDRODYNAMICS AS AN EFFECTIVE FIELD THEORY

Fluid dynamics is a field theory compatible with Noether's theorem and the fundamental spacetime symmetries. General covariance leads to the conservation of the stress energy tensor $\nabla_b T^{ab} = 0$. Additional internal symmetries of the matter under consideration, e. g.the $U(1)$ baryon number conservation, lead to additional conservation laws, such as the conservation of the particle current $\nabla_a J^a = 0$.

The fundamental assumption is that matter admits a description in terms of a small number of macroscopic variables. These are typically taken to be one timelike vector field u_a (normalised so that $u_a u^a = -1$), representing the fluid velocity, and two scalars – the temperature T, and the chemical potential μ. The most general stress energy tensor and particle number current written in terms of two scalars and one vector takes the following form

$$\begin{aligned} T^{ab} =& \mathscr{E} u^a u^b + \mathscr{P} \Delta^{ab} + \mathscr{Q}^a u^b + u^a \mathscr{Q}^b + \mathscr{T}^{ab} , \\ J^a =& \mathscr{N} u^a + \mathscr{J}^a , \end{aligned} \tag{9.1}$$

where $\mathcal{E}, \mathcal{P}, \mathcal{N}$ are arbitrary scalar functions of (T, μ, u_a), $\mathcal{Q}^a, \mathcal{J}^a$ are transverse vectors, i. e., $u_a \mathcal{Q}^a = u_b \mathcal{J}^b = 0$, and $\mathcal{T}^{ab}$ is a transverse and traceless symmetric tensor. Above $\Delta^{ab} = g^{ab} + u^a u^b$ is the projector onto the fluid's worldline. A hydrodynamic theory is specified once certain *constitutive relations*, relating the quantities $\mathcal{E}, \mathcal{P}, \mathcal{N}, \mathcal{Q}^a, \mathcal{J}^a, \mathcal{T}^{ab}$ to the thermodynamic variables T, μ, u_a are specified. Generically we say that a hydrodynamic theory is zeroth, first, or second-order if the constitutive relations involve no derivatives, first derivatives, or second derivatives, respectively, of the thermodynamic variables. Generically one may write

$$\begin{aligned} \mathscr{E} =& \varepsilon + \mathcal{E}^{(1)} + \mathscr{O}(\partial^2) , \quad \mathscr{P} = p + \mathcal{P}^{(1)} + \mathscr{O}(\partial^2) , \quad \mathscr{N} = n + \mathcal{N}^{(1)} + \mathscr{O}(\partial^2) , \\ \mathscr{Q}^a =& (\mathcal{Q}^a)^{(1)} + \mathscr{O}(\partial^2) , \quad \mathscr{J}^a = (\mathcal{J}^a)^{(1)} + \mathscr{O}(\partial^2) , \quad \mathscr{T}^{ab} = (\mathcal{T}^{ab})^{(1)} + \mathscr{O}(\partial^2) , \end{aligned} \tag{9.2}$$

where we note that there are no zeroth order contributions to the heat and particle number flux $\mathscr{Q}^a$, $\mathscr{J}^a$, and the stress tensor $\mathscr{T}^{ab}$, since one cannot construct transverse tensor fields without derivatives of the thermodynamic variables. Since we will only consider first order theories, we remove the superscript (1) from the dissipative corrections to the stress energy tensor, $\mathcal{E} \equiv \mathcal{E}^{(1)}$. Additionally we label ε, p, n the zeroth order values of the scalar quantities, whose interpretation is discussed below.

By performing this expansion in gradients, we are treating hydrodynamics as an effective field theory. The effective field theory framework allows us to formalise going from a microscopic theory of interacting particles to a hydrodynamic theory built upon thermodynamic variables. We construct a hydrodynamic theory by integrating out degrees of freedom up to a given power of the characteristic length scale of interactions in the microscopic theory, which can be taken to be the mean free path ℓ_{mfp}. At zeroth order we only retain the thermodynamic variables, which vary on lengthscales much larger than the mean free path. The gradient expansion becomes naturally an expansion in powers of ℓ_{mfp}, if we take into account that $|\partial_a T| \ll |T/\ell_{\text{mfp}}|$. The transport coefficients which will appear relating quantities like $\mathcal{E}$ to the thermodynamic variables can, thus, be related to n-point functions and correlators in the underlying microscopic theory. Knowledge of the chemical reaction rates can be used to directly estimate the scale of these transport coefficients, see [20, 210, 211].

The effective field theory of hydrodynamics is not completely free. In particular, a sensible physical requirement emerges by considering the entropy current [258]

$$TS^a = pu^a - T^{ab}u_b - \mu J^a \,, \tag{9.3}$$

with s The second-law of thermodynamics requires that the entropy is never decreasing. Therefore, one may naturally require (for a first-order theory) either of the following two conditions

$$\begin{aligned} &\text{Effective 2nd Law:} \qquad \nabla_a S^a \geq 0 + \mathscr{O}(\partial^3) \,, \\ &\text{Strict 2nd Law:} \qquad \nabla_a S^a \geq 0 \,. \end{aligned} \tag{9.4}$$

The first requirement takes into account that we have truncated the stress-energy tensor. As long as we are in the regime of validity of the effective field theory, i. e., as long as the gradients are small enough, then these two conditions for entropy production are equivalent. However the first condition allows for theories where entropy can decrease. This should *not* be read as a physical effect, but rather a smoking gun that one is applying the effective description beyond its regime of validity. On the other hand, the strict second law version may be more appealing, as it never leads to apparent violations of thermodynamics. Nevertheless, as we shall discuss below, it is too restrictive.

Zeroth order hydrodynamics, also known as the theory of a perfect fluid, corresponds to the following stress energy tensor and particle number current

$$T^{ab} = \varepsilon u^a u^b + p\Delta^{ab} \,, \qquad J^a = nu^a \,. \tag{9.5}$$

Locally we can construct a frame aligned with the fluid velocity, and flat coordinates, so that the stress energy tensor takes the form $T^a_b = \text{diag}(-\varepsilon, p, p, p)$, and $J^a = (n, 0, 0, 0)$. From the point of view of this frame, then ε clearly denotes the fluid's energy density, p the equilibrium pressure, and n the equilibrium density of the $U(1)$ charge, i. e., particle number density.

The equations of motion can be summarised as

$$\begin{aligned} u^a\nabla_a\varepsilon + (\varepsilon+p)\nabla_a u^a &= 0\,, \\ u^b\nabla_b u^a + \frac{\partial p}{\partial\varepsilon}\frac{\nabla^a_\perp\varepsilon}{\varepsilon+p} &= 0\,, \\ u^a\nabla_a n + n\nabla_a u^a &= 0\,, \end{aligned} \tag{9.6}$$

where $\nabla^a_\perp = \Delta^{ab}\nabla_b$ is the derivative orthogonal to the fluid flow. We can now show that this corresponds to a perfect fluid. The entropy current (9.3) is just

$$TS^a = (p+\varepsilon-\mu n)u^a \equiv Tsu^a\,, \tag{9.7}$$

with s the entropy density. It is now straightforward to show that the entropy current is covariantly conserved. Indeed, the equations of motion directly imply that

$$\nabla_a(TS^a) = u^a\nabla_a p - nu^a\nabla_a\mu = su^a\nabla_a T = S^a\nabla_a T\,, \implies \nabla_a S^a = 0\,. \tag{9.8}$$

where in the second equality we make use of the thermodynamic law $dp = Tds + nd\mu$. This immediately leads to the desired conservation law. As expected, zeroth-order hydrodynamics does not generate any entropy, and we are well justified labelling it as a perfect fluid [1].

9.3 RELATIVISTIC NAVIER-STOKES

9.3.1 *A First Approach*

Let us restrict ourselves for a moment to barotropic fluids, with equations of state $p = p(\varepsilon)$, where the speed of sound is simply $c_s^2 = dp/d\varepsilon$. In this case, we can set the chemical potential to zero $\mu = 0$, and the only thermodynamic variables are (ε, u^a). This is the regime that we will consider in subsequent chapters, although we will later present the more general formulation of first-order hydrodynamics. In this case, a naive generalization from Navier-Stokes to relativistic Navier-Stokes would prescribe the following constitutive relations

$$\mathcal{E} = \mathcal{Q}^a = 0\,, \qquad \mathcal{P} = -\zeta\vartheta\,, \qquad \mathcal{T}^{ab} = -2\eta\sigma^{ab}\,, \tag{9.9}$$

where $\vartheta = \nabla_a u^a$ is the fluid expansion, $\sigma^{ab} = \nabla^{(a}_\perp u^{b)} - \vartheta\Delta^{ab}/3$ is the shear, and ζ, η are the *bulk* and *shear* viscous coefficients. Notice how this new stress energy tensor explicitly depends on first-order derivatives, therefore leading to a first-order theory of hydrodynamics. This formulation was first introduced by Landau and Lifshitz [301], by requiring that there is no momentum in the fluid's local frame. The new equations of motion are

$$\begin{aligned} u^a\nabla_a\varepsilon + (\varepsilon+p)\vartheta &= \zeta\vartheta^2 + \frac{1}{2}\eta\sigma_{ab}\sigma^{ab}\,, \\ (\varepsilon+p)u^b\nabla_b u^a + c_s^2\nabla^a_\perp\varepsilon &= \zeta\vartheta u^b\nabla_b u^a + \nabla^a_\perp(\zeta\vartheta) + \Delta^a_b\nabla_c(\eta\sigma^{bc})\,. \end{aligned} \tag{9.10}$$

1 Shocks, being only weak solutions to the equations of motion, can generate entropy flux even for a perfect fluid.

We can notice two things from these equations. First of all, the entropy is no longer conserved. The entropy current remains given only by $S^a = su^a$, but its divergence can be shown to be, after an explicit calculation shown, e. g., in [53])

$$\nabla_a S^a = \frac{2\eta\sigma_{ab}\sigma ab}{T} + \frac{\zeta\vartheta^2}{T}\,. \tag{9.11}$$

The second-law is satisfied in a strict sense as long as $\eta, \zeta \geq 0$.

The second observation is that these equations are of mixed-order. The left-hand side contains first order derivatives – in particular, it captures the evolution of the energy density and fluid velocity along the flow direction. The right-hand side of the second equation, though, contains explicitly second derivatives, e. g., $\zeta\nabla^a_\perp\vartheta = \zeta\Delta^{ab}\nabla_b\nabla_c u^c$. The equations are of parabolic type, which means in particular that they are not hyperbolic in any of the senses discussed in Chapter 2. The initial value problem is *not* well-posed, which was understood early on [122, 295, 453], and lead to the development of alternative formulations of relativistic hydrodynamics to include the effects of dissipation, most notably the so-called Israel-Stewart theory [257, 259] (see also [351] for the non-relativistic case). This theory is a *second-order* theory, effectively promoting the viscous terms to new degrees of freedom, and prescribing their evolution in a particular way. Although this approach has enabled major advancements in relativistic hydrodynamics, Israel-Stewart theories have *not* been demonstrated to be well-posed in full generality (only recently in some specific cases, see e. g., Ref. [53]), and being second-order, they *effectively* include higher order deviations with respect to equilibrium. Is this really necessary? Here we argue that it is not, and that the key is to understand hydrodynamics as an effective field theory.

9.3.2 *A Minimal Frame Transformation*

In effective field theory, it is common to consider field redefenitions. Indeed, one may change the definition of the fundamental variables by a factor which depends on first-order gradients. For instance, suppose we do the following redefinition of the energy density

$$\varepsilon \to \varepsilon + a\vartheta\,, \tag{9.12}$$

where a is some coefficient that may depend on the state of the fluid. At equilibrium, $\vartheta = 0$, and the energy density retains its original physical meaning. The constitutive relations (9.9) change only by

$$\mathcal{E} \to a\vartheta\,, \qquad \mathcal{P} \to \mathcal{P} + c_s^2 a\vartheta\,. \tag{9.13}$$

We have *not* changed the physical content of the theory, but now the equations of motion will be different. This is a consequence of working with a particular truncation of an effective field theory to, in this case, first-order. This means that, whatever frame we choose (e.g. whatever value of a), the physical results should

not be very different, so long as we are within the regime of validity of first-order hydrodynamics. On the other hand, this changes the character of the equations, and in particular we can search for a frame transformation that renders the theory well-posed.

A *minimal* frame transformation that makes the theory well-posed was proposed in [49] and is given by

$$\varepsilon \to \varepsilon + \mathcal{A}\,, \qquad u^a \to u^a + \frac{q^a}{\varepsilon + p}\,, \tag{9.14}$$

with

$$\mathcal{A} = a_1\left(\eta + \frac{3}{4}\zeta\right)\left(\frac{u^a\nabla_a\varepsilon}{\varepsilon+p} + \vartheta\right), \qquad q^a = a_2\left(\eta + \frac{3}{4}\zeta\right)\left(u^b\nabla_b u^a + c_s^2\frac{\nabla_\perp^a\varepsilon}{\varepsilon+p}\right). \tag{9.15}$$

The constitutive relations in this frame, which we refer to as *minimal frame*, are

$$\mathcal{E} = \mathcal{A}\,, \qquad \mathcal{P} = c_s^2\mathcal{A} - \zeta\vartheta\,, \qquad \mathcal{Q}^a = q^a\,, \qquad \mathcal{T}^{ab} = -2\eta\sigma^{ab}\,. \tag{9.16}$$

The equations of motion generalise (9.10) but reduce to that setting $(a_1, a_2) = (0, 0)$, and we refer to [49] for their exact form. However, notice that for a perfect fluid, $\mathcal{A} = q^a = 0$ on-shell. Therefore the frame transformation (9.14) does *not* change the physical meaning. This is referred to as a Type II frame transformation in [49].

Remarkably, Ref. [49] demonstrates that these equations are (locally) well-posed if

$$a_1 \geq \frac{4}{3c_s^2}\,, \qquad a_2 \geq \frac{4a_1}{3(1-c_s^2)a_1 - 4c_s^2}\,. \tag{9.17}$$

Clearly, $(a_1, a_2) = (0, 0)$, corresponding to the theory introduced before, do *not* satisfy these constraints. This demonstrates that a well-posed first-order hydrodynamics theory *is* possible. We paid a price in the process: the constitutive relations are now notably more involved, and computing the entropy divergence shows that

$$\nabla_a S^a = \frac{2\eta\sigma_{ab}\sigma ab}{T} + \frac{\zeta\vartheta^2}{T} + \mathscr{O}(\partial^3) \geq 0 + \mathscr{O}(\partial^3)\,, \tag{9.18}$$

i. e., we now satisfy the 2nd law of thermodynamics only in an effective field theory sense. The reader may now judge whether this is more or less desirable than extending instead the system and treating a 2nd order theory such as Israel-Stewart hydrodynamics. Nevertheless, certain physical scenarios may prefer either approach.

9.3.3 *Landau-like and Eckart-like Frames*

Let us now consider a general fluid, i. e., $p = p(\varepsilon, n)$. The first attempts at describing the relativistic generalisation of Navier-Stokes hydrodynamics were carried out by Eckart [183] and Landau and Lifshitz [301]. The theories they obtained, i. e., the particular constitutive relations they proposed, lead to an ill-posed initial value

problem. Nevertheless, it is important to introduce them, as they consider two complementary viewpoints to look at hydrodynamics out of equilibrium.

As discussed before, Landau and Lifshitz consider a parametrization such that the velocity of a fluid element is such that there is no momentum in its local frame. This corresponds to fixing the heat flux $\mathcal{Q}^a = 0$. We refer to frames where this condition is satisfied as *Landau-like*. Instead, Eckart considers a frame where the local frame sees no particle number flux. This corresponds to choosing instead $\mathcal{J}^a = 0$. Frames satisfying this are said to be *Eckart-like*.

$$\text{Landau-like Frames:} \quad \mathcal{Q}^a = 0\,, \qquad \text{Eckart-like Frames:} \quad \mathcal{J}^a = 0\,. \tag{9.19}$$

For completeness, we write here the stress-energy tensor and particle number current proposed by both Eckart, and Landau and Lifshitz. However, we note that these stress-energy tensors lead to acausal propagation of degrees of freedom and an ill-posed initial value problem.

$$\begin{aligned}
T^{ab}_{\text{Landau}} =& \varepsilon u^a u^b + (p - \zeta\vartheta)\Delta^{ab} - \eta\sigma^{ab} + \mathscr{O}(\partial^2)\,,\\
J^a_{\text{Landau}} =& n u^a - \sigma T \nabla^a_\perp\left(\frac{\mu}{T}\right) + \mathscr{O}(\partial^2)\,,\\
T^{ab}_{\text{Eckart}} =& \varepsilon u^a u^b + (p - \zeta\vartheta)\Delta^{ab} + \mathcal{Q}^a_{\text{Eckart}} u^b + u^a \mathcal{Q}^b_{\text{Eckart}} - \eta\sigma^{ab} + \mathscr{O}(\partial^2)\,,\\
J^a_{\text{Eckart}} =& n u^a + \mathscr{O}(\partial^2)\,, \qquad \mathcal{Q}^a_{\text{Eckart}} = \kappa T \frac{\varepsilon + p}{n} \nabla^a_\perp\left(\frac{\mu}{T}\right).
\end{aligned} \tag{9.20}$$

Above, σ is the heat conductivity, and η, ζ are the shear and bulk viscosities, as in the previous case. One point to emphasize is that there is a frame transformation that maps the Eckart frame into the Landau frame [293]. We will now discuss some properties of first-order hydrodynamics in a general frame.

9.3.4 *Thermodynamics and Well Posedness*

Let us consider now the behaviour of small fluctuations around an equilibrium solution of a general first-order theory. For simplicity, we restrict in this section to fluctuations around flat spacetime, i. e., $g_{ab} = \eta_{ab} = \text{diag}(-1,1,1,1)$, where the equilibrium state is given by constant temperature, chemical potential, and background fluid velocity $u^a_0 \partial_a = \partial_t$. We consider a plane wave expansion of the form $\varepsilon = \varepsilon_0 + \epsilon\delta\varepsilon e^{i(kx-\omega t)}$, $u^a = u^a_0 + \epsilon\delta u^a e^{i(kx-\omega t)}$, where $|\epsilon| \ll 1$, and so on, with $\delta\varepsilon, \delta u^a$ constants.

The linearised equations of motion stemming from the linearisation of the conservation laws can be written as a matrix problem, $M_{IJ}\delta Y^J = 0$, where δY encapsulates all the perturbed quantities, and M_{IJ} is a matrix of coefficients. The full expression for M_{IJ} can be found in [241]. With a judicious choice of variables for δY, it can be shown that M_{IJ} takes a block diagonal form, with two distinct non-trivial blocks. One of them (which appears only once) can be associated to sound modes, and the other one, which appears with multiplicity 2 in $3+1$ dimensions, to shear or transverse modes [293].

Plane wave solutions exist only when $\det M_{IJ} = 0$, which lead to two distinct dispersion relations for sound modes $\omega_{\text{sound}}(k)$ and shear modes, $\omega_{\text{shear}}(k)$. We say that a hydrodynamic theory is *linearly stable* if $\Im(\omega(k)) \leq 0$ for all possible wavenumbers k – in essence, small plane wave fluctuations around an equilibrium solution do not grow. On the other hand, we say that a hydrodynamic theory is *causal* if $\Re(\omega(k))/|k| \to C < 1$ as $|k| \to \infty$, i. e.arbitrarily high frequency modes do not propagate faster than the speed of light. This point raises a clear concern, since any truncated gradient expansion will not be valid in the limit $k \to \infty$, whereas we are now requiring an ultraviolet condition to establish causality. Further discussions on causality criteria can be found in Ref [297].

Hiscock and Lindblom [241] remarkably showed that *any* first-order theory satisfying the second-law of thermodynamics in the strict sense (9.4) is linearly unstable. In essence, their analysis consists on writing the most general stress-energy tensor compatible with the strict formulation of the second law, and then proving that there always exist unstable modes, by computing the eigenvalues of the matrix M_{IJ}. The timescale of these unstable modes is remarkably short, casting doubts on the usefulness of these theories. As we have already anticipated, however, this issue is circumvented by an appropriate frame transformation. The condition imposed in [241] is, simply, too restrictive to allow for a stable, well-posed theory of first-order hydrodynamics.

9.3.5 *BDNK Hydrodynamics*

A number of works (see e. g. [209, 241, 304]) show that quite generically any first order theory compatible with the second law of thermodynamics in a strict sense, $\nabla_a S^a \geq 0$, cannot be causal and stable. Bemfica, Disconzi, and Noronha [52, 53, 55], and Kovtun [293] (hence the acronym BDNK) proved that sufficiently general frames lead to causal and stable first order hydrodynamics. This finding has led to a large flurry of activity in dissipative hydrodynamics, which we summarised in the next section. We highlight that BDNK hydrodynamics has been proven to be well-posed even when coupled to Einstein's equations [53, 249]. From the well-posedness point of view, at this point, one may conclude that first-order hydrodynamics stands on more solid ground than most second-order Israel-Stewart-like theories.

A very general class of frames (Eckart-like), which can be shown to lead to a causal and stable theory, is given by the following constitutive relations

$$\begin{aligned}
\mathcal{E} =& \tau_\varepsilon \left[u^a \nabla_a \varepsilon + (\varepsilon + p)\vartheta \right], \\
\mathcal{P} =& -\zeta\vartheta + \tau_p \left[u^a \nabla_a \varepsilon + (\varepsilon + p)\vartheta \right], \\
\mathcal{Q}^a =& \tau_Q (\varepsilon + p) u^b \nabla_b u^a + \beta_\varepsilon \Delta^{ab} \nabla_b \varepsilon + \beta_n \Delta^{ab} \nabla_b n, \\
\mathcal{T}^{ab} =& -2\eta\sigma^{ab},
\end{aligned} \tag{9.21}$$

where $\mathcal{N} = \mathcal{J}^a = 0$. The β coefficients are given by

$$\begin{aligned}\beta_\varepsilon =&\tau_Q\Big(\frac{\partial p}{\partial \varepsilon}\Big)_n + \frac{\sigma T(\varepsilon+p)}{n}\Big(\frac{\partial(\mu/T)}{\partial\varepsilon}\Big)_n,\\ \beta_n =&\tau_Q\Big(\frac{\partial p}{\partial n}\Big)_\varepsilon + \frac{\sigma T(\varepsilon+p)}{n}\Big(\frac{\partial(\mu/T)}{\partial n}\Big)_\varepsilon.\end{aligned} \tag{9.22}$$

The free transport coefficients of the BDNK theory are the three usual transport coefficients ζ, η, σ (bulk and shear viscosities, and heat conductivity), and three dissipation timescales $\tau_\varepsilon, \tau_p, \tau_Q$. These timescales multiply terms that vanish on-shell for a perfect fluid, i. e., they arise as a result of type II frame transformations, as in the minimal case. Therefore, one expects that changing the value of these τ_X coefficients does *not* change physical effects, as long as we remain within the regime of validity of first-order hydrodynamics.

Notice that these timescales multiply terms that are $\mathscr{O}(\partial^2)$ on-shell and thus are taken to be zero in Eckart hydrodynamics. However, keeping them at the level of the constitutive relations is necessary in order to guarantee causality and stability of the theory.

Causality, as defined above, i. e., requiring that in the ultraviolet limit degrees of freedom do not propagate faster than the speed of light, leads to the following constraints

$$\begin{aligned}\eta, \zeta, \sigma \geq& 0\,, \qquad \tau_\varepsilon, \tau_P, \tau_Q > 0\,,\\ (\varepsilon+p)\tau_Q >& \eta\,,\\ \mathcal{C}^2 \geq& 4(\varepsilon+p)\tau_\varepsilon\tau_Q\Big[\tau_P\Big((\varepsilon+p)c_s^2\tau_Q + \sigma\kappa_s\Big) - \beta_\varepsilon\Big(\zeta + \frac{4\eta}{3}\Big)\Big] \geq 0\,,\\ 2(\varepsilon+p)\tau_\varepsilon\tau_Q >& \mathcal{C} \geq 0\,,\\ (\varepsilon+p)\tau_\varepsilon\tau_Q + \sigma\kappa_s\tau_p >& \mathcal{C} - (\varepsilon+p)c_s^2\tau_p\tau_Q + \beta_\varepsilon\Big(\zeta + \frac{4\eta}{3}\Big)\,,\end{aligned} \tag{9.23}$$

where

$$\mathcal{C} = \tau_\varepsilon\Big((\varepsilon+p)c_s^2\tau_Q + \zeta + \frac{4\eta}{3} + \sigma\kappa_s\Big) + (\varepsilon+p)\tau_p\tau_Q\,, \tag{9.24}$$

and we have introduced the speed of sound for a general fluid

$$c_s^2 = \Big(\frac{\partial p}{\partial\varepsilon}\Big)_s = \Big(\frac{\partial p}{\partial\varepsilon}\Big)_n + \frac{n}{\varepsilon+p}\Big(\frac{\partial p}{\partial n}\Big)_\varepsilon, \tag{9.25}$$

and

$$\kappa_s = \frac{(\varepsilon+p)^2 T}{n}\Big(\frac{\partial(\mu/T)}{\partial\varepsilon}\Big)_s = \frac{(\varepsilon+p)^2 T}{n}\Big(\frac{\partial(\mu/T)}{\partial\varepsilon}\Big)_n + T(\varepsilon+p)\Big(\frac{\partial(\mu/T)}{\partial n}\Big)_\varepsilon. \tag{9.26}$$

Linear stability further imposes additional constraints on the transport coefficients, which for brevity we do not write here, but rather refer to Eq.(48) in Ref. [53]. It is remarkable that causality enforces that all the dissipation timescales must be strictly

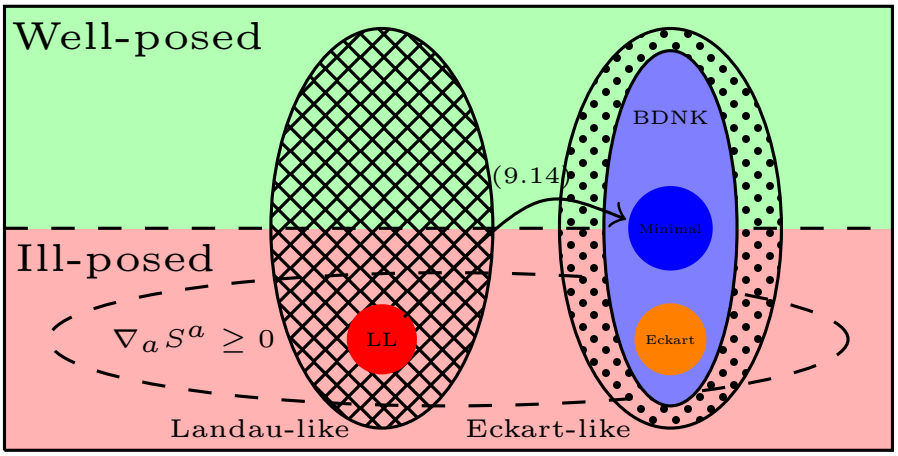

Figure 39 Schematic representation of the parameter space of first-order frames, distinguishing them as (locally) well or ill-posed. The cross-hatched region represents Landau-like frames, with $\mathcal{Q}^a = 0$, where the red dot is the Landau-Lifshitz hydrodynamics. The dotted region represents Eckart-like frames, with $\mathcal{J}^a = 0$. The orange dot represents Eckart hydrodynamics, the light blue region the BDNK constitutive relations (9.21), and the dark blue the minimal constitutive relations (9.16). The arrow indicates that this minimal hydrodynamics is obtained via a frame redefinition from Landau-Lifshitz hydrodynamics given explicitly in (9.14).

positive – under this conditions, the Eckart and Landau frames always exhibit acausal behaviour. We will later show how we recover these causal conditions by studying the causality of the equations describing linear propagations around the background of a spherically symmetric, self-gravitating fluid configuration. A summary of the different frame classes, their relations, and their well-posedness properties is shown in Fig. 39.

9.4 OUTLOOK AND STATE OF THE ART

Relativistic hydrodynamics is remarkably more complex than its Newtonian counterpart. One difficulty encountered in generalising the Navier-Stokes theory to the relativistic regime is the ill-posedness of the most trivial generalisations, and in fact, the apparent tension between the second-law of thermodynamics and well-posedness of first-order hydrodynamics. Recent works have now properly understood this tension, by noticing both that the second-law need not be satisfied strictly, but only up to certain order in the effective gradient expansion; and that frame transformations (field redefinitions) allow us to write equations of motion that define a causal, well-posed, and linearly stable Cauchy problem [55].

The remainder of this thesis builds upon this framework to study the dynamical properties of *neutron stars*, within the regime of validity of perturbation theory. However, recent years have seen remarkable progress in the context of first-order hydrodynamics. Here, we list some of these recent advancements. This list is not

meant to be exhaustive, but rather to serve as a starting point to investigate this fascinating field.

- **Numerics:** Numerically solving the well-posed equations of first-order hydrodynamics is one of the key advancements in this program. This problem was first tackled in a series of works [363–365], which, among other things, devised a conservative numerical scheme to evolve these equations. Within the context of heavy-ion collisions, numerical results were first obtained in [43]. More recent developments in the context of numerical solutions can be found in Refs. [50, 142, 267, 425].

- **Neutron Star Dynamics:** Beyond the works presented in the rest of this thesis, other works have begun exploring the consequences of first-order hydrodynamics in the perturbations of neutron stars. In particular, we highlight [90], which tackles some formal aspects of radial perturbations for small values of the viscosity, and [339], also studying radial perturbations within an approximated regime. Other works [123, 124] have demonstrated (within Israel-Stewart hydrodynamics) that viscosity plays a significant role in altering the postmerger GW emission in neutron star mergers. Therefore, further clarifying the role of viscosity in the dynamics of neutron stars and their GW emission appears as a promising direction, and a clear application of first-order hydrodynamics.

- **Heavy-Ion Collisions:** Within the context of heavy-ion collisions, we highlight the recent results of [49], reproducing experimental values of the quark-gluon plasma from first-order hydrodynamics.

- **Magnetohydrodynamics:** Recent work [31, 250] has extended these ideas to develop a causal and stable first-order theory of dissipative magnetohydrodynamics. This may encounter very relevant applications to study extreme astrophysical environments such as young neutron stars or accretion disks.

10

PERTURBATIONS OF VISCOUS STARS

Written while listening to music composed by Alban Berg and Arnold Schoenberg.

10.1 INTRODUCTION

Neutron stars (NSs) are the most compact known astrophysical objects, aside from BHs. The extreme densities achieved in their interiors make them a unique laboratory to study nuclear and particle physics in extreme regimes, unattainable with current experiments [393]. Neutron stars are cold — with temperatures ranging between $T \sim 10^8 - 10^9 \mathrm{K} \sim 0.01 - 0.1 \mathrm{MeV}$. Therefore by studying NS physics we probe a complementary regime to that achieved in heavy ion collisions, which produce short-lived nuclear matter at extreme temperatures $T \sim 150 - -600 \mathrm{MeV}$. GWs emitted when a NS merges with another NS or a BH provide a bright probe of cold nuclear physics at extreme densities, opening an avenue for new discoveries in the intersection between astrophysics and particle physics [26, 60].

One frontier in the study of NS physics is the role of viscosity or, generically, dissipative effects. The impact of shear viscosity is expected to be small compared to the damping produced by the emission of GWs [155, 156, 310], but it can be enhanced in the neutrino-dominated regime if there are relevant turbulent or non-axisymmetric instabilities [20, 181, 278, 305, 392]. Bulk viscosity is important due to the relevance of modified Urca processes [18–20, 93, 94, 123, 124, 346, 347], and hyperons and strange quarks [17, 132, 210, 211, 360]. Precision GW asteroseismology requires of a precise analysis of the impact of viscosity on the emission of GWs by NSs, extending beyond the estimates of classical works [155, 156, 310]. Building the foundations to tackle this gap is the goal of this Chapter. In addition, the possibility of exotic stars composed wholly or partially of dark matter, or other states of matter, where viscosity may play a more significant role, further reinforces the need to study systematically the impact of viscosity in the emission of GWs. A final motivation, already anticipated, is the interaction of GWs with viscous matter. The formalism developed in this chapter will allow us to later study the scattering of GWs off a viscous star, which will be the subject of subsequent chapters.

In order to do this, we need to specify a particular theory of dissipative hydrodynamics. As discussed in the previous chapter, the extensions of the Navier–Stokes hydrodynamics to the relativistic regime, first undertaken by Eckart [183] and Landau [301] are problematic: they lead to instabilities because of their acausal

character [240, 241]. Theories that include second-order gradients (Israel-Stewart theories [257]) can solve these problems, but at the cost of introducing a more complicated structure of differential equations. Recent progress in the perturbations of Israel-Stewart theories can be found in Ref. [172]. Here we focus instead on the BDNK hydrodynamics, which has the advantage of including only first-order gradients — thus leading to a simpler system of equations, structurally speaking — while providing a theory that can be causal and stable.

We expand on the formalism presented in Chapter 3 which builds upon a $2+2$ decomposition of the spherically symmetric background. Since we deal with fluids, whose velocity field determines a privileged direction in the Lorentzian sector of the metric, we introduce an oriented, normalised frame adapted to the fluid velocity. This is based on work by Gundlach and Martín-García [228, 331, 332], and allows us to reduce the linearised Einstein equations in the presence of a fluid source to scalar equations, in terms of gauge-invariant quantities.

In this chapter, we derive a coupled system of wave equations describing the dynamics of axial perturbations to a viscous stars. We identify one of the axial degrees of freedom with gravitational perturbations, whereas the other one is associated to a viscous mode, with no analogue in the case of a perfect fluid. This is akin to the appearance of a second sound mode for superfluid stars [23, 146, 311], or to the appearance of an unstable pair of modes in classical hydrodynamics for the Poiseuille flow, which are absent in the inviscid case [312]. Physically, this mode corresponds to a rotational motion in the star, which oscillates with a frequency proportional to the shear viscosity. Additionally we demonstrate that the even parity perturbations can be described by a mixed system composed of five coupled wave-like equations and one additional first-order equation (which can be interpreted as a constraint). By analysing their causal structure, we show that there are propagating degrees of freedom associated to (i) propagating GWs, (ii) a viscous mode induced by the shear viscosity, (iii) fluid density perturbations, which are modified due to the presence of bulk viscosity. Requiring that the propagation speed of each of this modes respects causality allows us to recover explicitly the causal constraints of the BDNK theory [54].

Throughout this chapter we make two simplifying assumptions. Firstly, we restrict to radiating modes, i. e., we do not discuss the dynamics of radial modes ($\ell = 0$ multipoles), or dipolar modes ($\ell = 1$), leaving that analysis for future work. Secondly, we assume that heat conductivity is negligible in the fluid — equivalently, that the temperature of the fluid is zero. This allows us to eliminate one of the transport coefficients of the BDNK theory and simplify somewhat the perturbative equations. However, our framework should be readily applicable including thermal effects.

10.2 PERTURBATIVE FORMALISM

We build upon the $2+2$ decomposition introduced in Chapter 3. Spacetime is decomposed as a warped product between a Lorentzian 2-manifold and a sphere, $\mathcal{M} = \mathcal{N}^2 \times_{r^2} \mathcal{S}^2$. Additionally we will introduce a frame on $\mathcal{N}^2$ adapted to the

background fluid velocity, which will allow us to reduce all the tensorial equations to scalar equations, while retaining gauge invariance.

10.2.1 *Background Geometry*

Recall that the background metric is decomposed as (3.1)

$$ds^2 = g_{AB}(y)dy^A dy^B + r^2(y)\mathring{\gamma}_{IJ}d\theta^I d\theta^J\,, \tag{10.1}$$

and we introduced $rv_A = \nabla_A r$. The key difference is that we now introduce a frame on the Lorentzian sector $\mathcal{N}^2$ given by the pair (u^A, n_A), where $u^A u_A = -1$ is a timelike vector, given by the background fluid velocity, and n_A is a spacelike vector orthogonal to it, i. e., $u^A n_A = 0$. The metric is given in terms of the frame by

$$g_{AB} = -u_A u_B + n_A n_B\,. \tag{10.2}$$

Additionally, there are only three other independent rank–2 tensors, which we label

$$p_{AB} = u_A u_B + n_A n_B\,, \quad q_{AB} = u_A n_B + n_A u_B\,, \quad \epsilon_{AB} = -u_A n_B + n_A u_B\,. \tag{10.3}$$

A general stress energy tensor can be written, in terms of these tensors, as

$$T_{\mu\nu}dx^\mu dx^\nu = \frac{1}{2}\Big(T_g g_{AB} + T_p p_{AB} - T_q q_{AB}\Big)dy^A dy^B + r^2 T_S \gamma_{IJ}d\theta^I d\theta^J\,, \tag{10.4}$$

i.e., it is fully characterised by the four scalars $\{T_g, T_p, T_q, T_S\}$. The normalisation of the previous expression is chosen so that, e. g., $q^{AB}T_{AB} = T_q$.

Additionally we introduce the frame derivatives

$$\delta f = u^A \nabla_A f \qquad \Delta f = n^A \nabla_A f\,, \tag{10.5}$$

and the scalars

$$U = u^A v_A\,, \quad W = n_A v^A\,, \quad \mu = \nabla_A u^A\,, \quad \nu = \nabla^A n_A\,. \tag{10.6}$$

Straightforward computations yield the following useful identities, which we will apply repeatedly in what follows

$$\begin{aligned} \nabla_A u_B =& n_B(\mu n_A - \nu u_A)\,, \qquad \nabla_A n_B = u_B(\mu n_A - \nu u_A)\,, \\ v^A v_A =& -U^2 + W^2\,, \qquad [\Delta, \delta]f = \mu\Delta f - \nu\delta f\,. \end{aligned} \tag{10.7}$$

Einstein equations (3.5) can be reduced to 4 scalar equations in terms of these variables and derivatives. Simply projecting (3.5) onto the projectors (10.3) and using (10.6)–(10.7) yields

$$\begin{aligned} \Delta W - \delta U + \nu W - \mu U + 2v^2 - r^{-2} =& 4\pi T_g\,, \\ -\Delta W - \delta U + \nu W + \mu U + v^2 - 2W^2 =& 4\pi T_p\,, \\ -\delta W - \Delta U + \mu W + \nu U - 2UW =& 4\pi T_q\,, \\ \Delta W - \delta U + \nu W - \mu U + v^2 - \frac{1}{2}R^{(2)} =& 8\pi T_S\,. \end{aligned} \tag{10.8}$$

These equations can be used to eliminate three of the first order frame derivatives of U, W. The only frame derivative that cannot be eliminated from these equations can be instead obtain from the other 3 via commutation relations (10.7):

$$\Delta U = (\mu - U)W - 2\pi T_q \,. \tag{10.9}$$

Finally, recall that for a two dimensional manifold, $R^{(2)} g_{AB} = 2R_{AB}$, so we can eliminate the Ricci scalar in terms of the scalars defined in (10.6) as

$$\frac{1}{2}R^{(2)} = \delta\mu - \Delta\nu + \mu^2 - \nu^2 = -\delta U + \Delta W + \nu W - \mu U + v^2 - 8\pi T_S \,. \tag{10.10}$$

We will use the last equality to eliminate every instance of $\delta\mu - \Delta\nu$.

10.2.2 *Linear Perturbations*

We consider linear perturbations to the spherically symmetric background introduced before, $g_{ab} = \mathring{g}_{ab} + \epsilon \dot{g}_{ab} + \mathscr{O}(\epsilon^2)$. Following Chapter 3, for an arbitrary metric perturbation, we can always find a unique gauge transformation (for multipoles with $\ell \geq 2$) that casts it into the RW gauge (3.16). Equivalently, by working in the RW gauge, our results can immediately be promoted to gauge-invariant expressions, with knowledge of the gauge transformations (3.12)–(3.13). The metric perturbation in the RW gauge can be written in terms of scalar variables as

$$\begin{aligned} \dot{g}_{ab}dx^a dx^b =& \dot{h}_{AB}\mathcal{Y} dy^A dy^B + 2\dot{k}_A \mathcal{X}_I dy^A dz^I + r^2 \dot{h}\mathcal{Y} q_{IJ} dz^I dz^J \,, \\ \dot{h}_{AB} =& \frac{1}{2}\Big(\dot{h}_g g_{AB} + \dot{h}_p p_{AB} - \dot{h}_q q_{AB}\Big) \,, \\ \dot{k}_A =& \dot{k}_n n_A - \dot{k}_u u_A \,. \end{aligned} \tag{10.11}$$

Similarly, the stress energy tensor is perturbed according to $T_{ab} = \mathring{T}_{ab} + \epsilon \dot{T}_{ab} + \mathscr{O}(\epsilon^2)$, where

$$\begin{aligned} \dot{T}_{ab}dx^a dx^b =& \frac{1}{2}\Big(\dot{t}_g g_{AB} + \dot{t}_p p_{AB} - \dot{t}_q q_{AB}\Big)\mathcal{Y} dy^A dy^B \\ &+ 2\Big[\Big(\dot{\vartheta}_n n_A - \dot{\vartheta}_u u_A\Big)\mathcal{X}_I + \Big(\dot{t}_n n_A - \dot{t}_u u_A\Big)\mathcal{Y}_I\Big] dy^A dz^I \\ &+ \Big[\dot{\vartheta}_S \mathcal{X}_{IJ} + r^2\Big(\dot{t}_S \mathcal{Y} q_{IJ} + \tilde{\dot{t}}_S \mathcal{Y}_{IJ}\Big)\Big] dz^I dz^J \,. \end{aligned} \tag{10.12}$$

Even (respectively odd) parity perturbations are governed by the $(\dot{h}, \dot{t})$ (resp. $(\dot{k}, \dot{\vartheta})$) variables). Recall that although we omit the harmonic indices ℓm, we assume that we work with a single harmonic, with $\ell \geq 2$. The linearised Einstein equations (3.17), which we wrote in Chapter 3 in tensorial form, can now be reduced to scalar equations. If we denote the linearised Einstein tensor as $\dot{G}_{ab} = \dot{G}^{\rm E}_{ab} + \dot{G}^{\rm O}_{ab}$, where the E and O labels stand for even and odd components, we can expand each of these as

$$\begin{aligned} \dot{G}^{\rm O}_{ab}dx^a dx^b =& \dot{K}_A \mathcal{X}_I dy^A dz^I + \dot{K}\mathcal{X}_{AB} dz^I dz^J \,, \\ \dot{K}_A =& \dot{K}_n n_A - \dot{K}_u u_A \,, \end{aligned} \tag{10.13}$$

for the odd sector, and

$$\begin{aligned}\dot{G}^{\rm E}_{ab}dx^a dx^b =&\dot{H}_{AB}\mathcal{Y}dy^A dy^B + 2\dot{H}_A\mathcal{Y}_I dy^A dz^I + r^2\Big[\dot{H}\mathcal{Y}q_{IJ} + \dot{\tilde{H}}\mathcal{Y}_{AB}\Big]dz^I dz^J\,,\\ \dot{H}_{AB} =&\frac{1}{2}\Big(\dot{H}_g g_{AB} + \dot{H}_p p_{AB} - \dot{H}_q q_{AB}\Big)\,,\\ \dot{H}_A =&\dot{H}_n n_A - \dot{H}_u u_A\,,\end{aligned} \tag{10.14}$$

for the even sector. The odd parity equations are given by

$$\begin{aligned}\dot{K}_u \equiv&\delta\Delta\dot{k}_n - \Delta^2\dot{k}_u + 2(\mu-U)\Delta\dot{k}_n + (2W-\nu)\delta\dot{k}_n - \nu\Delta\dot{k}_u + \Big(4\pi T_q + \Delta\mu - 2UW\Big)\dot{k}_n\\ &+\Big(4\pi(T_g - T_p + 4T_S) + 2(W^2+\mu U - \nu W) - v^2 - \Delta\nu + \frac{\ell(\ell+1)-1}{r^2}\Big)\dot{k}_u = 16\pi\dot{\vartheta}_u\,,\\ \dot{K}_n \equiv&\delta^2\dot{k}_n - \delta\Delta\dot{k}_u + \mu\delta\dot{k}_n - 2U\Delta\dot{k}_u + (2W-\nu)\delta\dot{k}_u + \Big(2UW - 4\pi T_q - \Delta\nu\Big)\dot{k}_u\\ &+\Big(4\pi(2T_g + T_p + 2T_S) + 2(\mu U - \nu W - W^2) + \Delta\nu + \nu^2 - \mu^2 + \frac{\ell(\ell+1)}{r}\Big)\dot{k}_n = 16\pi\dot{\vartheta}_n\,,\\ \dot{K} \equiv&\Delta\dot{k}_n + \nu\dot{k}_n - \delta\dot{k}_u - \mu\dot{k}_u = 8\pi\dot{\vartheta}_S\,.\end{aligned} \tag{10.15}$$

The even parity equations were first written in [331]. We recover them here, where the relation between our notation and theirs (MG) is $2\eta^{MG} \mapsto \dot{h}_g$, $2\phi^{MG} \mapsto \dot{h}_p$, $2\psi^{MG} \mapsto -\dot{h}_q$, $k^{MG} \mapsto \dot{h}_S$. For convenience, we write them below:

$$\begin{aligned}\dot{H}_g \equiv&-\delta^2\dot{h}_S + \Delta^2\dot{h}_S + U(\Delta\dot{h}_q - \delta\dot{h}_p) + W(\delta\dot{h}_q - \Delta\dot{h}_p) + (\nu+4W)\Delta\dot{h}_S - (\mu+4U)\delta\dot{h}_S\\ &+\dot{h}_p\Big(8\pi T_p + v^2 - 2\mu U - 2W(\nu+W)\Big) + 2\dot{h}_q\Big(\nu U + (\mu+U)W - 4\pi\dot{t}_q\Big)\\ &-\frac{1}{2r^2}\Big((\ell(\ell+1)+2)\dot{h}_g + 2(\ell(\ell+1)-2)\dot{h}_S\Big) = 8\pi\dot{t}_g\,,\\ \dot{H}_p \equiv&-\delta^2\dot{h}_S - \Delta^2\dot{h}_S + U(\delta\dot{h}_g - \Delta\dot{h}_q) + W(\delta\dot{h}_q + \Delta\dot{h}_g) + (\mu-2U)\delta\dot{h}_S + (\nu-2W)\Delta\dot{h}_S\\ &+\Big(8\pi T_g + 2\mu U - 2\nu W - v^2 + \frac{\ell(\ell+1)+2}{2r^2}\Big)\dot{h}_p = 8\pi\dot{t}_p\,,\\ \dot{H}_q \equiv&-2\dot{\Delta h}_S + U(\Delta\dot{h}_g - \Delta\dot{h}_p) + W(\delta\dot{h}_g + \delta\dot{h}_p) + 2\Big[(\nu-W)\delta\dot{h}_S - \Delta\dot{h}_S\Big]\\ &+\Big(8\pi T_G + 2\mu U - 2\nu W - v^2 + \frac{\ell(\ell+1)+2}{2r^2}\Big)\dot{h}_q = 8\pi\dot{t}_q\,,\\ \dot{H}_u \equiv&\Delta\dot{h}_q - \delta\dot{h}_g - \delta\dot{h}_p - 2\delta\dot{h}_S + 2\Big(U\dot{h}_g + \nu\dot{h}_q - \mu\dot{h}_P) = 32\pi\dot{t}_u\,,\\ \dot{H}_n \equiv&\Delta\dot{h}_p - \Delta\dot{h}_g - \delta\dot{h}_q - 2\Delta\dot{h}_S + 2\Big(W\dot{h}_g + \nu\dot{h}_p - \mu\dot{h}_q\Big) = 32\pi\dot{t}_n\,,\\ \dot{\tilde{H}}_S \equiv&\dot{h}_g = -16\pi r^2\dot{\tilde{t}}_S\,,\\ \dot{H}_S \equiv&2\Delta^2\dot{h}_S - \Delta^2\dot{h}_p + \Delta^2\dot{h}_g - 2\delta^2\dot{h}_S - \delta^2\dot{h}_p - \delta^2\dot{h}_g + 2\delta\Delta\dot{h}_q + 2\Big[(\nu+2W)\Delta\dot{h}_S - (\mu+2U)\delta\dot{h}_S\Big]\\ &-(3\mu+2U)\delta\dot{h}_p - (3\nu+2W)\Delta\dot{h}_p - \mu\delta\dot{h}_g + \nu\Delta\dot{h}_g + 2\Big[(2\mu+U)\Delta\dot{h}_q + (\nu+W)\delta\dot{h}_q\Big]\\ &+2\Big[4\pi(2T_S + T_P - T_G) + v^2 - 2\mu U - 2\nu W - 2\nu^2 - 2\Delta\nu - r^{-2}\Big]\dot{h}_p\\ &+2\Big[2\nu(\mu+U) + 2\mu W + \delta\nu - \Delta\mu - 4\pi T_q\Big]\dot{h}_q - \Big(16\pi T_S + \frac{\ell(\ell+1)}{r^2}\Big)\dot{h}_g + 32\pi T_S\dot{h}_S = 32\pi\dot{t}_S\,,\end{aligned}$$

(10.16)

In addition to Einstein equations, it will be useful to write the projections of the perturbation to the conservation of the stress energy tensor. Let us decompose it as

$$\big(\nabla^\nu T_{\mu\nu}\big)\,dx^\mu = \Big(\dot{B}_n n_A - \dot{B}_u u_A\Big)\mathcal{Y} dy^A + \Big(\dot{B}\mathcal{Y}_I + \dot{C}\mathcal{X}_I\Big)dz^I\,. \tag{10.17}$$

For the odd sector, this leads to a single equation

$$\begin{aligned}\dot{C} \equiv& \delta\dot{\vartheta}_u - \Delta\dot{\vartheta}_n + (\mu+2U)\dot{\vartheta}_u - (\nu+2W)\dot{\vartheta}_n + \frac{\ell(\ell+1)-2}{2r^2}\dot{\vartheta}_S \\ =& \, T_S(\delta\dot{k}_u - \Delta\dot{k}_n) + k_u\Big(\delta T_S + T_S(\mu+2U)\Big) - \dot{k}_n\Big(\Delta T_S + T_S(\nu+2W)\Big)\,,\end{aligned} \tag{10.18}$$

whereas for the even sector we have

$$\begin{aligned}\dot{B}_u \equiv& \frac{1}{2}\Big(\delta\dot{t}_g - \delta\dot{t}_p + \Delta\dot{t}_q\Big) + U\dot{t}_g - (\mu+U)\dot{t}_p + (\nu+W)\dot{t}_q - 2U\dot{t}_S - \frac{\ell(\ell+1)}{2}\dot{t}_u \\ =& \frac{1}{4}\Big[2T_g\delta\dot{h}_g + (2T_p - T_g)\delta\dot{h}_p - T_q\delta\dot{h}_q + (T_p + 2T_S - T_g)\delta\dot{h}_S\Big] \\ &- \frac{\dot{h}_q}{4}\Big[2UT_q - 2(T_g - T_p)(\nu+W) + \delta T_q - \Delta T_g + \Delta T_p\Big] \\ &- \frac{\dot{h}_p}{4}\Big[2(\mu+U)T_g - 2UT_p - 2(\nu+W)T_q + \delta T_g - \delta T_p - \Delta T_q\Big] \\ &- \frac{\dot{h}_g}{4}\Big[2T_p(\mu_U) - 2T_q(\nu+W) - 2UT_g - \delta T_g + \delta T_p - \Delta T_q\Big] - 2UT_S\dot{h}_S\,, \\ \dot{B}_n \equiv& \frac{1}{2}\Big(\Delta\dot{t}_g + \Delta\dot{t}_p - \delta\dot{t}_q\Big) + (\nu+W)\dot{t}_p - (\mu+U)\dot{t}_q - 2W\dot{t}_S + W\dot{t}_g \\ =& \frac{1}{4}\Big[2T_q(\delta\dot{h}_p + \delta\dot{h}_S) - (T_g + T_p)\delta\dot{h}_q + (T_g + 2T_p)\Delta\dot{h}_p - 2T_q\Delta\dot{h}_q + T_g\Delta\dot{h}_g \\ &+ 2(2T_S - T_g - T_p)\Delta\dot{h}_S\Big] \\ &- \frac{\dot{h}_g}{4}\Big[2(\mu+U)T_q - 2(\nu+W)T_P - 2WT_g + \delta T_q - \Delta T_g - \Delta T_p\Big] \\ &+ \frac{\dot{h}_p}{4}\Big[2\Big(\nu T_g + (\mu+U)t_q + W(t_g+t_p)\Big) + \delta T_q + \Delta T_g + \Delta T_p\Big] \\ &- \frac{\dot{h}_q}{4}\Big[2\Big((\mu+U)(T_g+t_p) + Wt_q\Big) + \delta T_g + \delta T_p + \Delta T_q\Big] - 2WT_S\dot{h}_S\,, \\ \dot{B} \equiv& \Delta\dot{t}_n - \delta\dot{t}_u + (\nu+2W)\dot{t}_n - (\mu+2U)\dot{t}_u - \frac{\ell(\ell+1)-2}{2}\dot{\tilde{t}}_S \\ =& \frac{1}{4}\Big[T_p\dot{h}_p - T_q\dot{h}_1 + (T_g - 2T_S)\dot{h}_g + T_S\dot{h}_S\Big]\,.\end{aligned} \tag{10.19}$$

We emphasize that these equations are valid in full generality — no assumptions have been made on the matter content, or on the background spacetime, beyond spherical symmetry. Below, we restrict them to a stationary spacetime sourced by a fluid, which will greatly simplify the algebra.

10.3 MATTER CONTENT

The matter content is specified by the BDNK stress energy tensor, discussed in great detail in Chapter 9. This stress energy tensor is given by the constitutive relations of (9.21), which lead to

$$T^{ab} = \Big(\varepsilon + \mathcal{E}\Big)u^a u^b + \Big(p + \mathcal{P}\Big)\Delta^{ab} + \mathcal{Q}^a u^b + u^a \mathcal{Q}^b + \mathcal{T}^{ab}\,, \tag{10.20}$$

where ε and p denote the energy density and pressure, respectively, $\Delta^{ab} = g^{ab} + u^a u^b$ is the projector onto the fluid's worldline, and

$$\begin{aligned}
\mathcal{E} =& \tau_\varepsilon \Big[u^a \nabla_a \varepsilon + (\varepsilon + p)\vartheta\Big]\,,\\
\mathcal{P} =& -\zeta\vartheta + \tau_p \Big[u^a \nabla_a \varepsilon + (\varepsilon + p)\vartheta\Big]\,,\\
\mathcal{Q}^a =& \tau_Q(\varepsilon + p)u^b \nabla_b u^a + \beta_\varepsilon \Delta^{ab}\nabla_b \varepsilon + \beta_n \Delta^{ab}\nabla_b n\,,\\
\mathcal{T}^{ab} =& -2\eta\sigma^{ab}\,.
\end{aligned} \tag{10.21}$$

The β coefficients are defined in (9.22). We now assume that we deal with a *cold* star, $T = 0$, and in addition, that we deal with barotropic matter, i. e., $p = p(\varepsilon)$. In that case, $\beta_n = 0$, and $\beta_\varepsilon = \tau_Q c_s^2$, where $c_s^2 = dp/d\varepsilon$ is the barotropic sound speed (9.25). This is the stress energy tensor whose perturbations will source metric perturbations.

10.3.1 *Background Stress Energy Tensor*

In spherical symmetry, it must be that the fluid velocity is purely on the Lorentzian plane, $u_a dx^a = u_A dy^A$, and thus, we can use it to generate a frame (the second vector of the frame can be defined to be simply $n_A = \epsilon_{AB}u^B$). If, in addition, the fluid is stationary, we immediately have that the fluid expansion vanishes, $\mu = \nabla_A u^A = 0$, and similarly all derivatives along the fluid flow vanish, $\delta\varepsilon = \delta p = 0$. We can also choose stationary coordinates such that the warping factor r does not change with the fluid flow. This leads to $U = 0$, which will allow us to greatly simplify the equations. In particular, a straightforward calculation shows that the components of the background stress energy tensor are, simply

$$T_g = p - \varepsilon\,, \quad T_p = p + \varepsilon\,, \quad T_q = -2\tau_Q\Big(\nu(\varepsilon + p) + c_s^2\Delta\varepsilon\Big)\,, \quad T_S = p\,. \tag{10.22}$$

Remarkably all viscous corrections vanish, except in T_q. However, Einstein equations on a stationary and spherically symmetric background (10.8) also enforce that $T_q = 0$. Plugging these into Einstein's equations leads to the closed-form system

$$\begin{aligned}
\Delta p =& -\nu(p + \varepsilon)\,,\\
\Delta\nu =& 4\pi(p + \varepsilon) - r^{-2}\,,\\
\Delta W =& 4\pi(p - \varepsilon) - \nu(W + 2\nu) + r^{-2}\,.
\end{aligned} \tag{10.23}$$

Plugging coordinate expressions for these equations will lead to the usual Tolman-Oppenheimer-Volkoff (TOV) equations.

10.3.2 *Perturbed Stress Energy Tensor*

Let us consider now perturbations to the matter content around an equilibrium solution, of the form $u_\mu = \mathring{u}_\mu + \epsilon \dot{u}_\mu$, $\varepsilon = \mathring{\varepsilon} + \epsilon\dot{\varepsilon}$, etc. Slightly abusing notation whenever we write, e. g., ε, we mean the background values. Then, the perturbations are simply given by

$$\begin{aligned} \dot{u}_\mu dx^\mu =& \left(\dot{\gamma} n_A + \frac{1}{2}\dot{g}_{AB}u^B\right)\mathcal{Y}dy^A + \left(\dot{\alpha}\mathcal{Y}_I + \dot{\beta}\mathcal{X}_I\right)dz^I\,, \\ \dot{\varepsilon} =& \dot{\omega}\varepsilon\mathcal{Y}\,, \qquad \dot{p} = c_s^2\dot{\varepsilon}\,. \end{aligned} \tag{10.24}$$

Odd parity perturbations are generated by $\dot{\beta}$, which captures differential rotation in the star, while even parity perturbations are governed by density perturbations $\dot{\omega}$, radial velocity perturbations $\dot{\gamma}$, associated to compression or expansion, and differential rotation governed by $\dot{\alpha}$. The components of the perturbed stress energy tensor (10.12) can be computed in a straightforward way, finding

$$\begin{aligned} \dot{\vartheta}_u =& -\varepsilon\dot{k}_u - (\varepsilon+p)\dot{\beta} - \tau_Q(\varepsilon+p)\left(\delta\dot{\beta} + \delta\dot{k}_u\right)\,, \\ \dot{\vartheta}_n =& pk_n - \eta\left[(\nu-2W)\dot{\beta} + \Delta\dot{\beta} + \delta\dot{k}_n\right]\,, \\ \dot{\vartheta}_S =& -2\eta\dot{\beta}\,, \end{aligned} \tag{10.25}$$

for the odd sector, and

$$\begin{aligned} \dot{t}_g =& \frac{1}{2}(\varepsilon+p)\dot{h}_p + \frac{1}{2}(p-\varepsilon)\dot{h}_g - (1-c_s^2)\varepsilon\dot{\omega} + (V_+ - 2\eta)\left(\frac{1}{2}W\dot{h}_q - \delta\dot{h}_S + \frac{\ell(\ell+1)\dot{\alpha}}{r^2} - 2W\dot{\gamma}\right) \\ &+ \frac{V_+}{4}\left(\nu\dot{h}_q - \delta\dot{h}_g - \delta\dot{h}_p + \Delta\dot{h}_q - 4\Delta\dot{\gamma} - 4\nu\dot{\gamma}\right) - \tau_-\left[\varepsilon\delta\dot{\omega} + \Delta\varepsilon\left(\dot{\gamma} - \frac{\dot{h}_q}{4}\right)\right]\,, \\ \dot{t}_p =& \frac{1}{2}(\varepsilon+p)\dot{h}_g + \frac{1}{2}(p-\varepsilon)\dot{h}_p + (1+c_s^2)\varepsilon\dot{\omega} + (V_- - 2\eta)\left(\frac{1}{2}W\dot{h}_q - \delta\dot{h}_S + \frac{\ell(\ell+1)\dot{\alpha}}{r^2} - 2W\dot{\gamma}\right) \\ &\frac{V_-}{4}\left(\nu\dot{h}_q - \delta\dot{h}_g - \delta\dot{h}_p + \Delta\dot{h}_q - 4\Delta\dot{\gamma} - 4\nu\dot{\gamma}\right) + \tau_+\left[\varepsilon\delta\dot{\omega} + \Delta\varepsilon\left(\dot{\gamma} - \frac{\dot{h}_q}{4}\right)\right]\,, \\ \dot{t}_q =& \frac{1}{2}(p-\varepsilon)\dot{h}_q - 2(\varepsilon+p)\dot{\gamma} - \frac{\tau_Q}{2}\Bigg[(\varepsilon+p)\left(\delta\dot{h}_q + 4\delta\dot{\gamma} + \Delta\dot{h}_g - \Delta\dot{h}_p\right) \\ &+ 4\left(c_s^2\varepsilon\Delta\dot{\omega} + \nu(p + c_s^2\varepsilon)\dot{\omega}\right)\Bigg]\,, \\ \dot{t}_u =& -(\varepsilon+p)\dot{\alpha} - \frac{\tau_Q}{4}\left[(\varepsilon+p)(\dot{h}_g - \dot{h}_p + 4\delta\dot{\alpha}) + 4c_s^2\varepsilon\dot{\omega}\right]\,, \\ \dot{t}_n =& \eta\left[\frac{\dot{h}_q}{4} - \Delta\dot{\alpha} - (\nu-2W)\dot{\alpha} - \dot{\gamma}\right]\,, \\ \dot{t}_S =& p\dot{h}_S + c_s^2\varepsilon\dot{\omega} - \frac{V - 2\eta - (\varepsilon+p)\tau_p}{4}\left(\delta\dot{h}_g + \delta\dot{h}_p - \Delta\dot{h}_q + 4\Delta\dot{\gamma} + \nu(\dot{h}_q - 4\dot{\gamma})\right) \\ &- (V - \eta - (\varepsilon+p)\tau_p)\left(\delta\dot{h}_S - \frac{W}{2}(\dot{h}_q - 4\dot{\gamma})\right) - \frac{\Delta\varepsilon\tau_p}{4}\left(\dot{h}_q - 4\dot{\gamma}\right)\,, \end{aligned}$$

(10.26)

for the even sector, where $\dot{\tilde{t}}_S = 0$, and we have introduced the short-hands

$$V = \zeta + \frac{4}{3}\eta\,, \quad \tau_\pm = \tau_\varepsilon \pm \tau_p\,, \quad V_\pm = V \pm (\varepsilon + p)\tau_\pm\,. \tag{10.27}$$

We have used the background equations of motion for a stationary spacetime in writing these. These expressions reduce to equations (76–82) in [332] in the inviscid limit. Plugging these expressions into eqs. (10.15), (10.16), (10.18), and (10.19) leads to a closed system of equations for the perturbed scalar variables in each sector. The rest of this chapter is devoted to unveiling the structure and, as best as possible, decoupling these systems of equations.

10.4 TRANSFORMATION TO A COORDINATE SYSTEM

It is often convenient to evaluate the expressions in a particular coordinate chart. We note that our expressions are valid for coordinate charts with the same domain of definition as the frame we introduced, this means, it may not be globally defined, e.g., both in the exterior and interior regions of a horizon. The issue of global definition of the frame is less important for spacetimes describing stars, which are our focus here. In this work we will work with static coordinates in the areal gauge, (t, r), valid everywhere but $r = 0$, where we must impose the regularity of our solutions. The frame we choose is

$$u_A dy^A = -e^{\nu/2} dt\,, \qquad n_A dy^A = e^{\lambda/2} dr\,, \tag{10.28}$$

The background metric is

$$g_{AB} dy^A dy^B = -e^\nu dt^2 + e^\lambda dr^2 = -e^\nu dt^2 + \left(1 - \frac{2M}{r}\right)^{-1} dr^2\,, \tag{10.29}$$

where

$$\lambda = -\log\left(1 - \frac{2M}{r}\right), \tag{10.30}$$

so that $M(r)$ denotes the mass contained inside a sphere of radius r. At the surface of the star, $r = R_S$, the metric must match smoothly the Schwarzschild metric in the exterior. Therefore, we must have that $e^\nu = 1 - 2M_S/R_S$, with M_S and R_S being the mass and the radius of the star, respectively. The background scalars are

$$\nu = \frac{\nu_{,r}}{2}\sqrt{1 - \frac{2M}{r}}\,, \qquad W = \frac{1}{r}\sqrt{1 - \frac{2M}{r}}\,, \tag{10.31}$$

with $\mu = U = 0$, and not to confuse the background scalar and the redshift factor. The frame derivatives, expressed in terms of coordinate derivatives, become

$$\delta X = -e^{-\nu/2}\frac{\partial X}{\partial t}\,, \qquad \Delta X = \sqrt{1 - \frac{2M}{r}}\frac{\partial X}{\partial r}\,. \tag{10.32}$$

We will also use the tortoise coordinate, defined through

$$\frac{d}{dr_\star} = e^{(\nu-\lambda)/2}\frac{d}{dr}\,. \tag{10.33}$$

Writing now eqs (10.23) in these coordinates we recover the TOV equations

$$\frac{dM}{dr} = 4\pi r^2\varepsilon\,, \qquad \frac{d\nu}{dr} = \frac{2e^{\lambda}}{r^2}\Big(M + 4\pi r^3 p\Big)\,, \qquad \frac{dp}{dr} = -\frac{\varepsilon+p}{2}\frac{d\nu}{dr}\,. \tag{10.34}$$

The TOV equations are solved once we specify an equation of state, and an initial condition. For barotropic matter this takes the form $p = p(\varepsilon)$, and a value for the central energy density ε_c. The integration is stopped once the pressure vanishes, condition that defines the surface of the star.

10.5 ODD PARITY PERTURBATIONS

Perturbations with odd parity are particularly simple. Already in the work of Thorne and Campolattaro [443] it was discussed that axial perturbations of a star are not dynamical — the only effect on the star is the onset of differential rotation. Later [285, 287] it was noticed that the spacetime of a star indeed has a class of strongly damped modes, dubbed w-modes or spacetime modes, corresponding to gravitational waves. However, for a perfect fluid, these spacetime modes barely couple to the motion inside the star, as discussed in Ref. [285]. By deriving the equations describing the propagation of axial perturbation in a viscous fluid we show that the situation changes if the fluid is viscous enough.

First, notice that we can use the equation $\dot{K}_n$ to eliminate $\dot{k}_u$ as

$$\frac{\partial k_u}{\partial t} = e^{-\lambda/2}\frac{\partial}{\partial r}\Big(r\dot{\psi}\Big) + 16\pi\eta e^{\nu/2}\dot{\beta}\,, \tag{10.35}$$

where we have introduced the master variable

$$\dot{\psi} = e^{\nu/2}\frac{\dot{k}_n}{r}\,. \tag{10.36}$$

The remaining equations, $\dot{K}_S$ and $\dot{\mathcal{C}}$ can be used to obtain a coupled system of wave equations for $\dot{\psi}$ and $\dot{\beta}$, given by

$$\begin{aligned} -\frac{\partial^2\dot{\psi}}{\partial t^2} + \frac{\partial^2\dot{\psi}}{\partial r_\star^2} - \mathcal{V}\dot{\psi} =& 16\pi\eta e^{\nu/2}\Big(\frac{\partial\dot{\psi}}{\partial t} + \mathsf{a}\dot{\beta}\Big)\,,\\ -\tau_{\mathrm{Q}}\frac{\partial^2\dot{\beta}}{\partial t^2} + \frac{\eta}{\varepsilon+p}\frac{\partial^2\dot{\beta}}{\partial r_\star^2} + \eta\Big(\mathsf{b}_1\frac{\partial\dot{\beta}}{\partial r_\star} + \mathsf{b}_2\frac{\partial\dot{\beta}}{\partial t} + \mathsf{b}_3\dot{\beta}\Big) =& \mathsf{c}_1\frac{\partial^2\dot{\psi}}{\partial t\partial r_\star} + \mathsf{c}_2\frac{\partial\dot{\psi}}{\partial t} + \mathsf{c}_3\frac{\partial\dot{\psi}}{\partial r_\star} + \mathsf{c}_4\dot{\psi}\,, \end{aligned} \tag{10.37}$$

where V is the usual Regge-Wheeler potential for a star [287]

$$\mathcal{V} = e^{\nu}\left(\frac{\ell(\ell+1)}{r^2} - \frac{6M}{r^3} + 4\pi(\varepsilon - p)\right)\,, \tag{10.38}$$

and the coefficients $\mathsf{a}, \mathsf{b}, \mathsf{c}$ are

$$
\begin{aligned}
\mathsf{a} =& -\frac{e^{\nu/2}}{r}\left(\frac{d\log\eta}{dr_\star}+\frac{1}{2}\frac{d\nu}{dr_\star}\right),\\
\mathsf{b}_1 =& \frac{4\pi r e^{(\nu+\lambda)/2}}{\mathcal{K}}\left(2\frac{d\log\eta}{dr_\star}+\frac{d\nu}{dr_\star}\right), \qquad \mathsf{b}_2 = -e^{\nu/2}\Big(\frac{1}{\eta}+16\pi\tau_Q\Big),\\
\mathsf{b}_3 =& -\frac{4\pi e^{(\nu-\lambda)/2}}{r\mathcal{K}}\left[2e^{\nu}\Big(1+e^{\lambda}(\ell(\ell+1)-1)\Big)+\left(4e^{(\nu+\lambda)/2}r-r^2e^{\lambda}\frac{d\nu}{dr_\star}\right)\frac{d\log\eta}{dr_\star}\right.\\
&\left.+re^{(\nu+\lambda)/2}\Big(\frac{d\lambda}{dr_\star}+3\frac{d\nu}{dr_\star}\Big)\right],\\
\mathsf{c}_1 =& re^{-\nu/2}\left(\tau-8\pi r e^{(\nu+\lambda)/2}\frac{\eta}{\mathcal{K}}\right),\\
\mathsf{c}_2 =& e^{-\lambda/2}\left[\tau_Q+4\pi r\left(re^{\lambda}\frac{d\nu}{dr_\star}-6e^{(\nu+\lambda)/2}\right)\frac{\eta}{\mathcal{K}}-8\pi r^2e^{\lambda}\frac{\eta}{\mathcal{K}}\frac{d\log\eta}{dr_\star}\right],\\
\mathsf{c}_3 =& r\,, \qquad \mathsf{c}_4 = e^{(\nu-\lambda)/2}\,.
\end{aligned}
\tag{10.39}
$$

We have introduced for convenience the short-hand

$$
\mathcal{K} = \frac{d\lambda}{dr_\star}+\frac{d\nu}{dr_\star} = 8\pi r e^{(\nu+\lambda)/2}(\varepsilon+p)\,. \tag{10.40}
$$

Axial perturbations are described thus by two degrees of freedom, governed by two coupled oscillator-like equations. An analysis of the characteristics of the problem will rapidly show two (pairs of) modes propagating with characteristic velocities 1 and $\sqrt{\eta/[\tau_Q(\varepsilon+p)]}$, respectively. We then predict a new family of modes, with no counterpart for a perfect fluid, since the restoring force is provided solely by shear viscosity. The existence of these modes could not have been predicted based solely on an analysis such as of Ref. [310]. Additionally, the fact that the dissipation timescale τ_Q appears in the propagation speed of these modes signals that they appear as a direct consequence of the BDNK formulation of hydrodynamics.

Notice that in the inviscid limit $\eta = \tau = 0$, the second master equation becomes just

$$
\frac{\partial\dot{\beta}}{\partial t} = re^{-\nu/2}\frac{\partial\dot{\psi}}{\partial r_\star}+e^{-\lambda/2}\dot{\psi} = e^{-\lambda/2}\frac{\partial}{\partial r}\Big(r\dot{\psi}\Big)\,. \tag{10.41}
$$

Therefore, using (10.35) this implies that, for a perfect fluid

$$
\frac{\partial\dot{\beta}}{\partial t} = \frac{\partial\dot{k}_u}{\partial t}\,, \tag{10.42}
$$

consistently with [443].

10.6 EVEN PARITY PERTURBATIONS

The sector of even parity perturbations is much richer in structure than the odd parity. When discussing modes, one typically encounters a fundamental mode (f-mode), together with a family of pressure modes (p-modes) [289]. Spacetime modes (w-modes) are also present in this case [287]. In the presence of a non-vanishing chemical potential, there appear also gravity modes (g-modes), as well as Rossby (r-modes) in the presence of rotation [287]. It is natural to expect this structure to become even more rich in the presence of viscosity. Thus, we first analyze in detail the perfect fluid case, recovering known results in the literature, before analyzing the viscous regime.

10.6.1 *Inviscid Regime*

Evidently $\dot{\tilde{H}}_S = 0$ implies $\dot{h}_g = 0$, regardless of the presence of viscous terms. Next, the equations $\dot{H}_n$, $\dot{\mathcal{B}}_n$, and $\dot{\mathcal{B}}_S$ can be used to eliminate three time derivatives,

$$\begin{aligned}
\frac{\partial \dot{h}_q}{\partial t} =& \frac{\partial \dot{h}_p}{\partial r_\star} - 2\frac{\partial \dot{h}_S}{\partial r_\star} + \dot{h}_p \frac{d\nu}{dr_\star}\,, \\
\frac{\partial \dot{\alpha}}{\partial t} =& e^{\nu/2}\left(\frac{\dot{h}_p}{4} - \dot{\omega}\right), \\
\frac{\partial \dot{\gamma}}{\partial t} =& \frac{1}{2}\frac{\partial \dot{h}}{\partial r_\star} - \frac{\partial \dot{\omega}}{\partial r_\star} - \frac{\dot{h}_p}{4}\frac{d\nu}{dr_\star}\,.
\end{aligned} \tag{10.43}$$

Above we write the equations in terms of the enthalpy perturbation

$$\dot{\omega} = \frac{c_s^2 \varepsilon \dot{\omega}}{\varepsilon + p}\,. \tag{10.44}$$

Plugging these expressions into $\dot{H}_g - \dot{H}_p$ we obtain a second order elliptic equation for $\dot{h}_S$

$$\begin{aligned}
\frac{\partial^2 \dot{h}}{\partial r^2} = \frac{1}{4r^2}\Bigg[& 2r\frac{\partial \dot{h}_p}{\partial r} + 2r\left(r\frac{d\lambda}{dr} - 6\right)\frac{\partial \dot{h}}{\partial r} + 2e^{\lambda}\Big(\ell(\ell+1)2\Big)\dot{h} \\
& - \frac{32\pi(\varepsilon + p)r^2 e^{\lambda}}{c_s^2}\dot{\omega} + e^{\lambda}\Big(\ell(\ell+1) + 2 - 16\pi r^2 \varepsilon\Big)\dot{h}_p\Bigg]\,.
\end{aligned} \tag{10.45}$$

This equation can be sometimes interpreted as a constraint, and used in combination with other equations to ensure a more accurate evolution of the system in numerical

This work	$\dot{h}_p$	$\dot{h}_q$	$\dot{h}$	$\dot{\omega}$	ν	λ
Ref. [353]	$2(\chi+k)$	2ψ	k	H	$2a$	$2b$

Table 2: Comparison between the notation of this work and the notation of [353].

implementations [353]. Finally we can use $\dot{H}_g$, $\dot{H}_S$, and $\dot{\mathcal{B}}_u$ to obtain three coupled wave equations for the remaining variables

$$
\begin{aligned}
-\frac{\partial^2\dot{h}}{\partial t^2}+\frac{\partial^2\dot{h}}{\partial r_\star^2} &= -\frac{2e^{(\nu-\lambda)/2}}{r}\frac{\partial\dot{h}}{\partial r_\star}+e^{\nu}\left[\frac{\ell(\ell+1)-2}{r^2}\dot{h}_S+8\pi(\varepsilon+p)\Big(1-\frac{1}{c_s^2}\Big)\dot{\omega}\right.\\
&\quad\left.+\frac{1}{r^2}\Big(e^{-\lambda}+4\pi r^2(\varepsilon+p)\Big)\dot{h}_p\right],\\
-\frac{\partial^2\dot{h}_p}{\partial t^2}+\frac{\partial^2\dot{h}_p}{\partial r_\star^2} &= e^{(\nu-\lambda)/2}\left[\Big(\frac{2}{r}+2\frac{d\nu}{dr}\Big)\frac{\partial\dot{h}_p}{\partial r_\star}-\Big(\frac{8}{r}-4\frac{d\nu}{dr}\Big)\frac{\partial\dot{h}}{\partial r_\star}\right]+e^{\nu}\left[16\pi(\varepsilon+p)\Big(1-\frac{1}{c_s^2}\Big)\dot{\omega}\right.\\
&\quad\left.+\left(\frac{4e^{-\lambda}}{r^2}-\frac{\ell(\ell+1)+4}{r^2}+8\pi(3\varepsilon+p)+e^{-\nu}\Big(\frac{d\nu}{dr_\star}\Big)^2\right)\dot{h}_p\right],\\
-\frac{\partial^2\dot{\omega}}{\partial t^2}+c_s^2\frac{\partial^2\dot{\omega}}{\partial r_\star^2} &= \frac{1-c_s^2}{8}\frac{d\nu}{dr_\star}\Big(4\frac{\partial\dot{h}}{\partial r_\star}-\frac{\partial\dot{h}_p}{\partial r_\star}\Big)+e^{\nu}\left[\left(\frac{c_s^2\ell(\ell+1)}{r^2}-4\pi(\varepsilon+p)(1+3c_s^2)\right)\dot{\omega}\right.\\
&\quad\left.+\left(2\pi c_s^2(\varepsilon+3p)-\frac{e^{-\nu}}{4}\Big(\frac{d\nu}{dr_\star}\Big)^2\right)\dot{h}_p\right].
\end{aligned}
\tag{10.46}
$$

These equations recover (9)–(11) in [353] with the correspondence between our variables and their notation written in Table 2.

We have three coupled wave equations and one additional elliptic equation. The latter can be used to effectively eliminate one of the equations. Therefore it is natural to expect two propagating degrees of freedom: one associated to gravitational perturbations, propagating at the speed of light, and one associated to enthalpy perturbations, propagating at the local sound speed. In the exterior, $\dot{\omega}=0$ and the problem can be further reduced to a single wave equation, the Zerilli equation, describing the propagation of GWs outside the star.

10.6.2 *Viscous Regime*

Viscous corrections turn the stress-energy tensor a first-order (in gradients) quantity, and thus its conservation law, e. g., $\dot{\mathcal{B}}_n$, becomes a second-order equation. This means that, unlike for the perfect fluid case, we cannot easily decouple the dynamics of

$\dot{\alpha}, \dot{\gamma}$. Viscosity promotes these to dynamical degrees of freedom, as in the axial sector. The only variable that can be decoupled in this case is $\dot{h}_q$, finding

$$\frac{\partial h_q}{\partial t} = \Big(\dots\Big)_{\text{P.F.}} + 8\pi\eta\left[e^{\nu/2}\Big(4\dot{\gamma} - \dot{h}_q - \frac{8e^{-\lambda/2}}{r}\dot{\alpha}\Big) + 4\frac{\partial\dot{\alpha}}{\partial r_\star} + 2\frac{d\nu}{dr_\star}\dot{\alpha}\right]. \tag{10.47}$$

The first term in brackets in the right-hand side denotes the value of the left-hand side for a perfect fluid, so that we only write explicitly the novel viscous corrections. We can also obtain easily the corrections to the elliptic equation for $\dot{h}$,

$$\begin{aligned}\frac{\partial^2\dot{h}}{\partial r^2} =& \Big(\dots\Big)_{\text{P.F.}} + \pi(\varepsilon+p)e^{\lambda/2}\tau_\varepsilon\left[\left(\frac{4}{r} + \Big(1-\frac{1}{c_s^2}\Big)\frac{d\nu}{dr}\right)(\dot{h}_q - 4\dot{\gamma})\right.\\ &\left. + \frac{8\ell(\ell+1)e^{\lambda/2}}{r^2}\dot{\alpha} - 2e^{(\lambda-\nu)/2}\Big(\frac{\partial\dot{h}_p}{\partial t} + 4\frac{\partial\dot{h}}{\partial t} + \frac{1}{c_s^2}\frac{\partial\dot{\omega}}{\partial t}\Big) + 2\frac{\partial\dot{h}_q}{\partial r} - 8\frac{\partial\dot{\gamma}}{\partial r}\right].\end{aligned} \tag{10.48}$$

The remaining equations, on the other hand, are very lengthy and unilluminating. We make their `Mathematica` expressions available in [1]. These equations are ready for their numerical solution once an equation of state, and a prescription for the transport coefficients is specified. However we can still learn much by studying the principal part of this system of equations. In particular we can learn about the propagating degrees of freedom, and the new speeds appearing into the system, as well as understand potential instabilities of the hydrodynamic formulation employed. Let us define $\vec{U}$ to be a vector that contains the five evolution variables, and let $\vec{V} = \partial_t\vec{U}$, and $\vec{W} = \partial_{r_\star}\vec{U}$. Then we have the following first order system,

$$\begin{aligned}\partial_t\vec{U} =& \vec{V}\,,\\ \partial_t\vec{W} =& \partial_{r_\star}\vec{V}\,,\\ \partial_t\vec{V} =& \mathbf{A}\partial_{r_\star}\vec{W} + \mathbf{B}\partial_{r_\star}\vec{V} + \mathbf{L}_1\vec{V} + \mathbf{L}_2\vec{W} + \mathbf{L}_3\vec{U}\,.\end{aligned} \tag{10.49}$$

The operators $\mathbf{L}_i$ are lower order terms, i.e., they do not affect the principal part, gathered in the matrices $\mathbf{A}$ and $\mathbf{B}$. Therefore, setting them to zero will not change the characteristics of the problem. For a similar reason, the first equation is always lower order. The minimal system to study can be written compactly as

$$\partial_t\begin{pmatrix}\vec{W}\\ \vec{V}\end{pmatrix} = \begin{pmatrix}0 & 1_5\\ \mathbf{A} & \mathbf{B}\end{pmatrix}\partial_{r_\star}\begin{pmatrix}\vec{W}\\ \vec{V}\end{pmatrix}, \tag{10.50}$$

where 1_5 denotes the five dimensional identity matrix. The matrices $\mathbf{A}$ and $\mathbf{B}$ are given explicitly by

$$\mathbf{A} = \begin{pmatrix}1 & 0 & 0 & 0 & 0\\ 0 & 1 & 64\pi\eta & 0 & 0\\ 0 & 0 & \frac{\eta}{(\varepsilon+p)\tau_Q} & 0 & 0\\ 0 & 0 & 0 & \frac{V-(\varepsilon+p)\tau_p}{(\varepsilon+p)\tau_Q} & 0\\ 0 & 0 & -8\pi c_s^2\eta\Big(1+\frac{\tau_Q}{\tau_\varepsilon}\Big) & 0 & -c_s^2\frac{\tau_Q}{\tau_\varepsilon}\end{pmatrix}, \tag{10.51}$$

and

$$\mathbf{B} = \begin{pmatrix} 0 & 0 & 0 & 0 & 0 \\ 0 & 0 & 0 & 0 & 0 \\ 0 & 0 & 0 & 0 & 0 \\ \frac{V-2\eta-(\varepsilon+p)\tau_p}{(\varepsilon+p)\tau_Q} & \frac{V-(\varepsilon+p)(\tau_p-\tau_Q)}{4(\varepsilon+p)\tau_Q} & 0 & 0 & -1-\frac{\tau_p}{c_s^2\tau_Q} \\ 0 & 0 & 0 & -c_s^2\left(1+\frac{\tau_Q}{\tau_\varepsilon}\right) & 0 \end{pmatrix} . \tag{10.52}$$

The eigenvalues of the matrix, λ_i, correspond to the characteristic speeds of the problem, $c_i^2 = \lambda_i^2$. These are given by

$$c^2_{\rm GW} = 1 \qquad c^2_{\rm Viscous} = \frac{\eta}{(\varepsilon+p)\tau_Q} , \qquad c^2_{\pm} = \frac{C_1 \pm C_2}{2(\varepsilon+p)\tau_\varepsilon\tau_Q} . \tag{10.53}$$

The GW eigenvalue appears with multiplicity two, corresponding to two degrees of freedom associated to the propagation of GWs. These are associated to $(\dot{h}, \dot{h}_p)$, and we know that one of them is actually non–propagating, because of the additional elliptic equation (10.48). There appears a new pair of eigenvalues, whose propagation speed is related to the ratio between shear viscosity and heat dissipation transport coefficient, similarly to the novel degree of freedom in the axial sector. We dub these modes viscous modes, and remark that they stop being dynamical in the perfect fluid limit. The restoring force for these modes, related to differential rotation induced by $\dot{\alpha}$, is provided by the shear viscosity. Finally, there is another pair of degrees of freedom, which involves a complicated combination of all transport coefficients, enclosed in C_1 and C_2. These are defined by

$$\begin{aligned} C_1 =& \tau_\varepsilon\Big((\varepsilon+p)c_s^2\tau_Q + V\Big) + (\varepsilon+p)\tau_p\tau_Q , \\ C_2 =& \sqrt{C_1^2 - 4c_s^2(\varepsilon+p)\tau_\varepsilon\tau_Q^2\Big((\varepsilon+p)\tau_p - V\Big)} . \end{aligned} \tag{10.54}$$

Out of these two degrees of freedom, one of them corresponds to enthalpy perturbations (i.e., modes associated to the $\dot{\omega}$ equation) in the perfect fluid case. These modes get modified slightly in the presence of viscosity. The other mode has no perfect fluid counterpart. A sensible guess is that it is related to expansive and compressive motion in the fluid (i.e., to the dynamics of $\dot{\gamma}$), where the bulk viscosity provides the restoring force.

We also want to highlight that the only causality constraints emerging from these analysis (which requires all the eigenvalues to be bounded, in absolute value, by unity), are

$$\begin{aligned} \tau_Q, \tau_\varepsilon, \tau_p >& 0 , \\ 0 \leq \eta \leq& (\varepsilon+p)\tau_Q , \\ C_1^2 \geq& 4c_s^2(\varepsilon+p)\tau_\varepsilon\tau_Q^2\Big((\varepsilon+p)\tau_p - V\Big) , \\ 0 \leq& C_1 + C_2 \leq 2(\varepsilon+p)\tau_\varepsilon\tau_Q . \end{aligned} \tag{10.55}$$

These constraints are identical to the causality constraints derived, in the context of the full non-linear theory, in [54]. The only difference is due to the last constraint, which is not evidently equivalent to the last constraint of [54], although it has a very similar structure. This shows a very nontrivial consistency check of our derivation. Notice that the constraints required for the nonlinear hydrodynamics theory to be causal are identical to the constraints of the theory linearized around any background (in particular, one that is flat) [54, 293].

10.7 CONCLUSIONS

In this chapter we have presented a formulation for the study of non-spherical perturbations of viscous stars, in BDNK hydrodynamics. This formulation allows us to obtain a well-posed and causal linearised theory, which in turn can be used to capture dissipative effects accurately. These may be important to alter and damp the oscillation frequencies of normal modes of neutron (or other compact) stars, with direct relevance for GW observations [60].

In the axial or odd sector we have shown that linearised perturbations are described by two coupled wave equations. One of them describes the modified propagation of GWs through the star, while the second wave equation governs differential rotation of the star. This mode only becomes dynamical when including dissipative effects, and it propagates at a velocity which depends on the local ratio between the shear viscosity and the heat dissipation rate τ_Q. We explore the consequences of these system of equations in the next chapters.

In the even or polar sector, the physics is richer. We first showed that our formulation recovers the results for a perfect fluid when setting all transport coefficients to zero. We provide a `Mathematica` notebook with the system of equations including viscosity, and have examined its causal structure in detail. We uncover two novel fluid modes: one of them associated with shear viscosity, and one of them likely associated to bulk viscosity. Additionally we have shown that the propagation speed of p-modes is altered in the presence of dissipative effects. Requiring that the propagation speeds of all modes of the system are bounded by the speed of light allows us to recover the BDNK causality constraints.

There are several limitations to this work, upon which this analysis can be improved. The first one is studying the nonradiating multipoles $\ell = 0, 1$. The $\ell = 0$ sector is particularly interesting as it is related to the radial stability of stars. Recent work in this direction has been tackled in Ref. [90]. Another aspect which we do not discuss in detail is the matching with perturbations in the exterior of the star, described by the Regge-Wheeler-Zerilli equations. We will discuss the axial case in the next chapter, whereas the even-parity case is left for future work. The inclusion of thermal effects — allowing for nonzero heat conductivity, and non-barotropic equations of state — and the effects of magnetic fields [31] are promising future directions that would allow us to more accurately predict the vibrational modes of neutron stars.

11

RESPONSE OF VISCOUS STARS

Written while listening to music composed by Johannes Brahms.

11.1 INTRODUCTION

The previous chapter 10 establishes a formalism to study the simultaneous perturbations of spacetime and viscous fluids. Crucially this enables us to undertake the main goal of this part of the thesis: to understand the interaction between GWs and viscous matter. Knowledge of the microscopic structure of matter, or of the large scale structure of our universe, and all the technology which our society is built upon, are possible thanks to the coupling between light and matter. Reflection and refraction of electromagnetic waves are consequences of Maxwell's equations, which are used to infer properties of the media, or sometimes nuisances that prevent us from understanding phenomena occurring at large distances. The interaction between GWs and matter, and the effects of matter in the generation of GWs is a burgeoning field of research [46, 167, 175, 178, 188, 194, 226, 237, 280, 370, 433, 434, 446, 447]. In an era of precision GW physics and multimessenger astrophysics, a precise understanding of the interaction of GWs and matter is necessary. We highlight four aspects where this is particularly relevant:

1. the physics of accretion disks. GWs passing through may result in a heat up of the disk, and as a consequence, in electromagentic signatures [279].

2. the physics of stars. Viscous dissipation plays an important role in spectroscopy [26, 155, 156, 310], can saturate f- and r-mode instabilities [27, 33, 156], or may quench the maximum-mass instability, possibly allowing for larger-mass neutron stars, as well as significantly impact the after-merger GW signal [124, 337, 347]. Previous works estimated the damping rate of stellar modes due to internal dissipative processes based on energy balance laws, motivated by the separation of scales between the mode oscillation rate and the viscous dissipation timescale [155, 156]. A self-consistent, relativistic calculation of the impact of viscosity on spectroscopy, in the context of a well posed relativistic theory is, surprisingly, lacking or treated only partially [227].

3. the physics of superradiance. Dissipation mechanisms hint towards amplification during the scattering of low-frequency GWs [83]. We will show that this is indeed the case in the following chapter.

4. the black hole paradigm. It has been argued that the rapid relaxation seen in GW events must be associated with horizons, or then with a material with abnormally large viscosity [466]. However, if electromagnetism is a good guide, highly viscous materials without horizons should be very good reflectors of GWs, possibly leading to characteristic signatures [384].

We begin by considering a toy model, due to Zeldovich [469], to explain why we expect highly dissipative objects to reflect radiation efficiently [384]. Next, we consider the scattering problem set-up, already introduced in chapter 3, in the spacetime of a viscous star, where the viscosity is described by BDNK hydrodynamics. The system of equations we consider is given in eqs. (10.37) in chapter 10. We discuss in detail the boundary conditions at the surface of the star, as well as our choice for the equation of state, and parametrization of the transport coefficients in the star. We compute the reflectivity of the star in the relativistic regime. Finally we discuss the quasinormal modes of viscous stars both in the decoupling regime (Cowling and inverse Cowling approximations) as well as in the coupled case.

11.2 REFLECTION FROM DISSIPATING MATERIALS

Let ψ be a scalar field propagating in flat space, which is scattered at a planar interface separating vacuum (region I, with $z > 0$), from a medium that absorbs the scalar field with a constant α (region II, with $z < 0$). If the medium is at rest, the scalar field propagation is well described by

$$\Box\psi + \alpha\partial_t\psi = 0\,. \tag{11.1}$$

Let us consider now a traveling wave ansatz

$$\begin{aligned}\psi =& A_{\rm in}e^{-i\omega t+ik_x x-ik_z z} + A_{\rm out}e^{-i\omega t+ik_x x+ik_z z} \qquad ({\rm region\,I})\\ \tilde{\psi} =& \mathcal{T}e^{-i\omega t+ik_x x-iKz}\,, \qquad ({\rm region\,II})\,.\end{aligned} \tag{11.2}$$

The equation of motion implies the following dispersion relations in each region

$$\begin{aligned}\omega^2 =& k_x^2 + k_z^2\,, \qquad ({\rm region\,I})\\ \omega^2 =& k_x^2 + K^2 + i\omega\alpha\,, \qquad ({\rm region\,II})\,.\end{aligned} \tag{11.3}$$

Now imposing that ψ and its derivative are continuous across the interface, we find

$$\begin{aligned}\left|\frac{A_{\rm out}}{A_{\rm in}}\right|^2 \to& \quad \frac{\omega^4\tilde{\alpha}^2}{16(\omega^2-k_x^2)^2} + \mathcal{O}(\tilde{\alpha}^4)\,, \qquad \tilde{\alpha}\to 0\\ \to& \quad 1 - \frac{2\sqrt{2(\omega^2-k_x^2)}}{\omega\sqrt{\tilde{\alpha}}} + \mathcal{O}(\tilde{\alpha}^{-1})\,, \quad \tilde{\alpha}\to\infty\,,\end{aligned} \tag{11.4}$$

where we have introduced the dimensionless parameter $\tilde{\alpha} = \alpha/\omega$.

At small $\tilde{\alpha}$, corresponding to $\alpha \ll \omega$, analogous to low-viscosity fluids, the reflectivity is small and the wave is almost perfectly transmitted from region I to

region II. However when the damping is large, $\alpha \gg \omega$, the situation is reversed and most of the incident wave is reflected back to region I.

This analysis extends in a straightforward way to spherical boundaries [98]. Notice that similar results are also obtained when studying the scattering of sound waves off planar interfaces separating a perfect fluid from a viscous one [340, 405] — in the regime where viscosity is large, sound waves are reflected off the interface. Highly absorbing materials are good reflectors of radiation. Notice that this behaviour should not come as a surprise: this is the same behaviour we observe for the reflection of electromagnetic waves off a perfect conductor.

11.3 SET-UP

We consider GWs scattering of a BDNK star. We restrict to axial parity perturbations, which are governed by a system of coupled wave equations of the form

$$\begin{aligned} -\frac{\partial^2\dot{\psi}}{\partial t^2}+\frac{\partial^2\dot{\psi}}{\partial r_\star^2}-\mathcal{V}\dot{\psi} =&16\pi\eta e^{\nu/2}\left(\frac{\partial\dot{\psi}}{\partial t}+\mathsf{a}\dot{\beta}\right), \\ -\tau_Q\frac{\partial^2\dot{\beta}}{\partial t^2}+\frac{\eta}{\varepsilon+p}\frac{\partial^2\dot{\beta}}{\partial r_\star^2}+\eta\left(\mathsf{b}_1\frac{\partial\dot{\beta}}{\partial r_\star}+\mathsf{b}_2\frac{\partial\dot{\beta}}{\partial t}+\mathsf{b}_3\dot{\beta}\right) =&\mathsf{c}_1\frac{\partial^2\dot{\psi}}{\partial t\partial r_\star}+\mathsf{c}_2\frac{\partial\dot{\psi}}{\partial t}+\mathsf{c}_3\frac{\partial\dot{\psi}}{\partial r_\star}+\mathsf{c}_4\dot{\psi}\,, \end{aligned} \tag{11.5}$$

where recall that $\dot{\psi}$ is a master variable related to the metric perturbation, and $\dot{\beta}$ is the perturbed angular velocity of the fluid inside the star. The coefficients are given in the previous chapter, eq. (10.39).

11.3.1 *Properties of the Star and Causality*

For simplicity, we focus on polytropic equations of state of the form

$$p=\kappa\varepsilon^{1+1/n}\,. \tag{11.6}$$

Unless otherwise specified, in this work we focus on a star with $n=0.8$, $\kappa=700\text{km}^{-2.5}$, and central density $\varepsilon_c=3\times10^{15}\text{gcm}^{-3}$, resulting in an object with mass $M_S=1.54M_\odot$, radius $R_S=8.78$km and compactness $M_S/R_S=0.259$. Although the star is relatively compact, these parameters render the star stable against radial perturbations [288], and are approximately compatible with current constraints.

Additionally we prescribe the following dependence for the transport coefficients

$$\eta=\hat{\eta}pR_S\,,\qquad \tau_Q=\hat{\tau}\frac{p}{\varepsilon}R_S\,, \tag{11.7}$$

with R_S the radius of the star. This parametrization has the advantage that the principal part of the β equation is regular even at the surface of the star, where $p,\varepsilon,p/\varepsilon\to0$. The BDNK causal constraints (9.23) enforce certain constrains upon the dimensionless coefficients $\hat{\eta}$ and $\hat{\tau}$. In order to find these, we need to specify additional dependences of *all* transport coefficients. Let us choose

$$\zeta=\hat{\zeta}pR_S\,,\qquad \tau_\varepsilon=\tau_Q\,,\qquad \tau_p=\frac{p}{\varepsilon}R_S\,. \tag{11.8}$$

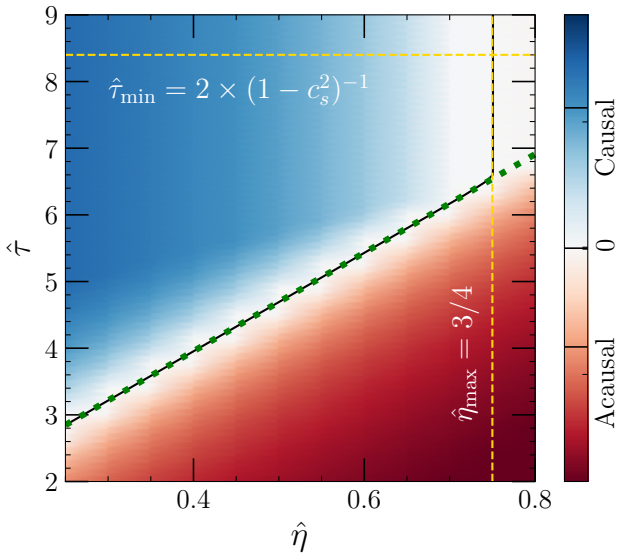

Figure 40 Regions of parameter space (assuming $\hat{\zeta} = 0$) where all causality constraints (11.9) are satisfied (blue), or where at least one of them is violated somewhere within the star (red). The yellow (respectively green) lines represent the analytical bounds of eq. (11.10) (resp. (11.11)).

We emphasize at this point that this prescription is arbitrary, as the BDNK transport coefficients have not yet been computed for nuclear matter composing a star — partial progress in this direction can be found in Refs. [363, 411]. Plugging this parametrization and the polytropic equation of state into the constraints (9.23) leads to

$$\begin{aligned} \hat{\eta} - \hat{\tau}\left(1 + \frac{c_s^2}{\Gamma}\right) &< 0\,, \\ \hat{\zeta} + \frac{4}{3}\hat{\eta} - \left(1 + \frac{c_s^2}{\Gamma}\right) &< 0\,, \\ \hat{\zeta} + \frac{4}{3}\hat{\eta} + \left(1 + \frac{c_s^2}{\Gamma}\right)\left(1 - 2\hat{\tau} + c_s^2\hat{\tau}\right) &< 0\,, \\ \left(\hat{\zeta} + \frac{4}{3}\hat{\eta}\right)(1 + c_s^2) - \left(1 + \frac{c_s^2}{\Gamma}\right)(1 - c_s^2)(\hat{\tau} - 1) &< 0\,, \end{aligned} \tag{11.9}$$

where $\Gamma = 1 + 1/n$ is the adiabatic index. A pair of sufficient but not necessary conditions is

$$\hat{\tau} > \max\left(\hat{\eta}, \hat{\zeta}, \frac{2}{1 - c_s^2}\right), \qquad 0 \leq \hat{\zeta} + \frac{4}{3}\hat{\eta} < 1 + \frac{c_s^2}{\Gamma}\,. \tag{11.10}$$

Further setting $\hat{\zeta} = 0$ we can prove that

$$\hat{\tau} > 1 + \frac{4\hat{\eta}}{3}\frac{\Gamma(1 + c_s^2)}{(1 - c_s^2)(c_s^2 + \Gamma)}\,. \tag{11.11}$$

These bounds are shown in detail in Fig. 40. Remarkably the total effective viscosity is bounded above in order to retain a causal theory, while the dissipation timescale

governed by $\hat{\tau}$ is bounded from below. Notice how these bounds are more strict than those that would emerge simply examining the causal character of (10.37) – which would lead only to $\hat{\tau} \geq \hat{\eta}$.

11.3.2 *Junction and Boundary Conditions*

In order to solve the system (10.37) we need to impose certain boundary conditions. First, at $r = 0$ we must impose regularity of the solutions. Regular solutions behave as $\dot{\psi}, \dot{\beta} \sim a_{\psi,\beta} r^{\ell+1}$. We enforce this by writing, close to the origin

$$\dot{\psi} = a_\psi r^{\ell+1}\left(1 + \sum_{n=1}^{N} a_\psi^{(n)} r^n\right), \qquad \dot{\beta} = a_\beta r^{\ell+1}\left(1 + \sum_{n=1}^{N} a_\beta^{(n)} r^n\right), \tag{11.12}$$

and solving the equations close to $r = 0$ for the coefficients $a^{(n)}_{\psi,\beta}$. We find that including the first $N = 4$ terms is enough to achieve accurate solutions.

At the surface of the star we must ensure that Israel's junction conditions are satisfied. These are given by requiring that the Einstein tensor $G_{r\mu}(R_+) - G_{r\mu}(R_-) = 0$ is continuous across the surface [256]. In order to enforce this it is sufficient to require that $\dot{T}_{r\mu} \propto \dot{\theta}_n = 0$. This condition reads

$$\eta\left[2r^2 e^{\lambda/2}\frac{d\dot{\psi}}{dt} + e^{\nu/2}\left(2r\frac{d\dot{\beta}}{dr} + \dot{\beta}(e^{\lambda} - 5)\right)\right] = 0\,. \tag{11.13}$$

This recovers the non-rotating limit of eq.(40) in [227] (see also [383]). Our parametrization of the viscosity (11.7) guarantees that this is satisfies, as $\eta = 0$ at the surface of the star. Junction conditions additionally require that $\dot{\psi}$ and its radial derivative are continuous across the surface of the star.

In the exterior region, $\dot{\beta} = 0$, and we only have to solve the RW equation for $\dot{\psi}$. At large distances we look for mononchromatic solutions (see the discussion of the scattering problem in chapter 3)

$$\dot{\psi} \sim A_{\rm in} e^{-i\omega t - i\omega r_\star} + A_{\rm out} e^{-i\omega t + i\omega r_\star}\,. \tag{11.14}$$

Based on this behaviour we define the reflectivity of the star as

$$\mathcal{R}^2(\omega) = \frac{|A_{\rm out}|^2}{|A_{\rm in}|^2}\,. \tag{11.15}$$

There is one last condition to take into account, stemming from the divergence of several lower-order coefficients in the $\dot{\beta}$ equation at the surface of the star. Requiring that $\dot{\beta}$ is regular in that limit enforces

$$z_S\frac{\partial\dot{\beta}}{\partial t} + \frac{M_S\hat{\eta}}{R_S}\frac{\partial\dot{\beta}}{\partial r_\star} + \frac{M_S(5M_S - 2R_S)\hat{\eta}}{R_S^3}\dot{\beta} = -\frac{M_S\hat{\eta}}{z_S}\frac{\partial\dot{\psi}}{\partial t} - R_S\frac{\partial\dot{\psi}}{\partial r_\star} - z_S^2\dot{\psi}\,, \tag{11.16}$$

where $z_S^2 = 1 - 2M_S/R_S$. We enforce this condition when solving the equation using the methods described below.

11.3.3 *Time Domain Implementation*

We first solve the system of equations in the time domain. To ensure regularity at the origin we re-scale the original variables as $\dot{\psi} = r^{\ell+1}\tilde{\psi}$ and $\dot{\beta} = r^{\ell+1}\tilde{\beta}$, and solve for $(\tilde{\psi}, \tilde{\beta})$ instead. We cast the system in first-order form and solve it employing the method of lines. Spatial derivatives are discretized using fourth order finite difference stencils, which make use of the fact that the functions have even parity close to the origin. In order to ensure numerical stability, we add numerical dissipation, through standard Kreiss-Oliger sixth order dissipation operators. The discretized equations are then evolved using an explicit, fourth order Runge–Kutta method. The time step is taken to be

$$\Delta t = \frac{\hat{\eta}}{2\hat{\tau}} \frac{\varepsilon_c}{\varepsilon_c + p_c} \Delta r_\star \,, \tag{11.17}$$

where ε_c, p_c are the central density and pressures, as to satisfy the Courant–Friedrichs–Levy condition everywhere in the star. We enforce the regularity condition at the surface (11.16) at each timestep, solving the discretized version of (11.16) and its time derivative to solve for $\tilde{\beta}$ and its derivative at the surface that satisfy the regularity condition.

We consider initial data that mimics a monochromatic pulse, but with compact support. In particular we consider

$$\dot{\psi}(t=0, r_\star) = \psi_0 \frac{(r_\star - r_1)^4 (r_2 - r_\star)^4}{r^{\ell+1} 2^8 (r_2 - r_1)^8} \cos\Big(\Omega r_\star\Big) \,, \tag{11.18}$$

where Ω is the driving frequency and $\psi = 0$ whenever $r_\star \notin [r_1, r_2]$. The initial data for the time derivative is taken so that the pulse is mostly incoming, $\partial_t \psi(t=0) = \partial_{r_\star} \psi$.

We test the convergence of the code by running it at different spatial resolutions, $\Delta r_\star = h, 2h, 4h$, with $h \sim 40$m. We measure the convergence order $\mathcal{Q}_h$ as

$$\mathcal{Q}_h = \log_2 \left(\frac{||\psi_{2h} - \psi_{4h}||}{||\psi_h - \psi_{2h}||} \right) . \tag{11.19}$$

We show the convergence order for a typical run in Fig. 41. The convergence is consistent with the expected fourth order convergence rate, except for at late times, where back-reflection from the outer boundary is present. Notice that this does not affect the time domain ringdown signal until much later times. We extract the reflectivity by computing the GW flux sufficiently far away (typically $r_{\rm ext} = 500$km. In particular, we compare the in-coming flux (flux between $t \in [0, t_1]$ and out-going flux ($t \in [t_1, t_2]$), where $t_{1,2}$ are estimated manually. Then the reflectivity is

$$\mathcal{R}^2 = \frac{\int_0^{t_1} \dot{E}_{\rm GW}(t') dt'}{\int_{t_1}^{t_2} \dot{E}_{\rm GW}(t') dt'} \,, \tag{11.20}$$

with

$$\dot{E}_{\rm GW} = \lim_{r\to\infty} \frac{1}{8\pi} \sum_{\ell m} \frac{(\ell+2)!}{(\ell-2)!} |\psi_{\ell m}|^2 \,. \tag{11.21}$$

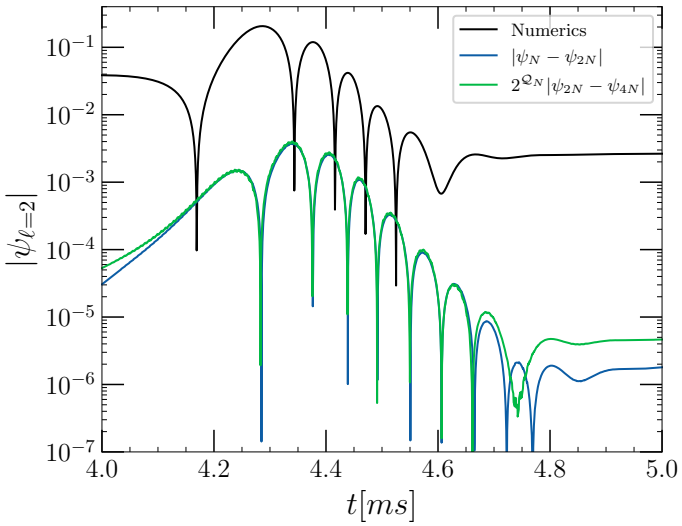

Figure 41 Ringdown signal extracted at $r_{\rm Ext} = 1000$km (black) for a high resolution run $h \sim 40$m (corresponding to $4N = 512$ points covering the interior of the star), and the difference between the extracted signal between runs with medium and low resolutions (blue), and medium and high resolution (green), rescaled by the convergence factor $2^{\mathcal{Q}}_h = 2^4$. The overlap between the blue and green lines signals that the code is convergenging at the expected rate.

11.3.4 *Frequency Domain Implementation*

We additionally solve the equations in the frequency domain, assuming a harmonic time dependence of the form $e^{-i\omega t}$ for both $\dot{\psi}$ and $\dot{\beta}$. The system reduces to a system of coupled ODEs. The ratio a_ψ/a_β is chosen such that the regularity condition at the surface (**??**) is satisfied. Particularly, the ratio is found using a Newton-Raphson method with an approximation to (**??**) at the surface obtained with a midpoint method from the last gridpoint before it. For scattering calculations, the integration for $\dot{\psi}$ is continued into the exterior region up to $r \sim 100 M_S$, where the reflectivity is computed as

$$\mathcal{R}^2 = \left| \frac{i\omega + \psi'/\psi}{i\omega - \psi'/\psi} \right|^2 , \tag{11.22}$$

averaging over several oscillations.

We have checked that the numerical implementation shows the expected convergence (in this case, second order, as the numerical integration scheme used is second order). An additional check has been performed to ensure that the truncation of the series expansion around the origin used to determine the functions at the first grid point introduces a negligible amount of error. A comparison between truncations using $N = 3$ and $N = 5$ shows that the relative different between the integrated functions is, at most, 10^{-6} throughout the entire domain.

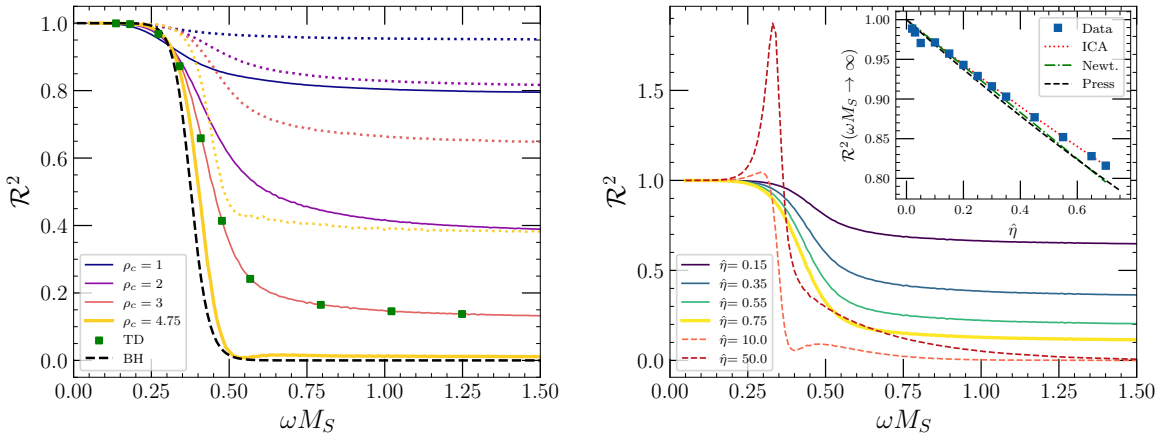

Figure 42 **Left:** Reflectivity $\mathcal{R}^2$ for a quadrupolar ($\ell = 2$) axial GW scattered off a compact, viscous star with $\kappa = 700\text{km}^{2.5}$, $n = 4/5$ and varying central density, in units of $10^{15}\text{g}\,\text{cm}^{-3}$, see legend. We set the transport coefficients to $\hat{\eta} = 0.7$ (solid lines), and $\hat{\eta} = 0.15$ (dotted lines), keeping $\hat{\tau} = 10$, as to ensure we are within the causal regime. The black dashed line is reflectivity of a non spinning black hole with mass M_S [83]. Green squares correspond to reflectivity extracted from time domain simulations for $\rho_c = 3$, showing excellent agreement between our two independent methods. **Right:** Same as on the left panel, but changing the value of the shear viscosity $\hat{\eta}$ as indicated in the legend. Dashed orange and red lines correspond to configurations which violate the BDNK causality bounds, and as a consequence result in amplification, $\mathcal{R}^2 > 1$. The inset panel shows the value of the reflectivity at large frequencies, $\omega M_S \gg 1$ showing good agreement with the Newtonian limit and the dispersion relation (11.23).

11.4 REFLECTIVITY OF A VISCOUS STAR

We can now address one of the main questions in this third part of the thesis: what is the interaction between GWs and a viscous, self-gravitating, compact fluid? Can a sufficiently viscous fluid reflect GWs? Our results are summarized in Fig. 42. When the radiation wavelength is large (small frequency), GWs barely interact with the star, and $\mathcal{R}^2 \simeq 1$. For inviscid materials, the same happens at *any* frequency: the wave penetrates the star but there is no dissipation, so it exits with a phase shift and no absorption.

In the presence of viscosity, GWs interact with the star material and get partially absorbed. Higher frequencies induce larger gradients and hence a more effective absorption, resulting in smaller reflection. This mimics the reflection properties of BHs (shown as a dashed black line in Fig. 42), for which the reflection coefficient vanish when $\omega M_S \gtrsim 1$. This is also achieved by increasing the star compactness.

In fact, Fig. 42 shows that stars close to the threshold of radial stability have a reflectivity curve similar to that of a non-rotating BH with the same mass. The large frequency reflectivity of viscous stars can be explained simply by recovering the dispersion relation satisfied by GWs passing through a viscous medium [384],

$$k^2 = \frac{\omega^2}{c^2}\left(1 + i\frac{16\pi G\eta}{\omega}\right). \tag{11.23}$$

This dispersion relation easily emerges taking the flat-space, dilute limit of (10.37), freezing the fluid degrees of freedom, i. e., $\dot{\beta} = 0$. At large frequencies $\omega \gg G\eta$, this dispersion relation would lead to $\mathcal{R}^2 = \exp(-16\pi R_S \eta)$, which captures accurately our results in the right panel of Fig. 42. Notice that this absorption features are different than the ones expected for models of exotic compact objects, based on a partially absorbing surface [324].

Based on well known properties of electric conductors, and on the examples we discussed concerning large dissipation, one is tempted to conclude that very viscous fluids reflect GWs. In fact Press used this behavior to hypothesize a material, "Respondium", able to reflect GWs or act as a waveguide [384]. Increasing the viscosity past the causal limit $\hat{\eta} > 3/4$, we observe a transition, which manifests itself in two ways: (a) low-frequency waves are amplified, $\mathcal{R}^2 > 1$, typical of systems with superluminal motion [83]; (b) at large frequencies, waves are no longer absorbed efficiently, but instead are better reflected at the surface of the star as η increases (cf. Fig. 42). Further evidence for efficient reflection is provided by the wavefunction ψ penetrating less efficiently into the star once viscosity increases past the causal bound. When attempting to reproduce these results from time domain scattering experiments, we find an instability, hinting towards the presence of unstable modes in the system. Therefore, highly viscous stars are, effectively, some kind of "Respondium material", and behave following the examples we worked out above. However, these properties are manifest only when violating the BDNK causality bounds, which are not present in the simplified examples. Therefore, exploring alternative parametrizations of the viscosity or numerical simulations of the full nonlinear problem is necessary to understand whether "Respondium"-like behavior is possible, while respecting causality.

11.5 QUASINORMAL MODES

We now turn our attention to the quasinormal modes of viscous stars. As discussed in chapter 3, QNMs correspond to frequencies ω_n for which the incident amplitude vanishes, $A_{\rm in}(\omega_n) = 0$ — these are the purely (damped) oscillatory frequencies of the star's spacetime. The fact that we deal with a coupled system, rather than a single equation, makes it challenging to numerically obtain the QNM frequencies of viscous stars. We have found and tracked the evolution of a spacetime mode, and confirmed its presence in time-domain evolution. However, we begin by discussing the QNMs in the decoupled limit, which allows us to study the properties of fluid viscous modes. These modes are a novel class of modes, without analogue in the perfect fluid case, and one of the new results presented in this thesis.

11.5.1 *Fluid Modes*

We consider the dynamics of perturbations in the decoupled case, setting $\dot{\psi} = 0$. This is reminiscent, although not exactly the same, as the Cowling approximation. The Cowling approximation consists on studying the perturbations of a relativistic

fluid around an equilibrium state in the curved background of a star, fixing the spacetime metric. Here we have derived eqs. (10.37) in full generality, and only at the end we set $\dot{\psi} = 0$. This consists on solving the second equation in (10.37) setting $c_i = 0$ for $i = 1, \ldots, 4$. We impose regularity at the origin and the condition (**??**) at the surface of the star.

We implement a spectral method decomposing the functions in Chebyshev polynomials. The equation is written as a generalized eigenvalue problem, in a first order formulation, i.e.,

$$\mathbf{L}\vec{U} = -i\omega\mathbf{B}\vec{U}\,, \tag{11.24}$$

where $\vec{U} = (\dot{\beta}, \partial_r\dot{\beta}, \partial_t\beta)$, ω is the complex QNM frequency, and the operators $\mathbf{L}$ and $\mathbf{B}$ are differential operators that implement the equations of motion and the boundary conditions. We have cross-checked that the spectrum obtained with this method is recovered by a simple shooting routine with high accuracy, as well as confirmed the stability of the recovered spectrum when increasing the number of collocation points used in the discretization.

Our results for the spectrum, for different values of $\hat{\eta}$, are shown in the left panel of fig. 43, where we decompose the complex QNM frequency as $\omega = 2\pi f - i/\tau$. First, we notice the appearance of non-oscillatory modes, with $f = 0$, which can be long lived for small values of $\hat{\eta}$ (we note that there is an additional non-oscillatory mode with damping time ~ 0.6ms for the $\hat{\eta} = 0.1$ case, which is outside the plot range of the figure). Secondly, we see that the oscillatory modes have a damping time which is comparable to that of spacetime modes, $\tau \sim 10^{-2}$ms. More interestingly, there is a large number of modes with a comparable damping time, but oscillatory frequencies extending from $f \sim 1 - 100$kHz. The physical interpretation is that the shear viscosity acts as a restoring force which makes these fluid modes oscillatory (unlike in the perfect fluid case). This restoring force is very effective, thus resulting in very efficient damping, as well as in rapidly oscillatory modes.

11.5.2 *Spacetime Modes*

Next we turn our attention to study the role of spacetime modes. This corresponds to the inverse Cowling approximation — setting the fluid perturbations to zero, $\dot{\beta} = 0$, and studying only the perturbations to the geometry. This approximation proved particularly useful to discern, e. g., the spacetime origin of w-modes [28]. We thus solve the first equation in (10.37) setting $\dot{\beta} = 0$, using a shooting method to extract the QNM frequencies. As $\hat{\eta} \to 0$ we recover the perfect fluid value of the fundamental spacetime mode, which is modified slightly in the presence of viscosity. This is shown in the right panel of Fig. 43. Remarkably viscosity only alters the frequency and damping time of this mode by a couple percent – this is in contrast with the fundamental fluid mode obtained in the previous subsection, which changes significantly as the viscosity increases.

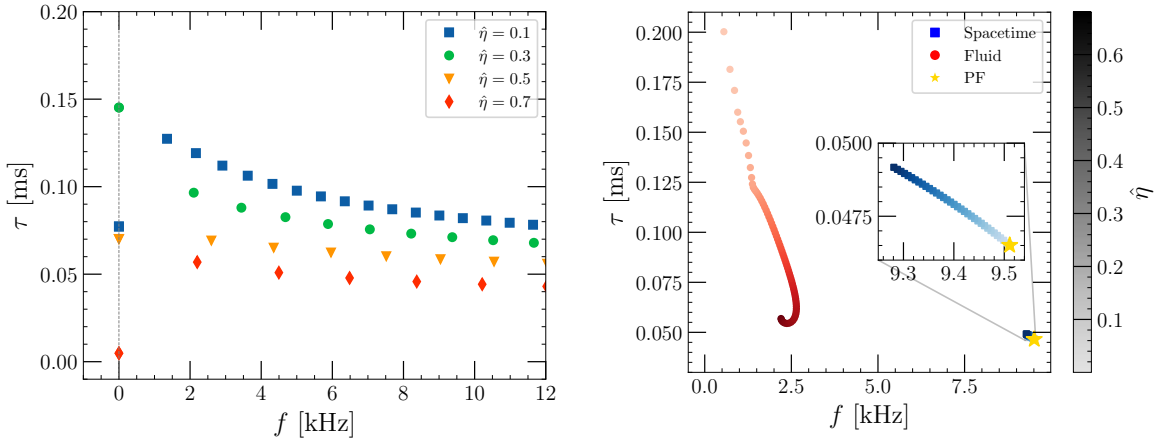

Figure 43 **Left:** Spectrum of the fluid modes for different values of the shear viscosity $\hat{\eta}$, as indicated in the legend, using always $\hat{\tau} = 10$. We observe the appearance of another set of purely damped modes along the axis, some of which are longer lived. **Right:** Frequency of the fundamental oscillatory mode in the spacetime spectrum (blue), and in the fluid spectrum (red), in the two decoupled limits, as a function of the shear viscosity $\hat{\eta}$. Darker colors correspond to larger viscosity values, as indicated by the colorbar. The yellow star marks the value of the fundamental spacetime mode for a perfect fluid. The inset zooms in to show the small variation of the spacetime mode with viscosity.

11.5.3 *Coupled System*

Finally we discuss the QNMs in the coupled system. Table 3 shows the value of the QNM frequency obtained for the least-damped spacetime mode for different values of the shear viscosity in the case where fluid and spacetime oscillations are coupled, and in the decoupled case where fluid motion is frozen. The last column shows the relative difference with respect to the QNM frequency in the perfect fluid case, which is, at most, less than 10%. Increasing the shear viscosity $\hat{\eta}$ results in a smaller real frequency and a longer damping time. It is perhaps surprising that the damping time of the QNM increases rather than decrease, but the variation is small enough to be most likely negligible for astrophysical purposes.

$\hat{\eta}$	$\hat{\tau} = 5$	ICA	$\delta\omega(\%)$
0.05	$(9.44, 46.5)$	$(9.49, 46.7)$	$(0.7, 0.4)$
0.25	$(9.24, 46.7)$	$(9.43, 47.5)$	$(2.9, 2.3)$
0.45	$(8.97, 47.0)$	$(9.36, 48.3)$	$(5.7, 4.1)$
0.65	$(8.78, 48.1)$	$(9.29, 49.0)$	$(8.4, 5.9)$

Table 3: Fundamental spacetime mode written as (f, τ), with f in kHz and τ in μs, for $\hat{\tau} = 5$ (second column), and in the inverse Cowling approximation (third column), for different values of $\hat{\eta}$. The last column shows the combined, relative difference between the QNM frequency and the one of the same mode for a perfect fluid, in percent value, for the two previous columns.

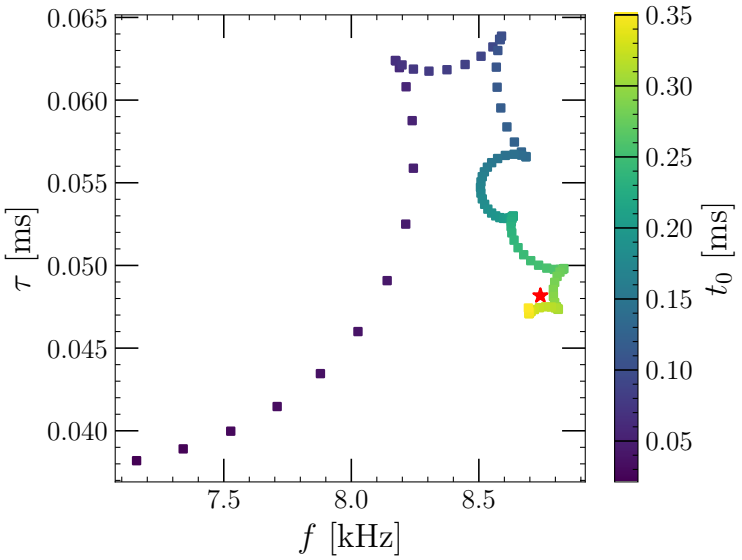

Figure 44 Extracted frequency and damping time for $\hat{\eta} = 0.7$ and $\hat{\tau} = 10$, varying the starting time of the fit t_0 (where $t_0 = 0$ corresponds to the peak of the signal). The red star corresponds to the frequency domain result for the fundamental spacetime mode. We observe very good agreement with this calculations when the starting time is late enough, as expected.

We show additional evidence of the existence of this mode in Fig. 44 by fitting time-domain simulations to a superposition of damped sinusoids. The recovered frequencies and damping time depend slightly on the starting time of the fit — this is likely due to the presence of additional shorter-lived modes in the system — but rapidly converges to the value we compute from the frequency domain calculation. This serves to cross-validate our results across our two independent methods.

The main takeaway is that axial spacetime modes are dominated by the gravitational potential of the star and thus, are not particularly sensitive to dissipative processes in the star. However this shows that, in principle, one can use the framework presented in the previous chapter 10, as well as in this chapter, to study the impact of viscosity on different mode families of realistic neutron stars. Quantifying the role of viscosity for the most relevant modes (in particular, f-modes), is a relevant task for precision GW asteroseismology which we plan to study in the future.

11.6 CONCLUSIONS

In this chapter we have presented new results describing the interaction of GW with matter. In particular we show that GWs interact in a nontrivial way with compact, viscous fluids. Viscosity induces absorption of GWs — we have calculated the precise response of compact, self-gravitating fluid configurations to impinging waves. Compactness enhances the absorption of GWs, to the point where extremely viscous and compact stars respond to GWs in a very similar manner to a black hole with the same mass. Additionally we show that once the viscosity becomes large

enough — outside the regime where hydrodynamics is causal — stars can amplify GWs. This is suspiciously similar to the overreflection found in the Poiseuille flow due to the Orr mechanism [239]. Our results motivate the study of amplification of GWs by rotating stars, which we undertake in the next chapter.

In the large frequency limit we recover results compatible with the dispersion relation first introduced by Press [384]. Our findings are consistent with past remarks [384]: a perfect reflector of GWs that does not violate energy conditions would be more compact than a black hole. An interesting open question is whether this requirement can be by-passed through quantum collective dynamics of matter reacting to GWs [35].

Absorption of GWs leads to heating of the star. For the maximum allowed $\hat{\eta} = 3/4$, $\eta_{\rm max} = 1.5 \times 10^{31} {\rm g/cm/s}$ is comparable to the effective viscosity of a BH with the same mass $\eta_{\rm BH} = 1.8 \times 10^{31} {\rm g/cm/s}$ [466]. This is much larger than the usual shear viscosity expected for a NS [466]. However, the absorption is suppressed by geometrical factors. For a supermassive BH coalescence of total mass $M = 10^6 M_\odot$ and a neutron star orbiting the binary at radius $10^3 M$, the fraction of GW energy released by the binary that impinges on the neutron star $\sim 10^{-16}$. It is very low-frequency radiation (in the low-frequency portion of Fig. 42) hence the energy absorbed is $\ll 10^{-14} M_\odot$.

However, during the inspiral stage of binary neutron star mergers, dissipative effects due to viscosity will alter the gravitational waveform through the dynamical tidal deformabilities [136, 238, 407, 410], opening the possibility of constraining the viscosities of neutron stars from gravitational wave observations.

We can extrapolate our results in the high-frequency regime to non self-gravitating, thin circumbinary accretion disks around a BH binary, for which $\eta = \alpha \rho \Omega H^2$ [32, 46, 424], with ρ the local disk density, Ω the Keplerian orbital velocity and H the disk height. Now,

$$M\eta = 5 \times 10^{-12} \frac{\alpha}{10^{-2}} \frac{M^2 \rho}{10^{-6}} \frac{M\Omega}{0.05} \left(\frac{H}{0.1M} \right)^2 . \tag{11.25}$$

We are now in the $\omega \gg \eta$ regime. Hence, we find that the ratio between the absorbed GW luminosity $\mathcal{L}_{\rm GW}^{\rm absorbed} \sim \mathcal{L}_{\rm GW}^{\rm peak} M\eta$ to the total disk luminosity $\mathcal{L}_{\rm accr} \sim \dot{M} = f_{\rm Edd} \dot{M}_{\rm Edd}$ is

$$\frac{\mathcal{L}_{\rm GW}^{\rm absorbed}}{\mathcal{L}_{\rm accr}} \sim 10^4 \frac{10^{-4}}{f_{\rm Edd}} \frac{10^6 M_\odot}{M} \frac{\alpha}{10^{-2}} \frac{M^2 \rho}{10^{-6}} \frac{M\Omega}{0.05} \left(\frac{H}{0.1M} \right)^2 , \tag{11.26}$$

where the peak GW luminosity for equal mass mergers $\mathcal{L}_{\rm GW}^{\rm peak} \sim 10^{23} \mathcal{L}_\odot$ [107]. GWs from mergers can heat up accretion disks to an important level, consistently with the findings in Ref. [279].

12

SUPERRADIANT AMPLIFICATION BY ROTATING STARS

Written while listening to music composed by Clara Schumann and Lili Boulanger.

12.1 INTRODUCTION

That sound waves scattering off moving interfaces can be amplified is a well known phenomena in fluid dynamics [340, 405]. In essence, sound waves scattering through a moving interface can extract energy from the interface if their momentum is low enough, getting dragged along in the interaction. In order to achieve this it is crucial that the system is dissipative, i. e., that waves can be absorbed in the interface. Zeldovich [469, 470] first realized that rotating BHs provide precisely both ingredients: their horizon is a moving (rotating), dissipative interface where low-frequency waves can be amplified. This amplification mechanism has since then been dubbed *superradiance* [48, 83, 386], and has vast implications in the physics of astrophysical BHs, e. g., related to the formation of jets [75], and for the search of ultralight bosons [34, 158]. We refer the curious reader to [83] and references therein for further details on superradiance in BH spacetimes.

In the previous chapter we have shown that a viscous, self-gravitating fluid can absorb GWs. It is then natural to ask oneself whether GWs are amplified if said object is rotating. The perturbative framework developed in previous chapters, augmented to account for the effects of rotation, provides a self-consistent framework to answer this question. This is remarkable, since it is a counterexample to two common misconceptions: (i) that superradiance is due to the presence of an ergoregion, and (ii) that superradiance relies on the existence of horizons. Both these facts had been proved previously [98, 166, 406]. However, examples of superradiance in horizonless spacetimes without ergoregions required the inclusion of electromagnetic fields, endowing the star with conducting properties [98, 406]. This chapter shows that this is not necessary if one allows the star to be viscous and, hence, dissipative. We will show that rotating stars can generically amplify low-frequency GWs. This is an important confirmation of Zeldovich's arguments for the generic amplification of waves off dissipative, moving interfaces.

Let us first review Zeldovich's argument [470]. Consider an axisymmetric, macroscopic body rotating uniformly and rigidly about its symmetry axis. Let S, T denote its mass, entropy, and temperature. Suppose now a wave packet with frequency $(\omega, \omega + d\omega)$ and azimuthal number m (which we will take to be positive) scatters

off this body with a certain power $P(\omega)d\omega$. Radiation with a specific frequency and azimuthal number carries angular momentum at a rate $(m/\omega)P(\omega)d\omega$. If we denote Z the fraction of the incident energy absorbed by the body, we have that its change in energy and angular momentum is

$$\dot{E} = ZPd\omega\,, \qquad \dot{J} = \frac{mZ}{\omega}Pd\omega\,. \tag{12.1}$$

We assume here that the frequency and multipolarity of the incident and scattered waves are the same. Changing to the frame corotating with the body, the change of energy is just

$$\dot{E}_0 = \dot{E} - \Omega\dot{J} = \dot{E}\left(1 - \frac{m\Omega}{\omega}\right) \tag{12.2}$$

which increases the entropy $\dot{S} = \dot{E}_0/T$ by an amount

$$\dot{S} = \frac{\omega - m\Omega}{\omega T}ZPd\omega\,. \tag{12.3}$$

Now the second law of thermodynamics $\dot{S} > 0$ allows for the wave to extract energy from the body, $Z < 0$, as long as $\omega < m\Omega$ (for positive frequency modes). Notably this argument neglects changes in the temperature of the object which we expect to be present in a dissipative, self-gravitating fluid. As a consequence, the superradiant condition $\omega < m\Omega$ may not be exactly satisfied for realistic systems with complex thermodynamics, but it should nevertheless be a good approximation.

Based on this thermodynamic argument, and in previous results [98, 406], we should expect superradiance to occur for generic rotating bodies. This applies, in particular, to BH mimickers that have free microstates—in particular, that they are not themselves microstates, such as fuzzballs [335] or topological stars [38]. For a self-gravitating body to mimic BH properties, one may expect that its entropy is large, $S \lesssim S_{\rm BH}$, and if the object also satisfies the Kovtun-Son-Starinets bound [291, 294], we can estimate the bodies shear viscosity as $\eta/\eta_{\rm BH} \gtrsim 4C^2 S/S_{\rm BH}$, where $C = M/R$ is the horizonless body compactness. Highly compact bodies with a large entropy *must* be very viscous, in particular much more so than neutron stars. Dissipative effects cannot be overlooked when studying the dynamics of black hole mimickers [11].

In this chapter we study in detail the impact of viscosity on the scattering of GWs off a rotating, self-gravitating fluid. We do so in the slowly-rotating limit, where we only keep terms that are linear in the bodies angular velocity Ω. This comes at a cost: recall that the superradiant threshold is $\omega < m\Omega$, and thus only frequencies that are $\mathcal{O}(\Omega)$ are amplified. Since the equations contain terms of the form ω^2, our perturbative expansion is formally inconsistent, and quantitative results must be taken with care. The main qualitative features presented here will hopefully survive a second-order in Ω expansion—as a historical note, the r-mode instability of rotating neutron stars was first observed in a first-order expansion in Ω, suffering the same limitation as this work [25], and it was later confirmed through a second-order expansion [27].

First, we review the structure of slowly rotating stars. We present a toy model, similar to the previous chapter, that allows us to illustrate some properties of the amplification factors and modes of rotating stars. Next, we briefly explain how to extend the perturbative framework to slowly rotating spacetimes, largely following [366]. Finally we present our results for the amplification factors, showing evidence of superradiant amplification, and interpret our findings.

12.2 SLOWLY ROTATING STARS

The metric of a slowly rotating star, to first order in the angular velocity Ω, is given by [235, 236]

$$ds^2 = -e^{\nu(r)}dt^2 + e^{\lambda(r)}dr^2 + r^2 d\Omega^2 - 2r^2\varpi(r)\sin^2\theta dt d\phi\,, \tag{12.4}$$

where $d\Omega^2$ is the area element of the round unit 2-sphere. The mass aspect $M(r)$ is defined through $e^{-\lambda} = 1 - 2M/r$. The stress-energy tensor T_{ab} describes a BDNK fluid (9.21), where the fluid velocity at equilibrium is given by

$$u = e^{-\nu/2}\Big(\partial_t + \Omega\partial_\phi\Big)\,. \tag{12.5}$$

Clearly this describes a self-gravitating fluid undergoing uniform rotation since Ω is a constant. That this is the expected equilibrium state for astrophysical self-gravitating fluids can be seen as follows. First, suppose there was some differential rotation, i. e., let $\Omega = \Omega(r)$. Two consecutive spherical shells of the star would shear against each other, so viscosity would efficiently act against this differential rotation on a timescale [438]. One can now estimate the timescale on which shear viscosity would damp away all differential rotation [155] as

$$\tau_\eta \sim 28\Big(\frac{10^{15}\mathrm{g\,cm^{-3}}}{\rho}\Big)^{5/4}\Big(\frac{T}{10^9\mathrm{K}}\Big)^2\Big(\frac{R}{10\mathrm{km}}\Big)\mathrm{yr}\,. \tag{12.6}$$

Hot young neutron stars would shed away their differential rotation during their first years of existence. As they cool down their outer core is expected to become superfluid, which admits a very accurate description in terms of uniform rotation on scales larger than the intervortex spacing (i. e., on scales of centimeters or meters). To conclude: shear viscosity, as well as other mechanisms, act efficiently to shed away all differential rotation in self-gravitating bodies. This is remarkably different in accretion disks—we will come back to this point later.

As in the previous chapter we will restrict to barotropic fluids where the equation of state is simply $p = p(\varepsilon)$, and the star can be assumed to be cold, with negligible heat conductivity $\sigma = 0$. The perturbative expansion we carry out assumes that $\Omega \ll \Omega_K = M_S^{1/2}R_S^{-3/2}$, where Ω_K is the (Keplerian) mass-shedding frequency of the star. To $\mathscr{O}(\Omega^0)$ Einstein equations reduce, evidently, to the usual Tolman-Oppenheimer-Volkoff equations (See (10.34) in chapter 10). The first order in Ω/Ω_K of Einstein equations leads to a second-order equation for the frame dragging coefficient

$$\varpi'' + 4\Big[\frac{1}{r} - \pi r e^{\lambda}(\rho + p)\Big]\varpi' + 16\pi e^{\lambda}(\rho + p)(\Omega - \varpi) = 0\,. \tag{12.7}$$

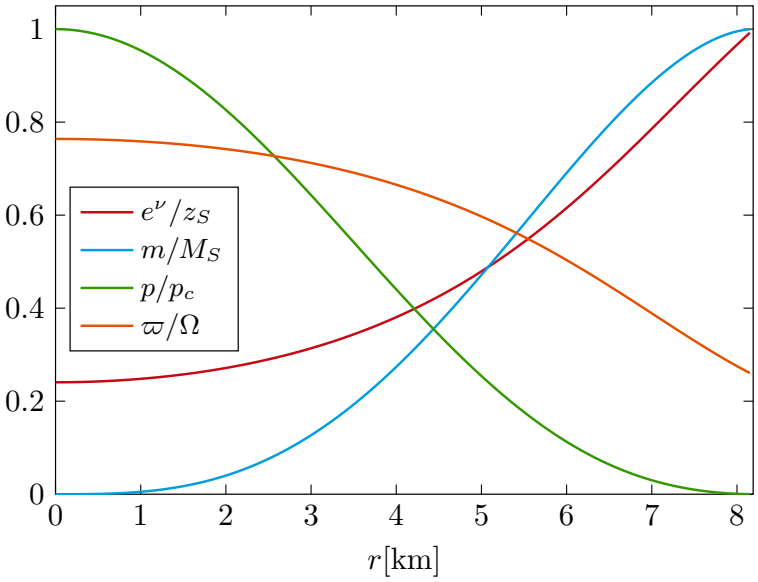

Figure 45 Radial profiles of the background functions of a slowly-rotating star with a polytropic equation of state and $n = 0.8$, $\kappa = 700\text{km}^{-2.5}$, and central density $\varepsilon = 3 \times 10^{15}\text{gcm}^{-3}$. We normalize the redshift factor, mass aspect, pressure, and frame-draggin function by the surface redshift, total mass, central pressure, and angular velocity, respectively.

After integrating the TOV equations, we integrate (12.7) for the auxiliary variable $\tilde{\varpi} = \Omega - \varpi$. The initial condition is $\tilde{\varpi}(0) = \tilde{\varpi}_0$, and $\tilde{\varpi}'(0) = 0$. Next we extract the angular momentum and angular velocity of the star requiring continuity with the exterior of a slowly rotating Schwarzschild spacetime (see section IVB in [462])

$$J = -\tilde{\varpi}'(R_S)\frac{R_S^4}{6}\,, \qquad \Omega = \tilde{\varpi}(R_S) + \frac{2J}{R_S^3}\,. \tag{12.8}$$

The quotient $J/\Omega = I$ determines the moment of the inertia of the star [235, 462]. In the following we will focus on polytropic equations of state (11.6), with $n = 0.8$, $\kappa = 700\text{km}^{-2.5}$, and central density $\varepsilon = 3 \times 10^{15}\text{gcm}^{-3}$. The radial profiles of the background variables are shown in Fig. 45, where $z_S = 1 - 2M_S/R_S$ is the redshift at the surface of the star.

12.3 TOY MODEL

We first examine a toy model inspired by Zeldovich's construction in [469]. Consider a scalar field Φ propagating in the background of a slowly-rotating star, with a non-minimal coupling to the rotation of the star that effectively accounts for absorption. This is governed by the equation of motion

$$\Box\Phi = \alpha u^{\mu}\nabla_{\mu}\Phi\,, \tag{12.9}$$

where $\alpha = \alpha(r)$ is a non-negative, purely radial function with units of frequency. It vanishes outside the star $\alpha(r > R_S) = 0$, and $\Box$ is the wave operator in the spacetime

of a slowly rotating star. Here u^μ is the fluid velocity, given in Eq. (12.5). Expanding in spherical harmonics $r\Phi = \sum_{\ell m} \phi_{\ell m} Y_{\ell m}$, neglecting mode coupling contributions, and transforming to the frequency domain, we find

$$\frac{d^2\phi}{dr_\star^2} + \Big(\omega^2 - \mathcal{V}\Big)\phi = i\alpha e^{\nu/2}(\omega - m\Omega)\phi\,, \tag{12.10}$$

where

$$\mathcal{V} = \frac{e^\nu}{r^2}\left[\ell(\ell+1) + \frac{2M}{r} + 4\pi(p-\rho)\right] + 2m\omega\varpi\,. \tag{12.11}$$

For low frequencies ($\omega < m\Omega$), the damping term on the right-hand side becomes an amplification term. We integrate numerically this equation ensuring regularity near the origin, and extract the reflectivity sufficiently far away from the star. In order to do so, notice that far away from the star,

$$\phi \xrightarrow{r\to\infty} A_{\rm in} e^{i\omega r_\star} + A_{\rm out} e^{-i\omega r_\star}\,. \tag{12.12}$$

We define the reflectivity of the star as $\mathcal{R}^2(\omega) = |A_{\rm out}/A_{\rm in}|^2$. We consider two models for dissipation: (i) $\alpha = \alpha_0/R_S$, a sharp cutoff at the surface of the star, and (ii) $\alpha = \alpha_0\sqrt{\rho}$, which smoothly approaches zero at the surface. The qualitative behavior for both models is identical—frequencies below the superradiant bound $\omega < m\Omega$ are amplified, whereas waves are absorbed by the star past this bound. Amplification increases with larger values of α, as one may naively expect. This confirms that low-frequency waves propagating in a dissipative, rotating system should be subject to superradiant amplification. This is true in the absence of horizons or ergoregions, as discussed in the Introduction.

For this simple toy model we can also find the associated scalar QNMs, corresponding to values of the frequency ω for which $A_{\rm in}(\omega) = 0$. This allows us to examine whether this system additionally possesses a superradiant *instability*. QNM frequencies with a positive imaginary part (signalling exponential growth) are clear smoking guns of a linear instability in the system. It is known [386] that a superradiant instability requires a mechanism that traps waves—otherwise, waves are scattered and amplified, but not in a runaway, unstable process. A natural mechanism that may lead to such trapping is the emergence of stable lightrings, which appear for extremely compact configurations. A constant density star $\rho = \rho_c$ will have a stable light ring whenever $R_S < 3M_S$ (to linear order in the rotation rate).

We adapt the previous method, shooting for the QNM frequency that satisfies this condition. By slowly changing the dissipation rate α and the angular velocity of the star Ω we can smoothly keep track of the evolution of the fundamental mode, shown in the right panel of fig. 46. As the figure shows, the real part of the frequency of the fundamental mode is always larger than the superradiant threshold, $\Re\omega > m\Omega$. In the regime where $\Omega \gg \Omega_{\rm sLR}$, the rescaled frequency $\Re\omega/(m\Omega) \to \mathcal{O}(1)$ asymptotes to a constant of order $\mathcal{O}(1)$, confirming the scaling $\omega \sim m(\Omega + \Omega_{\rm sLR})$. This behavior is independent of the compactness of the star, provided it has a stable light ring. Although not shown in the Figure, we report that the imaginary part depends only very weakly on Ω.

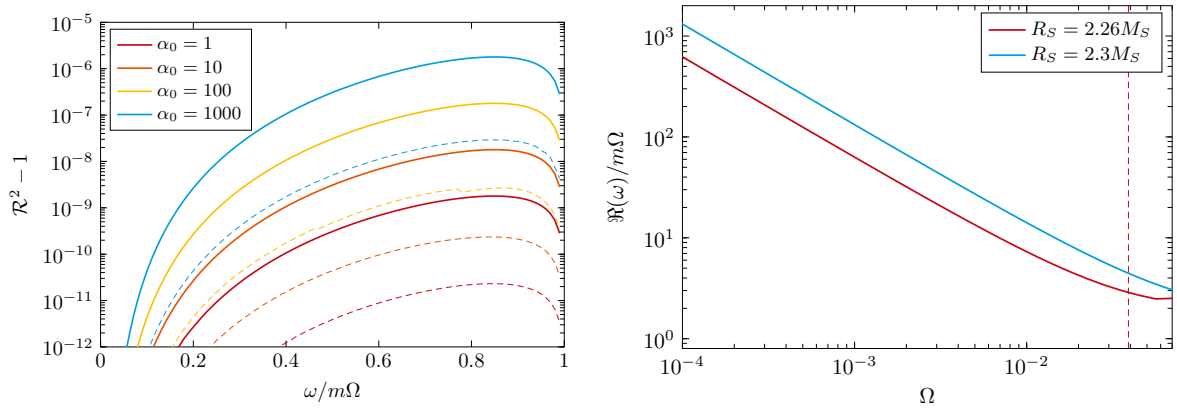

Figure 46 **Left:** Amplification factor $\mathcal{R}^2 - 1$ as a function of the dimensionless frequency $\omega/m\Omega$ for the toy model (12.9). Solid lines correspond to a constant α inside the star, which has a sharp cutoff at the surface, whereas dashed lines correspond to a smooth profile of α, which goes to zero smoothly towards the surface. The amplification factor scales proportionally with α, as expected. **Right:** Real part of the frequency of the fundamental mode, rescaled by $m\Omega$, for $m = 2$, as a function of the angular velocity of the star, Ω, for the model (12.9). The red (blue) lines correspond to constant density stars with radius $R_S = 2.26M_S$ ($R_S = 2.3M_S$). The dimensionless frequency $\Re\omega/m\Omega > 1$ is always larger than unity, signalling that the fundamental mode is outside the superradiant amplification threshold, even at relatively large angular velocities of the star.

12.4 AXIAL PERTURBATIONS OF SLOWLY ROTATING STARS

The theory of linear perturbations about a slowly rotating star was first studied in [131, 284]. One of the key differences with respect to perturbations about non-rotating, spherically symmetric spacetimes is that rotation provides a mechanism to couple different angular harmonics—spherical harmonics are no longer the harmonics that separate the equations of motion. To linear order in the rotation parameter the ℓth axial multipole couples to the $\ell \pm 1$th polar multipoles, and vice versa. For the purpose of this chapter, which is to study the response of a rotating star to incoming GWs, it is sufficient to focus on axial-led modes, neglecting the coupling to polar modes [366]. This coupling would be important in order to carry the calculation to second order in the rotation parameter.

Moreover, the framework developed in chapter 3, later refined in chapter 10 to the specific case of perturbations of spacetimes sourced by fluid matter, is not exactly suitable to discuss the slowly rotating case, as it relies so heavily on the spherical symmetry of the background. Although an extension of that framework to the slowly rotating case via a multiple parameter perturbative expansion is feasible, we leave that for future work, and follow here instead the formalism summarized in [366], which builds heavily upon [284]. As in the previous case we consider metric and fluid perturbations of the form

$$g_{ab} = \mathring{g}_{ab} + \epsilon \dot{h}_{ab}\,, \qquad u^a = \mathring{u}^a + \epsilon \dot{u}^a\,, \tag{12.13}$$

where the metric perturbation, in the RW gauge, is simply given by

$$\dot{h}_{AI} = \dot{h}^{\ell m}_{A}(r)\mathcal{X}^{\ell m}_{I}(z^J)e^{-i\omega t}\,, \tag{12.14}$$

where we recall that $A = 0, 1$ are the coordinates on the Lorentzian sector (t, r), and $I = 2, 3$ are the angular coordinates $z^I = (\theta, \phi)$. We omit the ℓ, m label, keeping in mind that the perturbation variables always refer to a concrete angular harmonic. The fluid perturbation admits a similar expansion

$$\delta u^a = e^{-\nu/2}e^{-i\omega t}\Big(e^{-\nu}\Big[\dot{\beta}(\Omega-\varpi)+\Omega\dot{h}_0\Big]\mathcal{X}_\phi, 0, \frac{\dot{\beta}}{r^2}\mathcal{X}_\theta, \frac{\dot{\beta}}{r^2\sin^2\theta}\mathcal{X}_\phi\Big)\,, \tag{12.15}$$

where the first component is such that $\delta(u_a u^a) = 0$. Einstein's equations can be written now in terms of the two metric perturbation components $\dot{h}_0, \dot{h}_1$, and the fluid perturbation $\dot{\beta}$. In particular, if we denote the linearised Einsten equations by $\dot{E}_{ab} = \dot{G}_{ab} - 8\pi\dot{T}_{ab}$, its components admit the following expansion in spherical harmonics

$$\begin{aligned}
\dot{E}_{A\theta} =& \tilde{\alpha}^A_{\ell m}\cos\theta\partial_\theta\mathcal{Y}_{\ell m} - \frac{\beta^A_{\ell m}}{\sin\theta}\partial_\phi\mathcal{Y}_{\ell m} + \eta^A_{\ell m}\sin\theta\mathcal{Y}_{\ell m} \\
&+ \chi^A_{\ell m}\sin\theta W_{\ell m} + \dots\,, \\
\dot{E}_{A\phi} =& \beta^A_{\ell m}\partial_\theta\mathcal{Y}_{\ell m} + \frac{\tilde{\alpha}^A_{\ell m}\cos\theta}{\sin\theta}\partial_\phi\mathcal{Y}_{\ell m} + \chi^A_{\ell m}X_{\ell m} + \dots\,, \\
\dot{E}_{\theta\phi} =& \frac{g_{\ell m}}{\sin\theta}\partial_\phi\mathcal{Y}_{\ell m} + \frac{t_{\ell m}}{\sin\theta}W_{\ell m} + \dots\,, \\
\dot{E}_{-} \equiv& \dot{E}_{\theta\theta} - \frac{\dot{E}_{\phi\phi}}{\sin^2\theta} = g_{\ell m}\partial_\theta\mathcal{Y}_{\ell m} - \frac{t_{\ell m}}{\sin^2\theta}X_{\ell m} + \dots\,,
\end{aligned} \tag{12.16}$$

where the dots denote terms of even-parity, and we have introduced

$$\begin{aligned}
X_{\ell m} =& 2\partial_\phi\Big(\partial_\theta - \cot\theta\Big)\mathcal{Y}_{\ell m}\,, \\
W_{\ell m} =& \Big(\partial^2_\theta - \cot\theta\partial_\theta - \frac{1}{\sin^2\theta}\partial^2_\phi\Big)\mathcal{Y}_{\ell m}\,.
\end{aligned} \tag{12.17}$$

Projecting these equations onto odd parity spherical harmonics leads to three equations, which, after neglecting the mode coupling between even and odd parity sectors, can be written as

$$\begin{aligned}
\ell(\ell+1)\beta^A_{\ell m} + im\Big[(\ell-1)(\ell+2)\chi^A_{\ell m} + \tilde{\alpha}^A_{\ell m} + \eta^A_{\ell m}\Big] =& 0\,, \\
\ell(\ell+1)t_{\ell m} + img_{\ell m} =& 0\,.
\end{aligned} \tag{12.18}$$

Similarly, if we let $\dot{C}_a = \Big(\nabla^b T_{ab}\Big)^{\cdot}$ be the linearization of the conservation of the stress-energy tensor, we can write

$$\begin{aligned}
\dot{C}_\theta =& \hat{\alpha}_{\ell m}\cos\theta\partial_\theta Y_{\ell m} - \frac{\hat{\beta}_{\ell m}}{\sin\theta}\partial_\phi Y_{\ell m} + \hat{\eta}_{\ell m}\sin\theta Y_{\ell m} \\
&+ \hat{\chi}_{\ell m}\sin\theta W_{\ell m} + \dots\,, \\
\dot{C}_\phi =& \hat{\beta}_{\ell m}\partial_\theta Y_{\ell m} + \frac{\hat{\alpha}_{\ell m}\cos\theta}{\sin\theta}\partial_\phi Y_{\ell m} + \hat{\chi}_{\ell m}X_{\ell m} + \dots\,,
\end{aligned} \tag{12.19}$$

leading to the equation

$$\ell(\ell+1)\hat{\beta}_{\ell m} + im\Big[(\ell-1)(\ell+2)\hat{\chi}_{\ell m} + \hat{\alpha}_{\ell m} + \hat{\eta}_{\ell m}\Big] = 0\,. \tag{12.20}$$

Therefore our task is reduced to computing the components of the linearised Einstein equations and the linearised conservation of the stress energy tensor in this expansion. The system of equations formed by (12.18)–(12.20) can now be used to derive a system of two coupled wave equations.

First, we can use the t component ($A = 0$) of the first equation in (12.18) to eliminate $\dot{h}_0$, and the r component ($A = 1$) to eliminate $\dot{h}_0'$, in terms of $\dot{\beta}, \dot{h}_1$. Plugging these back into the r component of (12.18) and into (12.20) leads to two coupled wave equations for the remaining variables. The second equation in (12.18) is used to verify the correctness of the derivation. Instead of using $\dot{h}_1$, we introduce a RW-like variable ψ defined as

$$\dot{h}_1 = re^{(\lambda-\nu)/2}\Big(1 - \frac{m\varpi}{\omega}\Big)\dot{\psi}\,. \tag{12.21}$$

In terms of this variable, the equations take the form

$$\begin{aligned}
\frac{d^2\dot{\psi}}{dr_\star^2} + \Big(\omega^2 c_\psi^{-2} - \mathcal{V}_\psi\Big)\dot{\psi} =& C_{11}\frac{d\dot{\psi}}{dr_\star} + C_{12}\frac{d\dot{\beta}}{dr_\star} + C_{13}\dot{\beta}\,,\\
\frac{d^2\dot{\beta}}{dr_\star^2} + \Big(\omega^2 c_Z^{-2} - \mathcal{V}_Z\Big)\dot{\beta} =& C_{21}\frac{dZ}{dr_\star} + C_{22}\frac{d\dot{\psi}}{dr_\star} + C_{23}\dot{\psi}\,,
\end{aligned} \tag{12.22}$$

where the coefficients C_{ij} are unilluminating and are given in an accompanying `Mathematica` notebook [1]. The propagation speed of each of the modes receives a purely imaginary correction with respect to their nonrotating value, $c_\psi^2 = 1 + i\Delta$, and $c_Z^2 = \eta[\tau_Q(p+\varepsilon)]^{-1}(1 - i\Delta)$, with

$$\Delta = \frac{16\pi m r^2 e^{-\nu/2}}{\ell(\ell+1)}\Big(\Omega - \varpi\Big)\Big[(\varepsilon + p)\tau_Q - \eta\Big]\,. \tag{12.23}$$

The nonrotating limit of Eqs. (12.22) recovers the equations of chapter 10 (see also ref. [395]), whereas the perfect fluid limit recovers the master equation of [284].

We study the scattering of waves off the star. As in the previous chapter, we consider solutions to (12.22) which are regular at the origin, and at large distances satisfy an expansion of the form (11.14). We then compute the reflectivity as in (11.15). In the exterior the propagation of GWs is governed by the slowly-rotating RW equation

$$\frac{d^2\dot{\psi}}{dr_\star^2} + \Big(\omega^2 - \frac{4m\omega J_S}{r^3} - \mathcal{V}_{\rm RW}\Big)\dot{\psi} = 0\,, \tag{12.24}$$

where

$$\mathcal{V}_{\rm RW} = f(r)\Big[\frac{\ell(\ell+1)}{r^2} - \frac{6M_S}{r^3} + \frac{24mJ_S(3r - 7M_S)}{\ell(\ell+1)\omega r^6}\Big]\,, \tag{12.25}$$

and $f(r) = 1 - 2M_S/r$. Since viscosity vanishes at the surface of the star, Israel junction conditions [256] are trivially satisfied. Regularity of the equations then imposes a boundary condition at the surface

$$A_1 \frac{d\dot{\beta}}{dr} + A_2 \dot{\beta} + A_3 \frac{d\dot{\psi}}{dr} + A_4 \dot{\psi} = 0\,, \tag{12.26}$$

where

$$\begin{aligned}
A_1 =& \hat{\eta}\ell(\ell+1)M_S R_S^4 z_S^3\,,\\
A_2 =& iR_S^2 z_S^2 \left[4mJ_S + 2i\ell(\ell+1)M_S R_S z_S \hat{\eta} - R_S^3\Big(\ell(\ell+1)\omega + 2m\Omega - m\ell(\ell+1)\Omega\Big)\right],\\
A_3 =& \ell(\ell+1)\Big(1 - \frac{m\Omega}{\omega}\Big) R_S^6 z_S^4\,,\\
A_4 =& \frac{2mJ_S}{\omega}\Big(6z_S^2 + iM_S R_S^2 z_S \ell(\ell+1)\omega\hat{\eta}\Big) + \ell(\ell+1)R_S^3\Big(1 - \frac{m\Omega}{\omega}\Big)\Big(z_S^2 - iM_S R_S^2 z_S \omega\hat{\eta}\Big)\,.
\end{aligned} \tag{12.27}$$

We adapt the shooting method implemented in the previous chapter to integrate the equations ensuring this boundary condition is satisfied. In particular, we use the `DifferentialEquations.jl` [391] package to solve the radial ODEs, and the `NLsolve.jl` [111] package to ensure the boundary conditions are satisfied. Our code is publicly available in [1], and has been tested against an independent routine written in `Mathematica`, in addition to reproducing the results of [80] in the nonrotating limit.

12.5 RESULTS

Our main result is shown in Fig. 47: rotating, viscous stars amplify radiation. This is evident in the inset of the left panel, where the reflectivity exceeds unity, $\mathcal{R}^2 > 1$, for frequencies $\omega \lesssim m\Omega$. We also find that the maximum amplification increases with the dimensionless shear viscosity. This parameter controls the absorption rate in the high-frequency limit [80, 384], supporting the idea that stronger absorption leads to shorter superradiant timescales. A similar result was found in Ref. [417], in the context of spinning black hole mimickers constructed from the membrane paradigm. The scattering of GWs off a membrane with with a given shear and bulk viscosity also showed the presence of superradiant amplification at low frequencies. However, this effect was classified as spurious in [417], because no ergoregions are present at linear order in the spin. As we argue here, superradiance requires no ergoregions—absorption (induced by viscosity) and rotation provide the necessary mechanism for superradiant amplification.

Amplification is not confined to the classical superradiant regime $0 < \omega < m\Omega$, unlike known literature on black holes [83], conducting stars [102], or what one may naively obtain by analyzing simplified models for dissipation (see Ref. [98]). The linear-in-spin approximation leads to an inconsistent expansion, which might

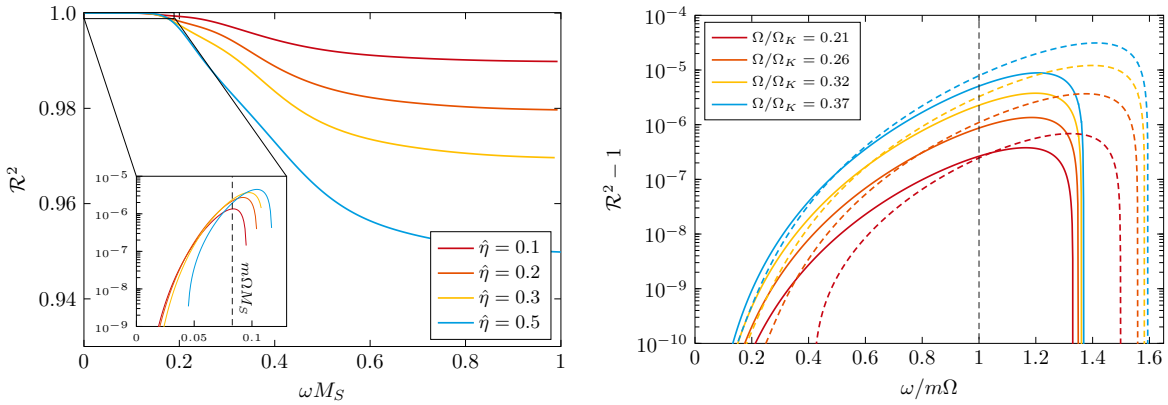

Figure 47 **Left:** Reflectivity as a function of the dimensionless frequency ωM_S, for different values of the dimensionless shear viscosity parameter $\hat{\eta}$. The inset shows the amplification $\mathcal{R}^2 - 1$ for frequencies lower than or comparable to the angular frequency of the star. In all three cases we observe superradiant amplification, though the superradiant region varies slightly in each case. We recover similar qualitative results as in [80] in the high-frequency limit, where viscosity induces absorption. In this case, $\hat{\tau} = 500$, and $\Omega/\Omega_K = 0.26$. **Right:** Amplification factor $\mathcal{R}^2 - 1$ as a function of the dimensionless frequency $\omega/m\Omega$, for different values of the angular velocity of the star Ω/Ω_K (see legend). Solid (dashed) lines correspond to $\hat{\eta} = 0.1(0.3)$, while $\hat{\tau} = 500$ is fixed.

explain these features: on the one hand, we include terms which are quadratic in $\omega \lesssim \Omega$, while neglecting terms of $\mathcal{O}(\Omega^2)$. This is a known issue [26, 368], which means that our quantitative results should be read with caution. Despite the thermodynamic arguments justifying the presence of amplification and our results, a second-order-in-spin calculation is required to confirm these results.

We investigate the dependence of superradiant amplification on parameter space more thoroughly in the right panel of Fig. 47. Although not shown in the Figure, we report a very mild dependence on $\hat{\tau}$. However, it is particularly challenging to obtain accurate solutions, including superradiance, in the regime where $\hat{\eta}/\hat{\tau}$ is large, or at very low frequencies $\omega \ll m\Omega_K$.

We find that the maximum amplification rate increases both with the rotation rate and the shear viscosity: higher angular velocities mean more angular momentum is available to be extracted from the star, whereas higher shear viscosity enhances the absorption cross-section [80]. We emphasize again that superradiant amplification occurs outside the classically allowed region, and this is enhanced by higher values of the dimensionless shear viscosity. On top of missing second-order-in-spin effects [26], this hints that the thermodynamic argument presented may need to account for nonequilibrium effects [169], possibly leading to a viscosity-dependent superradiant threshold. Once again, a second-order-in-spin calculation is urgent to clarify this.

Our results could be relevant for the physics of spinning ultracompact objects. When the object is so compact that an unstable light ring is present, a *stable* light ring must also feature in the geometry [152]. Perturbations around such objects decay logarithmically in time [58, 104, 272, 474]. The slow decay of linearized fluctuations

has led to the conjecture that nonlinearities may turn such objects unstable [104, 272], although recent results fail to find evidence of such instability [189, 329, 396]. Through numerical examination we found in previous sections that the frequency of *scalar* modes trapped in ultracompact objects scales as $\omega \sim m(\Omega_{\rm sLR} + \Omega)$, where $\Omega_{\rm sLR} = e^{\nu/2}/r$ is the angular frequency of the stable light ring in the nonrotating limit, and Ω is the angular speed of the object. We expect the same behaviour to occur for spacetime w-modes. By making the object compact enough, the lapse $e^{\nu} \to 0$ inside the object, so $\Omega_{\rm sLR}$ can be made parametrically small. However, the frame dragging term ensures that the frequency of these trapped modes always exceeds the superradiant threshold, $\omega > m\Omega$. Amplified waves are not trapped, and trapped radiation is not amplified. This supports the linear stability of ultracompact objects, even with rotation and dissipation, though it remains an open question whether an instability could be triggered in the rapidly rotating limit, when ergoregions may appear, or when accounting for nonlinear effects. One possible way an instability could develop is whenever the star features (gravity) g-modes due to stratification, which can have lower frequencies than $m\Omega$ (see Fig. 6 in Ref. [199]). A open question would be to determine whether g-modes become superradiantly unstable in the presence of viscosity.

The above concerns uniform rotation. From the above, it is also quite likely that differentially rotating stars may be strongly impacted by viscous instabilities. Indeed, the physics of viscous fluids may also render accretion disks—intrinsically differentially rotating structures—dynamically unstable.

12.6 CONCLUSIONS

In this chapter we have studied the superradiant amplification of GWs by rotating viscous stars. Building upon Zeldovich's arguments, we now provide a first-principled example where superradiant amplification of GWs occurs without horizons and without ergoregions. The only mechanism responsible for the superradiant amplification, as evidenced by the thermodynamic argument presented, is the combination of absorption (provided, in this case, by dissipative effects in the fluid), and frame-dragging. Together with the amplification of any massless field by black holes [83, 386], of sound waves by fluids [62, 105] (recently reported experimentally [449]), and of electromagnetic waves by conducting materials [51, 469] (recently reported experimentally [151]), our results paint a clear picture of energy extraction by spinning objects.

Noticeably, our findings for the regime of superradiant amplification are considerably more complex than previously reported in gravitational or electromagnetic wave superradiance. However, we find a similarly rich pattern in the amplification of sound waves at planar interfaces that separate an ideal fluid from a viscous one [340, 405]. A followup problem is to examine the backreaction of superradiant amplification onto the star, and consequent spindown, in the presence of dissipative effects.

Note that our analysis assumes slow rotation, retaining only terms linear in $\epsilon = \Omega/\Omega_K$. However, by examining the regime $\omega \lesssim \Omega$, we effectively incorporate some $\mathcal{O}(\epsilon^2)$ contributions, formally beyond our approximation. This issue is known from early studies of the r-mode instability [26]. Thus, results at high angular velocities or low frequencies should be considered merely informative, serving as a useful baseline. A second-order calculation, though technically challenging, would be a natural next step to better quantify the amplification of radiation by rotating, compact objects.

Part IV

CONCLUSION

También será posible / que esa hermosa mañana
ni tú, ni yo, ni el otro / la lleguemos a ver.
Pero habrá que forzarla / para que pueda ser.

— *José Antonio Labordeta*, Canto a la Libertad

13

FINAL WORDS

Written while listening to music composed by Gustav Mahler.

This thesis begun motivated by the counterintuitive dynamics of turbulence and by the fascinating description of the gravitational interaction provided by General Relativity. Moreover, this thesis has been carried out at a very particular moment in time. This moment marks a transition between the first steps of gravitational wave (GW) astronomy, and its adulthood. At this point in time, GWs are a reality. Their detection and remarkable agreement with predictions of General Relativity [4, 7] confirms that Einstein's theory is an accurate paradigm to describe even the nonlinear encounters and mergers of extremely compact objects such as black holes (BHs). The adulthood of GWs will answer key questions in the dynamics of stars and galaxies, will chart the cosmological evolution of the Universe, and may provide key insights towards understanding dark matter. However, a question hangs over this transitional moment, whispering *is this all?*. Obviously not.

Increased accuracy in GW observations will allow us to put General Relativity really under the microscope. The answer may lie in the next decimal place, and we ought to look for that. In particular, this enhanced precision will force us to understand the transition between a strongly nonlinear moment of spacetime (the BH merger), and an approximately linear or laminar regime. The questions that motivated this thesis on turbulence and nonlinear dynamics are just around the corner, and our theoretical understanding must rise to the occasion. Similarly, the next decades will likely see a revolution in our understanding of nuclear matter. GW observations of merging neutron stars, in correspondence with progress in particle physics experiments, will allow us to finally chart the phase diagram of quantum chromodynamics. The humble goal of this thesis has been to advance our knowledge of gravitation and the physics of BHs and neutron stars.

The first half of this thesis is devoted to the relaxation of BHs. The BH ringdown stands as one of the most promising laboratories to probe General Relativity and, in particular, to test the nonlinear dynamics of strong gravitational fields. Current Earth-based observations are reaching incredible accuracies, even in the BH ringdown. A remarkable example is the recent observation GW250114, achieving a signal to noise ratio ~ 40 in the ringdown alone [3]. This enabled the detection of two distinct characteristic modes (QNMs) of the remnant BH, although with limited accuracy. However, this heralds an era of multi-mode BH spectroscopy. The spaced-based observatory LISA is perhaps the most exciting prospect for ringdown physics. In

particular, ringdown GWs from merging supermassive BHs can be detected with LISA with a signal-to-noise ratio that is one or more orders of magnitude larger than GW250114 [67, 464]. This will enable extremely accurate BH spectroscopy measurements, entering uncharted territory.

General Relativity is a nonlinear theory, and thus it should not come out as a surprise that QNMs can couple nonlinearly. In nonlinear optics, for instance, this effect is just dubbed higher-harmonic generation, and is the technological basis behind, e. g., green laser pointers. Studying this effect in rotating BHs, and predicting the amplitudes of quadratic QNMs is one of the key results of the first half of this thesis. In Chapter 5 I present results obtained from the evolution of a perturbed rotating BH including second-order effects. Carefully extracting all possible mode content from the ringdown signal, these second-order effects demonstrate the existence of higher-harmonics, i. e., QQNMs. I demonstrate that the amplitude of the QQNMs is uniquely fixed by the amplitude of the parent modes and the BH spin. This means that by measuring these amplitudes from GW observations and contrasting them against theoretical results such as those presented in this thesis we can test a prediction of General Relativity in the nonlinear regime. Once again, LISA stands as a promising candidate to be able to carry out such tests [464].

Chapter 5 also shows interesting features of the excitation of these QQNMs in the high-frequency regime. This regime is not of direct relevance for astrophysical BH mergers, but it raises important questions about the nonlinear stability of BH spacetimes. Therefore, I explored in further detail these effects in Chapter 6. The key realisation is twofold: (i) the spacetime close to any null geodesic may be well approximated by a plane wave spacetime [374], and (ii) high-frequency perturbations to a BH are localised close to the light ring, which is a null geodesic. Chapter 5 therefore studies, for the first time, second-order gravitational perturbations on a plane wave spacetime in a systematic way. This enables the analytic calculation of QQNM amplitudes, albeit relative to a frame adapted to the plane wave geometry, and valid only at the light ring and not at infinity (where we observe the GW emission). However, the correspondence between BH perturbations and the dynamics of plane waves beyond the linear regime initiated here is a promising avenue to study nonlinear effects in BHs.

Next, the thesis moves on from higher harmonic generation to study another effect of relevance in the transition between the merger towards the BH ringdown. During the very first instants of the life of the "merged" BH, its mass and spin evolve significantly. Properly studying that regime would require pushing perturbation theory to third order, which is an open problem to this day. Instead, in Chapter 7 we study perturbations of an exact solution to Einstein equations (the *Vaidya* spacetime), describing a BH accreting a spherical shell of radiation. Although this is a simplification, it allows us to clearly show *spectral broadening*: the BH no longer oscillates with a concrete frequency, but rather with a frequency that evolves coherently with the accretion of mass. The results presented in this chapter demonstrate our ability to

model the time-evolution of the QNM frequencies, once we can model the growth of the ringing BH.

Finally, Chapter 8 directly aims to connect turbulent dynamics with GW physics. The setting is motivated by a conjecture related to the nonlinear stability of spacetimes featuring *stable trapping*, i. e., regions where GWs can be trapped for a long time. By studying a simplified wave equation, which aims to capture some features of Einstein's equations, our results show that once waves are trapped, they evolve according to a direct energy cascade. Chapter 8 directly shows that if confined, gravitational systems can lead to, e. g., Kolmogorov-Zakharov spectra, which are a clear smoking gun of turbulence.

Overall, this first part of the thesis begins to draw a coherent picture regarding nonlinear dynamics in the post-merger emission of GWs: (i) nonlinearities allow for mode coupling, which manifests itself more strongly in the higher harmonics of the signal, and will be observable in the near future, (ii) the dynamical evolution of the BH in the early ringdown may lead to spectral broadening, and therefore to time-dependent QNM amplitudes and frequencies, that will need to be modelled to achieve high-accuracy BH spectroscopy, and (iii) in the presence of trapping, the nonlinear development may be radically different. BHs are extremely *leaky* systems, as GWs are easily radiated towards infinity, or fall towards the horizon. However, BHs rotating close to the speed of light can confine GWs for a longer time, and we can expect stronger signatures of nonlinear phenomena, or event turbulence, in the ringdown of near-extremal BHs.

The second part of the thesis abandons vacuum to immerse itself in the dynamics of matter fields in General Relativity. Hydrodynamics provides the most general framework to study this, and in particular *dissipative* effects play a crucial role at coupling the dynamics of matter with the propagation of GWs [237], which is reviewed in Chapter 9. The model problem we consider is the perturbations of a neutron star, which is driven out of equilibrium by incoming GWs. Firstly, Chapter 10 sets the foundations to study problems like this. The result of this chapter is a set of master equations describing both spacetime and fluid perturbations of a spherically symmetric neutron star, capturing viscous effects in the context of a well-posed theory of first-order hydrodynamics. Therefore, the results of this chapter will be foundational towards future studies of the importance of viscosity in the dynamics of neutron stars.

Next, Chapter 11 solves the aforementioned equations in a particular sector, obtaining a number of novel results: (i) GWs can be absorbed by a neutron star, by depositing energy into differential rotation, which is in turn dissipated through shear viscosity, (ii) shear viscosity leads to the appearance of a new family of oscillation modes of the star, with frequencies that we estimate as $f_\eta \sim 1\text{kHz}$, and damping times that are strongly dependent on the scale of the viscous parameters, and (iii) other oscillation modes of the star such as spacetime (w-) modes are affected by the presence of viscosity. This paves the way to infer the scale of transport coefficients from GW asteroseismology. Finally, chapter 12 extends this discussion to slowly-rotating stars. This unveils a new phenomena: *superradiance*, demonstrating for the

first time the amplification of low-frequency GWs in the absence of ergoregions and horizons.

13.1 FUTURE DIRECTIONS

The research carried out in this thesis paves the way for a number of future research directions. These are very concisely summarised here.

13.1.1 *in Vacuum*

1. *Detection of QQNMs:* LISA and third-generation detectors will likely have enough sensitivity to enable the observation of QQNMs, emitted during the merger of supermassive BHs. Accurate measurements of their amplitudes can be contrasted with theoretical predictions and used as a novel test of General Relativity. However, further efforts in GW data analysis specific to these new detectors, as well as accurate and robust ringdown data analysis pipelines are absolutely necessary to make these measurements a reality. Some recent efforts in these directions are featured in Refs. [97, 380, 465].

2. *Nonlinear dynamics of near-extremal BHs:* Rapidly rotating BHs have much larger quality factors than non rotating BHs. This leaves more time for the nonlinear development of the spacetime disturbances after a BH merger. Superradiance [180] can also amplify frequencies close to the fundamental mode frequency in the near-extremal limit. All of these effects may lead to strongly nonlinear and possibly turbulent dynamics. The observational consequences are, nevertheless, limited by the existence or not of rapidly rotating BHs in the Universe. Radiation effects already seem to impose a sharp limit on the BH spin at $a/M \leq 0.998$ [442].

3. *Driven Turbulence:* Most theoretical studies have restricted their attention to the free relaxation of perturbed BHs. Although this is more comparable to astrophysical scenarios such as BH mergers, it is not necessarily the regime where one may expect nonlinear dynamics to take place. For instance, the nonlinear dynamics of the ocean is heavily influenced by strong winds driving and exciting surface waves. Triple systems are an astrophysically viable candidate to drive a BH spacetime possibly into the nonlinear regime [418]. Recently, Ref [323] has studied the development of an inverse turbulent cascade at the BH horizon by driving a non rotating BH with GWs from the boundary of a numerical simulation. This opens the door for many open questions regarding driving spacetimes with GWs.

4. *Higher Dimensions:* The turbulent dynamics in $2+1$ dimensional hydrodynamics is different than in $d+1$ with $d \geq 3$. Is it possible that 4 spacetime dimensions is special for gravitational physics? Studying nonlinear phenomena

in higher dimensions can potentially answer this question, but is a remarkably difficult problem, both perturbatively and numerically.

13.1.2 *non Vacuum*

1. *Nonlinear dynamics of charged BHs:* The simplest extension beyond vacuum General Relativity is possibly provided by the Einstein-Maxwell system. In particular, this allows to endow BHs with an electric (or magnetic) charge. Remarkably, recent research has shown that within this theory, extremal BHs can form dynamically in a finite amount of time from gravitational collapse [179, 270, 271]. The presence of additional matter fields can possibly enrich the nonlinear relaxation of BHs to equilibrium. Therefore, it is theoretically exciting to question whether BHs in vacuum behave fundamentally different to BHs coupled to matter fields.

2. *Tides of viscous neutron stars:* One of the main targets of GW observations of merging neutron stars is improving our understanding of matter beyond nuclear density. Current observations can give us information about the mass and radius of the star - information that is, in essence, sensitive to the equation of state. However, this is not sufficient to discern whether, e. g., there are deconfined quarks or hypernuclear matter in the core of neutron stars. The viscous transport coefficients provide complementary information to the equation of state, and are a particularly good probe of such physics [210, 211, 347]. One way to measure these viscous coefficients from GW observations is through the measurement of GW dephasing during the late inspiral. In the last stages of the inspiral, dissipative tidal effects and tidal heating (in essence, dephasing induced due to the friction between the tidal bulge and the star itself) are a clear observational signature that is directly linked to viscous coefficients [410]. A first-principles calculation of the dissipative tidal effects of a neutron star within a well-posed theory of hydrodynamics is still, remarkably, lacking.

3. *Modes of viscous neutron stars:* Another observational prospect of viscosity in the GW emission of neutron star mergers is the frequency of f-modes. These are the oscillation modes of the post-merger remnant (whenever it does not immediately collapse into a BH), and depend not only on the equation of state, but also on the scale of viscous effects [123, 124]. The framework developed in this thesis provides a natural starting point to quantifying the impact of viscosity on the f-modes of postmerger remnants.

4. *Accretion disks:* BHs may merge inside active galactic nuclei or accretion disks. The GWs they emit do not travel through vacuum, and they will perturb the disk out of equilibrium. The disk will later relax to equilibrium by emitting electromagnetic radiation that can possibly be observable [279, 280]. Properly studying the effect of GWs emitted inside and propagating through an accretion disk is a necessary step to quantify and model this electromagnetic

emission. Bright counterparts to BH mergers would enable measurements of the Hubble constant and directly link BH demographics to different formation channels, answering key questions in cosmology and galactic dynamics.

13.2 EPILOGUE

We are now leaving the "advent of GW astronomy" to enter into its adulthood. These cosmic messengers, first predicted more than 100 years ago, and observed for a decade now, are revolutionising our knowledge about the cosmos. It is impossible not to feel excited about the answers that we will have in a decade, with incredibly more accurate data enabled by upgrades to current detectors, as well as new GW observatories such as LISA [21], Cosmic Explorer [403], and Einstein Telescope [328]. Moreover, it is impossible not to feel excited about which questions we will be asking ourselves, enlightened by this new wealth of data. Only time will tell.

The conclusion of this PhD thesis means that, in a way, I am transitioning into my scientific adulthood. This thesis has given me the brilliant opportunity to study strong gravity systems from a variety of angles, balancing perturbation theory, numerics, data analysis, and observations; and tackling both the nonlinear dynamics of pure vacuum and the structure of some of the most complex stars in the cosmos. GW science is ultimately an interdisciplinar effort, where insights from high-energy physics, stellar dynamics, gravity, geometry, statistics, and computational physics are necessary and interplay with each other.

The previous list of open questions, which directly feeds from the research of this thesis, is just a small fraction of my own research interests. The whole landscape of GW observations offers a vast wealth of exciting questions, ripe to be answered. I find most beauty, and most pleasure, in tackling those problems where multiple fields and points of view collide, those nails for which not one hammer is good enough, and one may need to use the whole toolkit. I believe it is by bridging those ideas that science advances. This makes the challenge ever more difficult, but only more exciting, leaving only to hope that this road ahead is a long one, full of adventure, full of discovery.

BIBLIOGRAPHY

[1] Check the Center of Gravity webpage for publicly available material: https://the-center-of-gravity.com/.

[2] A. G. Abac et al. "GW231123: A Binary Black Hole Merger with Total Mass 190–265 $M_\odot$." In: *Astrophys. J. Lett.* 993.1 (2025), p. L25. DOI: 10.3847/2041-8213/ae0c9c. arXiv: 2507.08219 [astro-ph.HE].

[3] A. G. Abac et al. "GW250114: Testing Hawking's Area Law and the Kerr Nature of Black Holes." In: *Phys. Rev. Lett.* 135.11 (2025), p. 111403. DOI: 10.1103/kw5g-d732. arXiv: 2509.08054 [gr-qc].

[4] B. P. Abbott et al. "Observation of Gravitational Waves from a Binary Black Hole Merger." In: *Phys. Rev. Lett.* 116.6 (2016), p. 061102. DOI: 10.1103/PhysRevLett.116.061102. arXiv: 1602.03837 [gr-qc].

[5] B. P. Abbott et al. "Tests of general relativity with GW150914." In: *Phys. Rev. Lett.* 116.22 (2016). [Erratum: Phys.Rev.Lett. 121, 129902 (2018)], p. 221101. DOI: 10.1103/PhysRevLett.116.221101. arXiv: 1602.03841 [gr-qc].

[6] B. P. Abbott et al. "Gravitational Waves and Gamma-rays from a Binary Neutron Star Merger: GW170817 and GRB 170817A." In: *Astrophys. J. Lett.* 848.2 (2017), p. L13. DOI: 10.3847/2041-8213/aa920c. arXiv: 1710.05834 [astro-ph.HE].

[7] R. Abbott et al. "Tests of General Relativity with GWTC-3." In: (Dec. 2021). arXiv: 2112.06861 [gr-qc].

[8] R. Abbott et al. "Tests of general relativity with binary black holes from the second LIGO-Virgo gravitational-wave transient catalog." In: *Phys. Rev. D* 103.12 (2021), p. 122002. DOI: 10.1103/PhysRevD.103.122002. arXiv: 2010.14529 [gr-qc].

[9] Elcio Abdalla, Cecilia B. M. H. Chirenti, and Alberto Saa. "Quasinormal modes for the Vaidya metric." In: *Phys. Rev. D* 74 (2006), p. 084029. DOI: 10.1103/PhysRevD.74.084029. arXiv: gr-qc/0609036.

[10] Tim Adamo et al. "Amplitudes on plane waves from ambitwistor strings." In: *JHEP* 11 (2017), p. 160. DOI: 10.1007/JHEP11(2017)160. arXiv: 1708.09249 [hep-th].

[11] Niayesh Afshordi et al. "Black Holes Inside and Out 2024: visions for the future of black hole physics." In: ed. by Luca Buoninfante et al. Oct. 2024. arXiv: 2410.14414 [gr-qc].

[12] J. M. Aguirregabiria and C. V. Vishveshwara. "Scattering by black holes: A Simulated potential approach." In: *Phys. Lett. A* 210 (1996), pp. 251–254. DOI: 10.1016/0375-9601(95)00937-X.

[13] Ofer Aharony et al. "Loops in AdS from Conformal Field Theory." In: *JHEP* 07 (2017), p. 036. DOI: 10.1007/JHEP07(2017)036. arXiv: 1612.03891 [hep-th].

[14] Kazunori Akiyama et al. "First M87 Event Horizon Telescope Results. I. The Shadow of the Supermassive Black Hole." In: *Astrophys. J. Lett.* 875 (2019), p. L1. DOI: 10.3847/2041-8213/ab0ec7. arXiv: 1906.11238 [astro-ph.GA].

[15] Kazunori Akiyama et al. "First Sagittarius A* Event Horizon Telescope Results. VI. Testing the Black Hole Metric." In: *Astrophys. J. Lett.* 930.2 (2022), p. L17. DOI: 10.3847/2041-8213/ac6756. arXiv: 2311.09484 [astro-ph.HE].

[16] Steffen Aksteiner. "Geometry and analysis on black hole spacetimes." PhD thesis. Leibniz U., Hannover, 2014. DOI: 10.15488/8214.

[17] Mark G. Alford and Alexander Haber. "Strangeness-changing Rates and Hyperonic Bulk Viscosity in Neutron Star Mergers." In: *Phys. Rev. C* 103.4 (2021), p. 045810. DOI: 10.1103/PhysRevC.103.045810. arXiv: 2009.05181 [nucl-th].

[18] Mark G. Alford and Steven P. Harris. "Beta equilibrium in neutron star mergers." In: *Phys. Rev. C* 98.6 (2018), p. 065806. DOI: 10.1103/PhysRevC.98.065806. arXiv: 1803.00662 [nucl-th].

[19] Mark G. Alford, Simin Mahmoodifar, and Kai Schwenzer. "Large amplitude behavior of the bulk viscosity of dense matter." In: *J. Phys. G* 37 (2010), p. 125202. DOI: 10.1088/0954-3899/37/12/125202. arXiv: 1005.3769 [nucl-th].

[20] Mark G. Alford et al. "Viscous Dissipation and Heat Conduction in Binary Neutron-Star Mergers." In: *Phys. Rev. Lett.* 120.4 (2018), p. 041101. DOI: 10.1103/PhysRevLett.120.041101. arXiv: 1707.09475 [gr-qc].

[21] Pau Amaro-Seoane et al. "Laser Interferometer Space Antenna." In: (Feb. 2017). arXiv: 1702.00786 [astro-ph.IM].

[22] Lars Andersson et al. "Stability for Linearized Gravity on the Kerr Spacetime." In: *Ann. PDE* 11.1 (2025), p. 11. DOI: 10.1007/s40818-024-00193-w. arXiv: 1903.03859 [math.AP].

[23] N. Andersson and G. L. Comer. "On the dynamics of superfluid neutron star cores." In: *Mon. Not. Roy. Astron. Soc.* 328 (2001), p. 1129. DOI: 10.1046/j.1365-8711.2001.04923.x. arXiv: astro-ph/0101193.

[24] Nils Andersson. "Evolving test fields in a black hole geometry." In: *Phys. Rev. D* 55 (1997), pp. 468–479. DOI: 10.1103/PhysRevD.55.468. arXiv: gr-qc/9607064.

[25] Nils Andersson. "A New class of unstable modes of rotating relativistic stars." In: *Astrophys. J.* 502 (1998), pp. 708–713. DOI: 10.1086/305919. arXiv: gr-qc/9706075.

[26] Nils Andersson and Kostas D. Kokkotas. "Towards gravitational wave asteroseismology." In: *Mon. Not. Roy. Astron. Soc.* 299 (1998), pp. 1059–1068. DOI: 10.1046/j.1365-8711.1998.01840.x. arXiv: gr-qc/9711088.

[27] Nils Andersson and Kostas D. Kokkotas. "The R mode instability in rotating neutron stars." In: *Int. J. Mod. Phys. D* 10 (2001), pp. 381–442. DOI: 10.1142/S0218271801001062. arXiv: gr-qc/0010102.

[28] Nils Andersson, Kostas D. Kokkotas, and Bernard F. Schutz. "Space-time modes of relativistic stars." In: *Mon. Not. Roy. Astron. Soc.* 280 (1996), p. 1230. DOI: 10.1093/mnras/280.4.1230. arXiv: gr-qc/9601015.

[29] Marcus Ansorg and Rodrigo Panosso Macedo. "Spectral decomposition of black-hole perturbations on hyperboloidal slices." In: *Phys. Rev. D* 93.12 (2016), p. 124016. DOI: 10.1103/PhysRevD.93.124016. arXiv: 1604.02261 [gr-qc].

[30] Nima Arkani-Hamed and Juan Maldacena. "Cosmological Collider Physics." In: (Mar. 2015). arXiv: 1503.08043 [hep-th].

[31] Jay Armas and Filippo Camilloni. "A stable and causal model of magnetohydrodynamics." In: *JCAP* 10 (2022), p. 039. DOI: 10.1088/1475-7516/2022/10/039. arXiv: 2201.06847 [hep-th].

[32] Matias Montesinos Armijo. "Review: Accretion Disk Theory." In: (Mar. 2012). arXiv: 1203.6851 [astro-ph.HE].

[33] Phil Arras et al. "Saturation of the R mode instability." In: *Astrophys. J.* 591 (2003), pp. 1129–1151. DOI: 10.1086/374657. arXiv: astro-ph/0202345.

[34] Asimina Arvanitaki and Sergei Dubovsky. "Exploring the String Axiverse with Precision Black Hole Physics." In: *Phys. Rev. D* 83 (2011), p. 044026. DOI: 10.1103/PhysRevD.83.044026. arXiv: 1004.3558 [hep-th].

[35] Navdeep Arya and Magdalena Zych. "Selective Amplification of a Gravitational Wave Signal Using an Atomic Array." In: (Aug. 2024). arXiv: 2408.12436 [quant-ph].

[36] D. Ayzenberg et al. "Fundamental Physics Opportunities with the Next-Generation Event Horizon Telescope." In: (Dec. 2023). arXiv: 2312.02130 [astro-ph.HE].

[37] A Bachelot and J-P Nicolas. "Equation non linéaire de Klein-Gordon dans des métriques de type Schwarzschild." In: *Comptes rendus de l'Académie des sciences. Série 1, Mathématique* 316.10 (1993), pp. 1047–1050.

[38] Ibrahima Bah and Pierre Heidmann. "Topological Stars and Black Holes." In: *Phys. Rev. Lett.* 126.15 (2021), p. 151101. DOI: 10.1103/PhysRevLett.126.151101. arXiv: 2011.08851 [hep-th].

[39] Vishal Baibhav et al. "Agnostic black hole spectroscopy: Quasinormal mode content of numerical relativity waveforms and limits of validity of linear perturbation theory." In: *Phys. Rev. D* 108.10 (2023), p. 104020. DOI: 10.1103/PhysRevD.108.104020. arXiv: 2302.03050 [gr-qc].

[40] John G. Baker et al. "Gravitational wave extraction from an inspiraling configuration of merging black holes." In: *Phys. Rev. Lett.* 96 (2006), p. 111102. DOI: 10.1103/PhysRevLett.96.111102. arXiv: gr-qc/0511103.

[41] Venkat Balasubramanian et al. "Holographic Thermalization, Stability of Anti–de Sitter Space, and the Fermi-Pasta-Ulam Paradox." In: *Phys. Rev. Lett.* 113.7 (2014), p. 071601. DOI: 10.1103/PhysRevLett.113.071601. arXiv: 1403.6471 [hep-th].

[42] Jamie Bamber et al. "Quasinormal modes of growing dirty black holes." In: *Phys. Rev. D* 103.12 (2021), p. 124013. DOI: 10.1103/PhysRevD.103.124013. arXiv: 2103.00026 [gr-qc].

[43] Hans Bantilan, Yago Bea, and Pau Figueras. "Evolutions in first-order viscous hydrodynamics." In: *JHEP* 08 (2022), p. 298. DOI: 10.1007/JHEP08(2022)298. arXiv: 2201.13359 [hep-th].

[44] Leor Barack. "Late time dynamics of scalar perturbations outside black holes. 1. A Shell toy model." In: *Phys. Rev. D* 59 (1999), p. 044016. DOI: 10.1103/PhysRevD.59.044016. arXiv: gr-qc/9811027.

[45] Leor Barack. "Late time dynamics of scalar perturbations outside black holes. 2. Schwarzschild geometry." In: *Phys. Rev. D* 59 (1999), p. 044017. DOI: 10.1103/PhysRevD.59.044017. arXiv: gr-qc/9811028.

[46] Enrico Barausse, Vitor Cardoso, and Paolo Pani. "Can environmental effects spoil precision gravitational-wave astrophysics?" In: *Phys. Rev. D* 89.10 (2014), p. 104059. DOI: 10.1103/PhysRevD.89.104059. arXiv: 1404.7149 [gr-qc].

[47] Enrico Barausse et al. "Divergences in gravitational-wave emission and absorption from extreme mass ratio binaries." In: *Phys. Rev. D* 104.6 (2021), p. 064031. DOI: 10.1103/PhysRevD.104.064031. arXiv: 2106.09721 [gr-qc].

[48] James M. Bardeen, William H. Press, and Saul A Teukolsky. "Rotating black holes: Locally nonrotating frames, energy extraction, and scalar synchrotron radiation." In: *Astrophys. J.* 178 (1972), p. 347. DOI: 10.1086/151796.

[49] Yago Bea. "Relativistic Navier-Stokes description of the quark-gluon plasma radial flow." In: (Mar. 2025). arXiv: 2503.02931 [hep-ph].

[50] Yago Bea and Pau Figueras. "Field redefinitions and evolutions in relativistic Navier-Stokes." In: *JHEP* 11 (2024), p. 110. DOI: 10.1007/JHEP11(2024)110. arXiv: 2312.16671 [hep-th].

[51] Jacob D. Bekenstein and Marcelo Schiffer. "The Many faces of superradiance." In: *Phys. Rev. D* 58 (1998), p. 064014. DOI: 10.1103/PhysRevD.58.064014. arXiv: gr-qc/9803033.

[52] Fábio S. Bemfica, Marcelo M. Disconzi, and Jorge Noronha. "Causality and existence of solutions of relativistic viscous fluid dynamics with gravity." In: *Phys. Rev. D* 98.10 (2018), p. 104064. DOI: 10.1103/PhysRevD.98.104064. arXiv: 1708.06255 [gr-qc].

[53] Fabio S. Bemfica, Marcelo M. Disconzi, and Jorge Noronha. "Causality of the Einstein-Israel-Stewart Theory with Bulk Viscosity." In: *Phys. Rev. Lett.* 122.22 (2019), p. 221602. DOI: 10.1103/PhysRevLett.122.221602. arXiv: 1901.06701 [gr-qc].

[54] Fabio S. Bemfica, Marcelo M. Disconzi, and Jorge Noronha. "First-Order General-Relativistic Viscous Fluid Dynamics." In: *Phys. Rev. X* 12.2 (2022), p. 021044. DOI: 10.1103/PhysRevX.12.021044. arXiv: 2009.11388 [gr-qc].

[55] Fábio S. Bemfica et al. "Nonlinear Causality of General First-Order Relativistic Viscous Hydrodynamics." In: *Phys. Rev. D* 100.10 (2019). [Erratum: Phys.Rev.D 105, 069902 (2022)], p. 104020. DOI: 10.1103/PhysRevD.100.104020. arXiv: 1907.12695 [gr-qc].

[56] Paolo Benincasa. "Amplitudes meet Cosmology: A (Scalar) Primer." In: (Mar. 2022). DOI: 10.1142/S0217751X22300101. arXiv: 2203.15330 [hep-th].

[57] Gabriele Benomio. "The stable trapping phenomenon for black strings and black rings and its obstructions on the decay of linear waves." In: *Anal. Part. Diff. Eq.* 14.8 (2021), pp. 2427–2496. DOI: 10.2140/apde.2021.14.2427. arXiv: 1809.07795 [gr-qc].

[58] Gabriele Benomio et al. "Turbulence for spacetimes with stable trapping." In: *Phys. Rev. D* 111.10 (2025), p. 104037. DOI: 10.1103/PhysRevD.111.104037. arXiv: 2411.17445 [gr-qc].

[59] Roman Berens, Trevor Gravely, and Alexandru Lupsasca. "Gravitational waves on Kerr black holes: I. Reconstruction of linearized metric perturbations." In: *Class. Quant. Grav.* 41.19 (2024), p. 195004. DOI: 10.1088/1361-6382/ad6c9c. arXiv: 2403.20311 [gr-qc].

[60] Sebastiano Bernuzzi et al. "How loud are neutron star mergers?" In: *Phys. Rev. D* 94.2 (2016), p. 024023. DOI: 10.1103/PhysRevD.94.024023. arXiv: 1512.06397 [gr-qc].

[61] Emanuele Berti and Vitor Cardoso. "Quasinormal ringing of Kerr black holes. I. The Excitation factors." In: *Phys. Rev. D* 74 (2006), p. 104020. DOI: 10.1103/PhysRevD.74.104020. arXiv: gr-qc/0605118.

[62] Emanuele Berti, Vitor Cardoso, and Jose P. S. Lemos. "Quasinormal modes and classical wave propagation in analogue black holes." In: *Phys. Rev. D* 70 (2004), p. 124006. DOI: 10.1103/PhysRevD.70.124006. arXiv: gr-qc/0408099.

[63] Emanuele Berti, Vitor Cardoso, and Paolo Pani. "Breit-Wigner resonances and the quasinormal modes of anti-de Sitter black holes." In: *Phys. Rev. D* 79 (2009), p. 101501. DOI: 10.1103/PhysRevD.79.101501. arXiv: 0903.5311 [gr-qc].

[64] Emanuele Berti, Vitor Cardoso, and Andrei O. Starinets. "Quasinormal modes of black holes and black branes." In: *Class. Quant. Grav.* 26 (2009), p. 163001. DOI: 10.1088/0264-9381/26/16/163001. arXiv: 0905.2975 [gr-qc].

[65] Emanuele Berti, Vitor Cardoso, and Clifford M. Will. "On gravitational-wave spectroscopy of massive black holes with the space interferometer LISA." In: *Phys. Rev. D* 73 (2006), p. 064030. DOI: 10.1103/PhysRevD.73.064030. arXiv: gr-qc/0512160.

[66] Emanuele Berti and Antoine Klein. "Mixing of spherical and spheroidal modes in perturbed Kerr black holes." In: *Phys. Rev. D* 90.6 (2014), p. 064012. DOI: 10.1103/PhysRevD.90.064012. arXiv: 1408.1860 [gr-qc].

[67] Emanuele Berti et al. "Spectroscopy of Kerr black holes with Earth- and space-based interferometers." In: *Phys. Rev. Lett.* 117.10 (2016), p. 101102. DOI: 10.1103/PhysRevLett.117.101102. arXiv: 1605.09286 [gr-qc].

[68] Emanuele Berti et al. "Black hole spectroscopy: from theory to experiment." In: (May 2025). arXiv: 2505.23895 [gr-qc].

[69] Jérémy Besson and José Luis Jaramillo. "Quasi-normal mode expansions of black hole perturbations: a hyperboloidal Keldysh's approach." In: *Gen. Rel. Grav.* 57.7 (2025), p. 110. DOI: 10.1007/s10714-025-03438-6. arXiv: 2412.02793 [gr-qc].

[70] Swetha Bhagwat et al. "Ringdown overtones, black hole spectroscopy, and no-hair theorem tests." In: *Phys. Rev. D* 101.4 (2020), p. 044033. DOI: 10.1103/PhysRevD.101.044033. arXiv: 1910.08708 [gr-qc].

[71] Donato Bini et al. "Teukolsky master equation: De Rham wave equation for the gravitational and electromagnetic fields in vacuum." In: *Prog. Theor. Phys.* 107 (2002), pp. 967–992. DOI: 10.1143/PTP.107.967. arXiv: gr-qc/0203069.

[72] Piotr Bizoń, Maciej Maliborski, and Andrzej Rostworowski. "Resonant Dynamics and the Instability of Anti–de Sitter Spacetime." In: *Phys. Rev. Lett.* 115.8 (2015), p. 081103. DOI: 10.1103/PhysRevLett.115.081103. arXiv: 1506.03519 [gr-qc].

[73] Piotr Bizon and Andrzej Rostworowski. "On weakly turbulent instability of anti-de Sitter space." In: *Phys. Rev. Lett.* 107 (2011), p. 031102. DOI: 10.1103/PhysRevLett.107.031102. arXiv: 1104.3702 [gr-qc].

[74] *Black Hole Perturbation Toolkit*. (bhptoolkit.org).

[75] R. D. Blandford and R. L. Znajek. "Electromagnetic extractions of energy from Kerr black holes." In: *Mon. Not. Roy. Astron. Soc.* 179 (1977), pp. 433–456. DOI: 10.1093/mnras/179.3.433.

[76] Matthias Blau, Denis Frank, and Sebastian Weiss. "Fermi coordinates and Penrose limits." In: *Class. Quant. Grav.* 23 (2006), pp. 3993–4010. DOI: 10.1088/0264-9381/23/11/020. arXiv: hep-th/0603109.

[77] Matthias Blau and Martin O'Loughlin. "Homogeneous plane waves." In: *Nucl. Phys. B* 654 (2003), pp. 135–176. DOI: 10.1016/S0550-3213(03)00055-5. arXiv: hep-th/0212135.

[78] Matthias Blau et al. "Penrose limits and space-time singularities." In: *Class. Quant. Grav.* 21 (2004), p. L43. DOI: 10.1088/0264-9381/21/7/L02. arXiv: hep-th/0312029.

[79] Patrick Bourg et al. "Quadratic quasi-normal mode dependence on linear mode parity." In: (May 2024). arXiv: 2405.10270 [gr-qc].

[80] Valentin Boyanov et al. "Dynamical Response of Viscous Objects to Gravitational Waves." In: *Phys. Rev. Lett.* 135.15 (2025), p. 151402. DOI: 10.1103/smlr-v7b2. arXiv: 2411.16861 [gr-qc].

[81] John P Boyd. *Chebyshev and Fourier spectral methods*. Courier Corporation, 2001.

[82] Richard Brito, Alessandra Buonanno, and Vivien Raymond. "Black-hole Spectroscopy by Making Full Use of Gravitational-Wave Modeling." In: *Phys. Rev. D* 98.8 (2018), p. 084038. DOI: 10.1103/PhysRevD.98.084038. arXiv: 1805.00293 [gr-qc].

[83] Richard Brito, Vitor Cardoso, and Paolo Pani. "Superradiance: New Frontiers in Black Hole Physics." In: *Lect. Notes Phys.* 906 (2015), pp.1–237. DOI: 10.1007/978-3-319-19000-6. arXiv: 1501.06570 [gr-qc].

[84] David Brizuela, Jose M. Martin-Garcia, and Guillermo A. Mena Marugan. "High-order gauge-invariant perturbations of a spherical spacetime." In: *Phys. Rev. D* 76 (2007), p. 024004. DOI: 10.1103/PhysRevD.76.024004. arXiv: gr-qc/0703069.

[85] David Brizuela, Jose M. Martin-Garcia, and Manuel Tiglio. "A Complete gauge-invariant formalism for arbitrary second-order perturbations of a Schwarzschild black hole." In: *Phys. Rev. D* 80 (2009), p. 024021. DOI: 10.1103/PhysRevD.80.024021. arXiv: 0903.1134 [gr-qc].

[86] Bruno Bucciotti et al. "Amplitudes and polarizations of quadratic quasi-normal modes for a Schwarzschild black hole." In: *JHEP* 09 (2024), p. 119. DOI: 10.1007/JHEP09(2024)119. arXiv: 2406.14611 [hep-th].

[87] Bruno Bucciotti et al. "Quadratic quasinormal modes of a Schwarzschild black hole." In: *Phys. Rev. D* 110.10 (2024), p. 104048. DOI: 10.1103/PhysRevD.110.104048. arXiv: 2405.06012 [gr-qc].

[88] Bruno Bucciotti et al. "Ringdown nonlinearities in the eikonal regime." In: *Phys. Rev. D* 111.8 (2025), p. L081502. DOI: 10.1103/PhysRevD.111.L081502. arXiv: 2501.17950 [gr-qc].

[89] Alessandra Buonanno, Gregory B. Cook, and Frans Pretorius. "Inspiral, merger and ring-down of equal-mass black-hole binaries." In: *Phys. Rev. D* 75 (2007), p. 124018. DOI: 10.1103/PhysRevD.75.124018. arXiv: gr-qc/0610122.

[90] Daniel A. Caballero and Nicolás Yunes. "Neutron Star Radial Perturbations for Causal, Viscous, Relativistic Fluids." In: (June 2025). arXiv: 2506.09149 [gr-qc].

[91] Michel Cahen and Nolan Wallach. "Lorentzian symmetric spaces." In: *Bulletin of the American Mathematical Society* 76.3 (1970), pp. 585–591.

[92] Juan Calderón Bustillo, Paul D. Lasky, and Eric Thrane. "Black-hole spectroscopy, the no-hair theorem, and GW150914: Kerr versus Occam." In: *Phys. Rev. D* 103.2 (2021), p. 024041. DOI: 10.1103/PhysRevD.103.024041. arXiv: 2010.01857 [gr-qc].

[93] Giovanni Camelio et al. "Simulating bulk viscosity in neutron stars. I. Formalism." In: *Phys. Rev. D* 107.10 (2023), p. 103031. DOI: 10.1103/PhysRevD.107.103031. arXiv: 2204.11809 [gr-qc].

[94] Giovanni Camelio et al. "Simulating bulk viscosity in neutron stars. II. Evolution in spherical symmetry." In: *Phys. Rev. D* 107.10 (2023), p. 103032. DOI: 10.1103/PhysRevD.107.103032. arXiv: 2204.11810 [gr-qc].

[95] Manuela Campanelli and Carlos O. Lousto. "Second order gauge invariant gravitational perturbations of a Kerr black hole." In: *Phys. Rev. D* 59 (1999), p. 124022. DOI: 10.1103/PhysRevD.59.124022. arXiv: gr-qc/9811019.

[96] Manuela Campanelli et al. "Accurate evolutions of orbiting black-hole binaries without excision." In: *Phys. Rev. Lett.* 96 (2006), p. 111101. DOI: 10.1103/PhysRevLett.96.111101. arXiv: gr-qc/0511048.

[97] Lodovico Capuano et al. "Systematic bias in LISA ringdown analysis due to waveform inaccuracy." In: *Phys. Rev. D* 112.10 (2025), p. 104031. DOI: 10.1103/86yd-x1sl. arXiv: 2506.21181 [gr-qc].

[98] Vitor Cardoso, Richard Brito, and Joao L. Rosa. "Superradiance in stars." In: *Phys. Rev. D* 91.12 (2015), p. 124026. DOI: 10.1103/PhysRevD.91.124026. arXiv: 1505.05509 [gr-qc].

[99] Vitor Cardoso, Francisco Duque, and Gaurav Khanna. "Gravitational tuning forks and hierarchical triple systems." In: *Phys. Rev. D* 103.8 (2021), p. L081501. DOI: 10.1103/PhysRevD.103.L081501. arXiv: 2101.01186 [gr-qc].

[100] Vitor Cardoso, Edgardo Franzin, and Paolo Pani. "Is the gravitational-wave ringdown a probe of the event horizon?" In: *Phys. Rev. Lett.* 116.17 (2016). [Erratum: Phys.Rev.Lett. 117, 089902 (2016)], p. 171101. DOI: 10.1103/PhysRevLett.116.171101. arXiv: 1602.07309 [gr-qc].

[101] Vitor Cardoso, Shilpa Kastha, and Rodrigo Panosso Macedo. "Physical significance of the black hole quasinormal mode spectra instability." In: *Phys. Rev. D* 110.2 (2024), p. 024016. DOI: 10.1103/PhysRevD.110.024016. arXiv: 2404.01374 [gr-qc].

[102] Vitor Cardoso, Paolo Pani, and Tien-Tien Yu. "Superradiance in rotating stars and pulsar-timing constraints on dark photons." In: *Phys. Rev. D* 95.12 (2017), p. 124056. DOI: 10.1103/PhysRevD.95.124056. arXiv: 1704.06151 [gr-qc].

[103] Vitor Cardoso et al. "Geodesic stability, Lyapunov exponents and quasinormal modes." In: *Phys. Rev. D* 79.6 (2009), p. 064016. DOI: 10.1103/PhysRevD.79.064016. arXiv: 0812.1806 [hep-th].

[104] Vitor Cardoso et al. "Light rings as observational evidence for event horizons: long-lived modes, ergoregions and nonlinear instabilities of ultracompact objects." In: *Phys. Rev. D* 90.4 (2014), p. 044069. DOI: 10.1103/PhysRevD.90.044069. arXiv: 1406.5510 [gr-qc].

[105] Vitor Cardoso et al. "Detecting Rotational Superradiance in Fluid Laboratories." In: *Phys. Rev. Lett.* 117.27 (2016), p. 271101. DOI: 10.1103/PhysRevLett.117.271101. arXiv: 1607.01378 [gr-qc].

[106] Vitor Cardoso et al. "Gravitational-wave signatures of exotic compact objects and of quantum corrections at the horizon scale." In: *Phys. Rev. D* 94.8 (2016), p. 084031. DOI: 10.1103/PhysRevD.94.084031. arXiv: 1608.08637 [gr-qc].

[107] Vitor Cardoso et al. "Remarks on the maximum luminosity." In: *Phys. Rev. D* 97.8 (2018), p. 084013. DOI: 10.1103/PhysRevD.97.084013. arXiv: 1803.03271 [gr-qc].

[108] Vitor Cardoso et al. "Black holes in galaxies: Environmental impact on gravitational-wave generation and propagation." In: *Phys. Rev. D* 105.6 (2022), p. L061501. DOI: 10.1103/PhysRevD.105.L061501. arXiv: 2109.00005 [gr-qc].

[109] Vitor Cardoso et al. "Gravitational Waves from Extreme-Mass-Ratio Systems in Astrophysical Environments." In: *Phys. Rev. Lett.* 129.24 (2022), p. 241103. DOI: 10.1103/PhysRevLett.129.241103. arXiv: 2210.01133 [gr-qc].

[110] Vitor Cardoso et al. "Hushing black holes: Tails in dynamical spacetimes." In: *Phys. Rev. D* 109.12 (2024), p. L121502. DOI: 10.1103/PhysRevD.109.L121502. arXiv: 2405.12290 [gr-qc].

[111] Kristoffer Carlsson et al. *JuliaNLSolvers/NLsolve.jl: v4.0.0*. Version v4.0.0. May 2019. DOI: 10.5281/zenodo.2682214. URL: https://doi.org/10.5281/zenodo.2682214.

[112] Dean Carmi, Lorenzo Di Pietro, and Shota Komatsu. "A Study of Quantum Field Theories in AdS at Finite Coupling." In: *JHEP* 01 (2019), p. 200. DOI: 10.1007/JHEP01(2019)200. arXiv: 1810.04185 [hep-th].

[113] B. Carter. "Killing Tensor Quantum Numbers and Conserved Currents in Curved Space." In: *Phys. Rev. D* 16 (1977), pp. 3395–3414. DOI: 10.1103/PhysRevD.16.3395.

[114] Brandon Carter. "Global structure of the Kerr family of gravitational fields." In: *Phys. Rev.* 174 (1968), pp. 1559–1571. DOI: 10.1103/PhysRev.174.1559.

[115] Gregorio Carullo. "Enhancing modified gravity detection from gravitational-wave observations using the parametrized ringdown spin expansion coeffcients formalism." In: *Phys. Rev. D* 103.12 (2021), p. 124043. DOI: 10.1103/PhysRevD.103.124043. arXiv: 2102.05939 [gr-qc].

[116] Gregorio Carullo. "Black Hole Spectroscopy: from a mathematical problem to an observational reality." PhD thesis. U. Pisa (main), 2022.

[117] Gregorio Carullo, Walter Del Pozzo, and John Veitch. "Observational Black Hole Spectroscopy: A time-domain multimode analysis of GW150914." In: *Phys. Rev. D* 99.12 (2019). [Erratum: Phys.Rev.D 100, 089903 (2019)], p. 123029. DOI: 10.1103/PhysRevD.99.123029. arXiv: 1902.07527 [gr-qc].

[118] Gregorio Carullo, Walter Del Pozzo, and John Veitch. *pyRing: a time-domain ringdown analysis python package*. git.ligo.org/lscsoft/pyring. Version 2.3.0. July 2023. DOI: 10.5281/zenodo.8165508. URL: https://doi.org/10.5281/zenodo.8165508.

[119] Gregorio Carullo et al. "Empirical tests of the black hole no-hair conjecture using gravitational-wave observations." In: *Phys. Rev. D* 98.10 (2018), p. 104020. DOI: 10.1103/PhysRevD.98.104020. arXiv: 1805.04760 [gr-qc].

[120] Gregorio Carullo et al. "Constraints on Kerr-Newman black holes from merger-ringdown gravitational-wave observations." In: *Phys. Rev. D* 105.6 (2022), p. 062009. DOI: 10.1103/PhysRevD.105.062009. arXiv: 2109.13961 [gr-qc].

[121] Marc Casals and Adrian C. Ottewill. "High-order tail in Schwarzschild spacetime." In: *Phys. Rev. D* 92.12 (2015), p. 124055. DOI: 10.1103/PhysRevD.92.124055. arXiv: 1509.04702 [gr-qc].

[122] Carlo Cattaneo. "A form of heat-conduction equations which eliminates the paradox of instantaneous propagation." In: *Comptes rendus* 247 (1958), p. 431.

[123] Michail Chabanov and Luciano Rezzolla. "Impact of Bulk Viscosity on the Postmerger Gravitational-Wave Signal from Merging Neutron Stars." In: *Phys. Rev. Lett.* 134.7 (2025), p. 071402. DOI: 10.1103/PhysRevLett.134.071402. arXiv: 2307.10464 [gr-qc].

[124] Michail Chabanov and Luciano Rezzolla. "Numerical modeling of bulk viscosity in neutron stars." In: *Phys. Rev. D* 111.4 (2025), p. 044074. DOI: 10.1103/PhysRevD.111.044074. arXiv: 2311.13027 [gr-qc].

[125] Juno C. L. Chan et al. "Lensing and wave optics in the strong field of a black hole." In: (Feb. 2025). arXiv: 2502.14073 [gr-qc].

[126] Juno C. L. Chan et al. "Lensing and wave optics in the strong field of a black hole." In: *Phys. Rev. D* 112.6 (2025), p. 064009. DOI: 10.1103/6h6r-46cd. arXiv: 2502.14073 [gr-qc].

[127] S. Chandrasekhar and Steven L. Detweiler. "The quasi-normal modes of the Schwarzschild black hole." In: *Proc. Roy. Soc. Lond. A* 344 (1975), pp. 441–452. DOI: 10.1098/rspa.1975.0112.

[128] Subrahmanyan Chandrasekhar. *The mathematical theory of black holes*. 1985. ISBN: 978-0-19-850370-5.

[129] Subrahmanyan Chandrasekhar and Valeria Ferrari. "On the non-radial oscillations of a star. III. A reconsideration of the axial modes." In: *Proceedings of the Royal Society of London. Series A: Mathematical and Physical Sciences* 434.1891 (1991), pp. 449–457.

[130] Subrahmanyan Chandrasekhar and Valeria Ferrari. "On the non-radial oscillations of a star." In: *Proceedings of the Royal Society of London. Series A: Mathematical and Physical Sciences* 432.1885 (1991), pp. 247–279.

[131] Subrahmanyan Chandrasekhar and Valeria Ferrari. "On the non-radial oscillations of slowly rotating stars induced by the Lense-Thirring effect." In: *Proc. Roy. Soc. Lond. A* 433 (1991), pp. 423–440. DOI: 10.1098/rspa.1991.0056. URL: https://doi.org/10.1098/rspa.1991.0056.

[132] Debarati Chatterjee and Isaac Vidaña. "Do hyperons exist in the interior of neutron stars?" In: *Eur. Phys. J. A* 52.2 (2016), p. 29. DOI: 10.1140/epja/i2016-16029-x. arXiv: 1510.06306 [nucl-th].

[133] Samarth Chawla, Kwinten Fransen, and Cynthia Keeler. "The Penrose limit of the Weyl double copy." In: *Class. Quant. Grav.* 41.24 (2024), p. 245015. DOI: 10.1088/1361-6382/ad8f8c. arXiv: 2406.14601 [hep-th].

[134] Mark Ho-Yeuk Cheung et al. "Nonlinear Effects in Black Hole Ringdown." In: *Phys. Rev. Lett.* 130.8 (2023), p. 081401. DOI: 10.1103/PhysRevLett.130.081401. arXiv: 2208.07374 [gr-qc].

[135] Mark Ho-Yeuk Cheung et al. "Extracting linear and nonlinear quasinormal modes from black hole merger simulations." In: *Phys. Rev. D* 109.4 (2024). [Erratum: Phys.Rev.D 110, 049902 (2024)], p. 044069. DOI: 10.1103/PhysRevD.109.044069. arXiv: 2310.04489 [gr-qc].

[136] Horng Sheng Chia, Zihan Zhou, and Mikhail M. Ivanov. "Bring the Heat: Tidal Heating Constraints for Black Holes and Exotic Compact Objects from the LIGO-Virgo-KAGRA Data." In: (Apr. 2024). arXiv: 2404.14641 [gr-qc].

[137] E. S. C. Ching et al. "Late time tail of wave propagation on curved spacetime." In: *Phys. Rev. Lett.* 74 (1995), pp. 2414–2417. DOI: 10.1103/PhysRevLett.74.2414. arXiv: gr-qc/9410044.

[138] E. S. C. Ching et al. "Wave propagation in gravitational systems: Late time behavior." In: *Phys. Rev. D* 52 (1995), pp. 2118–2132. DOI: 10.1103/PhysRevD.52.2118. arXiv: gr-qc/9507035.

[139] E. S. C. Ching et al. "Quasinormal-mode expansion for waves in open systems." In: *Rev. Mod. Phys.* 70 (1998), p. 1545. DOI: 10.1103/RevModPhys.70.1545. arXiv: gr-qc/9904017.

[140] Cecilia Chirenti and Alberto Saa. "Quasinormal modes for the charged Vaidya metric." In: *J. Phys. Conf. Ser.* 314 (2011). Ed. by Victor Aldaya, Carlos Barcelo, and Jose Luis Jaramillo, p. 012086. DOI: 10.1088/1742-6596/314/1/012086. arXiv: 1012.5110 [gr-qc].

[141] P. L. Chrzanowski. "Vector Potential and Metric Perturbations of a Rotating Black Hole." In: *Phys. Rev. D* 11 (1975), pp. 2042–2062. DOI: 10.1103/PhysRevD.11.2042.

[142] Nicolas Clarisse et al. "Flux-Conservative BDNK Hydrodynamics and Shock Regularization." In: (Oct. 2025). arXiv: 2510.16603 [gr-qc].

[143] Teagan A. Clarke et al. "Toward a self-consistent framework for measuring black hole ringdowns." In: *Phys. Rev. D* 109.12 (2024), p. 124030. DOI: 10.1103/PhysRevD.109.124030. arXiv: 2402.02819 [gr-qc].

[144] J. M. Cohen and L. S. Kegeles. "Electromagnetic fields in curved spaces - a constructive procedure." In: *Phys. Rev. D* 10 (1974), pp. 1070–1084. DOI: 10.1103/PhysRevD.10.1070.

[145] Charles Collot, Helge Dietert, and Pierre Germain. "Stability and Cascades for the Kolmogorov–Zakharov Spectrum of Wave Turbulence." In: *Archive for Rational Mechanics and Analysis* 248.1 (2024), p. 7.

[146] G. L. Comer, David Langlois, and Lap Ming Lin. "Quasinormal modes of general relativistic superfluid neutron stars." In: *Phys. Rev. D* 60 (1999), p. 104025. DOI: 10.1103/PhysRevD.60.104025. arXiv: gr-qc/9908040.

[147] Gregory B. Cook. "Aspects of multimode Kerr ringdown fitting." In: *Phys. Rev. D* 102.2 (2020), p. 024027. DOI: 10.1103/PhysRevD.102.024027. arXiv: 2004.08347 [gr-qc].

[148] Roberto Cotesta et al. "Enriching the Symphony of Gravitational Waves from Binary Black Holes by Tuning Higher Harmonics." In: *Phys. Rev. D* 98.8 (2018), p. 084028. DOI: 10.1103/PhysRevD.98.084028. arXiv: 1803.10701 [gr-qc].

[149] Roberto Cotesta et al. "Analysis of Ringdown Overtones in GW150914." In: *Phys. Rev. Lett.* 129.11 (2022), p. 111102. DOI: 10.1103/PhysRevLett.129.111102. arXiv: 2201.00822 [gr-qc].

[150] Marco Crisostomi et al. "Neural Posterior Estimation with guaranteed exact coverage: the ringdown of GW150914." In: (May 2023). arXiv: 2305.18528 [gr-qc].

[151] Marion Cromb et al. "Creation of a black hole bomb instability in an electromagnetic system." In: (Mar. 2025). arXiv: 2503.24034 [quant-ph].

[152] Pedro V. P. Cunha, Emanuele Berti, and Carlos A. R. Herdeiro. "Light-Ring Stability for Ultracompact Objects." In: *Phys. Rev. Lett.* 119.25 (2017), p. 251102. DOI: 10.1103/PhysRevLett.119.251102. arXiv: 1708.04211 [gr-qc].

[153] Pedro V. P. Cunha et al. "Exotic Compact Objects and the Fate of the Light-Ring Instability." In: *Phys. Rev. Lett.* 130.6 (2023), p. 061401. DOI: 10.1103/PhysRevLett.130.061401. arXiv: 2207.13713 [gr-qc].

[154] C. T. Cunningham, R. H. Price, and V. Moncrief. "Radiation from collapsing relativistic stars. I - Linearized odd-parity radiation." In: *Astrophys. J.* 224 (1978), p. 643. DOI: 10.1086/156413.

[155] Curt Cutler and Lee Lindblom. "The effect of viscosity on neutron star oscillations." In: *Astrophysical Journal, Part 1 (ISSN 0004-637X), vol. 314, March 1, 1987, p. 234-241.* 314 (1987), pp. 234–241.

[156] Curt Cutler, Lee Lindblom, and Randall J Splinter. "Damping times for neutron star oscillations." In: *Astrophysical Journal, Part 1 (ISSN 0004-637X), vol. 363, Nov. 10, 1990, p. 603-611.* 363 (1990), pp. 603–611.

[157] Mihalis Dafermos and Igor Rodnianski. "Lectures on black holes and linear waves." In: *Clay Math. Proc.* 17 (2013). Ed. by David Ellwood et al., pp. 97–205. arXiv: 0811.0354 [gr-qc].

[158] T. Damour, N. Deruelle, and R. Ruffini. "On Quantum Resonances in Stationary Geometries." In: *Lett. Nuovo Cim.* 15 (1976), pp. 257–262. DOI: 10.1007/BF02725534.

[159] U. H. Danielsson, G. Dibitetto, and S. Giri. "Black holes as bubbles of AdS." In: *JHEP* 10 (2017), p. 171. DOI: 10.1007/JHEP10(2017)171. arXiv: 1705.10172 [hep-th].

[160] Ulf Danielsson and Suvendu Giri. "Observational signatures from horizonless black shells imitating rotating black holes." In: *JHEP* 07 (2018), p. 070. DOI: 10.1007/JHEP07(2018)070. arXiv: 1712.00511 [hep-th].

[161] Ulf Danielsson and Suvendu Giri. "Horizonless black hole mimickers with spin." In: *Phys. Rev. D* 109.2 (2024), p. 024038. DOI: 10.1103/PhysRevD.109.024038. arXiv: 2310.12148 [gr-qc].

[162] M. Davis et al. "Gravitational radiation from a particle falling radially into a schwarzschild black hole." In: *Phys. Rev. Lett.* 27 (1971), pp. 1466–1469. DOI: 10.1103/PhysRevLett.27.1466.

[163] Marina De Amicis et al. "Dynamical quasinormal mode excitation." In: (June 2025). arXiv: 2506.21668 [gr-qc].

[164] Walter Del Pozzo. *Bayesian inference and gravitational wave observations*. Lecture notes. Course notes. São Paulo, Brazil, 2015. URL: https://www.ictp-saifr.org/wp-content/uploads/2014/05/lectures.pdf.

[165] Walter Del Pozzo and John Veitch. *raynest: Parallel nested sampling in python*. https://pypi.org/project/raynest/1.0.0/. 2023.

[166] G. Denardo and R. Ruffini. "On the energetics of Reissner Nordstrøm geometries." In: *Phys. Lett. B* 45 (1973), pp. 259–262. DOI: 10.1016/0370-2693(73)90198-6.

[167] A. Derdzinski et al. "Evolution of gas disc–embedded intermediate mass ratio inspirals in the *LISA* band." In: *Mon. Not. Roy. Astron. Soc.* 501.3 (2021), pp. 3540–3557. DOI: 10.1093/mnras/staa3976. arXiv: 2005.11333 [astro-ph.HE].

[168] O. J. C. Dias and Jorge E. Santos. "AdS nonlinear instability: moving beyond spherical symmetry." In: *Class. Quant. Grav.* 33.23 (2016), 23LT01. DOI: 10.1088/0264-9381/33/23/23LT01. arXiv: 1602.03890 [hep-th].

[169] Oscar J. C. Dias, Roberto Emparan, and Alessandro Maccarrone. "Microscopic theory of black hole superradiance." In: *Phys. Rev. D* 77 (2008), p. 064018. DOI: 10.1103/PhysRevD.77.064018. arXiv: 0712.0791 [hep-th].

[170] Óscar J. C. Dias and Jorge E. Santos. "AdS nonlinear instability: breaking spherical and axial symmetries." In: *Class. Quant. Grav.* 35.18 (2018), p. 185006. DOI: 10.1088/1361-6382/aad514. arXiv: 1705.03065 [hep-th].

[171] Oscar J. C. Dias et al. "On the Nonlinear Stability of Asymptotically Anti-de Sitter Solutions." In: *Class. Quant. Grav.* 29 (2012), p. 235019. DOI: 10.1088/0264-9381/29/23/235019. arXiv: 1208.5772 [gr-qc].

[172] David Díaz-Guerra et al. "Gauge-invariant perturbations of relativistic non-perfect fluids in spherical spacetime." In: *Phys. Rev. D* 110.12 (2024), p. 124012. DOI: 10.1103/PhysRevD.110.124012. arXiv: 2410.18081 [gr-qc].

[173] Sam R. Dolan and Adrian C. Ottewill. "On an Expansion Method for Black Hole Quasinormal Modes and Regge Poles." In: *Class. Quant. Grav.* 26 (2009). Ed. by A. M. Uranga, p. 225003. DOI: 10.1088/0264-9381/26/22/225003. arXiv: 0908.0329 [gr-qc].

[174] Chris Doran. "A New form of the Kerr solution." In: *Phys. Rev. D* 61 (2000), p. 067503. DOI: 10.1103/PhysRevD.61.067503. arXiv: gr-qc/9910099.

[175] Francisco Duque et al. "Extreme-Mass-Ratio Inspirals in Ultralight Dark Matter." In: *Phys. Rev. Lett.* 133.12 (2024), p. 121404. DOI: 10.1103/PhysRevLett.133.121404. arXiv: 2312.06767 [gr-qc].

[176] Conor Dyson and Maarten van de Meent. "Kerr-fully diving into the abyss: analytic solutions to plunging geodesics in Kerr." In: *Class. Quant. Grav.* 40.19 (2023), p. 195026. DOI: 10.1088/1361-6382/acf552. arXiv: 2302.03704 [gr-qc].

[177] Conor Dyson et al. "Relativistic aerodynamics of spinning black holes." In: *Phys. Rev. D* 109.10 (2024), p. 104038. DOI: 10.1103/PhysRevD.109.104038. arXiv: 2402.07981 [gr-qc].

[178] Conor Dyson et al. "Environmental Effects in Extreme-Mass-Ratio Inspirals: Perturbations to the Environment in Kerr Spacetimes." In: *Phys. Rev. Lett.* 134.21 (2025), p. 211403. DOI: 10.1103/PhysRevLett.134.211403. arXiv: 2501.09806 [gr-qc].

[179] William E. East. "Gravitational collapse in the vicinity of the extremal black hole critical point." In: (Nov. 2025). arXiv: 2511.20567 [gr-qc].

[180] William E. East, Fethi M. Ramazanoğlu, and Frans Pretorius. "Black Hole Superradiance in Dynamical Spacetime." In: *Phys. Rev. D* 89.6 (2014), p. 061503. DOI: 10.1103/PhysRevD.89.061503. arXiv: 1312.4529 [gr-qc].

[181] William E. East et al. "Relativistic Simulations of Eccentric Binary Neutron Star Mergers: One-arm Spiral Instability and Effects of Neutron Star Spin." In: *Phys. Rev. D* 93.2 (2016), p. 024011. DOI: 10.1103/PhysRevD.93.024011. arXiv: 1511.01093 [astro-ph.HE].

[182] Lorenz Eberhardt, Shota Komatsu, and Sebastian Mizera. "Scattering equations in AdS: scalar correlators in arbitrary dimensions." In: *JHEP* 11 (2020), p. 158. DOI: 10.1007/JHEP11(2020)158. arXiv: 2007.06574 [hep-th].

[183] Carl Eckart. "The Thermodynamics of irreversible processes. 3.. Relativistic theory of the simple fluid." In: *Phys. Rev.* 58 (1940), pp. 919–924. DOI: 10.1103/PhysRev.58.919.

[184] Albert Einstein. "Näherungsweise integration der feldgleichungen der gravitation." In: *Sitzungsberichte der Königlich Preußischen Akademie der Wissenschaften* (1916), pp. 688–696.

[185] Albert Einstein. "Über gravitationswellen." In: *Sitzungsber. Preuss. Akad. Wiss.* 1 (1918), p. 154.

[186] Henriette Elvang and Yu-tin Huang. *Scattering Amplitudes in Gauge Theory and Gravity*. Cambridge University Press, Apr. 2015. ISBN: 978-1-316-19142-2, 978-1-107-06925-1.

[187] Miguel Escobedo and Juan Velázquez. *On the theory of weak turbulence for the nonlinear Schrödinger equation*. Vol. 238. 1124. American Mathematical Society, 2015.

[188] F Paul Esposito. "Absorption of gravitational energy by a viscous compressible fluid." In: *Astrophysical Journal, vol. 165, p. 165* 165 (1971), p. 165.

[189] Tamara Evstafyeva, Nils Siemonsen, and William E. East. "Assessing the stability of ultracompact spinning boson stars with nonlinear evolutions." In: (Aug. 2025). arXiv: 2508.11527 [gr-qc].

[190] V. Ferrari and K. D. Kokkotas. "Scattering of particles by neutron stars: Time evolutions for axial perturbations." In: *Phys. Rev. D* 62 (2000), p. 107504. DOI: 10.1103/PhysRevD.62.107504. arXiv: gr-qc/0008057.

[191] Valeria Ferrari and Bahram Mashhoon. "New approach to the quasinormal modes of a black hole." In: *Phys. Rev. D* 30 (1984), pp. 295–304. DOI: 10.1103/PhysRevD.30.295.

[192] Jose M. Figueroa-O'Farrill, Patrick Meessen, and Simon Philip. "Homogeneity and plane-wave limits." In: *JHEP* 05 (2005), p. 050. DOI: 10.1088/1126-6708/2005/05/050. arXiv: hep-th/0504069.

[193] Eliot Finch and Christopher J. Moore. "Searching for a ringdown overtone in GW150914." In: *Phys. Rev. D* 106.4 (2022), p. 043005. DOI: 10.1103/PhysRevD.106.043005. arXiv: 2205.07809 [gr-qc].

[194] Raphael Flauger and Steven Weinberg. "Gravitational Waves in Cold Dark Matter." In: *Phys. Rev. D* 97.12 (2018), p. 123506. DOI: 10.1103/PhysRevD.97.123506. arXiv: 1801.00386 [astro-ph.CO].

[195] Roger Fletcher. *Practical methods of optimization*. John Wiley & Sons, 2000.

[196] Kwinten Fransen. "Quasinormal modes from Penrose limits." In: *Class. Quant. Grav.* 40.20 (2023), p. 205004. DOI: 10.1088/1361-6382/acf26d. arXiv: 2301.06999 [gr-qc].

[197] Kwinten Fransen, David Pereñiguez, and Jaime Redondo-Yuste. "Perturbations of Plane Waves and Quadratic Quasinormal Modes on the Lightring." In: *JHEP* 2025.12 (Dec. 2025), p. 148. DOI: 10.1007/JHEP12(2025)148. arXiv: 2509.03598. URL: https://doi.org/10.1007/JHEP12(2025)148.

[198] Valeri P Frolov and Andrei Zelnikov. *Introduction to black hole physics*. OUP Oxford, 2011.

[199] Erich Gaertig and Kostas D. Kokkotas. "Relativistic g-modes in rapidly rotating neutron stars." In: *Phys. Rev. D* 80 (2009), p. 064026. DOI: 10.1103/PhysRevD.80.064026. arXiv: 0905.0821 [astro-ph.SR].

[200] Davide Gaiotto et al. "Twisted Traces on Abelian Quantum Higgs and Coulomb Branches." In: *Commun. Math. Phys.* 406.9 (2025), p. 202. DOI: 10.1007/s00220-025-05379-2. arXiv: 2308.15198 [hep-th].

[201] Sebastien Galtier and Sergey V. Nazarenko. "Direct Evidence of a Dual Cascade in Gravitational Wave Turbulence." In: *Phys. Rev. Lett.* 127.13 (2021), p. 131101. DOI: 10.1103/PhysRevLett.127.131101. arXiv: 2108.09158 [gr-qc].

[202] Walter Gautschi. "Computational aspects of three-term recurrence relations." In: *SIAM review* 9.1 (1967), pp. 24–82.

[203] Benoît Gay and Sébastien Galtier. "Gravitational wave turbulence: A multiple time scale approach for quartic wave interactions." In: *Phys. Rev. D* 109.8 (2024), p. 083531. DOI: 10.1103/PhysRevD.109.083531. arXiv: 2402.05614 [gr-qc].

[204] Benoît Gay and Sébastien Galtier. "Asymmetric dual cascade in gravitational wave turbulence." In: (Jan. 2025). arXiv: 2501.17023 [gr-qc].

[205] U. H. Gerlach and U. K. Sengupta. "GAUGE INVARIANT PERTURBATIONS ON MOST GENERAL SPHERICALLY SYMMETRIC SPACE-TIMES." In: *Phys. Rev. D* 19 (1979), pp. 2268–2272. DOI: 10.1103/PhysRevD.19.2268.

[206] U. H. Gerlach and U. K. Sengupta. "GAUGE INVARIANT COUPLED GRAVITATIONAL, ACOUSTICAL, AND ELECTROMAGNETIC MODES ON MOST GENERAL SPHERICAL SPACE-TIMES." In: *Phys. Rev. D* 22 (1980), pp. 1300–1312. DOI: 10.1103/PhysRevD.22.1300.

[207] Robert P. Geroch. "Spinor structure of space-times in general relativity. II." In: *J. Math. Phys.* 11 (1970), pp. 343–348. DOI: 10.1063/1.1665067.

[208] Robert P. Geroch, A. Held, and R. Penrose. "A space-time calculus based on pairs of null directions." In: *J. Math. Phys.* 14 (1973), pp. 874–881. DOI: 10.1063/1.1666410.

[209] Robert P. Geroch and L. Lindblom. "Dissipative relativistic fluid theories of divergence type." In: *Phys. Rev. D* 41 (1990), p. 1855. DOI: 10.1103/PhysRevD.41.1855.

[210] Suprovo Ghosh, Bikram Keshari Pradhan, and Debarati Chatterjee. "Tidal heating as a direct probe of strangeness inside neutron stars." In: *Phys. Rev. D* 109.10 (2024), p. 103036. DOI: 10.1103/PhysRevD.109.103036. arXiv: 2306.14737 [gr-qc].

[211] Suprovo Ghosh et al. "Tidal heating in binary inspiral of strange quark stars." In: *Phys. Rev. D* 112.8 (2025), p. 084072. DOI: 10.1103/h9r7-ld41. arXiv: 2504.07659 [gr-qc].

[212] G. W. Gibbons. "Quantized Fields Propagating in Plane Wave Space-Times." In: *Commun. Math. Phys.* 45 (1975), pp. 191–202. DOI: 10.1007/BF01629249.

[213] Matthew Giesler et al. "Overtones and nonlinearities in binary black hole ringdowns." In: *Phys. Rev. D* 111.8 (2025), p. 084041. DOI: 10.1103/PhysRevD.111.084041. arXiv: 2411.11269 [gr-qc].

[214] Simone Giombi, Charlotte Sleight, and Massimo Taronna. "Spinning AdS Loop Diagrams: Two Point Functions." In: *JHEP* 06 (2018), p. 030. DOI: 10.1007/JHEP06(2018)030. arXiv: 1708.08404 [hep-th].

[215] Suvendu Giri et al. "Exploring Black Hole Mimickers: Electromagnetic and Gravitational Signatures of AdS Black Shells." In: (May 2024). arXiv: 2405.08062 [gr-qc].

[216] Fernando Girotto and Alberto Saa. "Semi-analytical approach for the Vaidya metric in double-null coordinates." In: *Phys. Rev. D* 70 (2004), p. 084014. DOI: 10.1103/PhysRevD.70.084014. arXiv: gr-qc/0406067.

[217] Kostas Glampedakis and Nils Andersson. "Quick and dirty methods for studying black hole resonances." In: *Class. Quant. Grav.* 20 (2003), pp. 3441–3464. DOI: 10.1088/0264-9381/20/15/312. arXiv: gr-qc/0304030.

[218] Reinaldo J. Gleiser et al. "Second order perturbations of a Schwarzschild black hole." In: *Class. Quant. Grav.* 13 (1996), pp. L117–L124. DOI: 10.1088/0264-9381/13/10/001. arXiv: gr-qc/9510049.

[219] Goebel, C. J. "Comments on the "vibrations" of a Black Hole." In: *Astrophys. J. Lett.* 172 (1972), p. L95. DOI: 10.1086/180898. URL: https://ui.adsabs.harvard.edu/abs/1972ApJ...172L..95G.

[220] JN Goldberg and RK156679 Sachs. "Republication of: A theorem on Petrov types." In: *General Relativity and Gravitation* 41.2 (2009), pp. 433–444.

[221] Samuel E. Gralla and Alexandru Lupsasca. "Null geodesics of the Kerr exterior." In: *Phys. Rev. D* 101.4 (2020), p. 044032. DOI: 10.1103/PhysRevD.101.044032. arXiv: 1910.12881 [gr-qc].

[222] Finnian Gray et al. "Carrollian motion in magnetized black hole horizons." In: *Phys. Rev. D* 107.6 (2023), p. 064009. DOI: 10.1103/PhysRevD.107.064009. arXiv: 2211.13695 [gr-qc].

[223] Stephen R. Green, Stefan Hollands, and Peter Zimmerman. "Teukolsky formalism for nonlinear Kerr perturbations." In: *Class. Quant. Grav.* 37.7 (2020), p. 075001. DOI: 10.1088/1361-6382/ab7075. arXiv: 1908.09095 [gr-qc].

[224] Stephen R. Green et al. "Conserved currents for a Kerr black hole and orthogonality of quasinormal modes." In: *Phys. Rev. D* 107.6 (2023), p. 064030. DOI: 10.1103/PhysRevD.107.064030. arXiv: 2210.15935 [gr-qc].

[225] Phil Gregory. *Bayesian logical data analysis for the physical sciences: A comparative approach with Mathematica® support*. Cambridge University Press, 2005.

[226] L. P. Grishchuk and A. G. Polnarev. "Gravitational Waves and Their Interaction with Matter and Fields." In: *General Relativity and Gravitation II*. Ed. by A. Held. Vol. 2. Jan. 1980, p. 393.

[227] L. Gualtieri, J. A. Pons, and G. Miniutti. "Nonadiabatic oscillations of compact stars in general relativity." In: *Phys. Rev. D* 70.8, 084009 (Oct. 2004), p. 084009. DOI: 10.1103/PhysRevD.70.084009. arXiv: gr-qc/0405063 [gr-qc].

[228] Carsten Gundlach and Jose M. Martin-Garcia. "Gauge invariant and coordinate independent perturbations of stellar collapse. 1. The Interior." In: *Phys. Rev. D* 61 (2000), p. 084024. DOI: 10.1103/PhysRevD.61.084024. arXiv: gr-qc/9906068.

[229] Carsten Gundlach, Richard H. Price, and Jorge Pullin. "Late time behavior of stellar collapse and explosions: 1. Linearized perturbations." In: *Phys. Rev. D* 49 (1994), pp. 883–889. DOI: 10.1103/PhysRevD.49.883. arXiv: gr-qc/9307009.

[230] Carsten Gundlach, Richard H. Price, and Jorge Pullin. "Late time behavior of stellar collapse and explosions: 2. Nonlinear evolution." In: *Phys. Rev. D* 49 (1994), pp. 890–899. DOI: 10.1103/PhysRevD.49.890. arXiv: gr-qc/9307010.

[231] Guangzhou Guo, Peng Wang, and Yupeng Zhang. "Nonlinear Stability of Black Holes with a Stable Light Ring." In: (Mar. 2024). arXiv: 2403.02089 [gr-qc].

[232] Bertil Gustafsson, Heinz-Otto Kreiss, and Joseph Oliger. *Time dependent problems and difference methods*. Vol. 24. John Wiley & Sons, 1995.

[233] Jacques Hadamard. "Sur les problèmes aux dérivées partielles et leur signification physique." In: *Princeton university bulletin* (1902), pp. 49–52.

[234] Susan G. Hahn and Richard W. Lindquist. "The two-body problem in geometrodynamics." In: *Annals of Physics* 29.2 (Sept. 1964), pp. 304–331. DOI: 10.1016/0003-4916(64)90223-4.

[235] James B. Hartle. "Slowly rotating relativistic stars. 1. Equations of structure." In: *Astrophys. J.* 150 (1967), pp. 1005–1029. DOI: 10.1086/149400.

[236] James B. Hartle and Kip S. Thorne. "Slowly Rotating Relativistic Stars. II. Models for Neutron Stars and Supermassive Stars." In: *Astrophys. J.* 153 (1968), p. 807. DOI: 10.1086/149707.

[237] S. W. Hawking. "Perturbations of an expanding universe." In: *Astrophys. J.* 145 (1966), pp. 544–554. DOI: 10.1086/148793.

[238] Abhishek Hegade K. R., Justin L. Ripley, and Nicolás Yunes. "Dissipative tidal effects to next-to-leading order and constraints on the dissipative tidal deformability using gravitational wave data." In: *Phys. Rev. D* 110.4 (2024), p. 044041. DOI: 10.1103/PhysRevD.110.044041. arXiv: 2407.02584 [gr-qc].

[239] Werner Heisenberg. *Über stabilität und turbulenz von flüssigkeitsströmen*. Springer, 1985.

[240] W. A. Hiscock and L. Lindblom. "Stability and causality in dissipative relativistic fluids." In: *Annals Phys.* 151 (1983), pp. 466–496. DOI: 10.1016/0003-4916(83)90288-9.

[241] William A. Hiscock and Lee Lindblom. "Generic instabilities in first-order dissipative relativistic fluid theories." In: *Phys. Rev. D* 31 (1985), pp. 725–733. DOI: 10.1103/PhysRevD.31.725.

[242] Shahar Hod. "High order contamination in the tail of gravitational collapse." In: *Phys. Rev. D* 60 (1999), p. 104053. DOI: 10.1103/PhysRevD.60.104053. arXiv: gr-qc/9907044.

[243] Shahar Hod. "Wave tails in time dependent backgrounds." In: *Phys. Rev. D* 66 (2002), p. 024001. DOI: 10.1103/PhysRevD.66.024001. arXiv: gr-qc/0201017.

[244] Shahar Hod. "How pure is the tail of gravitational collapse?" In: *Class. Quant. Grav.* 26 (2009), p. 028001. DOI: 10.1088/0264-9381/26/2/028001. arXiv: 0902.0237 [gr-qc].

[245] Stefan Hollands and Vahid Toomani. "Metric reconstruction in Kerr spacetime." In: (May 2024). DOI: 10.1088/1361-6382/ad87a1. arXiv: 2405.18604 [gr-qc].

[246] Timothy J. Hollowood, Graham M. Shore, and Ross J. Stanley. "The Refractive Index of Curved Spacetime II: QED, Penrose Limits and Black Holes." In: *JHEP* 08 (2009), p. 089. DOI: 10.1088/1126-6708/2009/08/089. arXiv: 0905.0771 [hep-th].

[247] Seth Hopper. "Unbound motion on a Schwarzschild background: Practical approaches to frequency domain computations." In: *Phys. Rev. D* 97.6 (2018), p. 064007. DOI: 10.1103/PhysRevD.97.064007. arXiv: 1706.05455 [gr-qc].

[248] Gary T. Horowitz and Alan R. Steif. "Strings in Strong Gravitational Fields." In: *Phys. Rev. D* 42 (1990), pp. 1950–1959. DOI: 10.1103/PhysRevD.42.1950.

[249] Raphael E. Hoult and Pavel Kovtun. "Stable and causal relativistic Navier-Stokes equations." In: *JHEP* 06 (2020), p. 067. DOI: 10.1007/JHEP06(2020)067. arXiv: 2004.04102 [hep-th].

[250] Raphael E. Hoult and Pavel Kovtun. "Causality in dissipative relativistic magnetohydrodynamics." In: *JHEP* 04 (2025), p. 009. DOI: 10.1007/JHEP04(2025)009. arXiv: 2411.04966 [hep-th].

[251] Veronika E. Hubeny and Mukund Rangamani. "Causal structures of pp waves." In: *JHEP* 12 (2002), p. 043. DOI: 10.1088/1126-6708/2002/12/043. arXiv: hep-th/0211195.

[252] Kunihito Ioka and Hiroyuki Nakano. "Second and higher-order quasi-normal modes in binary black hole mergers." In: *Phys. Rev. D* 76 (2007), p. 061503. DOI: 10.1103/PhysRevD.76.061503. arXiv: 0704.3467 [astro-ph].

[253] Richard A. Isaacson. "Gravitational Radiation in the Limit of High Frequency. I. The Linear Approximation and Geometrical Optics." In: *Phys. Rev.* 166 (1968), pp. 1263–1271. DOI: 10.1103/PhysRev.166.1263.

[254] Richard A. Isaacson. "Gravitational Radiation in the Limit of High Frequency. II. Nonlinear Terms and the Ef fective Stress Tensor." In: *Phys. Rev.* 166 (1968), pp. 1272–1279. DOI: 10.1103/PhysRev.166.1272.

[255] Akihiro Ishibashi and Hideo Kodama. "Stability of higher dimensional Schwarzschild black holes." In: *Prog. Theor. Phys.* 110 (2003), pp. 901–919. DOI: 10.1143/PTP.110.901. arXiv: hep-th/0305185.

[256] W. Israel. "Singular hypersurfaces and thin shells in general relativity." In: *Nuovo Cim. B* 44S10 (1966). [Erratum: Nuovo Cim.B 48, 463 (1967)], p. 1. DOI: 10.1007/BF02710419.

[257] W. Israel. "Nonstationary irreversible thermodynamics: A Causal relativistic theory." In: *Annals Phys.* 100 (1976), pp. 310–331. DOI: 10.1016/0003-4916(76)90064-6.

[258] W. Israel. "Thermodynamics of relativistic systems." In: *Physica A: Statistical Mechanics and its Applications* 106.1 (1981), pp. 204–214. ISSN: 0378-4371. DOI: https://doi.org/10.1016/0378-4371(81)90220-X. URL: https://www.sciencedirect.com/science/article/pii/037843718190220X.

[259] W. Israel and J. M. Stewart. "Thermodynamics of nonstationary and transient effects in a relativistic gas." In: *Phys. Lett. A* 58.4 (1976), pp. 213–215. DOI: 10.1016/0375-9601(76)90075-X.

[260] Claudio Iuliano et al. "Extremal Black Hole Weather." In: (Dec. 2024). arXiv: 2412.02821 [gr-qc].

[261] José Luis Jaramillo, Rodrigo Panosso Macedo, and Lamis Al Sheikh. "Pseudospectrum and Black Hole Quasinormal Mode Instability." In: *Phys. Rev. X* 11.3 (2021), p. 031003. DOI: 10.1103/PhysRevX.11.031003. arXiv: 2004.06434 [gr-qc].

[262] E. T. Jaynes. *Probability Theory: The Logic of Science*. Cambridge, UK: Cambridge University Press, 2003. DOI: 10.1017/CBO9780511790423.

[263] Christian Baadsgaard Jepsen and Sarthak Parikh. "Propagator identities, holographic conformal blocks, and higher-point AdS diagrams." In: *JHEP* 10 (2019), p. 268. DOI: 10.1007/JHEP10(2019)268. arXiv: 1906.08405 [hep-th].

[264] Michael D. Johnson et al. "The Black Hole Explorer: motivation and vision." In: *Proc. SPIE Int. Soc. Opt. Eng.* 13092 (2024), p. 130922D. DOI: 10.1117/12.3019835. arXiv: 2406.12917 [astro-ph.IM].

[265] Daniel Kapec and Ahmed Sheta. "pp-Waves and the Hidden Symmetries of Black Hole Quasinormal Modes." In: (Dec. 2024). arXiv: 2412.08551 [hep-th].

[266] David J. Kaup. "Klein-Gordon Geon." In: *Phys. Rev.* 172 (1968), pp. 1331–1342. DOI: 10.1103/PhysRev.172.1331.

[267] Lennox S. Keeble and Frans Pretorius. "First-order viscous relativistic hydrodynamics on the two-sphere." In: *Phys. Rev. D* 112.12 (2025), p. 124034. DOI: 10.1103/d4wd-zj7w. arXiv: 2508.20998 [gr-qc].

[268] L. S. Kegeles and J. M. Cohen. "Constructive Procedure for Perturbations of space-times." In: *Phys. Rev. D* 19 (1979), pp. 1641–1664. DOI: 10.1103/PhysRevD.19.1641.

[269] Alex Kehagias, Davide Perrone, and Antonio Riotto. "Non-linear Quasi-Normal Modes of the Schwarzschild Black Hole from the Penrose Limit." In: (Mar. 2025). arXiv: 2503.09350 [gr-qc].

[270] Christoph Kehle and Ryan Unger. "Gravitational collapse to extremal black holes and the third law of black hole thermodynamics." In: (Nov. 2022). arXiv: 2211.15742 [gr-qc].

[271] Christoph Kehle and Ryan Unger. "Extremal black hole formation as a critical phenomenon." In: (Feb. 2024). arXiv: 2402.10190 [gr-qc].

[272] Joe Keir. "Slowly decaying waves on spherically symmetric spacetimes and ultracompact neutron stars." In: *Class. Quant. Grav.* 33.13 (2016), p. 135009. DOI: 10.1088/0264-9381/33/13/135009. arXiv: 1404.7036 [gr-qc].

[273] Bernard J. Kelly and John G. Baker. "Decoding mode mixing in black-hole merger ringdown." In: *Phys. Rev. D* 87.8 (2013), p. 084004. DOI: 10.1103/PhysRevD.87.084004. arXiv: 1212.5553 [gr-qc].

[274] R. P. Kerr and A. Schild. "Republication of: A new class of vacuum solutions of the Einstein field equations." In: *Gen. Rel. Grav.* 41.10 (2009), pp. 2485–2499. DOI: 10.1007/s10714-009-0857-z.

[275] Roy P. Kerr. "Gravitational field of a spinning mass as an example of algebraically special metrics." In: *Phys. Rev. Lett.* 11 (1963), pp. 237–238. DOI: 10.1103/PhysRevLett.11.237.

[276] Jirair K Kevorkian and Julian D Cole. *Multiple scale and singular perturbation methods*. Vol. 114. Springer Science & Business Media, 2012.

[277] Neev Khera, Sizheng Ma, and Huan Yang. "Quadratic Mode Couplings in Rotating Black Holes and Their Detectability." In: (Oct. 2024). arXiv: 2410.14529 [gr-qc].

[278] Kenta Kiuchi et al. "Efficient magnetic-field amplification due to the Kelvin-Helmholtz instability in binary neutron star mergers." In: *Phys. Rev. D* 92.12 (2015), p. 124034. DOI: 10.1103/PhysRevD.92.124034. arXiv: 1509.09205 [astro-ph.HE].

[279] Bence Kocsis and Abraham Loeb. "Brightening of an Accretion Disk Due to Viscous Dissipation of Gravitational Waves During the Coalescence of Supermassive Black Holes." In: *Phys. Rev. Lett.* 101 (2008), p. 041101. DOI: 10.1103/PhysRevLett.101.041101. arXiv: 0803.0003 [astro-ph].

[280] Bence Kocsis, Nicolas Yunes, and Abraham Loeb. "Observable Signatures of EMRI Black Hole Binaries Embedded in Thin Accretion Disks." In: *Phys. Rev. D* 84 (2011), p. 024032. DOI: 10.1103/PhysRevD.86.049907. arXiv: 1104.2322 [astro-ph.GA].

[281] Hideo Kodama and Akihiro Ishibashi. "A Master equation for gravitational perturbations of maximally symmetric black holes in higher dimensions." In: *Prog. Theor. Phys.* 110 (2003), pp. 701–722. DOI: 10.1143/PTP.110.701. arXiv: hep-th/0305147.

[282] Hideo Kodama and Akihiro Ishibashi. "Master equations for perturbations of generalized static black holes with charge in higher dimensions." In: *Prog. Theor. Phys.* 111 (2004), pp. 29–73. DOI: 10.1143/PTP.111.29. arXiv: hep-th/0308128.

[283] Hideo Kodama, Akihiro Ishibashi, and Osamu Seto. "Brane world cosmology: Gauge invariant formalism for perturbation." In: *Phys. Rev. D* 62 (2000), p. 064022. DOI: 10.1103/PhysRevD.62.064022. arXiv: hep-th/0004160.

[284] Y. Kojima. "Equations governing the nonradial oscillations of a slowly rotating relativistic star." In: *Phys. Rev. D* 46 (1992), pp. 4289–4303. DOI: 10.1103/PhysRevD.46.4289.

[285] Yasufumi Kojima. "Two Families of Normal Modes in Relativistic Stars." In: *Prog. Theor. Phys.* 79 (1988), p. 665. DOI: 10.1143/PTP.79.665.

[286] K. D. Kokkotas. "Pulsating relativistic stars." In: *Les Houches School of Physics: Astrophysical Sources of Gravitational Radiation*. Sept. 1995, pp. 89–102. arXiv: gr-qc/9603024.

[287] K. D. Kokkotas and B. F. Schutz. "W-modes: a new family of normal modes of pulsating relativistic stars." In: *Mon. Not. Roy. Astron. Soc.* 255.1 (1992), pp. 119–128. DOI: 10.1093/mnras/255.1.119.

[288] Kostas. D. Kokkotas and Johannes Ruoff. "Radial oscillations of relativistic stars." In: *Astron. Astrophys.* 366 (2001), p. 565. DOI: 10.1051/0004-6361:20000216. arXiv: gr-qc/0011093.

[289] Kostas D. Kokkotas and Bernd G. Schmidt. "Quasinormal modes of stars and black holes." In: *Living Rev. Rel.* 2 (1999), p. 2. DOI: 10.12942/lrr-1999-2. arXiv: gr-qc/9909058.

[290] AN Kolmogorov. "Local structure of turbulence in an incompressible viscous fluid at very high Reynolds numbers." In: *Soviet Physics Uspekhi* 10.6 (1968), p. 734.

[291] P. Kovtun, Dan T. Son, and Andrei O. Starinets. "Viscosity in strongly interacting quantum field theories from black hole physics." In: *Phys. Rev. Lett.* 94 (2005), p. 111601. DOI: 10.1103/PhysRevLett.94.111601. arXiv: hep-th/0405231.

[292] Pavel Kovtun. "Lectures on hydrodynamic fluctuations in relativistic theories." In: *J. Phys. A* 45 (2012), p. 473001. DOI: 10.1088/1751-8113/45/47/473001. arXiv: 1205.5040 [hep-th].

[293] Pavel Kovtun. "First-order relativistic hydrodynamics is stable." In: *JHEP* 10 (2019), p. 034. DOI: 10.1007/JHEP10(2019)034. arXiv: 1907.08191 [hep-th].

[294] Pavel Kovtun, Dam T. Son, and Andrei O. Starinets. "Holography and hydrodynamics: Diffusion on stretched horizons." In: *JHEP* 10 (2003), p. 064. DOI: 10.1088/1126-6708/2003/10/064. arXiv: hep-th/0309213.

[295] M Kranyš. "Relativistic hydrodynamics with irreversible thermodynamics without the paradox of infinite velocity of heat conduction." In: *Il Nuovo Cimento B (1965-1970)* 42 (1966), pp. 51–70.

[296] Juan A Valiente Kroon. *Conformal methods in general relativity*. Cambridge university press, 2017.

[297] Eckhard Krotscheck and Wolfgang Kundt. "Causality Criteria." In: *Communications in Mathematical Physics* 60 (1978), pp. 171–180. DOI: 10.1007/BF01609447.

[298] David Kubiznak et al. "Parallel-propagated frame along null geodesics in higher-dimensional black hole spacetimes." In: *Phys. Rev. D* 79 (2009), p. 024018. DOI: 10.1103/PhysRevD.79.024018. arXiv: 0811.0012 [gr-qc].

[299] Kei-ichiro Kubota et al. "Spin wave optics for gravitational waves lensed by a Kerr black hole." In: *Phys. Rev. D* 110.12 (2024), p. 124011. DOI: 10.1103/PhysRevD.110.124011. arXiv: 2408.03289 [gr-qc].

[300] Macarena Lagos and Lam Hui. "Generation and propagation of nonlinear quasinormal modes of a Schwarzschild black hole." In: *Phys. Rev. D* 107.4 (2023), p. 044040. DOI: 10.1103/PhysRevD.107.044040. arXiv: 2208.07379 [gr-qc].

[301] Lev Davidovich Landau and Evgenii Mikhailovich Lifshitz. *Fluid Mechanics: Volume 6*. Vol. 6. Elsevier, 1987.

[302] E. W. Leaver. "An Analytic representation for the quasi normal modes of Kerr black holes." In: *Proc. Roy. Soc. Lond. A* 402 (1985), pp. 285–298. DOI: 10.1098/rspa.1985.0119.

[303] Edward W. Leaver. "Spectral decomposition of the perturbation response of the Schwarzschild geometry." In: *Phys. Rev. D* 34 (1986), pp. 384–408. DOI: 10.1103/PhysRevD.34.384.

[304] Luis Lehner, Oscar A. Reula, and Marcelo E. Rubio. "Hyperbolic theory of relativistic conformal dissipative fluids." In: *Phys. Rev. D* 97.2 (2018), p. 024013. DOI: 10.1103/PhysRevD.97.024013. arXiv: 1710.08033 [gr-qc].

[305] Luis Lehner et al. "m=1 instability and gravitational wave signal in binary neutron star mergers." In: *Phys. Rev. D* 94.4 (2016), p. 043003. DOI: 10.1103/PhysRevD.94.043003. arXiv: 1605.02369 [gr-qc].

[306] Josef Lense and Hans Thirring. "Ueber den Einfluss der Eigenrotation der Zentralkoerper auf die Bewegung der Planeten und Monde nach der Einsteinschen Gravitationstheorie." In: *Phys. Z.* 19 (1918), pp. 156–163.

[307] Xiang Li et al. "Angular emission patterns of remnant black holes." In: *Phys. Rev. D* 105.2 (2022), p. 024016. DOI: 10.1103/PhysRevD.105.024016. arXiv: 2110.03116 [gr-qc].

[308] Steven L. Liebling and Carlos Palenzuela. "Dynamical boson stars." In: *Living Rev. Rel.* 26.1 (2023), p. 1. DOI: 10.1007/s41114-023-00043-4. arXiv: 1202.5809 [gr-qc].

[309] Halston Lim et al. "Exciting black hole modes via misaligned coalescences: II. The mode content of late-time coalescence waveforms." In: *Phys. Rev. D* 100.8 (2019), p. 084032. DOI: 10.1103/PhysRevD.100.084032. arXiv: 1901.05902 [gr-qc].

[310] L Lindblom and Steven L. Detweiler. "The quadrupole oscillations of neutron stars." In: *Astrophys. J. Suppl.* 53 (1983), pp. 73–92. DOI: 10.1086/190884.

[311] Lee Lindblom and Gregory Mendell. "The Oscillations of Superfluid Neutron Stars." In: *Astrophys. J.* 421 (Feb. 1994), p. 689. DOI: 10.1086/173682.

[312] R. S. Lindzen and J. W. Barker. "Instability and wave over-reflection in stably stratified shear flow." In: *Journal of Fluid Mechanics* 151 (Jan. 1985), pp. 189–217. DOI: 10.1017/S0022112085000921.

[313] Dong C Liu and Jorge Nocedal. "On the limited memory BFGS method for large scale optimization." In: *Mathematical programming* 45.1-3 (1989), pp. 503–528.

[314] Hong Liu. "Scattering in anti-de Sitter space and operator product expansion." In: *Phys. Rev. D* 60 (1999), p. 106005. DOI: 10.1103/PhysRevD.60.106005. arXiv: hep-th/9811152.

[315] L. London and E. Fauchon-Jones. "On modeling for Kerr black holes: Basis learning, QNM frequencies, and spherical-spheroidal mixing coefficients." In: *Class. Quant. Grav.* 36.23 (2019), p. 235015. DOI: 10.1088/1361-6382/ab2f11. arXiv: 1810.03550 [gr-qc].

[316] Lionel T. London. "A radial scalar product for Kerr quasinormal modes." In: (Dec. 2023). arXiv: 2312.17678 [gr-qc].

[317] Lionel London and Michelle Gurevich. "Natural polynomials for Kerr quasinormal modes." In: (Dec. 2023). arXiv: 2312.17680 [gr-qc].

[318] Lionel London, Deirdre Shoemaker, and James Healy. "Modeling ringdown: Beyond the fundamental quasinormal modes." In: *Phys. Rev. D* 90.12 (2014). [Erratum: Phys.Rev.D 94, 069902 (2016)], p. 124032. DOI: 10.1103/PhysRevD.90.124032. arXiv: 1404.3197 [gr-qc].

[319] Nicholas Loutrel et al. "Second Order Perturbations of Kerr Black Holes: Reconstruction of the Metric." In: *Phys. Rev. D* 103.10 (2021), p. 104017. DOI: 10.1103/PhysRevD.103.104017. arXiv: 2008.11770 [gr-qc].

[320] Miles Lucas et al. *TuringLang/NestedSamplers.jl: v0.8.1*. Version v0.8.1. Dec. 2021. DOI: 10.5281/zenodo.5808196. URL: https://doi.org/10.5281/zenodo.5808196.

[321] Alexandru Lupsasca et al. "The Black Hole Explorer: photon ring science, detection, and shape measurement." In: *Proc. SPIE Int. Soc. Opt. Eng.* 13092 (2024), 130926Q. DOI: 10.1117/12.3019437. arXiv: 2406.09498 [gr-qc].

[322] Sizheng Ma et al. "Quasinormal-mode filters: A new approach to analyze the gravitational-wave ringdown of binary black-hole mergers." In: *Phys. Rev. D* 106.8 (2022), p. 084036. DOI: 10.1103/PhysRevD.106.084036. arXiv: 2207.10870 [gr-qc].

[323] Sizheng Ma et al. "Emergent Turbulence in Nonlinear Gravity." In: (Aug. 2025). arXiv: 2508.13294 [gr-qc].

[324] Caio F. B. Macedo et al. "Spectral lines of extreme compact objects." In: *Phys. Rev. D* 98.10 (2018), p. 104034. DOI: 10.1103/PhysRevD.98.104034. arXiv: 1807.04762 [gr-qc].

[325] J. Madore. "The absorption of gravitational radiation by a dissipative fluid." In: *Communications in Mathematical Physics* 30.4 (1973), pp. 335–340. ISSN: 1432-0916. DOI: 10.1007/BF01645508. URL: https://doi.org/10.1007/BF01645508.

[326] Elisa Maggio. "Probing new physics on the horizon of black holes with gravitational waves." PhD thesis. Rome U., 2022. arXiv: 2211.16900 [gr-qc].

[327] Michele Maggiore. *Gravitational waves: Volume 1: Theory and experiments*. Vol. 1. Oxford university press, 2008.

[328] Michele Maggiore et al. "Science Case for the Einstein Telescope." In: *JCAP* 03 (2020), p. 050. DOI: 10.1088/1475-7516/2020/03/050. arXiv: 1912.02622 [astro-ph.CO].

[329] Gareth Arturo Marks et al. "Long-term stable nonlinear evolutions of ultracompact black-hole mimickers." In: (Apr. 2025). arXiv: 2504.17775 [gr-qc].

[330] Karl Martel and Eric Poisson. "Gravitational perturbations of the Schwarzschild spacetime: A Practical covariant and gauge-invariant formalism." In: *Phys. Rev. D* 71 (2005), p. 104003. DOI: 10.1103/PhysRevD.71.104003. arXiv: gr-qc/0502028.

[331] Jose M. Martin-Garcia and Carsten Gundlach. "All nonspherical perturbations of the Choptuik space-time decay." In: *Phys. Rev. D* 59 (1999), p. 064031. DOI: 10.1103/PhysRevD.59.064031. arXiv: gr-qc/9809059.

[332] Jose M. Martin-Garcia and Carsten Gundlach. "Gauge invariant and coordinate independent perturbations of stellar collapse. 2. Matching to the exterior." In: *Phys. Rev. D* 64 (2001), p. 024012. DOI: 10.1103/PhysRevD.64.024012. arXiv: gr-qc/0012056.

[333] Bahram Mashhoon. "Stability of charged rotating black holes in the eikonal approximation." In: *Phys. Rev. D* 31.2 (1985), pp. 290–293. DOI: 10.1103/PhysRevD.31.290.

[334] LJ Mason. "On Ward's integral formula for the wave equation in plane wave space-times." In: *Twistor Newsletter* 28 (1989), pp. 17–19.

[335] Samir D. Mathur. "The Fuzzball proposal for black holes: An Elementary review." In: *Fortsch. Phys.* 53 (2005). Ed. by E. Kiritsis, pp. 793–827. DOI: 10.1002/prop.200410203. arXiv: hep-th/0502050.

[336] Pawel O. Mazur and Emil Mottola. "Gravitational vacuum condensate stars." In: *Proc. Nat. Acad. Sci.* 101 (2004), pp. 9545–9550. DOI: 10.1073/pnas.0402717101. arXiv: gr-qc/0407075.

[337] B. McKernan et al. "Stars as resonant absorbers of gravitational waves." In: *Mon. Not. Roy. Astron. Soc.* 445 (2014), p. 74. DOI: 10.1093/mnrasl/slu136. arXiv: 1405.1414 [astro-ph.HE].

[338] Maarten van de Meent. "Analytic solutions for parallel transport along generic bound geodesics in Kerr spacetime." In: *Class. Quant. Grav.* 37.14 (2020), p. 145007. DOI: 10.1088/1361-6382/ab79d5. arXiv: 1906.05090 [gr-qc].

[339] Raissa F. P. Mendes et al. "Radial Oscillations of Viscous Neutron Stars: Zero Diffusion Case." In: (Sept. 2025). arXiv: 2509.12330 [gr-qc].

[340] John W. Miles. "Dispersive Reflection at the Interface between Ideal and Viscous Media." In: *Acoustical Society of America Journal* 26.6 (Jan. 1954), p. 1015. DOI: 10.1121/1.1907439.

[341] Yasushi Mino. "Perturbative approach to an orbital evolution around a supermassive black hole." In: *Phys. Rev. D* 67 (2003), p. 084027. DOI: 10.1103/PhysRevD.67.084027. arXiv: gr-qc/0302075.

[342] Keefe Mitman et al. "Nonlinearities in Black Hole Ringdowns." In: *Phys. Rev. Lett.* 130.8 (2023), p. 081402. DOI: 10.1103/PhysRevLett.130.081402. arXiv: 2208.07380 [gr-qc].

[343] Keefe Mitman et al. "A review of gravitational memory and BMS frame fixing in numerical relativity." In: *Class. Quant. Grav.* 41.22 (2024), p. 223001. DOI: 10.1088/1361-6382/ad83c2. arXiv: 2405.08868 [gr-qc].

[344] Keefe Mitman et al. "Probing the ringdown perturbation in binary black hole coalescences with an improved quasi-normal mode extraction algorithm." In: (Mar. 2025). arXiv: 2503.09678 [gr-qc].

[345] V. Moncrief. "Gravitational perturbations of spherically symmetric systems. I. The exterior problem." In: *Annals Phys.* 88 (1974), pp. 323–342. DOI: 10.1016/0003-4916(74)90173-0.

[346] Elias R. Most et al. "Projecting the likely importance of weak-interaction-driven bulk viscosity in neutron star mergers." In: *Mon. Not. Roy. Astron. Soc.* 509.1 (2021), pp. 1096–1108. DOI: 10.1093/mnras/stab2793. arXiv: 2107.05094 [astro-ph.HE].

[347] Elias R. Most et al. "Emergence of microphysical viscosity in binary neutron star post-merger dynamics." In: (July 2022). arXiv: 2207.00442 [astro-ph.HE].

[348] Pierre Mourier et al. "Quasinormal modes and their overtones at the common horizon in a binary black hole merger." In: *Phys. Rev. D* 103.4 (2021), p. 044054. DOI: 10.1103/PhysRevD.103.044054. arXiv: 2010.15186 [gr-qc].

[349] Gowtham Rishi Mukkamala and David Pereñiguez. "Decoupled gravitational wave equations in spherical symmetry from curvature wave equations." In: *JCAP* 01 (2025), p. 122. DOI: 10.1088/1475-7516/2025/01/122. arXiv: 2408.13557 [gr-qc].

[350] Shinji Mukohyama. "Gauge invariant gravitational perturbations of maximally symmetric space-times." In: *Phys. Rev. D* 62 (2000), p. 084015. DOI: 10.1103/PhysRevD.62.084015. arXiv: hep-th/0004067.

[351] Ingo Müller. "Zum paradoxon der wärmeleitungstheorie." In: *Zeitschrift für Physik* 198.4 (1967), pp. 329–344.

[352] Alessandro Nagar and Luciano Rezzolla. "Gauge-invariant non-spherical metric perturbations of Schwarzschild black-hole spacetimes." In: *Class. Quant. Grav.* 22 (2005). [Erratum: Class.Quant.Grav. 23, 4297 (2006)], R167. DOI: 10.1088/0264-9381/22/16/R01. arXiv: gr-qc/0502064.

[353] Alessandro Nagar et al. "Accretion driven gravitational radiation from non-rotating compact objects. Infalling quadrupolar shells." In: *Phys. Rev. D* 69 (2004), p. 124028. DOI: 10.1103/PhysRevD.69.124028. arXiv: gr-qc/0403077.

[354] Hiroyuki Nakano and Kunihito Ioka. "Second Order Quasi-Normal Mode of the Schwarzschild Black Hole." In: *Phys. Rev. D* 76 (2007), p. 084007. DOI: 10.1103/PhysRevD.76.084007. arXiv: 0708.0450 [gr-qc].

[355] Sergey Nazarenko. *Wave turbulence*. Vol. 825. Springer, 2011.

[356] Ezra Newman and Roger Penrose. "An Approach to gravitational radiation by a method of spin coefficients." In: *J. Math. Phys.* 3 (1962), pp. 566–578. DOI: 10.1063/1.1724257.

[357] Jean-Philippe Nicolas. "Non linear Klein-Gordon equation on Schwarzschild-like metrics." In: *Nonlinear Hyperbolic Problems: Theoretical, Applied, and Computational Aspects: Proceedings of the Fourth International Conference on Hyperbolic Problems, Taormina, Italy, April 3 to 8, 1992*. Ed. by Andrea Donato and Francesco Oliveri. Wiesbaden: Vieweg+Teubner Verlag, 1993, pp. 449–456. ISBN: 978-3-322-87871-7. DOI: 10.1007/978-3-322-87871-7_54. URL: https://doi.org/10.1007/978-3-322-87871-7_54.

[358] Hans-Peter Nollert. "TOPICAL REVIEW: Quasinormal modes: the characteristic 'sound' of black holes and neutron stars." In: *Class. Quant. Grav.* 16 (1999), R159–R216. DOI: 10.1088/0264-9381/16/12/201.

[359] Hans-Peter Nollert and Richard H. Price. "Quantifying excitations of quasinormal mode systems." In: *J. Math. Phys.* 40 (1999), pp. 980–1010. DOI: 10.1063/1.532698. arXiv: gr-qc/9810074.

[360] D. D. Ofengeim et al. "Bulk viscosity in neutron stars with hyperon cores." In: *Phys. Rev. D* 100.10 (2019), p. 103017. DOI: 10.1103/PhysRevD.100.103017. arXiv: 1911.08407 [astro-ph.HE].

[361] Sheehan Olver and Alex Townsend. "A fast and well-conditioned spectral method." In: *siam REVIEW* 55.3 (2013), pp. 462–489.

[362] J. R. Oppenheimer and H. Snyder. "On Continued gravitational contraction." In: *Phys. Rev.* 56 (1939), pp. 455–459. DOI: 10.1103/PhysRev.56.455.

[363] Alex Pandya, Elias R. Most, and Frans Pretorius. "Causal, stable first-order viscous relativistic hydrodynamics with ideal gas microphysics." In: *Phys. Rev. D* 106.12 (2022), p. 123036. DOI: 10.1103/PhysRevD.106.123036. arXiv: 2209.09265 [gr-qc].

[364] Alex Pandya, Elias R. Most, and Frans Pretorius. "Conservative finite volume scheme for first-order viscous relativistic hydrodynamics." In: *Phys. Rev. D* 105.12 (2022), p. 123001. DOI: 10.1103/PhysRevD.105.123001. arXiv: 2201.12317 [gr-qc].

[365] Alex Pandya and Frans Pretorius. "Numerical exploration of first-order relativistic hydrodynamics." In: *Phys. Rev. D* 104.2 (2021), p. 023015. DOI: 10.1103/PhysRevD.104.023015. arXiv: 2104.00804 [gr-qc].

[366] Paolo Pani. "Advanced Methods in Black-Hole Perturbation Theory." In: *Int. J. Mod. Phys. A* 28 (2013). Ed. by V. Cardoso et al., p. 1340018. DOI: 10.1142/S0217751X13400186. arXiv: 1305.6759 [gr-qc].

[367] Paolo Pani et al. "Gravitational wave signatures of the absence of an event horizon. I. Nonradial oscillations of a thin-shell gravastar." In: *Phys. Rev. D* 80 (2009), p. 124047. DOI: 10.1103/PhysRevD.80.124047. arXiv: 0909.0287 [gr-qc].

[368] Paolo Pani et al. "Perturbations of slowly rotating black holes: massive vector fields in the Kerr metric." In: *Phys. Rev. D* 86 (2012), p. 104017. DOI: 10.1103/PhysRevD.86.104017. arXiv: 1209.0773 [gr-qc].

[369] Rodrigo Panosso Macedo. "Hyperboloidal approach for static spherically symmetric spacetimes: a didactical introductionand applications in black-hole physics." In: *Phil. Trans. Roy. Soc. Lond. A* 382.2267 (2024), p. 20230046. DOI: 10.1098/rsta.2023.0046. arXiv: 2307.15735 [gr-qc].

[370] Demetrios Papadopoulos and F Paul Esposito. "Absorption of gravitational energy by a viscous compressible fluid in a curved spacetime." In: *Astrophysical Journal, Part 1 (ISSN 0004-637X), vol. 292, May 15, 1985, p. 330-338.* 292 (1985), pp. 330–338.

[371] G. Papadopoulos. "Separability, plane wave limits and rotating black holes." In: *Class. Quant. Grav.* 38.19 (2021), p. 195018. DOI: 10.1088/1361-6382/ac1cf8. arXiv: 2007.04702 [hep-th].

[372] Enrique Pazos et al. "Mode coupling of Schwarzschild perturbations: Ringdown frequencies." In: *Phys. Rev. D* 82 (2010), p. 104028. DOI: 10.1103/PhysRevD.82.104028. arXiv: 1009.4665 [gr-qc].

[373] R. Penrose. "The Nonlinear Graviton." In: *Gen. Rel. Grav.* 7 (1976), pp. 171–176. DOI: 10.1007/BF00763433.

[374] Roger Penrose. "A Remarkable property of plane waves in general relativity." In: *Rev. Mod. Phys.* 37 (1965), pp. 215–220. DOI: 10.1103/RevModPhys.37.215.

[375] Roger Penrose and Wolfgang Rindler. *Spinors and Space-Time*. Cambridge Monographs on Mathematical Physics. Cambridge, UK: Cambridge Univ. Press, Apr. 2011. ISBN: 978-0-521-33707-6, 978-0-511-86766-8, 978-0-521-33707-6. DOI: 10.1017/CBO9780511564048.

[376] David Pereñiguez. "Black hole perturbations and electric-magnetic duality." In: *Phys. Rev. D* 108.8 (2023), p. 084046. DOI: 10.1103/PhysRevD.108.084046. arXiv: 2302.10942 [gr-qc].

[377] D. Perrone, A. Kehagias, and A. Riotto. "Nonlinearities in Kerr Black Hole Ringdown from the Penrose Limit." In: (July 2025). arXiv: 2507.01919 [gr-qc].

[378] A. Z. Petrov. "The Classification of spaces defining gravitational fields." In: *Gen. Rel. Grav.* 32 (2000), pp. 1661–1663. DOI: 10.1023/A:1001910908054.

[379] Martin Pijnenburg et al. "Wave optics lensing of gravitational waves: Theory and phenomenology of triple systems in the LISA band." In: *Phys. Rev. D* 110.4 (2024), p. 044054. DOI: 10.1103/PhysRevD.110.044054. arXiv: 2404.07186 [gr-qc].

[380] Chantal Pitte et al. "Detectability of higher harmonics with LISA." In: *Phys. Rev. D* 108.4 (2023), p. 044053. DOI: 10.1103/PhysRevD.108.044053. arXiv: 2304.03142 [gr-qc].

[381] Alessia Platania and Jaime Redondo-Yuste. "Diverging black hole entropy from quantum infrared non-localities." In: *Phys. Lett. B* 857 (2024), p. 138993. DOI: 10.1016/j.physletb.2024.138993. arXiv: 2303.17621 [hep-th].

[382] Eric Poisson and W. Israel. "Inner-horizon instability and mass inflation in black holes." In: *Phys. Rev. Lett.* 63 (1989), pp. 1663–1666. DOI: 10.1103/PhysRevLett.63.1663.

[383] J. A. Pons et al. "Relativistic r-modes and shear viscosity: Regularizing the continuous spectrum." In: *Mon. Not. Roy. Astron. Soc.* 363 (2005), pp. 121–130. DOI: 10.1111/j.1365-2966.2005.09429.x. arXiv: astro-ph/0504062.

[384] W. H. Press. "ON GRAVITATIONAL CONDUCTORS, WAVEGUIDES, AND CIRCUITS." In: *Gen. Rel. Grav.* 11 (1979), pp. 105–109. DOI: 10.1007/BF00756582.

[385] William H. Press. "Long Wave Trains of Gravitational Waves from a Vibrating Black Hole." In: *Astrophys. J. Lett.* 170 (1971), pp. L105–L108. DOI: 10.1086/180849.

[386] William H. Press and Saul A. Teukolsky. "Floating Orbits, Superradiant Scattering and the Black-hole Bomb." In: *Nature* 238 (1972), pp. 211–212. DOI: 10.1038/238211a0.

[387] Frans Pretorius. "Evolution of binary black hole spacetimes." In: *Phys. Rev. Lett.* 95 (2005), p. 121101. DOI: 10.1103/PhysRevLett.95.121101. arXiv: gr-qc/0507014.

[388] Larry R. Price, Karthik Shankar, and Bernard F. Whiting. "On the existence of radiation gauges in Petrov type II spacetimes." In: *Class. Quant. Grav.* 24 (2007), pp. 2367–2388. DOI: 10.1088/0264-9381/24/9/014. arXiv: gr-qc/0611070.

[389] Richard H. Price. "Nonspherical Perturbations of Relativistic Gravitational Collapse. II. Integer-Spin, Zero-Rest-Mass Fields." In: *Phys. Rev. D* 5 (1972), pp. 2439–2454. DOI: 10.1103/PhysRevD.5.2439.

[390] Richard H. Price. "Nonspherical perturbations of relativistic gravitational collapse. 1. Scalar and gravitational perturbations." In: *Phys. Rev. D* 5 (1972), pp. 2419–2438. DOI: 10.1103/PhysRevD.5.2419.

[391] Christopher Rackauckas and Qing Nie. "DifferentialEquations.jl–a performant and feature-rich ecosystem for solving differential equations in Julia." In: *Journal of Open Research Software* 5.1 (2017).

[392] David Radice, Sebastiano Bernuzzi, and Christian D. Ott. "One-armed spiral instability in neutron star mergers and its detectability in gravitational waves." In: *Phys. Rev. D* 94.6 (2016), p. 064011. DOI: 10.1103/PhysRevD.94.064011. arXiv: 1603.05726 [gr-qc].

[393] David Radice et al. "Probing Extreme-Density Matter with Gravitational Wave Observations of Binary Neutron Star Merger Remnants." In: *Astrophys. J. Lett.* 842.2 (2017), p. L10. DOI: 10.3847/2041-8213/aa775f. arXiv: 1612.06429 [astro-ph.HE].

[394] Leonardo Rastelli and Xinan Zhou. "How to Succeed at Holographic Correlators Without Really Trying." In: *JHEP* 04 (2018), p. 014. DOI: 10.1007/JHEP04(2018)014. arXiv: 1710.05923 [hep-th].

[395] Jaime Redondo-Yuste. "Perturbations of relativistic dissipative stars." In: *Class. Quant. Grav.* 42.7 (2025), p. 075012. DOI: 10.1088/1361-6382/adbfef. arXiv: 2411.16841 [gr-qc].

[396] Jaime Redondo-Yuste and Alejandro Cárdenas-Avendaño. "Perturbative and nonlinear analyses of gravitational turbulence in spacetimes with stable light rings." In: *Phys. Rev. D* 111.12 (2025), p. 124009. DOI: 10.1103/hy3r-ww3w. arXiv: 2502.18643 [gr-qc].

[397] Jaime Redondo-Yuste and Vitor Cardoso. "Superradiant amplification by rotating viscous compact objects." In: *Phys. Rev. D* 112.6 (2025), p. L061501. DOI: 10.1103/gvd3-lqkv. arXiv: 2506.13850 [gr-qc].

[398] Jaime Redondo-Yuste and Luis Lehner. "Non-linear black hole dynamics and Carrollian fluids." In: *JHEP* 02 (2023), p. 240. DOI: 10.1007/JHEP02(2023)240. arXiv: 2212.06175 [gr-qc].

[399] Jaime Redondo-Yuste, David Pereñiguez, and Vitor Cardoso. "Ringdown of a dynamical spacetime." In: *Phys. Rev. D* 109.4 (2024), p. 044048. DOI: 10.1103/PhysRevD.109.044048. arXiv: 2312.04633 [gr-qc].

[400] Jaime Redondo-Yuste et al. "Eternal binaries." In: *Phys. Rev. D* 107.12 (2023), p. 124025. DOI: 10.1103/PhysRevD.107.124025. arXiv: 2304.02039 [gr-qc].

[401] Jaime Redondo-Yuste et al. "Spin dependence of black hole ringdown nonlinearities." In: *Phys. Rev. D* 109.10 (2024), p. L101503. DOI: 10.1103/PhysRevD.109.L101503. arXiv: 2308.14796 [gr-qc].

[402] Tullio Regge and John A. Wheeler. "Stability of a Schwarzschild singularity." In: *Phys. Rev.* 108 (1957), pp. 1063–1069. DOI: 10.1103/PhysRev.108.1063.

[403] David Reitze et al. "Cosmic Explorer: The U.S. Contribution to Gravitational-Wave Astronomy beyond LIGO." In: *Bull. Am. Astron. Soc.* 51.7 (2019), p. 035. arXiv: 1907.04833 [astro-ph.IM].

[404] Oscar A. Reula. "Strongly hyperbolic systems in general relativity." In: *J. Hyperbol. Diff. Equat.* 1.02 (2004), pp. 251–269. DOI: 10.1142/S0219891604000111. arXiv: gr-qc/0403007.

[405] Herbert S. Ribner. "Reflection, Transmission, and Amplification of Sound by a Moving Medium." In: *Acoustical Society of America Journal* 29.4 (Jan. 1957), p. 435. DOI: 10.1121/1.1908918.

[406] Maurício Richartz and Alberto Saa. "Superradiance without event horizons in General Relativity." In: *Phys. Rev. D* 88 (2013), p. 044008. DOI: 10.1103/PhysRevD.88.044008. arXiv: 1306.3137 [gr-qc].

[407] Justin L. Ripley, Abhishek Hegade K. R., and Nicolas Yunes. "Probing internal dissipative processes of neutron stars with gravitational waves during the inspiral of neutron star binaries." In: *Phys. Rev. D* 108.10 (2023), p. 103037. DOI: 10.1103/PhysRevD.108.103037. arXiv: 2306.15633 [gr-qc].

[408] Justin L. Ripley and Kent Yagi. "Black hole perturbation under a 2 + 2 decomposition in the action." In: *Phys. Rev. D* 97.2 (2018), p. 024009. DOI: 10.1103/PhysRevD.97.024009. arXiv: 1705.03068 [gr-qc].

[409] Justin L. Ripley et al. "Numerical computation of second order vacuum perturbations of Kerr black holes." In: *Phys. Rev. D* 103 (2021), p. 104018. DOI: 10.1103/PhysRevD.103.104018. arXiv: 2010.00162 [gr-qc].

[410] Justin L. Ripley et al. "A constraint on the dissipative tidal deformability of neutron stars." In: *Nature Astron.* 8.10 (2024), pp. 1277–1283. DOI: 10.1038/s41550-024-02323-7. arXiv: 2312.11659 [gr-qc].

[411] Gabriel S. Rocha, Gabriel S. Denicol, and Jorge Noronha. "Perturbative approaches in relativistic kinetic theory and the emergence of first-order hydrodynamics." In: *Phys. Rev. D* 106.3 (2022), p. 036010. DOI: 10.1103/PhysRevD.106.036010. arXiv: 2205.00078 [nucl-th].

[412] Andrzej Rostworowski. "Higher order perturbations of anti–de Sitter space and time-periodic solutions of vacuum Einstein equations." In: *Phys. Rev. D* 95.12 (2017), p. 124043. DOI: 10.1103/PhysRevD.95.124043. arXiv: 1701.07804 [gr-qc].

[413] Andrzej Rostworowski. "Towards a theory of nonlinear gravitational waves: A systematic approach to nonlinear gravitational perturbations in the vacuum." In: *Phys. Rev. D* 96.12 (2017), p. 124026. DOI: 10.1103/PhysRevD.96.124026. arXiv: 1705.02258 [gr-qc].

[414] Remo Ruffini and Silvano Bonazzola. "Systems of selfgravitating particles in general relativity and the concept of an equation of state." In: *Phys. Rev.* 187 (1969), pp. 1767–1783. DOI: 10.1103/PhysRev.187.1767.

[415] Michael P. Ryan. "Teukolsky equation and Penrose wave equation." In: *Phys. Rev. D* 10 (1974), pp. 1736–1740. DOI: 10.1103/PhysRevD.10.1736.

[416] R. K. Sachs. "Gravitational radiation." In: *Les Houches Summer Shcool of Theoretical Physics: Relativity, Groups and Topology*. 1964, pp. 523–564.

[417] M. V. S. Saketh and Elisa Maggio. "Quasinormal modes of slowly-spinning horizonless compact objects." In: *Phys. Rev. D* 110.8 (2024), p. 084038. DOI: 10.1103/PhysRevD.110.084038. arXiv: 2406.10070 [gr-qc].

[418] João S. Santos et al. "Gravitational Waves from Binary Extreme Mass Ratio Inspirals: Doppler Shift and Beaming, Resonant Excitation, Helicity Oscillations, and Self-Lensing." In: *Phys. Rev. Lett.* 135.21 (2025), p. 211402. DOI: 10.1103/qq3m-6phh. arXiv: 2506.14868 [gr-qc].

[419] Laura Sberna et al. "Nonlinear effects in the black hole ringdown: Absorption-induced mode excitation." In: *Phys. Rev. D* 105.6 (2022), p. 064046. DOI: 10.1103/PhysRevD.105.064046.

[420] Peter Schneider, Jürgen Ehlers, and Emilio E. Falco. *Gravitational Lenses*. Astronomy and Astrophysics Library. Springer, 1992. ISBN: 978-3-540-66506-9, 978-3-662-03758-4. DOI: 10.1007/978-3-662-03758-4.

[421] Oliver Schulz et al. "BAT.jl: A Julia-Based Tool for Bayesian Inference." In: *SN Computer Science* 2.3 (2021), p. 210. ISSN: 2661-8907. DOI: 10.1007/s42979-021-00626-4. URL: https://doi.org/10.1007/s42979-021-00626-4.

[422] Bernard F. Schutz and Clifford M. Will. "BLACK HOLE NORMAL MODES: A SEMIANALYTIC APPROACH." In: *Astrophys. J. Lett.* 291 (1985), pp. L33–L36. DOI: 10.1086/184453.

[423] Karl Schwarzschild. "On the gravitational field of a mass point according to Einstein's theory." In: *Sitzungsber. Preuss. Akad. Wiss. Berlin (Math. Phys.)* 1916 (1916), pp. 189–196. arXiv: physics/9905030.

[424] N. I. Shakura and R. A. Sunyaev. "Black holes in binary systems. Observational appearance." In: *Astron. Astrophys.* 24 (1973), pp. 337–355.

[425] Harry L. H. Shum et al. "Neutron star evolution with BDNK viscous hydrodynamics framework." In: (Sept. 2025). arXiv: 2509.15303 [gr-qc].

[426] Nils Siemonsen. "Nonlinear treatment of a black hole mimicker ringdown." In: (Apr. 2024). arXiv: 2404.14536 [gr-qc].

[427] Nils Siemonsen. "Ergoregion instability in bosonic stars: Scalar mode structure, universality, and weakly nonlinear effects." In: *Phys. Rev. D* 112.12 (2025), p. 124031. DOI: 10.1103/sbtt-jnjg. arXiv: 2510.07468 [gr-qc].

[428] Nils Siemonsen. "Weakly turbulent saturation of the nonlinear scalar ergoregion instability." In: (Oct. 2025). arXiv: 2510.07467 [gr-qc].

[429] Hector O. Silva, Abhirup Ghosh, and Alessandra Buonanno. "Black-hole ringdown as a probe of higher-curvature gravity theories." In: *Phys. Rev. D* 107.4 (2023), p. 044030. DOI: 10.1103/PhysRevD.107.044030. arXiv: 2205.05132 [gr-qc].

[430] Devinderjit Sivia and John Skilling. *Data analysis: a Bayesian tutorial*. OUP Oxford, 2006.

[431] John Skilling. "Nested sampling." In: *Bayesian inference and maximum entropy methods in science and engineering* 735 (2004), pp. 395–405.

[432] Ulrich Sperhake et al. "The High-energy collision of two black holes." In: *Phys. Rev. Lett.* 101 (2008), p. 161101. DOI: 10.1103/PhysRevLett.101.161101. arXiv: 0806.1738 [gr-qc].

[433] Lorenzo Speri et al. "Probing Accretion Physics with Gravitational Waves." In: *Phys. Rev. X* 13.2 (2023), p. 021035. DOI: 10.1103/PhysRevX.13.021035. arXiv: 2207.10086 [gr-qc].

[434] Thomas F. M. Spieksma et al. "Black Hole Spectroscopy in Environments: Detectability Prospects." In: *Phys. Rev. Lett.* 134.8 (2025), p. 081402. DOI: 10.1103/PhysRevLett.134.081402. arXiv: 2409.05950 [gr-qc].

[435] Seppe J. Staelens. "Search for growing angular modes in ultracompact boson star evolutions." In: Aug. 2025. arXiv: 2508.19460 [gr-qc].

[436] Leo C. Stein. "qnm: A Python package for calculating Kerr quasinormal modes, separation constants, and spherical-spheroidal mixing coefficients." In: *J. Open Source Softw.* 4.42 (2019), p. 1683. DOI: 10.21105/joss.01683. arXiv: 1908.10377 [gr-qc].

[437] Hans Stephani et al. *Exact solutions of Einstein's field equations*. Cambridge Monographs on Mathematical Physics. Cambridge: Cambridge Univ. Press, 2003. ISBN: 978-0-521-46702-5, 978-0-511-05917-9. DOI: 10.1017/CBO9780511535185.

[438] Nikolaos Stergioulas. "Rotating Stars in Relativity." In: *Living Rev. Rel.* 6 (2003), p. 3. DOI: 10.12942/lrr-2003-3. arXiv: gr-qc/0302034.

[439] JM Stewart. "Solutions of the wave equation on a Schwarzschild spacetime with localized energy." In: *Proceedings of the Royal Society of London. A. Mathematical and Physical Sciences* 424.1866 (1989), pp. 239–244.

[440] Edward Teo. "Spherical Photon Orbits Around a Kerr Black Hole." In: *Gen. Rel. Grav.* 35.11 (2003), pp. 1909–1926. DOI: 10.1023/A:1026286607562.

[441] S. A. Teukolsky. "Rotating black holes - separable wave equations for gravitational and electromagnetic perturbations." In: *Phys. Rev. Lett.* 29 (1972), pp. 1114–1118. DOI: 10.1103/PhysRevLett.29.1114.

[442] Kip S. Thorne. "Disk accretion onto a black hole. 2. Evolution of the hole." In: *Astrophys. J.* 191 (1974), pp. 507–520. DOI: 10.1086/152991.

[443] Kip S Thorne and Alfonso Campolattaro. "Non-radial pulsation of general-relativistic stellar models. I. Analytic analysis for L>= 2." In: *Astrophysical Journal, vol. 149, p. 591* 149 (1967), p. 591.

[444] Kip S Thorne, Charles W Misner, and John Archibald Wheeler. *Gravitation*. Freeman San Francisco, 2000.

[445] Paul Tod. "Spacetimes with all Penrose limits diagonalisable." In: *Class. Quant. Grav.* 37.7 (2020), p. 075021. DOI: 10.1088/1361-6382/ab738a. arXiv: 1909.07756 [gr-qc].

[446] Giovanni Maria Tomaselli, Thomas F. M. Spieksma, and Gianfranco Bertone. "The legacy of boson clouds on black hole binaries." In: (July 2024). arXiv: 2407.12908 [gr-qc].

[447] Giovanni Maria Tomaselli, Thomas F. M. Spieksma, and Gianfranco Bertone. "The resonant history of gravitational atoms in black hole binaries." In: (Mar. 2024). arXiv: 2403.03147 [gr-qc].

[448] Vahid Toomani et al. "New metric reconstruction scheme for gravitational self-force calculations." In: *Class. Quant. Grav.* 39.1 (2022), p. 015019. DOI: 10.1088/1361-6382/ac37a5. arXiv: 2108.04273 [gr-qc].

[449] Theo Torres et al. "Observation of superradiance in a vortex flow." In: *Nature Phys.* 13 (2017), pp. 833–836. DOI: 10.1038/nphys4151. arXiv: 1612.06180 [gr-qc].

[450] Theo Torres et al. "Regge pole description of scattering by dirty black holes." In: *Phys. Rev. D* 107.6 (2023), p. 064028. DOI: 10.1103/PhysRevD.107.064028. arXiv: 2211.17147 [gr-qc].

[451] Gabriele Travaglini et al. "The SAGEX review on scattering amplitudes." In: *J. Phys. A* 55.44 (2022), p. 443001. DOI: 10.1088/1751-8121/ac8380. arXiv: 2203.13011 [hep-th].

[452] P. Vaidya. "The Gravitational Field of a Radiating Star." In: *Proc. Natl. Inst. Sci. India A* 33 (1951), p. 264.

[453] NG Van Kampen. "A model for relativistic heat transport." In: *Physica* 46.2 (1970), pp. 315–332.

[454] Robert M. Wald. "Construction of Solutions of Gravitational, Electromagnetic, Or Other Perturbation Equations from Solutions of Decoupled Equations." In: *Phys. Rev. Lett.* 41 (1978), pp. 203–206. DOI: 10.1103/PhysRevLett.41.203.

[455] Robert M. Wald. *General Relativity*. Chicago, USA: Chicago Univ. Pr., 1984. DOI: 10.7208/chicago/9780226870373.001.0001.

[456] M. Walker and R. Penrose. "On quadratic first integrals of the geodesic equations for type [22] spacetimes." In: *Commun. Math. Phys.* 18 (1970), pp. 265–274. DOI: 10.1007/BF01649445.

[457] C. Warnick. "(In)completeness of Quasinormal Modes." In: *Acta Phys. Polon. Supp.* 15.1 (2022), p. 1. DOI: 10.5506/APhysPolBSupp.15.1-A13.

[458] B. Waugh and K. Lake. "Double Null Coordinates for the Vaidya Metric." In: *Phys. Rev. D* 34 (1986), pp. 2978–2984. DOI: 10.1103/PhysRevD.34.2978.

[459] Steven Weinberg. "Entropy generation and the survival of protogalaxies in an expanding universe." In: *Astrophys. J.* 168 (1971), p. 175. DOI: 10.1086/151073.

[460] J. A. Wheeler. "Geons." In: *Phys. Rev.* 97 (1955), pp. 511–536. DOI: 10.1103/PhysRev.97.511.

[461] Eugene P Wigner. "The unreasonable effectiveness of mathematics in the natural sciences." In: *Mathematics and science*. World Scientific, 1990, pp. 291–306.

[462] Kent Yagi and Nicolas Yunes. "I-Love-Q Relations in Neutron Stars and their Applications to Astrophysics, Gravitational Waves and Fundamental Physics." In: *Phys. Rev. D* 88.2 (2013), p. 023009. DOI: 10.1103/PhysRevD.88.023009. arXiv: 1303.1528 [gr-qc].

[463] Huan Yang, Aaron Zimmerman, and Luis Lehner. "Turbulent Black Holes." In: *Phys. Rev. Lett.* 114 (2015), p. 081101. DOI: 10.1103/PhysRevLett.114.081101.

[464] Sophia Yi et al. "Nonlinear quasinormal mode detectability with next-generation gravitational wave detectors." In: *Phys. Rev. D* 109.12 (2024), p. 124029. DOI: 10.1103/PhysRevD.109.124029. arXiv: 2403.09767 [gr-qc].

[465] Sophia Yi et al. "Systematic biases from the exclusion of higher harmonics in parameter estimation on LISA binaries." In: (Feb. 2025). arXiv: 2502.12237 [gr-qc].

[466] Nicolas Yunes, Kent Yagi, and Frans Pretorius. "Theoretical Physics Implications of the Binary Black-Hole Mergers GW150914 and GW151226." In: *Phys. Rev. D* 94.8 (2016), p. 084002. DOI: 10.1103/PhysRevD.94.084002. arXiv: 1603.08955 [gr-qc].

[467] Vladimir E Zakharov. "Weak turbulence in media with a decay spectrum." In: *Journal of Applied Mechanics and Technical Physics* 6.4 (1965), pp. 22–24.

[468] Vladimir E Zakharov, Victor S L'vov, and Gregory Falkovich. *Kolmogorov spectra of turbulence I: Wave turbulence*. Springer Science & Business Media, 2012.

[469] Ya. B. Zeldovich. "Generation of Waves by a Rotating Body." In: *Soviet Journal of Experimental and Theoretical Physics Letters* 14 (Aug. 1971), p. 180.

[470] Ya. B. Zeldovich. "Amplification of Cylindrical Electromagnetic Waves Reflected from a Rotating Body." In: *Soviet Journal of Experimental and Theoretical Physics* 35 (Jan. 1972), p. 1085.

[471] Anil Zenginoglu. "A Geometric framework for black hole perturbations." In: *Phys. Rev. D* 83 (2011), p. 127502. DOI: 10.1103/PhysRevD.83.127502. arXiv: 1102.2451 [gr-qc].

[472] F. J. Zerilli. "Gravitational field of a particle falling in a schwarzschild geometry analyzed in tensor harmonics." In: *Phys. Rev. D* 2 (1970), pp. 2141–2160. DOI: 10.1103/PhysRevD.2.2141.

[473] Frank J. Zerilli. "Effective potential for even parity Regge-Wheeler gravitational perturbation equations." In: *Phys. Rev. Lett.* 24 (1970), pp. 737–738. DOI: 10.1103/PhysRevLett.24.737.

[474] Zhen Zhong, Vitor Cardoso, and Elisa Maggio. "Instability of ultracompact horizonless spacetimes." In: *Phys. Rev. D* 107.4 (2023), p. 044035. DOI: 10.1103/PhysRevD.107.044035. arXiv: 2211.16526 [gr-qc].

[475] Hengrui Zhu et al. "Challenges in quasinormal mode extraction: Perspectives from numerical solutions to the Teukolsky equation." In: *Phys. Rev. D* 109.4 (2024), p. 044010. DOI: 10.1103/PhysRevD.109.044010. arXiv: 2309.13204 [gr-qc].

[476] Hengrui Zhu et al. "Nonlinear effects in black hole ringdown from scattering experiments: Spin and initial data dependence of quadratic mode coupling." In: *Phys. Rev. D* 109.10 (2024), p. 104050. DOI: 10.1103/PhysRevD.109.104050. arXiv: 2401.00805 [gr-qc].

[477] Yosef Zlochower et al. "Mode coupling in the nonlinear response of black holes." In: *Phys. Rev. D* 68 (2003), p. 084014. DOI: 10.1103/PhysRevD.68.084014. arXiv: gr-qc/0306098.